Proton Transfer in Peptide Systems

OLIVER RUPERT MAGUIRE

Proton Transfer in Peptide Systems

Oliver R. Maguire

Department of Chemistry

Durham University

2016

Submitted in partial fulfillment of the requirements for the Degree of

Doctor of Philosophy

Declaration

The work described in this thesis was carried out at the Department of Chemistry, Durham University, between October 2012 and October 2016, under the supervision of Dr. AnnMarie O'Donoghue. The material contained has not been previously submitted for a degree at this or any other university. All work has been carried out by the author unless otherwise indicated.

Statement of Copyright

In Memory of Mum and Oupa

“Peace I leave with you; my peace I give you. I do not give to you as the world gives.
Do not let your hearts be troubled and do not be afraid.”
John 14:27

“The cautious seldom err.”
Confucius

Abstract

This thesis details investigations into the proton transfer reactions of peptide systems and how this knowledge can be used to understand the chemical behaviour of peptides.

The acidity of the α-proton in peptides has an essential role in numerous biochemical reactions. The carbon acidity of cyclic dipeptides, diketopiperazines (DKPs), has been studied. Hydrogen deuterium exchange reactions monitored by ^{1}H NMR spectroscopy were used to measure second order rate constants for deprotonation by deuteroxide, k_{DO} (M^{-1} s^{-1}) at 25 ºC and I = 1.00 (KCl). Values recorded were between 1.12×10^{-1} – 1.02×10^{-3} M^{-1} s^{-1} and in the order of Prolyl > Glycyl > Alanyl > Tyrosyl. Prolyl residues had higher than expected kinetic acidities – this was attributed to a stereoelectronic effect; the other residues followed expected trends. Estimates for the pK_as were interpolated from a Brønsted relationship as pK_a = 18.8 – 23.7. It is posited that the stereoelectronic effect could play a role in enzyme catalysis by lowering the barrier to enolate formation.

The carbon acidity of triketopiperazines (TKPs), DKPs with an additional carbonyl, was also studied. Values of k_{DO} for the α-protons were between 5.09×10^{5} – 8.99×10^{6} M^{-1} s^{-1}. This is ~ 10^{6}-fold larger than that of the DKPs and was attributed to the early development of aromaticity in the transition state for the TKPs. A Brønsted relationship for carbon acids with aromatic enolates gave pK_a estimates between -3.35 – 4.39.

Native Chemical Ligation (NCL) is one of the two principle techniques used in the chemical synthesis of proteins and ligates an N-terminal cysteine thiolate with a C-terminal thioester that upon rearrangement forms the native amide bond. We have measured the pK_as of thiols in a series of cysteine derivatives using UV-Vis spectrophotometry at 25 °C and I = 0.3 (NaCl). Our results have been used to develop a detailed understanding of the mechanism of kinetically controlled NCLs.

Table of Contents

i Acknowledgements

A huge thank you to my supervisor, Dr. AnnMarie O'Donoghue, for all her help and support and for entrusting me with this project. I am incredibly grateful for her understanding, patience, encouragement, direction and mentorship. I have loved doing this PhD and I have been so lucky to have you as a supervisor. I would also like to thank Dr. David Hodgson for his encouragement and many helpful discussions. I thank the EPSRC and Durham University for funding as well.

A huge thank you to past and present members of the O'Donoghue and Hodgson research groups. Special mentions to: Dr. Richard Massey for his mentorship and guidance, David Wong-Pascua for outstanding company along the journey, Casey Banks for teaching me innumerable tricks around the lab, Peter Quinn for his friendship and many in-depth discussions on the intricacies of physical organic chemistry, David Tucker for his companionship and brightening our days with many amusing anecdotes, Vicki Linthwaite for being such a good laugh and a listening ear. Also to Beth Taylor for all her help on the TKPs and Jacob Grant for his good company. A big thank you to the Sandford group, particularly Toni Harsanyi and Craig Fisher, for being such good company in the lab and office and for allowing me to borrow various bits of glassware and chemicals.

A big thank you to Dr. Steven Cobb and Dr. Alex Hudson whose help was invaluable in the research into the cysteine derivatives and native chemical ligation and to Jingyi (Angela) Zong for her help in preparing the peptide systems. A thank you to the Beeby group for allowing me to use your balance – I could not have done any of the work without it. My thanks to Dr. Mark Fox for his help on performing DFT calculations.

I would also like to thank the incredible NMR service at the department: Dr. Alan Kenwright, Catharine Heffernan and Dr. Juan Aguilar for their help on all things NMR and for allowing me to hog NMR spectrometers even at silly hours in the morning. A big thank you to Dr. Aileen Congreave as well for all her help on the HPLC work and for devoting a good number of hours to helping me purify my various compounds. I'd

like to thank Jean Eccleston for helping me navigate through various bits of administration. Thank you to all the lab assistants as well for their bright company.

I'd like to thank the whole community of King's Church Durham for their all support and particularly to the Neville Terrace Cell group whose love and care has helped me persevere throughout the PhD. A special mention to Chris and Hannah Juby, Nate and Charissa Warne and Hannah and Ben Jiggins for their deep friendship and kindness to me.

A massive Thank You to all my friends: The whole Gap Year Group, especially Andrew Finlay and Louise Billingham, for their friendship, encouragement and being all-round fab – I love you all. To Joe Smith whose outstanding friendship and support has kept me going and I am extraordinarily blessed to have you as a friend. To Martin Dehnel-Wild and Heather Dehnel-Wild for their great company and being such good housemates. To Daniel Wright for a lovely year and a bit in the Deanery. To Michael and Jenny Sadgrove for allowing me to live in such an incredible home for so much of my studies. To everyone from John's for their friendship. To everyone from 48 Heron's Court for allowing me to stay with them for a few months at the end.

Finally, a huge thank you to my family. To Dad, whose unwavering love and support I could not do without. Thank you so much for everything. To my sister Clare, thank you for your wonderful friendship and for always giving me perspective on things – you are brilliant. To Nana, your love and company are a joy and thank you for allowing me to retreat regularly to the peacefulness of your home. To Oupa, whose fascination with the world taught me so much; I am very happy you got to see me start this journey and I wish you were here to share in the joy at end. And to my Mum, I miss you terribly, I will always be grateful for your love and everything you taught me, I know this work would make you proud.

ii Abbreviations

AcCl	Acyl Chloride
AcOH	Acetic Acid
AIBN	Azobisisobutyronitrile
Ala	Alanine
BAL	Backbone Amide Linked
CAN	Ceric ammonium nitrate
DCC	N,N'-Dicyclohexylcarbodiimide
DKPs	Diketopiperazines
DMF	Dimethylformamide
ee	enantiomeric excess
er	enantiomeric ratio
ES+	Electrospray following the positive ions
EtOAc	Ethyl Acetate
fb	Free base
Fmoc	Fluorenylmethyloxycarbonyl
Gly	Glycine
Gu.HCl	Guanidinium chloride
HMDS	Hexamethyldisilazane
HOMO	Highest Occupied Molecular Orbital
HRMS	High Resolution Mass Spectrometry
hv	Light
i-Pr	*iso*-propyl
KCL	Kinetically Controlled Ligation
LFER	Linear Free Energy Relationship
LHMDS	Lithium bis(trimethylsilyl)amide
LHS	Left Hand Side
LUMO	Lowest Unoccupied Molecular Orbital
MeOH	Methanol
MW	Microwave
NBS	N-Bromosuccinimide
NCL	Native Chemical Ligation
Pen	Penicillamine
Phe	Phenylalanine
PLP	Pyridoxal 5′-phosphate
PNS	Principle of Non-perfect Synchronisation
Pro	Proline
PyBOP	(Benzotriazol-1-yloxy)tripyrrolidinophosphoniu m hexafluorophosphate
PyBroP	Bromotripyrrolidino phosphonium hexafluorophosphate
RHS	Right Hand Side
SPPS	Solid Phase Peptide Synthesis
tBuOK	Potassium *tert*-butoxide
TFA	Trifluoroacetic Acid
Thz	Thiazolidine
TKP	Triketopiperazine
Tyr	Tyrosine
v/v	volume / volume
Xaa	Generic Amino Acid

1 Introduction

1.1 Overview

Proton transfer is ubiquitous throughout chemistry and the study of this process is central to an understanding of chemical reactions. This thesis details our investigations into the proton transfer reactions of peptide systems and how this knowledge can be used to understand the chemical behaviour of peptides. This chapter provides an overview of the historic research into proton transfer, which underpins all the main chapters in this thesis. A final section in this chapter also briefly covers linear free energy relationships and nucleophilicity, which are important for understanding how the results in Chapter 4 may be applied to peptide synthesis.

1.2 Proton Transfer

Our modern understanding of proton transfer stems from the seminal work by Brønsted[1] and Lowry[2] in the 1920s that first established the definitions of acidity and basicity. In their proton transfer model an acid (HA) is a proton donor and a base (B) is a proton acceptor (Equation 1.1).[3]

$$HA + B \rightleftharpoons A^- + BH^+ \qquad \text{(Equation 1.1)}$$

The acid dissociation constant, K_a, of a molecule is used to quantify acidity in solution where an acid donates a proton to the solvent (S) (Equations 1.2 and 1.3). The difference in the values of K_a between acids can vary by many orders of magnitude and therefore it is more convenient to use the negative logarithm of K_a, pK_a, to compare different acids (Equation 1.4).

$$HA + S \rightleftharpoons A^- + SH^+ \qquad \text{(Equation 1.2)}$$

$$K_a = \frac{[A^-][SH^+]}{[HA]} \qquad \text{(Equation 1.3)}$$

$$pK_a = -\log(K_a) \qquad \text{(Equation 1.4)}$$

The majority of pK_as available in the literature are for aqueous solution where water can act as both a conjugate acid via the hydronium ion, H_3O^+ p$K_a(H_3O^+)$ = - 1.74, and a base via the hydroxide ion, OH^- p$K_a(H_2O)$ = 15.74.[4] The conjugate acid hydronium ion is the strongest acid that can exist in aqueous solution and likewise the hydroxide ion is the strongest base. Acids with a pK_a lower than H_3O^+ will be deprotonated by solvent water and bases with a pK_a higher than OH^- will be protonated by solvent water. These limits enforce an accessible pH range of -1.74 – 15.74 in aqueous solutions. Many acidic heteroatoms in organic molecules have pK_as that are within the accessible pH range in water and consequently the extent of acid dissociation of these moieties is dependent upon the pH of the solution e.g. thiols, ammoniums, carboxylates. It should be noted that other pK_a scales do exist for other solvents such as DMSO,[5] DMF[6] and MeCN[7] but the focus of this thesis is on aqueous pK_as.

A seminal review by Eigen in 1964 review laid the foundation for understanding the kinetics of proton transfer.[8] If the basicity of the acceptor base is greater than that of the donor acid [pK_a(B) > pK_a(HA)] then the rate of proton transfer is diffusion controlled (~ 10^{11} s^{-1}) and independent of the difference in the acid and base pK_as. However, if the basicity of the donor acid is greater than that of the acceptor base [pK_a(HA) > pK_a(B)] then the rate of proton transfer will be proportional to the difference in the acid and base pK_as.[9] A more detailed overview of the elementary steps in the mechanism of proton transfer is laid out below in the context of carbon acids (Section 1.3.2.2.1).

In this thesis we have explored a variety of different acidic sites on peptides including protons on α-carbons, ammoniums and thiols. The heteroatom acids of thiols and ammoniums (Chapter 4) typically have pK_as within the accessible pH range of water with diffusion controlled proton transfer and therefore are underpinned by the above understanding of proton transfer. However, carbon acids (Chapters 2 and 3) usually have pK_as beyond the accessible pH range of water with kinetics of proton transfer that are below the rate of diffusion. Therefore the background to the more complicated proton transfer reactions of carbon acid requires further explanation, which is given in the Section below.

1.3 Proton transfer at carbon

Proton transfer processes underpin many vital biochemical transformations, such as the biosynthesis of amino acids[10] and the conversion of 2-phosphoglycerate to phosphoenolpyruvate in glycolysis.[11] In particular many biochemical transformations rely upon deprotonation at carbon and highly efficient enzymes have evolved to catalyse these reactions. Proton transfer at carbon is also vital in synthetic organic chemistry. For example, the classic aldol reaction and Claisen condensation are carbon-carbon bond forming reactions, which rely upon α-deprotonation of protons adjacent to carbonyl groups.[12]

The variation in the strength of carbon acids is substantial and covers a pK_a range of over 70 orders of magnitude (Figure 1.1). At the upper end of the pK_a range alkanes have been calculated to have a pK_a of ~ 45 – 71.[13] At the lower end cyclohexa-2,5-dienone, a tautomer of phenol, has a pK_a = - 2.89.[14]

Figure 1.1: Logarithmic scale showing the pK_a range covered by carbon acids. The acidic hydrogens are highlighted in red.[13-19]

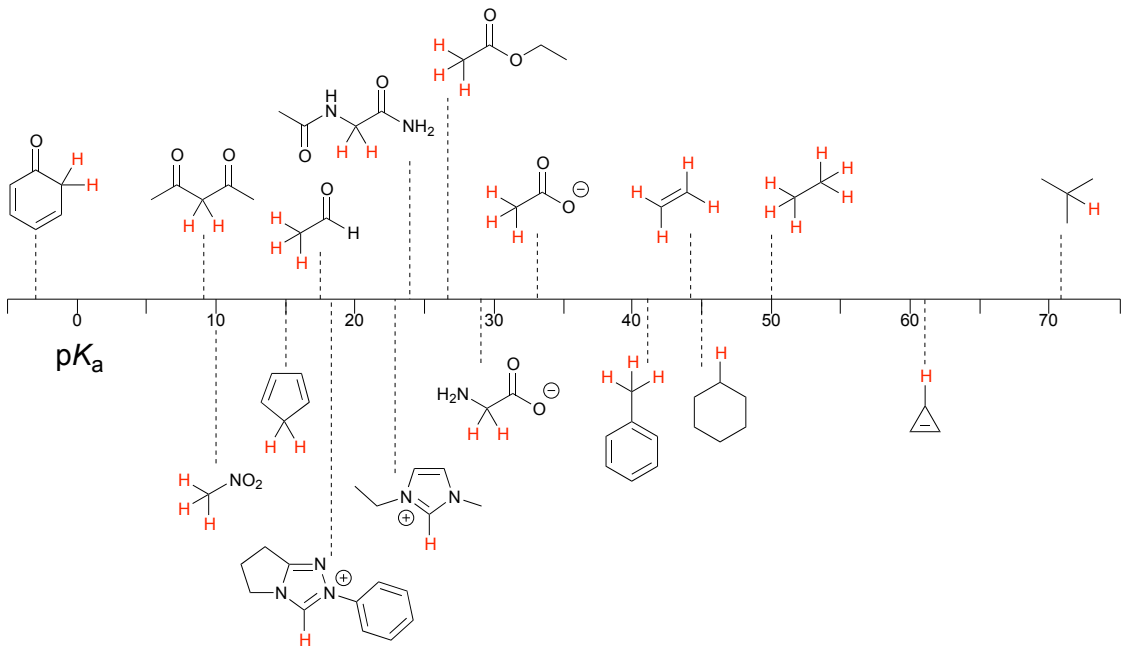

1.3.1 Factors affecting the pK_a of carbon acids

The chemical equation for the deprotonation of a carbon acid is shown in Scheme 1.1 and the equation for the dissociation constant, K_a, of the carbon acid is shown in Equation 1.5. The equilibrium in Equation 1.5 is affected by a number of different factors including the strength of the carbon-hydrogen sigma bond, $\sigma_{C–H}$, reaction conditions (e.g. temperature and the ionic strength of the solution) and the stability of the resulting carbanion. The stability of a proton in water is common across all acids and therefore does not influence the variation in the pK_a of the acids.

Scheme 1.1: The reaction for the deprotonation of a carbon acid in water.

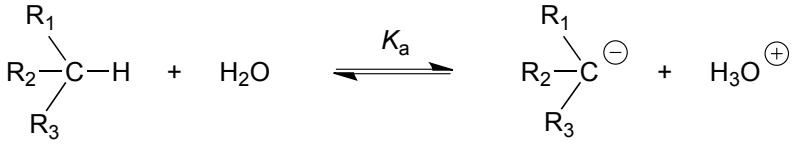

$$K_a = \frac{\left[(R_1,R_2,R_3)C^-\right][H_3O^+]}{[(R_1,R_2,R_3)CH]} \qquad \text{(Equation 1.5)}$$

The variation in the strength of a $\sigma_{C–H}$ between carbon acids is not substantial, for example an alkane $\sigma_{C–H}$ has a $\Delta H° = 101$ kcal mol^{-1} while a $\sigma_{C–H}$ adjacent to a carbonyl group has a $\Delta H° = 94$ kcal mol^{-1}. This variation is significantly smaller than the ~ 45 kcal mol^{-1} difference in pK_a between the two acids. A higher ionic strength in solution will lower the pK_a for the acid dissociation in Scheme 1.1 as the increased concentration of ions in solution will provide more stability to the carbanion and hydronium ion, primarily through electrostatic interactions. The effect of temperature on the pK_a of an acid can be complex. A higher temperature can lower the pK_a of an acid by making it easier to break the $\sigma_{C–H}$ bond, however, too high a value can reduce the hydrogen bonding ability of the solvent resulting in carbanion destabilisation and an increase in pK_a.

The primary determinant of the strength of a carbon acid is the stability of the carbanion conjugate base, $(R_1,R_2,R_3)C^-$ (Scheme 1.1). This is dependent upon the identity of the adjacent R-groups and the hybridisation at the carbanion. The presence of electron-withdrawing groups which can stabilise the formation of the carbanion by inductive and/or resonance effects will lower the pK_a of the carbon acid. The presence

of electron-donating groups, which destabilise the carbanion, usually by inductive effects, will raise the pK_a of the carbon acid.

Carbon acids on the lower end of the pK_a scale typically have one or more strong electron-withdrawing groups that can stabilise the carbanion by conjugation, e.g. nitromethane (pK_a = 10.2) and penta-2,4-dione (pK_a = 9.0). The conjugation transfers a significant proportion of the anionic charge onto a more electronegative atom thus stabilising the carbanion. The more electronegative atoms also have the added benefit of a stronger electron-withdrawing inductive effect that aids the stabilisation of the carbanion. The magnitude of stability typically conveyed by various functional groups is shown in Scheme 1.2.[20]

Scheme 1.2: Variation of α-proton acidity (pK_a) with functional group.[20] R = alkyl group and X = halogen atom.

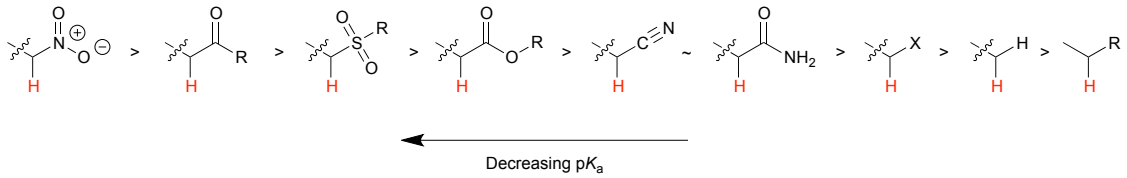

The hybridisation at the carbanion also affects the pK_a of the carbon acid. This can be seen in Scheme 1.3 which shows the effect that an increasing *s*-orbital character has upon the pK_a of the carbon acids ethane, ethylene and ethyne. The greater the *s*-orbital character the higher the effective nuclear charge in proximity to the lone pair of electrons and therefore the more stable the carbanion.

Scheme 1.3: The effect that an increasing *s*-orbital character of the carbanion has upon the pK_a of the carbon acid. The acidic protons are highlighted in red.[13]

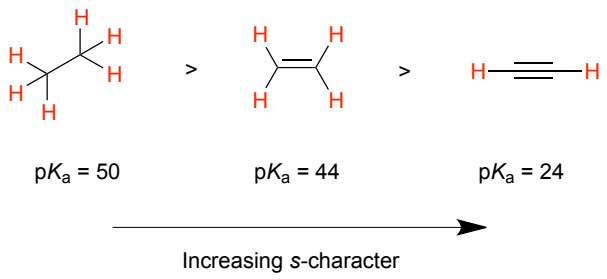

1.3.2 Determination of carbon acid pK_a

The approach taken to determining the pK_a of a carbon acid depends upon the magnitude. Stronger carbon acids, with pK_as in the normal pH range, have a detectable concentration of acid and conjugate base form in solution and equilibrium methods can be used to determine the pK_a. Weaker carbon acids, with pK_as above the normal pH range, require kinetic methods to determine pK_a as direct determination of the low carbanion concentration at equilibrium is impossible by existing analytical methods.[15]

1.3.2.1 Equilibrium methods to determine carbon acid pK_a

Equilibrium methods, typically involving spectrophotometric or electrochemical experiments, are used to measure pK_as for those carbon acids with values within the accessible pH range of water (-1.74 – 15.74). For example, the concentration of [$(R_1,R_2,R_3)C^-$] and [$(R_1,R_2,R_3)CH$] in solution may be determined via UV-Vis spectrophotometry and a pK_a value accessed by application of Equation 1.5. The spectrophotometric measurements can be performed either directly on the carbon acid if it has a chromophore or, alternatively, an indicator method can be used to indirectly access the concentrations of acid and conjugate base forms present in solution.[21]

1.3.2.2 Kinetic methods to determine carbon acid pK_a

For weaker carbon acids the concentration of the carbanion in solution will be below the detection limit of spectroscopic techniques – the lifetime of the carbanion is typically short and reverse reprotonation by solvent is rapid.[19] The kinetic approaches utilised to access the pK_a are based upon Scheme 1.4 and Equation 1.6, where K_a can be found from the ratio of the rate constant for the forward deprotonation reaction, k_f, and the rate constant for the reverse reprotonation reaction, k_r.

Scheme 1.4: The relationship between the rate constants of deprotonation, k_f, and reprotonation, k_r and the acid dissociation constant K_a for a carbon acid.

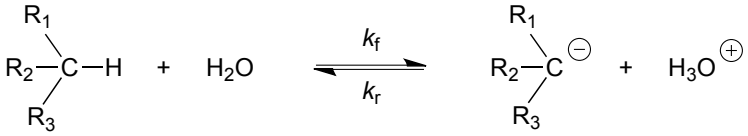

$$K_a = \frac{k_f}{k_r} \qquad \text{(Equation 1.6)}$$

The rest of this section will focus on α-carbonyl carbon acids that form an enolate conjugate base upon deprotonation as these are the predominant class of carbon acids that have been studied within this thesis. The majority of these carbon acids have pK_as outside the accessible pH range in water and thus require kinetic methods of analysis.

1.3.2.2.1 Determination of the rate constant for deprotonation of a carbon acid, k_f

The *modus operandi* of these kinetic techniques is to determine k_f by capturing the short-lived carbanion via a non-rate limiting reaction with a trapping agent. The k_f value may be accessed from the rate of formation of the trapped carbanion or the disappearance of trapping agent and/or monitoring the rate of disappearance of the carbon acid. A variety of trapping agents have been used including halogens, oxidants and isotopic labels.

In early carbon acidity studies halogenation reactions were widely employed to determine k_f. Scheme 1.5 shows an acid and a base catalysed halogenation reaction. Provided that the rate of halogenation $k_X[X_2]$ is non-rate limiting (i.e. a zero-order dependence upon $[X_2]$) the incorporation of the halogen into the carbon acid will be rate limited by deprotonation of the carbon acid such that $k_f = k_{H+}[H^+]$ for acid catalysis or $k_f = k_{HO}[OH^-]$ for base catalysis.[15]

Scheme 1.5: Enolate trapping via acid (a) and base (b) catalysed halogenation: determination of the rate constant for the deprotonation of an α-carbonyl carbon acid.

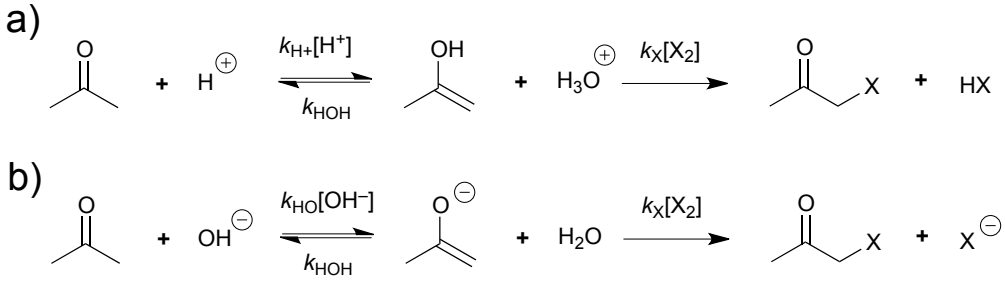

However, the halogenation reactions suffer from multiple drawbacks including i) multiple halogenations where more than one acidic proton is present at the site of interest, ii) lack of regiocontrol where multiple acidic sites are present in the molecule, and iii) side reactions such as oxidation by the halogenating agent.

Metal oxidation reactions have also been used to determine k_f. The validity of using an oxidant requires confidence that the oxidant is solely reacting with the carbanion and not with the carbon acid. Oxidants such as Cr(VI),[22,23] Mn(VIII)[24] and Ir(IV)[25,26] have been shown to react with the carbanion alone, while other oxidants such as V(V) and Co(III) oxidise the carbon acid.[27]

Since the advent of sensitive NMR spectroscopy in the 1970s isotope exchange techniques have been used to probe k_f. Isotope exchange techniques monitor the rate of incorporation of an isotope of hydrogen at the acidic site in the molecule. While tritium exchanges are more sensitive than deuterium exchanges, due to the radioactive nature of tritium, deuterium exchange reactions are often favoured. Deuterium exchange may be conveniently followed by ^{1}H NMR spectroscopy, which also allows for identification of the site(s) of deuteration. Disadvantages of tritium exchange include the requirement for careful separation of all labeled species, the necessity for disposal of radioactive waste and the greater expense of tritium containing reagents compared to their deuterated counterparts.

Scheme 1.6 outlines the mechanism for a deuteroxide-catalysed deuterium exchange of a carbonyl carbon acid. Initially, the carbon acid and deuteroxide diffuse together and subsequent proton transfer of α-proton to DO^- (k_p) leads to the enolate carbanion and HOD. The reaction can either reverse with reprotonation of the enolate (k_{DOH}) or can continue in the forward direction via solvent reorganisation (k_{reorg}) to place

a deuterium in the reactive position. Solvent reorganisation of the HOD molecule may involve rotation of the HOD molecule to place the deuterium in the reactive position or the diffusion of the HOD away and its replacement by a molecule of D_2O. The solvent reorganisation is considered irreversible because the concentration of deuterium in solution overwhelmingly exceeds the concentration of hydrogen in solution; thus HOD is essentially lost by dilution in bulk solvent (in a 99.9 % D_2O solution the concentration of D is 110.2 M). Deuteration of the carbanion gives an encounter complex between deuterated carbon acid and deuteroxide, which will diffuse apart to give free deuterated carbon acid in solution.

Scheme 1.6: The mechanism for base catalysed deuterium exchange of a carbonyl carbon acid. X = H or D.

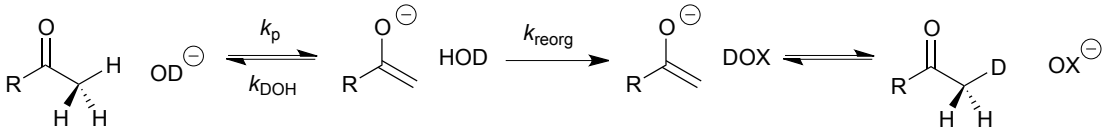

The disappearance of signal in the ^{1}H NMR spectrum with time will have an observed first order rate constant for exchange, k_{ex} (s^{-1}). For a base catalysed deuterium exchange k_{ex} can be comprised of three contributions: a solvent catalysed route, k_{D2O}, deuteroxide catalysed exchange, k_{DO}, and general base[1] catalysed exchange, k_{A-} (Equation 1.7).

$$k_{ex} = k_{D_2O} + k_{DO}[DO^-] + k_{A^-}[A^-] \qquad \text{(Equation 1.7)}$$

The extent of solvent catalysed exchange, k_{D2O}, for a carbonyl carbon acid is usually relatively small for weaker carbon acids and therefore Equation 1.7 normally simplifies to Equation 1.8.

$$k_{ex} = k_{DO}[DO^-] + k_{A^-}[A^-] \qquad \text{(Equation 1.8)}$$

The occurrence of general base catalysed exchange is dependent on the rate determining step in the overall mechanism. If deprotonation of the carbon acid is rate determining (i.e. the proton transfer step), k_p, then general base catalysis will be observed. Otherwise no general base catalysed exchange will be observed as there is

[1] A general base is any base apart from the base form of the solvent.

[2] See Section 1.4 for a more detailed description of Brønsted linear free energy relationships.

[3] Alcohols have a higher pK_a than thiols and therefore would be expected to be better nucleophiles.

pre-equilibrium formation of the carbanion. As will be seen later, either k_{DO} or k_{A-} can be used as k_f in order to determine the pK_a of the carbon acid.

1.3.2.2.2 Determination of the rate constant for reprotonation of the carbanion, k_r

In order to determine the pK_a of a carbon acid the reverse rate of reprotonation, k_r, is also required (Equation 1.6). The reverse rate of reprotonation for an enolate is usually extremely fast and therefore challenging to determine experimentally. Flash photolysis studies to establish the keto-enol equilibrium constant, K^E (Scheme 1.7), for simple carbonyl systems have been used to experimentally determine the rate constant for reprotonation of an enolate system.[11]

Scheme 1.7: The keto-enol equilibrium of acetone.

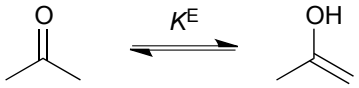

For example, Kresge and Wirz used the flash photolysis of methyl isobutyl ketone to generate the enol of acetone in aqueous alkaline solutions (Scheme 1.8, a).[28] The rate constant for the reprotonation of the enolate, k_{rp}, could be found from the observed first order rate constant for the tautomerisation of enol to keto form, k_{EK}, and the acid dissociation constant of the enol hydroxyl, K_a^E (Scheme 1.8, b and c; Equation 1.9).

Scheme 1.8: a) The mechanism for the generation of the enol form of acetone through flash photolysis of methyl isobutyl ketone. b) The enol to keto tautomerisation of acetone. c) The mechanism for the conversion of enol acetone to keto acetone in alkaline solutions.

a)

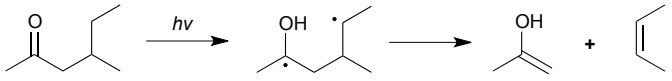

b)

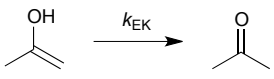

c)

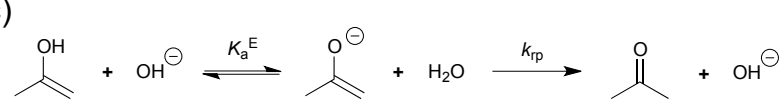

$$k_{EK} = k_{rp} K_a^E \quad \text{(Equation 1.9)}$$

The rate constant for the deprotonation of the α-carbon by hydroxide, k_{HO}, found from either halogenation or isotope exchange experiments, could then be combined with k_{rp} and the ionisation constant of water, K_w, to determine the K_a^K of the α-carbon proton (Equation 1.10).

$$K_a^K = \frac{k_{HO} K_w}{k_{rp}} \quad \text{(Equation 1.10)}$$

The K_a^K and K_a^E values could then be used to determine K^E from the thermodynamic cycle in Scheme 1.9 and Equation 1.11.

Scheme 1.9: Thermodynamic cycle for the relationship between the keto, enol and enolate forms of acetone.

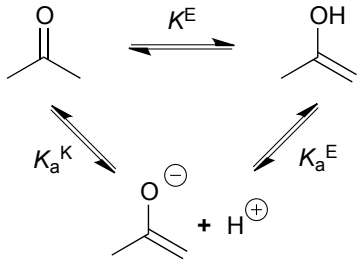

$$K^E = \frac{K_a^K}{K_a^E} \quad \text{(Equation 1.11)}$$

Flash photolysis methods have been used to determine K^E and pK_a values for a range of simple α-carbonyl carbon acids.[29,30] The flash photolysis method is an effective way to determine a variety of different rate constants associated with carbon acidity and keto-enol equilibria. However, broader applicability is restricted by i) the need to begin with an appropriate starting reagent that will generate the desired enol upon photolysis, and, ii) the determination of the rate constants is not trivial for molecules that have non-identical acidic α-protons on either side of the carbonyl or molecules with multiple acidic α-carbonyl sites.[30] Nevertheless there are multiple ways to circumvent the limitations of the flash photolysis setup. For simple neutral α-

carbonyl carbon acids a Brønsted linear free energy relationship[2] exists between the second order rate constants for hydroxide catalysed deprotonation, k_{HO}, and the pK_as of the carbon acids. (Equation 1.12; Figure 1.2; for a full list of k_{HO} and pK_a values see Chapter 2: Table 2.10).[15]

$$\log k_{HO} = \beta \, pK_a + \log(c) \qquad \text{(Equation 1.12)}$$

where β is the sensitivity constant. The pK_a values of the carbon acids in Figure 1.2 were determined by either flash photolysis or by equilibrium measurements for those carbon acids with a pK_a within the accessible pH range of water.

Figure 1.2: Brønsted relationship between the second order rate constant for hydroxide catalysed deprotonation, k_{HO}, and the pK_a values for a series of simple neutral α-carbonyl carbon acids whose acidic protons are highlighted in red (p = is a statistical correction for the number of acidic protons in the carbon acid).[15]

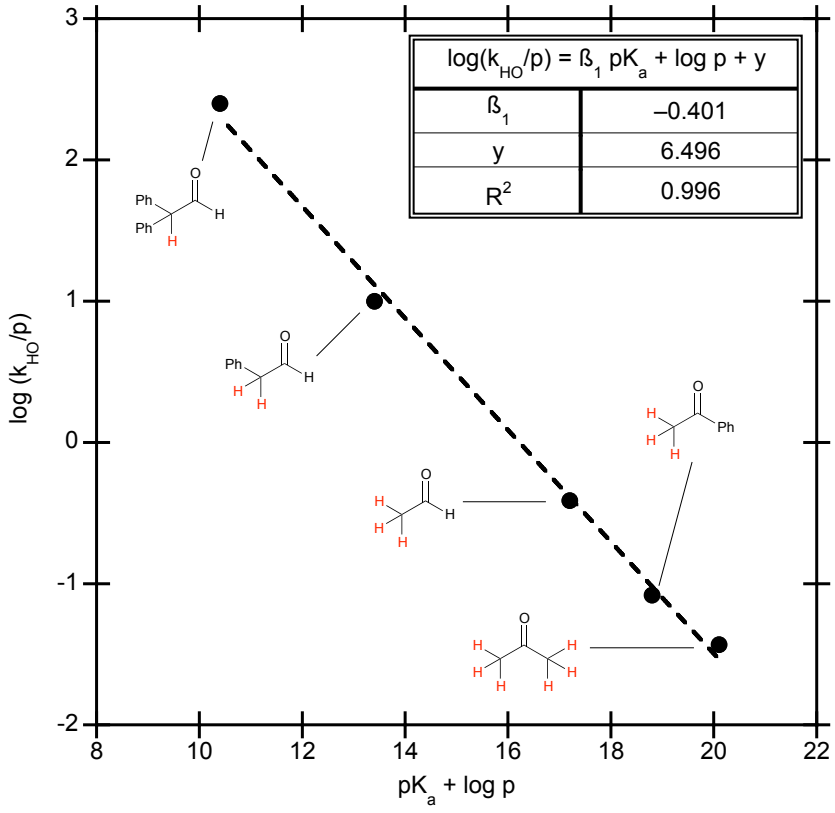

[2] See Section 1.4 for a more detailed description of Brønsted linear free energy relationships.

The Brønsted relationship in Figure 1.2 provides a simple tool by which estimates for the pK_a of other α-carbonyl based carbon acids of a similar structure may be interpolated or extrapolated. The β-value may be interpreted as the extent of proton transfer to the base at the transition state. The value of $\beta = 0.4$ in Figure 1.2 implies that the extent of proton transfer from the carbon acid to the hydroxide base is ~ 40 % complete at the transition state for these simple neutral α-carbonyl carbon acids. Richard has used this relationship to determine the pK_as for a variety of α-carbonyl carbon acids from the second order rate constant for hydroxide catalysed deprotonation, k_{HO}. This includes pK_a estimates for amino acids[31,32] and peptides.[33]

Richard has also developed a number of "clock" methods by which pK_a of carbon acid may be determined.[34] These methods use a rate constant for a known physical transport step as the rate constant for reprotonation of the carbanion. These rate constants for physical transport steps are known with good precision and are broadly independent of the structure carbanion. One "clock" that has been used is the rate constant for the dielectric relaxation of solvent water, which has a value of $k_{relax} = 10^{11}$ s^{-1}. For a carbanion whose reprotonation is limited by the reorganisation of the solvent, k_{reorg} in Scheme 1.6, the value of k_{relax} can be used as the rate constant for the reprotonation, k_{HOH}, i.e. $k_{HOH} = k_{reorg} = k_{relax}$. The p$K_a$ of carbon acid may then be found from Equation 1.13 (the logarithmic version of Equation 1.10).

$$pK_a = pK_w + \log\left(\frac{k_{HOH}}{k_{HO}}\right) \qquad \text{(Equation 1.13)}$$

This method was used by Richard to determine the pK_a of acetate ion as pK_a = 33.5.[19]

An alternative clock that has been used is the rate constant for the diffusion controlled encounter of ions, $k_{iondiff} = 5 \times 10^9$ M^{-1} s^{-1}. In the general base catalysed deprotonation of carbon acids the extent of proton transfer to the general base in the transition state may be determined from a Brønsted relationship. The Brønsted relationship is constructed from the conjugate acid pK_as of a series of structurally related general bases and the logarithm of the second order rate constant for general base catalysis, k_{A^-}. If a β-value ≥ 1 is observed, i.e. proton transfer is complete at the transition state, then this implies that the rate determining step to formation of free carbanion in solution is the diffusion apart of the carbanion and the conjugate acid of the general base (AH). The principle of microscopic reversibility requires that the

reverse reprotonation of the carbanion, k_{AH}, will be limited by the diffusion together of the conjugate acid of the general base (AH) and the carbanion (Scheme 1.10). The rate constant for the diffusion of two oppositely charged ions together, $k_{iondiff}$, may then be used for k_{AH} ($k_{AH} = k_{iondiff}$) and the pK_a of the carbon acid may be found from Equation 1.14, where K_a^{AH} is the ionization constant for the conjugate acid of the general base.

Scheme 1.10: Equation for the formation of an enolate from the reaction between the carbonyl carbon acid and a general base.

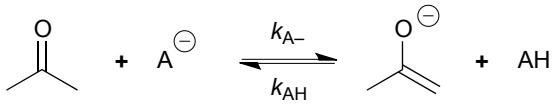

$$pK_a = pK_a^{AH} + \log\left(\frac{k_{AH}}{k_{A-}}\right) \qquad \text{(Equation 1.14)}$$

This ion diffusion clock was used to determine the pK_as of ethyl acetate pK_a = 25.6[16] and acetamide pK_a = 28.4.[19]

1.3.3 Summary of proton transfer at carbon

Understanding the fundamentals of carbon acidity remains an active area of research that is used to further our understanding of biological and synthetic processes. This section has detailed the various factors that affect carbon acidity and outlined a number of the methods that been employed to determine the thermodynamic and kinetic acidities of carbon acids.

1.4 Linear Free Energy Relationships, Nucleophilicity and pK_a

The relationship between chemical structure and reactivity may be probed by making small systematic alterations to the structure of a molecule and then monitoring the effect these changes have on the reaction rate and equilibrium constants.[35] If a change in molecular structure were to stabilise the transition state then the reaction rate will be greater as the rate constant, k, is increased. If a change in molecular structure were to stabilise the reactant state to a greater extent than the product state then this will shift the equilibrium towards reactants thereby lowering the equilibrium constant,

K. Often, but not always, changes to the structure will affect both *k* and *K*. This holds true provided that changes in structure affect the position of the transition state relative to the reactant and product state. The effect that a substituent has upon *k* and *K* may be quantified via a Linear Free Energy Relationship (LFER).

A LFER utilises the logarithms of *k* and *K*, which, according to Transition State Theory (TST), are directly proportional to the Gibbs free energy of activation, $\Delta G^{\ddagger}$, and the Gibbs free energy, ΔG, respectively, through Equation 1.15 and Equation 1.16:

$$\Delta G^{\ddagger} = -2.303\, RT \left(\log k - \log \frac{\kappa k_B T}{h}\right) \qquad \text{(Equation 1.15)}$$

$$\Delta G = -2.303\, RT \log K \qquad \text{(Equation 1.16)}$$

where *R* is the molar gas constant, *T* is the temperature, κ is the transmission coefficient, k_B is the Boltzmann constant and *h* is Planck's constant. κ in TST is taken as unity i.e. it is assumed that the transition state always proceeds to products.

A Brønsted LFER can be used to relate the rate constant, *k*, for a substitution reaction with the pK_a of either the nucleophile or leaving group. Equation 1.17 and Equation 1.18 show the Brønsted LFERs for a nucleophile and a leaving group respectively:

$$\log k = \beta_{NUC}\, pK_a + \log(c) \qquad \text{(Equation 1.17)}$$

$$\log k = -\beta_{LG}\, pK_a + \log(c) \qquad \text{(Equation 1.18)}$$

The sensitivity constants for the reaction, β_{NUC} and β_{LG}, quantify how sensitive the rate constant is to changes in the pK_a of the nucleophile and leaving group, respectively. The y-intercept of the LFER, log(c), simply gives the log(*k*) value for the substitution reaction when either the nucleophile or the leaving group has a pK_a = 0 (K_a = 1). Equation 1.17 shows that as the pK_a of a nucleophile increases so does the log(*k*) value; thus a nucleophile with a higher pK_a is a better nucleophile. Equation 1.18 shows that as the pK_a of a leaving group decreases the log(*k*) value increases; thus a leaving group with a lower pK_a is a better a leaving group.

Technically, a LFER for a substitution reaction would be best described by using the actual equilibrium constant for the substitution reaction. However, the effect that substituent changes on the nucleophile or leaving group have on the equilibrium constant for the substitution is considered to be similar to the effect that those changes would make to the pK_a of the nucleophile or leaving group. Therefore, the use of the pK_a of the nucleophile or leaving group in the Brønsted LFER is a convenient shortcut and avoids the necessity of measuring the equilibrium constant for each substitution reaction. The exception to the above is when the substitution reaction under study is the transfer of a proton between an acid (leaving group) and a base (nucleophile). In this case, the use of the pK_a in the Brønsted LFER is directly applicable to the relationship between the rate constant for the deprotonation of the acid by the base with the equilibrium constant for dissociation of the acid (i.e. K_a).

Thus, when observed, Brønsted LFERs can use the pK_a of a moiety on a molecule to estimate nucleophilicity. It should be stated that knowing the pK_a alone is not necessarily a good predictor of nucleophilicity, as the classic example of alcohols and thiols demonstrates.[3] However, within a class of nucleophiles, which have an identical nucleophilic heteroatom and a similar structure, the pK_a is generally a good predictor. Brønsted linear free energy relationships have been widely used in this thesis to estimate the nucleophilicity of molecules, to predict the reaction rates of bioconjugate additions and for extrapolation of carbon acid pK_a values.

[3] Alcohols have a higher pK_a than thiols and therefore would be expected to be better nucleophiles. However, experimentally thiols are better nucleophiles than alcohols in most cases. This is because the highest molecular orbital (HOMO) on a thiol has a better overlap with the lowest unoccupied molecular orbital (LUMO) on the electrophile than the HOMO of an alcohol does, and consequently is more reactive.

1.5 References:

(1) Brønsted, J. N. *Recueil des Travaux Chimiques des Pays-Bas* **1923**, 718.

(2) Lowry, T. M. *Chem. Ind.* **1923**, 43.

(3) Maguire, O. R., O'Donoghue A. C. in *Sustainable Catalysis: Without Metals or Other Endangered Elements*; North, M., Ed.; RSC Publishing: 2016; Vol. Part 2, p 38

(4) Jencks, W. Richard P. R. J. *Handbook of Biochemistry and Molecular Biology*, 1976.

(5) Bordwell, F. G. *Acc Chem Res* **1988**, *21*, 456.

(6) Kutt, A.; Leito, I.; Kaljurand, I.; Soovali, L.; Vlasov, V. M.; Yagupolskii, L. M.; Koppel, I. A. *J Org Chem* **2006**, *71*, 2829.

(7) Cox, R. A. *Angew Chem Int Ed* **2013**, *52*, 7638.

(8) Eigen, M. *Angew Chem Int Ed* **1964**, *3*, 1.

(9) Eigen, M. *Angew Chem Int Ed* **1965**, *4*, 791.

(10) Eliot, A. C.; Kirsch, J. F. *Annu Rev Biochem* **2004**, *73*, 383.

(11) Chiang, Y.; Kresge, A. J. *Science* **1991**, *253*, 395.

(12) Smith, B. M. March, J. *March's Advanced Organic Chemistry: Reactions, Mechanisms, and Structure 6th Ed.* ; John Wiley and Sons, 2007.

(13) Anslyn, E. V. D., Dougherty. A. *Modern Physical Organic Chemistry*, 2006.

(14) Capponi, M.; Gut, I. G.; Hellrung, B.; Persy, G.; Wirz, J. *Can J Chem* **1999**, *77*, 605.

(15) Keeffe, J. R.; Kresge, A. J. *The Chemistry of Enols*; John Wiley and Sons: Chichester, 1990.

(16) Amyes, T. L.; Richard, J. P. *J Am Chem Soc* **1996**, *118*, 3129.

(17) Higgins, E. M.; Sherwood, J. A.; Lindsay, A. G.; Armstrong, J.; Massey, R. S.; Alder, R. W.; O'Donoghue, A. C. *Chem Commun* **2011**, *47*, 1559.

(18) Massey, R. S.; Collett, C. J.; Lindsay, A. G.; Smith, A. D.; O'Donoghue, A. C. *J Am Chem Soc* **2012**, *134*, 20421.

(19) Richard, J. P.; Williams, G.; O'Donoghue, A. C.; Amyes, T. L. *J Am Chem Soc* **2002**, *124*, 2957.

(20) Higgins, E. M., Doctoral Thesis, Durham University, 2008.

(21) Delley, R. J.; O'Donoghue, A. C.; Hodgson, D. R. W. *J Org Chem* **2012**, *77*, 5829.

(22) Best, P. A.; Littler, J. S.; Waters, W. A. *J Chem Soc* **1962**, 822.

(23) Rocek, J.; Riehl, A. *J Am Chem Soc* **1966**, *88*, 4749.

(24) Littler, J. S. *J. Chem. Soc.* **1962**, 827.

(25) Cecil, R.; Fear, A. J.; Littler, J. S. *J Chem Soc B* **1970**, 632.

(26) Littler, J. S.; Quick, G. R.; Wozniak, D. *J Chem Soc Perk Trans 2* **1980**, 657.

(27) Littler, J. S. *J. Chem. Soc.* **1962**, 832.

(28) Chiang, Y.; Kresge, A. J.; Tang, Y. S.; Wirz, J. *J Am Chem Soc* **1984**, *106*, 460.

(29) Kresge, A. J.; Tobin, J. B. *J Am Chem Soc* **1990**, *112*, 2805.

(30) Keeffe, J. R.; Kresge, A. J.; Schepp, N. P. *J Am Chem Soc* **1990**, *112*, 4862.

(31) Rios, A.; Amyes, T. L.; Richard, J. P. *J Am Chem Soc* **2000**, *122*, 9373.

(32) Williams, G.; Maziarz, E. P.; Amyes, T. L.; Wood, T. D.; Richard, J. P. *Biochemistry* **2003**, *42*, 8354.

(33) Rios, A.; Richard, J. P.; Amyes, T. L. *J Am Chem Soc* **2002**, *124*, 8251.

(34) Richard, J. P.; Amyes, T. L.; Toteva, M. M. *Accounts Chem Res* **2001**, *34*, 981.

(35) Lassila, J. K.; Zalatan, J. G.; Herschlag, D. *Annual Review of Biochemistry, Vol 80* **2011**, *80*, 669.

2 Carbon Acidity of Diketopiperazines

2.0 Foreword

This chapter describes investigations into the carbon acidity of diketopiperazine systems. Section 2.1.1 – 2.1.5 overviews the literature concerning diketopiperazines including their synthesis, applications and properties. Section 2.1.6 outlines previous studies of carbon acidity. Section 2.2 describes the results of kinetic studies into the carbon acidity of diketopiperazines. The determination of the second order rate constants for deuteroxide catalysed exchange, k_{DO} (M^{-1} s^{-1}), via hydrogen deuterium exchange experiments are detailed in Section 2.2.4 – 2.2.10. The results are discussed in Section 2.3 and conclusions presented in Section 2.4. Experimental details are found in Section 2.5.

2.1 Introduction

2.1.1 Overview

Diketopiperazines (DKPs) are small cyclic dipeptides found in a variety of natural products and have more recently found application as enantioselective reagents and scaffolds for drug discovery.

Scheme 2.1: The three possible isomers of diketopiperazines.

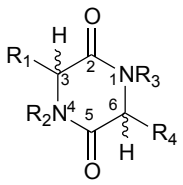

2,5-Diketopiperazine

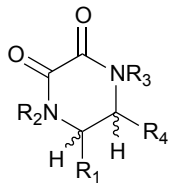

2,3-Diketopiperazine

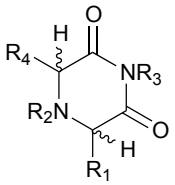

2,6-Diketopiperazine

Scheme 2.1 shows the three possible isomers of diketopiperazines all of which have been found in natural products. This work focuses on 2,5-diketopiperazines (DKPs) which are comprised of two amino acids fused together via two *cis*-peptide bonds to form a 6-membered ring. In this work DKPs will also be referred to as *cyclo*(L/D-Xaa-L/D-Xaa) or c(L/D-Xaa-L/D-Xaa), where Xaa is an unspecified amino acid.

This section will cover the chemistry, applications and properties of DKPs and previous studies into the carbon acidities of amino acids and small peptides. For a more detailed overview of DKPs the reader is referred to a recent review by Borthwick[36] and older reviews by Fischer[37] and Beshore.[38]

2.1.2 Synthesis of 2,5-Diketopiperazines

This section of the review will cover the synthetic approaches used to prepare DKPs.

2.1.2.1 Solution Phase Synthesis of DKPs

The dominant synthetic strategy in the preparation of DKPs involves the formation of the N1 – C2 amide bond (Scheme 2.1). Alternative cyclisation strategies

have been employed, such as N1 – C6 bond formation and tandem 2-bond cyclisations, but these reports are in the minority.[38] The father of peptide chemistry Emil Fischer first reported the synthesis of DKP c(Gly-Gly) in 1906 (Scheme 2.2).[39] Refluxing Gly-Gly dipeptide methyl ester in methanolic ammonia formed the DKP c(Gly-Gly).

Scheme 2.2: Fischer method for the synthesis of c(Gly-Gly) from the Gly-Gly dipeptide methyl ester.[39]

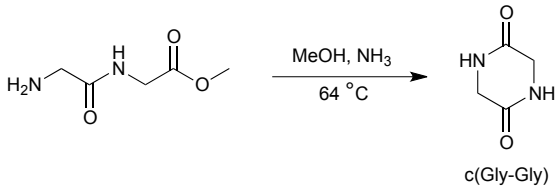

This method has been widely used to prepare DKPs but is hampered by accompanying racemisation at the α-position.[40] Performing the reaction at room temperature with a shortened reaction time (<4 h vs. 1 day) can be used mitigate the effect of racemisation (complete racemisation of certain DKPs was reduced to 1.5% racemisation) but at the expense of yield.[41]

The Nitecki method for DKP formation involves the cyclisation of the methyl ester dipeptide by refluxing with *sec*-butyl alcohol and toluene and is less prone to racemisation (Scheme 2.3).[40] This method has been used for the preparation of a range of DKPs.[42,43]

Scheme 2.3: Nitecki method for the synthesis of DKPs from methyl ester dipeptide.[40]

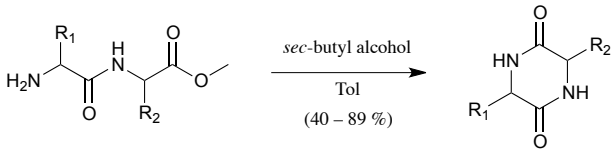

An alternative approach to overcome racemisation was proposed by Ueda where DKPs were prepared from a dipeptide ester by refluxing in methanol (Scheme 2.4).[44-46]

Scheme 2.4: Ueda method for DKP preparation from a methyl ester dipeptide.[44]

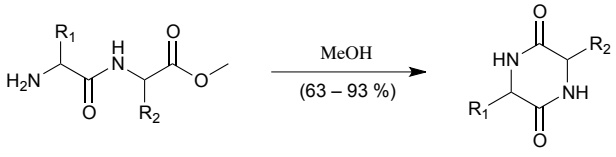

Using chiral HPLC, Ueda analysed the degree of racemisation resulting from each of the three aforementioned procedures. The Fischer, Nitecki and Ueda methods resulted in an average of 1.6 %, 1 % and 0.8 % racemisation respectively across a selection of DKPs based on alanine, leucine, phenylalanine, serine and valine residues.

Alternative solvents for the cyclisation of the methyl ester dipeptide have included 2-butanol/AcOH[47] and toluene.[48,49] More recently microwave methods have been used to accelerate the synthesis of DKPs from methyl ester derivatives.[50-52] The addition of ionic liquids to the microwave reaction was observed to increase the yields of DKPs with no discernable epimerisation (Scheme 2.5).

Scheme 2.5: Microwave assisted ionic liquid synthesis of DKPs.[50-52]

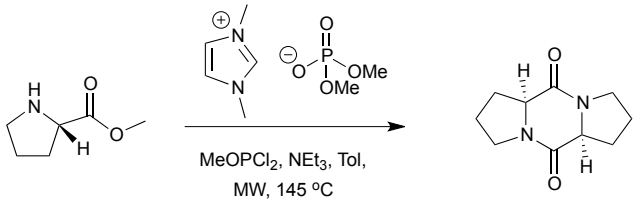

DKPs have also been prepared via activation of the carboxylic group. This is typically done in dilute conditions to prevent oligomerisation. For example, Scheme 2.6 shows the preparation of a Leuch's anhydride from an amino acid and phosgene which can then be transformed into a DKP by the addition of aziridine.[53-58]

Scheme 2.6: a) Preparation of an amino acid Leuch's anhydride. b) The synthesis of DKPs from Leuch's anhydride.[54]

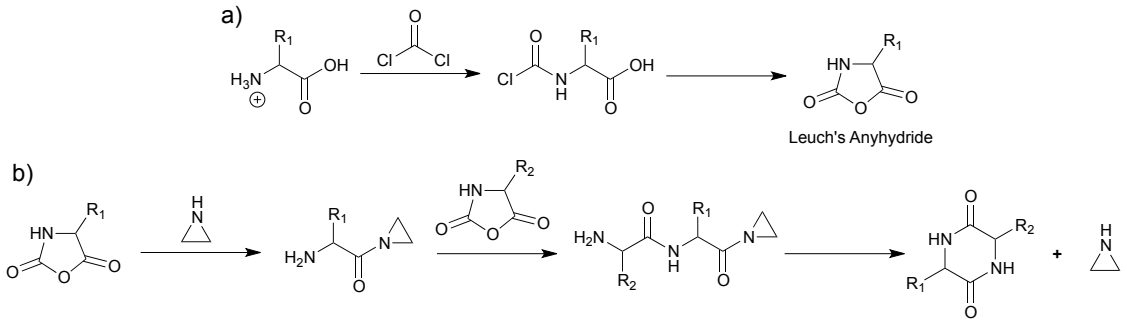

N-succinimido activation has been used in the formation of symmetrical DKPs.[54]

2.1.2.2 Solid-Phase Synthesis of DKPs

DKPs may also be accessed using solid-phase peptide synthesis (SPPS).[59] Katchalski first reported the use of SPPS in the preparation of DKPs upon a poly(nitrophenyl) resin (Scheme 2.7).[60]

Scheme 2.7: First reported synthesis of DKPs via SPPS on poly(nitrophenyl) resin.[60]

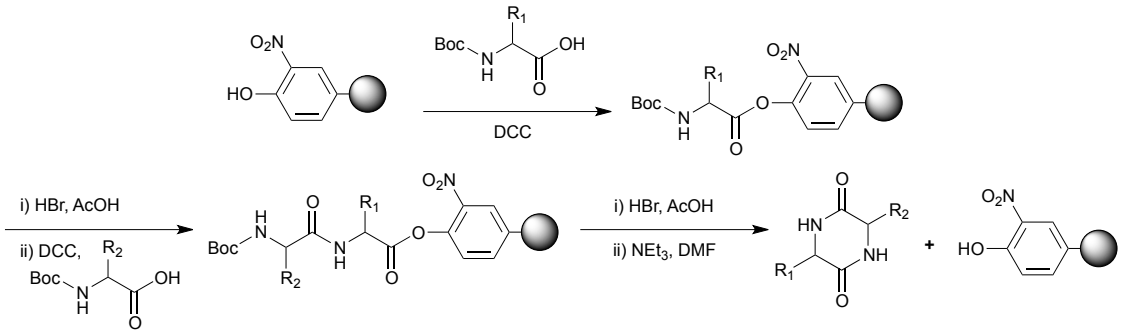

Merrifield reported DKPs as by-products in the synthesis of certain peptide sequences.[61] The presence of carboxylic acids catalysed the cyclisation process, which involved cleavage of a dipeptide chain from the resin (Scheme 2.8). It was found that sequences containing proline or sarcosine residues were more prone to DKP formation. A strategy for the synthesis of DKPs in the presence of acetic acid was subsequently developed.[62]

Scheme 2.8: Synthesis of DKPs via SPPS and catalysed by carboxylic acids.[61]

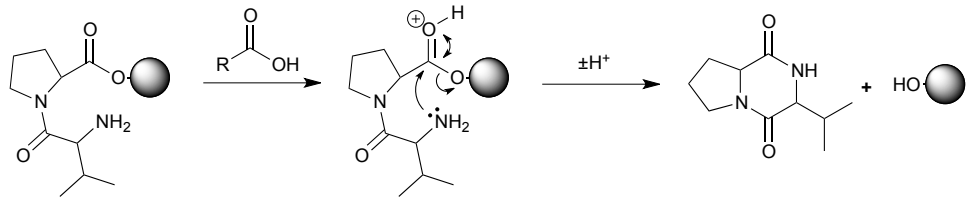

The Merrifield and alternative resins have been applied to the synthesis of a range of DKPs.[63,64] Formation of DKPs from SPPS may proceed via three routes: concomitant cleavage and cyclisation from the resin, DKP formation on resin followed by cleavage, and dipeptide cleavage from the resin followed by DKP formation in solution via cyclisation reaction. The first and second routes are ideal since only DKP is formed and side reactions such as oligomerisation are avoided.

Facile DKP ring synthesis is highly dependent upon the conformation adopted by the dipeptide when attached to the resin. The peptide bonds within the DKP ring are in a *cis*-conformation. This conformation is also required to facilitate the intramolecular attack by the N-terminus upon the carbonyl group in the cyclisation reaction. However, peptide bonds in the *trans*-conformation are favoured over *cis* by ~ 10.5 kJ mol^{-1} because of a reduction in steric interactions between α-substituents in adjacent residues, thus hindering the formation of DKPs.[65,66] DKP formation is known to be more facile with a di-substituted nitrogen in the peptide bond. While the *trans*-amide conformer is still favoured with a di-substituted nitrogen, the steric interactions between the nitrogen substituent and an α-substituent destabilise the *trans*-conformer. Thus the disparity between the stabilities of the *trans*- and *cis*-conformers is reduced and therefore the population of the *cis*-conformer in a peptide bond with a di-substituted nitrogen is increased relative to its mono-substituted nitrogen counterpart. This accounts for the observation by Merrifield that proline and sarcosine residues were prone to DKP formation.[61]

A number of groups have incorporated di-substituted nitrogen amides into DKP synthesis in order to take advantage of the more facile cyclisation. Three approaches have been used to do this: i) alkylation of the N-terminus of the amino acid on the resin, ii) the formation of a temporary di-substituted nitrogen amide through linking the amide nitrogen to the resin, and iii) multi-component reactions.

Permanent reductive alkylation of the N-terminus of the amino acid on the resin was used by Steele to prepare DKPs via SPPS (Scheme 2.9).[67] The unreactive secondary amine made peptide coupling challenging and required the use of a powerful peptide-coupling agent PyBroP. Boc deprotection and cleavage from resin occurred concomitantly in TFA, and reflux in toluene cyclised the DKP ring. Alkylation of the N-terminus has also been used by Szardenings[68-70] and Guo.[71]

Scheme 2.9: Synthesis of DKPs on a Wang resin via alkylation of the N terminus.[67]

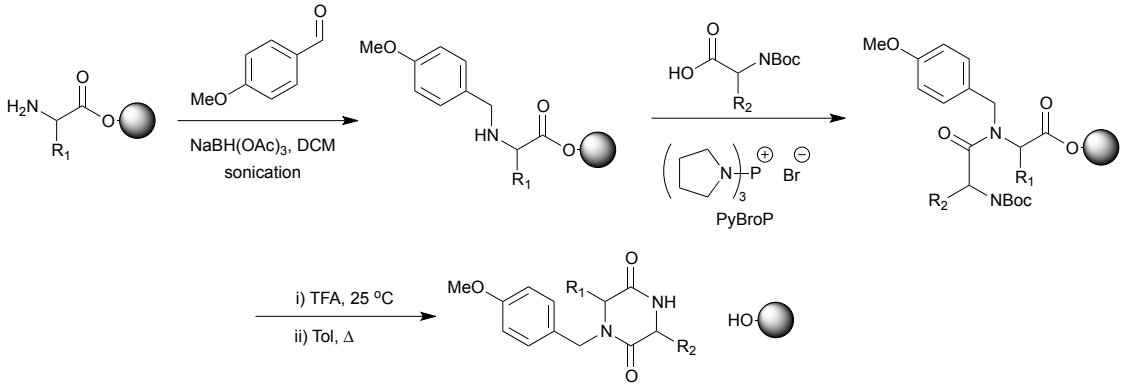

A temporary di-substituted nitrogen amide was used by Albericio and Barany to prepare DKPs in near quantitative yields through a temporary di-substituted nitrogen amide attached to a backbone amide linked (BAL) resin.[72,73] The BAL resin was reductively aminated with an allyl or methyl ester-protected C-terminus amino acid residue (Scheme 2.10). The secondary amine was then acylated using symmetric anhydrides of Fmoc protected amino acids. This was followed by Fmoc deprotection upon which spontaneous cyclisation occurred to form the DKP ring quantitatively. A series of DKPs were prepared using this method.[74]

Scheme 2.10: Synthesis of DKPs on BAL resin via temporary tertiary amide approach.

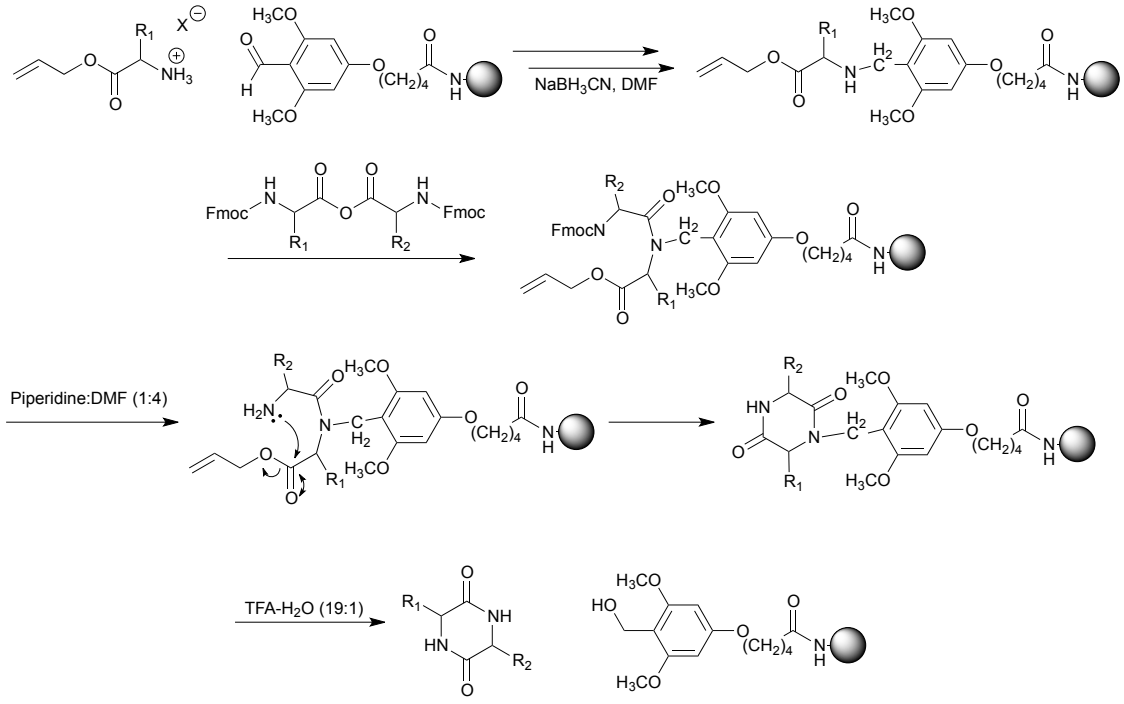

Finally, di-substituted nitrogen amides have been used in multicomponent reactions. Multicomponent reactions, as opposed to multi-step reactions, are a version of a one-pot synthesis where multiple starting materials react in a series of elementary steps to produce a target molecule.[75] Ideally, each step proceeds irreversibly thus driving the overall reaction to the desired product. A well-known example of a multicomponent reaction is the Ugi reaction – a 4-component condensation that can be used to form a dipeptide chain from an aldehyde, amine, carboxylic acid and isocyanide (Scheme 2.11).

Scheme 2.11: a) The Ugi reaction and b) the proposed mechanism.

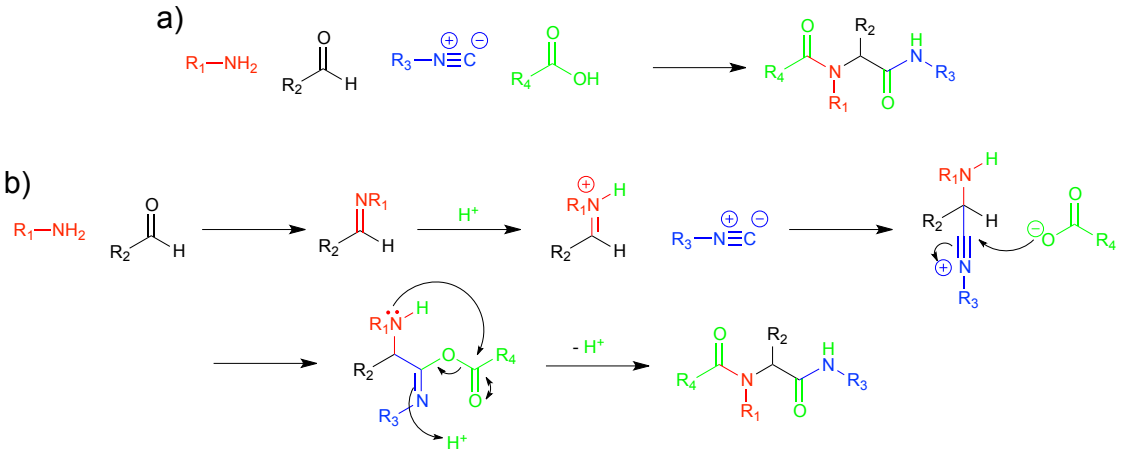

The Ugi reaction allows the formation of a di-substituted nitrogen amide without proceeding through an unreactive secondary amine. The Szardenings group took advantage of this reaction in the synthesis of a range of DKPs using SPPS and the Ugi reaction (Scheme 2.12).[68] This Ugi/De-Boc/Cyclise method has been applied to the synthesis of a range of different DKPs.[76,77]

Scheme 2.12: DKP formation via the Ugi/De-Boc/Cyclise reaction upon a resin.[68]

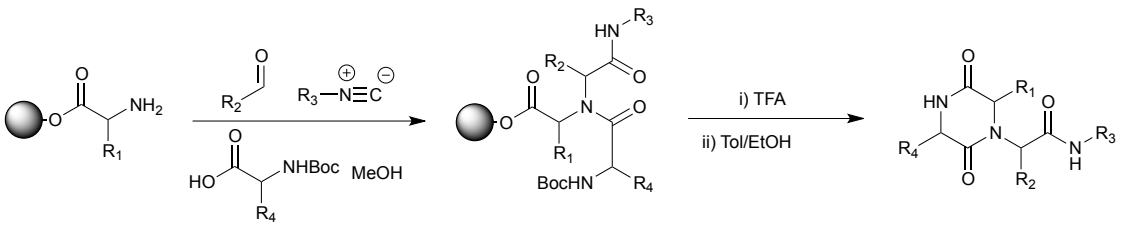

Blackwell has adapted the Ugi/De-Boc/Cyclise method in the incorporation of Fmoc rather than Boc protection.[78] The amine component was attached to a cellulose support via a photocleavable linker.[79] The Ugi reaction was then performed and the DKP assembled upon the support via microwave-assisted methanolysis. Free DKP was then produced by photocleavage from the support (Scheme 2.13). The microwave assisted solution synthesis of DKPs via the Ugi reaction has also been performed.[80]

Scheme 2.13: DKP formation via the Ugi reaction upon a cellulose resin.[79]

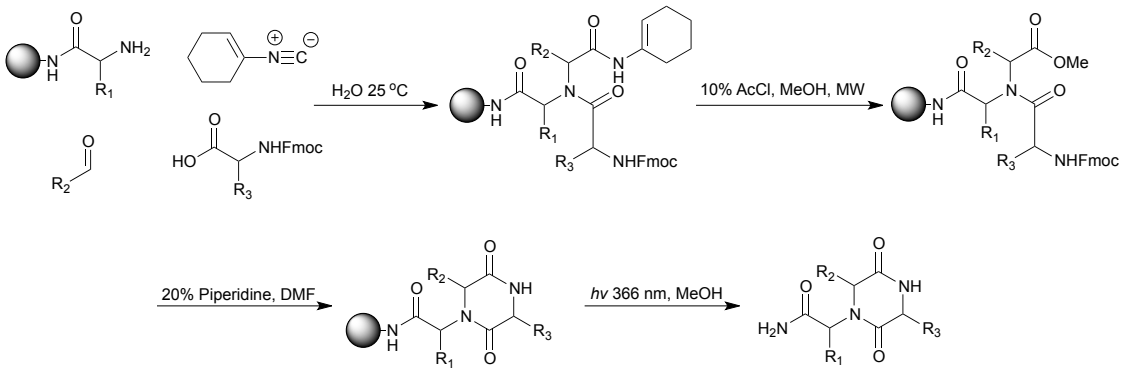

In summary, a diverse range of synthetic strategies have been used in the preparation of DKPs.

2.1.2.3 Kinetic Studies of DKP formation

DKP formation is problematic as a side reaction in peptide synthesis and as a source of degradation of peptides in storage. If unprotected, the N-terminus of the first residue may attack the carbonyl of the second residue in an intramolecular fashion leading to aminolysis of the peptide chain (Scheme 2.14). A number of kinetic studies have been undertaken in order to understand the mechanism of this process.

Scheme 2.14: Degradation of peptides via DKP formation.

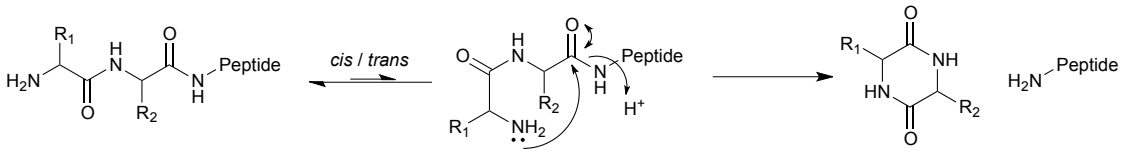

Capasso simulated peptide degradation by monitoring the rates of c(L-Ala-L-Pro) DKP formation from H-L-Ala-L-Pro-NH_2 via HPLC.[81] Both an acid and base catalysed routes for DKP synthesis were observed (Scheme 2.15).

Scheme 2.15: Mechanism for the aminolysis of a peptide chain via DKP formation. GBC = General Base Catalysis, GAC = General Acid Catalysis.[81]

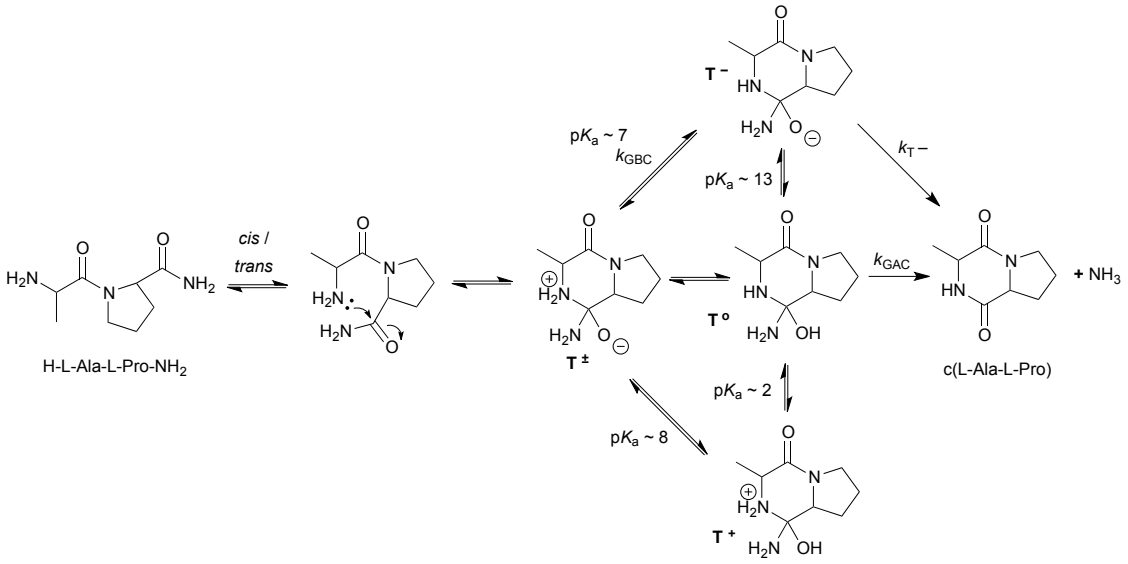

Under strongly acidic conditions the reaction proceeds along the $\mathbf{T^{\pm}} \rightleftarrows \mathbf{T^{+}} \rightleftarrows \mathbf{T^{o}} \rightarrow$ c(L-Ala-L-Pro) pathway. In mildly acidic conditions the reaction proceeds via the $\mathbf{T^{\pm}} \rightleftarrows \mathbf{T^{o}} \rightarrow$ c(L-Ala-L-Pro) pathway with rate determining $\mathbf{T^{\pm}} \rightleftarrows \mathbf{T^{o}}$. In mildly basic conditions the reaction also proceeds via $\mathbf{T^{\pm}} \rightleftarrows \mathbf{T^{o}} \rightarrow$ c(L-Ala-L-Pro) but there is a change in the rate determining step to $\mathbf{T^{o}} \rightarrow$ c(L-Ala-L-Pro) due to less efficient general acid catalysis. In highly basic conditions the reaction proceeds via $\mathbf{T^{\pm}} \rightleftarrows \mathbf{T^{-}} \rightarrow$ c(L-Ala-L-Pro) and above pH 13 the route $\mathbf{T^{\pm}} \rightleftarrows \mathbf{T^{o}} \rightleftarrows \mathbf{T^{-}} \rightarrow$ c(L-Ala-L-Pro) becomes accessible. Under strongly basic conditions *cis* / *trans* isomerisation becomes rate limiting. The rate of DKP formation was unsurprisingly slowest in acidic conditions due to protonation of the N terminus (pK_a = 7.8).

Borchardt investigated the rate of DKP formation using a series of c(Xaa-Pro) dipeptides with a *para*-nitroaniline leaving group.[82] The overall rate of DKP formation was dependent upon the identity of the Xaa residue. The clearest trend shown was an increase in cyclisation rate with increased steric bulk of the α-substituent. The minimisation of steric interactions in the dipeptide chain therefore appeared to favour DKP formation.

2.1.3 Further functionalisation of DKPs

Functionalisation of a DKP ring can be used to prepare natural products that incorporate DKP rings and to develop potential DKP-based drug molecules. DKP rings have three possible centres of reactivity: i) the secondary nitrogen, ii) the α-carbon and iii) the carbonyl carbon. In addition to this chemoselectivity, reactions at the α-carbon may also be stereocontrolled. A selection of reactions at the secondary nitrogen are detailed in Scheme 2.16.[83-85]

Scheme 2.16: Examples of possible reactions used to modify DKP rings at the secondary nitrogen.

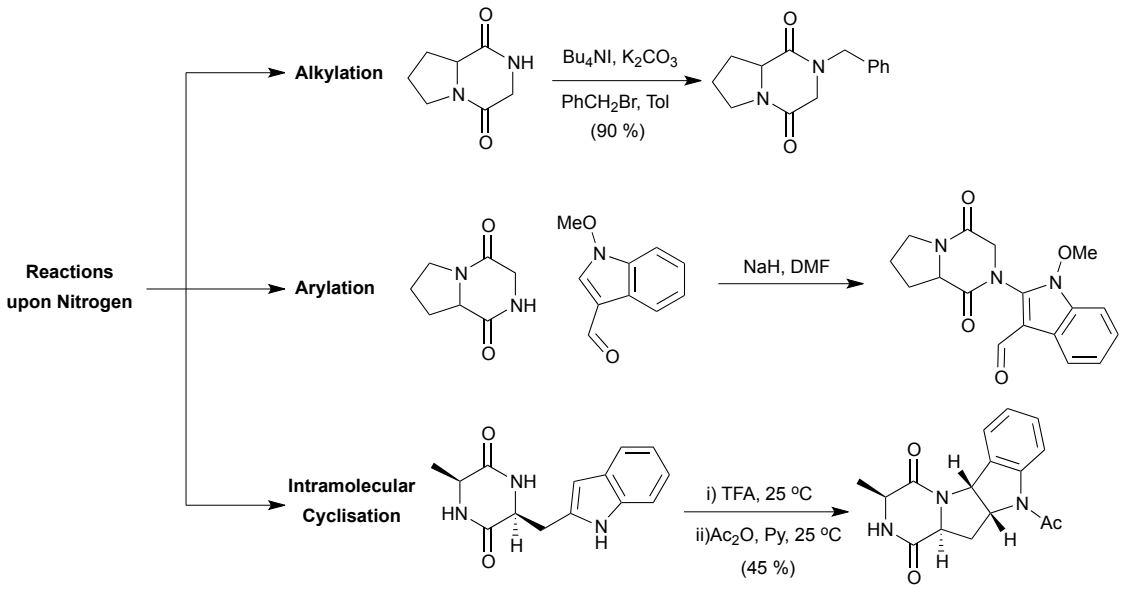

Examples of reactions at the α-carbon are shown in Scheme 2.17.

Scheme 2.17: Examples of reactions at the α-carbon on the DKP ring.

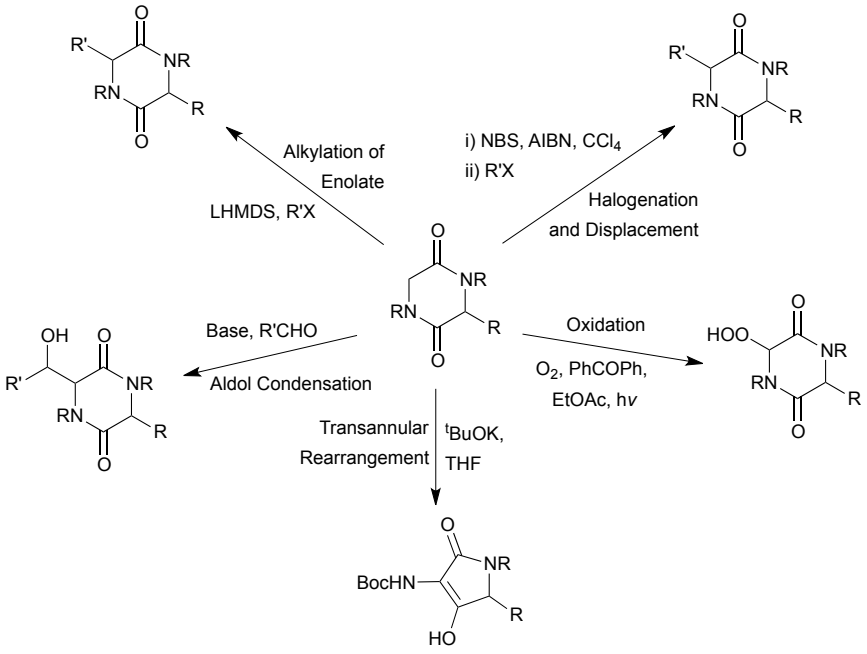

DKP rings have been used as chiral auxiliaries for the asymmetric synthesis of enantiopure amino acids. These reactions require asymmetric functionalisation of the α-carbon followed by acid catalysed ring opening at the carbonyl carbon (Scheme 2.18). The other amino acid residue in the DKP ring, typically valine, acts as a chiral auxiliary in the asymmetric functionalisation at the α-carbon.

Scheme 2.18: Typical route for the asymmetric synthesis of amino acids through a DKP ring with a valine synthon.

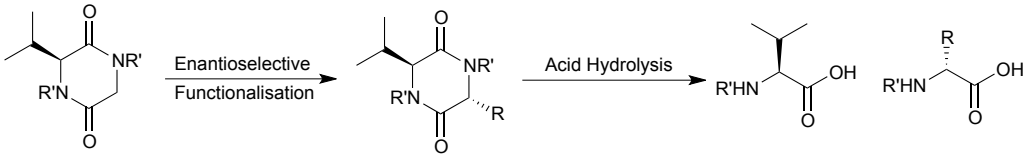

Nishiyama prepared phenylalanine and valine in high enantiopurity through the asymmetric hydrogenation of an α,β-unsaturated DKP ring (Scheme 2.19).[86,87]

Scheme 2.19: Synthesis of enantiopure amino acids via asymmetric hydrogenation. R= Ph- or Me_2CH-.[86,87]

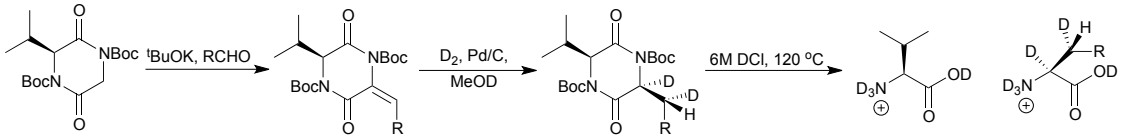

Davies has used a DKP chiral relay network to prepare amino acids with a high enantiopurity (Scheme 2.20).[88] The major product in the first step of the reaction is the *trans*-alkylated DKP ring. This diastereoselectivity is thought to arise through the enolate adopting a favoured conformation which reduces 1,2-torsional strain between the *para*-methoxybenzyl substituent on the N and the *iso*-Pr group of the valine residue (Scheme 2.21). In this conformation the *para*-methoxybenzyl substituent on the N is in an equatorial position and the *iso*-Pr group of the valine residue is in an axial position. This is unlike in the disfavoured enolate conformation where both substituents are in an equatorial position. The subsequent reaction of the favoured enolate conformer with the alkylating agent favours attack from the *Si* face so as to minimise steric interactions with the *iso*-Pr group ultimately leading to the *trans* product (Scheme 2.21).[89]

Scheme 2.20: Synthesis of enantiopure amino acids through a chiral relay network. R = alkyl.[88]

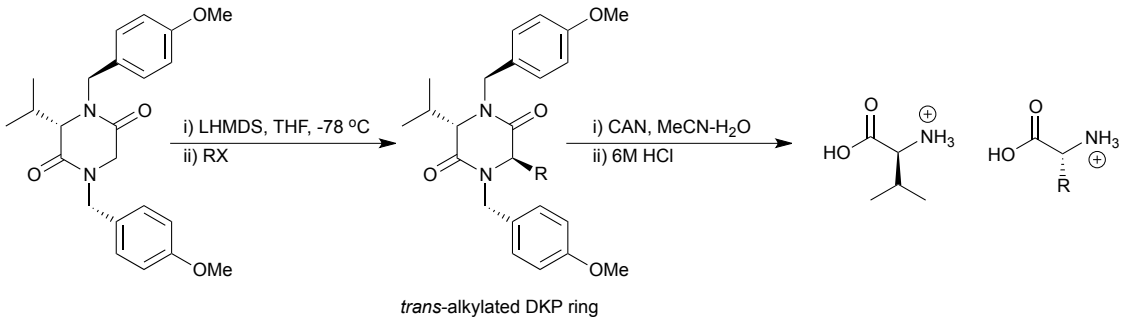

Scheme 2.21: Proposed origin of diastereoselectivity for alkylation of DKP.[89]

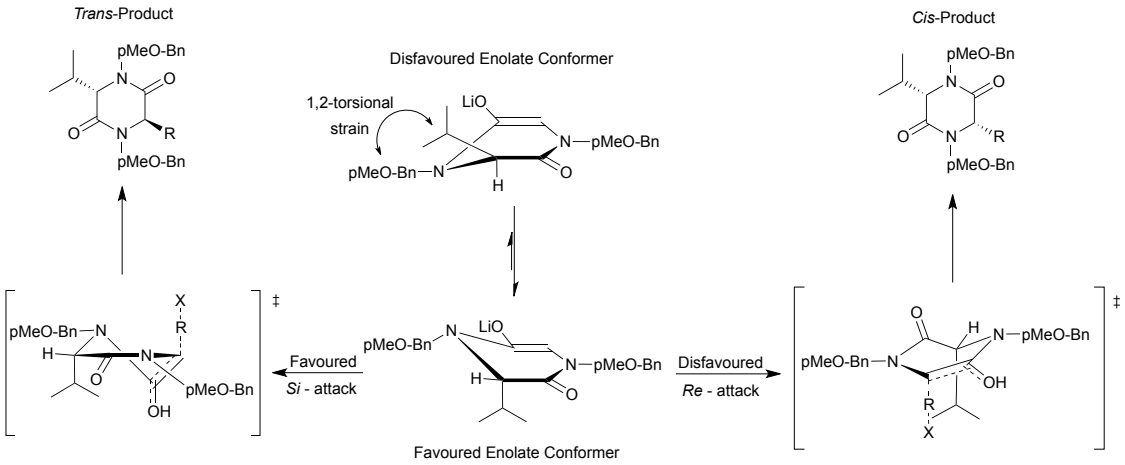

Davies has extensively reported a variety of routes for asymmetric amino acid synthesis.[90-93] Balducci has used the Davies synthesis in the homochiral synthesis of α-methylated amino acids.[94]

The various centres of reactivity in a DKP may therefore be used to functionalise DKP rings and utilises them in the synthesis of chiral amino acids.

2.1.4 Applications of DKPs

The majority of recent research into the application of DKPs has focused on the use of DKPs as scaffolds for low-molecular weight drug molecules. In addition to this a number of groups have also explored the applicability of DKPs in synthetic organic chemistry as catalysts and chiral auxiliaries.

2.1.4.1 Medicinal applications of DKPs

DKPs have been trialled as potential anti-cancer agents[95] including for breast cancer resistant proteins[96], for metalloproteinases inhibition[73] and to act as tubulin depolymerising agents.[97] DKPs have been found to act as peptide antibiotics,[98] antibacterial[99] and antifungal agents.[100] In many of these applications diastereomeric purity is key to the activity of the drug. An assessment of the pK_a of the α-carbon in a DKP can inform whether the efficacy of the drug is diminished by *in vivo* racemisation. DKPs may be used as convenient model peptides for peptidomimetics and are extensively found in bioactive natural products.[36]

2.1.4.2 Synthetic applications of DKPs

DKPs have been used as asymmetric organocatalysts to prepare chiral molecules in high yields and e.e.'s. Inoue reported the asymmetric synthesis of *R*-cyanohydrins with a c(L-Hys-L-Phe) catalyst in reasonable yields (> 40 %) and good enantioselectivities (< 90 %) (Scheme 2.22).[101] Houk has proposed that the origin of enantioselectivity is through a dimer formation of two catalyst molecules whereupon one imidazole guides the delivery of the nucleophile and the other acts as an acid.[278]

Scheme 2.22: Enantioselective synthesis of *R*-cyanohydrins with a DKP catalyst.[101]

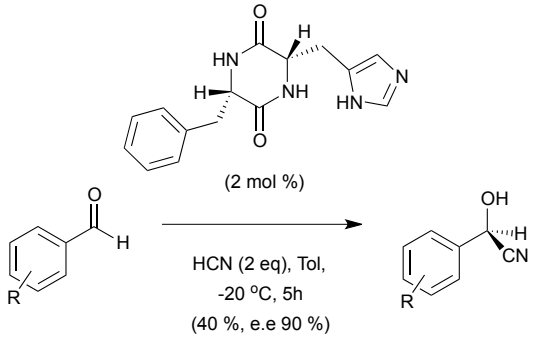

The DKP c(L-Arg-L-Phe) has been used in the Strecker reaction for the asymmetric synthesis of *S*-aminonitriles in high yields (> 90 %) and good ee's (> 92 %) (Scheme 2.23).[102]

Scheme 2.23: Enantioselective synthesis of *S*-aminonitriles in the Strecker synthesis with a DKP catalyst.[102]

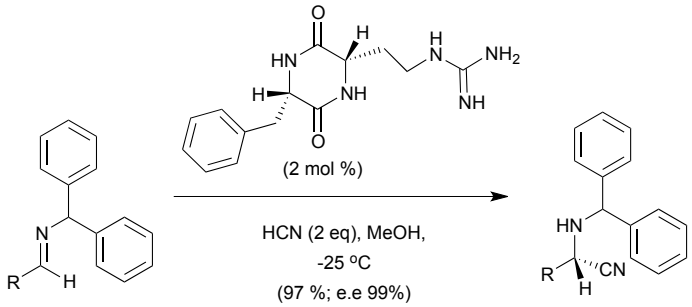

DKPs as chiral auxiliaries have been employed for the enantioselective epoxidation of enones (Scheme 2.24).[103]

Scheme 2.24: Chiral auxiliary c(Pro-Pro) peroxide catalyst for the epoxidation of enones.[103]

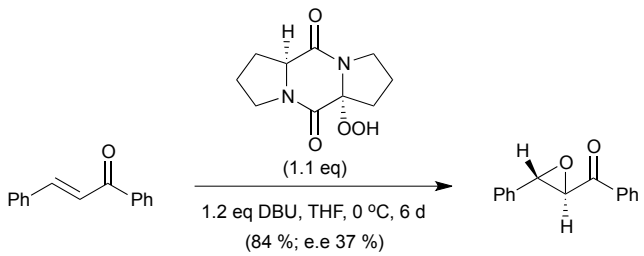

Further examples of synthetic applications of DKPs are found in the Borthwick review.[36]

2.1.5 Properties of DKPs

Early research relating to DKPs tended to focus on their molecular properties and in particular the conformations adopted by the DKP ring and side chains. This section overviews the conformations of the DKP ring, the conformations of DKP side chains and *cis* / *trans* isomerism in DKPs. As will be seen later the conformational properties of DKP rings holds substantial influence over the carbon acidity of the α-proton.

There are two stable conformations that the DKP ring can adopt: a planar and a boat conformation (Scheme 2.25). The two *cis* peptide bonds in the DKP ring favour a flat planar conformation of the DKP ring,[37] however, the nature of the favoured conformer is also dependent upon the identity of the side chains and the configurations at the α-carbons.

Scheme 2.25: The two major conformations for a DKP ring. Note that the Planar conformation is based upon a *cis*-DKP and the Boat conformation is based on a *trans*-DKP.

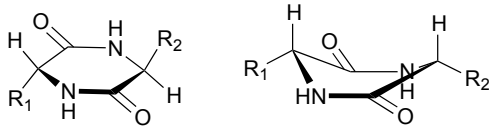

The planar conformation is adopted for amino acid residues whose side chains have little steric bulk or when the configurations at the α-carbons are asymmetric. The boat conformation is adopted for amino acid residues whose configurations at the α-carbons are identical. This conformation therefore places both side chains equatorial – minimising steric interactions. The extent of folding in the boat conformation is greatest for those amino acid residues with larger substituents and for DKPs that contain at least one proline residue.[104] The DKP and prolyl pyrrolidine ring conformations are interdependent: if the DKP ring adopts a boat conformation the pyrrolidine ring favours an envelope conformation, whereas a planar DKP ring results in a half chair conformation.[105]

The side chains of the DKP may adopt a number of possible conformations depending upon the nature of the substituent. Blout has analysed the possible rotamers

for a series of c(Pro-Xaa) DKPs using circular dichroism, ^{1}H NMR spectroscopy and *ab initio* calculations.[106,107] Three possible local energy minima rotamers were identified: an unfolded conformation and two folded conformations – with the R group(s) extending towards either nitrogen or oxygen (Scheme 2.26). For the majority of c(Pro-Xaa) DKPs studied the most favoured energy minima was one of two folded conformations (> 75 % of population).

Scheme 2.26: The three energy minima rotamers for c(Pro-Xaa) DKP.[106,107]

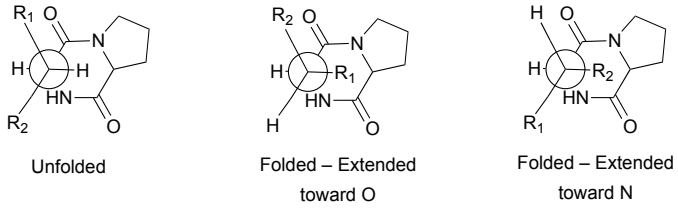

An aromatic side chain, such as in phenylalanine or tyrosine residues, favours the adoption of a folded rotamer thereby placing the aromatic ring above the DKP ring (Scheme 2.27). The preference for a folded rotamer is likely a result of the reduction in hydrophobic surface area that this conformer offers.

Scheme 2.27: Folded tyrosine rotamers for a) c(L-Tyr-D-Xaa) which prefers a planar conformation of the DKP ring and b) c(L-Tyr-D-Xaa) which prefers a boat conformation of the DKP ring.[106,107]

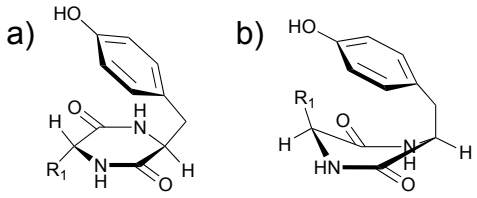

DKP rings show *cis* / *trans* isomerism depending upon the orientation of the side chains on the DKP ring (Scheme 2.28).[iv] In the *cis*-isomer the configuration at the two α-carbons are equivalent while in the *trans*-isomer the configurations are asymmetric. The preference for the *cis*- or *trans*-isomer depends upon the identity of the amino acid residues in the DKP ring. Eguchi has studied the equilibrium distributions of the *cis*- and *trans*-isomers for a variety of DKPs in ethanolic sodium

[iv] DKPs with at least one glycine residue are excluded from this isomerism.

ethoxide at 30 – 70 °C and aqueous solutions at 250 °C (Table 2.1).[105]

Scheme 2.28: *cis* / *trans* isomerism in DKPs.

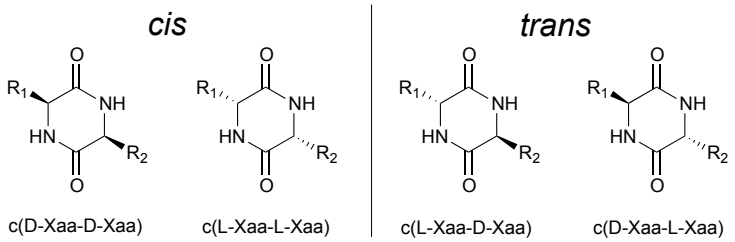

Table 2.1: The experimental equilibrium distributions of *cis*- and *trans*-isomers for a series of DKPs.[105]

DKP	*cis* / %	*trans* / %
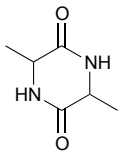 c(Ala-Ala)	48 [b] – 52.9 [a]	47.1 [a] – 52 [b]
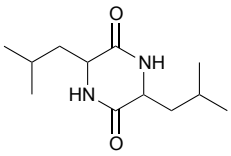 c(Leu-Leu)	48 [b] – 58.3 [a]	41.7 [a] – 52 [b]
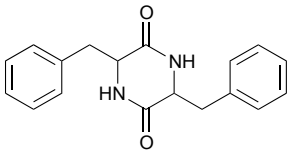 c(Phe-Phe)	46 [b] – 49.9 [a]	50.1 [a] – 54 [b]
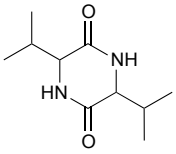 c(Val-Val)	24.1 [a] – 33 [b]	67 [b] – 75.9 [a]
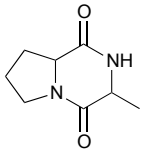 c(Pro-Ala)	42.8 [a] – 48 [b]	52 [b] – 57.2 [a]

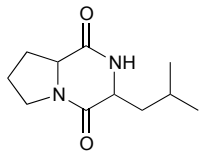 c(Pro-Leu)	15 [a] – 27 [b]	73 [b] – 85 [a]
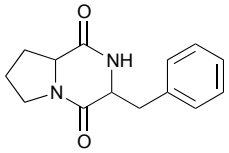 c(Pro-Phe)	9.1 [a] – 21 [b]	79 [b] – 90.9 [a]
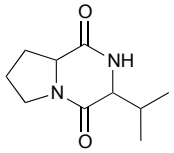 c(Pro-Val)	7.6 [a] – 19 [b]	81 [b] – 92.4 [a]
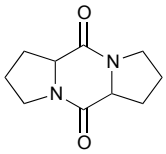 c(Pro-Pro)	> 99.5 [a b]	< 0.5 [a b]

[a] 0.1 M ethanolic sodium ethoxide in ethanol solution at 30 °C. [b] Aqueous solution at 250 °C.

For symmetric non-prolyl-containing DKPs with non-β-branched side chains there is an approximately equal distribution of both isomers, e.g. c(Ala-Ala). These DKP rings possess relatively high flexibility and therefore the stability of each isomer is near equivalent. For residues with β-branched side chains the *trans*-isomer is favoured in order to minimise steric interactions between the substituents, e.g. c(Val-Val).

For c(Pro-Xaa) DKPs with a single Pro residue the *trans*-isomer is preferred as it places the R-side chain and the carbonyl group in a staggered conformation as opposed to the eclipsed conformation that is found in the *cis*-isomer (Scheme 2.29). For c(Pro-Phe) the preference for the *trans*-isomer is also in part due to the tight placement of the phenyl group over the DKP ring thereby reducing the hydrophobic surface area.[106,107]

Scheme 2.29: Conformational preferences of c(Pro-Xaa).

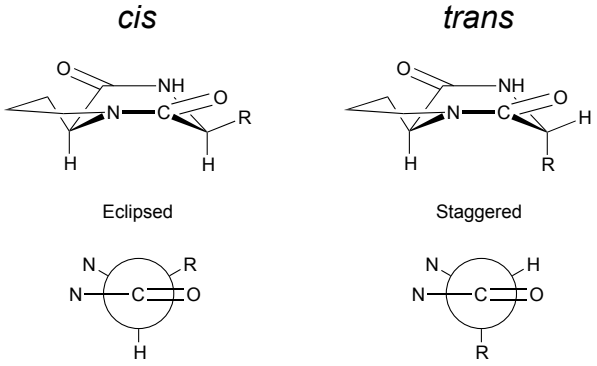

The only DKP that favoured the *cis*-isomer was c(Pro-Pro). *cis*-c(Pro-Pro) adopts a boat conformation while the *trans*-isomer contains a planar DKP ring.[108] As previously mentioned, if the DKP ring is planar the pyrrolidine ring of Pro will adopt a half chair conformation. Eguchi postulated that in order for the amide bonds to remain planar considerable strain is introduced into the half chair conformation of the pyrrolidine ring therefore disfavouring the *trans*-isomer.

The *cis*-isomer of c(Pro-Pro) have been extensively studied with NMR spectroscopy, Raman optical activity, UV-Vis circular dichroism and *ab initio* calculations.[109,110] The pyrrolidine ring can adopt three local energy minima conformations: Platter, Chair and Boat (Scheme 2.30).

Scheme 2.30: Conformations of *trans* c(Pro-Pro).

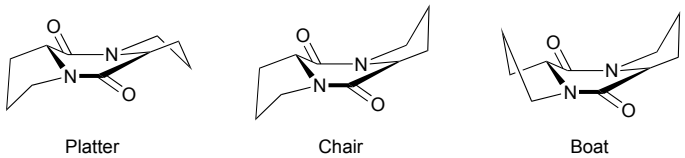

The population distribution amongst these three conformers is disputed. Budšínsky estimated a Platter : Chair : Boat distribution of 74 : 13 : 13 based upon agreements between ^{1}H NMR spectroscopy and *ab initio* calculations.[109] Thomasson estimated, however, that the population was evenly spread with each conformer comprising of a third of the total population based on circular dichroism measurements and *ab initio* calculations.[111]

The conformations of the DKP rings can affect the carbon acidity of the α-proton as will be seen later.

2.1.6 Carbon Acidity of Amino Acids and Peptides

The rise in applications of peptide chemistry has prompted research into the fundamental properties of peptide systems. The carbon acidity of the α-proton of an amino acid residue is of importance for the stereochemical integrity of peptide systems. In addition, the formation of the enolate is widely used in the biochemical transformation of peptide systems. Richard has examined how a range of different functional groups and ionization states affect the carbon acidity of the α-proton in a series of amino acid and small linear peptide systems. By using hydrogen deuterium exchange reactions monitored by ^{1}H NMR spectroscopy Richard determined the kinetic acidity of the α-protons (k_{HO}, second order rate constant for deprotonation by hydroxide) and estimated the thermodynamic acidity (pK_a) via a Brønsted relationship for simple neutral α-carbonyl carbon acids (Table 2.2).[112-114]

Table 2.2: Kinetic (k_{HO}) and thermodynamic (pK_a) acidities of the α-H_1 for amino acids, amino acid methyl esters and small peptides.

Entry	Carbon Acid	k_{HO}/p [a] (H_1) /M^{-1} s^{-1}	pK_a(H_1)
1 [b]	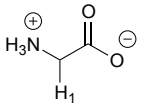	2.25×10^{-5}	29.2
2 [b]	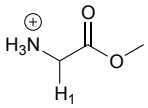	2.05	21.3
3 [d]	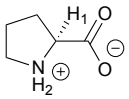	4.5×10^{-5}	29.0
4 [d]	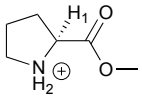	3.6	21
5 [c]	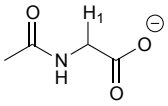	4.75×10^{-7}	31.1
6 [c]	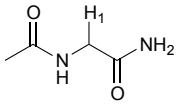	1.3×10^{-3}	23.9
7 [c]	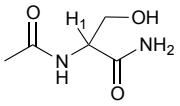	7.7×10^{-4}	24.1
8 [c]	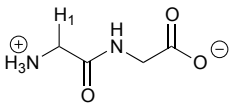	9.0×10^{-3}	27.0
9 [c]	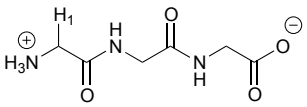	6.0×10^{-2}	25.4
10 [c]	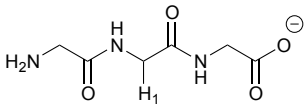	2.0×10^{-4}	25.9

[a] p = number of exchangeable protons, used to give the statistical corrected value. [b] Rios, A.; Amyes, T. L.; Richard, J. P. *J. Am. Chem. Soc.* **2000,** *122,* 9373 – 9385. [c] Rios, A.; Richard, J. P.; Amyes, T. L. *J. Am. Chem. Soc.* **2002**, *124*, 8251 – 8259. [d] Williams, G.; Maziarz III, E. P.; Amyes, T. L.; Wood, T. D.; Richard, J. P. *Biochemistry* **2003**, *42*, 8354 – 8361.

The range of kinetic acidities of α-protons in amino acid and peptide systems covers a breadth of 10^7 M^{-1} s^{-1} and depends significantly upon the proximity of neighbouring functional groups and their ionization states. The α-proton on the *N*-

acylated Gly anion (Table 2.2: Entry 5) has the lowest kinetic acidity ($k_{HO} = 4.75 \times 10^{-7}$ M^{-1} s^{-1}) as a result of the unfavourable formation of a carboxylate dianion in the enolate. Amidation of the C-terminus (Table 2.2: Entry 6 and 7) increases the kinetic acidity by four orders of magnitude ($k_{HO} \sim 1.00 \times 10^{-3}$ M^{-1} s^{-1}) compared to the *N*-acylated Gly anion.

For Gly and Pro zwitterions α-protons (Table 2.2: Entry 1 and 3) the low kinetic acidity ($\sim 10^{-5}$ M^{-1} s^{-1}) is also a reflection of the difficulty in forming a carboxylate dianion in the enolate. The presence of the cationic nitrogen in the zwitterions clearly stabilises the formation of the enolate as the kinetic acidity is two orders of magnitude greater than the *N*-acylated Gly anion.

For the cationic methyl esters of Gly and Pro ($k_{HO} \sim 2.8$ M^{-1} s^{-1}) (Table 2.2: Entry 2 and 4) the removal of the anionic C-terminus in the acid form and lack of dianionic carboxylate in the enolate increases the kinetic acidity by six orders of magnitude compared to their parent zwitterions. A comparison of the Gly and Pro systems indicates that the pyrrolidine ring has a modest effect (1.7 – 2.0 fold increase) upon the kinetic acidity of the α-proton.

The kinetic acidity of the α-proton in Gly-Gly linear dipeptide zwitterion (Table 2.2: Entry 8) is two orders of magnitude higher ($k_{HO} = 9.0 \times 10^{-3}$ M^{-1} s^{-1}) than the Gly zwitterion as there is now greater separation between the two anionic charges in the enolate. In the zwitterionic Gly-Gly-Gly linear tripeptide (Table 2.2: Entry 9) the further extension of the peptide chain increases the kinetic acidity by an order of magnitude ($k_{HO} = 6.0 \times 10^{-2}$ M^{-1} s^{-1}). The kinetic acidity of the anionic Gly-Gly-Gly linear tripeptide (Table 2.2: Entry 10) is 3.9 – 6.5 fold lower than the *N*-acylated amino acid amides (Table 2.2: Entry 6 and 7) as the enolate formed will be dianionic.

Richard observed that the effect of an α-NHAc and an α-NH_3^+ substituent on the acidity of a simple α-carbonyl carbon acid in aqueous solution were approximately the same at ~ 4.7 pK_a units (Scheme 2.31).

Scheme 2.31: The effect of the addition of an α-NHAc and an α-NH_3^+ upon the α-proton. p = number of exchangeable protons, used to give the statistical corrected value.

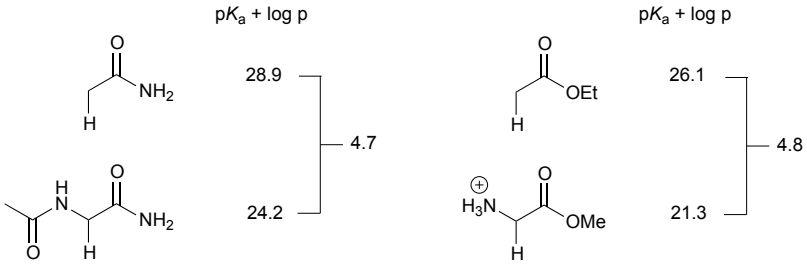

Both the neutral α-NHAc and the cationic α-NH_3^+ stabilise the formation of the carbanion to a similar degree which is unexpected due to the difference in charge between the two functional groups. Richard proposed that the greater than expected stabilisation from the α-NHAc arises from a greater contribution of the formally anionic resonance structure to the valence molecular wavefunction of the carbanion. In the formally anionic resonance structure both the resonance contributions and interactions between the positive and negative charges within the molecule could help stabilise the carbanion (Scheme 2.32).

Scheme 2.32: The anionic and formally anionic resonance structures of the α-NHAc enolate.

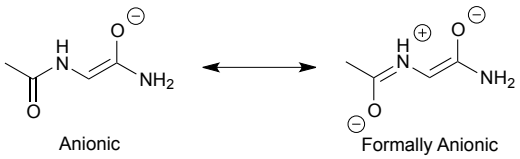

The aqueous pK_as of the α-protons in a series of DKPs have previously been computed via DFT calculations by Coote (Table 2.3).[115] The principle aim of the study was to explore the effect of N-substitution in the DKP ring on carbon acidity. As expected, the introduction of electron donating N-substituents, which decrease the stability of the enolate, increased the pK_as of the α-protons. Electron withdrawing N-substituents, which increase the stability of the enolate, decreased the pK_as of the α-protons. The calculated aqueous pK_as of the α-protons were expected to be of a similar value to the experimentally determined pK_a of N-acyl glycine amide (pK_a = 23.9) (Table 2.3: Entry 6). For c(Gly-Gly) (Table 2.3: Entry 1) this was indeed the case with

a calculated aqueous pK_a = 24.0. Upon addition of electron withdrawing substituents to one of the amide nitrogens a considerable drop of several pK_a units was found with pK_as of as low as 13.9 calculated.

Table 2.3: Calculated aqueous pK_as for DKP α-protons at 25 °C.[115]

DKP	pK_a	
	H_1	H_2
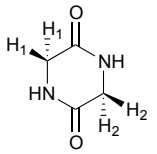	24.0	24.0
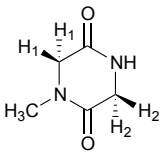	25.1	25.8
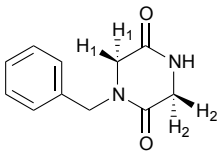	24.9	26.6
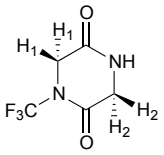	24.2	19.4
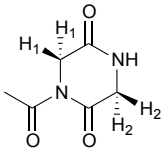	24.1	17.7
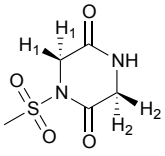	22.8	16.8
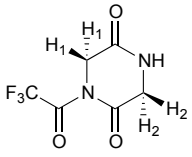	23.7	15.3
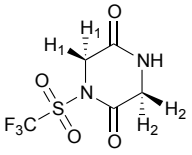	21.3	13.9

Unusually, the α-protons most affected by the addition of substituents to the amide nitrogen were not the adjacent proximal α-protons, H_1, but rather the more remote distal α-protons, H_2 (Scheme 2.33). This distal effect was observed with both electron withdrawing and donating substituents. For electron donating groups, such as methyl and benzyl, which destabilise the enolate, the pK_a of the distal H_2 protons increases more than the pK_a of the proximal H_1 protons by 0.7 – 1.7 pK_a units. For electron withdrawing groups the effect was substantially greater with the pK_a of the distal H_2 protons decreasing more than the pK_a of the proximal H_1 protons by 4.8 – 8.4 pK_a units.

Scheme 2.33: The proximal (H_1) and distal (H_2) protons on a DKP relative to the N-substituted amide nitrogen.

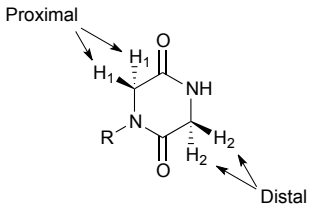

Coote and Easton postulated that the origin of this distal effect was due to the substitution on nitrogen affecting both resonance and inductive stabilisation of the distal enolate whilst only affecting inductive stabilisation of the proximal enolate. For an amide enolate there are three possible resonance forms (Scheme 2.34) and there is a competition between structures **A** and **C** for conjugation with the carbonyl bond. The population of structures **A** and **C** is affected by the ability of the carbanion and nitrogen lone pair to conjugate with the carbonyl, respectively. The addition of electron withdrawing substituents to the nitrogen reduces the ability of the nitrogen lone pair to conjugate to the carbonyl. Thus the enolate structure **A** is better able to conjugate to the carbonyl bond – increasing the stability of the carbanion.

Scheme 2.34: The three possible resonance structures for a DKP enolate.

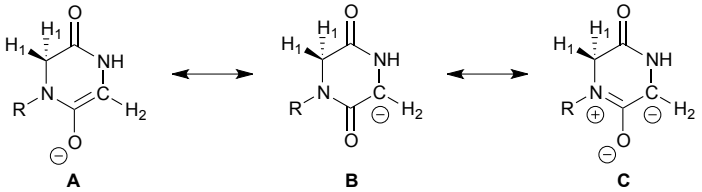

The difference in inductive effect from the substituted nitrogen upon the proximal and distal protons is small as the nitrogen is adjacent to both negatively charged regions of the respective enolates (Scheme 2.35). Thus, the ability of the substituted nitrogen to contribute to resonance stabilisation in the distal enolate causes the distal effect.

Scheme 2.35: The substituted nitrogen is adjacent to both the proximal and distal enolates.

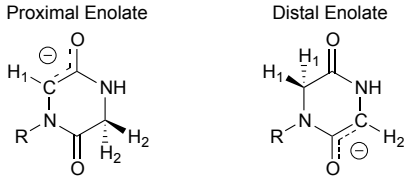

A subsequent study by Easton and Coote examined the kinetic acidity of N-substituted DKPs via hydrogen deuterium exchange reactions performed at 50 °C in d_6-acetone with a DBU base.[116] The kinetic acidities and calculated pK_as are shown in Table 2.4.

Table 2.4: The kinetic acidities and calculated aqueous pK_as values for a series of DKPs. Kinetic acidity values determined in d_6-acetone at 50 °C and calculated aqueous pK_as at 25 °C.[116]

DKP	Kinetic Acidity /M^{-1} s^{-1}	Calculated Aqueous pK_a
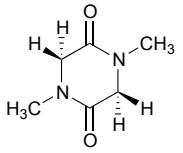	2.00×10^{-6}	26.6
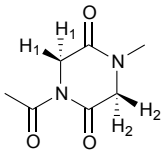	– (H_1) 5.01×10^{-2} (H_2)	25.8 (H_1) 18.4 (H_2)
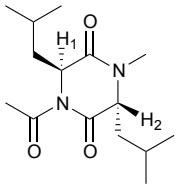	– (H_1) 2.30×10^{-2} (H_2)	28.4 (H_1) 17.1 (H_2)
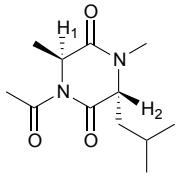	– (H_1) 3.40×10^{-2} (H_2)	28.2 (H_1) 18.2 (H_2)
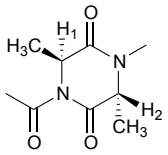	– (H_1) 5.90×10^{-2} (H_2)	28.6 (H_1) 18.4 (H_2)
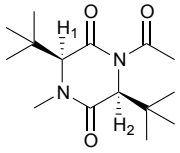	–	24.3 (H_1) 13.3 (H_2)
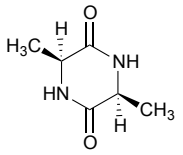	–	26.1
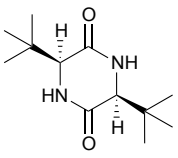	–	26.4

The difference in kinetic and thermodynamic acidity between the proximal and the distal protons for the N-acyl-N-methyl-c(Gly-Gly) DKP in Table 2.4: Entry 2 was

substantial. The difference in the calculated aqueous pK_as was 7.4 pK_a units and while deuterium exchange was observed for the distal protons no discernable exchange of the proximal protons was observed on the timescale of the experiment. Similar differences in kinetic acidities were also observed for a N-acyl-N-methyl-c(Leu-Leu), N-acyl-N-methyl-c(Ala-Leu) and N-acyl-N-methyl-c(Ala-Ala) (Table 2.4: Entries 3 – 5).

Easton and Coote then exploited both the difference in kinetic acidity and the *cis* / *trans* isomerism of DKPs to perform selective α-deuteration of N-methylated amino acids.[116] The procedure outlined in Scheme 2.36 involves initially preparing a *trans*-DKP from an (*R*/*S*)-N-methylated amino acid and either an alanine or leucine of opposite configuration (Scheme 2.36 a). The amide nitrogen is then acylated to give the *trans*-N-acyl-N-methyl-c(Xaa-Xaa). Subsequent reaction in a deuterated solvent in the presence of a base results in α-deuteration at the distal position (Scheme 2.36 b). The predominant product is the more stable *cis*-isomer of the DKP. The *cis*- and *trans*-isomers are then separated by chromatography and hydrolysed in acid to free the α-deuterated N-methylated amino acid (Scheme 2.36 c). This technique successfully prepared α-deuterated N-methylated amino acid with 95 – 99 % enantiomeric excesses.

Scheme 2.36: Preparation of α-deuterated N-methylated amino acids via DKPs. a) Synthesis of *trans*-N-acyl-N-methyl DKP. b) Deuterium exchange of distal α-protons. c) Hydrolysis of DKP to give the α-deuterated N-methylated amino acid.[116]

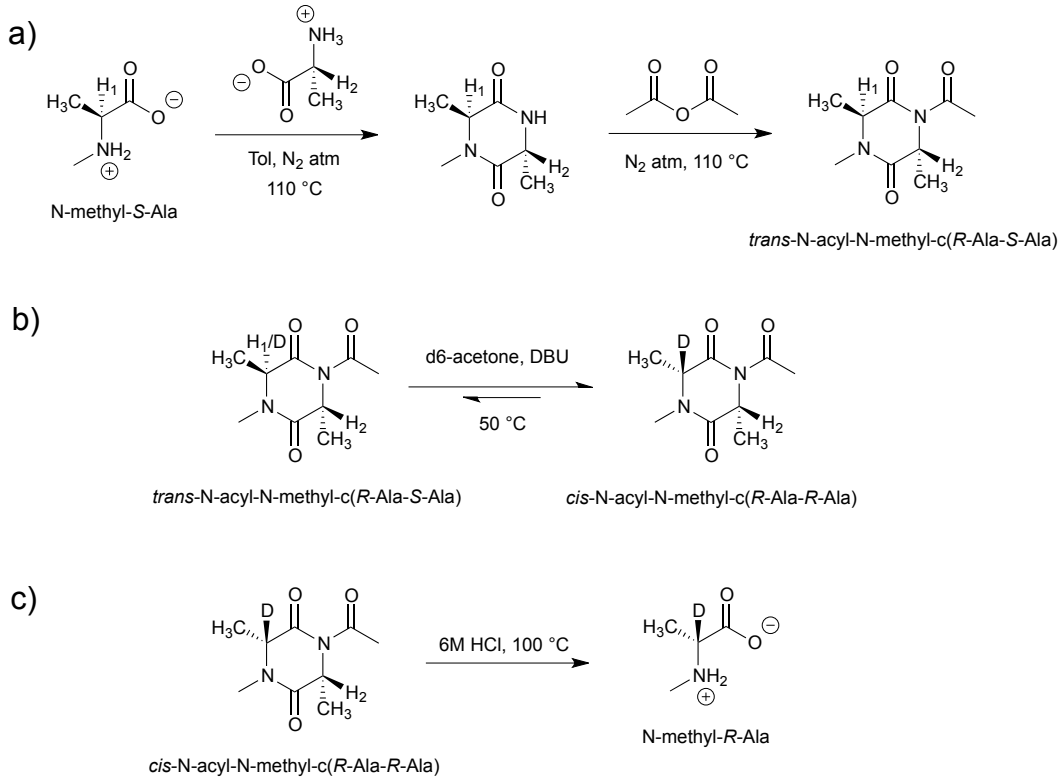

The higher than anticipated acidity in DKPs is not confined to the α-protons it has also been observed for the kinetic acidity of the amide proton. Robertson has utilised ^{1}H NMR saturation transfer and T_1 experiments to determine rate constants for specific acid catalysed (k_H), specific base catalysed (k_{OH}) and solvent induced (k_{H2O}) hydrogen deuterium exchange of the amide proton in 2-piperidone and c(Gly-Gly) DKP in D_2O (Table 2.5).[117] The mechanism for the specific base catalysis of the diketopiperazine is shown in Scheme 2.37.[118]

Table 2.5: Rate constants for hydrogen deuterium exchange of 2-piperidone and c(Gly-Gly) in D_2O at 25 °C.[117] Exchanging proton(s) highlighted in red.

Molecule	k_H /M^{-1} s^{-1}	k_{OH} /M^{-1} s^{-1}	k_{H2O} /s^{-1}
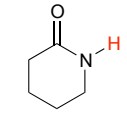 2-Piperidone	1.7×10^{-2}	0.79×10^{-7}	1.6×10^{2}
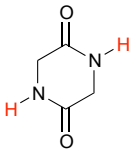 c(Gly-Gly)	3.9×10^{-2}	580×10^{-7}	7.7×10^{2}

Scheme 2.37: Mechanism for hydroxide catalysed exchange of amide proton in the diketopiperazine c(Gly-Gly).[118] rds = rate determining step.

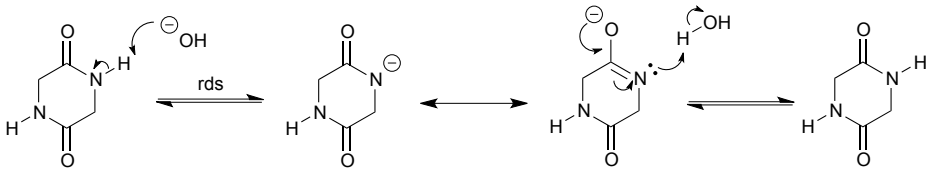

The effect of the additional amide group in c(Gly-Gly) upon the specific acid catalysed rate constant (k_H) is relatively small with only a two-fold increase in rate observed.

The effect on the specific base catalysis (k_{OH}) of the amide protons upon moving from the 2-piperidone amide to the c(Gly-Gly) was substantially larger with a 730-fold increase in rate observed. A previous study on the specific base catalysed exchange of amide protons in N-methylacetamide showed that the replacement of the methyl group with an acyl group resulted in only a 17-fold enhancement of k_{OH}.[119] The considerable difference between effect of an additional amide bond upon the linear and the cyclic systems could not be ascribed to the inductive effect alone. Robertson proposed that the additional rate enhancement in the cyclic DKP system was a result of additional electrostatic interactions between the amides.

Robertson calculated the free energy of the electrostatic interaction between the amide and the atoms in the opposite amide. A favourable interaction (ΔG = - 5.6 kcal mol^{-1}) is present between the amide δ^--nitrogen and the carbonyl δ^+-carbon on opposite amide. This interaction could stabilise the formation of the nitrogen anion in the rate

determining step therefore leading to a rate acceleration (Scheme 2.37). The absence of the additional amide group in 2-piperidone means that no electrostatic interaction is available to stabilise the amide nitrogen anion. In the linear system because the additional amide in N-acyl acetamide is not held in as close proximity as in the DKP any additional electrostatic interactions are attenuated (the magnitude of the free energy of electrostatic interaction is inversely proportionally to the distance between the point charges).

The above studies illustrate how the structure of the DKPs, particularly, the substituents on the nitrogen, can significantly affect the kinetic acidities of the α-carbon and amide protons. To date, however, there has been little consideration of how altering the R substituent at the α-carbon in DKPs affects the pK_as of the α-proton and the experimental aqueous pK_as of the α-carbon have not been determined.

2.2 Results

2.2.1 Overview

Hydrogen deuterium exchange experiments for a series of DKPs shown in Scheme 2.38 have been conducted in order to probe the effect of the R-substituent at the α-carbon on the acidity of the α-protons. Exchange of the α-protons for deuterium was monitored by ^{1}H NMR spectroscopy (400 and 500 MHz) at 25 °C and ionic strength I = 1.0 M (KCl) in carbonate and 3-chloro-quinuclidine buffers. From these data the first order and second order rate constants for deuteroxide catalysed exchange, k_{ex} and k_{DO}, were determined.

Scheme 2.38: The range of DKP substrates utilised for H-D exchange experiments.

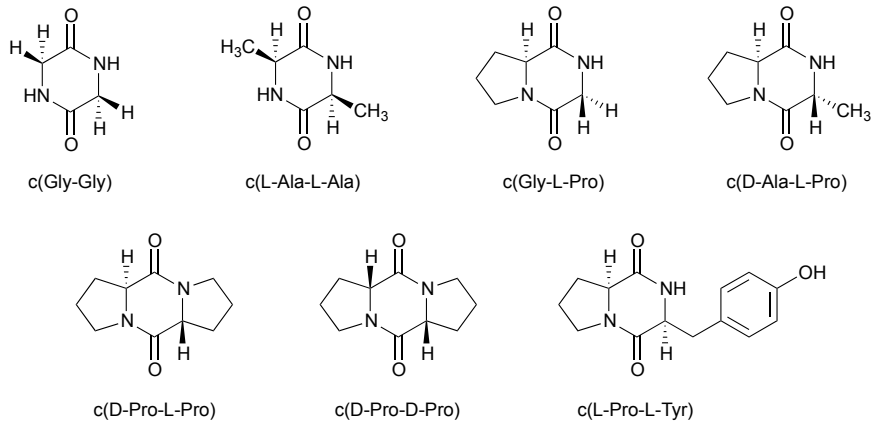

2.2.2 Synthesis of DKPs

c(D-Pro-L-Pro) and c(D-Pro-D-Pro) were prepared in yields of 15 % and 12 % based on starting reagents respectively via the method outlined in Scheme 2.39. Experimental details are provided in the Experimental Section 2.5.3.1 – 2.5.3.2.[v]

[v] We are grateful to Dr. Rachel Carr and Dr. Steven Cobb for recommending this synthetic route to c(D-Pro-L-Pro).

Scheme 2.39: Preparation of c(D-Pro-L-Pro). The synthesis of c(D-Pro-D-Pro) used an identical route but with L-Pro benzyl ester replaced with D-Pro benzyl ester.

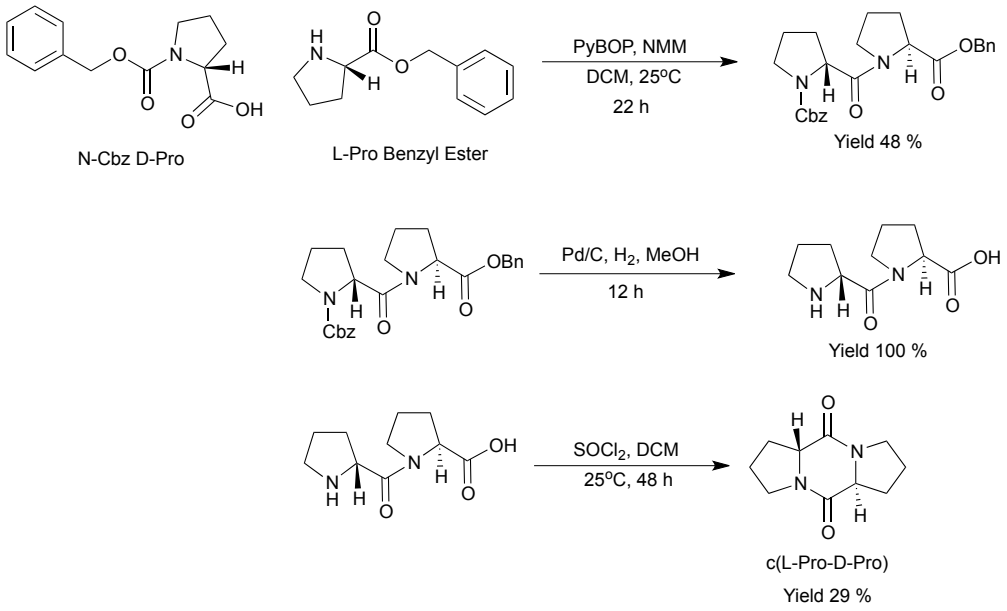

All other DKPs in Scheme 2.38 were purchased from either Bachem or Sigma Aldrich.

2.2.3 The deuterium exchange experiment

This section will detail how the hydrogen deuterium exchange experiments were performed and outline possible sources of experimental error.

2.2.3.1 Outline of the deuterium exchange experiment

Deuterium exchange reactions were carried out in carbonate ($KDCO_3$ / K_2CO_3) or 3-chloroquinuclidine buffered D_2O solutions in the p*D* range 9.35 – 10.98 at 25 °C and ionic strength I = 1.0 M. Reactions were initiated by the addition of buffer solution to the DKP and the internal standard (either tetramethylammonium deuteriosulfate or sodium trimethylsilylpropyl sulfonate). A portion of the resulting solution was extracted and placed in a sealed NMR tube and thermostated at 25 °C in a waterbath. The remainder of the solution was kept in the same waterbath and used to monitor the p*D* of the solution during the course of the reaction. To monitor the extent of deuterium exchange ^{1}H NMR spectroscopy was employed. The total acquisition time on the NMR

spectrometer for a single time point was ~ 25 min and 64 transients were taken over this period. To correct for any exchange that took place between the first and last transient the measurement times, *t*, for the exchange experiments were calculated from the mid-point of the acquisition.

The extent of deuterium exchange was evaluated by monitoring the disappearance of signal from α-protons relative to a peak from the internal standard. The fraction of non-exchanged α-protons at each time point, *f*(s), was determined via Equation 2.1:

$$f(\mathrm{s}) = \frac{(A_{\alpha-\mathrm{H}}/A_{\mathrm{int}})_t}{(A_{\alpha-\mathrm{H}}/A_{\mathrm{int}})_{t=0}} \qquad \text{(Equation 2.1)}$$

where $A_{\alpha\text{-H}}$ is the integral of the α-proton, A_{int} is the integral of the relevant peak on the internal standard and *t* is the time. Experimental pseudo first order rate constants of exchange, k_{ex}, of the α-protons were determined from the variation of *f*(s) with time via a fit of Equation 2.2 to the reaction data:

$$f(\mathrm{s}) = \exp\,(k_{\mathrm{ex}}t) \qquad \text{(Equation 2.2)}$$

The experimental pseudo first order rate of rate constant of exchange, k_{ex}, can potentially have kinetic contributions from the exchange pathways of three different components of solvent: acid catalysed, $k_{\mathrm{D+}}$, base catalysed, k_{DO} and solvent-promoted routes, k_{D2O}, Equation 2.3.

$$k_{\mathrm{ex}} = k_{\mathrm{D_2O}} + k_{\mathrm{D+}}[\mathrm{D^+}] + k_{\mathrm{DO}}[\mathrm{DO^-}] \qquad \text{(Equation 2.3)}$$

For the deuterium exchange of the α-protons in the DKPs, the values of k_{ex} increased with the p*D* of the solution indicating that the base catalysed rather than acid catalysed route was dominant. In addition, the solvent catalysed route for exchange is typically negligible for most weakly acidic carbon acids and therefore Equation 2.3 can be simplified to Equation 2.4.

$$k_{\mathrm{ex}} = k_{\mathrm{DO}}[\mathrm{DO^-}] \qquad \text{(Equation 2.4)}$$

Thus second order rate constants for deuteroxide-catalysed exchange, k_{DO}, can be determined as the slope of a linear correlation of k_{ex} and the concentration of deuteroxide ion. Basic buffer components may also contribute to k_{ex} (Equation 2.5):

$$k_{ex} = k_{DO}\left[DO^-\right] + k_{buff}[A^-] \qquad \text{(Equation 2.5)}$$

where k_{buff} is the second order rate constant for general base-catalysed exchange and $[A^-]$ is the concentration of the base form of the buffer.

2.2.3.2 Analysis of experimental error

There are several possible sources of experimental error:

- **Temperature variation:** The majority of the deuterium exchange experiments were carried out on a 400 MHz NMR spectrometer that was not thermostated. Care was taken to minimise the effect of temperature changes when the samples were removed from the waterbath. In transit between the lab and the NMR machine the sealed NMR tubes were carried in a container containing 25 °C water. The room which housed the NMR spectrometer was thermostated but the temperature did fluctuate by ~ ± 2 °C. The impact of the variation in temperature is expected to be minimal. The exchange experiments typically took two weeks to complete and with only one measurement taken a day (duration of acquisition ~ 25 min) the time spent out of the waterbath is less than 1.5 % of the total length of the experiment. The exchange experiments undertaken on a 500 MHz machine were thermostated at 25 °C.
- **Variation in p*D*:** For exchange reactions in 3-chloro-quinuclidine buffers there was no change in p*D* of the solutions over the two weeks. Small changes in p*D* (usually < 0.04) were sometimes observed for reactions in the carbonate buffers over the same timescale.
- **Variation in ionic strength:** In order to prepare the carbonate buffers ($KDCO_3$ / K_2CO_3) a concentrated DCl solution was added to a K_2CO_3 solution. Upon addition of DCl the solution did effervesce slightly. It is believed that a high local concentration of acid caused a sublimation reaction with the carbonate ($2D^+ + CO_3^{2-} \rightarrow D_2O + \uparrow CO_2$). The effect of this loss on the buffer capacity of

the solution is expected to be minimal as the concentration of buffer used was 0.185 M and little effervescence was observed. The effect of the loss on ionic strength will be higher than on buffer capacity as the contribution an ion makes to the ionic strength varies according to the square of its charge.[vi] Carbonate is a dianion and therefore makes a large contribution to ionic strength than a monocharged ion like K^+. Nevertheless, the loss of carbonate is not expected to significantly affect results, as the extent of effervescence observed was small.

- **Initial values at t = 0 s:** the integrals used for the $t = 0$ values were obtained from data acquired ~ 16 minutes after initiation of the exchange experiment. The error introduced due to this time delay in acquisition is negligible as the exchange experiments typically took two weeks to complete.

Overall the sources of experimental errors were minimised and their effect on the results of the deuterium exchange experiments is therefore believed to be small.

The following sections detail the deuterium exchange experiments performed for the DKPs in Scheme 2.38.

2.2.4 Carbon acidity of c(D-Pro-L-Pro)

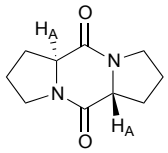

Pseudo first order rate constants for the deuteroxide catalysed exchange, k_{ex}, of the prolyl α-protons H_A of c(D-Pro-L-Pro) were determined in $KDCO_3$ buffered D_2O solutions (pD = 10.09 – 10.98) using ^1H NMR spectroscopy (400 and 500 MHz).

A representative set of spectra taken at three time points during the reaction at pD = 10.59 is shown in Figure 2.1. Deuterium exchange at the H_A position resulted in disappearance of the doublet of doublets due to H_A at 4.17 ppm over the course of the reaction. The level of exchange was monitored relative to a tetramethylammonium deuteriosulfate internal standard, whose methyl protons (3.14 ppm) are non-exchangeable. There are two possible products of exchange either c(D-Pro-D-Pro) or

[vi] Ionic strength is calculated via $I = \Sigma (n\ c\ z^2)$, where n is amount of the ion in the chemical formula, c = concentration of the ion and z is the charge on the ion.

c(L-Pro-L-Pro) both of which are diastereomers of c(D-Pro-L-Pro) (Scheme 2.40). c(D-Pro-L-Pro) was found to be unstable relative to the two diastereomers. Consequently, ^{1}H NMR spectra over the course of the reaction showed the disappearance of signals corresponding to the pyrrolidine ring protons (H_B, $H_{B'}$, H_C, $H_{C'}$, H_D and $H_{D'}$) on c(D-Pro-L-Pro) and the appearance of signals for analogous pyrrolidine ring protons (H_2, $H_{2'}$, H_3, $H_{3'}$, H_4 and $H_{4'}$) on c(D-Pro-D-Pro) / c(L-Pro-L-Pro) (Figure 2.1).

Figure 2.1: Representative ^{1}H NMR spectra at 500 MHz for the deuterium exchange reaction c(D-Pro-L-Pro) in $KDCO_3$ (50% free base, 0.185 M, p*D* = 10.59) buffered D_2O solution at 25 °C and ionic strength *I* = 1.0 M (KCl).

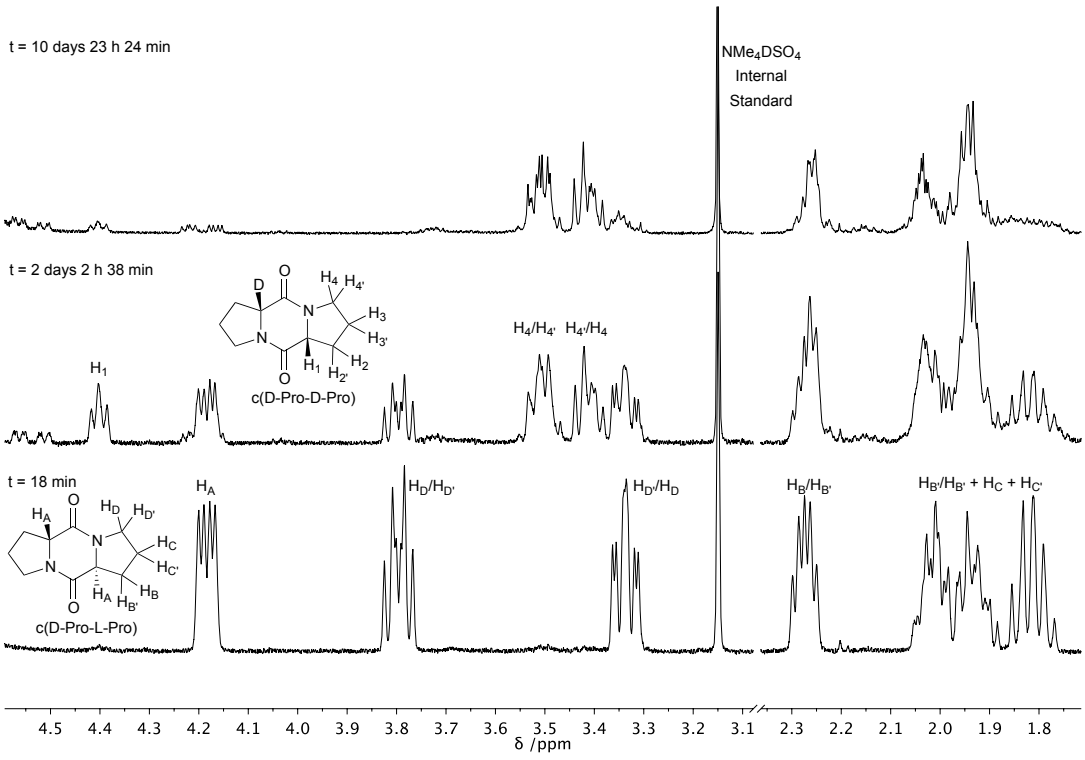

Scheme 2.40: Outcomes of the deuterium exchange reaction of c(D-Pro-L-Pro).

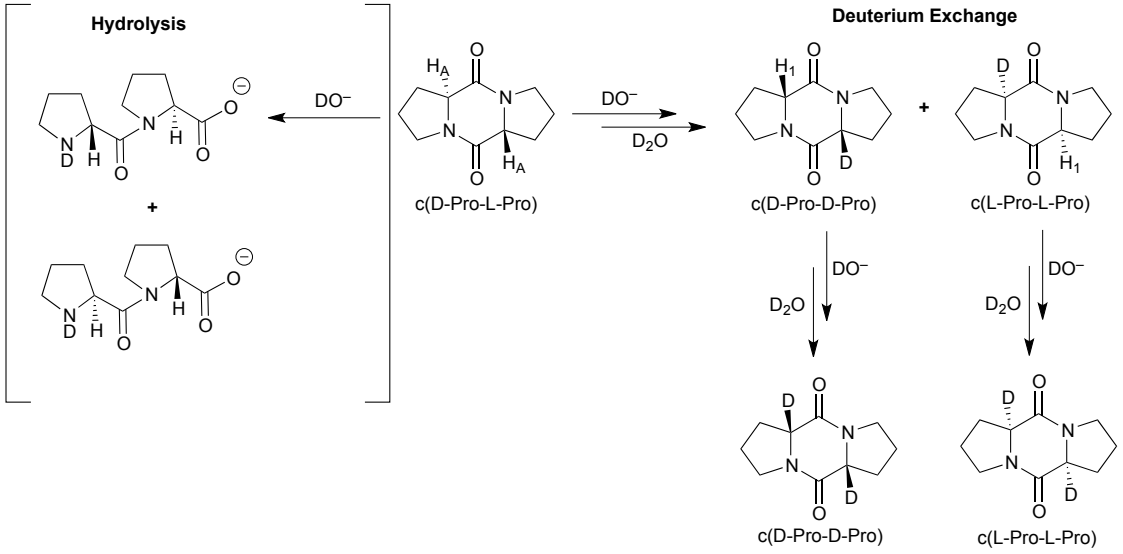

A minor amount of hydrolysis product (< 12 % after 10 days) was also observed in the ^{1}H NMR spectra. A proton on the hydrolysis product had an equivalent chemical shift to the H_A doublet of doublets. Consequently, deuterium exchange could not be precisely monitored via the H_A proton. Instead the exchange was followed via the disappearance of the multiplet for the pyrrolidine protons $H_D/H_{D'}$ (3.79 ppm) on c(D-Pro-L-Pro) and the appearance of the multiplet for the $H_4/H_{4'}$ (3.50 ppm) on c(D-Pro-D-Pro) / c(L-Pro-L-Pro). The rate limiting step for interconversion to the diastereomers will be deprotonation of H_A on c(D-Pro-L-Pro) and therefore $H_D/H_{D'}$ and $H_4/H_{4'}$ provide a reliable alternative assessment for deuterium exchange.

Experimentally observed first order rate constants for deuteroxide catalysed deuterium exchange, k_{ex}, of prolyl α-protons H_A of c(D-Pro-L-Pro) were determined from the fit of the fraction of protonated substrate remaining, f(s), for $H_D/H_{D'}$ c(D-Pro-L-Pro) and the fraction of deuterated product appearing, f(s)[vii], for $H_4/H_{4'}$ c(D-Pro-D-Pro) / c(L-Pro-L-Pro) to Equation 2.2 in Figure 2.2 and Figure 2.3, respectively. Reaction data and k_{ex} values for $H_D/H_{D'}$ and $H_4/H_{4'}$ over the pD range pD = 10.09 – 10.98 are shown in Table 2.5 and Table 2.6, respectively.

[vii] Calculated from f(s) = 1 – f(p), where f(p) is the fraction of product appearing.

Figure 2.2: Plot of the fraction, *f*(s), of $H_D/H_{D'}$ on c(D-Pro-L-Pro) not converted to c(D-Pro-D-Pro) / c(L-Pro-L-Pro) against time for c(D-Pro-L-Pro) (5.0 mM) in $KDCO_3$ (50 % fb, 0.185 M, p*D* = 10.59) buffered D_2O solution at *I* = 1.0 (KCl) and 25 ºC.

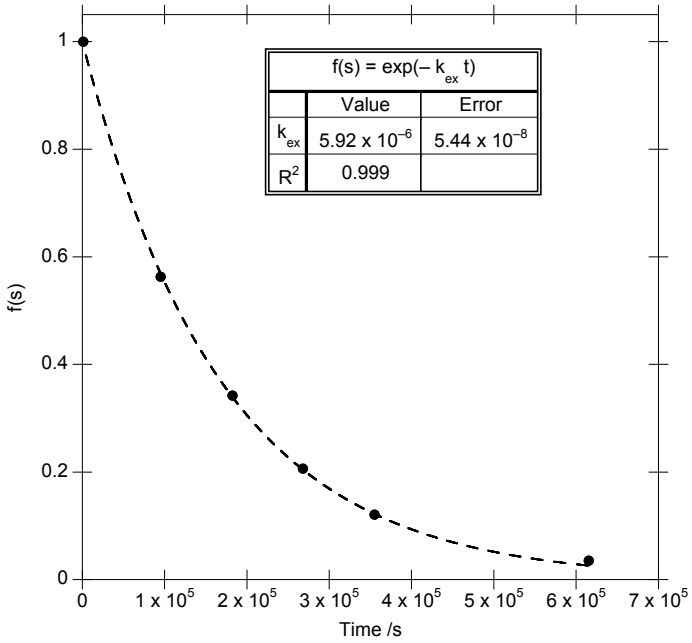

Figure 2.3: Plot of the inverse of the fraction, *f*(s), of $H_4/H_{4'}$ on c(D-Pro-D-Pro) / c(L-Pro-L-Pro) appearing against time for c(D-Pro-L-Pro) (5.0 mM) in $KDCO_3$ (50 % fb, 0.185 M, p*D* = 10.59) buffered D_2O solution at *I* = 1.0 (KCl) and 25 ºC.

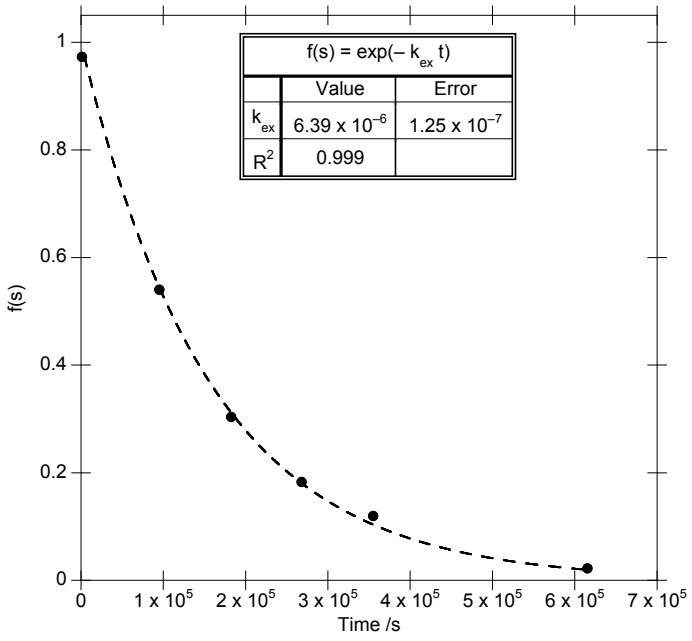

Table 2.5: Reaction data and observed first order rate constants (k_{ex}) for the deuterium exchange of the prolyl α-protons H_A in c(D-Pro-L-Pro) (5.0 mM) monitored via $H_D/H_{D'}$ pyrrolidine protons on c(D-Pro-L-Pro) in $KDCO_3$ (0.185 M, p*D* = 10.09 – 10.83) buffered D_2O solution, I = 1.0 (KCl) and 25 °C.

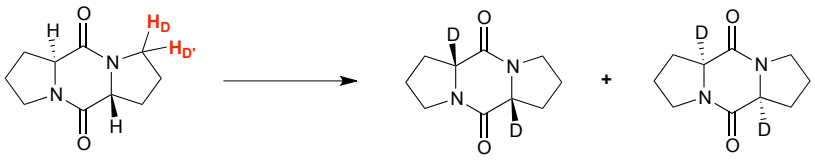

Experiment	Proton Chemical Shift /ppm	[DO^-] /M	Time /s	*f*(s)	k_{ex} /s^{-1}
70 % fb [a]	3.75 – 3.83	1.04×10^{-4} (p*D* 10.83)	1.00×10^{3}	1.00	1.05×10^{-5}
			9.48×10^{4}	0.38	
			1.82×10^{5}	0.15	
			2.68×10^{5}	0.06	
			3.55×10^{5}	0.02	
60 % fb	3.75 – 3.83	1.02×10^{-4} (p*D* 10.82)	1.19×10^{3}	1.00	9.84×10^{-6}
			1.25×10^{4}	0.89	
			1.93×10^{4}	0.83	
			7.93×10^{4}	0.45	
			9.33×10^{4}	0.40	
			1.06×10^{5}	0.35	
			1.64×10^{5}	0.19	
			1.82×10^{5}	0.17	
			1.92×10^{5}	0.15	
			2.52×10^{5}	0.09	
			2.67×10^{5}	0.07	
			3.38×10^{5}	0.03	
			3.66×10^{5}	0.02	
50 % fb	3.75 – 3.83	5.97×10^{-5} (p*D* 10.59)	1.07×10^{3}	1.00	5.92×10^{-6}
			9.50×10^{4}	0.56	
			1.82×10^{5}	0.34	
			2.68×10^{5}	0.21	
			3.55×10^{5}	0.12	
			6.15×10^{5}	0.04	
35 % fb	3.75 – 3.83	4.27×10^{-5}	1.06×10^{3}	1.00	4.26×10^{-6}

		(p*D* 10.44)	9.75×10^4	0.65	
			1.85×10^5	0.45	
			2.76×10^5	0.31	
			3.68×10^5	0.21	
			6.23×10^5	0.08	
			7.08×10^5	0.06	
			7.86×10^5	0.04	
			8.75×10^5	0.05	
			9.72×10^5	0.02	
20 % fb	3.75 – 3.83	3.81×10^{-5}	1.06×10^3	1.00	3.86×10^{-6}
		(p*D* 10.39)	9.56×10^4	0.69	
			1.81×10^5	0.50	
			2.73×10^5	0.35	
			3.64×10^5	0.25	
			6.19×10^5	0.09	
			7.05×10^5	0.07	
			7.84×10^5	0.04	
			8.77×10^5	0.03	
			9.68×10^5	0.02	
22 % fb	3.75 – 3.83	1.91×10^{-5}	1.19×10^3	1.00	2.09×10^{-6}
		(p*D* 10.09)	1.81×10^4	0.98	
			7.80×10^4	0.85	
			1.63×10^5	0.58	
			2.56×10^5	0.71	
			3.37×10^5	0.49	
			6.01×10^5	0.28	
			6.83×10^5	0.24	
			7.76×10^5	0.19	
			8.56×10^5	0.16	
			9.42×10^5	0.13	
			1.22×10^6	0.08	
			1.40×10^6	0.06	

[a] fb = free base.

Table 2.6: Reaction data and observed first order rate constants (k_{ex}) for the deuterium exchange of the prolyl α-protons H_A in c(D-Pro-L-Pro) (5.0 mM) monitored via $H_4/H_{4'}$ pyrrolidine protons on c(D-Pro-D-Pro) / c(L-Pro-L-Pro) in $KDCO_3$ (0.185 M, p*D* = 10.09 – 10.83) buffered D_2O solution, I = 1.0 (KCl) and 25 °C.

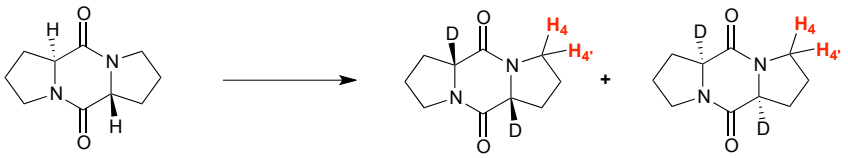

Experiment	Proton Chemical Shift /ppm	[DO^-] /M	Time /s	*f*(s)	k_{ex} /s^{-1}
70 % fb [a]	3.46 – 3.53	1.04×10^{-4}	1.00×10^{3}	0.96	1.09×10^{-5}
		(p*D* 10.83)	9.48×10^{4}	0.35	
			1.82×10^{5}	0.14	
			2.68×10^{5}	0.07	
			3.55×10^{5}	0.05	
60 % fb	3.46 – 3.53	1.02×10^{-4}	1.19×10^{3}	0.96	9.70×10^{-6}
		(p*D* 10.82)	1.25×10^{4}	0.87	
			1.93×10^{4}	0.82	
			7.93×10^{4}	0.46	
			9.33×10^{4}	0.39	
			1.06×10^{5}	0.36	
			1.64×10^{5}	0.21	
			1.82×10^{5}	0.17	
			1.92×10^{5}	0.16	
			2.52×10^{5}	0.08	
			2.67×10^{5}	0.08	
			3.38×10^{5}	0.07	
			3.66×10^{5}	0.06	
			6.03×10^{5}	0.00	
50 % fb	3.46 – 3.53	5.97×10^{-5}	1.07×10^{3}	0.97	6.39×10^{-6}
		(p*D* 10.59)	9.50×10^{4}	0.54	
			1.82×10^{5}	0.30	
			2.68×10^{5}	0.18	
			3.55×10^{5}	0.12	
			6.15×10^{5}	0.02	

35 % fb	3.46 – 3.53	4.27×10^{-5}	1.06×10^{3}	0.96	4.56×10^{-6}
		(p*D* 10.44)	9.75×10^{4}	0.64	
			1.85×10^{5}	0.44	
			2.76×10^{5}	0.28	
			3.68×10^{5}	0.19	
			6.23×10^{5}	0.05	
			7.08×10^{5}	0.04	
			7.86×10^{5}	0.03	
			8.75×10^{5}	0.01	
20 % fb	3.46 – 3.53	3.81×10^{-5}	1.06×10^{3}	0.96	4.44×10^{-6}
		(p*D* 10.39)	9.56×10^{4}	0.65	
			1.81×10^{5}	0.46	
			2.73×10^{5}	0.29	
			3.64×10^{5}	0.22	
			6.19×10^{5}	0.06	
			7.05×10^{5}	0.03	
22 % fb	3.46 – 3.53	1.91×10^{-5}	1.19×10^{3}	1.00	2.47×10^{-6}
		(p*D* 10.09)	1.81×10^{4}	0.92	
			7.80×10^{4}	0.82	
			1.63×10^{5}	0.55	
			2.56×10^{5}	0.68	
			3.37×10^{5}	0.43	
			6.01×10^{5}	0.22	
			6.83×10^{5}	0.18	
			7.76×10^{5}	0.14	
			8.56×10^{5}	0.12	
			9.42×10^{5}	0.10	
			1.22×10^{6}	0.02	

[a] fb = free base.

Figure 2.4 and Figure 2.5 show the dependence of k_{ex} on the concentration of deuteroxide for H_A in c(D-Pro-L-Pro). Second order rate constants for deuteroxide-catalysed-exchange of $k_{DO} = 9.69 \times 10^{-2}$ M^{-1} s^{-1} for $H_D/H_{D'}$ and $k_{DO} = 9.31 \times 10^{-2}$ M^{-1} s^{-1} for $H_4/H_{4'}$ are obtained from the slopes of linear fits of the reaction data to Equation 2.4. These k_{DO} values are in good agreement.

Figure 2.4: Plot of the dependence of k_{ex} upon [DO^-] for the deuterium exchange of the prolyl α-protons H_A in c(D-Pro-L-Pro) (5.0 mM) monitored via $H_D/H_{D'}$ protons on c(D-Pro-L-Pro) in $KDCO_3$ (0.185 M, pD = 10.09 – 10.83) buffered D_2O solution, I = 1.0 (KCl) and 25 ºC.

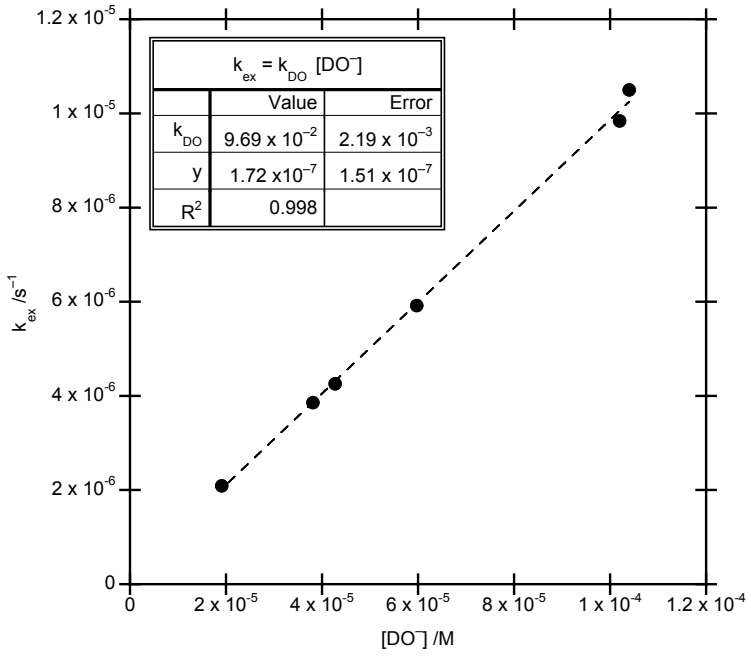

Figure 2.5: Plot of the dependence of k_{ex} upon [DO^-] for the deuterium exchange of the prolyl α-protons H_A in c(D-Pro-L-Pro) (5.0 mM) monitored via $H_4/H_{4'}$ protons on c(D-Pro-D-Pro) / c(L-Pro-L-Pro) in $KDCO_3$ (0.185 M, pD = 10.09 – 10.83) buffered D_2O solution, I = 1.0 (KCl) and 25 ºC.

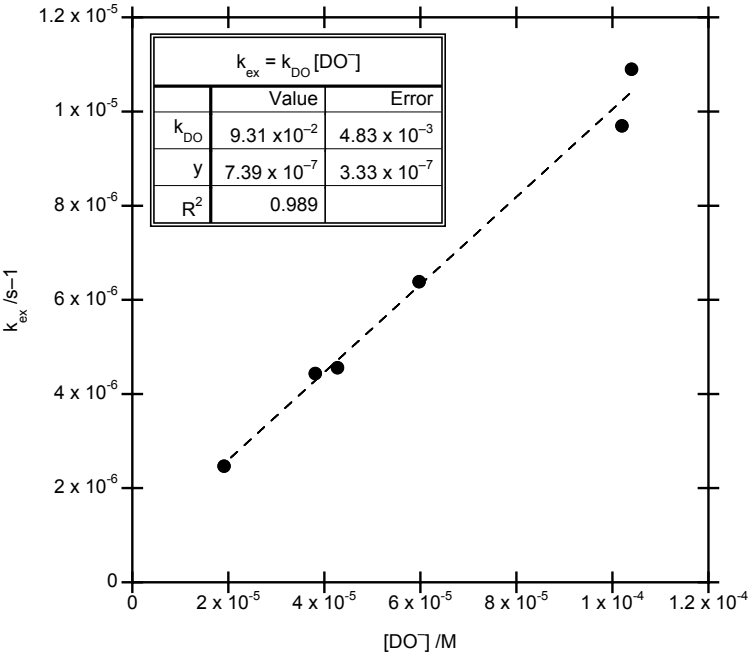

Figures 2.4 and 2.5 also indicate that buffer catalysis is insignificant as i) both fits intersect the y-axis close to the origin, and ii) no upwards curvature of reaction data is observed at higher concentrations of the free base form of the buffer [CO_3^{2-}].

For a more definitive assessment of the contribution of buffer catalysis, deuterium exchange reactions were undertaken in a series of solutions with an identical buffer ratio (to maintain a relatively constant p*D* and therefore a consistent contribution of $k_{DO}[DO^-]$ to k_{ex}, Equation 2.5) and a varying total concentration of buffer, [$KDCO_3$].[viii] The exchange reactions were performed at 70 % free base $KDCO_3$ over the [$KDCO_3$] range 0.07 – 0.37 M. Ideally, the p*D* should remain constant as the concentration of the buffer changes, however, experimentally the p*D* varied unavoidably by 0.13 units. Therefore it was necessary to determine whether the relatively small differences in k_{ex} between solutions were due to changes in [CO_3^{2-}] or changes in [DO^-].

Figures 2.6 and 2.8 show the dependence of k_{ex} for $H_D/H_{D'}$ and $H_4/H_{4'}$ on CO_3^{2-} concentration (Appendix I.1.1: Table I.1 – I.2) while Figures 2.7 and 2.9 show the dependence on deuteroxide concentration. In the former case, the fit of the data would give $k_{buff} = 1.64 \times 10^{-5} – 1.88 \times 10^{-5}$ M^{-1} s^{-1}. However, the fit of the data in the latter case gives $k_{DO} = 9.36 \times 10^{-2} – 1.05 \times 10^{-1}$ M^{-1} s^{-1} which are in good agreement with the k_{DO} values determined in Figure 2.4 and Figure 2.5 above. Consequently, it appears more likely that the changes in k_{ex} observed in the experiments to determine buffer catalysis are due to the changes in deuteroxide concentration between the different concentrations of buffer rather than the buffer itself.

[viii] There are two possible bases in $KDCO_3$ buffer: KCO_3^- and CO_3^{2-}. Only CO_3^{2-} is considered in determining buffer catalysis because it is a significantly stronger base than KCO_3^- as pK_a (HCO_3^-) = 10.33 while pK_a (H_2CO_3) = 3.58.

Figure 2.6: Plot of the dependence of k_{ex} upon $[CO_3^{2-}]$ for the deuterium exchange of the prolyl α-protons H_A in c(D-Pro-L-Pro) (5.0 mM) monitored via $H_D/H_{D'}$ pyrrolidine protons on c(D-Pro-D-Pro) / c(L-Pro-L-Pro) in 70 % free base $KDCO_3$ (0.07 – 0.37 M, pD = 10.85 – 10.98) buffered D_2O solution, I = 1.0 (KCl) and 25 ºC.

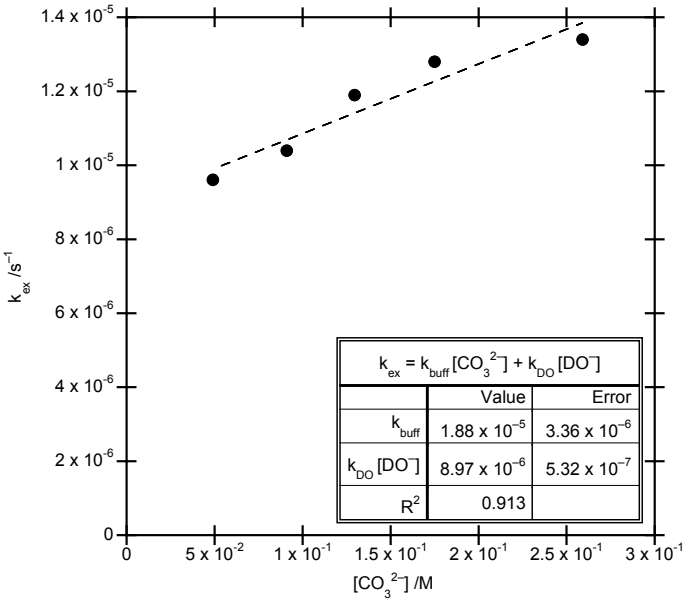

Figure 2.7: Plot of the dependence of k_{ex} upon $[DO^-]$ for the deuterium exchange of the prolyl α-protons H_A in c(D-Pro-L-Pro) (5.0 mM) monitored via $H_D/H_{D'}$ pyrrolidine protons on c(D-Pro-D-Pro) / c(L-Pro-L-Pro) in 70 % free base $KDCO_3$ (0.07 – 0.37 M, pD = 10.85 – 10.98) buffered D_2O solution, I = 1.0 (KCl) and 25 ºC.

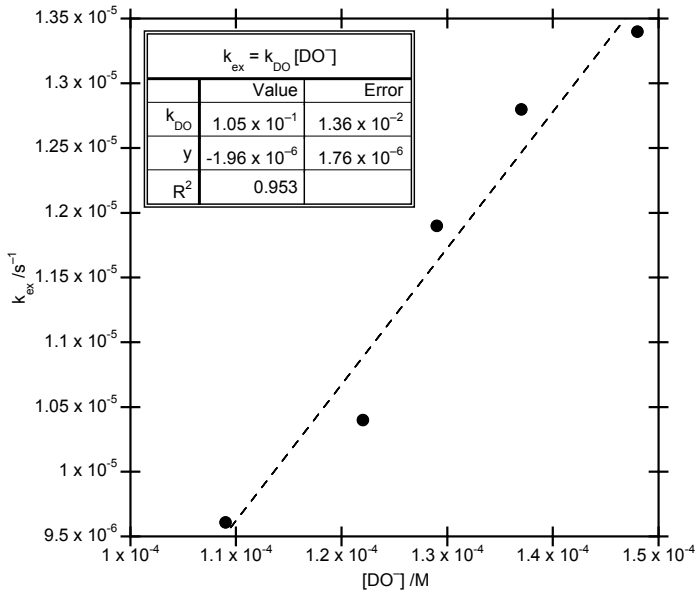

Figure 2.8: Plot of the dependence of k_{ex} upon $[CO_3^{2-}]$ for the deuterium exchange of the prolyl α-protons H_A in c(D-Pro-L-Pro) (5.0 mM) monitored via $H_4/H_{4'}$ pyrrolidine protons on c(D-Pro-D-Pro) / c(L-Pro-L-Pro) in 70 % free base $KDCO_3$ (0.07 – 0.37 M, pD = 10.85 – 10.98) buffered D_2O solution, I = 1.0 (KCl) and 25 ºC.

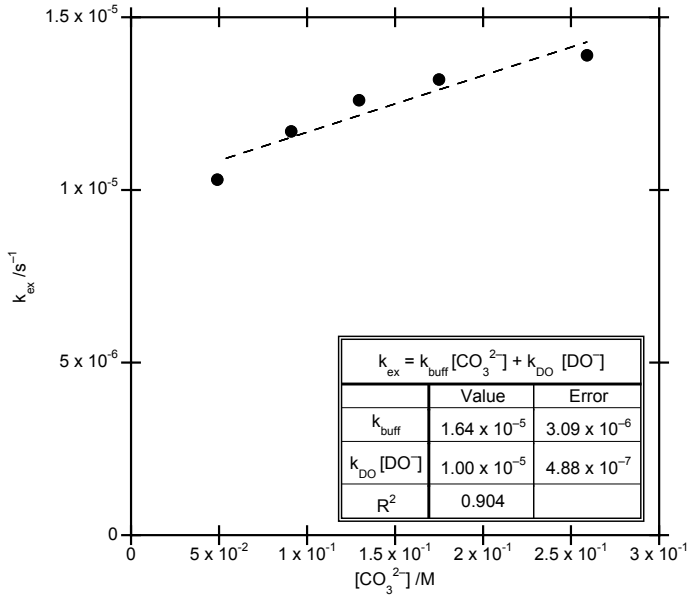

Figure 2.9: Plot of the dependence of k_{ex} upon $[DO^-]$ for the deuterium exchange of the prolyl α-protons H_A in c(D-Pro-L-Pro) (5.0 mM) monitored via $H_4/H_{4'}$ pyrrolidine protons on c(D-Pro-D-Pro) / c(L-Pro-L-Pro) in 70 % free base $KDCO_3$ (0.07 – 0.37 M, pD = 10.85 – 10.98) buffered D_2O solution, I = 1.0 (KCl) and 25 ºC.

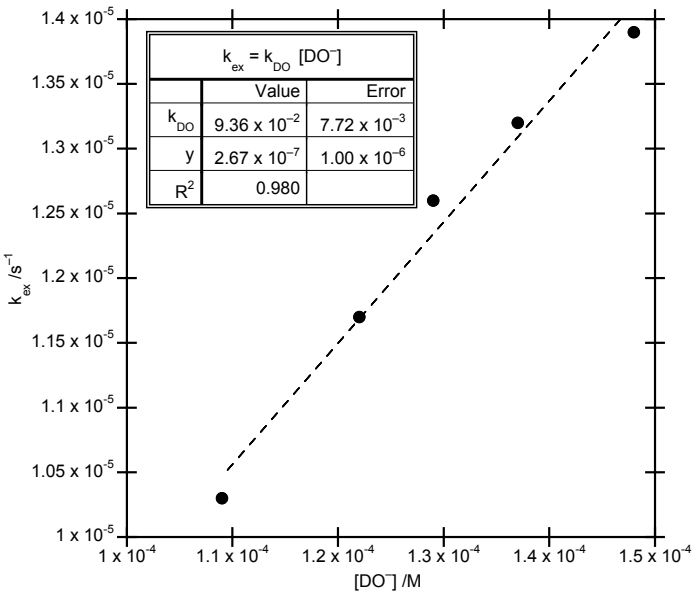

2.2.5 Carbon acidity of c(D-Pro-D-Pro)

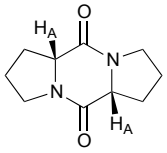

Pseudo first order rate constants for the deuteroxide catalysed exchange, k_{ex}, of the prolyl α-protons H_A of c(D-Pro-D-Pro) were determined in $KDCO_3$ buffered D_2O solutions (p*D* = 10.16 – 10.81) using ^1H NMR spectroscopy (400 MHz).

A representative set of spectra taken at three time points during the reaction at p*D* = 10.60 is shown in Figure 2.10. Deuterium exchange at the H_A position resulted in disappearance of the doublet of doublets due to H_A at 4.49 ppm over the course of the reaction. The level of exchange was monitored relative to a tetramethylammonium deuteriosulfate internal standard, whose methyl protons (3.21 ppm) are non-exchangeable. The disappearance of the doublet of doublets due to H_A was used to monitor the extent of exchange. No changes in the integrated areas from the pyrrolidine ring protons (H_B, $H_{B'}$, H_C, $H_{C'}$ H_D and $H_{D'}$) on c(D-Pro-D-Pro) were observed. The product of deuterium exchange will solely be deuterated c(D-Pro-D-Pro) (Scheme 2.41). No hydrolysis of c(D-Pro-D-Pro) was observed.

Figure 2.10: Representative ^{1}H NMR spectra at 400 MHz for the deuterium exchange reaction c(D-Pro-D-Pro) (5.0 mM) in $KDCO_3$ (50% free base, pD = 10.60, 0.185 M), 25 °C and ionic strength I = 1.0 M (KCl).

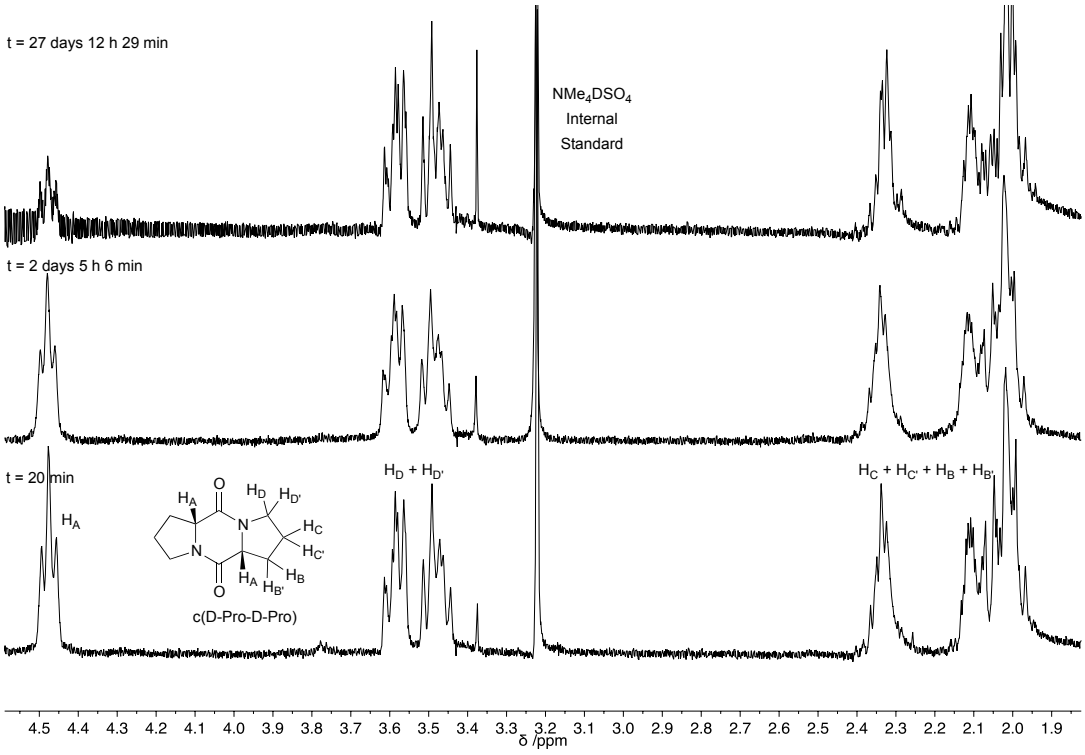

Scheme 2.41: Outcomes of the deuterium exchange reaction of c(D-Pro-D-Pro).

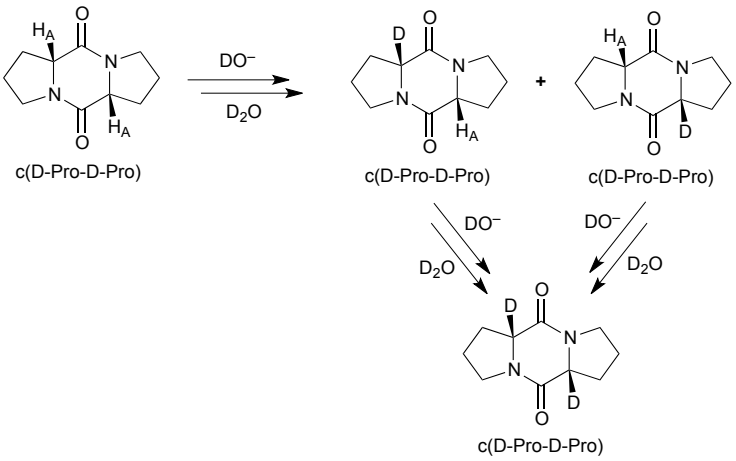

Experimentally observed first order rate constants for deuteroxide-catalysed deuterium exchange, k_{ex}, of prolyl α-protons H_A of c(D-Pro-D-Pro) were determined from the fit of the fraction of protonated substrate remaining, f(s), for H_A c(D-Pro-D-

Pro) to Equation 2.2. Reaction data and k_{ex} values for H_A over the pD range pD = 10.16 – 10.81 are shown in Appendix I.2.1: Table I.3.

Figure 2.11 shows the dependence of k_{ex} on the concentration of deuteroxide for H_A. A value of $k_{DO} = 8.62 \times 10^{-3}$ M^{-1} s^{-1} is obtained as the slope of a linear fit of the reaction data to Equation 2.4. Again, there was no indication of buffer catalysis of the deuterium exchange reaction of c(D-Pro-D-Pro). Given that no buffer catalysis was observed for c(D-Pro-L-Pro) which had a higher k_{DO} value further checks for buffer catalysis of c(D-Pro-D-Pro) were deemed unnecessary.

Figure 2.11: Plot of the dependence of k_{ex} upon [DO^-] for the deuterium exchange of the prolyl α-protons H_A in c(D-Pro-D-Pro) (5.0 mM) in $KDCO_3$ (0.185 M, pD = 10.16 – 10.81) buffered D_2O solution, I = 1.0 (KCl) and 25 ºC.

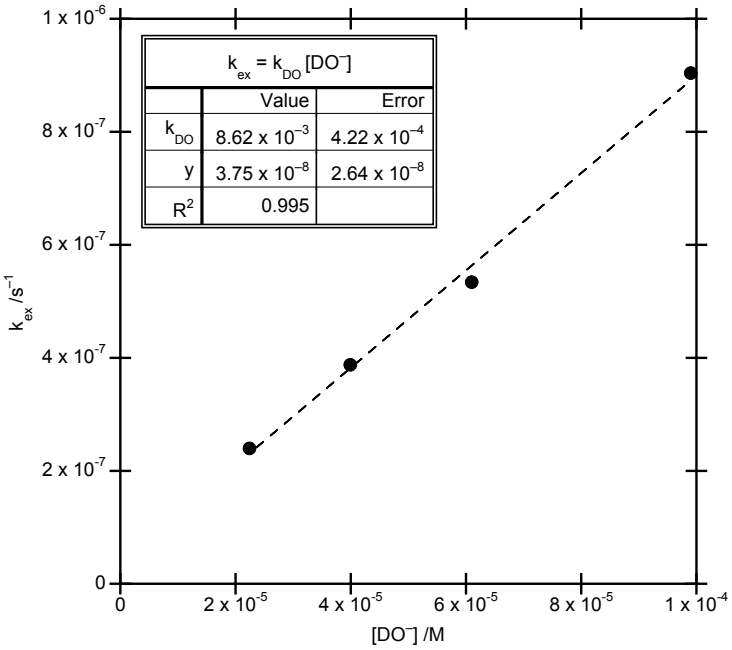

2.2.6 Carbon acidity of c(D-Ala-L-Pro)

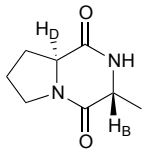

Pseudo first order rate constants for the deuteroxide catalysed exchange, k_{ex}, of the prolyl α-proton H_D and alanyl α-proton H_B of c(D-Ala-L-Pro) were determined in

$KDCO_3$ buffered D_2O solutions (p*D* = 10.12 – 10.98) using ^1H NMR spectroscopy (400 MHz).

2.2.6.1 c(D-Ala-L-Pro) Prolyl α-proton

A representative set of spectra taken at three time points during the reaction at p*D* = 10.58 is shown in Figure 2.12. Deuterium exchange at the H_D position on c(D-Ala-L-Pro) resulted in disappearance of the doublet of doublets due to H_D at 4.30 ppm over the course of the reaction. The level of exchange was monitored relative to a tetramethylammonium deuteriosulfate internal standard, whose methyl protons (singlet, 3.14 ppm) are non-exchangeable. The products of deuterium exchange at H_D position on c(D-Ala-L-Pro) are deuterated c(D-Ala-L-Pro) and c(D-Ala-D-Pro) (Scheme 2.42). Over the course of the reaction the equilibrium distribution of the diastereomers c(D-Ala-L-Pro) and c(D-Ala-D-Pro) is approached.[ix] Consequently, ^1H NMR spectra over the course of the reaction showed the disappearance of the doublet corresponding to the alanyl methyl group (H_A) and the multiplet prolyl pyrrolidine ring protons (H_E, $H_{E'}$, H_F, $H_{F'}$, H_G and $H_{G'}$) on c(D-Ala-L-Pro) and the appearance of the doublet for the analogous methyl (H_1) and the multiplets for the analogous pyrrolidine ring protons (H_5, $H_{5'}$, H_6, $H_{6'}$, H_7 and $H_{7'}$) on c(D-Ala-D-Pro) (Figure 2.12). A minor amount of hydrolysis product (< 10 % after 11 days) was also observed in the ^1H NMR spectra.

[ix] The enantiomer of c(D-Ala-L-Pro), i.e. c(L-Ala-D-Pro), and the enantiomer of c(D-Ala-D-Pro), i.e. c(L-Ala-L-Pro), will also be formed by deprotonation at the α-positions.

Figure 2.12: Representative ^{1}H NMR spectra at 400 MHz for the deuterium exchange reaction of c(D-Ala-L-Pro) (5.0 mM) in $KDCO_3$ (50% free base, p*D* = 10.58, 0.185 M), 25 °C and ionic strength *I* = 1.0 M (KCl).

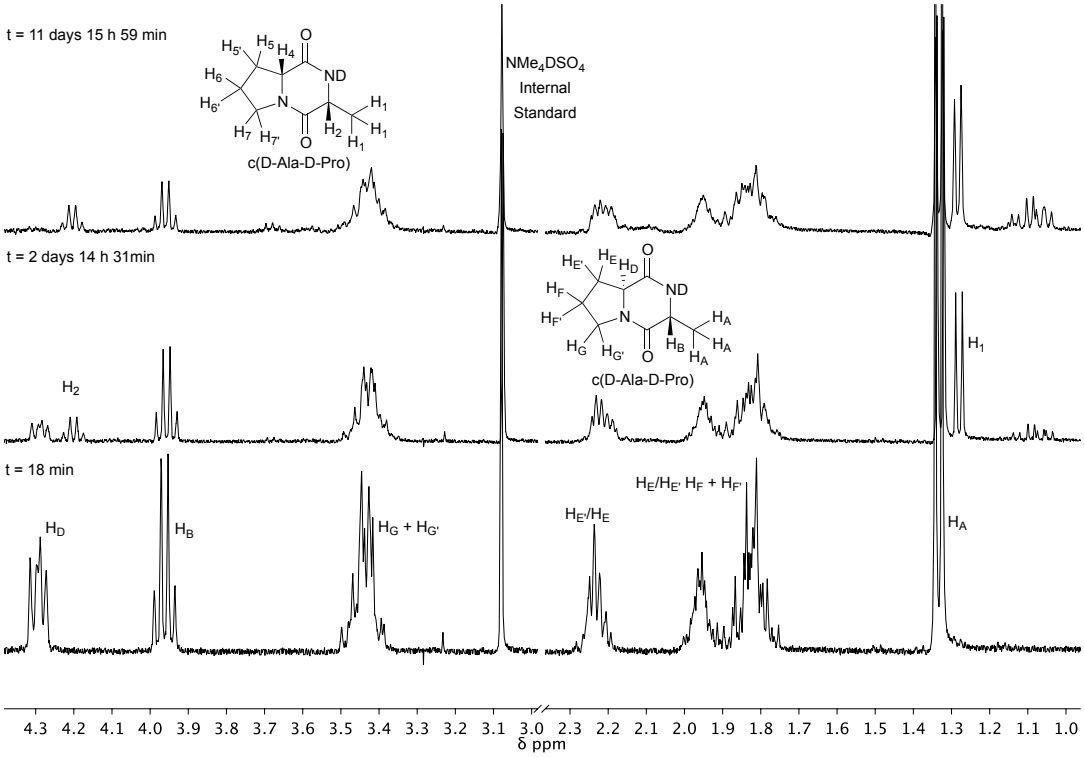

Scheme 2.42: Outcomes of the deuterium exchange reactions of c(D-Ala-L-Pro).

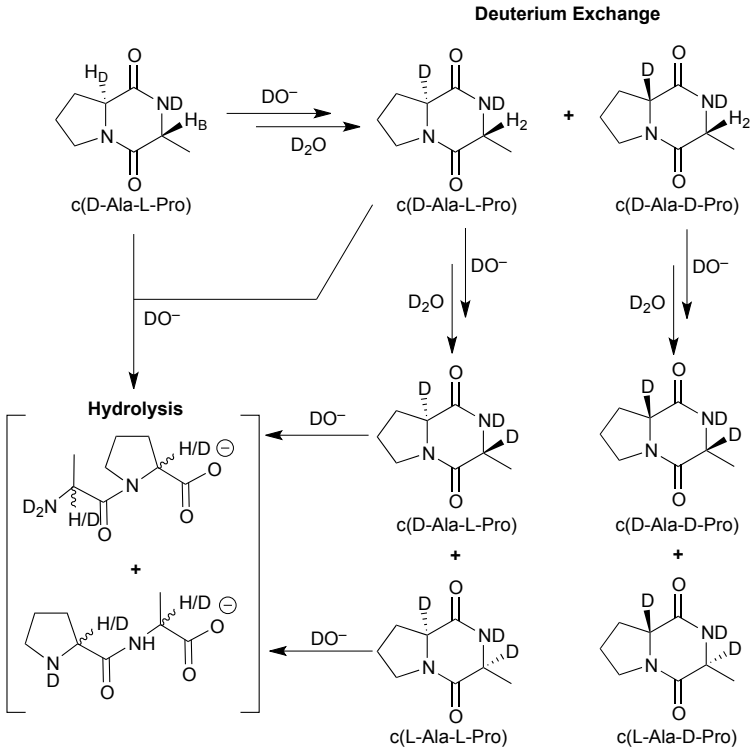

Pseudo first order rate constants for exchange were determined by monitoring the disappearance of signal from the prolyl proton H_D (4.30 ppm) on c(D-Ala-L-Pro) and the appearance of the methyl protons H_1 (1.29 ppm) on the product c(D-Ala-D-Pro)[x] (Figure 2.12). The rate limiting step for formation of c(D-Ala-D-Pro) will be deprotonation of c(D-Ala-L-Pro) and therefore H_1 provides an alternative assessment for k_{ex}. Experimentally observed first order rate constants for deuteroxide catalysed deuterium exchange, k_{ex}, of prolyl α-protons H_A of c(D-Ala-L-Pro) were determined from the fit of the fraction of protonated substrate remaining, $f(s)$, for H_D c(D-Ala-L-Pro) and the fit of the fraction of deuterated product appearing, $f(s)$, for H_1 c(D-Ala-D-Pro) to Equation 2.2. Reaction data and k_{ex} values for H_D and H_1 over the p*D* range p*D* = 10.12 – 10.98 are shown in Appendix I.3.1: Table I.4 and Table I.5, respectively.

Figure 2.13 and Figure 2.14 show the dependence of k_{ex} on the concentration of deuteroxide for H_D and H_1 (Appendix I.3.1: Table I.4 and Table I.5). Values of k_{DO} = 9.45×10^{-2} M^{-1} s^{-1} for H_D and $k_{DO} = 1.18 \times 10^{-1}$ M^{-1} s^{-1} for H_1 are obtained as the slope of a linear fit of the reaction data to Equation 2.4, which are in good agreement.

Figure 2.13: Plot of the dependence of k_{ex} upon $[DO^-]$ for the deuterium exchange of the prolyl α-proton H_D in c(D-Ala-L-Pro) (5.0 mM) in $KDCO_3$ (0.185 M, p*D* = 10.12 – 10.98) buffered D_2O solution, I = 1.0 (KCl) and 25 ºC.

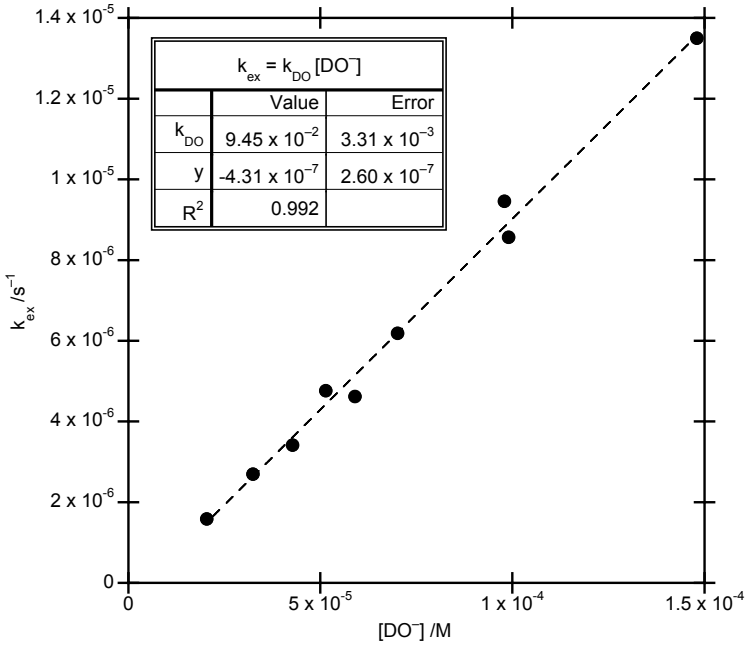

[x] Minor amount of c(L-Ala-L-Pro) may also be present here.

Figure 2.14: Plot of the dependence of k_{ex} upon [DO^-] for the deuterium exchange of the prolyl α-proton H_D in c(D-Ala-L-Pro) (5.0 mM) monitored via H_1 methyl protons on c(D-Ala-D-Pro) in $KDCO_3$ (0.185 M, p*D* = 10.12 – 10.98) buffered D_2O solution, *I* = 1.0 (KCl) and 25 ºC.

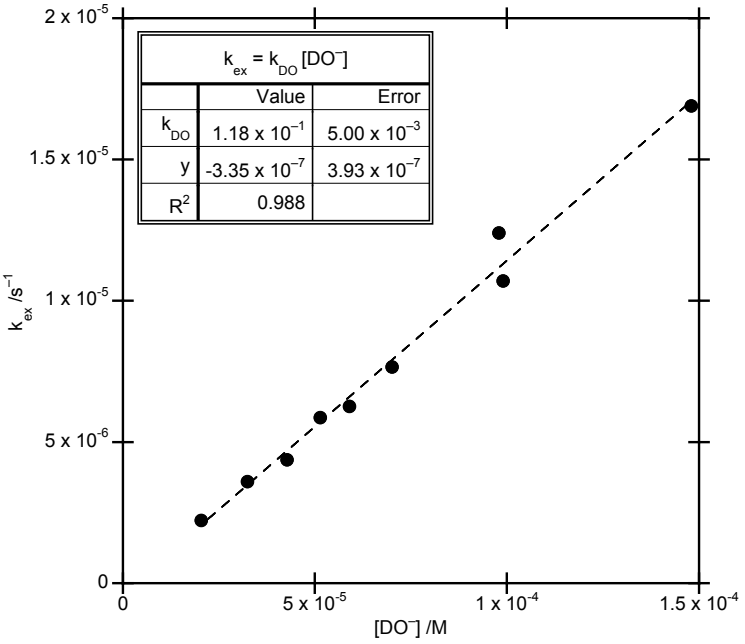

As mentioned in previous sections Figures 2.13 and 2.14 indicate that there is insignificant buffer catalysis of hydrogen-deuterium exchange of the prolyl α-proton of c(D-Ala-L-Pro) as i) both fits intersect the y-axis close to the origin, and ii) no upwards curvature at higher concentrations of free base form of the buffer [CO_3^{2-}] is observed. To further probe the role of buffer species, exchange reactions were undertaken in a series of solutions with an identical buffer ratio and a varying total concentration of buffer, [$KDCO_3$]. The H / D exchange reactions were performed at both 20 % free base and 70 % free base $KDCO_3$ over the [$KDCO_3$] range 0.07 – 0.37 M. Experimentally, the p*D* varied by 0.07 – 0.14 units upon dilution at constant ionic strength. As before, it was necessary to ascertain whether the differences in k_{ex} between solutions were due to changes in [CO_3^{2-}] or changes in [DO^-]. Figure 2.15, Figure 2.17, Figure 2.19 and Figure 2.21 show the dependence of k_{ex} on the [CO_3^{2-}] (Appendix I.3.2: Table I.6 – I.7) while Figure 2.16, Figure 2.18, Figure 2.20 and Figure 2.22 show the dependence of k_{ex} on the [DO^-]. In the former four Figures the fits of the data would give k_{buff} = 1.97 ×

10^{-5} – 2.93 × 10^{-5} M^{-1} s^{-1}.[xi] However, the fits of the data in the latter four Figures gives k_{DO} = 1.02 × 10^{-1} – 1.54 × 10^{-1} M^{-1} s^{-1} which are in good agreement with the k_{DO} values determined in Figures 2.13 and 2.14 above. Consequently, it appears more likely that the observed changes in k_{ex} are due to the changes in [DO^-] rather than [CO_3^{2-}].

Figure 2.15: Plot of the dependence of k_{ex} upon [CO_3^{2-}] for the deuterium exchange of the prolyl α-proton H_D in c(D-Ala-L-Pro) (5.0 mM) in $KDCO_3$ (70 % free base, 0.07 – 0.37 M, p*D* = 10.85 – 10.98) buffered D_2O solution, *I* = 1.0 (KCl) and 25 ºC.

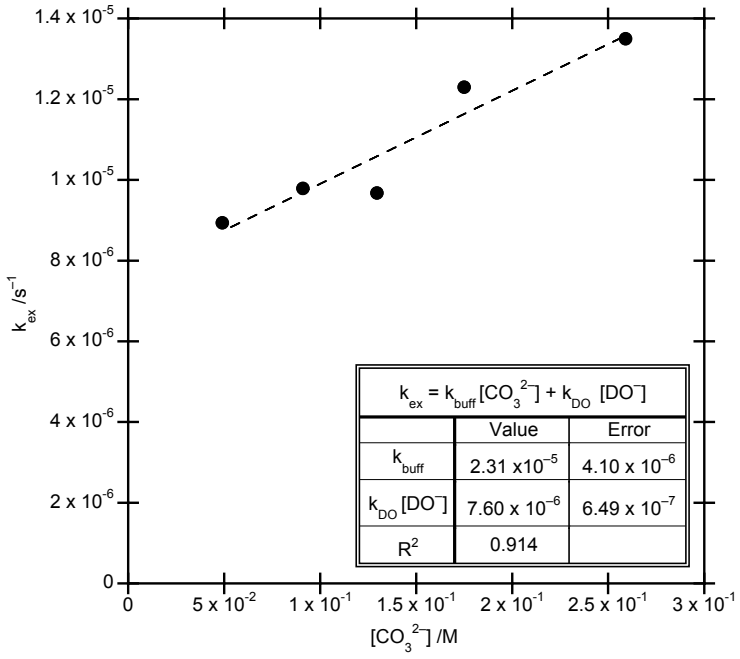

[xi] Figure 2.18 does have two data points for 0.185 M and 0.13 M whose p*D* is identical and for H_1 the k_{ex} = 6.90 × 10^{-6} M^{-1} s^{-1} and k_{ex} = 6.35 × 10^{-6} M^{-1} s^{-1} respectively, but this only amounts to a < 8 % difference in the k_{ex}.

Figure 2.16: Plot of the dependence of k_{ex} upon [DO^-] for the deuterium exchange of the prolyl α-proton H_D in c(D-Ala-L-Pro) (5.0 mM) in $KDCO_3$ (70 % free base, 0.07 – 0.37 M, pD = 10.85 – 10.98) buffered D_2O solution, I = 1.0 (KCl) and 25 ºC.

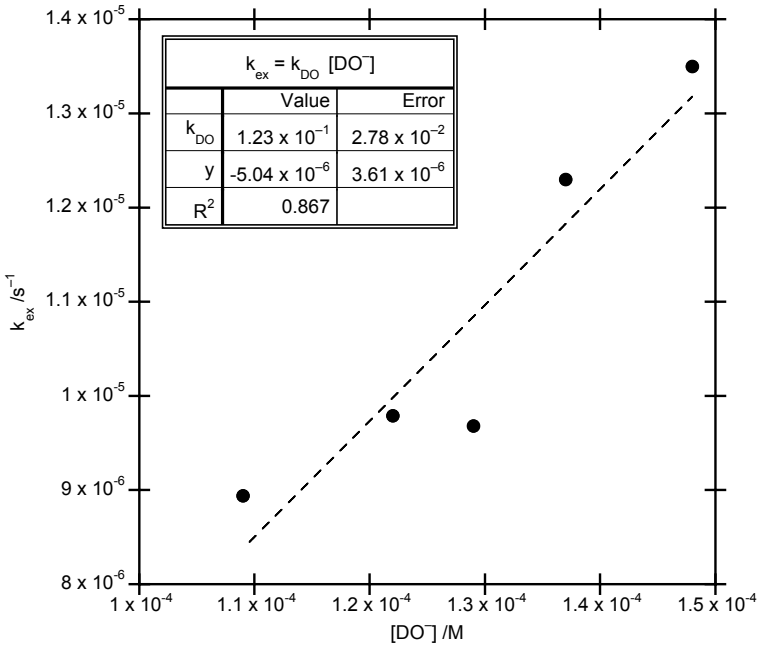

Figure 2.17: Plot of the dependence of k_{ex} upon [CO_3^{2-}] for the deuterium exchange of the prolyl α-proton H_D in c(D-Ala-L-Pro) (5.0 mM) in $KDCO_3$ (20 % free base, 0.07 – 0.37 M, pD = 10.59 – 10.66) buffered D_2O solution, I = 1.0 (KCl) and 25 ºC.

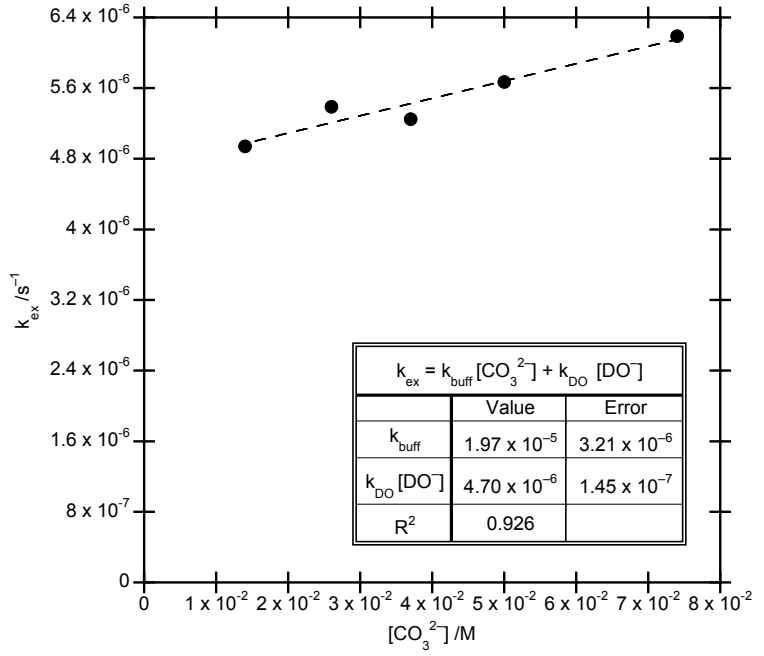

Figure 2.18: Plot of the dependence of k_{ex} upon [DO^-] for the deuterium exchange of the prolyl α-proton H_D in c(D-Ala-L-Pro) (5.0 mM) in $KDCO_3$ (20 % free base, 0.07 – 0.37 M, p*D* = 10.59 – 10.66) buffered D_2O solution, *I* = 1.0 (KCl) and 25 ºC.

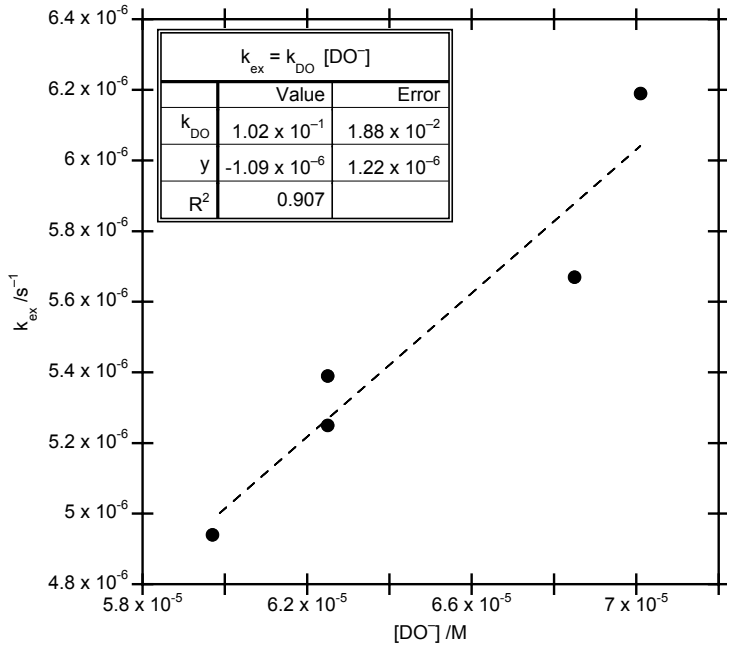

Figure 2.19: Plot of the dependence of k_{ex} upon [CO_3^{2-}] for the deuterium exchange of the prolyl α-proton H_D in c(D-Ala-L-Pro) (5.0 mM) monitored via H_1 methyl protons on c(D-Ala-D-Pro) in $KDCO_3$ (70 % free base, 0.07 – 0.37 M, p*D* = 10.85 – 10.98) buffered D_2O solution, *I* = 1.0 (KCl) and 25 ºC.

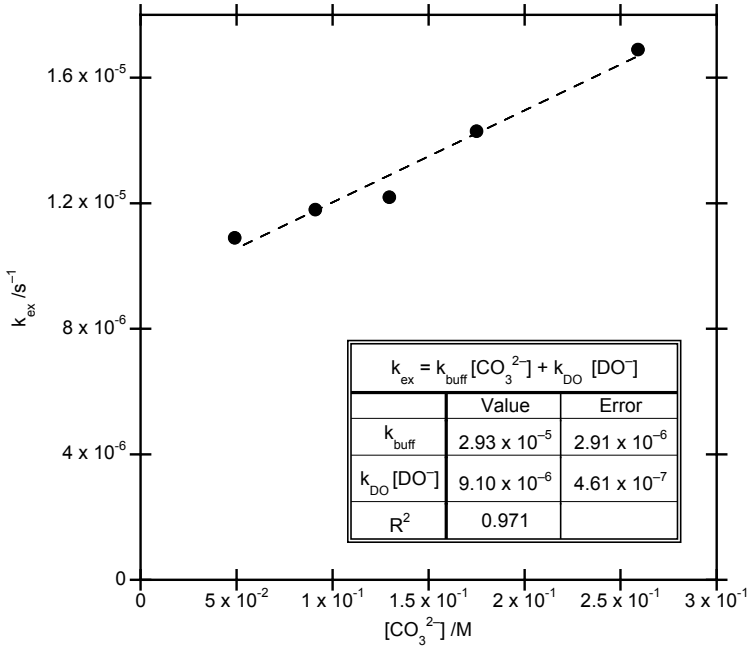

Figure 2.20: Plot of the dependence of k_{ex} upon [DO^-] for the deuterium exchange of the prolyl α-proton H_D in c(D-Ala-L-Pro) (5.0 mM) monitored via H_1 methyl protons on c(D-Ala-D-Pro) in $KDCO_3$ (70 % free base, 0.07 – 0.37 M, pD = 10.85 – 10.98) buffered D_2O solution, I = 1.0 (KCl) and 25 ºC.

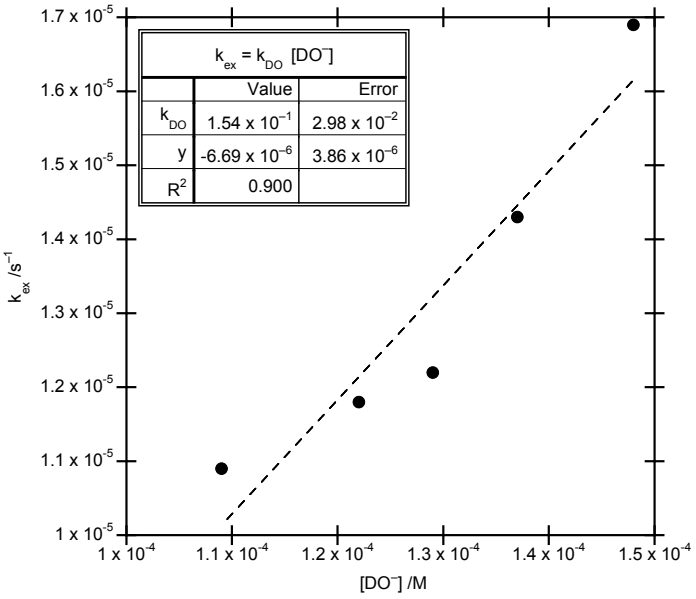

Figure 2.21: Plot of the dependence of k_{ex} upon [CO_3^{2-}] for the deuterium exchange of the prolyl α-proton H_D in c(D-Ala-L-Pro) (5.0 mM) monitored via H_1 methyl protons on c(D-Ala-D-Pro) in $KDCO_3$ (20 % free base, 0.07 – 0.37 M, pD = 10.59 – 10.66) buffered D_2O solution, I = 1.0 (KCl) and 25 ºC.

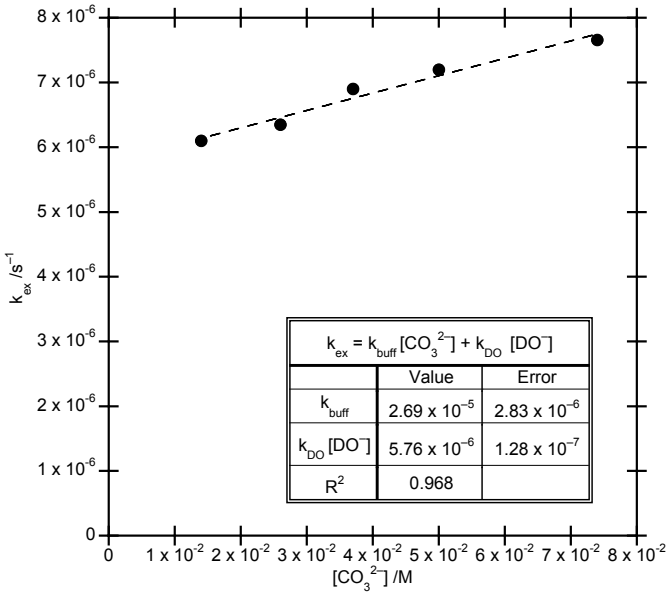

Figure 2.22: Plot of the dependence of k_{ex} upon [DO^-] for the deuterium exchange of the prolyl α-proton H_D in c(D-Ala-L-Pro) (5.0 mM) monitored via H_1 methyl protons on c(D-Ala-D-Pro) in $KDCO_3$ (20 % free base, 0.07 – 0.37 M, pD = 10.59 – 10.66) buffered D_2O solution, I = 1.0 (KCl) and 25 ºC.

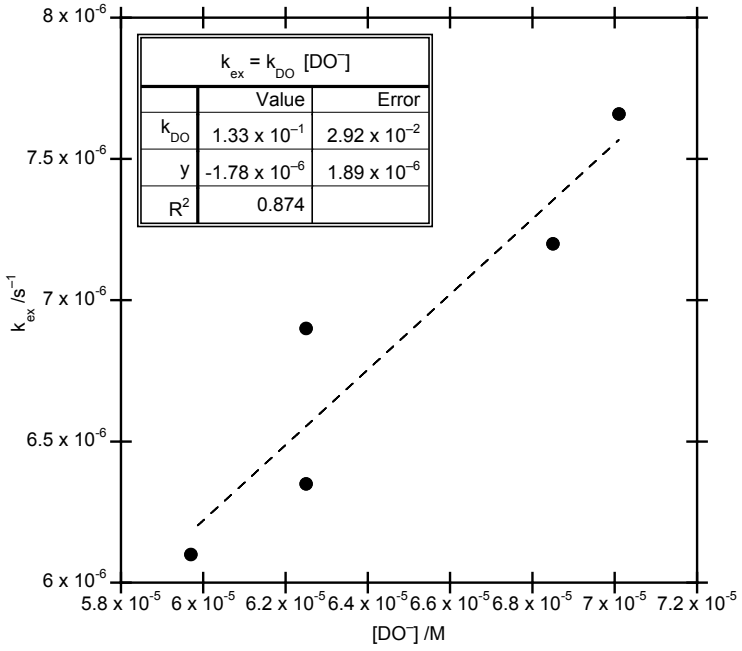

2.2.6.2 c(D-Ala-L-Pro) Alanyl α-proton

The second order rate constant for the deuteroxide catalysed exchange, k_{DO}, for the alanyl α-proton of c(D-Ala-L-Pro) H_B may also be estimated from the deuterium exchange reaction data. This cannot be done by only monitoring the decrease in the integration from H_B as the interconversion to the c(D-Ala-D-Pro) diastereomer (via deprotonation of the prolyl α-proton in c(D-Ala-L-Pro) and subsequent reprotonation upon the opposite face) also decreases the magnitude of the H_B peak. By summating the integral areas for the multiplets of both H_B (3.96 ppm, Figure 2.12) on c(D-Ala-L-Pro) and H_2 (4.21 ppm, Figure 2.12) on c(D-Ala-D-Pro) and assuming that $k_{DO}(H_B) \sim k_{DO}(H_2)$ an estimate for k_{DO} may be found for the alanyl α-proton in c(D-Ala-L-Pro).
The reaction data and k_{ex} values are shown in Appendix I.3.3: Table I.10. Figure 2.23 shows the dependence of k_{ex} upon the concentration of deuteroxide and the fit of these data gives $k_{DO} = 5.51 \times 10^{-3}$ M^{-1} s^{-1}.

Figure 2.23: Plot of the dependence of k_{ex} upon [DO^-] for the deuterium exchange of the alanyl α-proton H_B in c(D-Ala-L-Pro) (5.0 mM) in $KDCO_3$ (0.185 M, p*D* = 10.12 – 10.98) buffered D_2O solution, *I* = 1.0 (KCl) and 25 ºC.

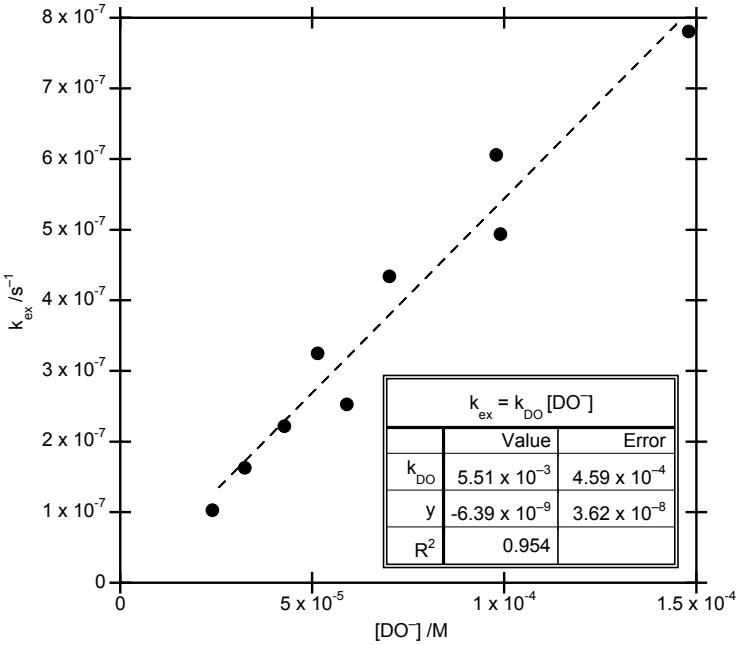

2.2.7 Carbon acidity of c(L-Pro-L-Tyr)

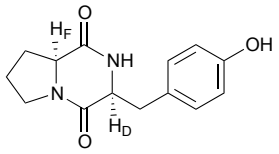

Pseudo first order rate constants for the deuteroxide catalysed exchange, k_{ex}, of the prolyl α-proton H_F and tyrosyl α-proton H_D of c(L-Pro-L-Tyr) were determined in $KDCO_3$ buffered D_2O solutions (p*D* = 10.30 – 10.94) using ^1H NMR spectroscopy (400 MHz).

2.2.7.1 c(L-Pro-L-Tyr) Prolyl α-proton

A representative set of spectra taken at three time points during the reaction at p*D* = 10.57 is shown in Figure 2.24. Deuterium exchange at the H_D position on c(L-Pro-L-Tyr) resulted in disappearance of the doublet of doublets due to H_D at 4.30 ppm over the course of the reaction. The level of exchange was monitored relative to a tetramethylammonium deuteriosulfate internal standard, whose methyl protons (singlet,

3.14 ppm) are non-exchangeable. The products of deuterium exchange at H_D position on c(L-Pro-L-Tyr) are deuterated c(L-Pro-L-Tyr) and c(D-Pro-L-Tyr) (Scheme 2.43). Over the course of the reaction the equilibrium distribution of the diastereomers c(L-Pro-L-Tyr) and c(D-Pro-L-Tyr) is approached. Consequently, ^{1}H NMR spectra over the course of the reaction showed the disappearance of the doublet of doublets corresponding to the tyrosyl methylene group (H_C and $H_{C'}$) and the multiplet prolyl pyrrolidine ring protons (H_G, $H_{G'}$, H_I, $H_{I'}$ H_J and $H_{J'}$) on c(L-Pro-L-Tyr) and the appearance of the doublet of doublets for the analogous methylene (H_3 and $H_{3'}$) and the multiplets for the analogous pyrrolidine ring protons (H_7, $H_{7'}$, H_8, $H_{8'}$ H_9 and $H_{9'}$) on c(D-Pro-L-Tyr) (Figure 2.24).

Figure 2.24: Representative ^{1}H NMR spectra at 400 MHz for the deuterium exchange reaction of c(L-Pro-L-Tyr) (5.0 mM) in $KDCO_3$ (p*D* = 10.57, 50% free base, 0.185 M), 25 °C and ionic strength *I* = 1.0 M (KCl).

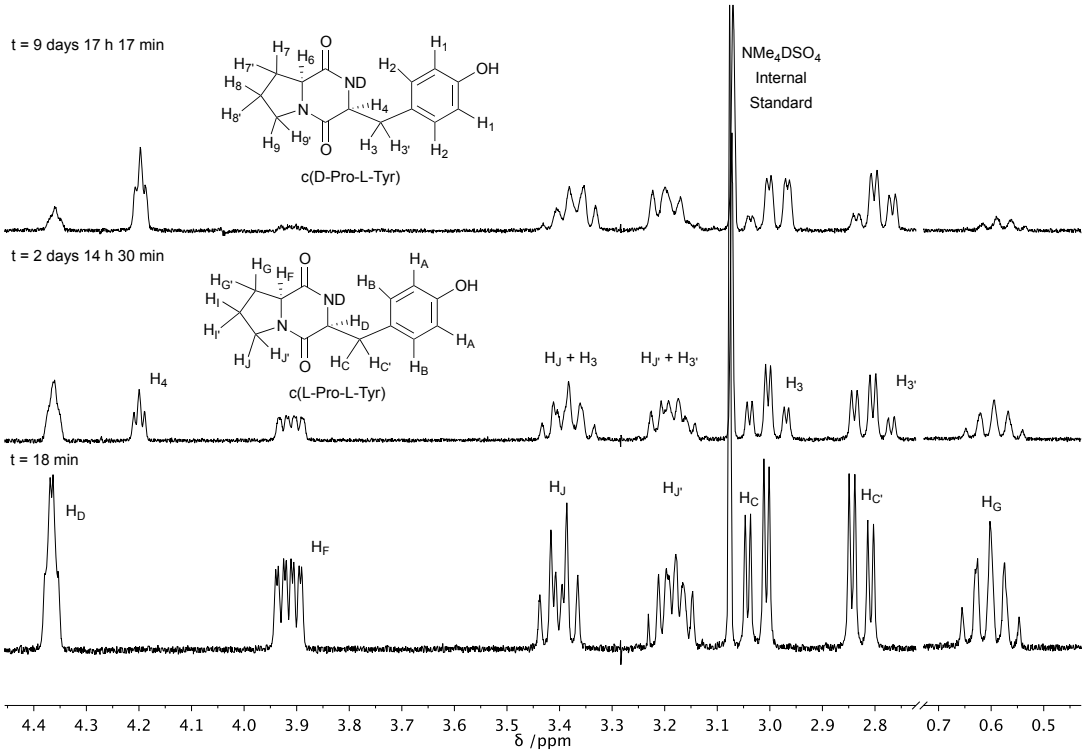

Scheme 2.43: Outcomes of the deuterium exchange reactions of c(L-Pro-L-Tyr).

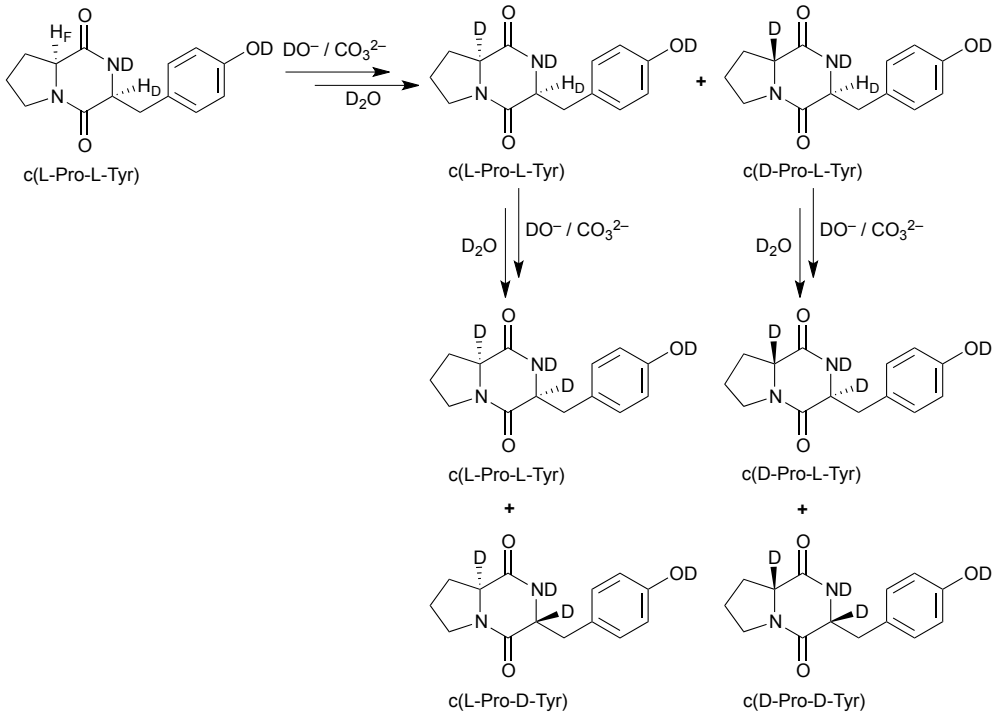

The phenol group on the amino acid tyrosine has a pK_a = 10.07 which is within 2 pK_a units of the pD range (pD = 10.30 – 10.94) used in the exchange experiments. Thus, both neutral and anionic c(L-Pro-L-Tyr) are present in solution. A negative charge on the DKP molecule would reduce the kinetic acidity of the α-protons, particularly the tyrosyl α-proton. We were interested in obtaining the kinetic acidity of the α-protons solely from neutral c(L-Pro-L-Tyr). The concentration of neutral c(L-Pro-L-Tyr) decreases as the pD of the solution is increased and therefore first order observed rate constant for exchange, k_{ex}, will not be directly comparable. To correct for this phenolic acid dissociation, the k_{ex} values must be divided by the fraction of neutral c(L-Pro-L-Tyr) present in solution, f_{OH}, to give the corrected first order observed rate constant for exchange, k_{ex}' (Equation 2.6).

$$k'_{ex} = \frac{k_{ex}}{f_{OH}} \qquad \text{(Equation 2.6)}$$

The fraction of neutral c(L-Pro-L-Tyr) present in solution can be found from the pK_a of the tyrosyl phenol group in c(L-Pro-L-Tyr). A UV-Visible spectrophotometric experiment was performed to determine the pK_a of the tyrosyl phenol group. The changes in absorption from the anionic phenol group (λ_{max} = 293 nm) over the pD range

p*D* = 4.89 – 14.01 were measured (Figure 2.25). In order to solubilise c(L-Pro-L-Tyr) a 9 : 1 D_2O : d_3-MeCN solution was required.

Figure 2.25: Plot of the dependence of absorption from phenol group in c(L-Pro-L-Tyr) (0.8 mM)[xii] upon the p*D* of solution (p*D* = 4.89 – 14.01) with λ_{max} = 293 nm in a 9 : 1 D_2O : d_3-MeCN solution, I = 1.0 M, at 25 °C.

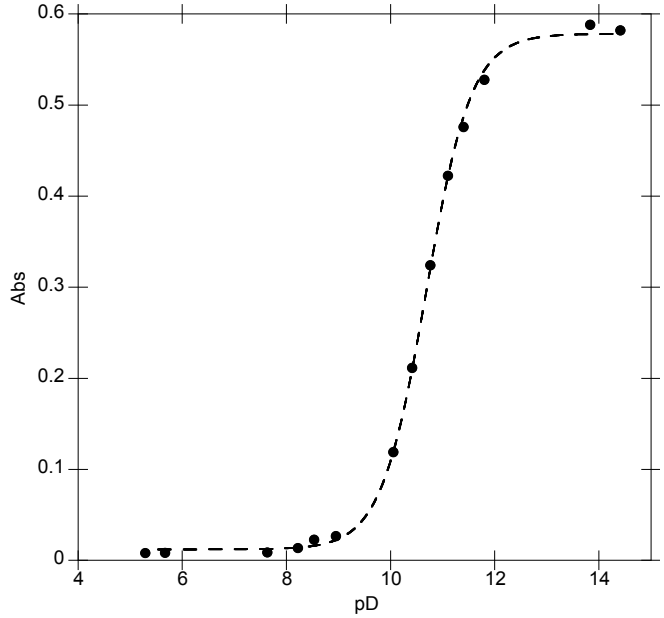

$A_{obs} = (K_a * A_{max} + A_{min} * 10^{-pD}) / (10^{-pD} + K_a)$

	Value	Error
K_a	2.07×10^{-11}	7.29×10^{-13}
A_{max}	5.78×10^{-1}	3.88×10^{-3}
A_{min}	1.23×10^{-2}	2.70×10^{-3}
R^2	0.999	

The data in Figure 2.25 was fitted to Equation 2.7 to determine the pK_a, where A_{max} is the absorbance when all tyrosyl phenol group in c(L-Pro-L-Tyr) is fully deprotonated and A_{min} is the absorbance when all tyrosyl phenol group in c(L-Pro-L-Tyr) is fully protonated. The fit gives a pK_a = 10.68 for the tyrosyl phenol group in c(L-Pro-L-Tyr).

[xii] This c(L-Pro-L-Tyr) concentration of 0.8 mM is lower than that used in the deuterium exchange experiments. The d_3-MeCN co-solvent was required in order to prepare a 20.0 mM c(L-Pro-L-Tyr) stock solution. It was also necessary to prepare the buffer solutions with 9 : 1 D_2O : d_3-MeCN in order to able to remove contribution that d_3-MeCN makes to the absorbance in the spectrum.

$$A_{\text{obs}} = \frac{K_{\text{a}}\, A_{\text{max}} + A_{\text{min}}\, 10^{-\text{p}D}}{10^{-\text{p}D} + K_{\text{a}}} \qquad \text{(Equation 2.7)}$$

This pK_a is for 9 : 1 D_2O : d_3-MeCN solution but the pK_a in a 100 % D_2O is expected to be very similar. Acid dissociation constants are typically not substantially affected by the addition of a co-solvent until the composition of the co-solvent increases above 40 % v/v. In all subsequent Figures in this section the corrected first order observed rate constant for exchange, k_{ex}', are plotted rather than k_{ex}.

In order to determine the second order rate constant for deuteroxide catalysed exchange, k_{DO}, for the prolyl α-proton of c(L-Pro-L-Tyr) H_F the hydrogen deuterium exchange reactions were performed in $KDCO_3$ buffers over the pD range 10.30 – 10.94. The corrected first order rate constant for exchange, k_{ex}', was determined by monitoring exchange of the prolyl proton H_F on c(L-Pro-L-Tyr). Figure 2.26 shows the dependence of k_{ex}' on the concentration of deuteroxide for H_F (Appendix I.4.1: Table I.11). The fit of the data gives a value of $k_{DO} = 1.19 \times 10^{-1}$ M^{-1} s^{-1} for H_F.

Figure 2.26: Plot of the dependence of k_{ex}' upon [DO^-] for the deuterium exchange of the prolyl α-proton H_F in c(L-Pro-L-Tyr) (5.0 mM) in $KDCO_3$ (0.185 M, pD = 10.30 – 10.81) buffered D_2O solution, I = 1.0 (KCl) and 25 ºC.

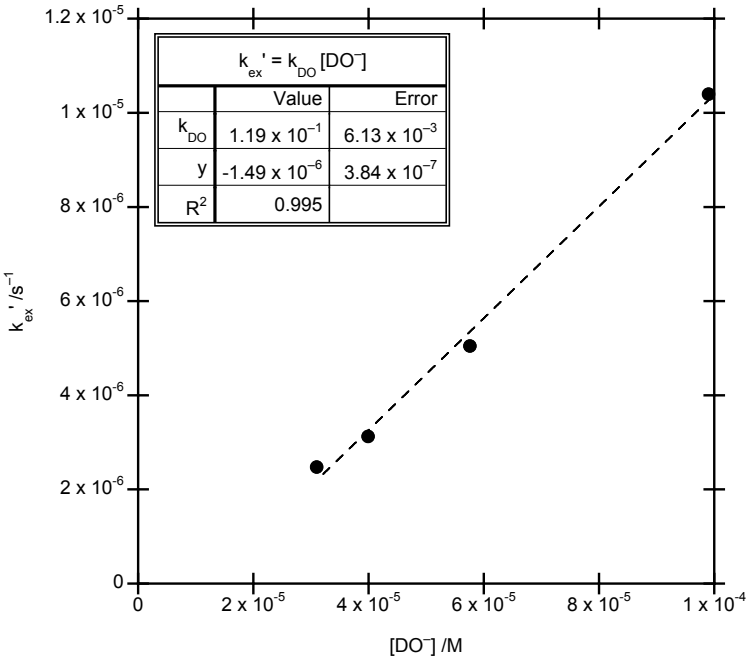

As for other DKP substrates, H / D exchange reactions were also undertaken in a series of solutions with an identical buffer ratio and a varying total concentration of buffer, [$KDCO_3$]. The H / D exchange reactions were performed at both 70 % free base and 20 % free base $KDCO_3$ over the [$KDCO_3$] range 0.12 – 0.37 M (experimentally, the p*D* varied by 0.09 – 0.11). Figures 2.27 and 2.28 show the dependence of k_{ex}' on the [CO_3^{2-}] (Appendix I.4.2: Table I.12 – I.13) while Figure 2.29 and Figure 2.30 show the dependence of k_{ex}' on the [DO^-]. In the former Figures the fit of the data would give $k_{buff} = 1.79 \times 10^{-5} – 4.51 \times 10^{-5}$ M^{-1} s^{-1}. However, the fit of the data in the latter Figures gives $k_{DO} = 1.65 \times 10^{-1} – 2.20 \times 10^{-1}$ M^{-1} s^{-1} which are in reasonable agreement with the $k_{DO} = 1.19 \times 10^{-1}$ M^{-1} s^{-1} determined in Figure 2.26 above. Thus, like in the other DKP substrates, the changes in k_{ex} observed in the above experiments are most likely due changes in [DO^-] rather than buffer concentration.

Figure 2.27: Plot of the dependence of k_{ex} upon [CO_3^{2-}] for the deuterium exchange of the prolyl α-proton H_F in c(L-Pro-L-Tyr) (5.0 mM) in $KDCO_3$ (70 % free base, 0.13 – 0.37 M, p*D* = 10.83 – 10.94) buffered D_2O solution, *I* = 1.0 (KCl) and 25 ºC.

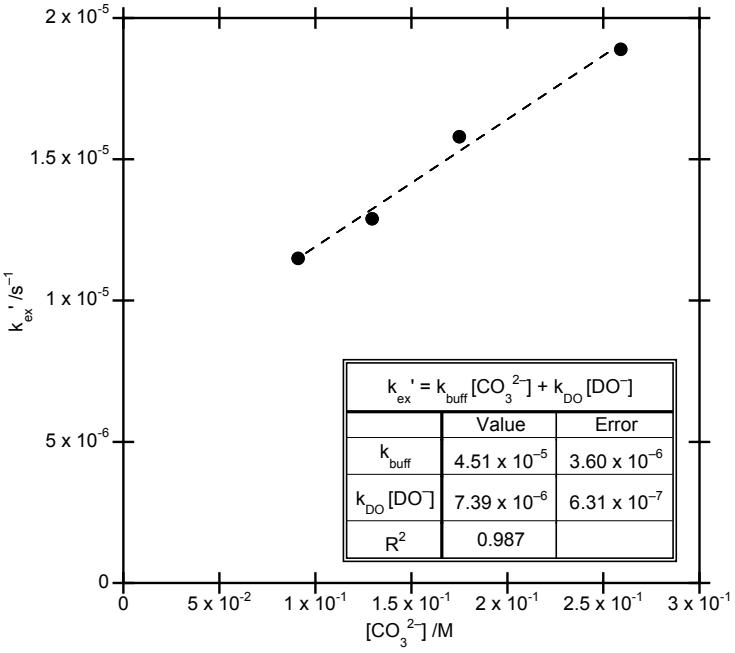

Figure 2.28: Plot of the dependence of k_{ex} upon $[CO_3^{2-}]$ for the deuterium exchange of the prolyl α-proton H_F in c(L-Pro-L-Tyr) (5.0 mM) in $KDCO_3$ (20 % free base, 0.12 – 0.37 M, pD = 10.19 – 10.28) buffered D_2O solution, I = 1.0 (KCl) and 25 ºC.

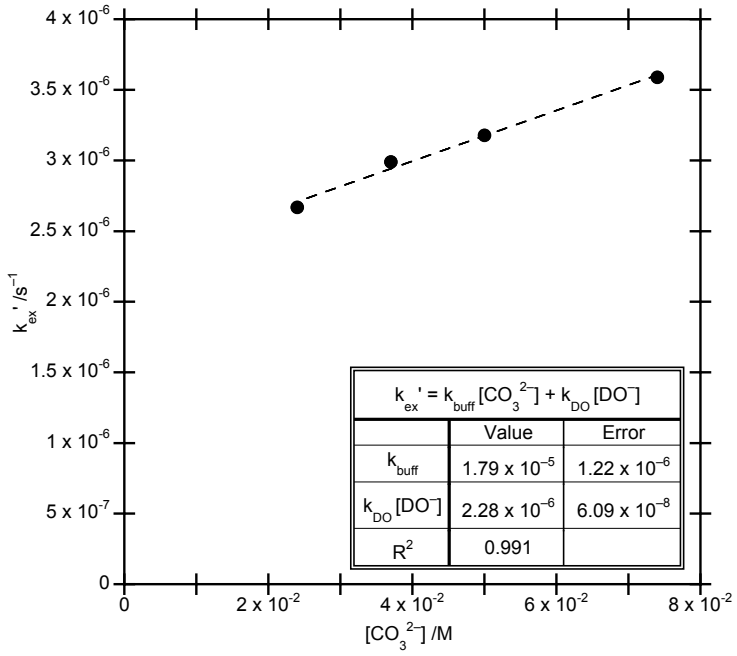

Figure 2.29: Plot of the dependence of k_{ex} upon $[DO^-]$ for the deuterium exchange of the prolyl α-proton H_F in c(L-Pro-L-Tyr) (5.0 mM) in $KDCO_3$ (70% free base, 0.13 – 0.37 M, pD = 10.83 – 10.94) buffered D_2O solution, I = 1.0 (KCl) and 25 ºC.

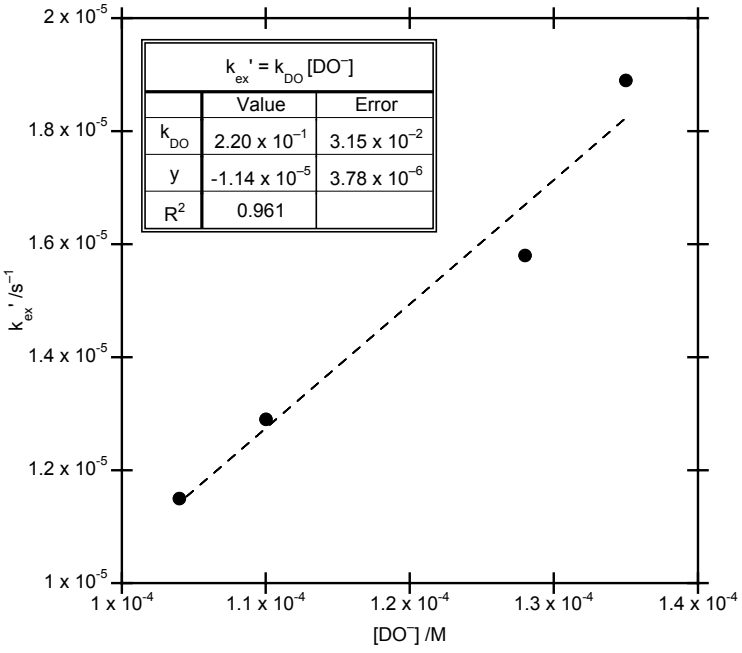

Figure 2.30: Plot of the dependence of k_{ex} upon [DO^-] for the deuterium exchange of the prolyl α-proton H_F in c(L-Pro-L-Tyr) (5.0 mM) in $KDCO_3$ (20% free base, 0.12 – 0.37 M, p*D* = 10.19 – 10.28) buffered D_2O solution, I = 1.0 (KCl) and 25 ºC.

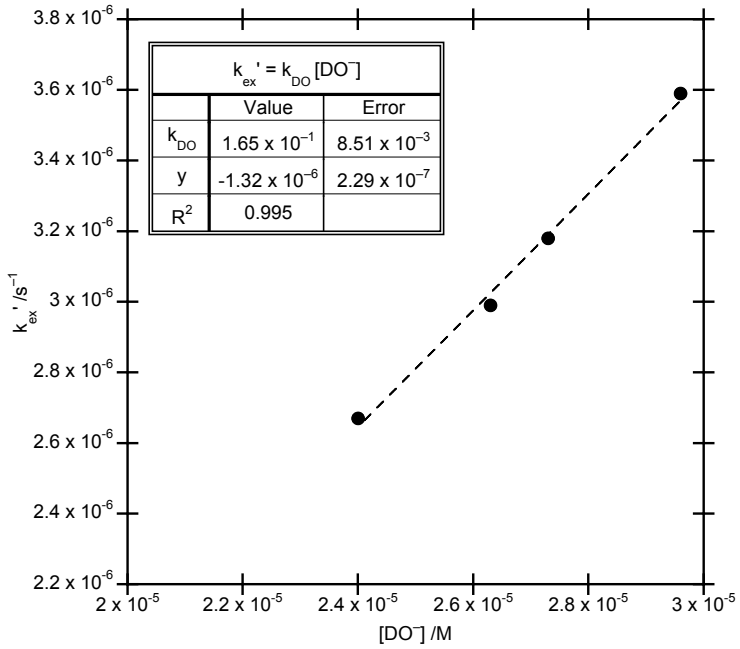

2.2.7.2 c(L-Pro-L-Tyr) Tyrosyl α-proton

In order to determine the second order rate constant for deuteroxide catalysed exchange, k_{DO}, for the tyrosyl α-proton of c(L-Pro-L-Tyr) H_D the hydrogen deuterium exchange reactions were performed in $KDCO_3$ buffers over the p*D* range 10.23 – 10.85. The corrected first order observed rate constant for exchange, k_{ex}', was determined by monitoring exchange of the summated integral area from prolyl proton H_D on c(L-Pro-L-Tyr) and H_4 on c(D-Pro-L-Tyr) (Appendix I.4.3: Table 1.14). This approach assumes that k_{ex}' values for H_D on c(L-Pro-L-Tyr) and H_4 on c(D-Pro-L-Tyr) are equivalent. Figure 2.31 shows the dependence of k_{ex}' on the concentration of deuteroxide for H_D and the fit of the reaction data to Equation 2.4 gives $k_{DO} = 2.09 \times 10^{-3}$ M^{-1} s^{-1}.

Figure 2.31: Plot of the dependence of k_{ex}' upon [DO^-] for the deuterium exchange of the prolyl α-protons H_D in c(L-Pro-L-Tyr) and H_4 in c(D-Pro-L-Tyr) (5.0 mM) in $KDCO_3$ (0.185 M, p*D* = 10.23 – 10.85) buffered D_2O solution, at I = 1.0 (KCl) and 25 ºC.

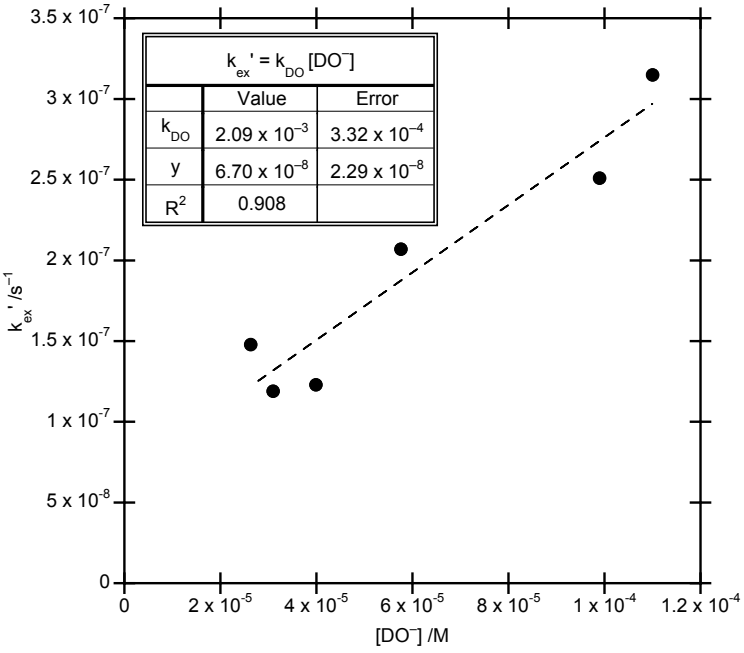

2.2.8 Carbon acidity of c(Gly-L-Pro)

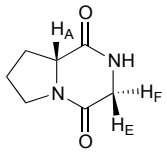

Pseudo first order rate constants for the deuteroxide catalysed exchange, k_{ex}, of the prolyl α-proton H_A and glycyl α-protons H_E and H_F of c(Gly-L-Pro) were determined in $KDCO_3$ buffered D_2O solutions (p*D* = 10.39 – 10.83) using ^1H NMR spectroscopy (400 MHz).

2.2.8.1 c(Gly-L-Pro) Prolyl α-proton

A representative set of spectra taken at three time points during the reaction at p*D* = 10.12 is shown in Figure 2.32. Deuterium exchange at the H_A position on c(Gly-L-Pro) resulted in disappearance of the doublet of doublets due to H_A at 4.25 ppm over the course of the reaction. The level of exchange was monitored relative to a

tetramethylammonium deuteriosulfate internal standard, whose methyl protons (singlet, 3.14 ppm) are non-exchangeable. The products of deuterium exchange at H_A position on c(Gly-L-Pro) are deuterated c(Gly-L-Pro) and deuterated c(Gly-D-Pro), which are enantiomers and therefore have equivalent chemical shift (Scheme 2.44). It is expected that the equilibrium concentration of each enantiomer will be identical. No changes in the integrated areas from the pyrrolidine ring protons (H_B, $H_{B'}$, H_C, $H_{C'}$, H_D and $H_{D'}$) on c(Gly-L-Pro) and no hydrolysis were observed.

Figure 2.32: Representative ^{1}H NMR spectra at 400 MHz for the deuterium exchange reaction of c(Gly-L-Pro) (5.0 mM) in $KDCO_3$ (50% free base, 0.185 M, p*D* = 10.12) at 25 °C and ionic strength *I* = 1.0 M (KCl).

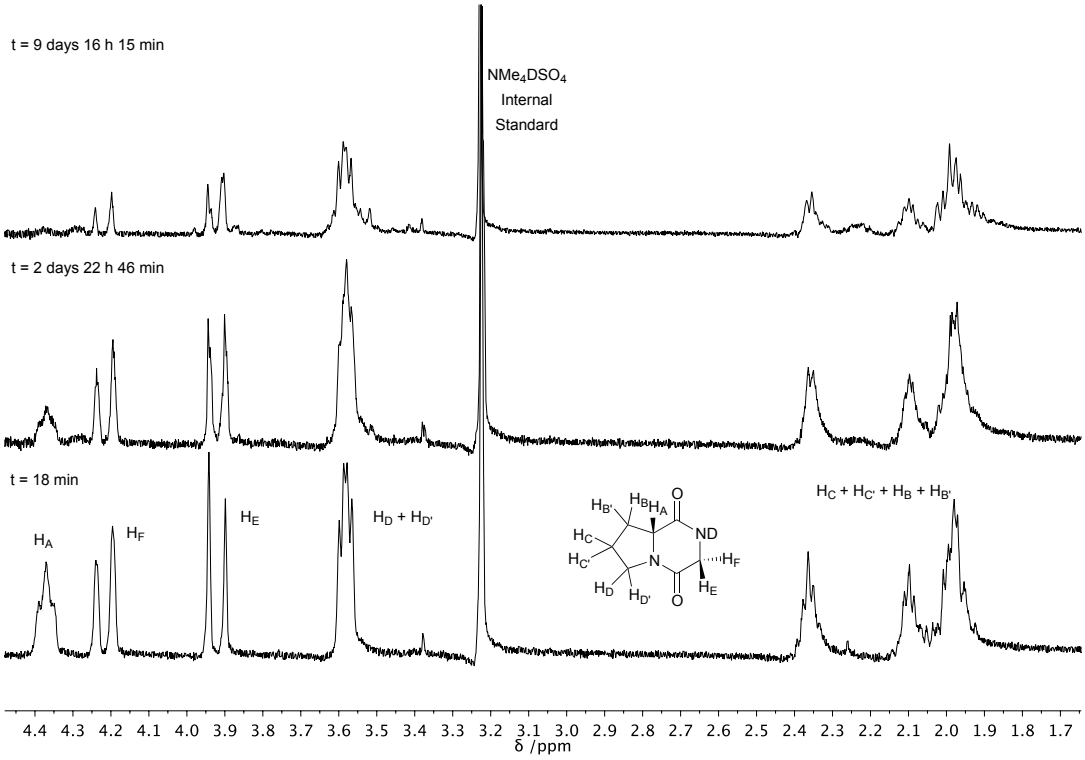

Scheme 2.44: Outcomes of the deuterium exchange reactions of c(Gly-L-Pro).

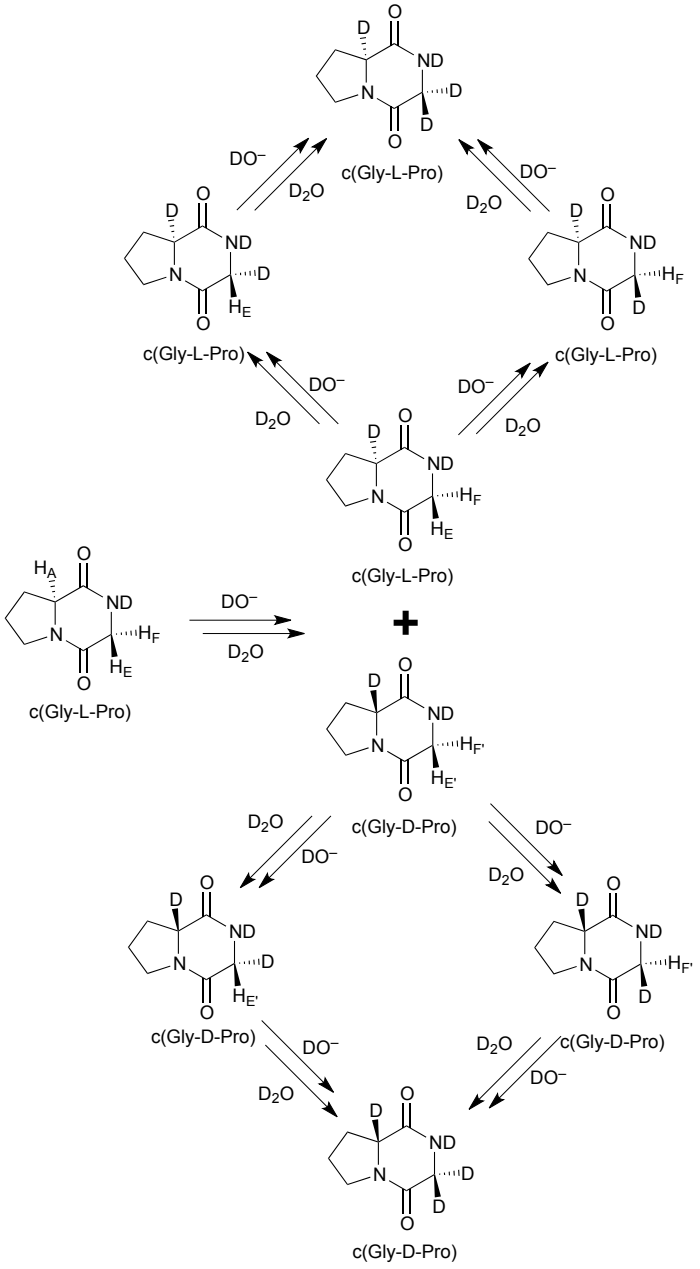

Experimentally observed first order rate constants for deuteroxide catalysed deuterium exchange, k_{ex}, of the prolyl α-proton H_A of c(Gly-L-Pro) were determined from the fit of the fraction of protonated substrate remaining, $f(s)$, for H_A c(Gly-L-Pro) to Equation 2.2. Reaction data and k_{ex} values for H_A over the pD range pD = 9.99 – 10.43 are shown in Appendix I.5.2: Table I.15.

Figure 2.33 shows the dependence of k_{ex} on the concentration of deuteroxide for H_A. The fit of the reaction data to Equation 2.4 gives a value of $k_{DO} = 1.87 \times 10^{-1}$ M^{-1} s^{-1} for H_A. The fit of the data in Figure 2.33 crosses close to the origin and the lack of

upward curvature at higher concentrations of deuteroxide indicate that insignificant buffer catalysis is present for exchange of H_A.

Figure 2.33: Plot of the dependence of k_{ex} upon [DO^-] for the deuterium exchange of the prolyl α-proton H_A in c(Gly-L-Pro) (5.0 mM) in $KDCO_3$ (0.185 M, pD = 10.39 – 10.83) buffered D_2O solution, I = 1.0 (KCl) and 25 ºC.

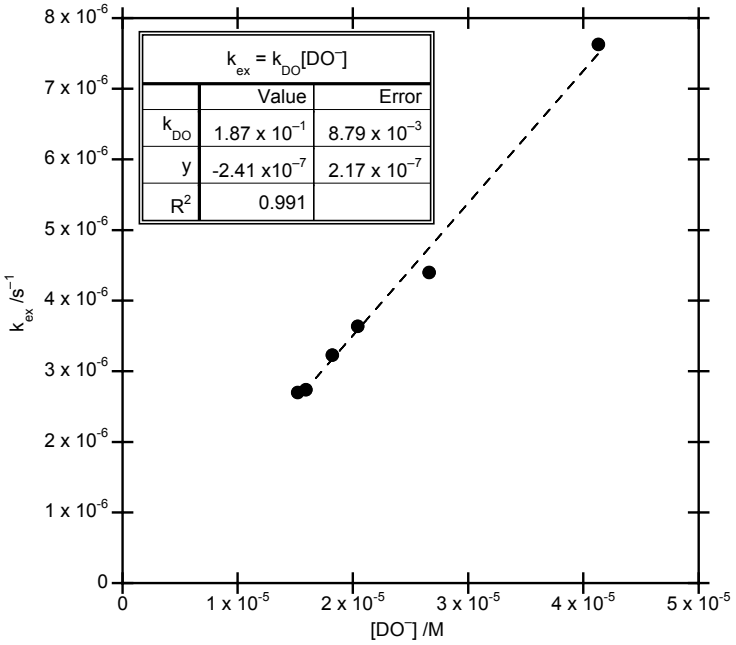

2.2.8.2 c(Gly-L-Pro) Glycyl α-protons

Deuterium exchange at the H_E and H_F position on c(Gly-L-Pro) resulted in disappearance of the doublets at 3.77 ppm and 4.06 ppm, respectively, over the course of the reaction (Figure 2.32). The signals are also due to the $H_{E'}$ and $H_{F'}$ protons on c(Gly-D-Pro) [xiii]. As c(Gly-L-Pro) and c(Gly-D-Pro) are enantiomers, deuterium exchange at the H_E and $H_{E'}$, and, H_F and $H_{F'}$ protons should be equivalent. The level of exchange was monitored relative to a tetramethylammonium deuteriosulfate internal standard, whose methyl protons (singlet, 3.14 ppm) are non-exchangeable. The products of deuterium exchange at H_E and H_F positions on c(Gly-L-Pro) are deuterated c(Gly-L-Pro) (Scheme 2.44, top half) and deuterated c(Gly-D-Pro) (Scheme 2.44, bottom half), which are enantiomers possessing equivalent ^{1}H NMR chemical shift.

[xiii] c(Gly-D-Pro) in solution arises from interconversion of c(Gly-L-Pro) to c(Gly-D-Pro), via exchange at the prolyl α-proton H_A.

Experimentally observed first order rate constants for deuteroxide catalysed deuterium exchange, k_{ex}, of glycyl α-proton H_E and H_F of c(Gly-L-Pro) were determined from the fit of the fraction of protonated substrate remaining, f(s), for H_E c(Gly-L-Pro) to Equation 2.2. Reaction data and k_{ex} values for H_E over the pD range pD = 9.99 – 10.43 are shown in Appendix I.5.3: Table I.16 and Table I.17. Figure 2.34 and 2.35 shows the dependence of k_{ex} on the concentration of deuteroxide for H_E and H_F. The fit of the reaction data to Equation 2.4 gives values of $k_{DO} = 2.09 \times 10^{-2}$ M^{-1} s^{-1} for H_E and $k_{DO} = 6.59 \times 10^{-2}$ M^{-1} s^{-1} for H_F.

Figure 2.34: Plot of the dependence of k_{ex} upon [DO^-] for the deuterium exchange of the glycyl α-proton H_E in c(Gly-L-Pro) (5.0 mM) in $KDCO_3$ (0.185 M, pD = 10.39 – 10.83) buffered D_2O solution, I = 1.0 (KCl) and 25 ºC.

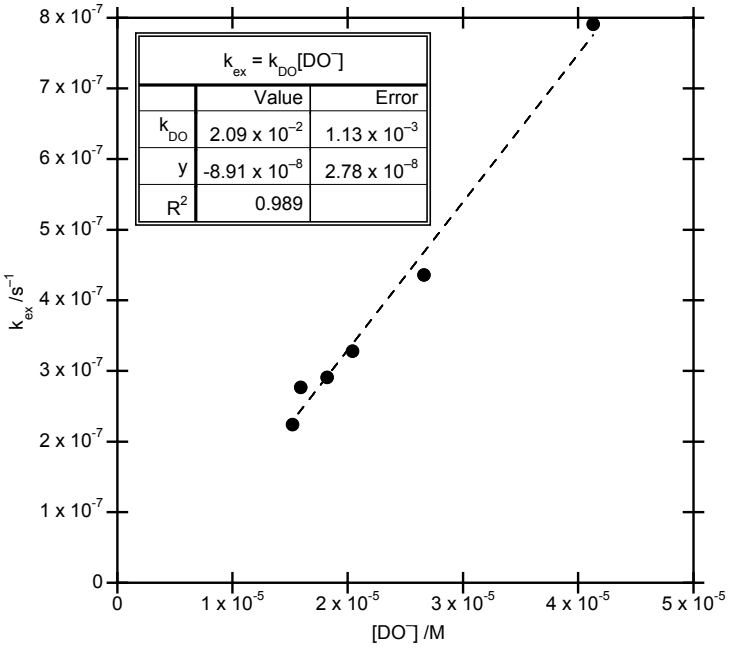

Figure 2.35: Plot of the dependence of k_{ex} upon [DO^-] for the deuterium exchange of the glycyl α-proton H_F in c(Gly-L-Pro) (5.0 mM) in $KDCO_3$ (0.185 M, pD = 10.39 – 10.83) buffered D_2O solution, I = 1.0 (KCl) and 25 ºC.

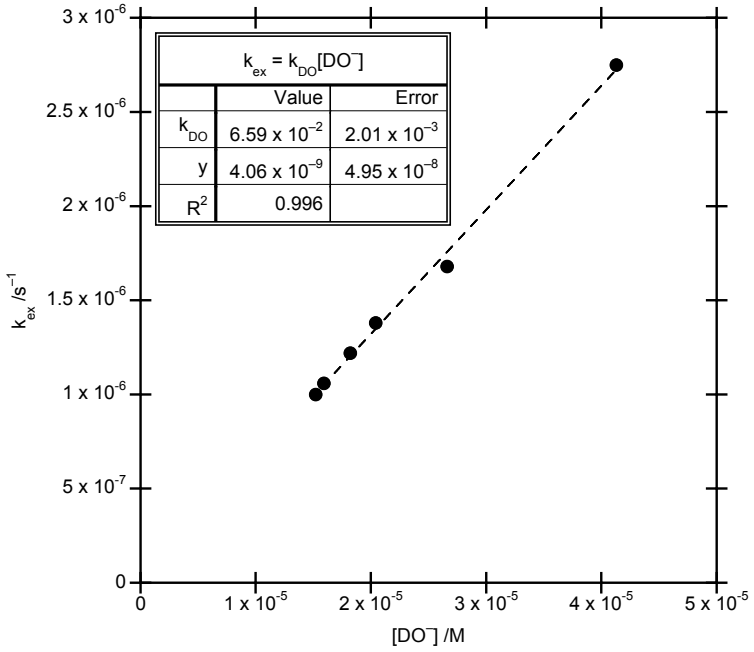

2.2.9 Carbon acidity of c(Gly-Gly)

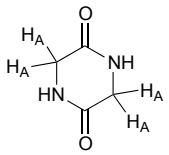

Pseudo first order rate constants for the deuteroxide catalysed exchange, k_{ex}, of the glycyl α-proton H_A of c(Gly-Gly) were determined in 3-chloroquinuclidine buffered D_2O solutions (pD = 9.35 – 10.82) using ^1H NMR spectroscopy (500 MHz).

A representative set of spectra taken at three time points during the reaction at pD = 10.19 is shown in Figure 2.36. Deuterium exchange at the H_A position on c(Gly-Gly) resulted in disappearance of the H_A singlet at 4.15 ppm over the course of the reaction. The level of exchange was monitored relative to a sodium trimethylsilylpropyl sulfonate internal standard, whose methyl protons (singlet, 0.11 ppm) are non-exchangeable. The product of deuterium exchange at H_A position on c(Gly-Gly) is deuterated c(Gly-Gly) (Scheme 2.45). As deuterium exchange progresses, an additional peak from the H_A protons appears at 4.62 ppm. This upfield peak is a triplet (albeit poorly resolved in Figure 2.36) that appears due to the coupling between the D and H

in the singly exchanged α-CHD product.[113] A small but appreciable amount of the hydrolysis product, dipeptide Gly-Gly, was also observed at 3.89 ppm.

Figure 2.36: Representative ^{1}H NMR spectra at 500 MHz for the deuterium exchange reaction of c(Gly-Gly) (20.0 mM) in 3-chloroquinuclidine (0.15 M, 70% fb, pD = 10.19) at 25 °C and I = 1.0 M (KCl).

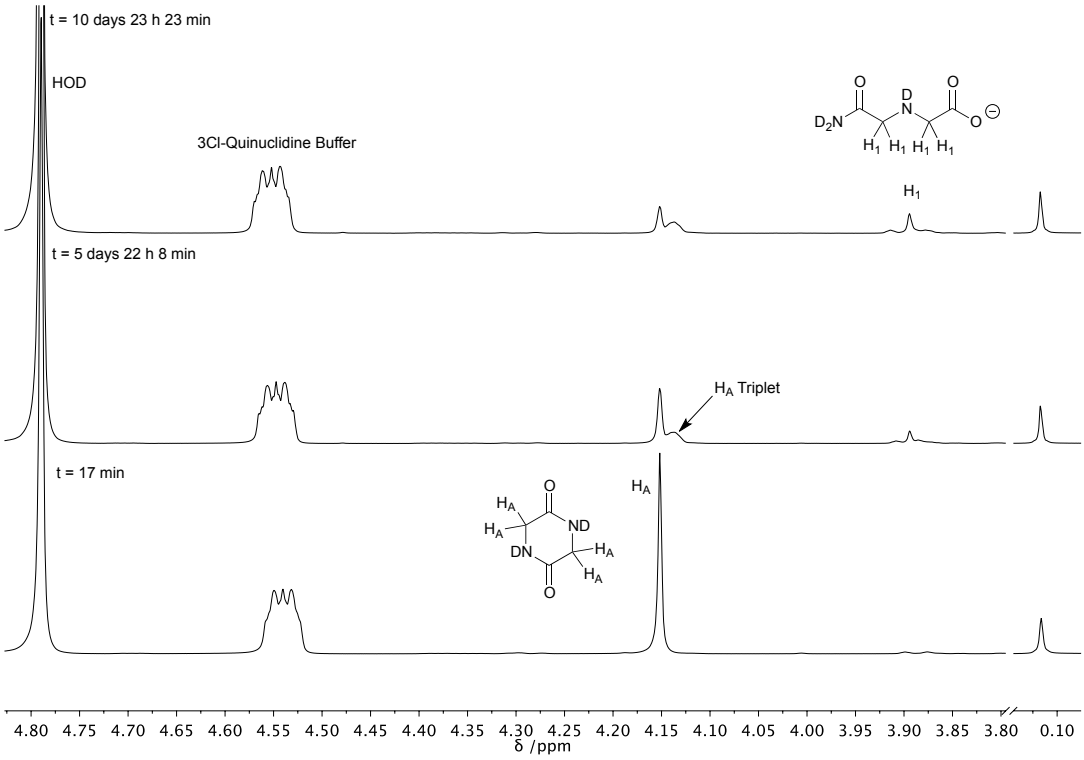

Scheme 2.45: Outcomes of the deuterium exchange reactions of c(Gly-Gly).

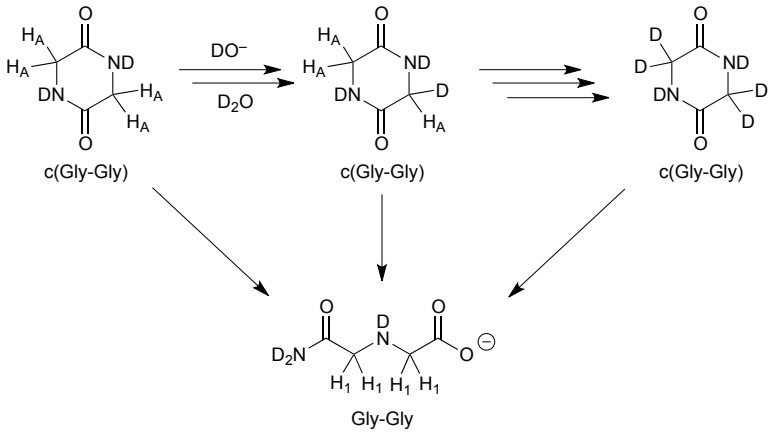

Experimentally observed first order rate constants for deuteroxide catalysed deuterium exchange, k_{ex}, of glycyl α-proton H_A c(Gly-Gly) were determined from the

fit of Equation 2.2 to the fraction of protonated substrate remaining, $f(s)$, for H_A c(Gly-Gly). Reaction data and k_{ex} values for H_A over the pD range pD = 9.35 – 10.82 are shown in Appendix I.6.1: Table I.18. Figure 2.37 shows the dependence of k_{ex} on the concentration of deuteroxide for H_A. The fit of the reaction data to Equation 2.4 to the data gives a value of $k_{DO} = 6.33 \times 10^{-2}$ M^{-1} s^{-1} for H_A.

Figure 2.37: Plot of the dependence of k_{ex} upon [DO^-] for the deuterium exchange of the glycyl α-proton H_A in c(Gly-Gly) (20.0 mM) in 3-chloroquinuclidine (0.15 M, pD = 10.19 – 10.82) at 25 °C and I = 1.0 M (KCl).

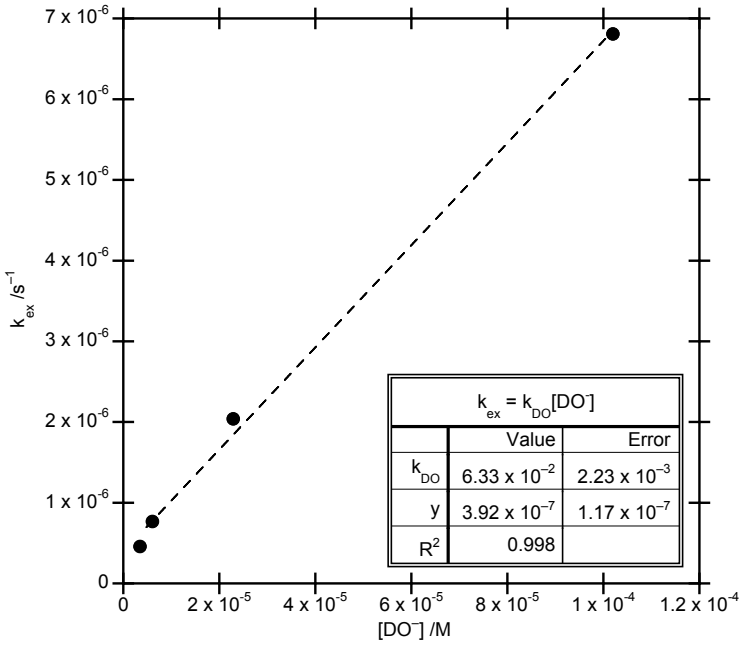

2.2.10 Carbon acidity of c(L-Ala-L-Ala)

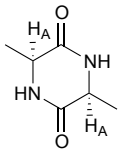

Pseudo first order rate constants for the deuteroxide catalysed exchange, k_{ex}, of the alanyl α-proton H_A of c(L-Ala-L-Ala) were determined in 3-chloroquinuclidine buffered D_2O solutions (pD = 9.35 – 10.81) using ^1H NMR spectroscopy (500 MHz).

A representative set of spectra taken at three time points during the reaction at pD = 10.17 is shown in Figure 2.38. Deuterium exchange at the H_A position on c(L-Ala-L-Ala) resulted in disappearance of the H_A quartet at 4.27 ppm over the course of

the reaction. The level of exchange was monitored relative to a trimethylsilylpropyl sulfonate internal standard, whose methyl protons (singlet, 0.11 ppm) are non-exchangeable. The products of deuterium exchange at H_A position on c(L-Ala-L-Ala) are deuterated c(L-Ala-L-Ala) and c(D-Ala-L-Ala) (Scheme 2.46). Consequently, ^{1}H NMR spectra over the course of the reaction showed the disappearance of the doublet corresponding to the methyl protons H_B at 1.58 ppm and the appearance of the doublet for the analogous methyl H_2 at 1.56 ppm (Figure 2.38).

Figure 2.38: Representative ^{1}H NMR spectra at 500 MHz for the deuterium exchange reaction of c(L-Ala-L-Ala) (20.0 mM) in 3-chloroquinuclidine (0.15 M, 70% fb, p*D* = 10.17) at 25 °C and *I* = 1.0 M (KCl).

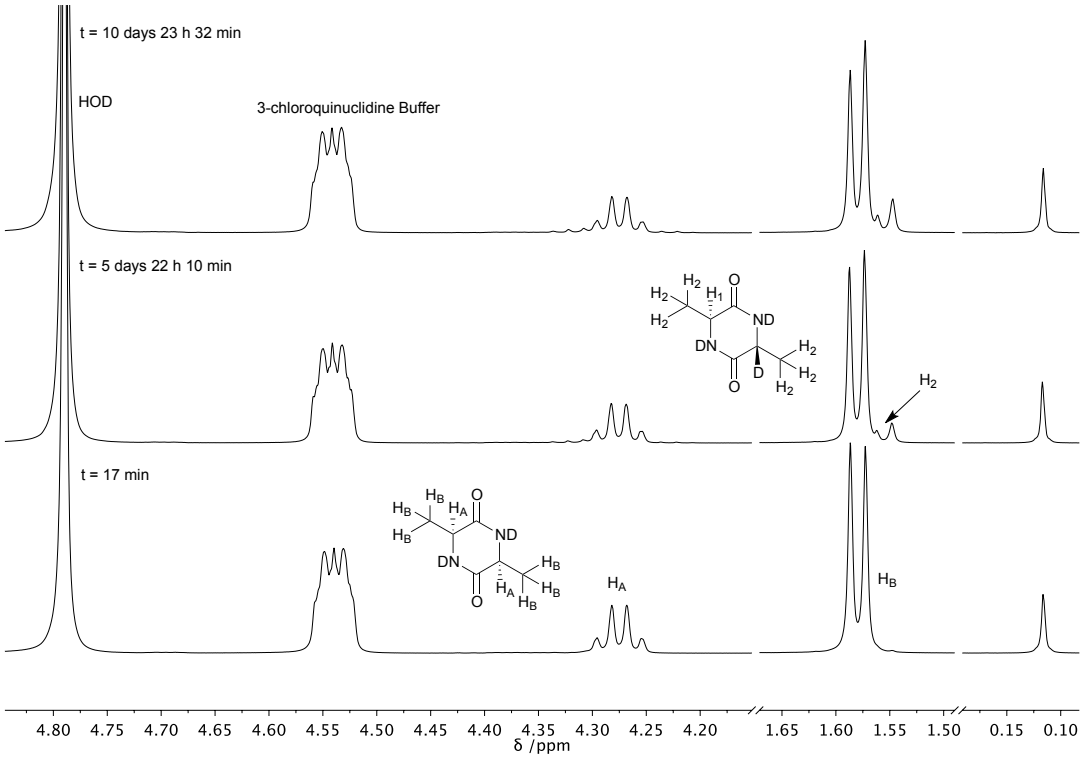

Scheme 2.46: Outcomes of the deuterium exchange reactions of c(L-Ala-L-Ala).

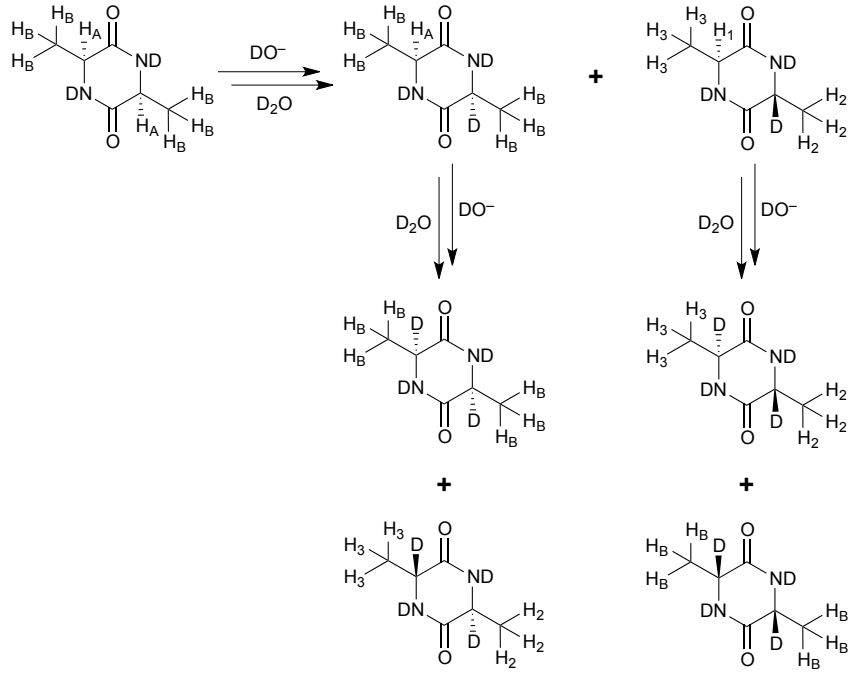

Experimentally observed first order rate constants for deuteroxide catalysed deuterium exchange, k_{ex}, of the alanyl α-proton H_A c(L-Ala-L-Ala) were determined from the fit of the fraction of protonated substrate remaining, f(s), for H_A c(L-Ala-L-Ala) to Equation 2.2. Reaction data and k_{ex} values for H_A over the pD range pD = 9.35 – 10.81 are shown in Appendix I.7.1: Table I.19. Figure 2.39 shows the dependence of k_{ex} on the concentration of deuteroxide for H_A. A value of $k_{DO} = 7.80 \times 10^{-3}$ M^{-1} s^{-1} for H_A was obtained.

Figure 2.39: Plot of the dependence of k_{ex} upon [DO^-] for the deuterium exchange of the alanyl α-proton H_A in c(L-Ala-L-Ala) (20.0 mM) in 3-chloroquinuclidine (0.15 M, pD = 9.35 – 10.81), at 25 °C and I = 1.0 M (KCl).

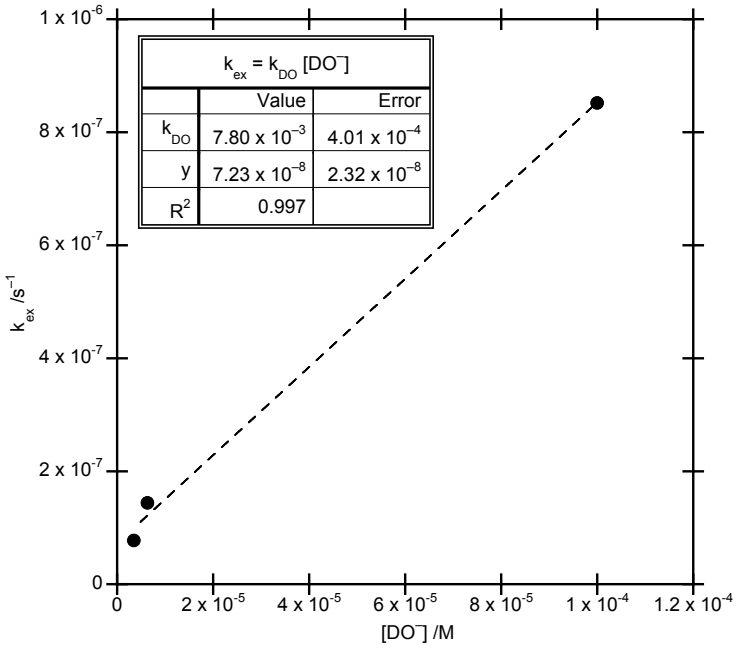

2.3 Discussion

2.3.1 Kinetic acidities of DKPs

A summary of the second order rate constants for deuteroxide-catalysed exchange, k_{DO}, determined as described in Section 2.2, are shown in Table 2.7. In order to make an accurate comparison between the different DKPs the k_{DO} values are statistically corrected to give k_{DO}/p values (Table 2.7), where p is the number of acidic α-protons in a DKP.

Table 2.7: Kinetic acidities, k_{DO} and k_{DO}/p of the DKPs studied at 25 °C and I = 1.0 M (KCl).

Carbon Acid	k_{DO} /M^{-1} s^{-1}	k_{DO}/p [a] /M^{-1} s^{-1}
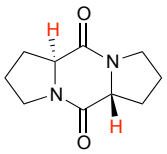 c(D-Pro-L-Pro)	9.69×10^{-2}	4.85×10^{-2}
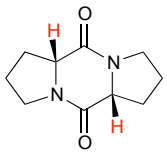 c(D-Pro-D-Pro)	8.62×10^{-3}	4.31×10^{-3}
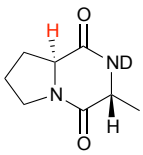 c(D-Ala-**L-Pro**)	9.45×10^{-2}	9.45×10^{-2}
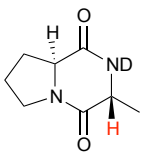 c(**D-Ala**-L-Pro)	5.51×10^{-3}	5.51×10^{-3}
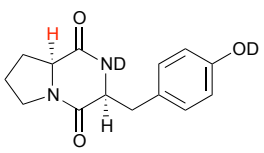 c(**L-Pro**-L-Tyr)	1.19×10^{-1}	1.19×10^{-1}

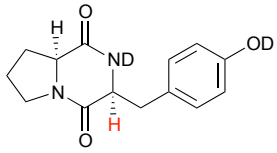 c(L-Pro-**L-Tyr**)	2.09×10^{-3}	2.09×10^{-3}
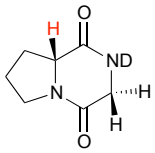 c(Gly-**L-Pro**)	1.87×10^{-1}	1.87×10^{-1}
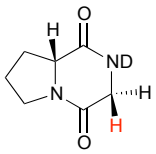 c(**Gly**-L-Pro)	2.09×10^{-2}	2.09×10^{-2}
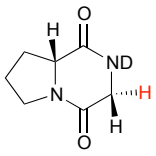 c(**Gly**-L-Pro)	6.59×10^{-2}	6.59×10^{-2}
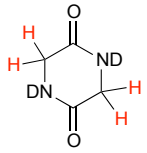 c(Gly-Gly)	6.33×10^{-2}	1.58×10^{-2}
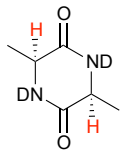 c(L-Ala-L-Ala)	7.80×10^{-3}	3.90×10^{-3}

[a] p = number of acidic protons; used to statistically correct the kinetic acidities.

2.3.1.1 Order of kinetic acidities by residue

For the DKPs studied the order of the k_{DO}/p values in decreasing magnitude is:

c(Gly-**L-Pro**) > c(**L-Pro**-L-Tyr) > c(D-Ala-**L-Pro**) > c(**Gly**-L-Pro) > c(D-Pro-L-Pro) > c(**Gly**-L-Pro) > c(Gly-Gly) > c(**D-Ala**-L-Pro) > c(D-Pro-D-Pro) > c(L-Ala-L-Ala) > c(L-Pro-**L-Tyr**)

The trend in the acidity of the α-proton(s) in the amino acid residues studied is:

Prolyl > Glycyl > Alanyl > Tyrosyl

Table 2.8 shows a comparison of average k_{DO}/p values per amino acid residue.

Table 2.8: The mean k_{DO}/p value for each amino acid residue and a comparison of the relative kinetic acidities of the DKPs at 25 °C and I = 1.0 M (KCl).

	Mean k_{DO}/p [b] /M^{-1} s^{-1}	Relative Kinetic Acidities compared to Tyr	Ala	Gly
Pro	1.12×10^{-1} [a]	110.6	23.9	3.3
Gly	3.42×10^{-2}	33.7	7.3	1.0
Ala	4.71×10^{-3}	4.6	1.0	
Tyr	1.02×10^{-3}	1.0		

[a] The k_{DO} value for c(D-Pro-D-Pro) was excluded in the calculation of the mean k_{DO} for prolyl residues as it was substantially lower (43-fold) than in the other DKPs. [b] p = number of acidic protons; used to statistically correct the kinetic acidities.

The tyrosyl α-proton is the least acidic in the series. This may in part be ascribed to inductive destabilisation of the enolate by the methylene and aryl ring. Additionally, the formation of a tyrosyl enolate in aqueous solution may be disfavoured by the hydrophobicity of the attached phenol ring. Madison has shown that the phenyl ring in c(L-Pro-L-Phe) overwhelmingly favours (> 99 %) being placed above the central DKP ring as it reduces the hydrophobic surface area presented to the aqueous solvent.[106,107] A phenol ring in a tyrosyl residue is expected to adopt a similar conformation. The stabilisation of the tyrosyl α-carbanion by the formation of the enolate requires the geometry at α-carbon to change from sp^3 to sp^2 (Scheme 2.47). This results in the phenol ring projecting more into the bulk solvent away from the DKP ring, which increases the hydrophobic surface area and raises the barrier to deprotonation.

Scheme 2.47: Orientation of the phenol ring in the c(Pro-Tyr) DKP systems and corresponding enolate.

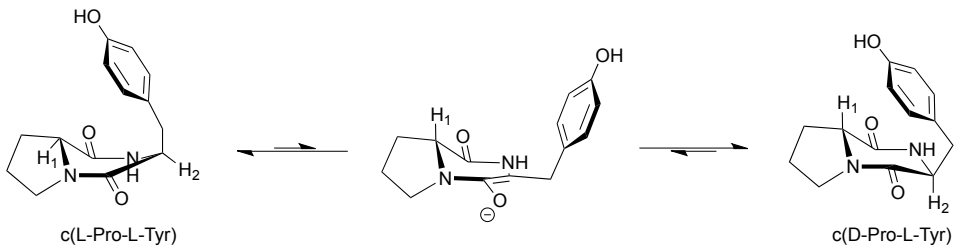

The alanyl residue is ~ 7-fold less acidic than the glycyl residue (Table 2.8). The majority of this difference is expected to originate from the inductive destabilisation of the DKP enolate by the methyl group of the alanyl residue. Steric hindrance by this methyl group may also be considered, however, this group is on the opposite face of the DKP ring to the alanyl α-proton. The most favourable angle of approach for the deuteroxide base when removing the α-proton will be at 180° to the σ_{C-H} bond – in order to maximise the orbital overlap with the σ^*_{C-H}. This will place the deuteroxide on the opposite side of the DKP to the methyl group and thus steric hindrance of deprotonation is unlikely.

2.3.1.2 Enhanced kinetic acidity of prolyl α-proton

The prolyl residue has an unexpectedly high kinetic acidity being 110-fold, 24-fold and 3-fold kinetically more acidic than the tyrosyl, alanyl and glycyl residues, respectively (Table 2.8). In principle, in comparison to the methyl group in the alanyl residue the pyrrolidine ring should have a similar – if not greater – inductive destabilisation effect upon formation of the DKP enolate. In addition, the pyrrolidine is sterically bulkier than the methyl group. Both of these factors should result in the prolyl α-proton being less kinetically acidic than the alanyl residue. Possible explanations for this enhanced kinetic acidity are outlined below and include a consideration of the conformational effects of a fused pyrrolidine and DKP ring structure, the equilibrium between *cis* and *trans* isomers of DKPs and stereoelectronic effects.

A comparison of the kinetic acidities of c(D-Pro-L-Pro) and c(D-Pro-D-Pro) shows that the α-proton of c(D-Pro-L-Pro) ($k_{DO} = 9.69 \times 10^{-2}\,M^{-1}\,s^{-1}$) is 11-fold more acidic than c(D-Pro-D-Pro) ($k_{DO} = 8.62 \times 10^{-3}\,M^{-1}\,s^{-1}$). Deprotonation of the α-carbon proceeds to a common enolate and therefore the difference in kinetic acidity must be derived from reactant destabilisation in c(D-Pro-L-Pro) (Scheme 2.48).[xiv] Eguchi has examined the *cis* / *trans* equilibrium between the c(D-Pro-L-Pro) [*trans*] and c(D-Pro-D-Pro) [*cis*] and found that the equilibrium overwhelmingly favours the *cis* isomer. Experiments showed that > 99.5 % of the DKP is in the *cis*-isomer and a difference in stability of $\Delta G_{exp} > 3.2$ kcal mol^{-1} was found between the two isomers.[105] A DFT calculation to compare the stability of the two isomers calculated that the difference in

[xiv] This could alternatively be expressed as reactant stabilisation of the c(D-Pro-D-Pro).

stability between the two isomers was ΔG_{calc} = 4.04 kcal mol^{-1} which is in good agreement with the experimental value.[xv] [120] Further evidence of the overwhelming preference for c(D-Pro-D-Pro) was seen in the ^{1}H NMR spectra of the deuterium exchange of c(D-Pro-D-Pro) where no appearance of signals for c(D-Pro-L-Pro) was observed.

Scheme 2.48: Comparison of the reactant stability of c(D-Pro-L-Pro) and c(D-Pro-D-Pro) and the effect on enolate formation. c(D-Pro-D-Pro) is more stable because the pyrrolidine rings can both adopt the more stable envelope conformation as opposed to the half-chair conformation in c(D-Pro-L-Pro).

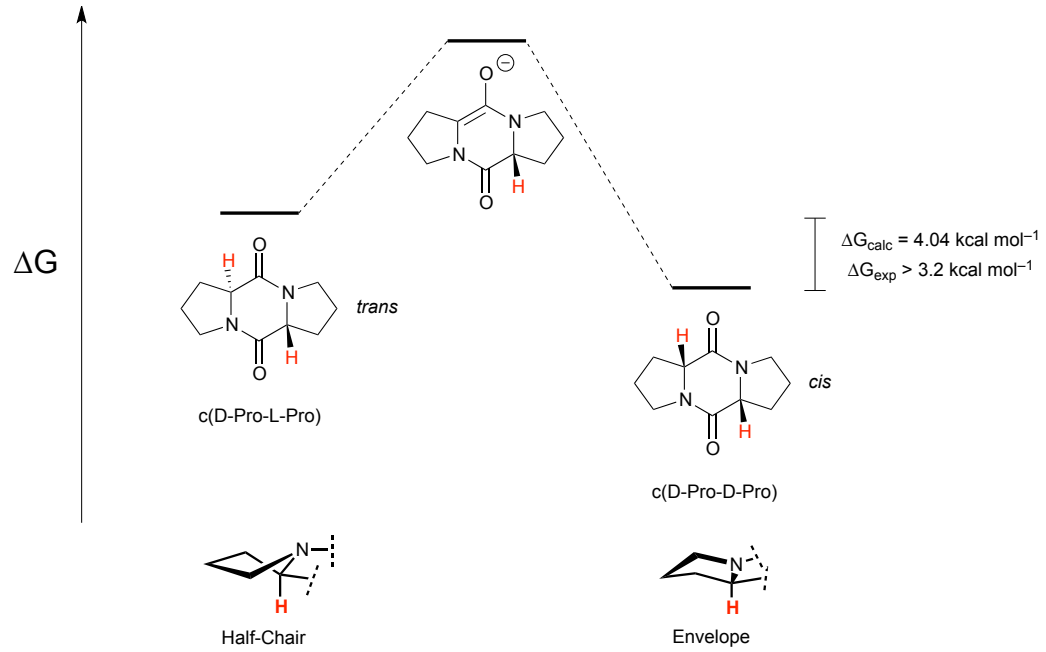

The preference for the *cis* isomer is a result of the interplay of conformational preferences in the pyrrolidine and DKP rings. In order to keep the preferred planar amide bond geometry of *trans* c(D-Pro-L-Pro) the DKP ring must adopt a planar conformation. However, this places both pyrrolidine rings of the prolyl residues into disfavoured half-chair conformations. In the *cis* c(D-Pro-D-Pro) the amide bonds can

[xv] Gaussian 09. Optimised Structures calculated at B3LYP level with a 6-31+G(d) Basis set in an aqueous CPCM at 25 °C. Free energy calculation performed at G3MP2B3 level with identical basis set and conditions.

be kept close to planar with the DKP ring in a chair conformation which therefore allows the pyrrolidine rings to adopt the more stable envelope conformations.

The free energy of activation energy for the deprotonation by deuteroxide can be found using the Eyring equation (Equation 2.8):

$$k = \frac{\kappa k_B T}{h} \exp\left(-\frac{\Delta G^{\ddagger}}{RT}\right) \qquad \text{(Equation 2.8)}$$

where k is the rate constant, κ is the transmission coefficient, k_B is the Boltzmann constant, T is the temperature, h is Planck's constant, R is the molar gas constant and $\Delta G^{\ddagger}$ is the Gibbs free energy of activation. κ was taken as unity for the Gibbs free energy of activation calculations below i.e. it was assumed that the transition state always proceeded to products.

Using this equation, the activation free energies may be calculated as $\Delta G^{\ddagger}$ = 18.84 kcal mol^{-1} for c(D-Pro-L-Pro) and $\Delta G^{\ddagger}$ = 20.27 kcal mol^{-1} for c(D-Pro-D-Pro). Thus, the difference in activation energies is only $\Delta\Delta G^{\ddagger}$ = 1.43 kcal mol^{-1} which is 1.77 – 2.61 kcal mol^{-1} smaller than the above experimental and calculated differences in stability between c(D-Pro-L-Pro) and c(D-Pro-D-Pro). Thus the difference in reactant stability is not fully translated into $\Delta\Delta G^{\ddagger}$. This indicates that there are one or more other factors that counterbalance the differences in energies between the deprotonation transition states for the two isomers.

The α-proton in the prolyl residue of c(L-Pro-L-Tyr) has the second highest k_{DO} value of the residues studied. Reactant destabilisation of c(L-Pro-L-Tyr) may also contribute to the high kinetic acidity in this case. Eguchi determined that in c(Phe-Pro) the preference for the *trans*- over the *cis*-isomer is as high as 9 : 1 due to the hydrophobic phenyl ring being able to sit more closely over the DKP in the *trans*-isomer (Scheme 2.49).

Scheme 2.49: The preference for the *trans* c(D-Pro-L-Tyr) over *cis* c(L-Pro-L-Tyr) is driven by the orientation of the phenol ring in closer proximity to the DKP ring in c(D-Pro-L-Tyr).

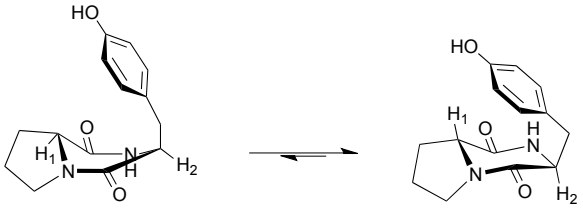

A similar preference was observed in the ^{1}H NMR spectra for the deuterium exchange experiments of c(L-Pro-L-Tyr) where the equilibrium distribution of *trans* c(D-Pro-L-Tyr) and *cis* c(L-Pro-L-Tyr) after complete exchange of the α-proton was 87 % : 13 %. In c(D-Pro-L-Tyr) the phenol ring can reside more closely over the DKP ring and therefore reduce the hydrophobic surface area presented to the aqueous solvent. This relative destabilisation of c(L-Pro-L-Tyr) may therefore help lower the barrier to removal of the α-proton.

The aforementioned effects of conformational preference and reactant destabilisation are likely to play a partial role in determining the acidity of the prolyl α-protons. However, such effects cannot account for the high kinetic acidity of the α-protons in the prolyl residues of c(D-Ala-L-Pro) and c(Gly-L-Pro). Eguchi determined that the distribution of *cis* / *trans* isomers in c(Ala-Pro) is ~ 50 : 50 and therefore c(D-Ala-L-Pro) and c(D-Ala-D-Pro) should be of similar stabilities. c(Gly-L-Pro) lacks any such isomerism and has a relatively flexible DKP ring due to the glycyl residue, easily facilitating a stable conformation.

A stereoelectronic effect is instead proposed to explain the high kinetic acidity of the prolyl α-protons. The first indication of the presence of a stereoelectronic effect that influences the carbon acidity of DKPs came from the two glycyl α-protons in c(Gly-L-Pro), which were found to have a 3.1-fold difference in kinetic acidities. The NOESY spectrum of c(Gly-L-Pro) in Figure 2.40 shows the glycyl α-proton at 4.03 ppm has a larger interaction with the prolyl α-proton at 4.17 ppm than the other glycyl α-proton at 3.74 ppm, and consequently is spatially closer. The glycyl α-proton at 4.03 ppm has a $k_{DO} = 6.59 \times 10^{-2}\,M^{-1}\,s^{-1}$ while the glycyl α-proton at 3.74 ppm has a lower $k_{DO} = 2.09 \times 10^{-2}\,M^{-1}\,s^{-1}$. It is posited that in c(Gly-L-Pro) the glycyl α-proton at 4.03

ppm is on the same face of the DKP ring as the prolyl α-proton and is thus placed in a position where there is increased orbital overlap between the σ_{C-H} bond and $\pi^*_{C=O}$ bond (H_3, Scheme 2.50 a). This will aid enolate formation as the transfer of electron density in the deprotonation transition state from σ_{C-H} bond to $\pi^*_{C=O}$ will be more facile. This stereoelectronic effect therefore potentially lowers the barrier to deprotonation for the glycyl α-proton at 4.03 ppm compared to glycyl α-proton at 3.74 ppm, which leads to the difference in the kinetic acidity between the two glycyl α-protons.

Figure 2.40: NOESY spectrum for c(Gly-L-Pro) in D_2O. The prolyl α-proton (H_1, Scheme 2.50) is at 4.17 ppm, one glycyl α-proton (H_3, Scheme 2.50) is at 4.03 ppm and one glycyl α-proton (H_2, Scheme 2.50) is at 3.74 ppm.

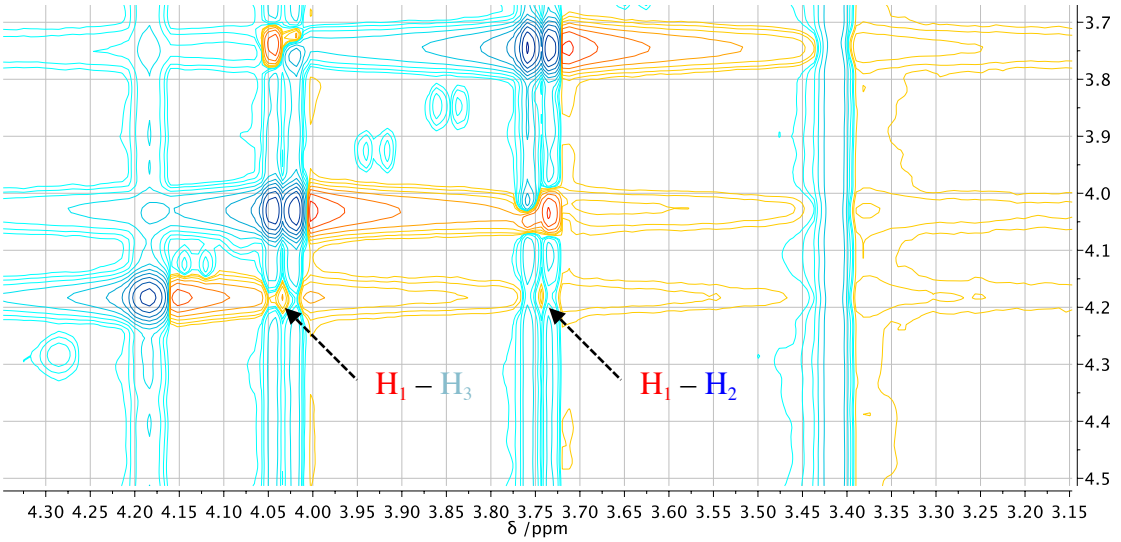

Scheme 2.50: A possible stereoelectronic effect to account for the difference in kinetic acidities between the glycyl α-protons in c(Gly-L-Pro) and the enhanced acidity of the prolyl α-proton. The structure on the left indicates the line of sight for a) glycyl α-protons, and b) prolyl α-proton. The antibonding orbital on the nitrogen has been omitted for clarity.

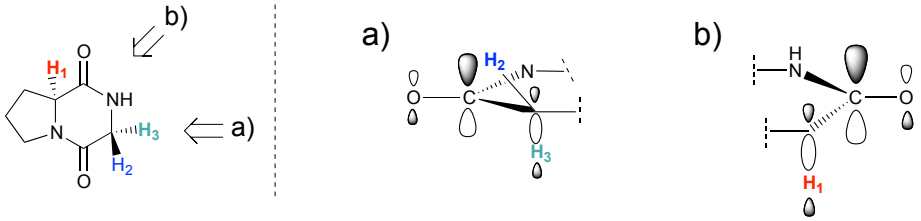

Further evidence for the existence of the stereoelectronic effect can be seen from the glycyl H_3 proton having a higher chemical shift (4.03 ppm) than the glycyl H_2 proton (3.74 ppm). This indicates that the C–H_3 bond is more elongated than the C–H_2 bond which could be accounted for by a donation of electron density from the σ_{C-H3} to the $\pi^*_{C=O}$ bond.

This stereoelectronic effect could also contribute to the enhanced kinetic acidity of the prolyl α-proton (H_1, Scheme 2.50 b). The pyrrolidine ring could lock the prolyl α-proton into a favourable position for deprotonation – enhancing the orbital overlap between the σ_{C-H} and $\pi^*_{C=O}$ bonds and lowering the barrier to enolate formation.

2.3.1.3 Comparison to linear peptides

Richard has measured the second order rate constants for deuteroxide-catalysed deprotonation of the α-protons for a series of linear peptide systems in aqueous solution – including *N*-acyl glycine amide.[113] *N*-acyl glycine amide is a linear analogue of a DKP and can be used to probe the effect of cyclisation on carbon acidity (Table 2.9).

Table 2.9: Comparison of DKP k_{DO} values with k_{DO} of N-acyl glycine amide.

Carbon Acid	k_{DO} /M^{-1} s^{-1}	k_{DO}/p [a] /M^{-1} s^{-1}	k_{DO}/p relative to *N*-Acyl Glycine Amide k_{DO}/p [a]
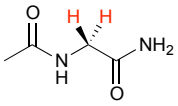 *N*-acyl glycine amide	2.6×10^{-3} [b]	1.3×10^{-3}	1.0
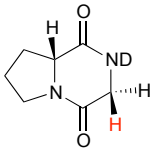 c(Gly-L-Pro)	2.09×10^{-2}	2.09×10^{-2}	16.1
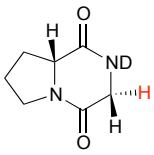 c(Gly-L-Pro)	6.59×10^{-2}	6.59×10^{-2}	50.7
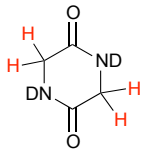 c(Gly-Gly)	6.33×10^{-2}	1.58×10^{-2}	12.2

[a] p = number of acidic protons; used to statistically correct the kinetic acidities. [b] Rios, A.; Richard, J. P.; Amyes, T. L. *J. Am. Chem. Soc.* **2002**, *124*, 8251 – 8259.

The glycyl α-proton experiences a 12 – 51-fold increase in kinetic acidity upon cyclisation. This is equivalent to a drop of $\Delta\Delta G^{\ddagger}$ = 1.48 – 2.43 kcal mol^{-1} in the free energy of activation for deprotonation of the DKP relative to the linear peptide. A stereoelectronic effect could play a role in decreasing the barrier for the DKP system whereby fixed placement of the α-proton into a more favourable position for enolate formation helps lower the barrier. Related to the stereoelectronic benefit of a fixed orientation, there could be a lowering of the entropy of activation in the DKP versus the linear system due to less rotational flexibility in the former case. Finally, electrostatic stabilisation from the δ^{+}-carbonyl carbon in the neighbouring amide group could help stabilise the formation of the enolate, as posited by Robertson.[117]

Previous studies by Richard of the kinetic acidities of the amino acids glycine and proline showed near identical k_{DO} value (~ 4.5×10^{-5} M^{-1} s^{-1}) for the α-protons.[112,114] Consequently, it is reasonable to assume that an N-acyl proline amide system would

also have a k_{DO} similar to that of the *N*-acyl glycine amide. Based on these assumptions, it can be calculated that the prolyl α-proton in a DKP would experience an increase in k_{DO} of 37 – 144-fold compared to the linear system. The more substantial cyclic/linear difference for the prolyl DKP could be attributed to a greater stereoelectronic effect.

2.3.2 Mechanism of hydrogen deuterium exchange

The kinetic acidity values, k_{DO}, can inform the mechanism of proton transfer for DKPs. The free energy profile for a hydrogen deuterium exchange reaction catalysed by both deuteroxide and buffer is shown in Scheme 2.51.[121] Initially, the carbon acid diffuses together with either a molecule of deuteroxide or buffer to form an encounter complex (**1** and **2**).[xvi] Subsequently, the carbon acid is deprotonated to form the carbanion and HOD **3** or AH **4**. The reaction can either reverse with reprotonation of the carbanion or can continue in the forward direction via solvent reorganisation to place a deuterium in the reactive position. In this step the HOD molecule may either rotate to place the deuterium in the reactive position or the HOD may diffuse away and be replaced by a D_2O. The protonated buffer AH must be replaced by a deuteriated analogue AD – assuming the buffer has only one acidic site. The solvent reorganisation is considered irreversible because the concentration of deuterium in solution overwhelmingly exceeds the concentration of hydrogen in solution when the reaction involves millimolar concentrations of substrate; thus HOD and AH are essentially lost by dilution in bulk solvent.[xvii] The carbanion is deuterated in **5** and **6** to give the encounter complex between deuterated carbon acid and either deuteroxide or buffer, **7** and **8**, which will diffuse apart to give free deuterated carbon acid in solution.[xviii]

[xvi] Diffusion to form the encounter complex is not shown in Scheme 2.51.

[xvii] In a 99.9 % D_2O the concentration of D is 110.17 M. The typical concentration of acidic H in DKP is 5.00 mM in the exchange reactions. This means that the concentration of D is 22000-fold greater than that of H.

[xviii] Again, diffusion to separate encounter complex not shown in Scheme 2.51.

Scheme 2.51: Relative free energy profile for the hydrogen deuterium exchange of a carbon acid catalysed by deuteroxide and buffer. X = H or D.

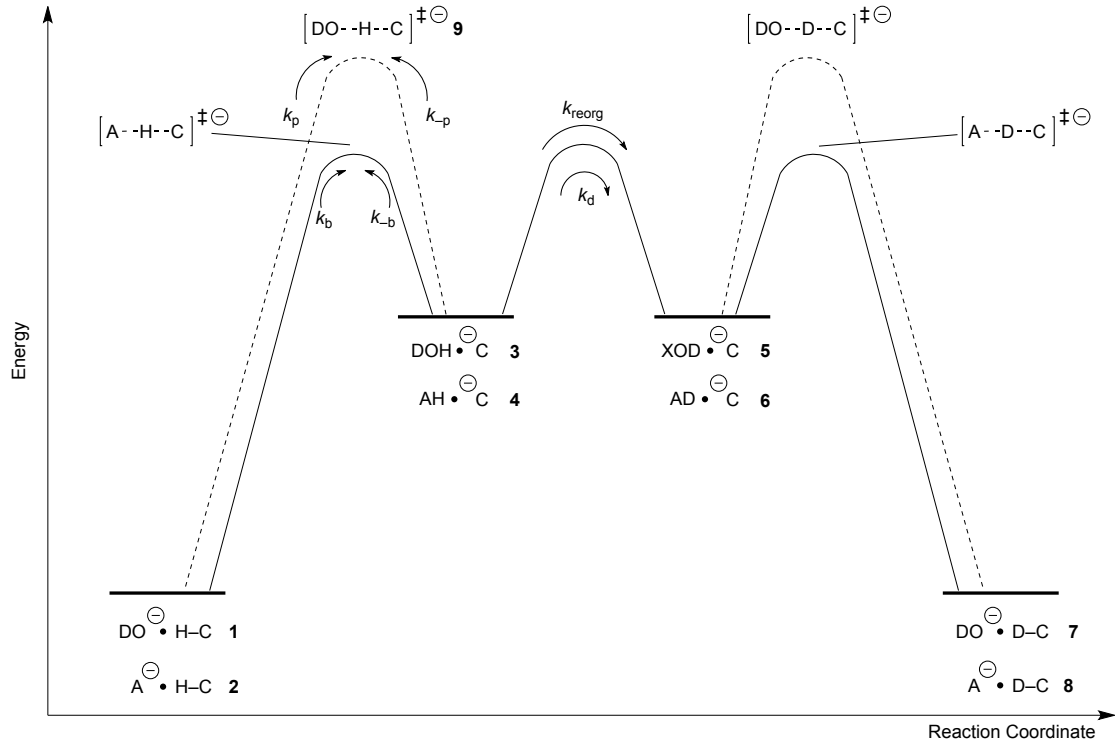

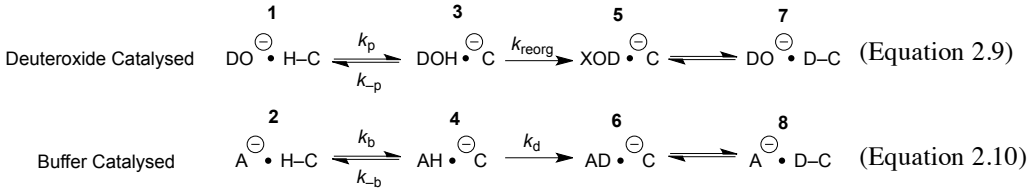

The microscopic rate constants for the deuteroxide and buffer catalysed reactions are defined in Equations 2.9 and Equations 2.10 (Scheme 2.51): k_p is the rate constant for deprotonation of the carbon acid by deuteroxide in the encounter complex, k_{-p} is the rate constant for reprotonation of the conjugate base of the carbon acid (the carbanion) by HOD, k_b is the rate constant for deprotonation of the carbon acid by buffer, k_{-b} is the rate constant for reprotonation of the conjugate base of the carbon acid by protonated buffer, k_d is the rate constant for replacement of protonated buffer by deuteronated buffer and k_{reorg} is the rate constant for solvent reorganisation which is experimentally determined to be $k_{reorg} \sim 10^{11}$ s^{-1}.[122-124]

Using the steady state approximation for the formation of **3** and **4** and taking the k_{reorg} step to be irreversible, the microscopic rate constants are related to the second order

rate constant for deuteroxide and buffer catalysed deuterium exchange, k_{DO} and k_{A^-}, by Equation 2.11 and Equation 2.12.

$$k_{DO} = \frac{k_p\, k_{reorg}}{k_{-p} + k_{reorg}} \quad \text{(Equation 2.11)}$$

$$k_{A^-} = \frac{k_b\, k_d}{k_{-b} + k_d} \quad \text{(Equation 2.12)}$$

Equation 2.11 and Equation 2.12 are valid provided that deprotonation of carbon acid and solvent reorganisation or reorganisation of buffer are both partially rate determining. If reorganisation is rate determining then $k_{-p} >> k_{reorg}$ and $k_{-b} >> k_d$ and thus Equation 2.11 and Equation 2.12 become Equation 2.13 and Equation 2.14:

$$k_{DO} = \frac{k_p\, k_{reorg}}{k_{-p}} = K_p\, k_{reorg} \quad \text{(Equation 2.13)}$$

$$k_{A^-} = \frac{k_b\, k_d}{k_{-b}} = K_b\, k_d \quad \text{(Equation 2.14)}$$

where K_p and K_b are the pre-equilibrium constants for formation of carbanion in the deuteroxide and buffer catalysed reaction. As k_d is smaller than k_{reorg}, no buffer catalysis will be observed if solvent reorganisation is rate determining as the deuteroxide catalysed pathway will be kinetically favoured.

If deprotonation of the carbon acid is rate determining then $k_{reorg} >> k_{-p}$ and $k_d >> k_{-b}$ and Equation 2.11 and Equation 2.12 become Equation 2.15 and Equation 2.16:

$$k_{DO} = \frac{k_p\, k_{reorg}}{k_{reorg}} = k_p \quad \text{(Equation 2.15)}$$

$$k_{A^-} = \frac{k_b\, k_d}{k_d} = k_b \quad \text{(Equation 2.16)}$$

When deprotonation of the carbon acid is rate determining, buffer catalysis will be observed as the buffer catalysed route offers a lower energy path for the deuterium exchange relative to the deuteroxide catalysed pathway (Scheme 2.51).

The rate determining step in the proton transfer is dependent upon the stability of the carbonyl carbanion. For highly unstable carbanions solvent reorganisation is rate determining, for more stable carbanions deprotonation is rate determining and for carbanions of intermediate stability both deprotonation and solvent reorganisation are partially rate determining. In order to determine which mechanism is active in the hydrogen deuterium exchange of DKPs the k_{DO} values must be compared to those for other simple neutral α-carbonyl carbon acids whose mechanism of exchange is already known.

Brønsted linear free energy relationships (and observed deviations from linearity) can be used to give insight into the mechanism of proton transfer. Richard has shown that there is a Brønsted relationship between the kinetic acidity, k_{HO}, and the pK_a of the α-protons in a series of simple neutral α-carbonyl carbon acids (Equation 2.17, Table 2.10, Figure 2.41 ●).[113] The β value of β = - 0.401 in Equation 2.17 indicates that in the transition state the progression of proton transfer to the base is ~ 40 % complete.

$$\log \frac{k_{HO}}{p} = -0.401(pK_a + \log p) + 6.496 \qquad \text{(Equation 2.17)}$$

Table 2.10: Kinetic acidities, k_{DO} and k_{HO}, and thermodynamic acidities, pK_a, of α-carbonyl carbon acids and TKPs at 25 ºC.

Entry	Carbon Acid [a]	k_{DO} /M^{-1} s^{-1}	k_{HO} /M^{-1} s^{-1}	pK_a
1 [j]	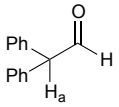	-	254	10.4 [h]
2 [j]	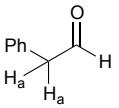	-	20.0	13.1 [h]
3 [j]	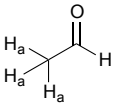	-	1.17	16.7 [h]
4 [j]	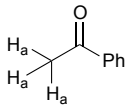	-	2.50×10^{-1}	18.3 [h]
5 [j]	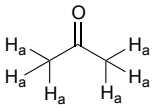	-	2.20×10^{-1}	19.3 [h]
6 [k]	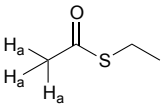	-	2.00×10^{-2}	21.0
7 [l]	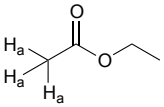	1.7×10^{-3} [b]	1.20×10^{-3} [e]	25.6 [i]
8 [m]	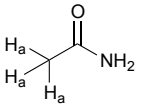	1.9×10^{-5} [b]	9.50×10^{-6} [f]	28.4 [i]
9 [n]	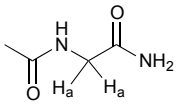	2.6×10^{-3}	1.3×10^{-3}	23.9 [i]
10 [m]	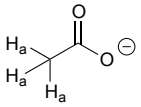	8.4×10^{-9}	3.5×10^{-9}	33.5

[a] H_a = the acidic protons. [b] k_{DO} determined in D_2O solutions at I = 1.0. [c] k_{DO} determined in 60 : 40 D_2O : d_3-MeCN at I = 0.06. [d] k_{DO} determined in 60 : 40 D_2O : d_3-MeCN at I = 0.20. [e] Secondary solvent isotope effect k_{DO} / k_{HO} = 1.4. [f] Secondary solvent isotope effect k_{DO} / k_{HO} = 2.4. [g] Secondary solvent isotope effect k_{DO} / k_{HO} = 1.46. [h] Experimentally determined pK_a. [i] Extrapolated from Equation 2.17, which is found to not be valid. [j] Keeffe, J. R.; Kresge, A. J. In *The Chemistry of Enols*; Rappoport, Z., Ed.; John Wiley and Sons: Chichester, **1990**; 399 – 480. [k] Amyes, T. L.; Richard, J. P. *J. Am. Chem. Soc.* **1992**, *114*, 10297 – 10302. [l] Amyes, T. L.; Richard, J. P. *J. Am. Chem. Soc.* **1996**, *118*, 3129 – 3141. [m] Richard, J. P.; Williams, G.; O'Donoghue, A. C.; Amyes, T. L. *J. Am. Chem. Soc.* **2002**, *124*, 2957 – 2968. [n] d Rios, A.; Richard, J. P.; Amyes, T. L. *J. Am. Chem. Soc.* **2002**, *124*, 8251 – 8259.

Figure 2.41: Brønsted linear free energy relationship between $\log(k_{HO}/p)$ and pK_a for a series of simple neutral α-carbonyl carbon acids (●) (Equation 2.17, Table 2.10). The dependence of the log of the reverse rate of reprotonation, k_{HOH}, on the pK_a (■) is also shown. p = number of acidic protons. Figure reproduced from Richard, J. P.; Williams, G.; O'Donoghue, A. C.; Amyes, T. L. *J. Am. Chem. Soc.* **2002**, *124*, 2957 – 2968. Reproduced with permission from the ACS.

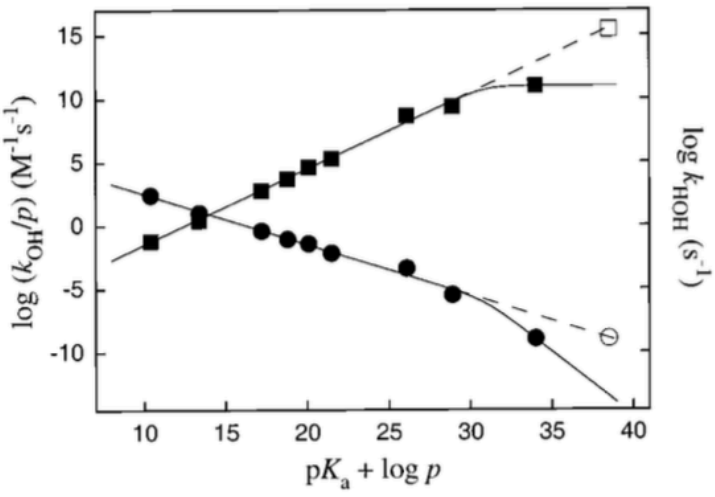

A linear relationship exists over the $\log(k_{HO}/p)$ range from -5.5 – 2.5 (or, pK_a = 10 – 30). However, for $\log(k_{HO}/p) < -5.5$ (or $pK_a > 30$) there is a downward curvature in the Brønsted plot. To explain this downward curvature one needs to consider Equation 2.18 which shows the relationship between pK_a, k_{HO}, the reverse rate of reprotonation, k_{HOH}, and the ionic product of water, K_w[xix].

$$pK_a = pK_w + \log\left(\frac{k_{HOH}}{k_{HO}}\right) \qquad \text{(Equation 2.18)}$$

Equation 2.18 was used to calculate k_{HOH} values from the experimentally determined k_{HO} and pK_a values for the carbon acids in Table 2.10. This relationship is also shown in Figure 2.41 (■). There is a clear linear increase in k_{HOH} with pK_a up until $k_{HOH} = 10^{11}$ s^{-1} whereupon the relationship levels off. The reason for the plateau is the physical limit placed upon the reverse rate of reprotonation of the carbanion by the rate constant of solvent reorganisation, $k_{reorg} \sim 10^{11}$ s^{-1}. This limit exists because it is not physically

[xix] $K_w = 10^{-14}$ M^2

possible for a solvent molecule to be placed into a reactive position for reprotonation of the carbanion faster than the solvent itself can reorganise (Scheme 2.51: step **3** → **5**). Thus Equation 2.18 and the limit from k_{reorg} cause the downward curvature in the Brønsted relationship in Figure 2.41.

Figure 2.41 can be used to assess whether the rate determining step in hydrogen deuterium exchange of DKPs is solvent reorganisation, deprotonation of the carbon acid, or a combination of deprotonation and solvent reorganisation. For highly unstable carbanions the rate determining step in deprotonation is solvent reorganisation and therefore, according to the principle of microscopic reversibility, the rate determining step for the reverse reprotonation of the carbanion will also be solvent reorganisation. Thus if the k_{HO} value of the carbanion places it on the downward curvature section of Figure 2.41 then solvent reorganisation is the rate determining step in the exchange mechanism. If, however, the k_{HO} value of the carbanion places it on the Brønsted relationship of Equation 2.17 then either deprotonation is rate limiting or both deprotonation and solvent reorganisation are rate limiting. The onset of the downward curvature in Figure 2.41 occurs at $k_{DO} < 7.0 \times 10^{-6}$ M^{-1} s^{-1}, therefore for any k_{DO} larger than this the hydrogen deuterium exchange is not expected to have solvent reorganisation as the rate determining step. The DKPs have $k_{DO} > 2.09 \times 10^{-3}$ M^{-1} s^{-1} which substantially exceeds this lower threshold and therefore the rate determining step in DKPs is not solvent reorganisation. No significant buffer catalysis was observed for the DKPs and thus deprotonation of the DKPs is not the rate determining step. Therefore, the only remaining option is that both deprotonation and solvent reorganisation are both partially rate determining in the hydrogen deuterium exchange of DKPs assuming the same linear Brønsted relationship applies.

2.3.3 Second order rate constants for hydroxide catalysed exchange, k_{HO}, and thermodynamic acidities, pK_as, of DKPs

DKPs are simple neutral α-carbonyl carbon acids and therefore the Brønsted relationship (Equation 2.17, Figure 2.41) can be used to estimate pK_a values for the α-protons of the DKPs. This first requires conversion of the second order rate constants for deuteroxide-catalysed exchange, k_{DO}, into second order rate constants for hydroxide-catalysed exchange, k_{HO} M^{-1} s^{-1}. This may be done via a secondary solvent isotope effect.

Secondary solvent isotope effects range between $k_{DO} / k_{HO} = 1.36 – 2.4$ for the deprotonation of carbon acids.[xx] Deuteroxide in D_2O is a stronger base than hydroxide in H_2O, hence $k_{DO} > k_{HO}$. The secondary solvent isotope is sensitive to which microscopic rate constant is the rate determining step for deuterium exchange. When solvent reorganisation, k_{reorg}, is rate determining the full secondary solvent isotope effect of $k_{DO} / k_{HO} = 2.4$ will apply, as complete proton transfer in the pre-equilibrium formation of the carbanion means that the full difference in basicity between deuteroxide and hydroxide will be observed. When deprotonation of the carbon acid is rate determining, k_p, the secondary solvent isotope effect will be $k_{DO} / k_{HO} = 1.36 – 1.48$,[xxi] as proton transfer is only partially complete at the transition state, **9** (Scheme 2.51). Thus the full difference in basicity between deuteroxide and hydroxide is not observed. If both solvent reorganisation and deprotonation of the carbon acid are partially rate determining then an intermediate value of $k_{DO} / k_{HO} \sim 2.0$ can be used for the secondary solvent isotope effect.

Given that the rate determining step in the mechanism for hydrogen deuterium exchange of the DKPs was both partially deprotonation and solvent reorganisation an intermediate secondary solvent isotope effect of $k_{DO} / k_{HO} = 2.0$ was used to convert the k_{DO} values into k_{HO} values (Table 2.11).

[xx] i) $k_{DO} / k_{HO} = 1.4$ for racemization of the anion of mandelic acid at 100 ºC [Pocker, Y. *Chem. Ind.* (*London*) **1958**, 1117 – 1118]; ii) base-catalyzed bromination of acetone at 25 ºC $k_{DO} / k_{HO} = 1.46$ [Pocker, Y. *Chem. Ind.* (*London*) **1959**, 1383 – 1384]; iii) $k_{DO} / k_{HO} = 2.4$ [Gold, V.; Grist, S. *J. Chem. Soc., Perkin Trans. 2* **1972**, 89 – 95]; iv) detritiation of phenylacetylene at 25 ºC $k_{DO} / k_{HO} = 1.36$ [Kresge, A. J.; Lin, A. C. *J. Am. Chem. Soc.* **1975**, *97*, 6257 – 6258]; v) detritiation of chloroform at 25 ºC $k_{DO} / k_{HO} = 1.48$ [*ibid*].

[xxi] Dependent upon the extent of proton transfer in the transition state of the reaction. See above the note.

Table 2.11: Kinetic acidities, k_{DO} and k_{HO}, and thermodynamic acidities, pK_a, of DKPs studied at 25 °C and I = 1.0 M (KCl). Calculated pK_as from Coote and Easton are also shown.

Carbon Acid	k_{DO} /M^{-1} s^{-1}	k_{HO} /M^{-1} s^{-1}	k_{HO}/p /M^{-1} s^{-1}	pK_a
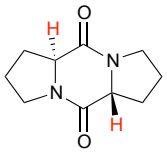 c(D-Pro-L-Pro)	9.69×10^{-2}	4.85×10^{-2}	2.42×10^{-2}	20.0
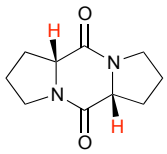 c(D-Pro-D-Pro)	8.62×10^{-3}	4.31×10^{-3}	2.16×10^{-3}	22.6
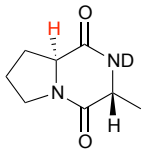 c(D-Ala-**L-Pro**)	9.45×10^{-2}	4.73×10^{-2}	4.73×10^{-2}	19.6
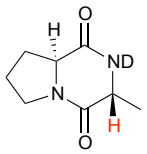 c(**D-Ala**-L-Pro)	5.51×10^{-3}	2.76×10^{-3}	2.76×10^{-3}	22.6
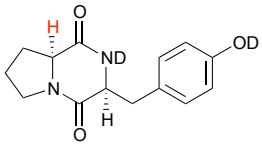 c(**L-Pro**-L-Tyr)	1.19×10^{-1}	5.95×10^{-2}	5.95×10^{-2}	19.3
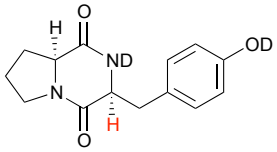 c(L-Pro-**L-Tyr**)	2.09×10^{-3}	1.05×10^{-3}	1.05×10^{-3}	23.7
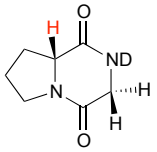 c(Gly-**L-Pro**)	1.87×10^{-1}	9.35×10^{-2}	9.35×10^{-2}	18.8
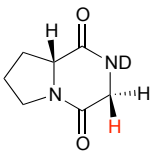 c(**Gly**-L-Pro)	2.09×10^{-2}	1.05×10^{-2}	1.05×10^{-2}	21.2

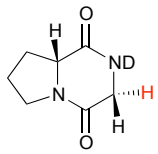 c(**Gly**-L-Pro)	6.59×10^{-2}	3.30×10^{-2}	3.30×10^{-2}	19.9
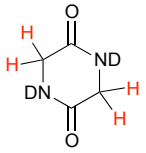 c(Gly-Gly)	6.33×10^{-2}	3.17×10^{-2}	7.91×10^{-3}	20.9
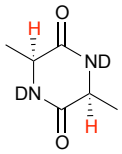 c(L-Ala-L-Ala)	7.80×10^{-3}	3.90×10^{-3}	1.95×10^{-3}	22.7
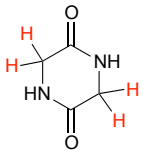 c(Gly-Gly) [c]	–	–	–	24.0 [b]
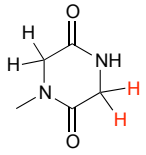 N-methyl c(Gly-Gly) [c]	–	–	–	25.8 [b]
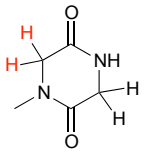 N-methyl c(Gly-Gly) [c]	–	–	–	25.1 [b]
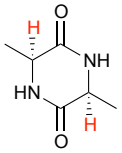 c(L-Ala-L-Ala) [d]	–	–	–	26.1 [b]

[a] p = number of acidic protons; used to statistically correct the kinetic acidities. [b] Calculated aqueous pK_a at 25 °C. [c] Ho, J.; Easton, C. J.; Coote, M. L. *J. Am. Chem. Soc.* **2010**, *132*, 5515 – 5521. [d] Ho, J.; Coote, M. L.; Easton, C. J. *J. Org. Chem.* **2011**, *76*, 5907 – 5914.

The k_{HO}/p values and the Brønsted relationship in Figure 2.42 were then used to interpolate estimates for the pK_a values of the DKP α-protons (Table 2.11). The prolyl α-protons have pK_as = 18.8 – 22.6, the glycyl α-protons have pK_as = 19.9 – 21.2, the alanyl α-protons have pK_as = 22.6 – 22.7 and the tyrosyl α-proton have a pK_a = 23.7.

Figure 2.42: Brønsted linear free energy relationship between $\log(k_{HO}/p)$ and pK_a for a series of simple neutral α-carbonyl carbon acids (●) (Equation 2.17, Table 2.10). The interpolated pK_a values for the DKPs (○) are shown (Table 2.11). p = number of acidic protons.[113]

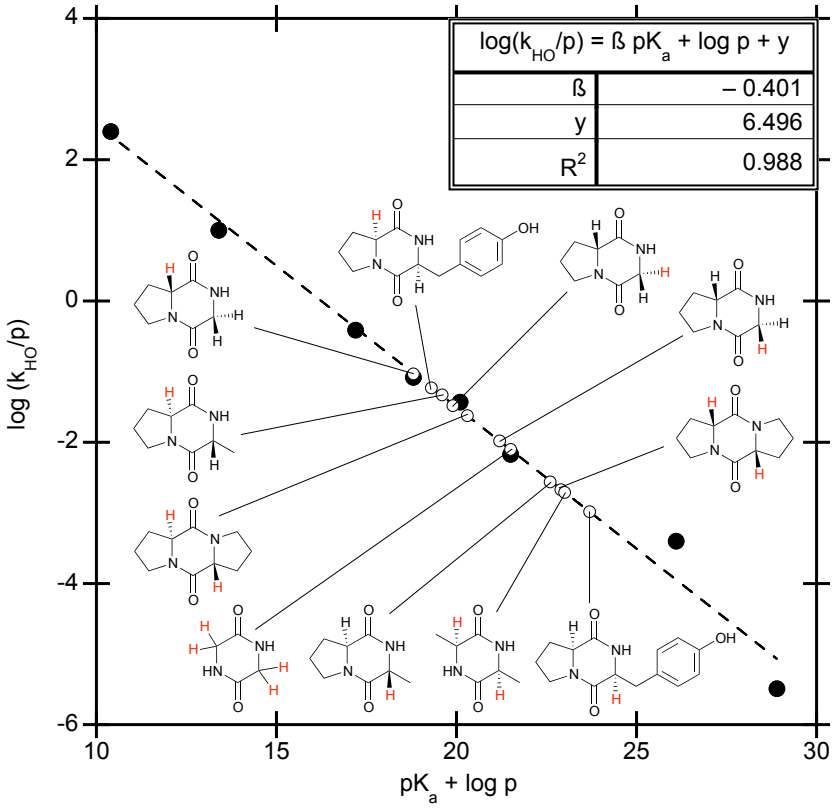

2.3.3.1 Validity of the application of the neutral α-carbonyl carbon acid Brønsted to DKPs

The validity of Brønsted relationships is dependent upon a number of assumptions that are outlined below regarding the relationship between the Gibbs free energy of activation ($\Delta G^{\ddagger}$), which is proportional to log k, and the thermodynamic Gibbs free energy of the reaction (ΔG), which is proportional to pK_a (Chapter 1: Section 1.4). An adaption of Marcus' theory of electron transfer to proton transfer reactions is used to quantify this relationship.[125,126] The $\Delta G^{\ddagger}$ is related to ΔG by a quadratic function:

$$\Delta G^{\ddagger} = \Delta G_{\circ}^{\ddagger}\left(1 + \frac{\Delta G}{4\,\Delta G_{\circ}^{\ddagger}}\right)^{2} \qquad \text{(Equation 2.19)}$$

where $\Delta G^{\ddagger}_{o}$ is the intrinsic barrier to the reaction. The intrinsic barrier is the kinetic barrier to the reaction when the overall thermodynamic Gibbs free energy change is 0 (ΔG = 0 kJ mol^{-1}). For a reaction series with structurally related reactants the intrinsic barrier is expected to remain constant. Thus, for the deprotonation by hydroxide of the series of structurally related neutral α-carbonyl carbon acids in Table 2.10 and Figure 2.41 (●) there ought to be a consistent intrinsic barrier. Equation 2.19 implies that there will be curvature in the relationship between $\Delta G^{\ddagger}$ and ΔG and therefore in Figure 2.41 (●) there should be negative curvature in the relationship between log k_{HO} and pK_a.[xxii] However, this is not observed and Richard has shown that there is a poor fit of the data in Table 2.10 to Marcus theory.[121] One reason for this is that proton transfer at carbon is slow; thus it is difficult to cover a pK_a range wide enough that the curvature in the fit is perceptible. Richard also noted that "the expected increasingly sharp decreases in rate constant and increases in reaction barrier predicted by the Marcus equation as the proton transfer becomes increasingly uphill thermodynamically are offset or balanced by decreases in the intrinsic barrier to enolization."[121] Richard posited that the decrease in the intrinsic barriers were a result of changes in the extent of resonance stabilisation in the carbanion and reactant state throughout the series of neutral α-carbonyl carbon acids in Table 2.10. Greater resonance stabilisation in the carbanion will cause an increase in the intrinsic barrier while greater resonance stabilisation in the reactant state will lead to a decrease in the intrinsic barrier. The changes in intrinsic barrier result in the linear Brønsted relationship of Equation 2.17 providing a better fit of the data than Marcus theory.

The above estimations for the pK_as of the DKPs are based upon the assumption that the intrinsic barrier to deprotonation for the DKPs are equivalent or closely similar to that for the other simple neutral α-carbonyl carbon acids which compose the Brønsted relationship in Equation 2.17. This may not be correct as the aforementioned stereoelectronic effect could lower the intrinsic barrier to deprotonation by hydroxide. For the neutral α-carbonyl carbon acids prior to enolate formation the α-H must rotate into a position where the σ_{C-H} and $\pi^*_{C=O}$ orbitals have maximum overlap. In the DKPs the α-H is essentially preorganised by the stereoelectronic effect into an optimal position for enolate formation. This will lower the intrinsic barrier to deprotonation in

[xxii] For deprotonation by oxyanion bases apart from hydroxide, curvature in the Brønsted relationship is observed. Guthrie, P. J. *Can. J. Chem.* **1979**, *57*, 1177 – 1185.

the DKPs relative to the neutral α-carbonyl carbon acid principally by reducing the entropy of activation.

If the intrinsic barrier were lowered then this would require a new Brønsted relationship for the DKPs. The thermodynamic driving force for deprotonation would not be expected to differ substantially between the neutral α-carbonyl carbon acids and the DKPs as both proceed from a neutral carbon acid to an anionic enolate and thus the pK_a for both be similar. However, a lower intrinsic barrier would increase the value of log k_{HO} and thus lead to a positive deviation from the Brønsted relationship in Figure 2.42.

Richard has previously assessed the effect that an α-cationic group can have upon the acidity of the α-proton of a carbonyl carbon acid.[112] A cationic charge will lower the intrinsic barrier to deprotonation by hydroxide by stabilising both the developing negative charge on the carbanion and the hydroxide in the transition state. Figure 2.43 (■) and Equation 2.20 show the Brønsted relationship for cationic α-carbonyl carbon acids. In comparison to the neutral α-carbonyl carbon acids Figure 2.43 (●) there is a positive deviation in the Brønsted relationship for the cationic α-carbonyl carbon acids. This deviation is similar to that which might be expected from a lower intrinsic barrier in the DKPs, however, the magnitude of the positive deviation from an adjacent cationic charge is expected to be significantly larger than for the stereoelectronic effect in the DKPs.

$$\log\frac{k_{HO}}{p} = -0.444(\mathrm{p}K_a + \log p) + 10.044 \qquad \text{(Equation 2.20)}$$

Figure 2.43: Brønsted linear free energy relationship between $\log(k_{HO}/p)$ and pK_a for a series of simple neutral α-carbonyl carbon acids (●) (Equation 2.17, Table 2.10) and cationic α-carbonyl carbon acids (■) (Equation 2.20). *p* = number of acidic protons.[112]

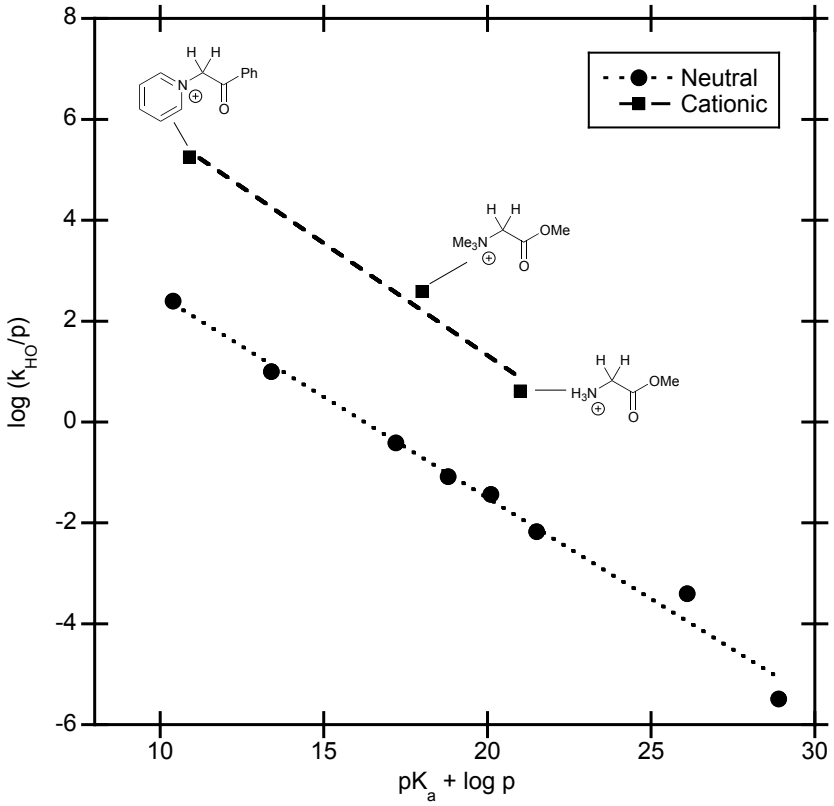

$\log(k_{HO}/p) = ß\ pK_a + \log p + y$	
ß	– 0.401
y	6.496
R^2	0.988

$\log(k_{HO}/p) = ß^+\ pK_a + \log p + y$	
$ß^+$	-0.444
y	10.044
R^2	0.979

From the cationic Brønsted relationship in Equation 2.20 estimates for the pK_a values of the DKP α-protons are in the range of pK_a = 26.1 – 30.0. This is felt to be an overestimate as these pK_a values are above that of the *N*-acyl glycine amide (pK_a = 23.9). Given that both *N*-acyl glycine amide and DKPs are neutral α-carbonyl carbon acids and that the DKPs have k_{DO} values up to 144-fold larger than the linear system the pK_a values for the DKPs are expected to be below that of *N*-acyl glycine amide. Nevertheless, the positive deviation in the postulated Brønsted relationship for the DKPs that includes the lower intrinsic barrier may cause a small increase in the pK_a values for the DKPs in Table 2.11.

2.3.3.2 Comparison of DKP pK_a to previous computational estimates

Table 2.11 also shows a selection of the calculated aqueous pK_as from Coote and Easton. The calculated aqueous pK_as are substantially higher than the experimental pK_a estimated from the experimental k_{DO} values and the Brønsted relationship. For example, c(Gly-Gly) has an experimental pK_a = 20.9 while the calculated pK_a = 24.0, a difference of 3.1 pK_a units. Likewise, for c(L-Ala-L-Ala) the experimental pK_a = 22.7 while the calculated pK_a = 26.1, a difference of 3.4 pK_a units. Assuming the application of the linear Brønsted relationship above for neutral α-carbonyl acids is also valid for DKPs then the calculations underestimate the stability of the DKP enolates by $\Delta\Delta G \sim$ 4.2 – 4.6 kcal mol^{-1}. One possible explanation for this could be that the calculations failed to fully account for all solute-solvent interactions. The calculations were performed with a polarizable continuum medium to replicate the effect of solvent water. However, this method does not include any explicit solvent molecules and therefore cannot account for solute-solvent hydrogen bonding which could stabilise the enolate.

Coote and Easton identified a distal effect in DKPs where substitution on a nitrogen amide affected the pK_a of the distal protons to a greater extent than the proximal protons (Scheme 2.52).[115,116] For example, the pK_a of the distal protons (H_2) of *N*-methyl-c(Gly-Gly) are affected more than the proximal protons (H_1) by the electron donating methyl group attached to the amide nitrogen (Scheme 2.52). Coote and Easton proposed that the distal effect was predominately due to a resonance effect. The distal enolate can adopt three possible resonance structures (Scheme 2.53). The higher the contribution of resonance form **C** to the DKP conjugate base the less the carbanion can be stabilised by the enolate resonance form **A**. In the case of *N*-methyl-c(Gly-Gly) formation of resonance form **C** is more favourable as the electron-donating methyl group stabilises the cationic charge formed upon donation of the nitrogen lone pair to form the π-bond. Consequently, this lowers the contribution of resonance form **A** and therefore destabilises the distal protons raising their pK_a.

Scheme 2.52: The proximal (H_1) and distal (H_2) protons on a DKP relative to the N-substituted amide nitrogen. The pK_as of the proximal and distal protons *N*-methyl-c(Gly-Gly) and c(Gly-L-Pro) are also shown.

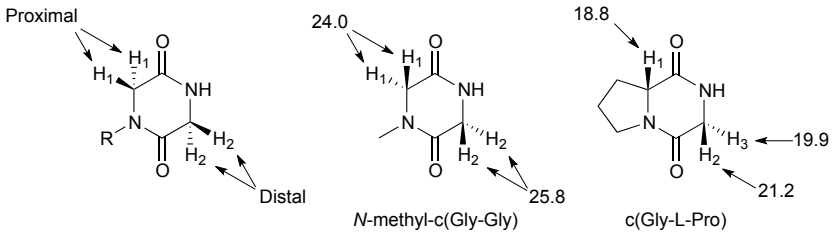

Scheme 2.53: The three possible resonance structures for a DKP enolate.

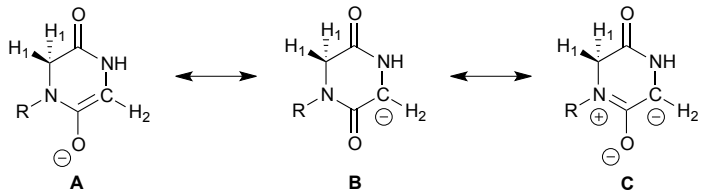

While the DKPs examined by Coote and Easton, which displayed the distal effect, were not used in this study the c(Xaa-L-Pro) DKPs can be used to gain insight of the effect of alkylation on the amide. c(Gly-L-Pro) studied in this work shows some evidence for the distal effect. The pK_a of the distal protons in c(Gly-L-Pro) are 1.1 – 1.4 pK_a units higher than the proximal prolyl α-proton. However, c(Gly-L-Pro) is a more complex system than *N*-methyl-c(Gly-Gly) and therefore other factors such as the aforementioned stereoelectronic effect may also be responsible for the difference in the pK_as between the proximal and distal protons.

2.3.4 Relevance to biochemical reactions

A variety of biochemical processes such as epimerisation, β-replacement and transamination reactions rely upon the deprotonation of the α-proton in amino acid or peptide systems.[127] Epimerisation enzymes, for example, are used to convert either monomeric L-amino acids into D-amino acids or the corresponding L/D conversion in peptides.[128,129] Life overwhelmingly utilises L-amino acids in proteins but prokaryotic organisms do include D-amino acids in peptide sequences. Typically, an epimerisation enzyme uses a cofactor such as pyridoxal 5′-phosphate, PLP, to lower the pK_a of the α-proton (Scheme 2.54). PLP reacts with the amine group on the amino acid to form a

Schiff base which lowers the pK_a of the α-proton to pK_a ~ 17 from pK_a of ~ 29 for the zwitterionic form of the amino acid.

Scheme 2.54: The mechanism for the epimerisation of amino acids with the cofactor PLP.[127]

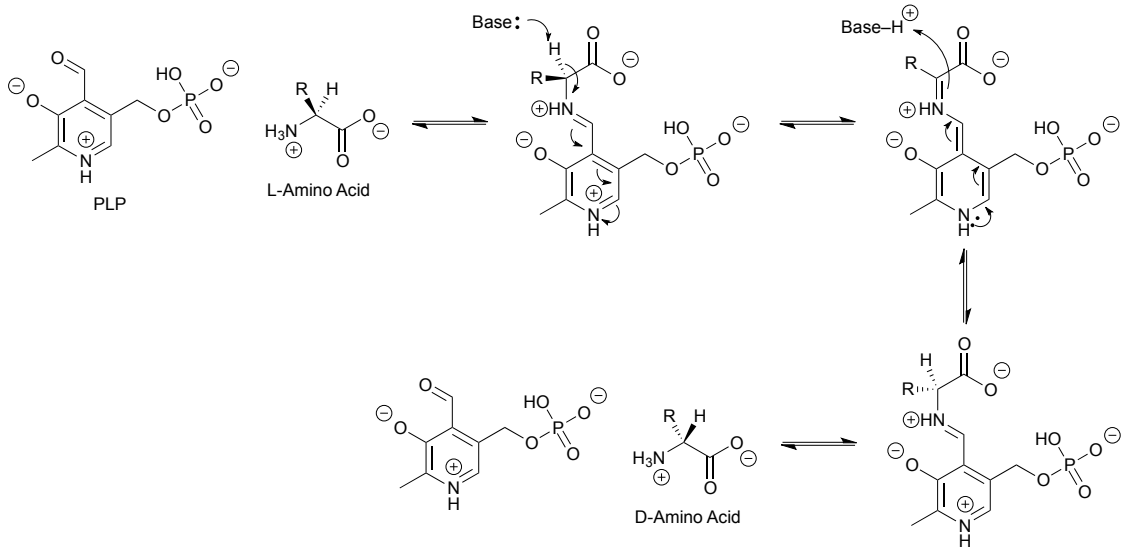

PLP can act as a cofactor for a number of different enzymatic reactions including the aforementioned deprotonation at the α-carbon but also decarboxylation of the α-carbon carboxylate and transamination of the α-carbon amine.[127] Dunathan has proposed that this diversity of function is in part regulated by the stereoelectronic overlap between the α-carbon substituent and the imine-pyridine π-system.[130] The substituent parallel to the π-system will have the greatest orbital overlap and will, in part, dictate which of the three possible reactions occurs. This hypothesis has been confirmed from the crystal structures of enzymes with their substrates or substrate analogues.[131] While the majority of epimerisation enzymes make use of the PLP cofactor to catalyse the deprotonation at the α-carbon there are a number of enzymes that require no cofactor for epimerization. This includes the epimerisation enzymes for proline, aspartic acid and glutamic acid.[132,133]

The difference between epimerisation with and without a cofactor can be seen by comparing alanine racemase and proline racemase along with the rates of deprotonation of an amino acid in water. The deprotonation of zwitterionic proline in water (k_{HO} = 4.5 × 10^{-11} M^{-1} s^{-1}) is ~ 6 × 10^{13}-fold smaller than the deprotonation by proline racemase (k_{cat} = 2600 s^{-1}).[114] The enzyme lowers the barrier to deprotonation by

~ 19 kcal mol^{-1}. For alanine racemase $k_{cat}/K_M = 4 \times 10^5$ M^{-1} s^{-1} is 2×10^8-fold faster than the deprotonation of a glycine-PLP analogue by phosphate dianion $k_B = 1.7 \times 10^{-3}$ M^{-1} s^{-1}.[134] This corresponds to the PLP lowering the barrier to deprotonation by the enzyme by ~ 11 kcal mol^{-1}. Thus the PLP cofactor contributes slightly over half the transition state stabilisation required to deprotonate the α-carbon of an amino acid with the burden on the alanine racemase enzyme about 8 kcal mol^{-1} smaller than that for proline racemase.[135]

The absence of a cofactor for proline racemase requires the enzyme to have alternative approaches to stabilise the transition state for deprotonation of the α-carbon of an amino acid. These include: i) the zwitterionic enol product being more tightly bound within the active site, ii) hydrogen bonding to the carbonyl oxygen of proline and iii) the closer proximity between the cationic nitrogen and the anionic enolate enhancing the electrostatic interaction relative to the anionic carboxylate and the cationic nitrogen in the amino acid zwitterion.[114] Richard has largely ruled out the possibility of Brønsted base catalysis by amino acid residues within the active site. The active site of proline racemase has two catalytic thiols, one of which accepts a proton from proline on one face and the other thiol donates a proton to the opposite face (Scheme 2.55).[132] The absence of buffer catalysis in the deprotonation of the α-carbon in proline zwitterion and the fact that thiolate anions are poor bases led to Richard concluding that deprotonation catalysed by amino acid side residues does not significantly affect the barrier to deprotonation. The use of thiolate bases within the active site is posited to have evolved due to the active site having a low dielectric constant which favors the formation of the more diffuse thiolate anion as opposed to, for example, an oxygen anion base.

Scheme 2.55: Mechanism for the epimerisation of proline within the active site of proline racemase. For clarity proline is presented as a solid bar.[132]

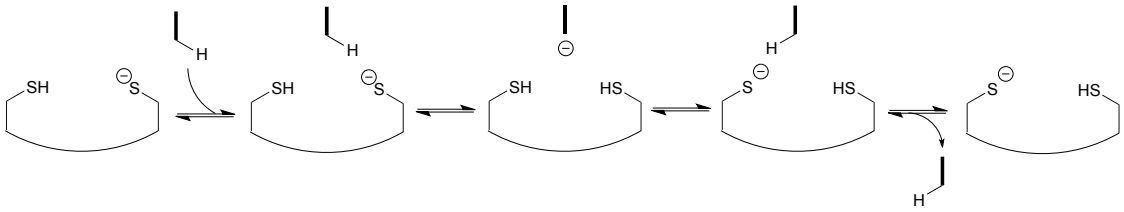

This study into DKPs indicates an additional method for rate enhancement in an amino acid racemase which lacks a cofactor. The restrictions on the conformation of an amino acid residue within a DKP has been shown to enhance the kinetic acidity of the α-proton by up to 144-fold and reduces the barrier to deprotonation by up to ~ 2.9 kcal mol^{-1}. This enhancement, which in part has been attributed to a stereoelectronic effect, could be present within a racemase enzyme if the residues within the active site of the enzyme correctly orientate the carbonyl group of the carboxylate into a position that maximises the overlap between the σ_{C-H} and $\pi^*_{C=O}$ bonds. This could therefore contribute up to ~ 2.9 kcal mol^{-1} of stabilisation to the transition state for deprotonation within the active site. While it should be noted that DKPs are neutral α-carbonyl carbon acids rather than formally neutral zwitterionic carbonyl carbon acids this should not prevent a stereoelectronic effect being present in the deprotonation reaction at an enzyme active site.

2.3.5 Pharmaceutical Application

As outlined in the introduction the potential to use DKPs as low-molecular weight drug molecules has been explored. The DKP structure is a convenient scaffold upon which to build 3D drug molecules. Critical to the efficacy of these DKP drugs is the stereochemical integrity of the α-positions on the DKP rings. The k_{HO} values in this work can be used to establish the half-life of the α-position. The half-life of the most acidic α-proton in this study, the prolyl α-proton on c(L-Pro-L-Tyr), at physiological pH (7.36) was found to be ~ 370 days. Therefore there should be little concern that *in vivo* racemisation will harm the efficacy of DKP-based drug molecules.

2.4 Summary

Hydrogen deuterium exchange reactions have been used to measure the second order rate constants for the deuteroxide-catalysed exchange, k_{DO} (M^{-1} s^{-1}), of the α-protons in a series of diketopiperazines. Kinetic acidities in the range of $k_{DO} = 2.09 \times 10^{-3} - 1.87 \times 10^{-1}$ M^{-1} s^{-1} have been determined. The order of kinetic acidity of amino acid residues was found to be Prolyl > Glycyl > Alanyl > Tyrosyl. A combination of minimisation of hydrophobic surface area and inductive effects could account for the order of Glycyl > Alanyl > Tyrosyl. However, the prolyl α-protons were found to be substantially more acidic than expected. A stereoelectronic effect, first noticed in the glycyl residue, which enhances the overlap between the σ_{C-H} of the α-proton and $\pi^*_{C=O}$ of the adjacent amide carbonyl, is proposed to be responsible for the enhanced acidity.

The DKP α-protons are up to 144-fold more acidic than related linear peptide systems which is proposed to be a result of the stereoelectronic effect and stabilising electrostatic interactions within the DKP ring.

The mechanism for hydrogen deuterium exchange in DKPs appears to involve both partially rate limiting deprotonation of the carbon acid by deuteroxide and partially rate limiting solvent reorganisation. The evidence for this is twofold with: i) an absence of buffer catalysed exchange which eliminates deprotonation of the carbon acid being solely rate limiting, and ii) the magnitude of the k_{DO} values for DKPs being ~ 300-fold greater than the k_{DO} values for other similar α-carbonyl carbon acids which have rate limiting solvent reorganisation – thus eliminating solvent reorganisation from being solely rate limiting. Consequently, an intermediate secondary solvent isotope effect of $k_{DO} / k_{HO} = 2.0$ was used to convert the k_{DO} values into second order rate constants for hydroxide-catalysed exchange, k_{HO} (M^{-1} s^{-1}).

Estimate for the pK_as of the α-protons were interpolated from a Brønsted relationship for simple neutral α-carbonyl carbon acids and the DKP α-protons were found to have pK_as in the range of pK_a = 18.8 – 23.7. These pK_as are ~ 3.3 pK_a units lower than previous computational estimates for the pK_a of DKPs and demonstrate that the DKP enolates are ~ 4.4 kcal mol^{-1} more stable than previously thought.

The relevance of these results to enzyme catalysis has been explored. It is suggested that the observed stereoelectronic effect found in DKPs systems could offer an alternative/additional explanation for the origin of the reduction in the barrier to enolate formation in proline racemases, which catalyse the epimerisation reaction of proline in the absence of a cofactor.

2.5 Experimental

2.5.1 General Instrumentation

NMR: Synthetic and Kinetic NMR spectra were recorded on Bruker Ultrashield 400 MHz, Varian 400 MHz and Oxford Varian Unity Inova 500 MHz NMR spectrometers. High Resolution ^{1}H NMR, ^{13}C NMR, COSY, HSQC, HMBC spectra were recorded on a Varian Inova 700 MHz NMR spectrometer. NMR samples were prepared in D_2O and $CDCl_3$. All chemical shifts are reported relative to residual solvent peaks of δ_H 4.79 ppm for D_2O and δ_H 7.26 ppm and δ_C 77.2 ppm for $CDCl_3$.

Mass Spectrometry: A Waters TQD mass spectrometer was used to record low resolution mass spectrums. A Thermo-Finnigan LTQ FT mass spectrometer was used to record high resolution mass spectrums

UV-Vis Spectrophotometry: A Cary 100 UV-Vis spectrophotometer with a temperature regulated cuvette holder and attached heating unit was used to collect all absorbance spectra.

pH Measurement: A MeterLab™ PHM 290 pH-Stat Controller equipped with a radiometer combination electrode filled with saturated KCl solution was used to measure pH.

Melting Point: Melting point measurements were made on a Gallenkamp melting point apparatus.

2.5.2 Materials

NMR Solvents: d2-Deuterium oxide (99.9 atom % D) and d_3-acetonitrile (99.8 atom % D) was purchased from Goss Scientific. Chloroform-d_1 (99.8 atom % D), potassium deuteroxide (99.8 atom % D, 40 wt %) and deuterium chloride (99 atom % D, 35 wt %) were purchased from Sigma-Aldrich. A stock solution of 2 M potassium chloride was prepared by dissolving solid potassium chloride in D_2O. Stock solutions of potassium

deuteroxide and deuterium chloride were prepared by dissolving concentrated potassium deuteroxide and deuterium chloride in D_2O and then titrating against volumetric hydrochloric acid and volumetric sodium hydroxide solutions respectively to determine the concentration of KOD and DCl.

Synthetic Reagents: L-Proline benzyl ester hydrochloride salt, D-proline benzyl ester hydrochloride salt, *N*-carboxybenzyl-D-proline and (benzotriazol-1-yloxy)-tripyrrolidinophosphonium hexafluorophosphate (PyBOP) were purchased from TCI UK. Dichloromethane AR grade, ethyl acetate reagent grade, methanol HPLC-grade were purchased from Fisher Scientific. Pd/C 10 % catalyst and thionyl chloride were purchased from Sigma Aldrich.

Kinetic Experiments: Potassium carbonate, 3-chloroquinuclidine hydrogen chloride salt, potassium chloride, tetramethylammonium hydrogensulfate, sodium trimethylsilylpropyl sulfonate and c(Gly-Gly) were purchased from Sigma Aldrich. c(D-Ala-L-Pro), c(L-Ala-L-Ala), c(L-Pro-L-Tyr) and c(Gly-L-Pro) were purchased from Bachem.

2.5.3 DKP Synthesis

2.5.3.1 Synthesis of c(D-Pro-L-Pro)

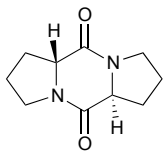

A round bottom flask was charged with L-proline benzyl ester hydrochloride salt (243 mg, 1.0 mmol) which was then partially dissolved in 5 mL of dry dichloromethane. *N*-Methylmorpholine (110 μL, 1.0 mmol, 1 eq) was added along with *N*-carboxybenzyl-D-proline (250 mg, 1.0 mmol, 1 eq) to the solution. (Benzotriazol-1-yloxy)tripyrrolidinophosphonium hexafluorophosphate, PyBOP, (570 mg, 1.1 mmol, 1.1 eq) was added to the solution and the reaction was left to stir at 25 °C under an inert argon atmosphere for 22 h. Solvent was removed under reduced pressure to give a viscous yellow oil. Upon dissolving the crude yellow oil in ethyl acetate a white precipitate was formed and this was removed via gravity filtration. Oil was purified

upon a silica column (ethyl acetate 100 %) to give benzyl-2-([2-benzyloxycarbonylpyrrodin-1-yl]carbonyl)pyrrolidine-1-carboxylate (211 mg, 0.5 mmol, 48 % Yield, Rf 0.35).

This procedure was repeated with 1 eq of PyBOP (520 mg, 1.0 mmol) to give benzyl-2-([2-benzyloxycarbonylpyrrodin-1-yl]carbonyl)pyrrolidine-1-carboxylate (135 mg, 0.3 mmol, 31 % Yield).

Both of the benzyl-2-([2-benzyloxycarbonylpyrrodin-1-yl]carbonyl)pyrrolidine-1-carboxylate were combined and dissolved in HPLC grade methanol (15 mL). Pd/C 10 % catalyst (83 mg) was added and solution was subjected to hydrogenation at 40 bar pressure for 12 h. Solution was gravity filtered three times to remove Pd/C catalyst and then solvent was evaporated off under reduced pressure to leave a white solid, 1-([pyrrodin-2-yl]carbonyl)pyrrolidine-2-carboxylic acid (179 mg, 0.8 mmol, 100 % Yield).

1-([Pyrrodin-2-yl]carbonyl)pyrrolidine-2-carboxylic acid (179 mg , 0.8 mmol) was dissolved in 5 mL of dichloromethane and thionyl chloride (70 μL, 1.0 mmol, 1.2 eq) was added dropwise and the solution was left to stir for 48 h at 25 ºC. The solvent was removed under reduced pressure to leave a light brown solid, which was dissolved again in dichloromethane and extracted with 5 % aqueous HCl solution. The organic layer was removed and concentrated under reduced pressure to leave the title compound as a light yellow solid (48 mg, 0.25 mmol, 29 % Yield [yield compared to starting reagents 15 %]). The enantiopurity of the c(D-Pro-L-Pro) was confirmed using chiral HPLC. **^{1}H NMR** (400 MHz, D_2O): δ_H 1.66-2.00 (6H, m), 2.15-2.23 (2H, m), 3.43-3.52 (2H, m), 3.88-3.98 (2H, m), 4.29-4.36 (2H, m); ***m/z*** (ES+): $[M–H]^+$ $C_{10}H_{15}N_2O_2$ requires 194.2 found 194.2. Melting Point: 188 – 190 ºC (Literature: 179 – 181 ºC).[107]

2.5.3.2 Synthesis of c(D-Pro-D-Pro)

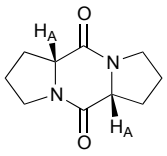

c(D-Pro-D-Pro) was prepared using an identical method to c(D-Pro-L-Pro) as detailed above, but with D-proline benzyl ester hydrochloride salt used as a starting reagent

instead. The title compound was a white solid (31 mg, 0.40 mmol, 40 % Yield [yield compared to starting reagents 12 %]). The enantiopurity of the c(D-Pro-D-Pro) was confirmed using chiral HPLC. **^{1}H NMR** (400 MHz, D_2O): δ_H 1.95-2.15 (6H, m), 2.27-2.40 (2H, m), 3.41-3.52 (2H, m), 3.55-3.63 (2H, m), 4.44-4.52 (2H, m); ***m/z*** (ES+): $[M–H]^+$ $C_{10}H_{15}N_2O_2$ requires 194.2 found 194.2.

2.5.4 Kinetic Experiments

2.5.4.1 Solution Preparation

Potassium carbonate ($KDCO_3$ / K_2CO_3) buffer solutions were prepared by dissolving solid potassium carbonate in D_2O. Deuterium chloride solution was used to adjust the percentage of free base form of the buffer. A 2 M potassium chloride solution was employed to adjust to ionic strength I = 1.0.

3-Chloroquinuclidine buffer solutions were prepared from 3-chloroquinuclidine deuterium chloride salt (prepared from 3-chloroquinuclidine hydrogen chloride salt by exchanging the hydron for a deuteron with D_2O on a freeze dryer apparatus) and a potassium deuteroxide solution. A 2 M potassium chloride solution was employed to adjust to ionic strength I = 1.0.

Tetramethylammonium deuteriosulfate and sodium trimethylsilylpropyl sulfonate internal standard solutions were prepared with D_2O and a 2 M potassium chloride solution to adjust to ionic strength I = 1.0.

2.5.4.2 Measurement of pH

The pH of the buffered solutions was determined using a MeterLab™ PHM 290 p*H*-Stat Controller equipped with a radiometer combination electrode filled with saturated KCl solution at 25 ºC. The pH meter was calibrated with pH 7 potassium phosphate and pH 12.45 saturated calcium hydroxide solutions. The p*D* values were calculated by adding 0.4 to the pH meter reading.[136] An activity coefficent for the deuteroxide ion (γ_{DO}) of 0.722 and a pK_w(D_2O) = 14.951 was used to determine the concentration of deuteroxide ion from Equation 2.21:

$$\gamma_{OH}[OD^-] = 10^{[pD - pK_{w(D_2O)}]} \qquad \text{(Equation 2.21)}$$

2.5.4.3 NMR conditions

The hydrogen deuterium exchange experiments were carried out on either a Varian 400 MHz or a Varian 500 MHz NMR spectrometer. A pulse sequence with a 20 s relaxation delay, an acquisition time of 4 s and a 90º pulse angle was employed. A total of 64 transients were taken for each spectrum (a total acquisition time of ~ 25 min 30 s). ^{1}H NMR spectral baselines were subject to a first-order drift correction before integration of the peak areas. The integration of substrate peak areas was compared to the peaks of the tetramethylammonium deuteriosulfate or sodium trimethylsilylpropyl sulfonate internal standard with an arbitrary value of 1000 for the integration of the internal standard.

2.5.5 UV-Vis Spectrophotometric determination of the tyrosyl phenolic pK_a on c(L-Pro-L-Tyr)

A 20 mM stock solution of c(L-Pro-L-Tyr) was prepared by dissolving 26.09 mg (106.8 mmol) of c(L-Pro-L-Tyr) in 5.00 mL of 9 : 1 D_2O : d_3-MeCN. Buffer solutions (KAcO/AcOH, $N(EtOD)_3/N(EtOD)_3D^+$, $KDCO_3/K_2CO_3$ and KOD) with a 9 : 1 D_2O : d_3-MeCN solvent composition were prepared over the pH range pH = 5.29 – 14.41. A solution of 2 M potassium chloride in 9 : 1 D_2O : d_3-MeCN was used to bring the ionic strength to I = 1.0 M.

All absorbance spectra were obtained on a Cary 100 UV-Vis spectrophotometer. A 1.0 mL cuvette was filled with a buffer solution and placed in the temperature regulated cuvette holder of the UV-Vis spectrophotometer. The solution was allowed to equilibrate to 25 °C prior to recording the absorbance spectrum over the wavelength range 190 – 400 nm (the UV-Vis spectrophotometer had been zeroed against air). 41 μL of the 20 mM c(L-Pro-L-Tyr) stock solution was added to the cuvette to give a 0.8 mM solution of c(L-Pro-L-Tyr) and the cuvette inverted several times to ensure good mixing. The absorbance spectrum over the wavelength range 190 – 400 nm was once again taken and the previous absorbance spectrum of the solution was manually subtracted from this to leave just the absorbance from c(L-Pro-L-Tyr). This procedure was repeated for every buffer prepared in the pH range pH = 5.29 – 14.41. The absorbance from the phenolate group was located at λ = 293 nm. The plot of the

changes in absorbance at 293 nm with pH is shown in Figure 2.25 and Equation 2.7 was used to determine the pK_a of the phenol on the tyrosyl residue.

2.6 References

(36) Borthwick, A. D. *Chem Rev* **2012**, *112*, 3641.

(37) Fischer, P. M. *J Pept Sci* **2003**, *9*, 9.

(38) Dinsmore, C. J.; Beshore, D. C. *Tetrahedron* **2002**, *58*, 3297.

(39) Fischer, E. *Ber Dtsch Chem Ges* **1906**, *39*, 2893.

(40) Nitecki, D. E.; Halpern, B.; Westley, J. W. *J Org Chem* **1968**, *33*, 864.

(41) Izumiya, N.; Lee, S.; Kanmera, T.; Aoyagi, H. *J Am Chem Soc* **1977**, *99*, 8346.

(42) Woodard, R. W. *J Org Chem* **1985**, *50*, 4796.

(43) Eriksson, J.; Arvidsson, P. I.; Davidsson, O. *Chem-Eur J* **1999**, *5*, 2356.

(44) Ueda, T.; Saito, M.; Kato, T.; Izumiya, N. *B Chem Soc Jpn* **1983**, *56*, 568.

(45) Iyer, M. S.; Lipton, M. A. *Bioorg Med Chem Lett* **1993**, *3*, 2061.

(46) Hendea, D.; Laschat, S.; Baro, A.; Frey, W. *Helv Chim Acta* **2006**, *89*, 1894.

(47) Le, T. X. H.; Bussolari, J. C.; Murray, W. V. *Tetrahedron Lett* **1997**, *38*, 3849.

(48) Bull, S. D.; Davies, S. G.; Epstein, S. W.; Ouzman, J. V. A. *Tetrahedron-Asymmetry* **1998**, *9*, 2795.

(49) Saleki, M.; Colgin, N.; Kirby, J. A.; Cobb, S. L.; Ali, S. *MedChemComm* **2013**, *4*, 860.

(50) Tullberg, M.; Grotli, M.; Luthman, K. *Tetrahedron* **2006**, *62*, 7484.

(51) Tullberg, M.; Grotli, M.; Luthman, K. *J Org Chem* **2007**, *72*, 195.

(52) Santagada, V.; Fiorino, F.; Perissutti, E.; Severino, B.; Terracciano, S.; Cirino, G.; Caliendo, G. *Tetrahedron Lett* **2003**, *44*, 1145.

(53) Daly, W. H.; Poche, D. *Tetrahedron Lett* **1988**, *29*, 5859.

(54) Rosenmund, P.; Kaiser, K. *Angew Chemie Int Ed* **1970**, *9*, 162

(55) Schollkopf, U.; Groth, U.; Westphalen, K. O.; Deng, C. *Synthesis-Stuttgart* **1981**, 969.

(56) Schollkopf, U. *Tetrahedron* **1983**, *39*, 2085.

(57) Oya, M.; Katakai, R.; Nakai, H.; Iwakura, Y. *Chem Lett* **1973**, 1143.

(58) Gonzalez, A.; Vorobeva, S. L.; Linares, A. *Tetrahedron-Asymmetry* **1995**, *6*, 1357.

(59) O'Neill, J. C.; Blackwell, H. E. *Comb Chem High T Scr* **2007**, *10*, 857.

(60) Fridkin, M.; Patchorn, A.; Katchals, E. *J Am Chem Soc* **1965**, *87*, 4646.

(61) Gisin, B. F.; Merrifield, R. B. *J Am Chem Soc* **1972**, *94*, 3102.

(62) Suzuki, K.; Sasaki, Y.; Endo, N.; Mihara, Y. *Chem Pharm Bull* **1981**, *29*, 233.

(63) Kowalski, J.; Lipton, M. A. *Tetrahedron Lett* **1996**, *37*, 5839.

(64) Flanigan, E.; Marshall, G. R. *Tetrahedron Lett* **1970**, 2403.

(65) Ramachandran, G. N.; Mitra, A. K. *J Mol Biol* **1976**, *107*, 85.

(66) Li, Y.; Garrell, R. L.; Houk, K. N. *J Am Chem Soc* **1991**, *113*, 5895.

(67) Gordon, D. W.; Steele, J. *Bioorg Med Chem Lett* **1995**, *5*, 47.

(68) Szardenings, A. K.; Burkoth, T. S.; Lu, H. H.; Tien, D. W.; Campbell, D. A. *Tetrahedron* **1997**, *53*, 6573.

(69) Szardenings, A. K.; Harris, D.; Lam, S.; Shi, L. H.; Tien, D.; Wang, Y. W.; Patel, D. V.; Navre, M.; Campbell, D. A. *J Med Chem* **1998**, *41*, 2194.

(70) Szardenings, A. K.; Antonenko, V.; Campbell, D. A.; DeFrancisco, N.; Ida, S.; Shi, L. H.; Sharkov, N.; Tien, D.; Wang, Y. W.; Navre, M. *J Med Chem* **1999**, *42*, 1348.

(71) Guo, T.; Adang, A. E. P.; Dong, G.; Fitzpatrick, D.; Geng, P.; Ho, K. K.; Jibilian, C. H.; Kultgen, S. G.; Liu, R. Y.; McDonald, E.; Saionz, K. W.; Valenzano, K. J.; van Straten, N. C. R.; Xie, D.; Webb, M. L. *Bioorg Med Chem Lett* **2004**, *14*, 1717.

(72) Jensen, K. J.; Alsina, J.; Songster, M. F.; Vagner, J.; Albericio, F.; Barany, G. *J Am Chem Soc* **1998**, *120*, 5441.

(73) del Fresno, M.; Alsina, J.; Royo, M.; Barany, G.; Albericio, F. *Tetrahedron Lett* **1998**, *39*, 2639.

(74) del Fresno, M.; Fernandez-Forner, D. B.; Miralpeix, M.; Segarra, V.; Ryder, H.; Royo, M.; Albericio, F. *Bioorg Med Chem Lett* **2005**, *15*, 1659.

(75) Domling, A.; Ugi, I. *Angew Chem Int Ed* **2000**, *39*, 3168.

(76) Hulme, C.; Peng, J.; Morton, G.; Salvino, J. M.; Herpin, T.; Labaudiniere, R. *Tetrahedron Lett* **1998**, *39*, 7227.

(77) Wyatt, P. G.; Allen, M. J.; Borthwick, A. D.; Davies, D. E.; Exall, A. M.; Hatley, R. J. D.; Irving, W. R.; Livermore, D. G.; Miller, N. D.; Nerozzi, F.; Sollis, S. L.; Szardenings, A. K. *Bioorg Med Chem Lett* **2005**, *15*, 2579.

(78) Lin, Q.; Blackwell, H. E. *Chem Commun* **2006**, 2884.

(79) Bowman, M. D.; Jeske, R. C.; Blackwell, H. E. *Org Lett* **2004**, *6*, 2019.

(80) Cho, S.; Keum, G.; Kang, S. B.; Han, S. Y.; Kim, Y. *Mol Divers* **2003**, *6*, 283.

(81) Capasso, S.; Vergara, A.; Mazzarella, L. *J Am Chem Soc* **1998**, *120*, 1990.

(82) Goolcharran, C.; Borchardt, R. T. *J Pharm Sci* **1998**, *87*, 283.

(83) Guenoun, F.; Zair, T.; Lamaty, F.; Pierrot, M.; Lazaro, R.; Viallefont, P. *Tetrahedron Lett* **1997**, *38*, 1563.

(84) Somei, M.; Hamamoto, S.; Nakagawa, K.; Yamada, F.; Ohta, T. *Heterocycles* **1994**, *37*, 719.

(85) Caballero, E.; Avendano, C.; Menendez, C. *Tetrahedron-Asymmetry* **1998**, *9*, 967.

(86) Oba, M.; Nakajima, S.; Nishiyama, K. *Chem Commun* **1996**, 1875.

(87) Oba, M.; Terauchi, T.; Owari, Y.; Imai, Y.; Motoyama, I.; Nishiyama, K. *J Chem Soc Perk Trans 1* **1998**, 1275.

(88) Bull, S. D.; Davies, S. G.; Parkin, R. M.; Sanchez-Sancho, F. *J Chem Soc Perk T 1* **1998**, 2313.

(89) Bull, S. D.; Davies, S. G.; Garner, A. C.; Parkes, A. L.; Roberts, P. M.; Sellers, T. G. R.; Smith, A. D.; Tamayo, J. A.; Thomson, J. E.; Vickers, R. J. *New J Chem* **2007**, *31*, 486.

(90) Bull, S. D.; Davies, S. G.; Garner, A. C.; Savory, E. D.; Snow, E. J.; Smith, A. D. *Tetrahedron-Asymmetry* **2004**, *15*, 3989.

(91) Davies, S. G.; Rodriguez-Sola, H.; Tamayo, J. A.; Cowley, A. R.; Concellon, C.; Garner, A. C.; Parkes, A. L.; Smith, A. D. *Org Biomol Chem* **2005**, *3*, 1435.

(92) Bull, S. D.; Davies, S. G.; Epstein, S. W.; Garner, A. C.; Mujtaba, N.; Roberts, P. M.; Savory, E. D.; Smith, A. D.; Tamayo, J. A.; Watkin, D. J. *Tetrahedron* **2006**, *62*, 7911.

(93) Davies, S. G.; Garner, A. C.; Ouzman, J. V. A.; Roberts, P. M.; Smith, A. D.; Snow, E. J.; Thomson, J. E.; Tamayo, J. A.; Vickers, R. J. *Org Biomol Chem* **2007**, *5*, 2138.

(94) Balducci, D.; Lazzari, I.; Monari, M.; Piccinelli, F.; Porzi, G. *Amino Acids* **2010**, *38*, 829.

(95) Zhao, S.; Smith, K. S.; Deveau, A. M.; Dieckhaus, C. M.; Johnson, M. A.; Macdonald, T. L.; Cook, J. M. *J Med Chem* **2002**, *45*, 1559.

(96) van Loevezijn, A.; Allen, J. D.; Schinkel, A. H.; Koomen, G. J. *Bioorg Med Chem Lett* **2001**, *11*, 29.

(97) Kanzaki, H.; Yanagisawa, S.; Nitoda, T. *Biosci Biotech Bioch* **2004**, *68*, 2341.

(98) Brogan, A. P.; Widger, W. R.; Bensadek, D.; Riba-Garcia, I.; Gaskell, S. J.; Kohn, H. *J Am Chem Soc* **2005**, *127*, 2741.

(99) Park, D. K.; Lee, K. E.; Baek, C. H.; Kim, I. H.; Kwon, J. H.; Lee, W. K.; Lee, K. H.; Kim, B. S.; Choi, S. H.; Kim, K. S. *J Bacteriol* **2006**, *188*, 2214.

(100) Izumida, H.; Nishijima, M.; Takadera, T.; Nomoto, A. M.; Sano, H. *J Antibiot* **1996**, *49*, 829.

(101) Oku, J. I.; Inoue, S. *J Chem Soc Chem Comm* **1981**, 229.

(102) Iyer, M. S.; Gigstad, K. M.; Namdev, N. D.; Lipton, M. *J Am Chem Soc* **1996**, *118*, 4910.

(103) Kienle, M.; Argyrakis, W.; Baro, A.; Laschat, S. *Tetrahedron Lett* **2008**, *49*, 1971.

(104) Karle, I. L. *J Am Chem Soc* **1972**, *94*, 81.

(105) Eguchi, C.; Kakuta, A. *J Am Chem Soc* **1974**, *96*, 3985.

(106) Madison, V.; Young, P. E.; Blout, E. R. *J Am Chem Soc* **1976**, *98*, 5358.

(107) Young, P. E.; Madison, V.; Blout, E. R. *J Am Chem Soc* **1976**, *98*, 5365.

(108) Young, P. E.; Madison, V.; Blout, E. R. *J Am Chem Soc* **1973**, *95*, 6142.

(109) Bour, P.; Sychrovsky, V.; Malon, P.; Hanzlikova, J.; Baumruk, V.; Pospisek, J.; Budesinsky, M. *J Phys Chem A* **2002**, *106*, 7321.

(110) Carlson, K. L.; Lowe, S. L.; Hoffmann, M. R.; Thomasson, K. A. *J Phys Chem A* **2006**, *110*, 1925.

(111) Carlson, K. L.; Lowe, S. L.; Hoffmann, M. R.; Thomasson, K. A. *J Phys Chem A* **2005**, *109*, 5463.

(112) Rios, A.; Amyes, T. L.; Richard, J. P. *J Am Chem Soc* **2000**, *122*, 9373.

(113) Rios, A.; Richard, J. P.; Amyes, T. L. *J Am Chem Soc* **2002**, *124*, 8251.

(114) Williams, G.; Maziarz, E. P.; Amyes, T. L.; Wood, T. D.; Richard, J. P. *Biochemistry* **2003**, *42*, 8354.

(115) Ho, J. M.; Easton, C. J.; Coote, M. L. *J Am Chem Soc* **2010**, *132*, 5515.

(116) Ho, J.; Coote, M. L.; Easton, C. J. *J Org Chem* **2011**, *76*, 5907.

(117) Forsyth, W. R.; Robertson, A. D. *J Am Chem Soc* **1996**, *118*, 11337.

(118) Perrin, C. L.; Johnston, E. R.; Lollo, C. P.; Kobrin, P. A. *J Am Chem Soc* **1981**, *103*, 4691.

(119) Molday, R. S.; Kallen, R. G. *J Am Chem Soc* **1972**, *94*, 6739.

(120) Gaussian 09, F., M. J.; Trucks, G. W.; Schlegel, H. B.; Scuseria, G. E.; Robb, M. A.; Cheeseman, J. R.; Scalmani, G.; Barone, V.; Mennucci, B.; Petersson, G. A.; Nakatsuji, H.; Caricato, M.; Li, X.; Hratchian, H. P.; Izmaylov, A. F.; Bloino, J.; Zheng, G.; Sonnenberg, J. L.; Hada, M.; Ehara, M.; Toyota, K.; Fukuda, R.; Hasegawa, J.; Ishida, M.; Nakajima, T.; Honda, Y.; Kitao, O.; Nakai, H.; Vreven, T.; Montgomery, J. A., Jr.; Peralta, J. E.; Ogliaro, F.; Bearpark, M.; Heyd, J. J.; Brothers, E.; Kudin, K. N.; Staroverov, V. N.; Kobayashi, R.; Normand, J.; Raghavachari, K.; Rendell, A.; Burant, J. C.; Iyengar, S. S.; Tomasi, J.; Cossi, M.;

Rega, N.; Millam, J. M.; Klene, M.; Knox, J. E.; Cross, J. B.; Bakken, V.; Adamo, C.; Jaramillo, J.; Gomperts, R.; Stratmann, R. E.; Yazyev, O.; Austin, A. J.; Cammi, R.; Pomelli, C.; Ochterski, J. W.; Martin, R. L.; Morokuma, K.; Zakrzewski, V. G.; Voth, G. A.; Salvador, P.; Dannenberg, J. J.; Dapprich, S.; Daniels, A. D.; Farkas, Ö.; Foresman, J. B.; Ortiz, J. V.; Cioslowski, J.; Fox, D. J. Gaussian, Inc., Wallingford CT, 2009.

(121) Amyes, T. L.; Richard, J. P. *J Am Chem Soc* **1996**, *118*, 3129.

(122) Giese, K.; Kaatze, U.; Pottel, R. *J Phys Chem* **1970**, *74*, 3718.

(123) Kaatze, U. *J Chem Eng Data* **1989**, *34*, 371.

(124) Kaatze, U.; Pottel, R.; Schumacher, A. *J Phys Chem* **1992**, *96*, 6017.

(125) Marcus, R. A. *J Phys Chem-Us* **1968**, *72*, 891.

(126) Cohen, A. O.; Marcus, R. A. *J Phys Chem* **1968**, *72*, 4249.

(127) Eliot, A. C.; Kirsch, J. F. *Annu Rev Biochem* **2004**, *73*, 383.

(128) Heck, S. D.; Siok, C. J.; Kelbaugh, P. R.; Thadeio, P. F.; Welch, M. J.; Williams, R. D.; Ganong, A. H.; Kelly, M. E.; Lanzetti, A. J.; Phillips, D.; Ahlijanian, M. K. *Science* **1994**, *266*, 1464.

(129) Heck, S. D.; Faraci, W. S.; Kelbaugh, P. R.; Saccomano, N. A.; Thadeio, P. F.; Volkmann, R. A. *P Natl Acad Sci USA* **1996**, *93*, 4036.

(130) Dunathan, H. C. *P Natl Acad Sci USA* **1966**, *55*, 712.

(131) Kirsch, J. F.; Eichele, G.; Ford, G. C.; Vincent, M. G.; Jansonius, J. N.; Gehring, H.; Christen, P. *J Mol Biol* **1984**, *174*, 497.

(132) Albery, W. J.; Knowles, J. R. *Biochemistry-Us* **1986**, *25*, 2572.

(133) Tanner, M. E. K., G. L. *Comprehensive Biological Catalysis*; Academic Press: San Diego, 1998; Vol. 2.

(134) Toth, K.; Amyes, T. L.; Wood, B. M.; Chan, K.; Gerlt, J. A.; Richard, J. P. *J Am Chem Soc* **2007**, *129*, 12946.

(135) Richard, J. P.; Amyes, T. L.; Crugeiras, J.; Rios, A. *Bba-Proteins Proteom* **2011**, *1814*, 1419.

(136) Glasoe, P. K.; Long, F. A. *J Phys Chem* **1960**, *64*, 188.

(278) Schoenebeck, F.; Houk, K. N. *J. Org. Chem.* **2009**, *74*, 1464 – 1472.

3 Carbon Acidity of Triketopiperazines

3.0 Foreword

This chapter describes investigations of the carbon acidity of triketopiperazine systems. Section 3.1 overviews previous research relating to triketopiperazines including their synthesis and applications. Section 3.2 describes the results of kinetic studies of the carbon acidity of diketopiperazines. The determination of the second order rate constants for buffer catalysed exchange, k_{A^-} (M^{-1} s^{-1}), and the second order rate constants for deuteroxide catalysed exchange, k_{DO} (M^{-1} s^{-1}), via hydrogen deuterium exchange experiments are detailed in Section 3.2. The results are discussed in Section 3.3 and conclusions presented in Section 3.4. Experimental details are found in Section 3.5.

3.1 Introduction:

3.1.1 Triketopiperazines

Triketopiperazines (TKPs) are masked amino acids similar in structure to diketopiperazines but with an imidic carbonyl at the C2 position instead of a second amino acid (Scheme 3.1). Whilst TKPs have been known since 1917, they have received little attention due to the instability of the TKP ring, which is prone to hydrolysis (at the C2 imidic carbonyl) unless isolated in dry conditions or in strongly acidic solutions. More recently TKPs have shown synthetic potential for creating unusual moieties found in natural products and for enantioselective Michael additions to create complex cyclic carbon skeletons. The following introduction will describe the various synthetic approaches that have been employed to prepare TKPs and the most recent applications of TKPs in synthesis.

Scheme 3.1: Base structure of Triketopiperazines (TKPs).

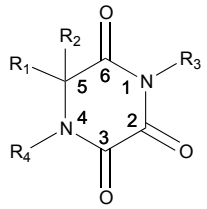

3.1.2 Synthesis of Triketopiperazines

Bornwater first reported the synthesis of a phenylalanine-based TKP in 1917 by reacting phenylalanine amide with oxalyl chloride (Scheme 3.2).[137]

Scheme 3.2: Bornwater synthesis of phenylalanine-based TKP.[137]

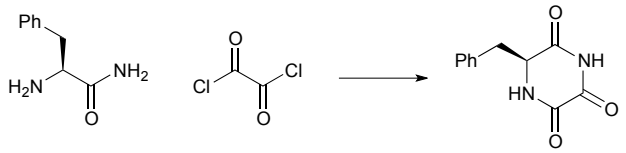

Later, Safir in the search for other barbituric acid drug like molecules obtained the phenylalanine TKP from the sodium methoxide catalysed reaction of phenylalanine

amide with oxalyl ethyl ester (Scheme 3.3).[138] [xxiii] While the reaction gave reasonable yields, ~ 60 %, the sodium salts obtained were prone to hydrolysis when placed in any aqueous solution that was not strongly acidic.

Scheme 3.3: Safir synthesis of phenylalanine TKP.[138]

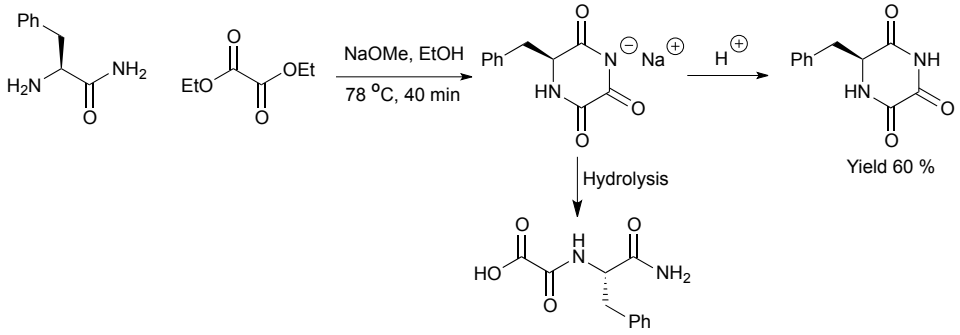

A more unusual TKP synthesis has been achieved by Makino *et al* who used a solid phase resin to construct the TKP ring (Scheme 3.4).[139] The TKP was built starting from a secondary amine group on the support onto which 4-nitrophenylacetic acid was added via DIC catalysed amide bond formation. Reduction of the nitro group to aniline allowed a subsequent amide bond to be formed with an amino acid. When the Fmoc amine on the amino acid was deprotected the TKP ring was formed via reaction with oxalyl diimidazole. A combinatorial library of TKPs was then created by replacing the naphthalene ring with various heterocycles and altering the identity of the Fmoc protected amino acid.

Makino noted that cyclisation to the TKP ring proceeded best when the terminal amine of the amino acid was alkylated (R_2 = alkyl). Alkylation increases the *cis* conformation of the amide bond and places the imidazole ester into a favourable position for a cyclisation reaction with the internal amide nitrogen. Semi-empirical computational studies on these TKP rings suggested that the most stable conformation of the TKP ring occurs when a planar structure is formed. If another ring was fused to the TKP as in the case of proline, where the pyrrolidine ring is fused at C5 and N4, then this prevents the TKP adopting a planar structure. Deformations to the planarity of the 2,3-diketo moiety were particularly destabilising.

[xxiii] Safir was unable to reproduce Bornwater's reaction.

Scheme 3.4: Solid phase synthesis of TKP by Makino.[139]

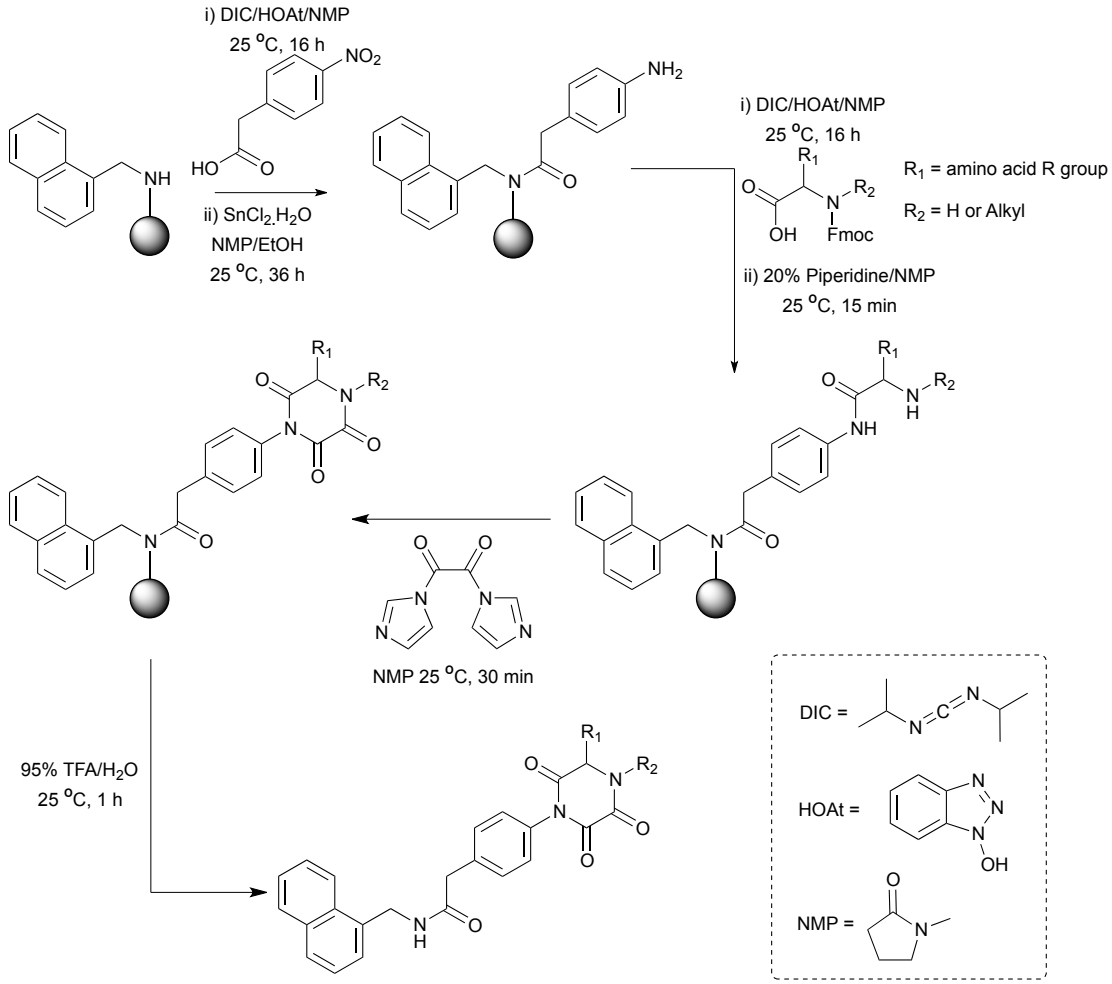

TKP rings are found in a number of natural products that exhibit pharmacological properties including Gliocladin C,[140] dithiosecoemestrin[141] and neoechinulin E[142,143] (Scheme 3.5). Gliocaldin C is a hexahydropyrroloindoline alkaloid, which has been found to be cytotoxic to leukemia cells and has been targeted by a number of groups as a scaffold for the construction of other C3–C3' indole alkaloids.

Scheme 3.5: Natural products containing TKP rings.[140-143]

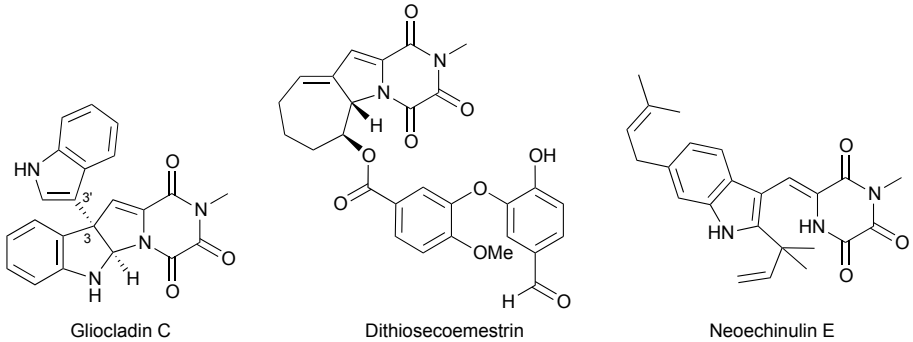

Gliocladin C Dithiosecoemestrin Neoechinulin E

Overman first reported the synthesis of Gliocladin C starting from oxindole and with the formation of the TKP ring in the final step (Scheme 3.6).[144] The pyrrolidine ring forms an amide bond with ethyl oxalyl chloride and subsequent cyclisation via the secondary amide nitrogen in the presence of hexamethyldisilazane (HMDS) yields the TKP.

Scheme 3.6: Synthesis of TKP ring in Gliocladin C by Overman.[144]

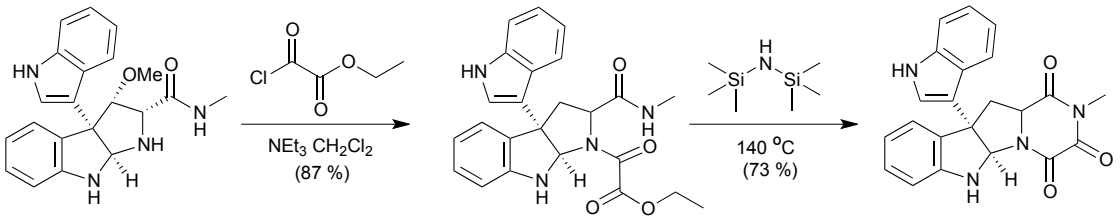

Overman has reported a second synthesis of Gliocladin C in which a TKP ring is initially formed from an amino acid amide and oxalyl diimidazole, akin to Makino, but is then masked as an iminoyl methyl ester by trimethyloxonium tetrafluoroborate in order to prevent ring opening (Scheme 3.7).[145] The TKP ring is then revealed in the final step of the reaction during the formation of the pyrrolidine ring in Gliocladin C.

Scheme 3.7: Overman's second synthesis of Gliocladin C using a masked TKP ring.[145]

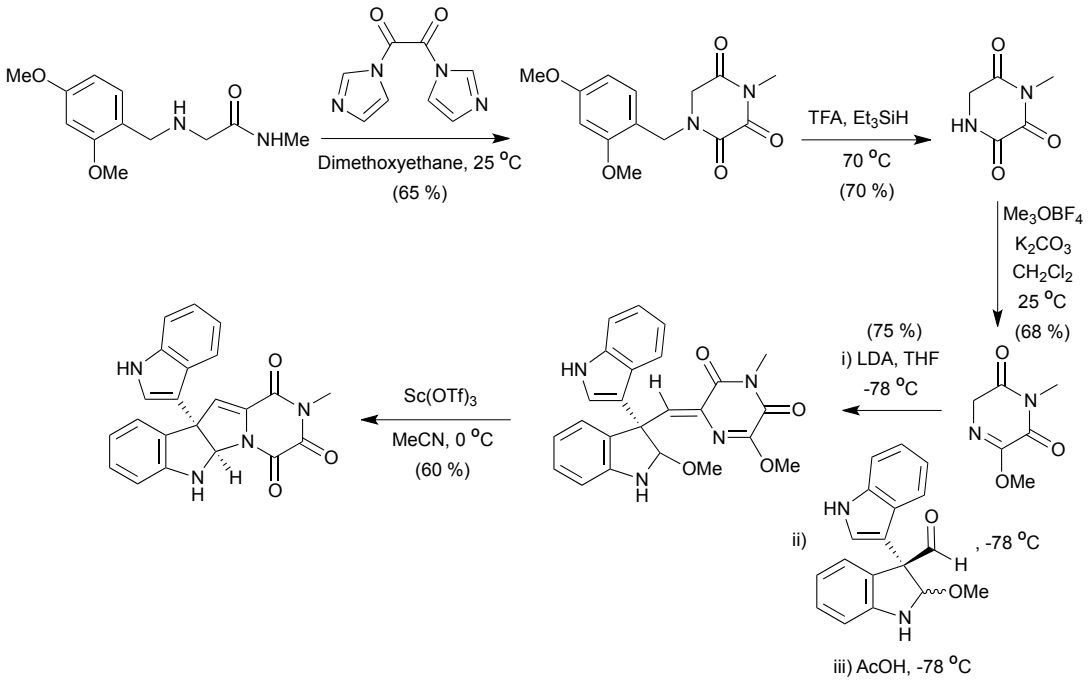

Stephenson *et al* have reported a 10-step route to Gliocladin C starting from a commercially available tryptophan methyl ester.[146] The TKP ring formation is shown in Scheme 3.8 and involves the initial formation of an imine via reaction of the amine with *N*-bromosuccinimide followed by elimination of HBr. The imine is then reacted with ethyl oxalyl chloride that subsequently cyclises with the secondary amide in a microwave procedure.

Scheme 3.8: Synthesis of TKP ring in Stephenson route to Gliocladin C.[146]

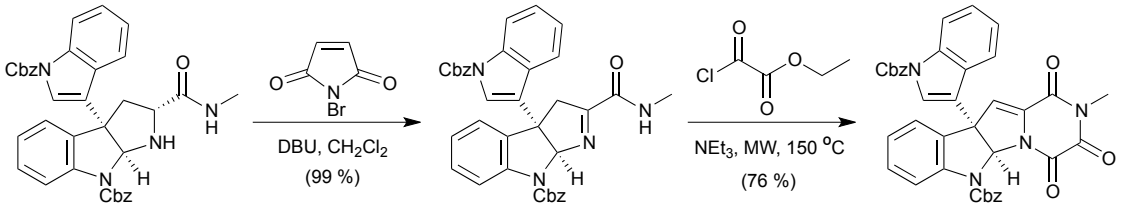

Movassaghi has developed a synthesis of Gliocladin C that starts from a diketopiperazine diol (Scheme 3.9).[147] One hydroxyl group is first dehydrated and then the second is oxidised to the carbonyl by 2-iodoxybenzoic acid.

Scheme 3.9: Gliocladin C synthesis from a DKP diol by Movassaghi.[147]

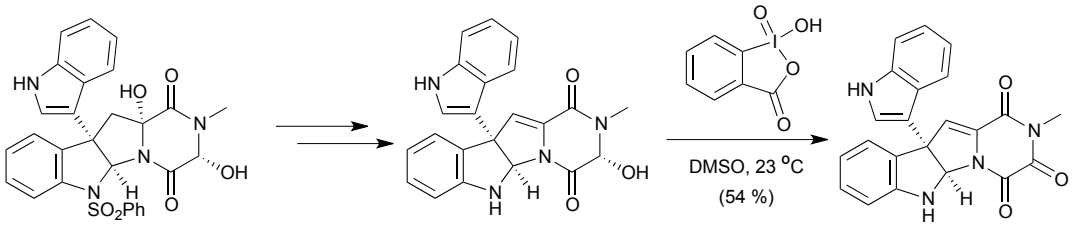

3.1.3 Applications of TKPs

3.1.3.1 Natural Product and Drug Synthesis

TKPs are particularly important in the synthesis of epidithiodioxopiperazines – a class of fungal metabolites that have potency against a variety of cancer cells (Scheme 3.10).[148,149] The biological activity of epidithiodioxopiperazines arises from the disulfide-bridged diketopiperazine fragment.[150] A TKP ring is the base structure from which this fragment may be constructed whereby the C2 and C5 positions are stereoselectively thiolated and then oxidised to give the epidithiodioxopiperazine.[145]

Scheme 3.10: Use of TKPs in the synthesis of the natural product Epidithiodioxopiperazine.[148,149]

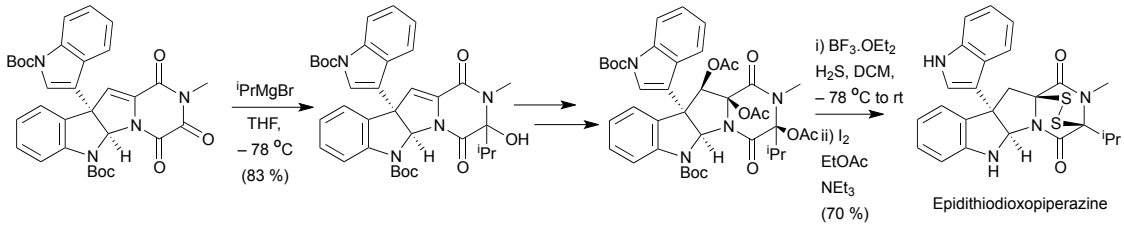

3.1.3.2 TKPs in Organic Synthesis

Boa has studied how TKPs react with various alkylating agents with the intention of alkylating exclusively on the N1 position (Scheme 3.11).[151] The results varied significantly depending upon the identity of the base and alkylating agent used. In the presence of a strong base, such as sodium hydride, and methyl iodide, methylation successfully occurred at the N1 position (Scheme 3.11a). Using methyl bromoacetate as the alkylating agent gave the expected mono-alkylated N1 product and a minor amount of the bis-alkylated product via alkylation at the C5 position (Scheme 3.11b).

An attempt to solely get the mono-alkylated product by using the weaker base, potassium carbonate, failed and in the presence of two equivalents of methyl bromoacetate only the bis-alkylated product was formed (Scheme 3.11c). In a subsequent study by Boa, no alkylation occurred with non-activated alkyl halides, e.g. methyl iodide, when potassium carbonate instead of sodium hydride was used as a base (Scheme 3.11d).[152] In order for alkylation to occur with less reactive electrophiles the anion must have a sufficiently long lifetime for the reaction to occur. In the case of sodium hydride the anion is irreversibly formed, as the proton is lost via evolution of hydrogen. However, for potassium carbonate the reverse protonation of the anion can occur, which prevents alkylation.

Scheme 3.11: Alkylation of TKPs by Boa.[151]

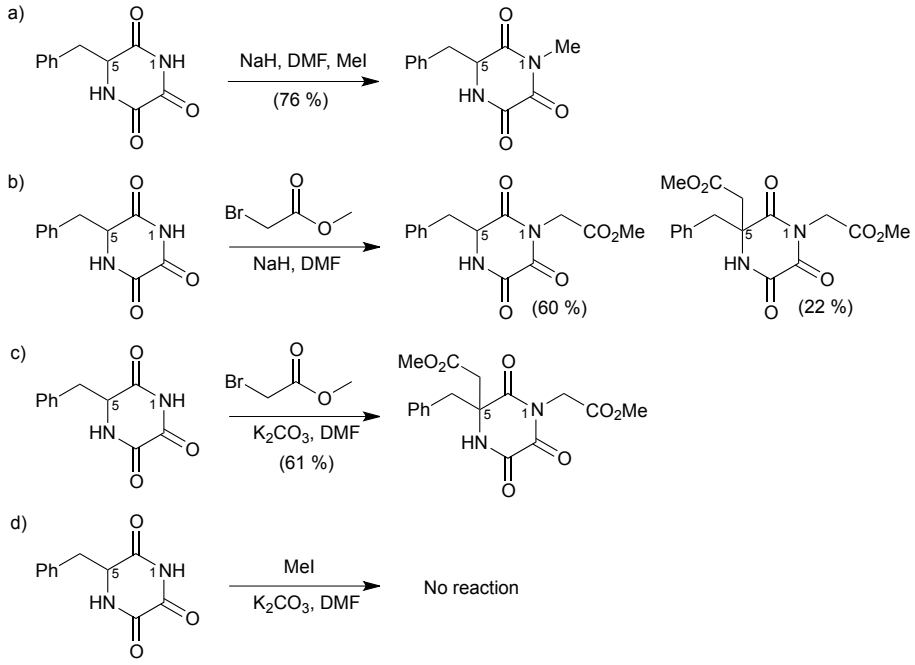

These results suggest a relatively high acidity of the TKP C5 proton relative to other carbon acids, as potassium carbonate was sufficiently basic to enable quantitative alkylation, whilst no alkylation is observed at N4. Boa has theorised that the higher acidity of the C5 proton is due to the formation of an aromatic enolate intermediate (Scheme 3.12). However, attempts to trap this intermediate with trimethylsilyl chloride (TMS-Cl) failed.

Scheme 3.12: Theorised aromatic enolate intermediate of the TKP and trapping attempt with TMS-Cl.

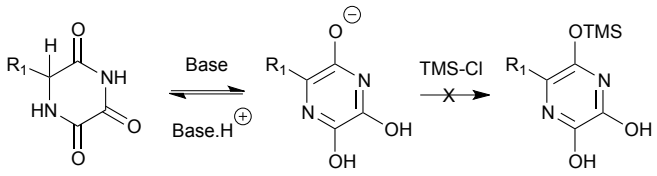

Simpkins *et al* have used TKPs in Michael addition reactions to access various natural product motifs.[153] Bifunctional cinchona alkaloid based catalysts had previously been shown to enantioselectively catalyse Michael additions and were successfully applied to the reaction of TKPs and enone Michael acceptors (Scheme 3.13).[154,155]

Scheme 3.13: Michael additions with TKP donors and enone acceptors catalysed by bifunctional cinchona alkaloid catalysts.[153]

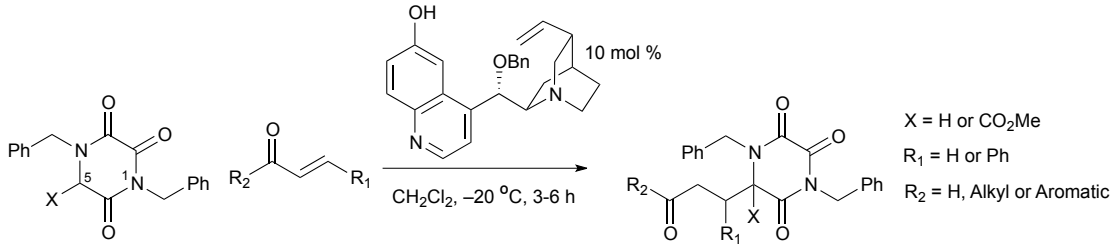

The reaction of the doubly activated TKP X = CO_2Me, with a variety of enones gave good yields (> 87 %) and excellent enantioselectivities (er > 96 %) at the C5 position on the TKP ring (Scheme 3.13). Upon switching to a glycine based TKP (X = H) the yields (> 80 %) and enantioselectivities (er > 88 %) decreased modestly. The lower enantioselectivity for the glycine TKP was attributed to a scrambling reaction between the product and the catalyst upon deprotonation at the C5 position. X-Ray crystallography revealed that the (*S*)-configuration at the C5 position on the TKP ring was favoured.

Simpkins *et al* have proposed that the enantioselectivity exhibited by these reactions arises from a network of hydrogen bonds formed between the catalyst and the reactants (Scheme 3.14).[153] The catalyst straddles both the reactants with the protonated quinuclidine amine stabilising the formation of the enolate (the quinuclidine in a previous step having removed the proton from the α-carbon of the TKP) and the hydroxyl on the quinoline stabilising the formation of the oxygen anion on the enone acceptor. The chiral centre in the middle of the bifunctional catalyst allows for the reactants to be arranged in a manner such that only one enantiomer of the product is formed. The use of TKPs as donors in Michael additions is unusual as it is a rare example of an amidic-based donor.[156] The large activation energy required to disrupt the conjugation in the amide normally precludes the use of amide enolates in synthesis.

Scheme 3.14: Proposed model for the interaction between the cinchona alkaloid catalyst and reactants.[153] Used with permission from the RSC.

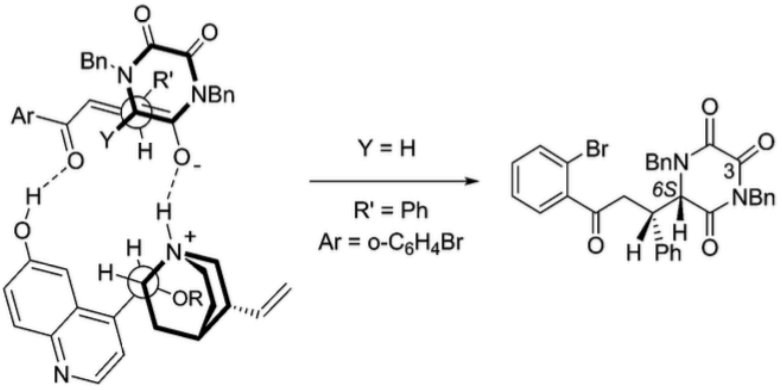

The chemistry of the TKP Michael additions was extended to a variety of other Michael acceptors including vinyl sulfone, acrylonitrile and acrylate esters. The products of the Michael additions were used to access a variety of different DKP-based natural product motifs including a bridged ether DKP (Scheme 3.15) and a neat one pot cascade reaction to form a bicyclo[2.2.2]diazaoctane DKP structure that proceeded with excellent diastereoselectivity despite the need to form three new stereogenic centres (Scheme 3.16).

Scheme 3.15: Bridged ether DKP synthesis based upon TKP Michael addition product.

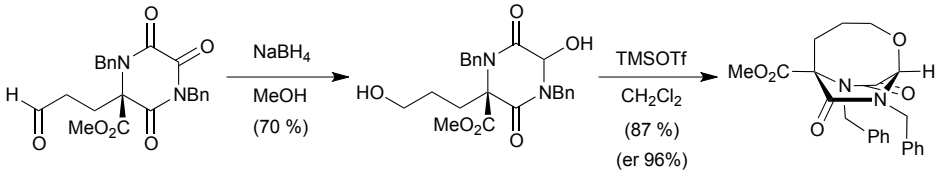

Scheme 3.16: Bicyclo[2.2.2]diazaoctane DKP synthesis.[153]

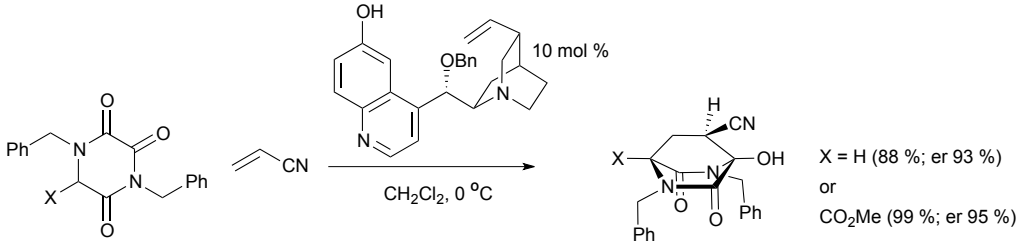

3.2 Results

The aforementioned synthetic work by Simpkins and Boa highlighted that the C5 proton(s) in a TKP ring are considerably more acidic and prone to enolate formation than normal neutral α-carbonyl carbon acids. In this work we probe the kinetic acidity (k_{HO}, M^{-1} s^{-1}) of the C5 proton(s) using a Glycyl (Gly) **10** TKP and a Prolyl (Pro) **11** TKP (Scheme 3.17). We are grateful to the Simpkins' group for the preparation and donation of TKPs **10** and **11**. Preliminary work by Taylor indicated kinetic acidities of $k_{HO} \sim 10^4 - 10^5$ M^{-1} s^{-1}, which are 6 – 7 orders of magnitude higher than for the most acidic DKP.[157] A more thorough investigation was required to confirm these estimations. Kinetic acidity was measured using H / D exchange reactions akin to those detailed in Chapter 2 for studies on DKPs.

Scheme 3.17: Glycyl (**10**) and prolyl (**11**) TKP studied.

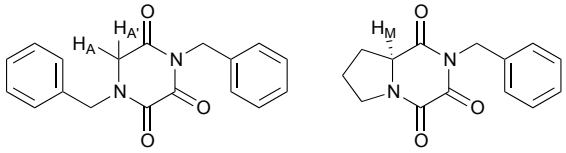

3.2.1 Deuterium exchange reactions of TKPs followed by ^{1}H NMR spectroscopy

The deuterium exchange reactions for a Glycyl TKP **10** and a Prolyl TKP **11** were monitored by ^{1}H NMR spectroscopy in buffered potassium acetate solutions in D_2O. Owing to the poor solubility of **10** and **11** in D_2O, deuterated acetonitrile (d_3-MeCN) was employed as a co-solvent (40 % v/v). Exchange reactions were monitored in a thermostated 500 MHz NMR spectrometer at 25 ºC. The ionic strength was maintained at $I = 0.06$ for **10** and $I = 0.2$ for **11** with the lower ionic strength for **10** due its lower solubility. Due to low quantities of **10** and **11** available for study, exchange reactions were monitored in sealed NMR tubes rather than sampling larger reaction volumes. From these data, observed first order rate constants for deuterium exchange, k_{ex} (s^{-1}), second order rate constants for buffer catalysed exchange, k_{A-} (M^{-1} s^{-1}), and second order rate constants for deuteroxide catalysed exchange, k_{DO} (M^{-1} s^{-1}), were

determined. Due to the lability of the C5-proton towards deuterium exchange, these reactions were conducted at relatively low p*D* values (pD 4.76 – 6.29). By contrast, corresponding DKP exchange reactions were monitored at p*D* 9.35 – 10.98.

The deuterium exchange reaction may be either acid or base catalysed;[xxiv] both routes are shown in Scheme 3.18. The microscopic rate constants in Scheme 3.18 are: k_p^a is for deprotonation of the cationic intermediate **10-HD** by D_2O, k_{-p}^a is for reprotonation of the enol to give **10-HD** by HOD_2^+, k_p is for deprotonation of **10** by DO^-, k_{-p} is for reprotonation of the enolate by HOD, k_{reorg} is for solvent reorganisation of a HOD molecule and k_g is the rate constant for the facilitated diffusion via the Grotthuss mechanism of proton transfer.[158] Both routes are irreversible as the H^+ is diluted substantially in bulk solvent. For the analogous buffer catalysed routes, D_3O^+ and DO^- may be replaced by the general acids and bases, DA and A^-, respectively.

[xxiv] Solvent catalysed exchange is omitted here because it was negligible for the TKPs **10** and **11** (Section 3.2.3 and Section 3.2.5).

Scheme 3.18: a) Acid and b) base catalysed routes for deuterium exchange reactions involving **10**. X = H or D.

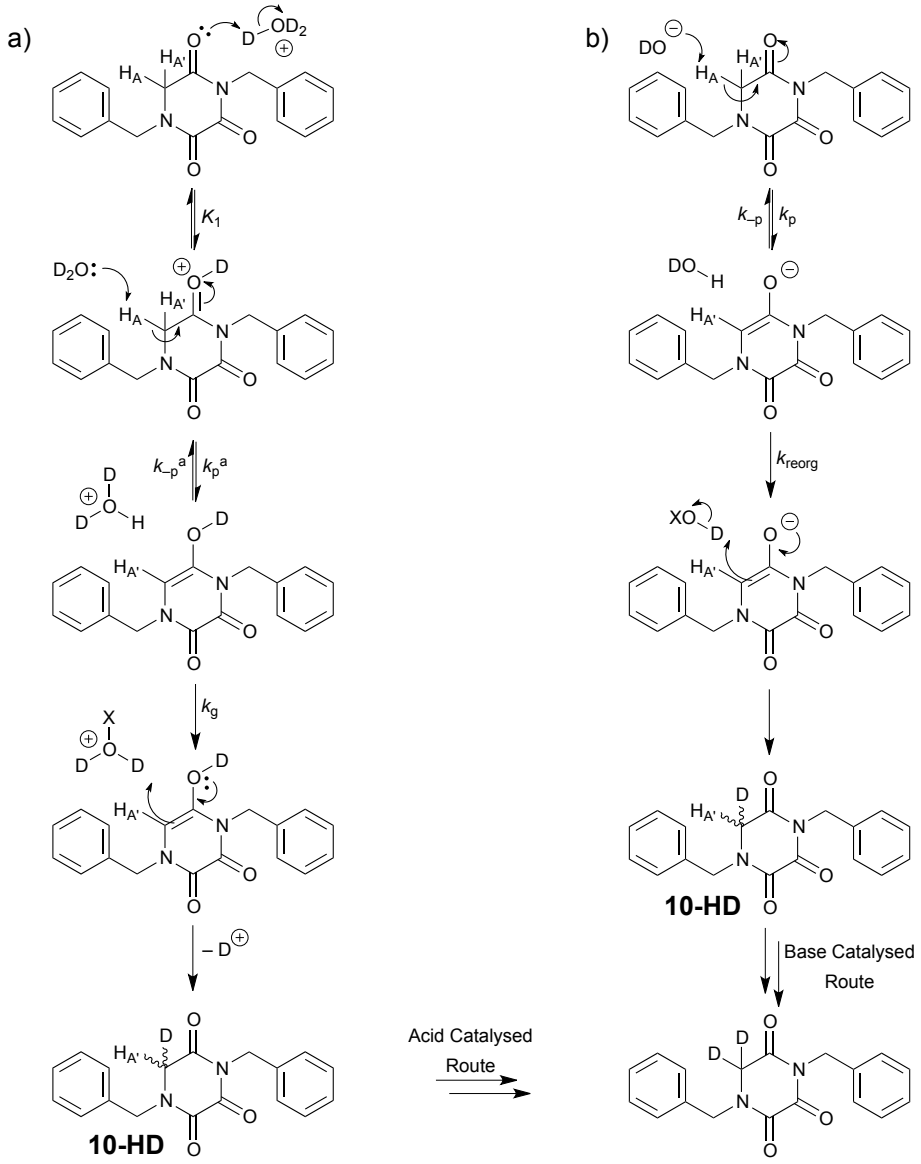

These microscopic rate constants contribute to the observed first order rate constant for deuterium exchange, k_{ex}, determined by ^{1}H NMR spectroscopy, by following the disappearance of signal from the acidic proton(s) (H_A and $H_{A'}$) over time (Equation 3.1).

$$-\frac{\mathrm{d}[\mathrm{CH_AH_{A'}}]}{\mathrm{d}t} = k_{\mathrm{ex}}[\mathrm{CH_AH_{A'}}] \qquad \text{(Equation 3.1)}$$

The k_{ex} value is comprised of both specific and general catalysis components. Reactions which are specific acid or base catalysed show a kinetic dependence on only

$[D_3O^+]$ or $[DO^-]$, respectively. Reactions additionally involving general acid and base catalysis show a kinetic dependence upon both $[D_3O^+]$ and [DA], and, $[DO^-]$ and $[A^-]$, respectively. In specific catalysis proton transfer is not involved in the rate determining step and catalysis is from either D_3O^+ or DO^-. In general catalysis proton transfer is involved in the rate determining step and catalysis is either from D_3O^+ and the deuterated acid form of the buffer, DA, or from DO^- and the conjugate base form of the buffer A^-. In the case of the acid catalysed route in Scheme 3.18 k_{ex} is:

$$k_{ex} = k_{D_2O} + k_{D+}[D^+] + k_{DA}[DA] \qquad \text{(Equation 3.2)}$$

where k_{D2O} is the second order rate constant for the solvent promoted exchange, k_{D+} is the second order rate constant for D^+ catalysed exchange and k_{DA} is the second order rate constant for buffer catalysed exchange by DA. For the base catalysed exchange k_{ex}:

$$k_{ex} = k_{D_2O} + k_{DO}[DO^-] + k_{A-}[A^-] \qquad \text{(Equation 3.3)}$$

where k_{DO} is the second order rate constant for deuteroxide-catalysed exchange and k_{A-} is the second order rate constant for buffer catalysed exchange by A^-.

Previous work by Taylor on **10** and **11** had shown that k_{ex} increased as the p*D* increased indicating that a base catalysed exchange was active (Table 3.1).[157] However, the contributions of buffer catalysis, k_{A-}, and deuteroxide catalysis, k_{DO}, to k_{ex} were not elucidated. Deuterium exchange reactions to both verify the original data and also to determine k_{A-} and k_{DO} were therefore undertaken.

Table 3.1: k_{ex} values for deuterium exchange in potassium acetate and deuterium chloride solutions for 6 mM glycyl TKP (**10**) and 6 mM prolyl TKP (**11**) with 40 % d_3-MeCN, I = 0.06 (KCl) and 25 ºC. Data taken from Bethany Taylor's MChem Thesis 2014.

TKP	Solution[a]	pD	k_{ex} / s^{-1}
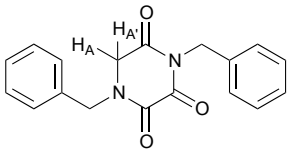	50 % fb 0.05 M KOAc	5.99	3.69×10^{-4}
	30 % fb 0.05 M KOAc	5.67	2.04×10^{-4}
	15 % fb 0.05 M KOAc	5.49	1.65×10^{-4}
	10 % fb 0.05 M KOAc	4.94	8.50×10^{-5}
	5 % fb 0.05 M KOAc	4.40	2.98×10^{-5}
	0.025 M DCl	1.80	25.1×10^{-7}
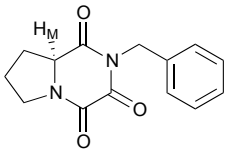	30 % fb 0.05 M KOAc	5.54	6.18×10^{-4}
	15 % fb 0.05 M KOAc	4.77	1.76×10^{-4}
	5 % fb 0.05 M KOAc	4.35	4.64×10^{-5}
	0.025 M DCl	1.85	1.25×10^{-6}

[a] %fb = % base form of the buffer.

3.2.2 First order rate constants for deuterium exchange, k_{ex}, of Glycyl TKP

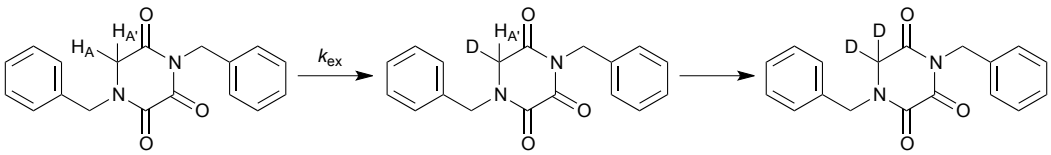

In order to determine k_{A-} for **10** a series of exchange reactions were performed in potassium acetate buffered solutions with an identical buffer ratio (75 % free base) but varying total concentration of buffer (0.025 M – 0.05 M). The identical buffer ratio maintained a consistent pD between solutions and thus kept $k_{DO}[DO^-]$ of Equation 3.3 constant. Thus any alterations in the rate of exchange will be due to the differences in the concentration of the free base form of the buffer.

First order rate constants for deuterium exchange, k_{ex}, were determined by ^{1}H NMR spectroscopy and a representative set of spectra are shown in Figure 3.1. The exchangeable α-protons H_A and $H_{A'}$ appear as a singlet at 4.76 ppm just upfield of the

HOD peak. As deuterium exchange progresses, an additional peak from the α-protons appears at 4.74 ppm. This upfield peak is a triplet (albeit poorly resolved in Figure 3.2) that appears due to the coupling between the D and H of α-CHD.[159] The methylene protons from the benzyl groups, H_C and H_D, appear as singlets at 5.10 ppm and 5.38 ppm, respectively, while the aromatic protons appear at 7.71 – 7.86 ppm.

Figure 3.1: Representative ^{1}H NMR spectra at 500 MHz for the hydrogen deuterium exchange of glycyl TKP (**10**) (3.29 mM) in acetic acid buffer (0.025 M, 75 % fb) with 40 % d_3-MeCN co-solvent at p*D* = 6.28, *I* = 0.06 (KCl) and 25 ºC.

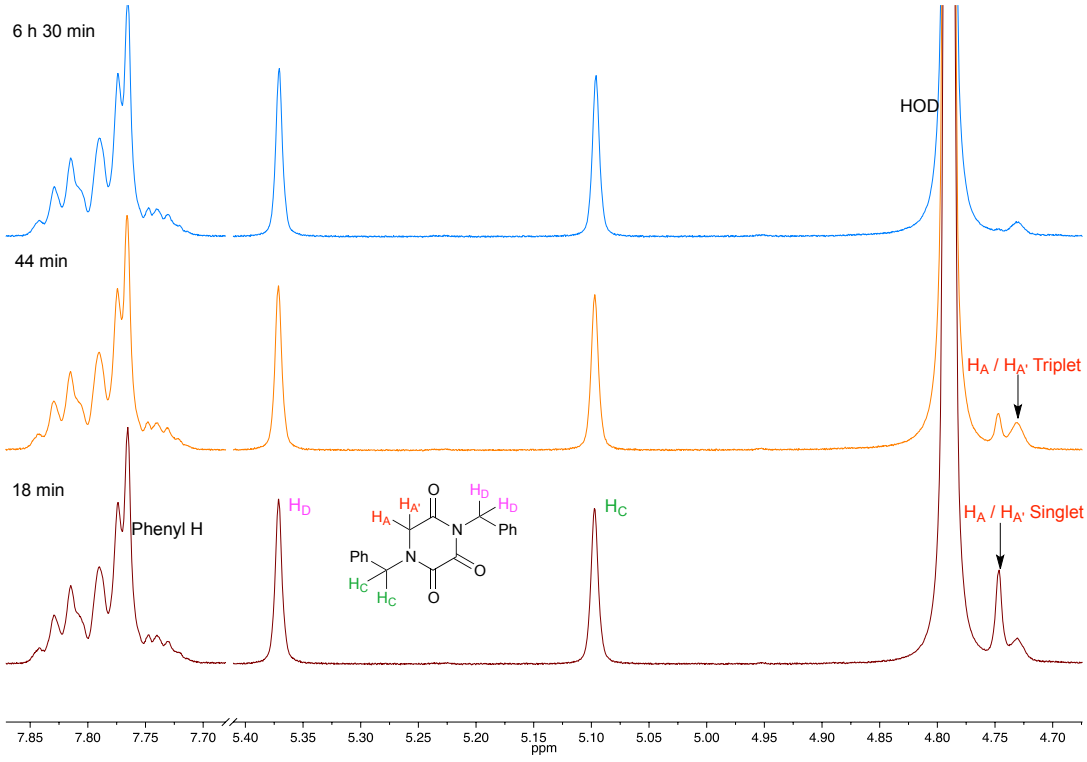

The integrated area of the H_A and $H_{A'}$ singlet ($A_{HA/HA'}$) decreased relative to the methylene peaks (A_{CH2}) and the fraction of unexchanged substrate *f*(s) was determined according to Equation 3.4. No parallel reactions were observed during the course of the exchange reaction and therefore it was acceptable to use the methylene peaks as references to monitor the disappearance of H_A and $H_{A'}$. The observed first order rate constants for deuterium exchange, k_{ex}, were determined from a fitting of Equation 3.5 to a plot of *f*(s) vs. time (Figure 3.2).

$$f(\mathrm{s}) = \frac{(A_{\mathrm{H_A/H_{A'}}}/A_{\mathrm{CH_2}})_t}{(A_{\mathrm{H_A/H_{A'}}}/A_{\mathrm{CH_2}})_{t=0}} \qquad \text{(Equation 3.4)}$$

$$f(\mathrm{s}) = \mathrm{e}^{-k_{\mathrm{ex}}t} \qquad \text{(Equation 3.5)}$$

The reaction data and observed first order rate constants for deuterium exchange (k_{ex}) are shown in Table 3.2 and Appendix II Figures II.1 – II.2.

Figure 3.2: Plot of the fraction of remaining unexchanged α-protons H_A and $H_{A'}$ against time for glycyl TKP (**10**) (3.29 mM) in acetic acid buffer (0.025 M, 75 % fb) with 40 % d_3-MeCN co-solvent at p*D* = 6.28, *I* = 0.06 (KCl) and 25 ºC.

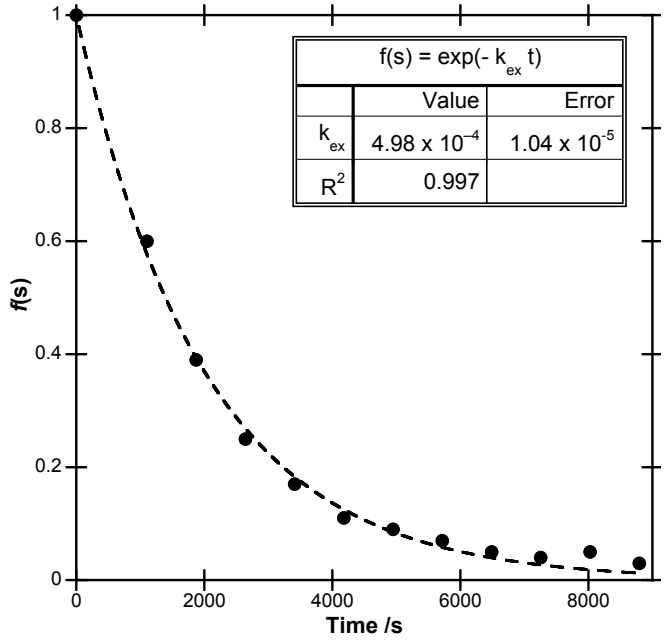

Table 3.2: Reaction data and observed first order rate constants (k_{ex}) for the deuterium exchange of the α-protons H_A and $H_{A'}$ in glycyl TKP (**10**) (3.29 mM) in acetic acid buffer (0.0250 – 0.0500 M, 75 % fb) with 40 % d_3-MeCN co-solvent, I = 0.06 (KCl) and 25 ºC.

$[KOAc]_{Tot}$ /M	$[AcO^-]$ /M	$[DO^-]$ /M	Time /s	f(s)	k_{ex} /s^{-1}
0.0500	0.0375	3.03×10^{-10} (pD = 6.29)	0	1.00	6.02×10^{-4}
			1194	0.74	
			1963	0.54	
			2732	0.39	
			3501	0.33	
			4270	0.26	
			5039	0.22	
			5808	0.17	
			6577	0.14	
			7346	0.11	
			8115	0.09	
			8884	0.08	
			9653	0.08	
			10422	0.07	
			11191	0.05	
			11960	0.06	
			12729	0.06	
			13498	0.05	
			14267	0.03	
0.0375	0.0281	3.07×10^{-10} (pD = 6.29)	0	1.00	4.98×10^{-4}
			1104	0.60	
			1873	0.39	
			2642	0.25	
			3411	0.17	
			4180	0.11	
			4949	0.09	
			5718	0.07	
			6487	0.05	
			7256	0.04	
			8025	0.05	
			8794	0.03	
0.0250	0.0188	2.96×10^{-10} (pD = 6.28)	0	1.00	3.76×10^{-4}
			864	0.75	

1633	0.54
2402	0.39
3171	0.29
3940	0.21
4709	0.16
5478	0.12
6247	0.1
7016	0.08
7785	0.07
8554	0.06
9323	0.05
10092	0.04
10861	0.04
11630	0.03
12399	0.04

The second order rate constant for the buffer catalysed exchange k_{A^-} was determined from plotting k_{ex} against the concentration of the free base form of the buffer and fitting the data to Equation 3.3 (Figure 3.3). From the plot a value of $k_{A^-} = 1.21 \times 10^{-2}\ M^{-1}\ s^{-1}$ is found for the α-protons H_A and $H_{A'}$.

Figure 3.3: Plot of the dependence of k_{ex} upon the concentration of the free base form of the buffer for glycyl TKP (**10**) (3.29 mM) in acetic acid buffer (0.0250 – 0.0500 M, 75 % fb) with 40 % d_3-MeCN co-solvent, I = 0.06 (KCl) and 25 ºC.

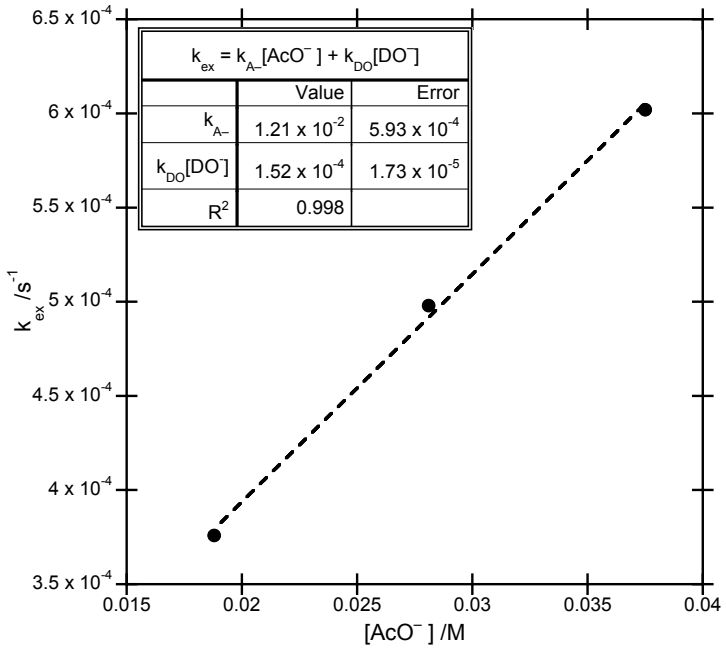

3.2.3 Estimates for the second order rate constant for deuteroxide catalysed exchange, k_{DO}, for Glycyl TKP

The previously obtained k_{ex} values in Table 3.1 were used in conjunction with k_{A-} to obtain an estimate for the buffer independent first order rate constants for exchange, k_{ex}' (Equation 3.3 and Table 3.3).

An estimate for the second order rate constant for deuteroxide catalysed exchange, k_{DO}, was then found from plotting k_{ex}' against the concentration of deuteroxide (Figure 3.4) and linearly fitting the data according to Equation 3.3. The k_{DO} value for the α-protons H_A and $H_{A'}$ in the glycine TKP is estimated to be $k_{DO} = 5.09 \times 10^5$ M^{-1} s^{-1}. The linear fit crosses the y-axis at ~ 0 and therefore the extent of solvent catalysed exchange by D_2O is negligible.

Table 3.3 k_{ex} values and contributions of buffer catalysis (k_{A^-}[KOAc]) and deuteroxide catalysis (k_{ex}') to deuterium exchanges of the α-protons H_A and $H_{A'}$ glycyl TKP (**10**) (3.29 mM) in acetic acid buffer with 40 % d_3-MeCN co-solvent, I = 0.06 (KCl) and 25 ºC.

[KOAc] /M	[DO^-] /M	k_{ex} /s^{-1}	k_{A^-}[KOAc] /s^{-1}	k_{ex}' / s^{-1}	%Buffer catalysis	% DO^- catalysis
0.0375	3.03×10^{-10}	6.02×10^{-4}	4.54×10^{-4}	1.48×10^{-4}	75	25
0.0250	1.03×10^{-10}	3.69×10^{-4} [b]	3.03×10^{-4}	6.65×10^{-5}	82	18
0.0150	4.92×10^{-11}	2.04×10^{-4} [b]	1.82×10^{-4}	2.25×10^{-5}	89	11
0.0075	9.16×10^{-12}	8.50×10^{-5} [b]	9.08×10^{-5}	-5.75×10^{-6}	107	-7
0.0025	2.64×10^{-12}	2.98×10^{-5} [b]	3.03×10^{-5}	-4.50×10^{-7}	102	-2

[a] $k_{A^-} = 1.21 \times 10^{-2}$ M^{-1} s^{-1}. [b] Data taken from Bethany Taylor's MChem Thesis 2014.

Figure 3.4: Plot of the estimated buffer independent first order rate constants of exchange (k_{ex}') against the concentration of deuteroxide for glycyl TKP (**10**) (3.29 mM) in acetic acid buffer with 40 % d_3-MeCN co-solvent, I = 0.06 (KCl) and 25 ºC.

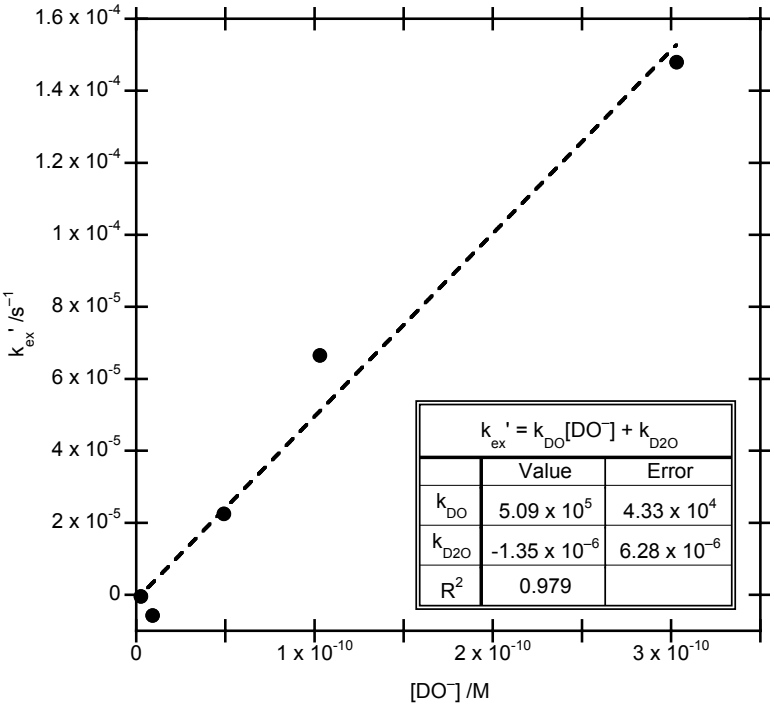

3.2.4 First order rate constants for deuterium exchange, k_{ex}, for Prolyl TKP

In order to determine the kinetic acidity of the α-proton H_M in the proline TKP (**11**) deuterium exchange reactions were carried out in potassium acetate buffered D_2O solutions with 40 % d_3-MeCN co-solvent in the range p*D* 4.76 – 5.28. In order to delineate the contributions of deuteroxide ($k_{DO}[DO^-]$) and buffer ($k_{A^-}[KOAc]$) components to the k_{ex} values (Equation 3.3), exchange was monitored in potassium acetate solutions at four different free base percentages (15 %, 20 %, 25 % and 30 %), and at every percentage free base four different concentrations of total buffer (0.20 M, 0.15 M, 0.125 M, 0.10 M) were used. First order rate constants for deuterium exchange, k_{ex}, were determined by ^{1}H NMR spectroscopy and a representative set of spectra are shown in Figure 3.5. The α-proton H_M signal is at 4.93 ppm and decreases as exchange progresses.

Figure 3.5: Representative ^{1}H NMR spectra at 500 MHz for the hydrogen deuterium exchange of prolyl TKP (**11**) (3.93 mM) in acetic acid buffer (0.2 M, 15 % fb, p*D* = 4.78) with 40 % d_3-MeCN co-solvent, *I* = 0.2 (KCl) and 25 °C.

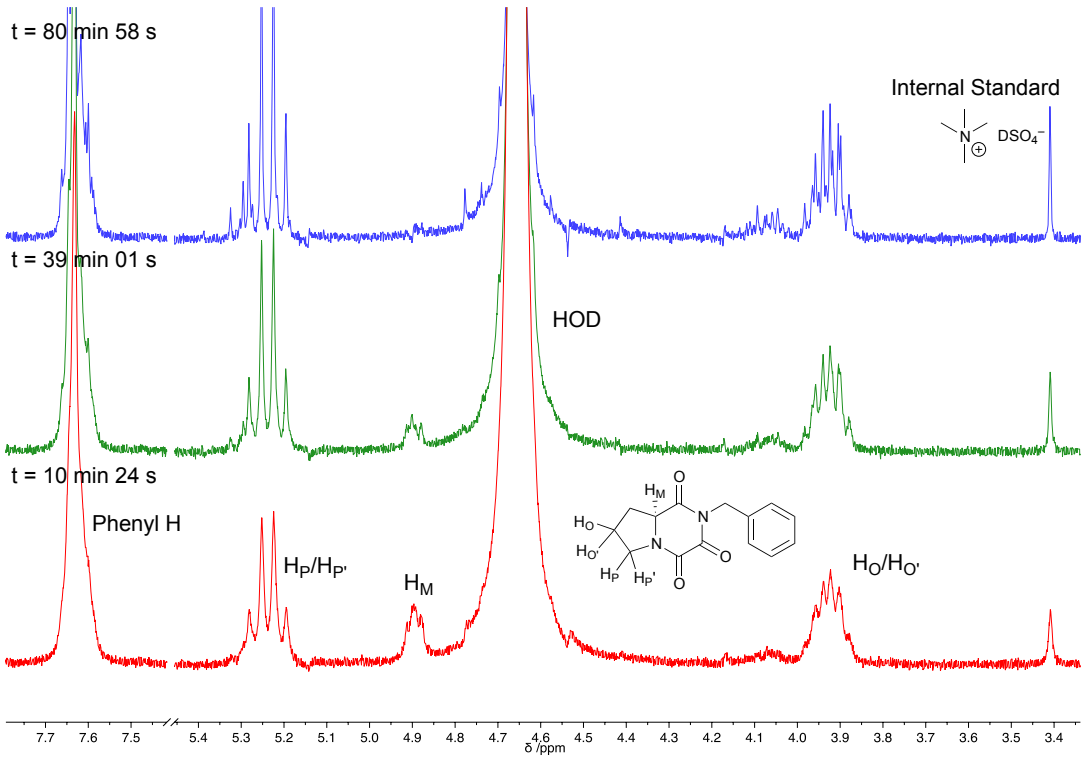

The integrated area of the H_M triplet decreased relative to the tetramethylammonium deuteriosulfate internal standard and the fraction of unexchanged substrate *f*(s) was determined according to Equation 3.5.[xxv] The observed first order rate constants for deuterium exchange, k_{ex}, were determined from a fitting of Equation 3.5 to a plot of *f*(s) vs. time (Table 3.4). The reaction data and observed first order rate constants for deuterium exchange (k_{ex}) for all exchange reactions are shown in Appendix II: Figure II.3 – Figure II.18 and Table II.1 – Table II.3.

3.2.5 Second order rate constants for buffer catalysed, k_{A^-}, and deuteroxide catalysed, k_{DO}, exchange for Prolyl TKP

Under all conditions buffer catalysis of deuterium exchange is clearly observed for prolyl TKP **11**. The second order rate constants for buffer catalysed exchange were determined using Equation 3.3 and plotting the k_{ex} against the concentration of the free base form of the buffer Figure 3.7 and Table 3.8. Figure 3.8 is identical to Figure 3.7 but with two anomalous data points (15 % fb 0.20 M KOAc, and, 25 % fb 0.20 M KOAc) removed.

The value for k_{A^-} should not change between the different percentage free base solutions.[xxvi] Gratifyingly, for experiments in 20 % and 30 % free base, the values for k_{A^-} are closely similar at 1.66×10^{-2} M^{-1} s^{-1} and 1.62×10^{-2} M^{-1} s^{-1} respectively (Figure 3.7). The k_{A^-} values for 15 % and 25 % free base in Figure 3.7 were below this k_{A^-} value ($k_{A^-} = 3.43 \times 10^{-3}$ M^{-1} s^{-1} and $k_{A^-} = 1.00 \times 10^{-2}$ M^{-1} s^{-1}, respectively). For 25 % free base it was found that omitting the k_{ex} value for 0.20 M 25 % fb KOAc (Figure 3.8) led to a rise in k_{A^-} to 1.54×10^{-2} M^{-1} s^{-1} which is consistent with the k_{A^-} values for 20 % and 30 % free base above. For 15 % free base omitting the k_{ex} value for 0.20 M 15 % fb KOAc gave $k_{A^-} = 1.00 \times 10^{-2}$ M^{-1} s^{-1} which still remains below the k_{A^-} values for 20 %, 25 % and 30 % free base above (Figure 3.8).

The origin of the inconsistent k_{A^-} value for 15 % free base is presumed to be due to the poor fitting of the data for the 15 % free base. Unfortunately, due to the limited amounts of material available the experiment could not be repeated.

[xxv] In Equation 3.5 A_{CH2} is replaced by A_{Int} for the area of the internal standard peak for **11**.

[xxvi] Assuming only general base catalysis was active and no general acid catalysis was present.

Figure 3.7: Plot of k_{ex} of the α-proton H_M in prolyl TKP (**11**) (3.93 mM) against free base buffer concentration in a series of acetic acid buffer solutions with 40 % d_3-MeCN co-solvent, $I = 0.2$ (KCl) and 25 °C.

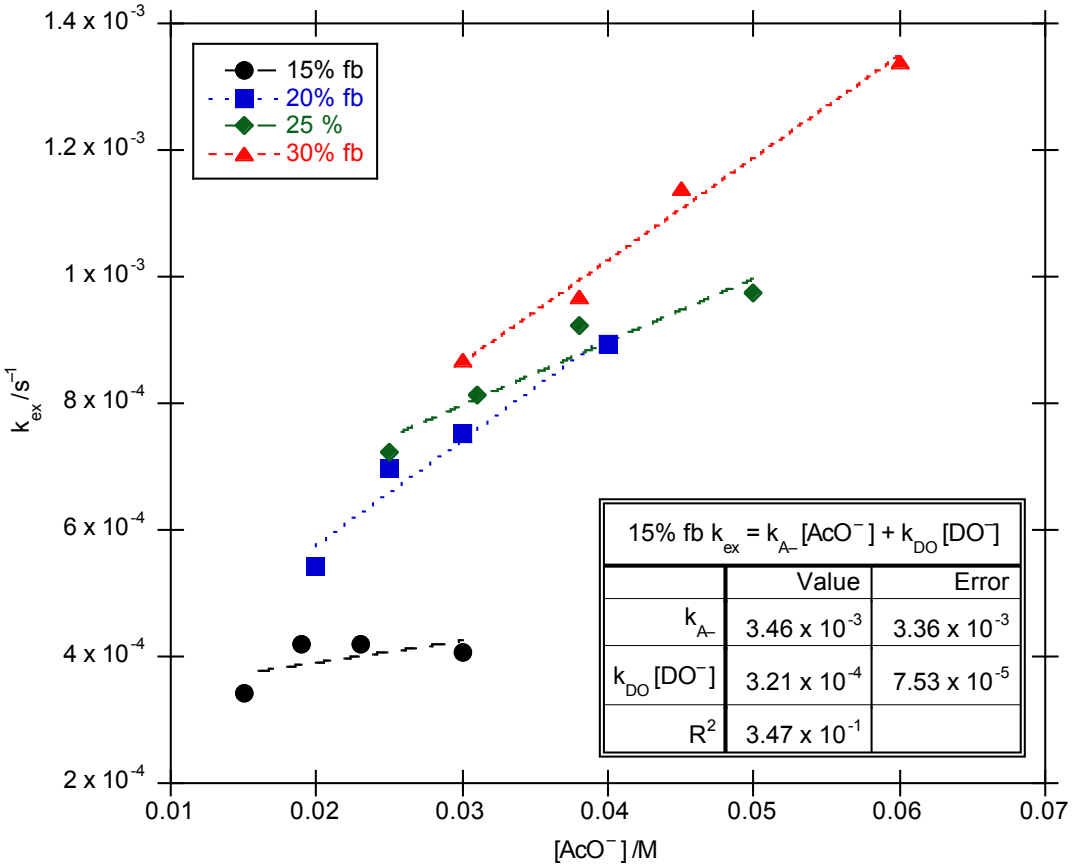

20% fb $k_{ex} = k_{A^-}[AcO^-] + k_{DO}[DO^-]$		
	Value	Error
k_{A^-}	1.66×10^{-2}	2.56×10^{-3}
$k_{DO}[DO^-]$	2.43×10^{-4}	7.6×10^{-5}
R^2	0.955	

25% fb $k_{ex} = k_{A^-}[AcO^-] + k_{DO}[DO^-]$		
	Value	Error
k_{A^-}	1.00×10^{-2}	2.17×10^{-3}
$k_{DO}[DO^-]$	4.97×10^{-4}	8.06×10^{-5}
R^2	0.914	

30% fb $k_{ex} = k_{A^-}[AcO^-] + k_{DO}[DO^-]$		
	Value	Error
k_{A^-}	1.62×10^{-2}	1.38×10^{-3}
$k_{DO}[DO^-]$	3.79×10^{-4}	6.16×10^{-5}
R^2	0.986	

Figure 3.8: Plot of k_{ex} of the α-proton H_M in prolyl TKP (**11**) (3.93 mM) against free base buffer concentration in a series of acetic acid buffer solutions with 40 % d_3-MeCN co-solvent, I = 0.2 (KCl) and 25 ºC. The value for 15% fb the [KOAc] = 0.2 M and 25% fb the [KOAc] = 0.2 M have been omitted from this plot. Full data is in Figure 3.7.

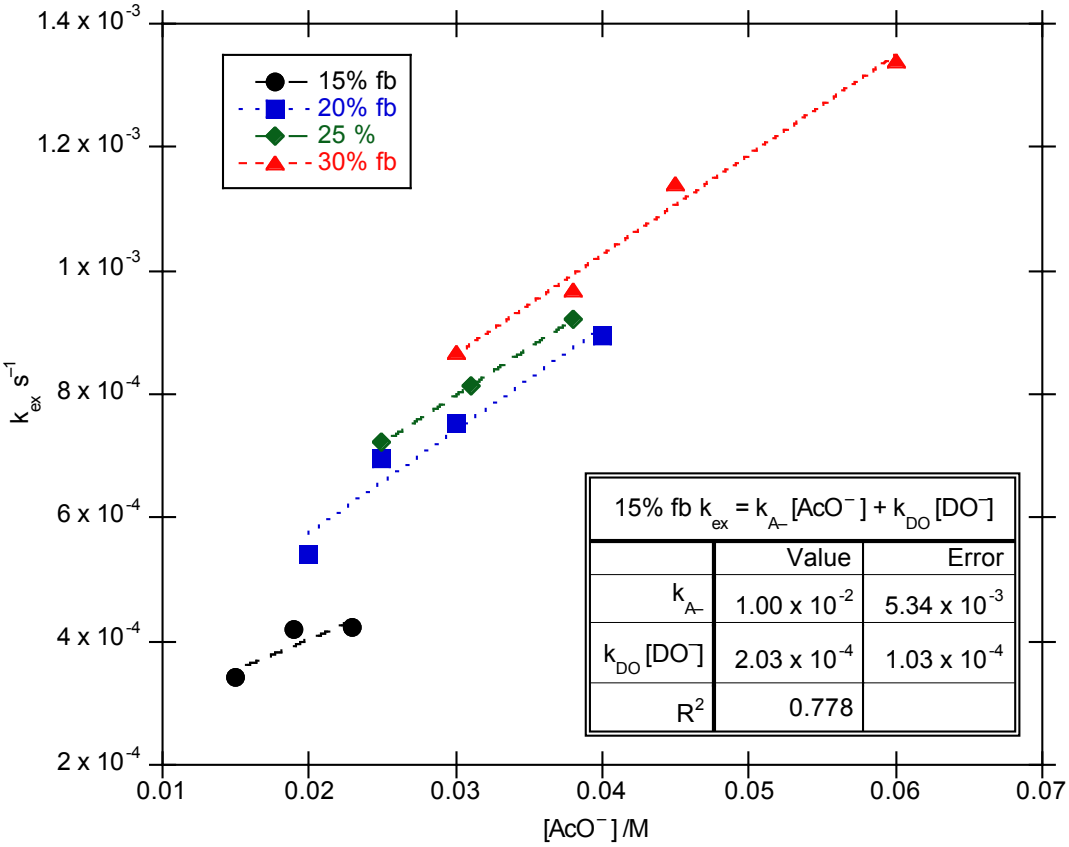

15% fb $k_{ex} = k_{A-}[AcO^-] + k_{DO}[DO^-]$	Value	Error
k_{A-}	1.00×10^{-2}	5.34×10^{-3}
$k_{DO}[DO^-]$	2.03×10^{-4}	1.03×10^{-4}
R^2	0.778	

20% fb $k_{ex} = k_{A-}[AcO^-] + k_{DO}[DO^-]$	Value	Error
k_{A-}	1.66×10^{-2}	2.56×10^{-3}
$k_{DO}[DO^-]$	2.43×10^{-4}	7.6×10^{-5}
R^2	0.955	

25% fb $k_{ex} = k_{A-}[AcO^-] + k_{DO}[DO^-]$	Value	Error
k_{A-}	1.54×10^{-2}	2.05×10^{-4}
$k_{DO}[DO^-]$	3.36×10^{-4}	6.5×10^{-6}
R^2	1.00	

30% fb $k_{ex} = k_{A-}[AcO^-] + k_{DO}[DO^-]$	Value	Error
k_{A-}	1.62×10^{-2}	1.38×10^{-3}
$k_{DO}[DO^-]$	3.79×10^{-4}	6.16×10^{-5}
R^2	0.986	

Table 3.4: k_{ex}, k_{buff} and k_{ex}' values for the deuterium exchange of the α-proton H_M in 3.93 mM prolyl TKP (**11**) in a set of different percentage free base acetic acid buffer solutions with 40 % d_3-MeCN co-solvent, I = 0.2 (KCl) and 25 ºC.

% fb	[KOAc] /M	[AcO^-] /M	[DO^-] /M	k_{ex} /s^{-1}	k_{A-} /M^{-1} s^{-1}	k_{ex}' /s^{-1}
15	0.200	0.030	8.95×10^{-12}	4.06×10^{-4} [a]	1.00×10^{-2} [a] (3.46×10^{-3}) [b]	2.03×10^{-4}
	0.150	0.023	9.05×10^{-12}	4.21×10^{-4}		
	0.125	0.019	8.95×10^{-12}	4.18×10^{-4}		
	0.100	0.015	8.85×10^{-13}	3.41×10^{-4}		
20	0.200	0.040	1.50×10^{-11}	8.93×10^{-4}	1.66×10^{-2}	2.43×10^{-4}
	0.150	0.030	1.49×10^{-11}	7.53×10^{-4}		
	0.125	0.025	1.47×10^{-11}	6.96×10^{-4}		
	0.100	0.020	1.49×10^{-11}	5.42×10^{-4}		
25	0.200	0.050	2.25×10^{-11}	9.73×10^{-4} [a]	1.54×10^{-2} [a] (1.00×10^{-2}) [b]	3.36×10^{-4}
	0.150	0.038	2.17×10^{-11}	9.22×10^{-4}		
	0.125	0.031	2.15×10^{-11}	8.12×10^{-4}		
	0.100	0.025	2.15×10^{-11}	7.22×10^{-4}		
30	0.200	0.060	3.03×10^{-11}	1.34×10^{-3}	1.62×10^{-2}	3.79×10^{-4}
	0.150	0.045	3.00×10^{-11}	1.14×10^{-3}		
	0.125	0.038	2.93×10^{-11}	9.68×10^{-4}		
	0.100	0.030	2.90×10^{-11}	8.67×10^{-4}		

[a] Anomalous results omitted during fitting in Figure 3.8. [b] Value for k_{A-} without anomalous results removed.

From the y-intercepts in Figure 3.9 buffer independent first order rate constants for exchange, k_{ex}' (s^{-1}), were determined. The gradient of a plot of k_{ex}' against the

concentration of deuteroxide gave the second order rate constant for deuteroxide catalysed exchange for the α-proton H_M in the proline TKP of $k_{DO} = 8.99 \times 10^6$ M^{-1} s^{-1}.

The first order rate constant for the solvent catalysed deprotonation, k_{D2O} (s^{-1}), is found from the y-intercept of Figure 3.9 where $k_{D2O} = 1.21 \times 10^{-4}$ s^{-1}. The second order rate constant for solvent catalysis, k_{D2O}' (M^{-1} s^{-1}), may be found from Equation 3.6.

$$k_{D2O} = k_{D2O}'[D_2O] \qquad \text{(Equation 3.6)}$$

where the concentration of D_2O in a 60 : 40 D_2O : d_3-MeCN solution is 33.08 M. Thus $k_{D2O}' = 3.66 \times 10^{-6}$ M^{-1} s^{-1}.

Figure 3.9: Plot of the buffer independent first order rate constants of exchange (k_{ex}') against the concentration of deuteroxide for prolyl TKP (**11**) (3.93 mM) in acetic acid buffer solutions with 40 % d_3-MeCN co-solvent, I = 0.2 (KCl) and 25 ºC.

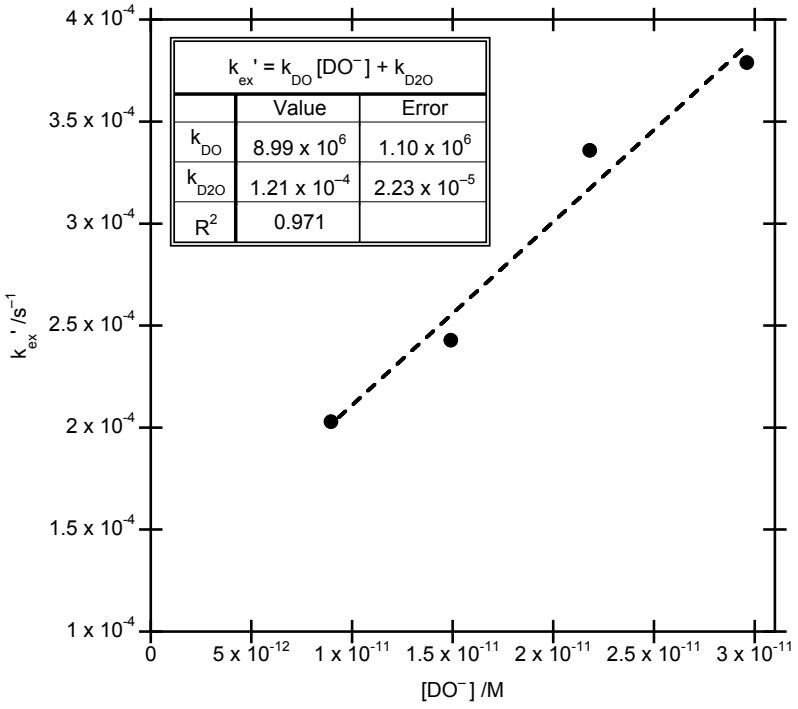

3.3 Discussion

3.3.1 Comparison between Glycyl and Prolyl TKP

Scheme 3.19: Glycyl (**10**) and Prolyl (**11**) TKP studied.

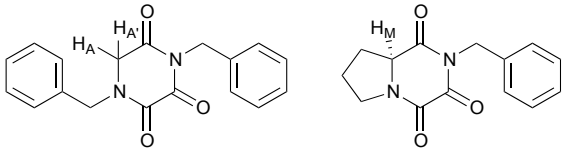

10 **11**

A comparison of the second order rate constants for deuteroxide catalysed exchange, k_{DO}, or kinetic acidities, show that the α-proton of the prolyl TKP **11** (k_{DO} = 8.99 × 10^6 M^{-1} s^{-1}) is 18-fold kinetically more acidic towards DO^- than the glycyl TKP **10** α-protons (k_{DO} = 5.09 × 10^5 M^{-1} s^{-1}). The higher kinetic acidity of prolyl TKP **11** may be attributed to destabilisation of the parent TKP by the presence of a fused pyrrolidine and TKP ring. As indicated in calculations by Makino, the TKP ring prefers to have a planar conformation in order to maximise the overlap between the various π bonds.[139] However, the fusion of the pyrrolidine ring from proline was shown to enforce a non-planar, less stable conformation on the TKP ring. This reactant destabilisation could be responsible for the higher kinetic acidity of the prolyl α-proton relative to the glycyl α-protons. However, within the enolate formed from **11**, competing effects of ring strain should act in opposing directions: there will be a relief of ring strain within the TKP ring which can adopt its preferred planar conformation, but there will be an introduction of ring strain into the pyrrolidine ring caused by the formation of an sp^2 carbon at the C2 position. The aforementioned stereoelectronic effect could also play a role in enhancing the k_{DO} of **11** relative to **10** (Chapter 2: Section 2.3.1.2). In the DKPs this resulted in a 3 – 12-fold (average 3.3-fold) enhancement of k_{DO} for prolyl residues compared to glycyl residues. The 18-fold difference seen for the TKPs indicates that additional factors are also present.

For the second order rate constant for buffer catalysed exchange, k_{A-}, while the α-proton of the prolyl TKP **11** (k_{A-} = 1.61 × 10^{-2} M^{-1} s^{-1})[xxvii] is more acidic to the acetate buffer than the glycyl TKP **10** α-protons (k_{A-} = 1.21 × 10^{-2} M^{-1} s^{-1}) the extent of

[xxvii] Mean of k_{A-} values of 20 %, 25 % and 30 % fb KOAc solutions in Table 3.4.

this difference is much smaller in comparison to that for k_{DO}, only 1.33-fold larger for k_{A^-} vs. 18-fold larger for k_{DO}. Whilst the TKP enolates formed from the reaction with deuteroxide and acetate anion are identical formally, the transition states for the deuteroxide and buffer catalysed reactions are expected to be different, as the extent of proton transfer varies with the strength of the base. Proton transfer is expected to be more advanced for the stronger base deuteroxide in the transition state than in the weaker base acetate. Consequently, the transition state is expected to be more product-like and hence closer in structure to the enolate. The greater difference in stabilities of the glycyl and prolyl enolates is therefore manifested more fully for the deuteroxide catalysed reaction than the buffer catalysed reaction. Although this explanation assumes that the difference in stabilities of the enolates is greater than the difference in stabilities of the acid form.

The prolyl TKP **11** is also more sensitive to the change of base from acetate to deuteroxide than the glycyl TKP **10** (5.58×10^8-fold increase for **11** vs. 4.21×10^7-fold increase for **10**). The origin of this could be due to several factors. Potentially, greater hindrance from the pyrrolidine ring in **11** results in a more substantial increase in rate upon moving from the larger acetate to the smaller deuteroxide base in **11** compared to **10**.

3.3.2 Kinetic (k_{DO} and k_{HO}) and thermodynamic acidity (pK_a) of TKPs

3.3.2.1 Mechanism of hydrogen deuterium exchange

The kinetic acidity values, k_{DO}, may be used to access information about the mechanism of proton transfer for TKPs. The free energy profile for a hydrogen deuterium exchange reaction catalysed by both deuteroxide and buffer is shown in Scheme 3.20.[160] Initially, the carbon acid diffuses together with either a molecule of deuteroxide or buffer to form an encounter complex (**1** and **2**).[xxviii] Subsequently, the carbon acid is deprotonated to form the carbanion and HOD **3** or AH **4**. The reaction can either reverse with reprotonation of the carbanion or can continue in the forward direction via solvent reorganisation to place a deuterium in the reactive position. In this step the HOD molecule may either rotate to place the deuterium in the reactive position

[xxviii] Diffusion to form the encounter complex is not shown in Scheme 3.20.

or the HOD may diffuse away and be replaced by a D_2O. The protonated buffer AH must be replaced by a deuteronated buffer AD – assuming the buffer has only one acidic site. The solvent reorganisation is considered irreversible because the concentration of deuterium in solution overwhelmingly exceeds the concentration of hydrogen in solution; thus HOD and AH are essentially lost by dilution in bulk solvent.[xxix] The carbanion is deuterated in **5** and **6** to give the encounter complex between deuterated carbon acid and either deuteroxide or buffer, **7** and **8**, which will diffuse apart to give free deuterated carbon acid in solution.[xxx]

Scheme 3.20: Relative free energy profile for the hydrogen deuterium exchange of a carbon acid catalysed by deuteroxide and buffer. X = H or D.

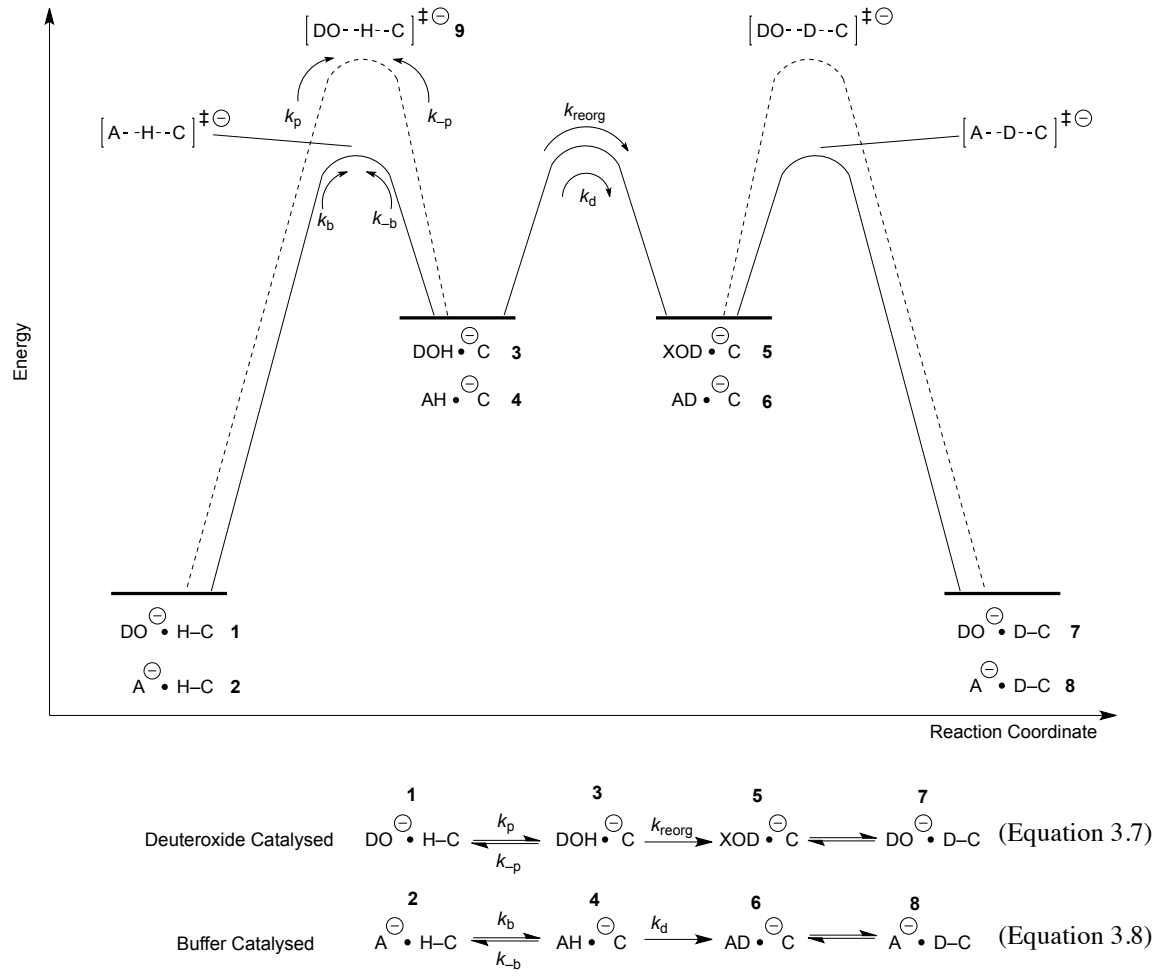

[xxix] In a 60 : 40 D_2O : d3-MeCN solution prepared from 99.9 % D_2O the concentration of D is 66.10 M. The concentrations of acidic H in Gly TKP **10** and Pro TKP **11** in the exchange reactions were 6.58 mM and 3.93 mM respectively. This means that the concentration of D to H is 10046-fold and 20091-fold greater for Gly TKP **10** and Pro TKP **11** respectively.

[xxx] Again, diffusion to separate encounter complex not shown in Scheme 3.20.

The microscopic rate constants for the deuteroxide and buffer catalysed reactions are defined in Equations 3.7 and 3.8 (Scheme 3.20): k_p is the rate constant for deprotonation of the carbon acid by deuteroxide in the encounter complex, k_{-p} is the rate constant for reprotonation of the conjugate base of the carbon acid by HOD, k_b is the rate constant for deprotonation of the carbon acid by buffer, k_{-b} is the rate constant for reprotonation of the conjugate base of the carbon acid by protonated buffer, k_d is the rate constant for replacement of protonated buffer by deuteronated buffer and k_{reorg} is the rate constant for solvent reorganisation which is experimentally determined to be $k_{reorg} \sim 10^{11}$ s^{-1}.[161-163]

Using the steady state approximation for the formation of **3** and **4** and taking the k_{reorg} step to be irreversible the microscopic rate constants are related to the second order rate constant for deuteroxide and buffer catalysed deuterium exchange, k_{DO} and k_{A^-}, by Equation 3.9 and Equation 3.10.

$$k_{DO} = \frac{k_p\, k_{reorg}}{k_{-p} + k_{reorg}} \qquad \text{(Equation 3.9)}$$

$$k_{A^-} = \frac{k_b\, k_d}{k_{-b} + k_d} \qquad \text{(Equation 3.10)}$$

Equation 3.9 and Equation 3.10 are valid provided that deprotonation of carbon acid, k_p, and solvent reorganisation, k_{reorg} (reorganisation of buffer, k_d) are both partially rate determining. If solvent reorganisation is rate determining then $k_{-p} >> k_{reorg}$ and $k_{-b} >> k_d$ and thus Equations 3.9 and 3.10 become Equations 3.11 and 3.12, respectively:

$$k_{DO} = \frac{k_p\, k_{reorg}}{k_{-p}} = K_p\, k_{reorg} \qquad \text{(Equation 3.11)}$$

$$k_{A^-} = \frac{k_b\, k_d}{k_{-b}} = K_b\, k_d \qquad \text{(Equation 3.12)}$$

where K_p and K_b are the pre-equilibrium constants for formation of carbanion in the deuteroxide and buffer catalysed reaction. k_d is smaller than k_{reorg} and consequently, no buffer catalysis will be observed if solvent reorganisation is rate determining as the deuteroxide catalysed pathway will be kinetically favoured.

If deprotonation of the carbon acid is rate determining then $k_{reorg} >> k_{-p}$ and $k_d >> k_{-b}$ and Equations 3.9 and 3.10 become Equations 3.13 and 3.14, respectively:

$$k_{DO} = \frac{k_p\, k_{reorg}}{k_{reorg}} = k_p \qquad \text{(Equation 3.13)}$$

$$k_{A^-} = \frac{k_b\, k_d}{k_d} = k_b \qquad \text{(Equation 3.14)}$$

When deprotonation of the carbon acid is rate determining buffer catalysis will be observed as the buffer catalysed route offers a lower energy path for the deuterium exchange relative to the deuteroxide catalysed pathway (Scheme 3.20). Both the glycyl and prolyl TKPs displayed buffer catalysed deuterium exchange, which indicates that deprotonation of the carbon acid, k_p, is rate determining.

3.3.2.2 The effect of solvent conditions on k_{DO}

The k_{DO} values above are for a 60 : 40 D_2O : d_3-MeCN solution. In order to make comparisons to the other carbon acids whose k_{DO} values were recorded in 100 % D_2O it is necessary to adjust the k_{DO} values of the TKPs to account for this. A previous study by O'Donoghue on the carbon acidity of triazolium ions showed that there was between a 1.2 – 5.4-fold increase in k_{DO} upon moving from 100 % D_2O to a 2 : 1 D_2O : d_3-MeCN solution.[164] Deuteroxide is a stronger base in a mixed solvent than it is in pure D_2O as the poorer hydrogen bonding ability of the mixed solvent destabilises the deuteroxide. Unfortunately, due to solubility, it was not possible to determine a k_{DO} value in 100 % D_2O for the TKPs. To overcome this we have used the 5.4-fold difference in k_{DO} determined by O'Donoghue to convert our k_{DO} values for 60 : 40 D_2O : d_3-MeCN into k_{DO} values for 100 % D_2O.

There are a number of caveats to the validity of applying this conversion factor for k_{DO} to our TKP systems. The conversion factor was determined for a solution with a composition of 66 % d_3-MeCN compared to our 60 % d_3-MeCN and thus deuteroxide will be a marginally stronger base in the previous study. The impact of this would be to slightly lower the conversion factor for our work, but this difference is not considered to have a significant effect.

There is also a difference in structure and charge (cationic vs. neutral) between the triazolium ions and our TKP carbon acids. The difference in the stability of the reactant state in the two different solvent conditions (100 % D_2O and the D_2O : d_3-MeCN) will be larger for triazolium ions than for TKPs. This is because stabilisation of the cationic charge on the triazolium ions will be significantly less in the mixed solvent system than in D_2O. For the TKPs the reactant state is neutral and therefore the corresponding difference will not be substantial. Consequently, the difference in the activation barrier for deprotonation between the two solvent systems will be greater for the triazolium ions than the TKPs and therefore the difference in k_{DO} will also be greater for the triazolium ions.

The effect of solvent change on the transition state will be the reverse of that for the reactant state. In the triazolium ions the cationic acid goes to a neutral conjugate base via a formally neutral transition state while for the TKPs the neutral acid goes to an anionic enolate conjugate base via an anionic transition state. The extent of change in the solvent shell required to stabilise the transition state of the triazolium ions will be less than that of the TKPs. Thus the change in solvent from 100 % D_2O to the mixed solvent will have a greater effect on the stability of the TKP transition state. Therefore, with regards to transition state stability, the TKPs should have a greater difference in k_{DO} for the different solvent systems compared to the triazolium ions.

It is anticipated that the effect of the change in solvent systems on reactant state and transition state stability will cancel each other out and thus overall there should be no difference in the conversion factor for k_{DO} between the triazolium ion and TKPs.

There is a difference in the rate limiting step for hydrogen deuterium exchange between the triazolium ions and the TKPs. The triazolium ions have rate limiting solvent reorganisation while the TKPs have rate limiting proton transfer (Scheme 3.20). It is not anticipated that the change in solvent will affect which step in the mechanism is rate limiting, but the change in solvent will affect the stability of the deuteroxide. For the triazolium ions proton transfer to the deuteroxide is complete at the rate limiting step and therefore the difference in stability of the deuteroxide between the solvent systems is fully reduced, which should reduce the difference in the k_{DO} between the different solvent systems for the triazolium ions. However, for the TKPs proton transfer to the deuteroxide is only partially complete in the rate limiting step and therefore the difference in stability of the deuteroxide in the different solvent systems is expressed at

the rate limiting step. This should therefore increase the difference in k_{DO} between the different solvent systems for the TKPs.

Taking the above factors into account we believe that the k_{DO} conversion factor for the TKPs will be at the higher end (or above) of the range of conversion factors found for the triazolium ions. Therefore we chose a conversion factor of 5.4 to adjust our k_{DO} values into estimates for the k_{DO} in 100 % D_2O. This gives $k_{DO} = 9.43 \times 10^4$ M^{-1} s^{-1} for glycyl TKP **10** and 1.66×10^6 M^{-1} s^{-1} for prolyl TKP **11**. These k_{DO} values will be used henceforth within this Discussion.

3.3.2.3 Comparison of kinetic acidities, k_{DO}, of TKPs to DKPs

The effect of an additional carbonyl in the TKP ring compared to the DKP ring on the kinetic acidity, k_{DO}, may be found by comparing k_{DO} values for **10** and **11** in comparison to c(Gly-Gly) and c(Gly-L-Pro) (Table 3.5). The prolyl α-proton in **11** is 10^6-fold more acidic than in c(Gly-L-Pro) and the glycyl α-protons in **10** are also 10^6-fold more acidic than in c(Gly-Gly). The extra carbonyl group therefore has a dramatic effect upon the kinetic acidity of the α-protons. It should be noted that the k_{DO} values for the TKPs are at ionic strength $I = 0.06 – 0.20$ while the k_{DO} values DKPs are at $I =$ 1.0 and therefore the comparisons must take this difference in the conditions into account. However, the change in ionic strength is not expected to affect k_{DO} on the order 10^6-fold and thus the overwhelming majority of this change can be attributed to the differences in structure.

In addition, there was no clear evidence for buffer catalysed exchange in the DKPs while this is present in the TKPs. This points to a change in mechanism for the deprotonation from partially rate determining deprotonation *and* solvent reorganisation in the DKPs to rate determining deprotonation in the TKPs.

Table 3.5: Comparison of DKP and TKP second order rate constants for deuteroxide catalysed exchange at 25 °C.

Carbon Acid	k_{DO}/p [a] /M^{-1} s^{-1}	Relative to c(Gly-Gly)	Relative to c(Gly-L-Pro)
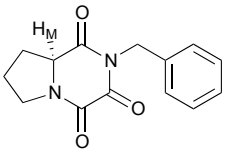 Pro TKP	1.66×10^{6}	1.05×10^{8}	8.88×10^{6}
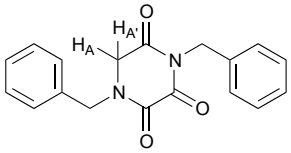 Gly TKP	9.34×10^{4}	5.91×10^{6}	4.99×10^{5}
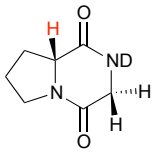 c(Gly-L-Pro)	1.87×10^{-1}	11.84	1.00
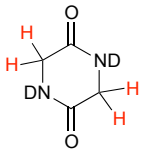 c(Gly-Gly)	1.58×10^{-2}	1.00	–

[a] p = number of acidic protons; used to statistically correct the kinetic acidities.

3.3.2.4 Comparison of kinetic acidities, k_{HO}, of TKPs to other carbonyl carbon acids

The second order rate constants for hydroxide-catalysed deprotonation, k_{HO} (M^{-1} s^{-1}), of a variety of other carbon acids have been determined experimentally by a number of research groups (Table 3.6). In order to compare our TKP data with relevant literature values, a conversion of k_{DO} into k_{HO} values is first required.

The second order rate constants for deuteroxide-catalysed exchange, k_{DO} M^{-1} s^{-1}, may be converted into second order rate constants for hydroxide-catalysed deprotonation, k_{HO} M^{-1} s^{-1}, using a secondary solvent isotope effect. Secondary solvent isotope effects range between k_{DO} / k_{HO} = 1.36 – 2.4 for the deprotonation of carbon

acids.[xxxi] Deuteroxide in D_2O is a stronger base than hydroxide in H_2O, hence $k_{DO} > k_{HO}$. The secondary solvent isotope is sensitive to which microscopic rate constant is the rate determining step for deuterium exchange. When solvent reorganisation, k_{reorg}, is rate determining the full secondary solvent isotope effect of $k_{DO} / k_{HO} = 2.4$ will apply, as complete proton transfer in the pre-equilibrium formation of the carbanion means that the full difference in basicity between deuteroxide and hydroxide will be observed. When deprotonation of the carbon acid is rate determining, k_p, the secondary solvent isotope effect will be $k_{DO} / k_{HO} = 1.36 - 1.48$,[xxxii] as proton transfer is only partially complete at the transition state, **9** (Scheme 3.20). Thus the full difference in basicity between deuteroxide and hydroxide is not observed. If both solvent reorganisation and deprotonation of the carbon acid are partially rate determining then an intermediate value of $k_{DO} / k_{HO} \sim 2.0$ can be used for the secondary solvent isotope effect.

For the TKPs, as buffer catalysis is clearly observed, the rate determining step is deprotonation of the carbon acid, k_p, and thus a secondary solvent isotope effect at the lower end of $k_{DO} / k_{HO} = 1.46$[xxxiii] is chosen to convert k_{DO} to k_{HO}. This gives a $k_{HO} = 6.40 \times 10^4$ M^{-1} s^{-1} for glycyl TKP **10** and a $k_{HO} = 1.14 \times 10^6$ M^{-1} s^{-1} for prolyl TKP **11** (Table 3.6). These values are based upon the assumption that the secondary solvent isotope effect is not significantly affected when transferring from aqueous to a 60 : 40 D_2O : d_3-MeCN / H_2O : MeCN solution.[165]

Comparisons of the kinetic acidities, k_{HO}, of the TKPs with those of related α-carbonyl carbon acids are shown in Table 3.6. It is apparent that the kinetic acidities of the TKPs are between $10^5 - 10^{13}$-fold more acidic than most related α-carbonyl carbon acids. The k_{HO} value of 2.0×10^6 M^{-1} s^{-1} for deprotonation of cyclohexa-2,5-dienone to form phenolate anion (Table 3.6, Entry 10) is the carbon acid that is closest in kinetic acidity.[166]

[xxxi] i) $k_{DO} / k_{HO} = 1.4$ for racemization of the anion of mandelic acid at 100 ºC [Pocker, Y. *Chem. Ind.* (*London*) **1958**, 1117 – 1118]; ii) base-catalyzed bromination of acetone at 25 ºC $k_{DO} / k_{HO} = 1.46$ [Pocker, Y. *Chem. Ind.* (*London*) **1959**, 1383 – 1384]; iii) $k_{DO} / k_{HO} = 2.4$ [Gold, V.; Grist, S. *J. Chem. Soc., Perkin Trans. 2* **1972**, 89 – 95]; iv) detritiation of phenylacetylene at 25 ºC $k_{DO} / k_{HO} = 1.36$ [Kresge, A. J.; Lin, A. C. *J. Am. Chem. Soc.* **1975**, *97*, 6257 – 6258]; v) detritiation of chloroform at 25 ºC $k_{DO} / k_{HO} = 1.48$ [*ibid*].

[xxxii] Dependent upon the extent of proton transfer in the transition state of the reaction. See above the note.

[xxxiii] For base-catalyzed bromination of acetone at 25 ºC $k_{DO} / k_{HO} = 1.46$ [Pocker, Y. *Chem. Ind.* (*London*) **1959**, 1383 – 1384]. This value was chosen because it involves deprotonation of a carbonyl carbon acid at 25 ºC and as is the closest equivalent to deprotonation of TKPs.

Table 3.6: Kinetic acidities, k_{DO} and k_{HO}, and thermodynamic acidities, pK_a, of carbonyl carbon acids and TKPs at 25 ºC.

Entry	Carbon Acid [a]	k_{DO} /M^{-1} s^{-1}	k_{HO} /M^{-1} s^{-1}	pK_a
1 [j]	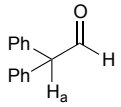	-	254	10.4 [h]
2 [j]	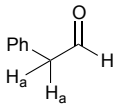	-	20.0	13.1 [h]
3 [j]	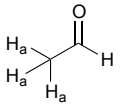	-	1.17	16.7 [h]
4 [j]	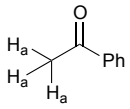	-	2.50×10^{-1}	18.3 [h]
5 [j]	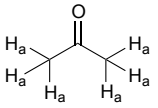	-	2.20×10^{-1}	19.3 [h]
6 [k]	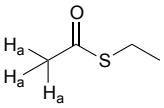	-	2.00×10^{-2}	21.0
7 [l]	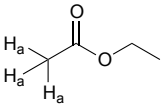	1.7×10^{-3} [b]	1.20×10^{-3} [e]	25.6 [i]
8 [m]	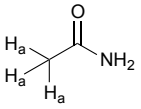	1.9×10^{-5} [b]	9.50×10^{-6} [f]	28.4 [i]
9 [n]	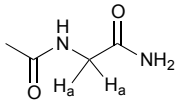	2.6×10^{-3}	1.3×10^{-3}	23.9 [i]
10 [o]	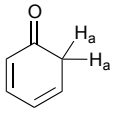	-	2.0×10^{6}	- 2.89 [h]
11	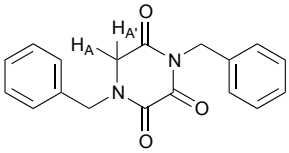	9.34×10^{4} [c]	6.40×10^{4} [g]	(4.71) [i]
12	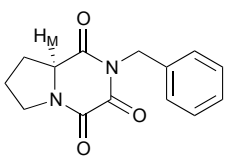	1.66×10^{6} [d]	1.14×10^{6} [g]	(1.14) [i]

[a] H_a = the acidic protons. [b] k_{DO} determined in D_2O solutions at I = 1.0. [c] k_{DO} determined in 60 : 40 D_2O : d_3-MeCN at I = 0.06 and converted to 100 % D_2O by dividing by 5.4. [d] k_{DO} determined in 60 : 40 D_2O : d_3-MeCN at I = 0.20 and converted to 100 % D_2O by dividing by 5.4. [e] Secondary solvent isotope effect k_{DO} / k_{HO} = 1.4. [f] Secondary solvent isotope effect k_{DO} / k_{HO} = 2.4. [g] Secondary solvent isotope effect k_{DO} / k_{HO} = 1.46. [h] Experimentally determined pK_a. [i] Extrapolated from Equation 3.15, which is found to not be

valid. [j] Keeffe, J. R.; Kresge, A. J. In *The Chemistry of Enols*; Rappoport, Z., Ed.; John Wiley and Sons: Chichester, **1990**; 399 – 480. [k] Amyes, T. L.; Richard, J. P. *J. Am. Chem. Soc.* **1992**, *114*, 10297 – 10302. [l] Amyes, T. L.; Richard, J. P. *J. Am. Chem. Soc.* **1996**, *118*, 3129 – 3141. [m] Richard, J. P.; Williams, G.; O'Donoghue, A. C.; Amyes, T. L. *J. Am. Chem. Soc.* **2002**, *124*, 2957 – 2968. [n] d Rios, A.; Richard, J. P.; Amyes, T. L. *J. Am. Chem. Soc.* **2002**, *124*, 8251 – 8259. [o] Capponi, M.; Gut, I. G.; Hellrung, B.; Persy, G.; Wirz, J. *Can. J. Chem.* **1999**, *77*, 605 – 613.

3.3.2.5 Origin of enhanced kinetic acidity in TKPs

There are two factors that could be responsible for the dramatic increase in kinetic acidity in the TKPs compared to similar α-carbonyl carbon acids: an enhanced inductive effect and aromaticity. The additional carbonyl in the TKP ring will increase the electron withdrawing inductive effect, which will in turn help stabilise the formation of the carbanion in the transition state. However, the additional carbonyl is located upon the opposite side of the TKP ring to the acidic protons, which should limit the magnitude of the inductive effect due to the large distance from the site of deprotonation.

In addition to the inductive effect the possibility of an aromatic enolate for the TKPs may also enhance the kinetic acidity. Boa has proposed that the enolate of the TKP could have an aromatic structure, which could help stabilise the formation of the intermediate (Scheme 3.12).[151] The enolates, **12** and **13**, and the equivalent aromatic structures, **14** and **15**, for **10** and **11** are shown in Scheme 3.21. In order for aromaticity to enhance the kinetic acidity it must be present in the transition state as well as the intermediate.

Scheme 3.21: The TKP enolates, **12** and **13**, and proposed aromatic resonance structures, **14** and **15**.

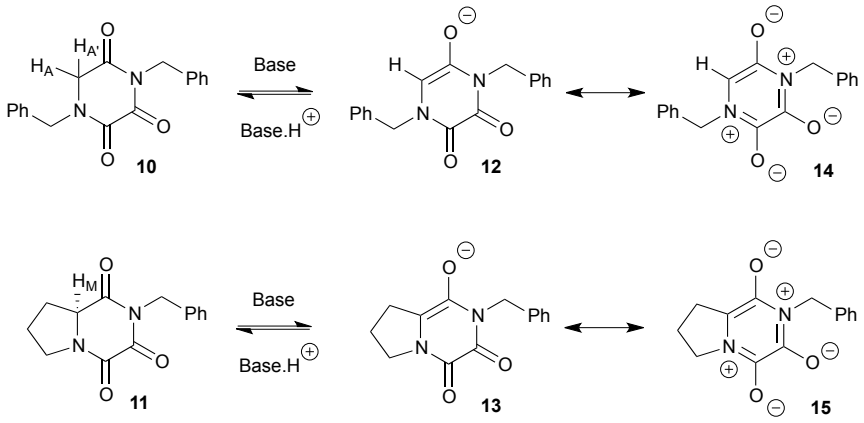

The contribution of aromaticity to transition state stabilisation is well known e.g. in Diels Alder reactions. However, the formation of the aromatic resonance structures **14** and **15** is unlikely to be as facile because: i) a significant reorganisation of charge around the TKP ring is required in order to form the two additional anionic charges at the remaining carbonyl oxygens and two cationic charges at the nitrogens; and ii) the reorganisation of solvent required to accommodate such a highly charged species will also be significant. Both of these processes would increase the work required to form the transition state, increase the barrier for proton transfer and therefore likely decreasing the kinetic acidity. To evaluate these various processes taking place in the formation of a transition state requires consideration of the Principle of Non-perfect Synchronisation (PNS).[167,168]

In even simple reactions such as proton transfer there are multiple concurrent processes occurring, e.g. bond formation/cleavage, solvation/desolvation and delocalisation/localisation of charge, which affect the stability of the transition state. The PNS acknowledges that these processes do not necessarily make equivalent progress in the transition state. Consequently, a reaction may have imbalanced transition state, where the main process, usually bond formation/cleavage, is ahead of other processes, such as delocalisation of charge. The effect of these processes on the intrinsic rate constant, k_0,[xxxiv] is that "a product-stabilizing factor whose development at the transition state is late [i.e. lags behind the main process] always lowers k_0, whereas a product-stabilizing factor that develops early [i.e. ahead of the main process] enhances k_0."[168]

Previous studies of proton transfer reactions with carbon acids, such as aryl nitromethanes (Scheme 3.22), have indicated that charge delocalisation to give the oxyanion form of the nitroenolate typically lags behind bond cleavage as only partial formation of the carbon-carbon double bond and partial cleavage of the nitrogen oxygen double bond in the transition state causes the negative charge to be localised upon the carbanion.[169] In addition, the change in solvation due to charge development is expected to lag behind charge delocalisation. Both of these processes increase the intrinsic barrier to proton transfer and lower k_0. This is particularly pertinent to deprotonation of the TKPs.

[xxxiv] The intrinsic rate constant is directly related to the Gibbs free energy of activation required to overcome the intrinsic barrier for a reaction where there is no thermodynamic driving force, i.e. $\Delta G = 0$ kJ mol^{-1}.

Scheme 3.22: The mechanism and transition state for the deprotonation of aryl nitromethane by base B.[169]

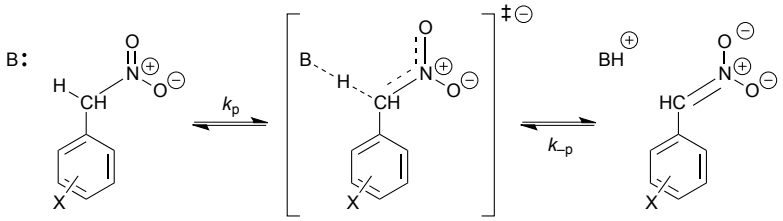

The kinetic acidities, k_{HO}, of the TKPs reflect the magnitude of the activation barrier to form the transition state in proton transfer. The large reorganisation of charge and solvation required to form the aromatic enolates of the TKPs would appear to be incongruous with the large values of k_{HO} determined, as the reorganisation would likely destabilise the formation of the transition state. However, the above does not consider the significant stabilising effect that aromaticity may have on a transition state.

A study by Bernasconi of the relative effects on the transition state of product aromaticity, product resonance and charge delocalisation,[xxxv] indicated that aromaticity is decoupled from resonance and charge delocalisation.[170] The transition state for the gas phase proton transfer between a 2,4-cyclopentadiene and a cyclopentadienyl anion was calculated (Scheme 3.23). Various indicators, including the geometries and aromatic indices, found that the transition state was closer to the aromatic conjugate base product than the acid reactant. Examinations of the charges on atoms in the transition state indicated that the negative charge was localised upon the acidic carbon C1. It was therefore concluded that the aromaticity and resonance / charge delocalisation were not coupled. Bernasconi suggested from the calculations that only minor progress to the formation of aromatic molecular orbitals is required in order for the transition state to take advantage of aromaticity for stabilisation, which is also supported by experimental observations.[171] The aromaticity in the transition state was found to lower the intrinsic barrier to the reactions and therefore increase the k_0.

[xxxv] The latter two will increase the intrinsic barrier as work is required to move electron density around the molecule.

Scheme 3.23: The deprotonation of 2,4-cyclopentdiene by cyclopentdienyl anion and transition state for the reaction. Reproduced with permission from the ACS.[170]

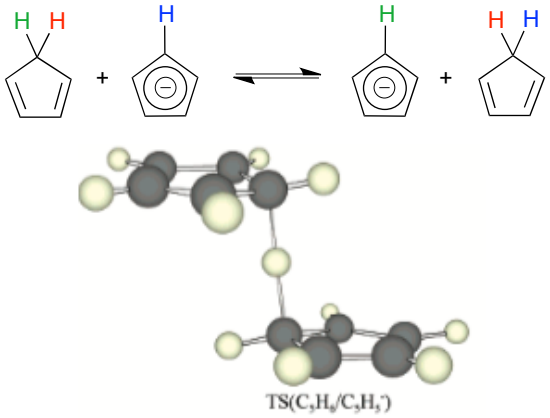

While the calculations were performed in the gas phase the decrease in intrinsic barriers has also been observed experimentally in solution (Scheme 3.24). This has been attributed, at least in part, to aromaticity stabilising the transition state. For example, the order of intrinsic barriers for deprotonation of furan **16**, selenophene **17** and thiophene **18** coordinated to a rhenium metal centre is shown to be **18** > **17** > **16**. Although there are additional contributing factors to the intrinsic barrier for proton transfer the aforementioned order is identical to that of the magnitude of aromaticity in these compounds.[172] Likewise, benzothiophen-3(2*H*)-one **20** has a lower intrinsic barrier to deprotonation than benzofuran-3(2*H*)-one **19**, which again follows the trend in aromaticity.[173]

Scheme 3.24: Examples of solution phase proton transfer reactions that show lower than expected intrinsic barriers. This is attributed, in part, to aromaticity stabilising the transition state.[172,173]

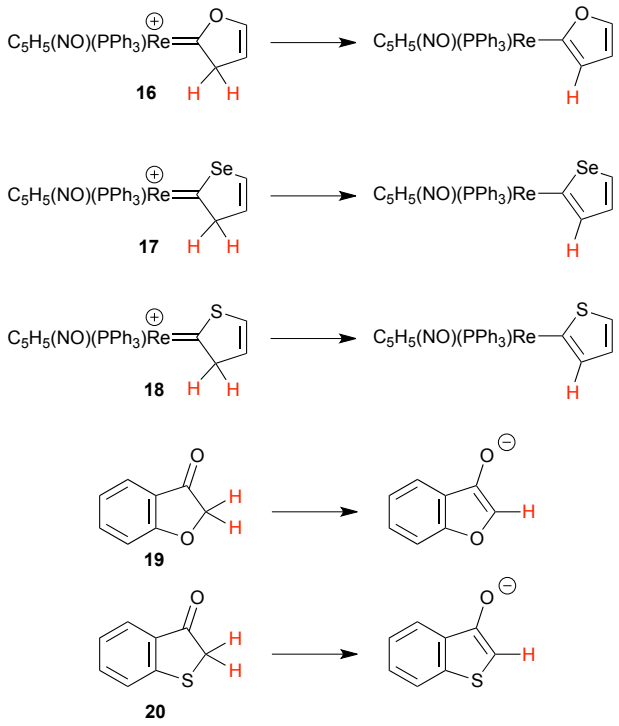

Returning to the TKP aromatic enolates, if only a small degree of formation of the aromatic molecular orbitals is required to take advantage of aromaticity in the transition state then this could explain the significant enhancement of k_{HO} values relative to other carbon acids. The k_{HO} value of 2.0×10^6 M^{-1} s^{-1} for deprotonation of cyclohexa-2,5-dienone to give the aromatic phenolate anion compares favourably with the $k_{HO} = 6.40 \times 10^4$ M^{-1} s^{-1} for glycyl TKP **10** and $k_{HO} = 1.66 \times 10^6$ M^{-1} s^{-1} for prolyl TKP **11**.[166]

3.3.2.6 Thermodynamic acidity pK_a of TKPs

A Brønsted relationship exists between the experimentally determined kinetic acidities and the pK_as of the carbon acids in Table 3.6, Entries 1 – 5:

$$\log\frac{k_{HO}}{p} = -0.401(pK_a + \log p) + 6.496 \qquad \text{(Equation 3.15)}$$

where p is the number of acidic protons in the carbon acid[xxxvi] and the Brønsted coefficient β_1 = - 0.401. An estimate for the pK_a of glycyl and prolyl TKP may be found by extrapolating the Brønsted relationship to give glycyl TKP pK_a = 4.71 and prolyl TKP pK_a = 1.14.

The validity of using this Brønsted relationship for the pK_as of TKPs is questionable. In order to determine the values the relationship must be extrapolated out by a further 5 – 9 pK_a units beyond the nearest α-carbonyl carbon acid (Figure 3.10). In addition, the possible aromatic nature of the TKP enolates means the intrinsic barriers for proton transfer for TKPs have additional influences to those encountered by the other neutral monocarbonyl acids. In order to test the validity of this Brønsted relationship the experimentally known k_{HO} value (2.0×10^6 M^{-1} s^{-1}) for cyclohexa-2,5-dienone was inserted into Equation 3.15 which yielded a pK_a = 0.98.[166] This value is 3.87 pK_a units above the experimentally determined value of pK_a = - 2.89 and therefore the Brønsted relationship in Equation 3.15 does not appear to be valid for carbon acids whose enolates have an aromatic character and whose transition states are also expected to display a level of aromaticity.

[xxxvi] Required to give a statistical correction to the values so that they are equivalent to a single proton.

Figure 3.10: Plot of the Brønsted relationship (Equation 3.15) between the kinetic acidities, k_{HO}, and thermodynamic acidities, pK_a, for the carbonyl carbon acids in Table 3.6, Entries 1 – 5. The extrapolated plots to determine possible pK_as for glycyl TKP **10** and prolyl TKP **11** from Equation 3.15 are shown. The plot of experimental k_{HO} and pK_a for cyclohexa-2,5-dienone is also shown. p = number of acidic protons.

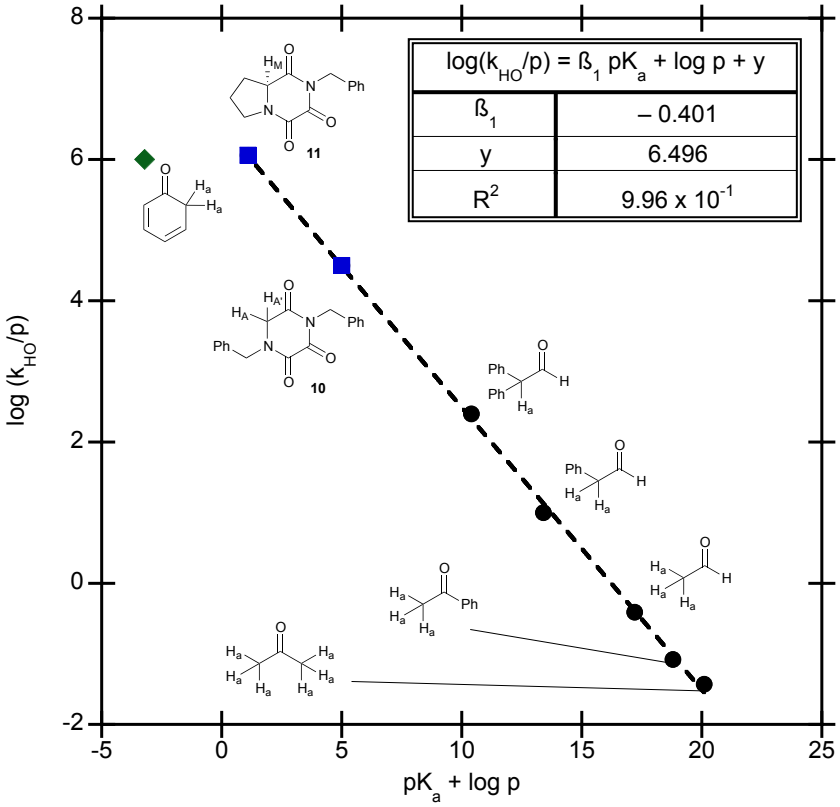

A more appropriate Brønsted relationship may be found using the kinetic and thermodynamic acidities of carbonyl carbon acids with aromatic enolates (Table 3.7).

Table 3.7: Kinetic acidities, k_{HO}, and thermodynamic acidities, pK_a, of carbonyl carbon acids and TKPs whose conjugate bases are aromatic, at 25 ºC.

Entry	Carbon Acid [a]	k_{HO} /M^{-1} s^{-1}	pK_a
1 [b]	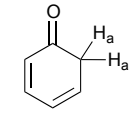	2.0×10^6	- 2.89
2 [c]	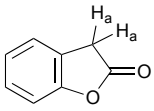	2.24×10^3	11.87
3 [c]	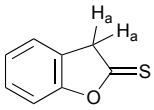	8.32×10^4	2.81
4 [c]	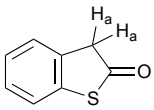	9.55×10^3	8.85
5 [d]	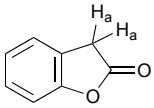	2.44×10^3	11.68
6 [d]	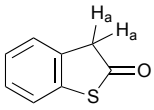	1.05×10^4	8.83
7 [e]	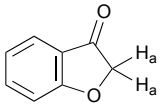	83.7	11.71
8 [e]	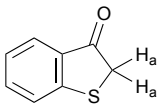	2.30×10^3	9.45 [g]
9 [f]	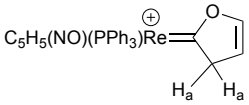	1.99×10^3	5.78
10 [f]	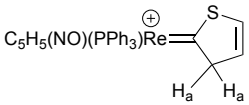	2.37×10^4	2.51
11 [f]	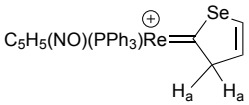	1.61×10^4	4.17
12	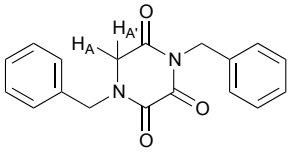	6.40×10^4	4.15 [h] 4.39 [i]
13	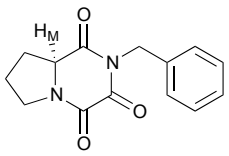	1.14×10^6	- 3.35 [h] - 3.35 [i]

[a] H_a = number of acidic protons. [b] Capponi, M.; Gut, I. G.; Hellrung, B.; Persy, G.; Wirz, J. *Can. J. Chem.* **1999**, *77*, 605 – 613. [c] Kresge, A. J.; Meng, Q. *J. Am. Chem. Soc.* **2002**, *124*, 9189 – 9198. [d]

Bernasconi, C. F.; Zheng, H. *J. Org. Chem.* **2006**, *71*, 8203 – 8211. [e] Bernasconi, C. F.; Pérez-Lorenzo, M. *J. Am. Chem. Soc.* **2007**, *129*, 2704 – 2712. [f] Bernasconi, C. F.; Ragains, M. L.; Bhattacharya, S. *J. Am. Chem. Soc.* **2003**, *125*, 12328 – 12336. [g] Estimated from a fitting in reference 'e'. [h] Interpolated from Equation 3.16. [I] Interpolated from Equation 3.17.

The Brønsted relationship in Equation 3.16 is constructed from Table 3.7 Entries 1 – 6, 8. The carbon acids based upon the rhenium carbene complexes cannot be included in the relationship because i) the acid form is cationic while the other α-carbonyl carbon acids in Table 3.7 are neutral and ii) the organometallic nature of the carbon acids from coordination to the metal centre is expected to alter the behaviour compared to the organic carbon acids. Benzofuran-3(2*H*)-one was also omitted because of its abnormally low kinetic acidity, which is attributed to weak type 2 π-donor effects (Table 3.7, Entry 7).[173]

$$\log \frac{k_{\mathrm{HO}}}{p} = -0.199(\mathrm{p}K_{\mathrm{a}} + \log p) + 5.39 \qquad \text{(Equation 3.16)}$$

where p is the number of acidic protons in the carbon acid and the Brønsted coefficient β_2 = - 0.199. Using Equation 3.16 the pK_as for the TKPs may be interpolated to give a pK_a = 4.15 for glycyl TKP **10** and extrapolated to give a pK_a = - 3.35 for prolyl TKP **11** (Figure 3.11).

Figure 3.11: Plot of the Brønsted relationship (Equation 3.16) between the kinetic acidities, k_{HO}, and thermodynamic acidities, pK_a, for the carbonyl carbon acids in Table 3.7: Entries 1 – 6, 8 (See Table 3.7 footnotes for references). Plots for the interpolated pK_as for glycyl TKP **10** and prolyl TKP **11** from Equation 3.16 are shown. p = number of acidic protons.

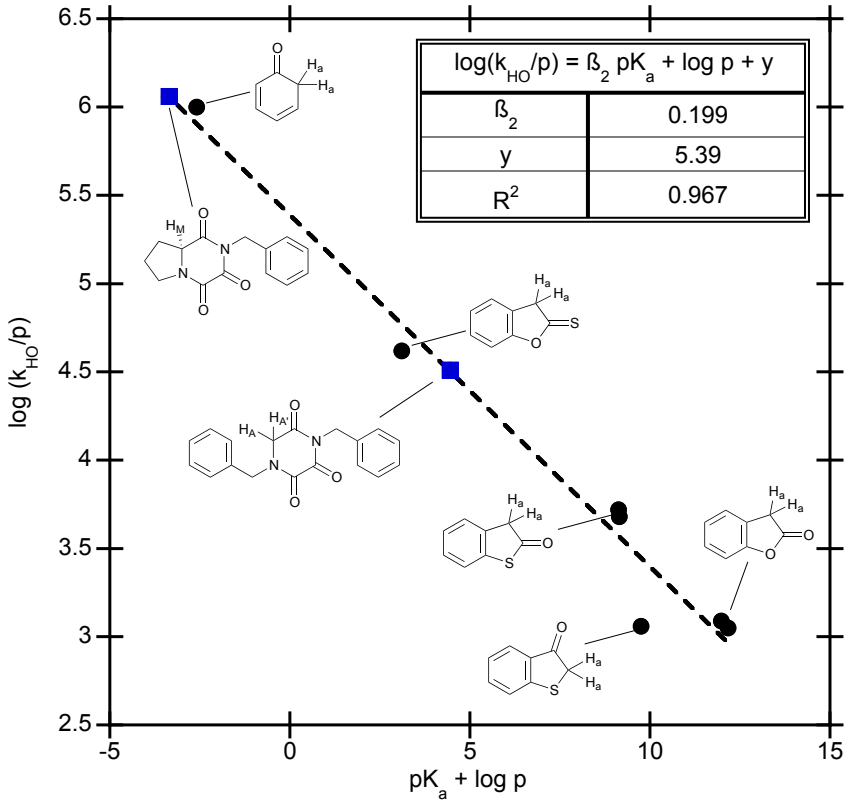

The removal of benzothiophene-3(2*H*)-one, Table 3.7, Entry 8, allows the construction of a Brønsted relationship with a better R^2 value, 0.992 vs. 0.967:

$$\log\frac{k_{\mathrm{HO}}}{p} = -0.193(\mathrm{p}K_{\mathrm{a}} + \log p) + 5.41 \qquad \text{(Equation 3.17)}$$

where p is number of acidic protons and the Brønsted coefficient β_3 = - 0.193. Using Equation 3.17 the pK_as for the TKPs may be interpolated to give a pK_a = 4.39 for glycyl TKP **10** and extrapolated to give a pK_a = - 3.35 for prolyl TKP **11** (Figure 3.12).[xxxvii] If

[xxxvii] The unadjusted k_{DO} values for 60 : 40 D_2O : d_3-MeCN were also input into Equation 3.17 to give pK_a estimates for the glycyl TKP pK_a = - 0.28 and prolyl TKP pK_a = - 8.00. These values are substantially smaller than the pK_a estimates from the adjusted k_{DO} values and given the observation of the deuterated

the extrapolated pK_a value for prolyl TKP is correct then this would make it the most acidic α-carbonyl based carbon acid to date.

The value of β_3 = - 0.193 indicates that in the transition state the progression of proton transfer to the base is ~ 19 % complete. This is lower than the β = - 0.401 value (Equation 3.15) or ~ 40 % proton transfer to the base in the transition state for the simple α-carbonyl carbon acids and indicates that the aromatic carbon acids have earlier transition states than their non-aromatic cousins.

Figure 3.12: Plot of the Brønsted relationship (Equation 3.16) between the kinetic acidities, k_{HO}, and thermodynamic acidities, pK_a, for the carbonyl carbon acids in Table 3.7 Entries 1 – 6 (See Table 3.7 footnotes for references). Plots for the interpolated pK_as for glycyl TKP **10** and prolyl TKP **11** from Equation 3.16 are shown. p = number of acidic protons.

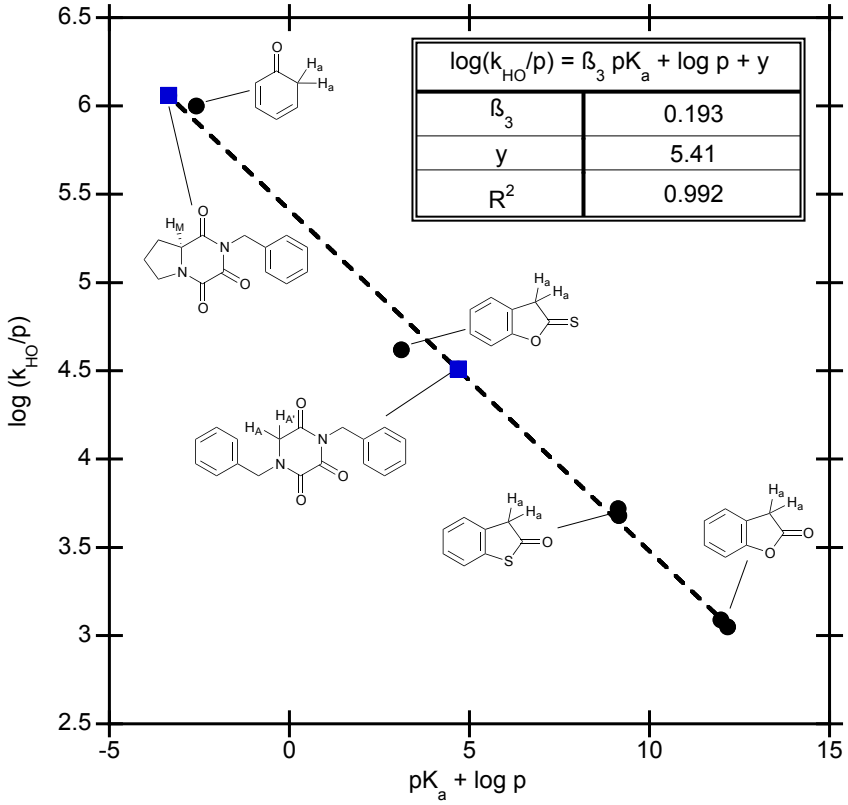

The reliability of the pK_a values for glycyl TKP pK_a = 4.15 – 4.39 and prolyl TKP pK_a = - 3.35 derived from Equation 3.16 and Equation 3.17 are expected to higher

acid form of the TKP in the ^{1}H NMR spectroscopy suggests that a conversion factor is required to adjust the k_{DO} values for 60 : 40 D_2O : d_3-MeCN into k_{DO} values for 100 % D_2O (Section 3.3.2.2).

than that derived for Equation 3.15, as these values are estimated from Brønsted relationships constructed from carbon acids with aromatic enolates rather than carbon acids with a simple α-carbonyl enolate. The reliability of the glycyl TKP pK_a value is also higher because it is an interpolation in Equation 3.16 and Equation 3.17 and not an extrapolation as in Equation 3.15. While the pK_a value for prolyl TKP is an extrapolation it is only 0.46 pK_a units outside of the interpolation range of the Brønsted relationship and there is believed to be a reasonable estimate.

Figure 3.13 shows a comparison of the Brønsted relationships for α-carbonyl carbon acids (Normal, Equation 3.15) and aromatic enolates (Aromatic, Equation 3.16). For the α-carbonyl carbon acids the magnitude of k_{HO} and pK_a is dependent upon changes in surrounding moieties that affect k_{HO} and pK_a through inductive, resonance and electrostatic effects. For the carbon acids with aromatic enolates the changes in k_{HO} and pK_a are dependent upon the aforementioned factors as well as aromaticity. The estimate for the pK_a of the glycyl TKP does not significantly differ between the Brønsted relationships for α-carbonyl carbon acids (Equation 3.15) and for aromatic enolates (Equations 3.16 and 3.17), with the pK_a = 4.71 vs. 4.15 – 4.39, respectively. For the prolyl TKPs there is a more significant difference with pK_a = 1.14 vs. - 3.35, respectively. The intersection between the two Brønsted relationships in Figure 3.13 occurs close to both pK_a estimates for the glycyl TKP. This indicates that the proposed aromaticity in the enolate does not significantly enhance the stability of the glycyl TKP enolate relative to a glycyl enolate that has no aromaticity present. However, the ~ 4.5 pK_a unit difference in the values of the prolyl TKPs indicates that aromaticity would significantly stabilise the enolate.

Figure 3.13: Comparison of the Brønsted relationships for α-carbonyl carbon acids (Equation 3.15) and aromatic enolates (Equations 3.16).

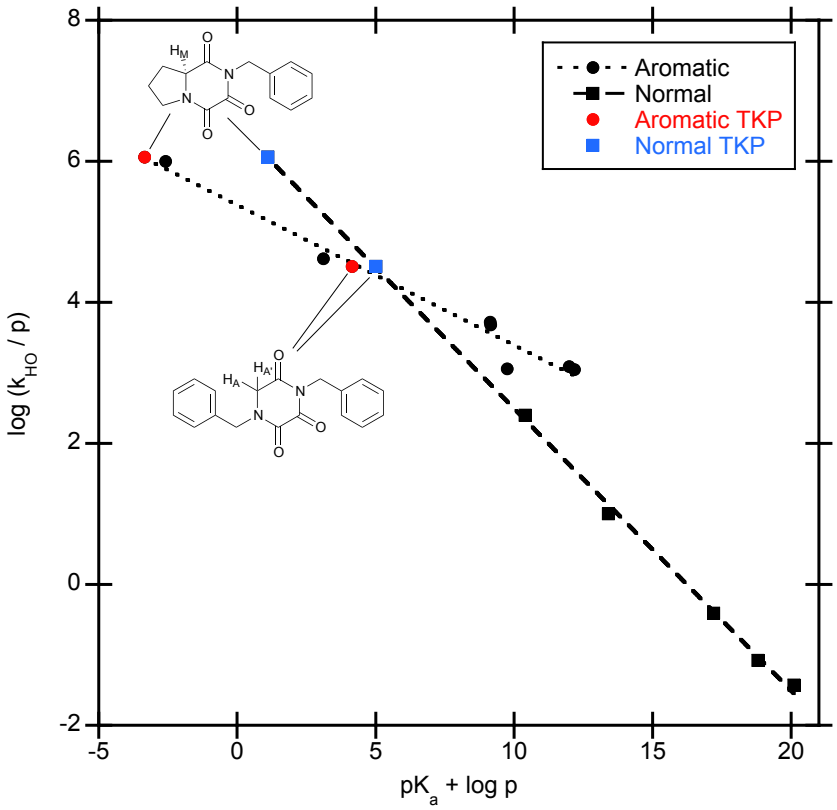

Normal

$\log(k_{HO}/p) = ß_1\, pK_a + \log p + y$	
$ß_1$	– 0.401
y	6.496
R^2	0.988

Aromatic

$\log(k_{HO}/p) = ß_2\, pK_a + \log p + y$	
$ß_2$	– 0.199
y	5.39
R^2	0.967

The pK_a estimate for the glycyl TKP is ~ 16.5 pK_a units lower than c(Gly-Gly) DKP. The enhanced acidity of the TKP is attributed principally to the additional carbonyl in the ring allowing an aromatic enolate to form. The near equivalence of the pK_a estimates in both Brønsted relationships could suggest that the aromaticity is unnecessary. However, this would require the additional carbonyl in the TKP ring to stabilise the enolate via an alternative mechanism. One possibility for this could be a change in the stability of the various resonance forms of the TKP enolate in a similar fashion to that proposed by Coote and Easton (Chapter 2: Section 2.16 and Section 2.3.3.2).[174] A selection of resonance forms for the glycyl TKP carbanion is shown in Scheme 3.25. The additional carbonyl could potentially increase the proportion of the enolate resonance form **23** by disfavouring the resonance form **22** by destabilising the

formation of the cationic nitrogen. Also, the additional carbonyl could also help stabilise the resonance form **24** by withdrawing electron density from the adjacent amide and therefore increase the proportion of the cationic amide resonance form, which could help stabilise the formation to the carbanion. Whether these effects stabilise the glycyl TKP by ~ 16.5 pK_a units relative to the glycyl DKP is doubtful. Coote and Easton have calculated that strongly electron withdrawing groups on the nitrogen may reduce the pK_a of the distal protons by 4.6 ($-CF_3$) – 10.1 ($-SO_2CF_3$) units. While this effect is not an exact comparison to the additional carbonyl in the TKPs, as substitution is located on the nitrogen and not the adjacent carbon, both changes in substitution are adjacent to the amide group and thus the additional lowering of pK_a by 6.4 – 11.9 units from the carbonyl is beyond what might reasonably be expected from changes in the distribution of resonance forms. It is also worth noting that the resonance effects on the prolyl TKP are expected to be similar to that of the glycyl TKP as it also contains two secondary nitrogens. If no aromaticity was present in the prolyl TKP then the further lowering of the pK_a by ~ 3.6 units is difficult to account for. In the DKPs the stereoelectronic effect results in a difference of up to 2.4 units between the prolyl and glycyl pK_as but the additional 1.2 units of difference for the TKPs is inexplicable.

Including aromaticity results in a 7.5 – 7.7 pK_a unit difference between the prolyl and glycyl TKPs. This difference is more substantial than that observed in the DKPs. This difference does assume a consistent intrinsic barrier for deprotonation by hydroxide between the prolyl and glycyl TKPs. Given the possible presence of the stereoelectronic effect in the prolyl TKP the intrinsic barrier could be lower which would result in a positive deviation of the aromatic Brønsted relationships. Therefore, given the shallower gradient of the aromatic Brønsted relationships, this will shift the pK_a of the prolyl TKP higher than would be expected for the α-carbonyl carbon acids Brønsted relationship, and hence closer to that of the glycyl TKP.

Scheme 3.25: A selection of possible resonance forms for the glycyl TKP carbanion.

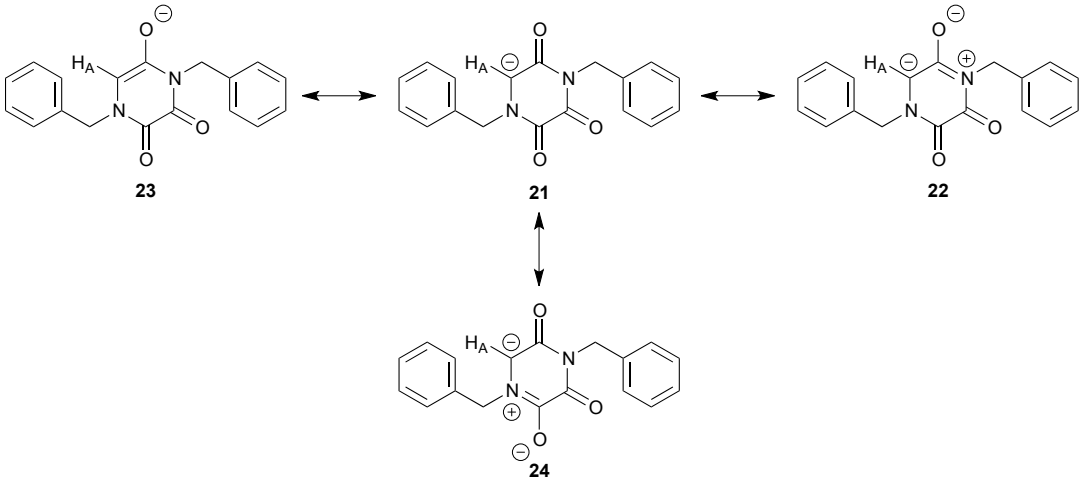

One implication of the above pK_a values for the TKPs is that in solutions whose pH is more than two pH units above the pK_a of the TKP at equilibrium the enolate should be the only species present in solution. The deuterium exchange reactions for the glycyl TKP were carried out at p*D* 6.28 – 6.29 and for the prolyl TKP at p*D* 4.76 – 5.29. Thus deprotonation of the TKPs at these p*D*s should in both cases result in the enolate species being favoured in solution. In principle this ought to be seen in the ^{1}H NMR spectra. For the glycyl TKP there is no substantial change over time in the chemical shift of any of the remaining protons on the TKP in the (Figure 3.1). Indeed the appearance of an upfield triplet for CHD from coupling of the remaining H to the D indicates the deuteration of the enolate occurs and the TKP is not trapped in enolate form upon deprotonation. For the prolyl TKP there is again no substantial change over time in the chemical shift of the any of the observable protons in the (Figure 3.5). The protons that should experience the most significant chemical shift upon enolate formation ought to be the methylene protons adjacent to the α-proton and the benzyl methylene protons on N1 (Scheme 3.1). We believe that the benzyl methylene protons are hidden under the HOD peak and so any change from enolate formation cannot be observed. The chemical shift of the methylene protons adjacent to the α-protons is not altered. This could either suggest that in the enolate the anionic charge is heavily localised upon the carbonyl oxygen rather than the α-carbon and therefore does not significantly affect the chemical shift of the methylene protons, or, it would suggest that the acid form is favoured more than expected in solution and that the pK_a estimate for the prolyl TKP is too low.

Attempts were made to observe the enolate of the Glycyl TKP using UV-Vis spectrophotometry (data not shown). However, increasing the pH of the solution caused a decrease in absorbance rather than the expected increase from the formation of the enolate. Based on the work by Taylor, this was attributed to a hydrolysis reaction, which caused the ring opening of the TKP.[157] Taylor observed complete hydrolysis in potassium carbonate buffered solutions above p*D* = 10.79 and partial hydrolysis in acetate buffered solutions after 22 days (p*D* = 4.95) via ^{1}H NMR spectroscopy and mass spectrometry. The molecular ion for the possible hydrolysis products **25**, **26** and **27** was identified (Scheme 3.26).

Scheme 3.26: Possible hydrolysis products for the ring opening of the Glycyl TKP **1** ring. Each product **25**, **26** and **27** has an equivalent mass of [MH^{+}] = 328 *m/z* which was identified via mass spectrometry of the deuterated buffer solutions.[157]

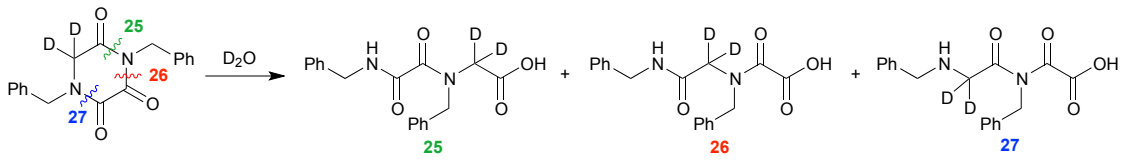

3. 4 Summary

In conclusion we have used hydrogen deuterium exchange experiments to determine second order rate constants for deuteroxide catalysed and buffer catalysed exchange, k_{DO} and k_{A-}, for the α-protons on a glycyl **10** TKP ($k_{DO} = 5.09 \times 10^5$ M^{-1} s^{-1}, $k_{A-} = 7.21 \times 10^{-2}$ M^{-1} s^{-1}) and prolyl **11** TKP ($k_{DO} = 8.99 \times 10^6$ M^{-1} s^{-1}, $k_{A-} = 1.61 \times 10^{-2}$ M^{-1} s^{-1}). Potential explanations for the greater kinetic acidity of the prolyl **11** TKP relative to the glycyl **10** TKP, including reactant destabilisation, have been proposed. The k_{DO} values for a 60 : 40 D_2O : d_3-MeCN solution were converted to a k_{DO} value for a 100 % D_2O solution to give $k_{DO} = 9.34 \times 10^4$ M^{-1} s^{-1} for glycyl **10** TKP and 1.66×10^6 M^{-1} s^{-1} prolyl **11** TKP.

The effect of an additional carbonyl group on a DKP ring in the TKPs increases the kinetic acidity, k_{DO}, of the α-protons by 10^7-fold.

The mechanism for proton transfer in TKPs was found to have rate determining deprotonation of the carbon acid as there was clear evidence for buffer catalysed exchange. A secondary solvent isotope effect of $k_{DO} / k_{HO} = 1.46$ was therefore used to convert the k_{DO} values into second order rate constants for hydroxide catalysed exchange, k_{HO} as proton transfer is only partially complete at the transition state of the rate determining step.

The kinetic acidity, k_{HO} (M^{-1} s^{-1}), of the TKPs (glycyl TKP **10** $k_{HO} = 6.40 \times 10^4$ M^{-1} s^{-1}; prolyl TKP **11** $k_{HO} = 1.14 \times 10^6$ M^{-1} s^{-1}) is similar to that of carbon acids that have aromatic enolates. An aromatic enolate is possible for TKPs although this requires significant reorganisation of charge and solvent. The Principle of Non-perfect Synchronisation and previous work by Bernasconi on the early formation of aromaticity in the transition state was used to justify the explanation that aromaticity is responsible for the significantly enhanced kinetic acidity of the TKPs relative to DKPs and other simple α-carbonyl carbon acids.

A Brønsted relationship based upon carbon acids with aromatic enolates was constructed for the first time and used to estimate the pK_a of the TKPs as glycyl **10** TKP pK_a = 4.15 – 4.39 and prolyl **11** TKP pK_a = - 3.35.

3.5 Experimental

3.5.1 General Instrumentation

NMR: Kinetic NMR spectra were recorded on an Oxford Varian Unity Inova 500 MHz NMR spectrometer. NMR samples were prepared in 60 : 40 D_2O : d_3-acetonitrile. All chemical shifts are reported relative to the residual solvent peak of δ_H 4.79 ppm for D_2O.

3.5.2 Materials

NMR Solvents: d_2-Deuterium oxide (99.9 atom % D) and d_3-acetonitrile (99.8 atom % D) were purchased from Goss Scientific. Deuterium chloride (99 atom % D, 35 wt %) was purchased from Sigma-Aldrich. A stock solution of 2 M potassium chloride were prepared by dissolving solid potassium chloride in D_2O. A stock solution of deuterium chloride was prepared by a dissolving concentrated deuterium chloride solution in D_2O and then titrating against volumetric sodium hydroxide solutions to determine the concentration of DCl.

Kinetic Experiments: Potassium acetate, potassium chloride and tetramethylammonium hydrogensulfate was purchased from Sigma Aldrich. Glycyl TKP and prolyl TKP were donated by Prof. Nigel Simpkins.

3.5.3 Kinetic Experiments

The methodology for kinetic experiments on the TKPs was near identical to that used for the kinetic experiments on DKPs.

3.5.3.1 Solution Preparation

Potassium acetate (KAcO / AcOH) buffer solutions were prepared from dissolving solid potassium acetate and 60 : 40 D_2O : d_3-acetonitrile. Deuterium chloride solution

was used to adjust the percentage of free base form of the buffer. A 2 M potassium chloride solution was used to adjust the ionic strength of the solution.

A tetramethylammonium deuteriosulfate internal standard solution was prepared with D_2O.

3.5.3.2 Measurement of pH

The pH of the buffered solutions was determined using a MeterLab™ PHM 290 p*H*-Stat Controller equipped with a radiometer combination electrode filled with saturated KCl solution at 25 ºC. The pH meter was calibrated with pH 4 phthalate and pH 7 potassium phosphate solutions. The p*D* values were calculated by adding 0.4 to the pH meter reading.[175] It was necessary to correct the p*D* values as the solutions contained 40% d_3-MeCN. Bosch *et al* have shown that the difference between the pH of a solution containing 40% MeCN and the pH recorded with a glass electrode containing 100% H_2O is δ = - 0.175 pH units; this correction was added to the observed p*D* [p*D*(obs)] values to give the corrected p*D* [p*D*(corr)] values for the 60 : 40 D_2O : d_3-MeCN solution (Equation 3.19).[176]

$$\mathrm{p}D(\mathrm{corr}) = \mathrm{p}D(\mathrm{obs}) + \delta = \mathrm{p}D(\mathrm{obs}) - 0.175 \qquad \text{(Equation 3.19)}$$

The autoprotolysis constant of water, K_s, varies with solvent composition. Aslan has shown that for a 60 : 40 H_2O : MeCN solution at 25 ºC and I = 0.1 ($NaClO_4$) the autoprotolysis constant of water is pK_s(H_2O : MeCN) = 14.74.[177] To convert this into the autoprotolysis constant for D_2O in a 60 : 40 H_2O : MeCN, pK_s(D_2O : MeCN), we assumed that the ratio of $K_s(H_2O) / K_s(D_2O) = 10^{-14} / 10^{-14.87} = 7.40$ in was the same for a H_2O / D_2O acetonitrile mixed solvent, i.e. $K_s(H_2O : MeCN) / K_s(D_2O : MeCN) = 7.40$, and therefore taking p$K_s$($H_2O$: MeCN) = 14.74 from Aslan above the pK_s(D_2O : MeCN) = 15.61. It is assumed that the use of d_3-MeCN rather than MeCN will not substantially affect this value.

In order to determine the concentration of deuteroxide present in a 60 : 40 D_2O : d_3-MeCN solution Euation 3.20 was used. A previously determined activity coefficent for the deuteroxide ion (γ_{DO}) in a 2 : 1 D_2O : d_3-MeCN solution of γ_{DO} = 1.56 was used in conjunction with the p*D*(corr) and pK_s(D_2O : MeCN) values from above to determine the concentration of deuteroxide ion.[164]

$$[OD^-] = \frac{10^{[pD(corr) - pK_s(D_2O:MeCN)]}}{\gamma_{OD}} \quad \text{(Equation 3.20)}$$

3.5.3.3 NMR conditions

The hydrogen deuterium exchange experiments were usually carried out on an Oxford Varian Unity Inova 500 MHz NMR spectrometer with a thermostated probe. A pulse sequence with a 20 s relaxation delay, an acquisition time of 4 s and a 90 º pulse angle. A total of 32 transients were taken for each spectrum (a total acquisition time of ~ 12 min 45 s). The measurement times, *t*, for the exchange experiments were calculated from the mid-point of the acquisition. ^{1}H NMR spectral baselines were subject to a first-order drift correction before integration of the peak areas. The integration of substrate peak areas was compared to the peaks of the tetramethylammonium deuteriosulfate internal standard with an arbitrary value of 1000 for the integration of the internal standard.

To initiate an exchange reaction the TKP was initially dissolved in a small volume (< 20 μL) of d_3-acetonitrile. 2.0 mL of the buffer solution was then added followed by the internal standard solution. 0.7 mL of this solution was then placed within an NMR tube and this was immediately placed within the thermostated NMR spectrometer. The spectrometer was then reshimmed and the exchange was subsequently monitored. Periodically throughout the experiment ~ 4 acquisitions the probe was reshimmed to correct for any drift in the magnetic field. The remaining 1.3 mL of the solution was used to monitor the pH of the solution throughout the exchange experiment. Little to no change was observed in the pH of the solutions between the beginning and end of the experiments.

3.6 References:

(137) Bornwater, J. T. *Rec Trav Chim Pays-Bas* **1917**, *36*, 250.

(138) Safir, S. R.; Hlavka, J. J.; Williams, J. H. *J Org Chem* **1953**, *18*, 106.

(139) Makino, S.; Nakanishi, E.; Tsuji, T. *Synlett* **2003**, 817.

(140) Usami, Y.; Yamaguchi, J.; Numata, A. *Heterocycles* **2004**, *63*, 1123.

(141) Seya, H.; Nozawa, K.; Nakajima, S.; Kawai, K. I.; Udagawa, S. I. *J Chem Soc Perk Trans 1* **1986**, 109.

(142) Casnati, G.; Pochini, A.; Ungaro, R. *Gazz Chim Ital* **1973**, *103*, 141.

(143) Marchelli, R.; Dossena, A.; Pochini, A.; Dradi, E. *J Chem Soc Perk Trans 1* **1977**, 713.

(144) Overman, L. E.; Shin, Y. *Org Lett* **2007**, *9*, 339.

(145) DeLorbe, J. E.; Jabri, S. Y.; Mennen, S. M.; Overman, L. E.; Zhang, F. L. *J Am Chem Soc* **2011**, *133*, 6549.

(146) Furst, L.; Narayanam, J. M. R.; Stephenson, C. R. J. *Angew Chem Int Ed* **2011**, *50*, 9655.

(147) Boyer, N.; Movassaghi, M. *Chem Sci* **2012**, *3*, 1798.

(148) Yanagihara, M.; Sasaki-Takahashi, N.; Sugahara, T.; Yamamoto, S.; Shinomi, M.; Yamashita, L.; Hayashida, M.; Yamanoha, B.; Numata, A.; Yamori, T.; Andoh, T. *Cancer Sci* **2005**, *96*, 816.

(149) Block, K. M.; Wang, H.; Szabo, L. Z.; Polaske, N. W.; Henchey, L. K.; Dubey, R.; Kushal, S.; Laszlo, C. F.; Makhoul, J.; Song, Z. H.; Meuillet, E. J.; Olenyuk, B. Z. *J Am Chem Soc* **2009**, *131*, 18078.

(150) Jiang, C.-S. G., Y.-W. *Mini-Rev. Med. Chem.* **2011**, *11*, 728

(151) Bailey, C.; Baker, E.; Hayler, J.; Kane, P. *Tetrahedron Lett* **1999**, *40*, 4847.

(152) Bailey, P. D.; Bannister, N.; Bernad, M.; Blanchard, S.; Boa, A. N. *J Chem Soc Perk Trans 1* **2001**, 3245.

(153) Cabanillas, A.; Davies, C. D.; Male, L.; Simpkins, N. S. *Chem Sci* **2015**, *6*, 1350.

(154) Wang, Y.; Liu, X. F.; Deng, L. *J Am Chem Soc* **2006**, *128*, 3928.

(155) Wang, B. M.; Wu, F. H.; Wang, Y.; Liu, X. F.; Deng, L. *J Am Chem Soc* **2007**, *129*, 768.

(156) Tan, B.; Hernandez-Torres, G.; Barbas, C. F. *Angew Chem Int Ed* **2012**, *51*, 5381.

(157) Taylor, B., Master's Thesis, Durham University, 2014.

(158) de Grotthuss, C. J. T. *Ann. Chim.* **1806**, *58*, 54

(159) Rios, A.; Richard, J. P.; Amyes, T. L. *J Am Chem Soc* **2002**, *124*, 8251.

(160) Amyes, T. L.; Richard, J. P. *J Am Chem Soc* **1996**, *118*, 3129.

(161) Giese, K.; Kaatze, U.; Pottel, R. *J Phys Chem* **1970**, *74*, 3718.

(162) Kaatze, U. *J Chem Eng Data* **1989**, *34*, 371.

(163) Kaatze, U.; Pottel, R.; Schumacher, A. *J Phys Chem* **1992**, *96*, 6017.

(164) Massey, R. S.; Collett, C. J.; Lindsay, A. G.; Smith, A. D.; O'Donoghue, A. C. *J Am Chem Soc* **2012**, *134*, 20421.

(165) Delley, R. J.; O'Donoghue, A. C.; Hodgson, D. R. W. *J Org Chem* **2012**, *77*, 5829.

(166) Capponi, M.; Gut, I. G.; Hellrung, B.; Persy, G.; Wirz, J. *Can J Chem* **1999**, *77*, 605.

(167) Bernasconi, C. F. *Accounts Chem Res* **1987**, *20*, 301.

(168) Bernasconi, C. F. *Accounts Chem Res* **1992**, *25*, 9.

(169) Bordwell, F. G.; Boyle, W. J. *J Am Chem Soc* **1972**, *94*, 3907.

(170) Bernasconi, C. F.; Wenzel, P. J.; Ragains, M. L. *J Am Chem Soc* **2008**, *130*, 4934.

(171) Tsuji, T.; Okuyama, M.; Ohkita, M.; Kawai, H.; Suzuki, T. *J Am Chem Soc* **2003**, *125*, 951.

(172) Bernasconi, C. F.; Ragains, M. L.; Bhattacharya, S. *J Am Chem Soc* **2003**, *125*, 12328.

(173) Bernasconi, C. F.; Perez-Lorenzo, M. *J Am Chem Soc* **2007**, *129*, 2704.

(174) Ho, J. M.; Easton, C. J.; Coote, M. L. *J Am Chem Soc* **2010**, *132*, 5515.

(175) Glasoe, P. K.; Long, F. A. *J Phys Chem* **1960**, *64*, 188.

(176) Gagliardi, L. G.; Castells, C. B.; Rafols, C.; Roses, M.; Bosch, E. *Anal Chem* **2007**, *79*, 3180.

(177) Kilic, E.; Aslan, N. *Microchim Acta* **2005**, *151*, 89.

4 Cysteine Derivative Acidity and Native Chemical Ligation

4.0 Foreword

This chapter describes investigations into the pK_a of various cysteine derivatives and its application to native chemical ligation (NCL) – a technique used in the chemical synthesis of proteins. Section 4.1 details recent developments in the area of native chemical ligation. Section 4.2.1 – 4.2.3 describes the results of UV-Vis spectrophotometry experiments to determine the pK_a of various cysteine derivatives. These results are discussed in Section 4.3 and the implications for native chemical ligation are outlined in the Discussion (Section 4.3.5) and Conclusion (Section 4.4). Experimental details are presented in Section 4.5.

4.1 Introduction

4.1.1 Protein Synthesis

Proteins are highly versatile biological macromolecules with cellular functions that range from catalysis, *e.g.* enzymes which undertake the biochemistry of cells, to structure *e.g.* collagen. The function and properties of proteins is related to their primary, secondary, tertiary and quaternary structures and considerable research effort is expended upon elucidating these structure/function relationships.[178]

One approach to tackle this problem is to make modifications to the structure of the protein and observe how these changes affect the function relative to the original "wild type". The most common approach to modifying the structure is to use recombinant-DNA based molecular biology. In this technique the DNA that encodes for the protein is incorporated into the plasmid of *Escherichia coli* (or similar bacteria), which will then go onto express the protein on scale. Mutations to the protein can be performed by altering the base pairing in the DNA to encode for a different amino acid to the wild type. While this technique has had great success in illuminating the structure/function relationship of a vast number of proteins it does have a number of limitations. Apart from a few exceptions, one drawback is the inability to incorporate non-native amino acids into the proteins using molecular biology. This therefore limits modification to the 20 naturally occurring amino acids. Another drawback is that many proteins require site-specific post-translational modification, which is not always possible within the cell.

The total chemical synthesis of proteins circumvents the restrictions of molecular biology allowing much greater control over the structure of protein. Fine control of the amino acid sequence is possible and non-native amino acids can be readily incorporated into structure.[179] There have been two key developments in the chemical synthesis of proteins. The first is Solid Phase Peptide Synthesis[180] and the second is Native Chemical Ligation.[181]

Prior to the 1960s the chemical synthesis of peptides and proteins was performed in solution.[182,183] Fischer, the founder of peptide chemistry, had used this approach and his work set the methodological precedent for peptide synthesis.[184,185] This technique had a number of notable successes including the first synthesis of the

hormone oxytocin (a 9-mer polypeptide) by du Vigneaud[186] and in the synthesis of the 124-mer ribonuclease A.[187] However, this technique has drawbacks including: 1) Lack of enantiopurity during peptide bond formation, where racemisation of the C-terminal residue can occur during the coupling amino acids, 2) Difficulty in purification of protected peptides, 3) Poor solubility of peptide fragments which hinders coupling reactions.

The publication of the first Solid Phase Peptide Synthesis (SPPS) by Merrifield in 1963 revolutionised the peptide synthesis field.[180] The process outlined in Scheme 4.1 involves initially tethering the C-terminus of an amino acid to a polymer support. An excess of the N-protected amino acid next in the sequence is added along with a coupling reagent to link the two amino acids. The polymer support may then be filtered and washed to remove starting materials and byproducts. The N-terminus of the nascent peptide chain is deprotected, usually by base-catalysed cleavage. After further filtering and washing a new amino acid can be added to the chain. The above steps are iterated in order to produce the desired polypeptide chain. Finally, the peptide can be cleaved from the polymer support – normally this linker is acid sensitive so as to make it orthogonal to the base-catalysed deprotection of amino acids. The resulting free peptide chains in solution can then be easily purified by high pressure liquid chromatography (HPLC).

Scheme 4.1: Outline of the various stages of Solid Phase Peptide Synthesis (SPPS).

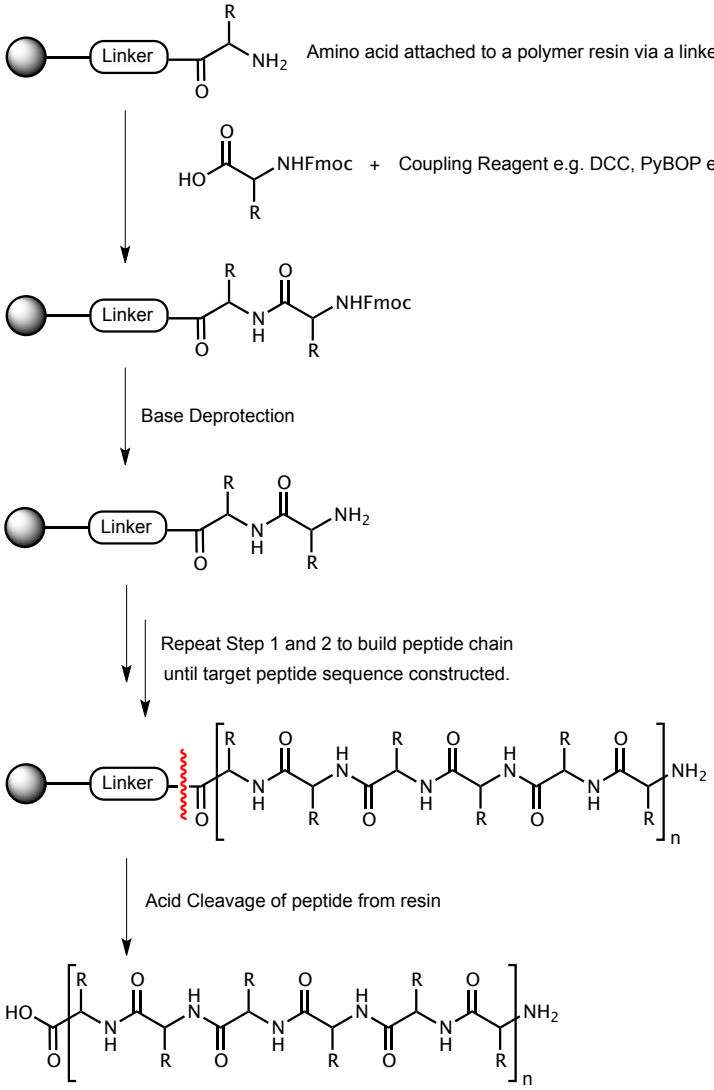

In comparison to solution phase synthesis, SPPS is a higher yielding technique because there is limited loss of material during the synthesis, as the peptide is bound to the polymer support. Purification steps are significantly easier with only filtering and washing required. The insolubility of peptides is also circumvented as the peptides remain on the polymer support.

SPPS has one major drawback: it is limited to producing peptide chains that are at most 50 residues in length. The origin of this restriction is due to the interaction and folding together of adjacent chains on the polymer support, which becomes more significant as the peptide increases in length. This can result in the reactive N-terminus of some peptide chains becoming hidden amongst other chains on the polymer support. Subsequent coupling of other amino acids to these chain ends may then no longer be

possible, leading to deletions in the sequence that upon cleavage from the support gives an impure mixture of peptide chains of different lengths (See Scheme 4.2 for a schematic representation of this). The purification of this mixture can be extremely challenging as all peptide chains share an identical sequence for the first 45 – 50 residues and thus tend to behave similarly in chromatography.

SPPS is an excellent technique to access medium sized polypeptides and thus chemists in the 1980s believed that the most promising route to larger peptides would be to find an efficient technique to link several chains together. This convergent approach is known to be more effective than stepwise synthetic strategies because of easier purification of products and a more efficient use of starting materials.[188] This aim was achieved with the advent of peptide ligation chemistry in the early 1990s.

Scheme 4.2: Schematic representation of the 45 – 50 amino acid residue limit for SPPS.

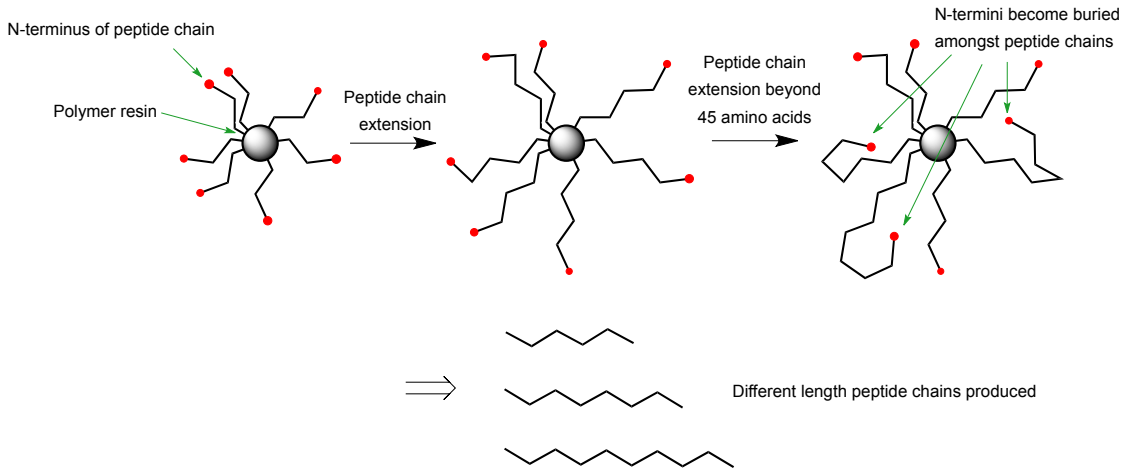

4.1.2 Native Chemical Ligation

Effective peptide ligation is based upon the identification of a chemoselective reaction between two functional groups that will exclusively react together and remain unreactive to any other reagents present in solution. The earliest peptide ligations focused upon linking peptide chains together with a non-native covalent linker. Kent and co-workers reported the first ligation technique based upon the chemoselective reaction between a peptide thiocarboxylate with a bromoacetyl-peptide in a low pH aqueous solution (Scheme 4.3).[189] The chemoselectivity of this reaction arises from the combination of a soft thiocarboxylate nucleophile with a soft bromo-acetyl

electrophile. An HIV-1 protease prepared using this technique had identical reactivity to the wild type despite the presence of a thioester to link the two peptide chains rather than the native amide bond. Alternative ligation approaches based upon different chemoselective reactions were also developed in the early 1990s e.g. an oxime based linker, prepared from an aminooxyacetyl-peptide and a glyoxyl-peptide (Scheme 4.4).[190]

Scheme 4.3: First example of a ligation employed by Kent to link two peptide chains by a thioester linkage.[189]

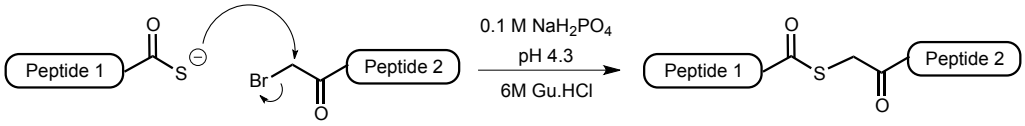

Scheme 4.4: Oxime based ligation for combining peptide chains.[190]

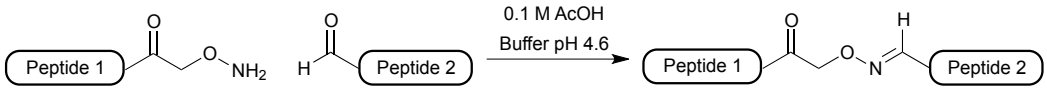

The main criticism of the above ligation techniques was that a native amide bond was not used to link the chains, which therefore had the potential to change the behaviour of the resulting peptide. The publication of the Native Chemical Ligation (NCL) technique in 1994 by Kent, Dawson and co-workers addressed this concern and made the most significant impact upon the field of peptide chemistry since SPPS.[181] In NCL two peptide chains, one with a N-terminal cysteine and the other with C-terminal thioester, are ultimately ligated together by a native amide bond (Scheme 4.5a). The mechanism proposed for this reaction involves first the chemoselective transthioesterification reaction between the thiol/thiolate of the N-terminal cysteine and the C-terminal thioester (Scheme 4.5b). The resulting thioester then undergoes a rapid and irreversible intramolecular S-to-N acyl shift to produce the native peptide bond.

Scheme 4.5: a) Native Chemical Ligation (NCL) of two peptide fragments; b) Proposed mechanism for NCL.[181]

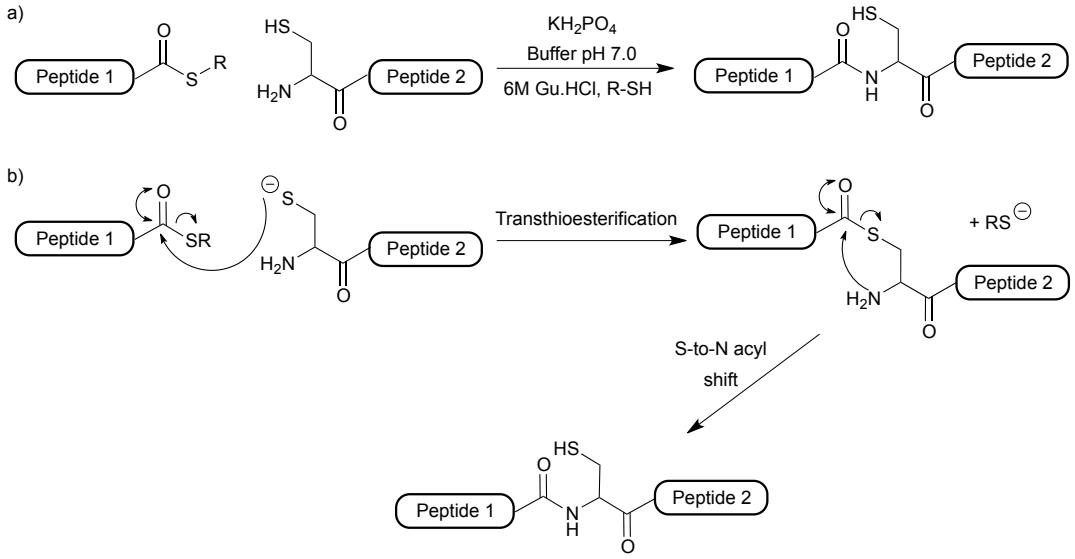

NCL has a number of distinct advantages over other ligation techniques:

1) Importantly, the bond produced that links the peptide fragments is a native amide bond – identical to the wild type peptide.
2) The peptide chain obtained is the final product and requires no further deprotection or conversion steps.
3) The amide bond formation step is irreversible under the conditions of the NCL, which leads to a high yielding reaction.
4) NCL is performed in a phosphate buffer at pH 7.0 in the presence of an external thiol (R-SH) and 6 M guanidine.HCl at 25 – 37 °C. These conditions are relatively mild and prevent peptide degradation. The external thiol is added to prevent oxidative disulfide bond formation between the N-terminus cysteines. The 6 M guanidine.HCl acts as a chaotropic reagent, preventing aggregation of peptide chains and leading to a higher concentration of free peptide in solution which accelerates the ligation.
5) The final product can easily be separated by HPLC from starting materials and characterised using HPLC-electrospray mass spectrometry.
6) The starting peptide chains can be efficiently prepared solely from SPPS.

Kent successfully applied NCL to the synthesis of a 72-mer Interlukin-8 peptide whose properties were identical to the naturally occurring Interlukin-8 peptide. The

coupling of NCL with SPPS has afforded chemists relatively easy access to peptide chains of up to 150 amino acids residues in length – approximately three times the size of those previously obtainable by SPPS alone. Since development NCL has undergone various optimisations and the breadth of applicability has been probed. A selection of key developments is outlined below.

4.1.3 Thiol Additives

The preparation of appropriate thioesters for NCL is arguably the most challenging aspect of the technique. There are two main classes of thioesters prepared for NCL: alkyl thioesters and aryl thioesters. Alkyl thioesters are more stable in preparation, purification and storage than aryl thioesters. Aryl thioesters are significantly more reactive in NCL than alkyl thioesters due to a lower thiol pK_a and hence a superior leaving group ability. Other non-thioester C-termini for NCL have also been developed (See Section 4.1.6.3). In a follow-up to the original report of NCL, Dawson, Kent and co-workers demonstrated that the addition of thiophenol to NCL could accelerate the reaction by over four-fold (Scheme 4.6).[191] The origin of this rate acceleration was the activation of the C-terminus thioester by displacement of the benzyl mercaptan alkyl thioester by thiophenol to give the phenyl thioester. This introduced a new thiol-thioester exchange step into the mechanism of NCL, which permitted the *in situ* preparation of a more reactive aryl thioester.

Scheme 4.6: Mechanism of NCL in the presence of an aryl thiol additive. The thiol-thioester exchange step is introduced prior to transthioesterification.

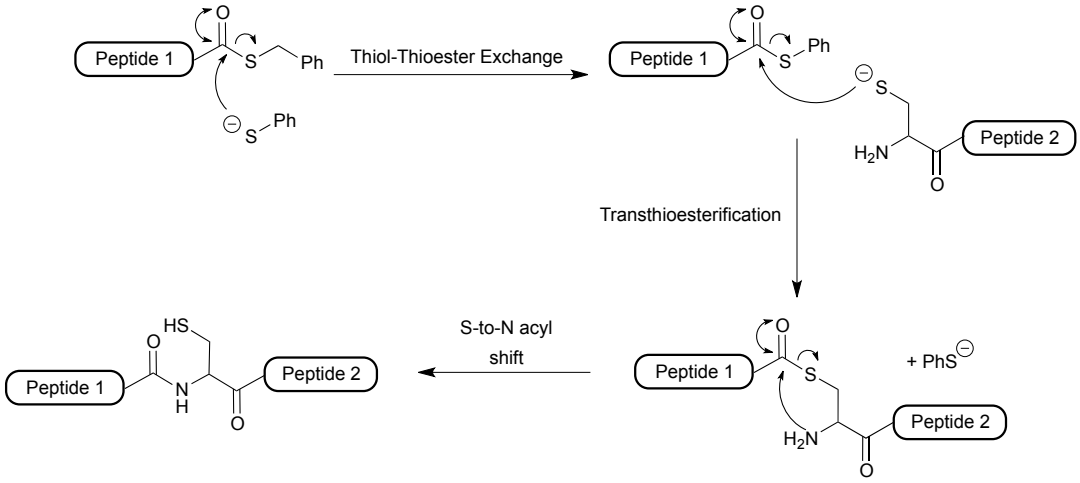

The use of thiophenol does have disadvantages: i) it has an unpleasant odour and ii) it is poorly soluble in aqueous media. The lower solubility limits the concentration in solution and thus places a ceiling on the level of rate acceleration possible. These disadvantages prompted Kent to conduct a screening of a range of aryl and alkyl thiols to identify a more appropriate additive.[192] The thiol additive's role in catalysing the reaction is twofold:

1) The thiol additive displaces an alkyl thiol during the thiol-thioester exchange step. Therefore, the additive must be a sufficiently good nucleophile to readily attack the alkyl-thioester. Thiols with a higher pK_a are better nucleophiles and hence more appropriate for this step of the reaction.
2) The thiol additive is displaced from the thioester by the N-terminal cysteine thiolate during the transthioesterification step. Therefore, the additive must be a sufficiently good leaving group to readily depart upon attack of the cysteine. Thiols with a low pK_a will be better leaving groups and hence more appropriate for this step of the reaction.

To balance these two conflicting demands, it was anticipated that a thiol additive with an intermediate pK_a would be effective at undertaking both roles.

Ligation reactions with various aryl and alkyl thiols were performed and monitored over time via electrospray mass spectrometry and analytical HPLC. The concentration of thiol-thioester exchange intermediate and the final ligation product present could be identified and quantified using these techniques.

Figure 4.1 shows how the pK_a of a variety of thiols affects the completion of ligation, and, as anticipated, thiols with intermediate pK_as of 6.50 – 8.75 showed the most rapid conversions. While alkyl thiols proved to be poor catalysts for ligation they did show the highest amount of thiol-thioester exchange presumably due to their higher nucleophilicities. For the aryl thiols no build-up of the thiol thioester exchange product was observed, which indicates that the rate determining step of the reaction for these catalysts is initial thiol-thioester exchange not transthioesterification as in the case of alkyl thiol catalysts. Rate determining thiol-thioester exchange is more desirable as the addition of more readily available aryl thiol catalyst can accelerate the reaction. This would be unfeasible for the alkyl thiol catalysts as variation of the concentration of N-terminal cysteine peptide would be required in order to accelerate the rate determining transthioesterification step.

Figure 4.1: Fraction of peptide ligation after two hours as a function of thiol additive pK_a.[192]

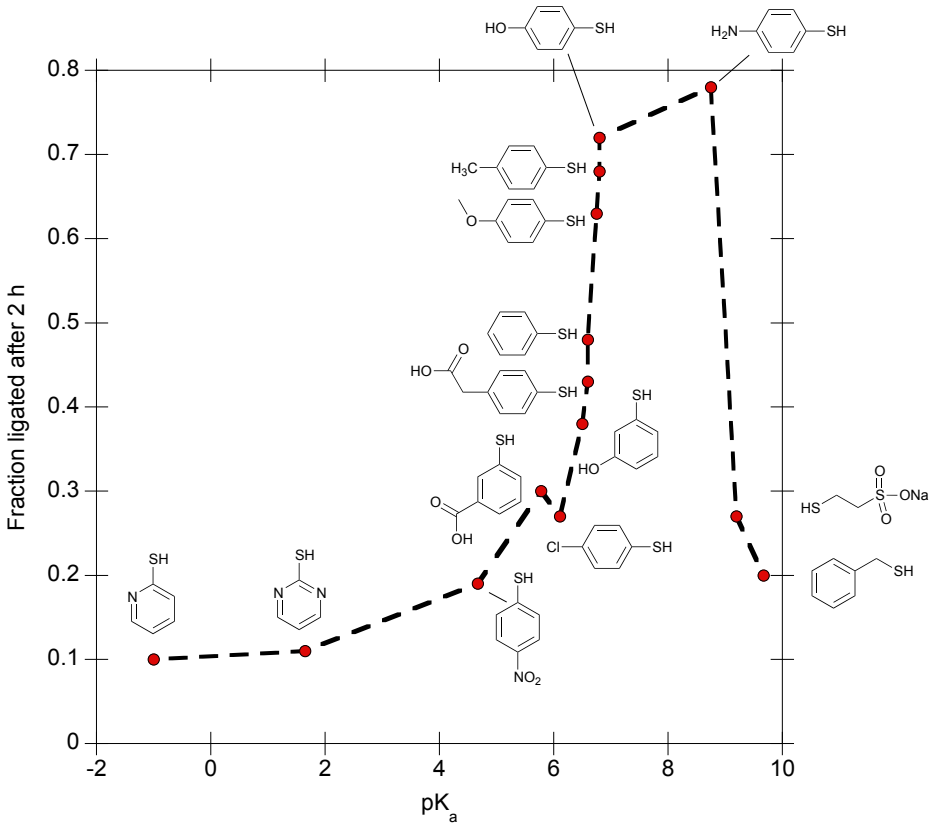

Of the aryl thiol catalysts, (4-amino)thiophenol (pK_a = 8.75) proved to give the greatest acceleration of the ligation reaction. However, 4-(carboxymethyl)-thiophenol

(MPAA, pK_a = 6.60) was chosen as the optimal catalyst due to greater solubility in aqueous media and wider commercial availability (Scheme 4.7).

Scheme 4.7: Optimal thiol additive for NCL MPAA [4-(carboxymethyl)-thiophenol] pK_a = 6.60.

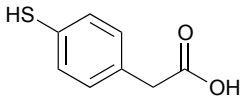

4.1.4 The Effect of the Identity of the C-terminal residue on NCL

The rate of NCL is dependent upon the identity of the C-terminal residue of the thioester. Dawson has exhaustively probed how the completion times of ligation are affected by the identity of the amino acid present at the C-terminal using a model ligation reaction between a LYRA-X[xxxviii] peptide thioester and a CRANK[xxxix] cysteine peptide. The completion times for ligation were monitored using both the appearance of LYRAX-C(=O)-N(H)-CRANK product and the disappearance of benzylmercaptan thioester LYRA-X starting material. Based upon the time taken for ligation to go to completion Dawson grouped the 20 native amino acids studied into four: ≤ 4 h, ≤ 9 h, ≤ 24 h and ≥ 48 h (Scheme 4.8).[193]

The completion times for each terminal amino acid were dependent upon several different factors. The extent of steric hindrance of the C-terminus thioester appeared to be the most significant factor. In particular, amino acids with branching on the β-carbon (valine, threonine, isoleucine) or a bulky alkyl chain (leucine) had the slowest completion times ≥ 48 h. Despite no branching at the β-carbon, proline showed the longest completion times; the proposed origin of this is detailed below. Those amino acids with longer unbranched side chains (asparagine, aspartic acid, glutamine, glutamic acid, lysine, arginine) and serine took ≤ 24 h to go to completion.

[xxxviii] 5-mer peptide: H-Leu-Tyr-Arg-Ala-Xaa-S(Benzyl)

[xxxix] 5-mer peptide: H-Cys-Arg-Ala-Asn-Lys-OH

Scheme 4.8: The four groups of C-terminal residues (≤ 4 h, ≤ 9 h, ≤ 24 h and ≥ 48 h) based upon the time required for the ligation to go to completion.[193]

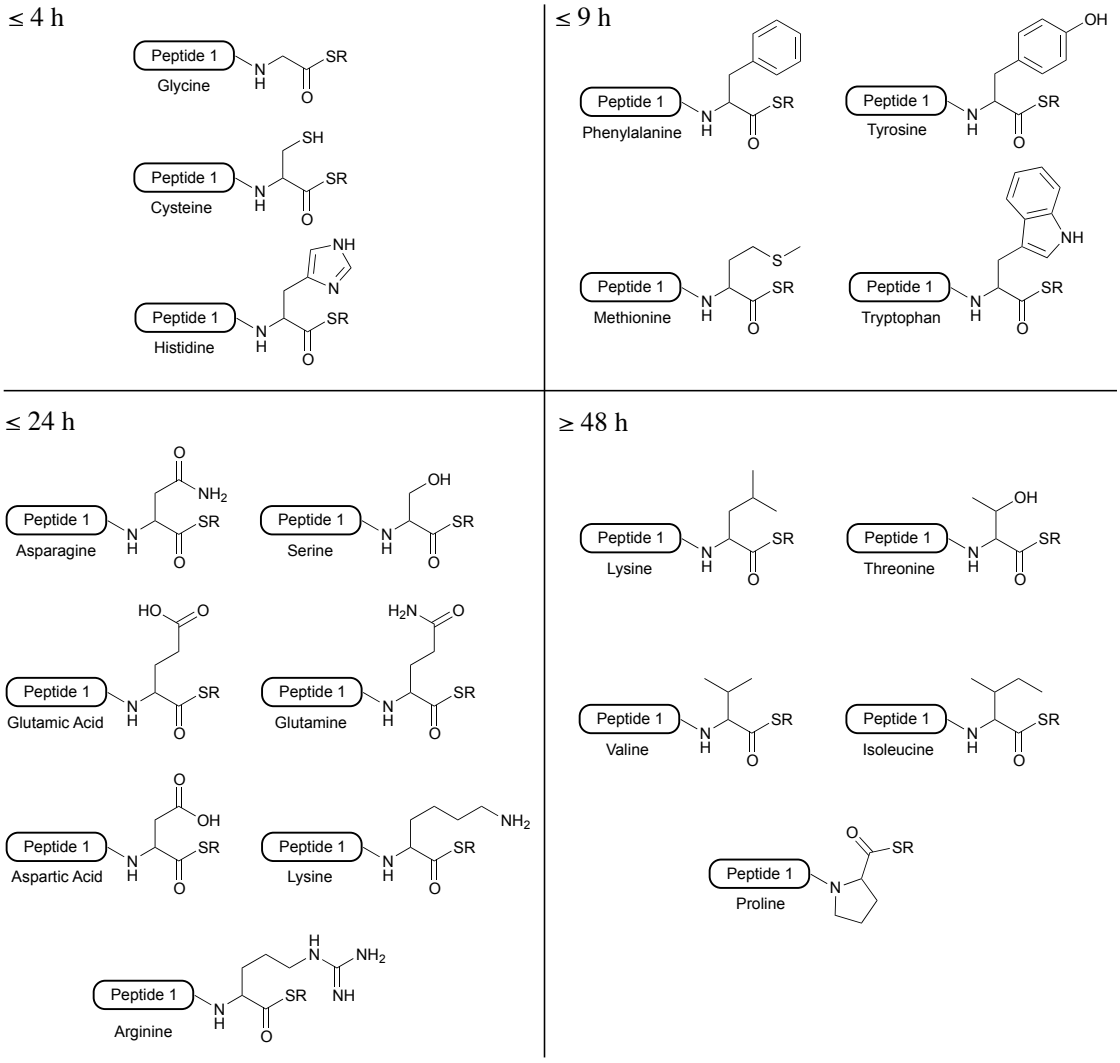

Unexpectedly, the amino acids with larger aromatic groups (phenylalanine, tyrosine, tryptophan) had shorter completion times (≤ 9 h) than might be expected from their steric bulk. While no justification for this behaviour was proposed by the authors, the greater hydrophobicity of the side groups could cause closer folding of the side chain to the peptide chain thereby exposing the C-terminus thioester. Alanine and methionine also had ligations that took ≤ 9 h, which is anticipated from the reduced smaller steric bulk of the side chains.

The amino acids with the overall shortest completion times (≤ 4 h) were glycine, cysteine and histidine. Glycine has the smallest side chain steric bulk of any amino acid and consequently the fast ligation is expected. For cysteine and histidine the short completion times were proposed to be due to side chain participation of the thiol

and imidazole, respectively, in the transthioesterification step (Scheme 4.10). This could be more rigorously tested via monitoring the actual rate of ligation, rather than just ligation times, and probing whether general base catalysis by an exogenous thiol or imidazole additive is observed.

Scheme 4.10: Potential side chain participation in NCL for histidine. The imidazole nitrogen could catalyse the rate limiting transthioesterification step via intramolecular deprotonation of the thiol on cysteine.

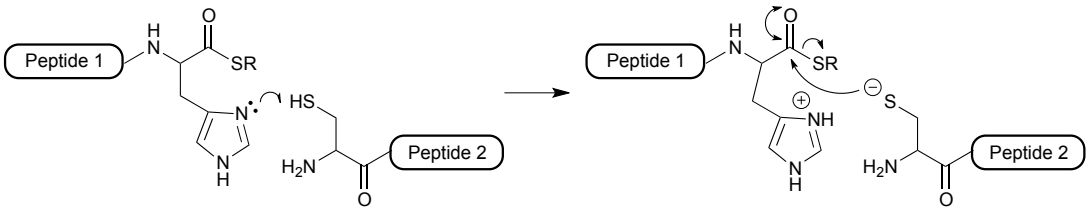

The origin of the anomalously slow rate of ligation with prolyl C-terminal thioesters was recently ascribed to the influence of n-to-π* interactions by Kent.[194] In a series of kinetic experiments Kent compared the ligation rates for a C-terminal prolyl, alanyl, methylated alanyl and other alkyl thioesters (Scheme 4.11). The peptide-alanyl-thioester, **29**, was found to have a ligation rate ~200-fold larger than the peptide-prolyl-thioester, **28**. By contrast, only a two-fold difference in reactivity was observed between the alkyl mimics **30** and **31** which therefore highlighted differences in N-reactivity as an important factor and thus a possible differential role for n-to-π* (thioester) interactions.

Scheme 4.11: Prolyl **28** and alanyl **29** thioesters and prolyl **30** and alanyl **31** hydrocarbon mimic thioesters used by Kent to ascertain origin of poor ligation rate at prolyl C-terminus.[194]

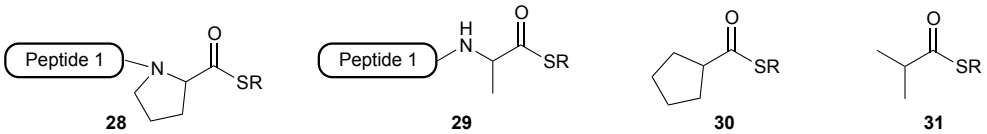

Hydrogen bonding from the NH group is possible in alanine residues, however, is absent in proline residues due to the secondary nature of the amine group. To probe how the lack of hydrogen bonding affected the ligation rates an *N*-methylated alanine

analogue peptide thioester, **29**, was analysed. However, the rate constants measured were only 0.69 fold smaller than for the peptide-alanyl-thioester, which could be attributed to the reduced electrophilicity of the thioester from the presence of the inductively donating methyl group.

The effect of the neighbouring peptide bond was next probed. For the alanyl alkyl mimic **31** there was a 20-fold decrease in ligation rate relative to the peptide-alanyl-thioester **29** as the removal of the electron-withdrawing amide bond decreases the electrophilicity of the thioester carbonyl. However, for the hydrocarbon prolyl mimic **30** the ligation rate increased by 25-fold upon removal of the amide and therefore the carbonyl group on the prolyl nitrogen was responsible for the slow rate of ligation. It was proposed that n-to-π* interactions (donation of electron density from the lone pairs on the carbonyl oxygen to the π* orbital in the carbonyl, Scheme 4.12) were the origin of the actual slower ligation rate. The n-to-π* interactions may slow the rate of ligation by both the reduction in electrophilicity of the carbonyl oxygen and the steric blocking of the Bürgi-Dunitz angle on one face of the thioester.

Scheme 4.12: n-to-π* interaction between lone pair on oxygen and the π* orbital of the thioester bond.

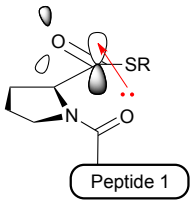

A recent publication by Otaka has shown, however, that by both altering the identity of the penultimate C-terminal amino acid next to the terminal prolyl residue and conditions the rate of ligation with a prolyl thioester can be improved by 3 – 22 fold.[195] These results are a significant improvement upon previous ligations at prolyl thioesters and would change the Dawson categorisation of prolyl from ≥ 48 h to ≤ 24 h.

4.1.5 Further Mechanistic Studies of NCL

Kent and co-workers have experimentally verified portions of the proposed mechanism for NCL, Scheme 4.13.[192] In order to further assess the validity of the

mechanism Fu has computationally examined each step of the NCL mechanism using DFT at the B3LYP level and approximating the effects of solvation in water with a polarizable continuum medium (PCM) model.[196]

Scheme 4.13: Mechanism for NCL showing experimentally observed intermediates and rate determining steps.

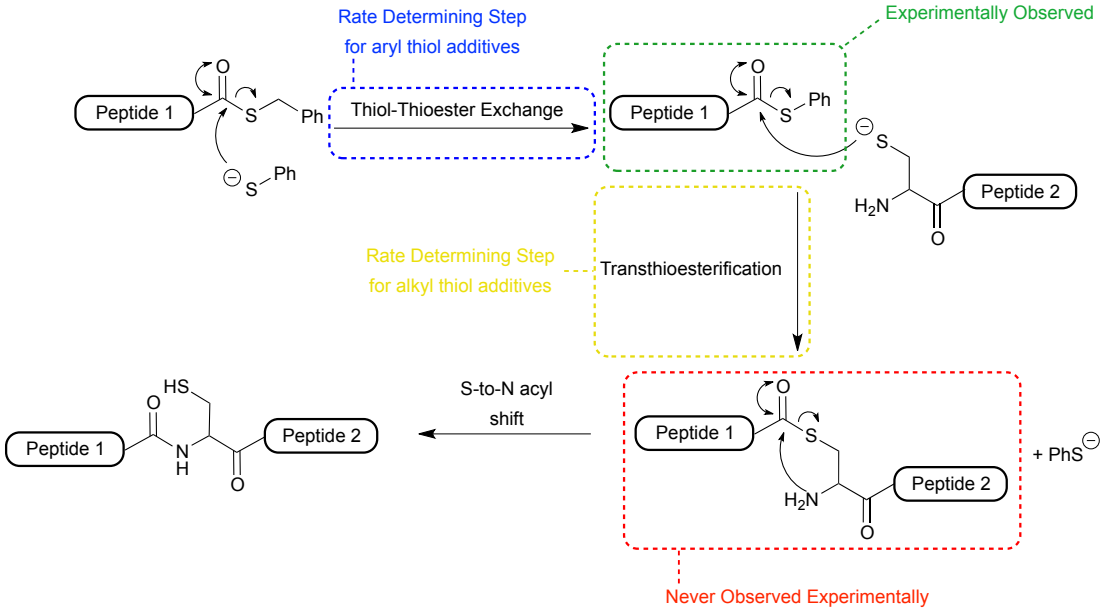

In these computational studies, the concerted or stepwise nature of the thiol-thioester exchange step was assessed and whether the thiol additive nucleophile attacked as a thiol or a thiolate (Scheme 4.14). The calculation failed to identify a stepwise transition state and only concerted transition states were observed. The transition state for the reaction involving thiolate was 20.4 kcal mol^{-1} more stable than that for the thiol with the resulting peptide aryl-thioester 1.9 kcal mol^{-1} less stable than the peptide alkyl-thioester. Fu attributed the concerted mechanism and lack of identification of any stepwise transition states or intermediates to the larger atom radius of the S atoms destabilising the formation of the tetrahedral intermediate.

Scheme 4.14: Possible routes for the thiol-thioester exchange reaction between an aryl-thiol additive and an alkyl-thiol thioester.

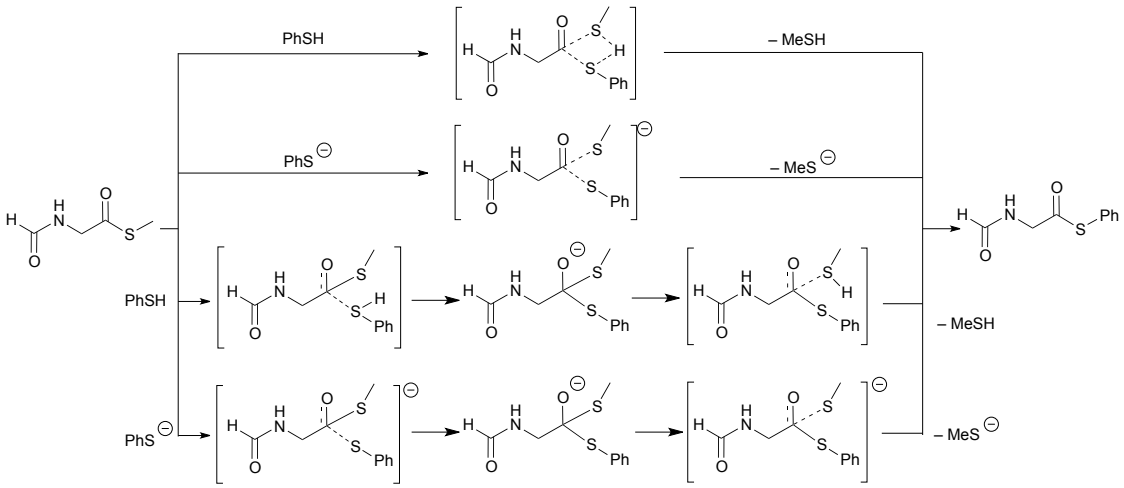

The transthioesterification step between the cysteine and the aryl-peptide thioester was examined with the thiol in both protonated and deprotonated forms (Scheme 4.15). Once again, the reaction was found to be a concerted process with the anionic transition state (Scheme 4.15 lower route) 25.1 kcal mol^{-1} more stable than the neutral transition state (Scheme 4.15 upper route) and the resulting transthioesterification intermediate having an identical energy to the peptide aryl-thioester within error. The concerted mechanism for this step of NCL was again attributed to the larger radii of S atoms destabilising the tetrahedral intermediate.

Scheme 4.15: Possible routes for the transthioesterification reaction between a cysteine and an aryl-thiol thioester.

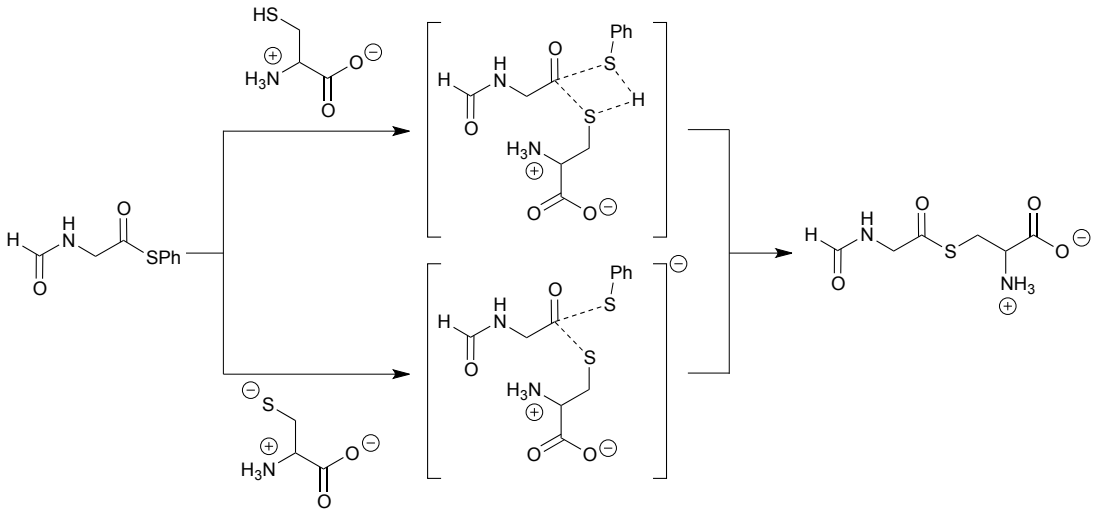

The S-to-N acyl shift step was found to occur via a stepwise reaction where the ammonium was initially deprotonated and then the amine proceeds to attack the thioester to form a thiazolidine ring tetrahedral intermediate (Scheme 4.16). This intermediate then decomposed to form the native amide bond via a transition state that has a transannular hydrogen bond. The zwitterionic intermediate is then converted to neutral form via two proton transfers.

Scheme 4.16: Calculated pathway for the S-to-N acyl shift step of NCL.

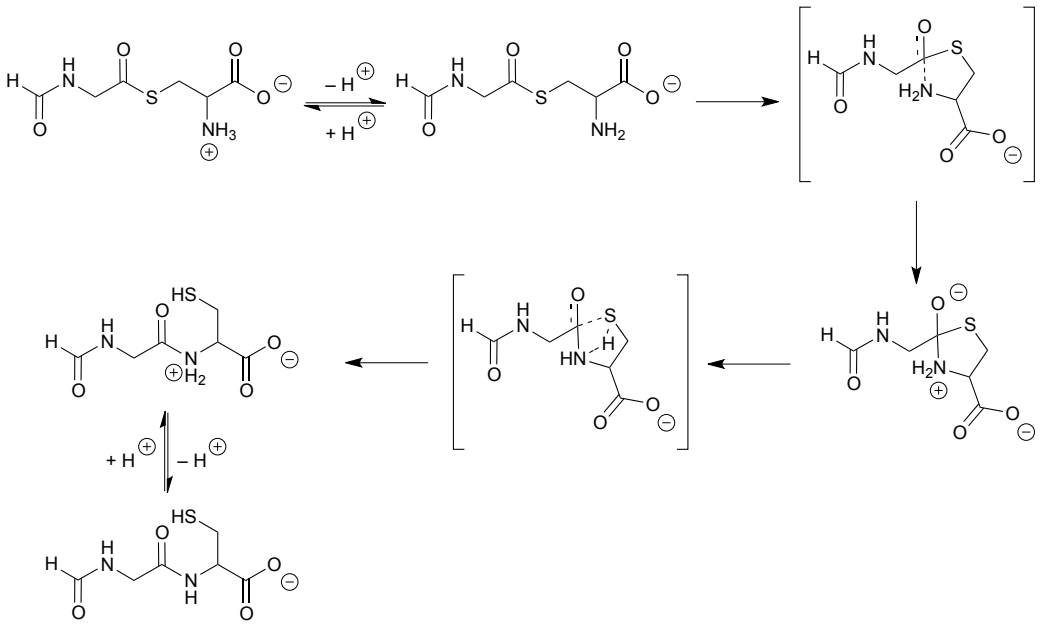

The calculated free energy profile for the NCL of a peptide-alkyl-thioester with cysteine in the presence of an aryl-thiol additive is shown in Scheme 4.17. The barriers to the thiol-thioester exchange, transthioesterification and S-to-N acyl shift are 29.4, 22.6 and 23.7 kcal mol^{-1} respectively and 27.5, 24.8 and 31.1 kcal mol^{-1} for the barriers to the reverse reactions.

Scheme 4.17: Free energy profile for the NCL of a peptide-alkyl-thioester with cysteine in the presence of an aryl-thiol additive. Values in brackets are the free energies in kcal mol^{-1}. The calculation of the free energy values shown in the profile also took account of all other molecules present in the reaction (e.g. the first step also includes the energy of cysteine), however, for clarity these have been omitted.[196]

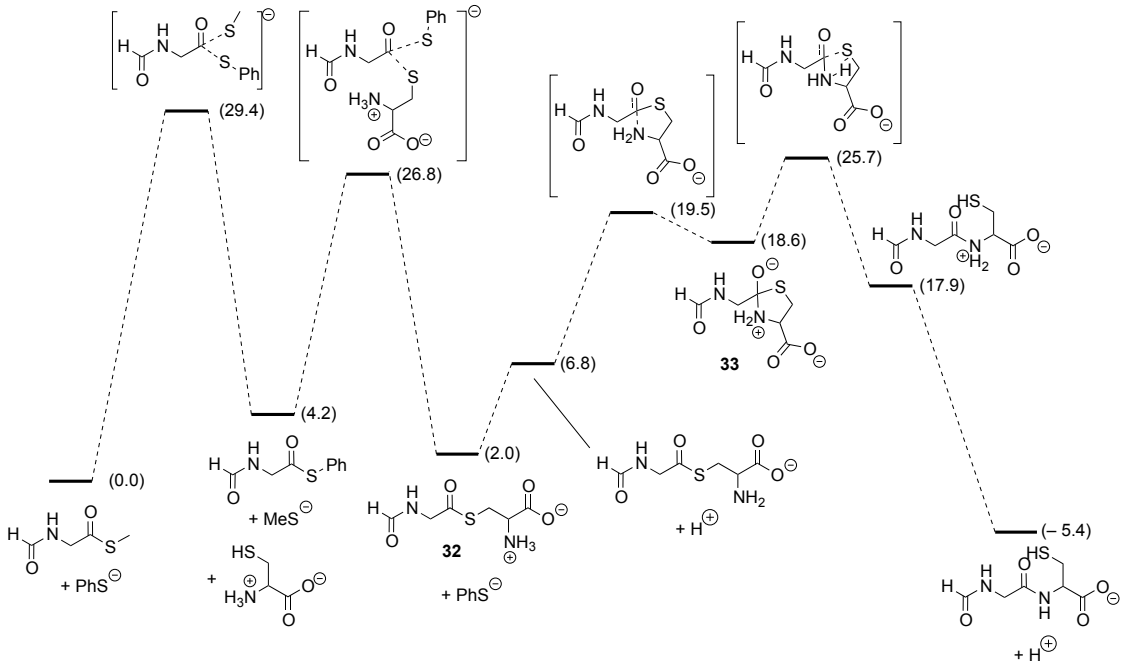

The order identified for the magnitude of activation barriers in the forward direction in the computational study is corroborated by experimental observations with the rate-determining step in the forward direction correctly calculated to be the thiol-thioester exchange. The absence of the intermediates **32** and **33** (Scheme 4.17) in experimental observations is consistent with the calculated barriers in the forward direction of both transthioesterification (22.6 kcal mol^{-1}) and S-to-N acyl shift (23.7 kcal mol^{-1}) being smaller than the competing reverse reactions of thiol thioester exchange (27.5 kcal mol^{-1}) and transthioesterification (24.8 kcal mol^{-1}). The largest barrier in the reverse direction is for the N-to-S acyl shift (31.1 kcal mol^{-1}) and is consistent with NCL being an irreversible reaction. Computations to study how the identity of the C-terminus amino acid affected the activation barrier to ligation were also consistent with experimental observations.[193]

The computational study identified a number of species that are consistent with previous experimental studies of thiol and thioester reactions. The lower barrier for the

thiolate nucleophile, as opposed to thiol nucleophile, for both the thiol thioester exchange and transthioesterification is consistent with a number of experimental studies that show for a reaction between an alkyl thiol and various electrophiles the observed rates of reaction show a linear dependence upon the concentration of thiolate in solution.[197,198]

Likewise, for the S-to-N acyl shift step, the identification of rate limiting departure of the thiolate from the zwitterionic tetrahedral intermediate is consistent with experiment. Castro has shown that for the aminolysis of aryl-thioacetates by secondary amines the breakdown of the zwitterionic tetrahedral intermediate by thiolate departure is rate limiting (Scheme 4.18).[199,200] An examination of microscopic rate constants for the reaction also found that the rate of expulsion of the aryl-thiolate was faster than the rate of deprotonation of the zwitterionic tetrahedral intermediate by a base.[xl]

Scheme 4.18: Aminolysis reactions of aryl-thioacetates by secondary amines studied by Castro.[199,200]

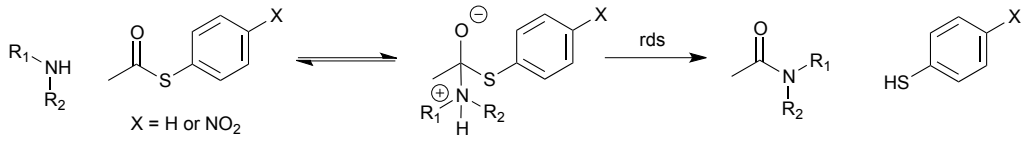

While Castro's work focused on aryl thiols and secondary amines the mechanism is not expected to differ for the S-to-N acyl shift in NCL, which has an alkyl thiol and a primary amine, because:

a) The increase in the pK_a of the leaving group in going from an aryl to an alkyl thiol is not expected to change the mechanism. The effect of leaving group pK_a on the mechanism was probed by Castro using phenyl thioacetate (thiophenol pK_a = 6.62) and *p*-nitrophenyl thioacetate (*p*-nitrothiophenol pK_a = 4.50). The breakdown of the zwitterionic tetrahedral intermediate by departure of thiolate was almost always rate limiting for both thioesters.[201]

[xl] An examination of the kinetics showed rate limiting breakdown of the zwitterionic intermediate that was pH independent and first order dependent upon amine (if the amine acted as a base then there would be a second order dependence on the amine). Therefore deprotonation of the zwitterionic intermediate to form an anionic intermediate does not occur.

The only exception to this was when *p*-nitrophenyl thioacetate was lysed by a secondary amine with a high (conjugate acid) pK_a. In this case the zwitterionic tetrahedral intermediate formation was rate limiting. For phenyl thioacetate the rate determining step remained unchanged when it was lysed by the same secondary amine. Therefore only decreasing the pK_a of the leaving group alters the rate determining step of reaction between a N nucleophile and a thioester leaving group. Alkyl thiols have higher pK_as than thiophenol and therefore the rate limiting step is expected to be breakdown of zwitterionic tetrahedral intermediate by departure of thiolate.

b) The switch from secondary to primary amines is also not expected to affect the mechanism. Primary amines typically have lower conjugate acid pK_as than secondary amines and hence are better leaving groups than secondary amines. Therefore breakdown of the zwitterionic tetrahedral intermediate by departure of the amine nucleophile is likely to be more facile than breakdown by departure of thiolate. Thus this increases the likelihood that the breakdown by departure of thiolate is rate determining.

Despite the above correlations with experiment there are two key problems with the computational results. First, the computed barrier to N-to-S acyl shift (31.1 kcal mol^{-1}) is only 1.7 kcal mol^{-1} larger than for the reverse of thiol-thioester exchange (29.4 kcal mol^{-1}) (Scheme 4.17). Experimentally, the reverse of thiol-thioester exchange is observed, while the reverse of the amide bond formation is not. Consequently, one would expect that the difference in the height of these barriers to be considerably greater.

The second, more critical, issue with the computational results is the identification of a concerted mechanism for the thiol-thioester exchange and transthioesterification steps. All previous experimental studies of reactions between a thiol and an alkyl / aryl thioester have identified the presence of a stepwise mechanism where the reaction proceeds via a tetrahedral intermediate **34** (Scheme 4.19).[202] Jencks and co-workers extensively studied the reaction between *p*-nitrophenyl thioacetate and a series of thiolate anions to establish whether the mechanism for these biologically relevant reactions was stepwise or concerted.[201]

Scheme 4.19: Stepwise mechanism for thiol thioester exchange.

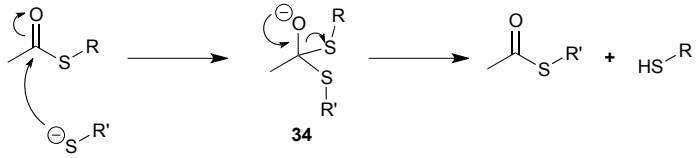

In a stepwise mechanism a change in the rate determining step is expected as either the pK_a of the conjugate acid of the attacking nucleophile thiolate, or, the pK_a of the conjugate acid of the thiolate leaving group is varied (Scheme 4.20). For nucleophiles with a pK_a higher than that of the leaving group the attack of the nucleophile will be rate determining, as the barrier to the forward departure of the leaving group from the tetrahedral intermediate will be smaller than the barrier to the loss of nucleophile ($k_2 > k_{-1}$) (Scheme 4.20 Left). For nucleophiles with a pK_a below that of the leaving group the departure of the leaving group becomes rate determining, as the barrier to loss of the nucleophile from the tetrahedral intermediate is smaller than the barrier for loss of the leaving group ($k_2 < k_{-1}$) (Scheme 4.20 Right). In the latter case, the rate of the reaction would be expected to show a strong dependence upon the pK_a of the nucleophile, while in the former case, the rate of reaction should be relatively insensitive to the pK_a of the nucleophile. In a concerted mechanism no change in the rate determining step of the reaction should be observed and the reaction should show a consistent linear dependence upon the pK_a of the nucleophile.

Scheme 4.20: Variation of the rate determining step for the thiol thioester exchange due to alteration of the thiolate nucleophile and thiolate leaving group. Reproduced with permission from the ACS.[201]

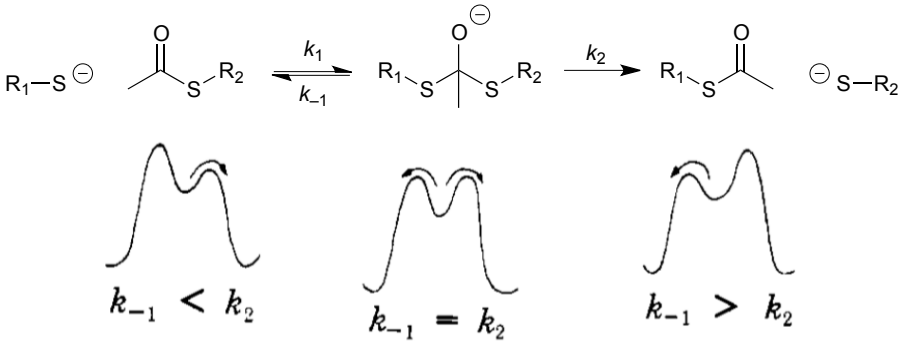

A Brønsted plot for the reaction between *p*-nitrophenyl thioacetate and a series of thiolate anion nucleophiles is shown in Figure 4.2. There are two distinct regions in

the plot centred on the pK_a of *p*-nitrophenyl thiol (pK_a = 4.50). Above this pK_a the β_{nuc} = 0.27 showing that the rate of exchange is only loosely related to the pK_a of the thiolate nucleophile. Below this pK_a the β_{nuc} = 1.0 which shows that the rate of exchange has a strong dependence upon the pK_a of the thiolate nucleophile.[xli] The non-linear behaviour is indicative of a change in rate determining step for the reaction, from leaving group departure, when nucleophile pK_a < 4.50 ($k_2 < k_{-1}$), to nucleophilic attack, when nucleophile pK_a > 4.50 ($k_2 > k_{-1}$). Consequently, a stepwise mechanism, which proceeds via a tetrahedral intermediate, is strongly supported rather than a concerted mechanism. Douglas has similar evidence for a stepwise and non-concerted mechanism in related hydrolyses of alkyl and aryl thioesters.[203-205]

Figure 4.2: Brønsted plot for the reaction of a series of thiol anion nucleophiles with *p*-nitrophenyl acetate thioester. Reproduced with permission from the ACS.[201]

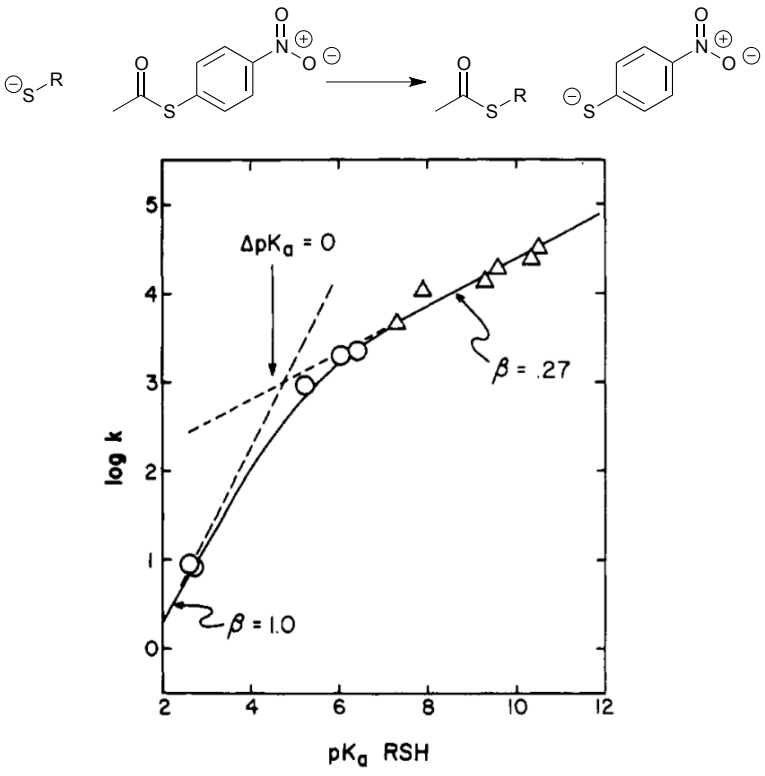

[xli] It may seem counterintuitive that the β_{nuc} is smaller (β_{nuc} = 0.27) for rate determining nucleophilic attack than for rate determining leaving group departure (β_{nuc} = 1.0). This is the case because the β_{nuc} value represents the sensitivity of the rate constant and pK_a to a change in substituents on the nucleophile. When nucleophilic attack is rate determining there is only partial loss of negative charge on the nucleophile (and only partial bond formation to the nucleophile) in the transition state and therefore the sensitivity to changes in substituents upon the nucleophile is weaker. When leaving group departure is rate determining there is complete loss of negative charge on the nucleophile (and complete bond formation to the nucleophile) in the transition state and thus changes in the substituents on the nucleophile will have a greater affect upon the rate.

Thus, the concerted mechanisms proposed by Fu based on calculations do not stand up to experimental scrutiny, as the larger radii of sulfur atoms has demonstrably been shown not to preclude a stepwise mechanism from being possible. A potential source of these errors may be the use of a polarizable continuum medium instead of explicit solvent water molecules to model the aqueous environment. Consequently, the calculations cannot account for specific hydrogen bonding interactions between water and the various intermediates and transition states. Another possible source of error is the use of cysteine and not a cysteine peptide in the transthioesterification and S-to-N acyl shift reactions. The extra anionic charge on the carboxylate of cysteine and the absence of an adjacent amide bond to the thiol and amine groups may have affected the results.

4.1.6 Developments to extend the NCL technique

Since the development of NCL many advances have focused upon extending the technique beyond the original Xaa-Cys bond formation. Its adaption has led to new strategies for *de novo* peptide synthesis. Major developments are presented below.

4.1.6.1 Extension of NCL to non-Cysteine Residues

One of the initial limitations of the NCL technique was the requirement for a cysteine residue in the peptide sequence. Not all proteins contain a cysteine residue and cysteine comprises only 1.7 % of all amino acid residues found in natural proteins.[206] For those proteins that do contain cysteine, the location of the cysteine residue(s) within the primary sequence is not necessarily appropriate for application of NCL. Two main strategies have been devised to overcome this limitation: i) the use of acyl transfer auxiliaries, and ii) the use of thiol analogues of amino acids with subsequent desulfurization.

4.1.6.1.1 Acyl Transfer Auxiliaries

Canne reported the first use of acyl transfer auxiliaries in NCL where an oxyalkyl thiol auxiliary was used to facilitate ligations between a C-terminal thioester and a non-cysteine N-terminal peptide (Scheme 4.21).[207] The oxyalkyl thiol was

covalently linked to the amine at the N-terminus of a peptide and could be removed with zinc under acidic conditions. Various iterations of this idea were developed (Scheme 4.22) including N^{α}-1-(4-methoxyphenyl)-2-mercaptoethyl,[208,209] N^{α}-2-mercaptobenzylamine,[210] N^{α}-2-phenyl ethanethiol,[211] N^{α}-4,5-dimethoxy-2-mercaptobenzyl[212] and a N^{α}-3,4,5-trimethoxy-2-mercaptobenzyl.[213] The main advantage of the latter systems is that they could be selectively cleaved using only trifluoroacetic acid.

Scheme 4.21: First auxiliary mediated ligation developed by Canne.[207] The oxyalkyl thiol takes part in the transthioesterification reaction with the thioester. The resulting ligated thioester subsequently undergoes a S-to-N acyl shift to form the amide bond, and the auxiliary may then be removed.

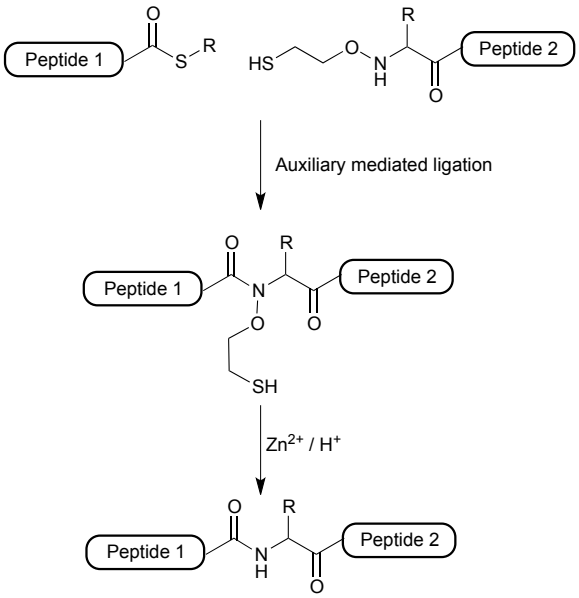

Scheme 4.22: Examples of auxiliaries developed for auxiliary mediated ligation.

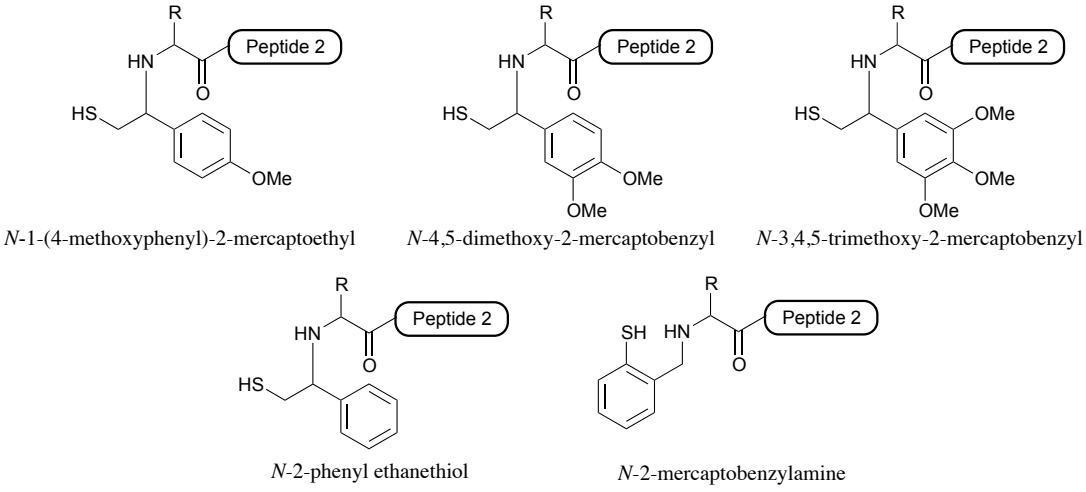

Thiol auxiliaries have not been widely applied because of a number of limitations.[214] The greater steric bulk provided by the auxiliary makes this methodology acutely sensitive to the identity of the C-terminal and N-terminal amino acid and a requirement of a successful ligation is that one of these two residues must be a glycine. Even marginal increases in steric bulk such as two alanine residues results in no reaction.[213] While ligations can occur between a glycine and a more sterically bulky amino acid (e.g. lysine or glutamine), yields are usually low to medium and a mixture of products can result as the rate of C-terminal thioester of hydrolysis becomes similar to the rate of ligation.[215] Competitive hydrolysis suggests that there is a change in the rate determining step from transthioesterification to N-to-S acyl shift in the more hindered ligations.

Another limitation with auxiliary-mediated ligations is that during acid cleavage of the auxiliary from the peptide chain, an N-to-S acyl shift may occur (Scheme 4.23).[216] This reaction is irreversible due to complete protonation of the amine in the strongly acidic conditions. Danishefsky has shown that methylation of the mercaptobenzyl prior to acid cleavage mitigates this.[215]

Scheme 4.23: Irreversible N-to-S acyl shift seen during deprotection of auxiliary ligated peptides.

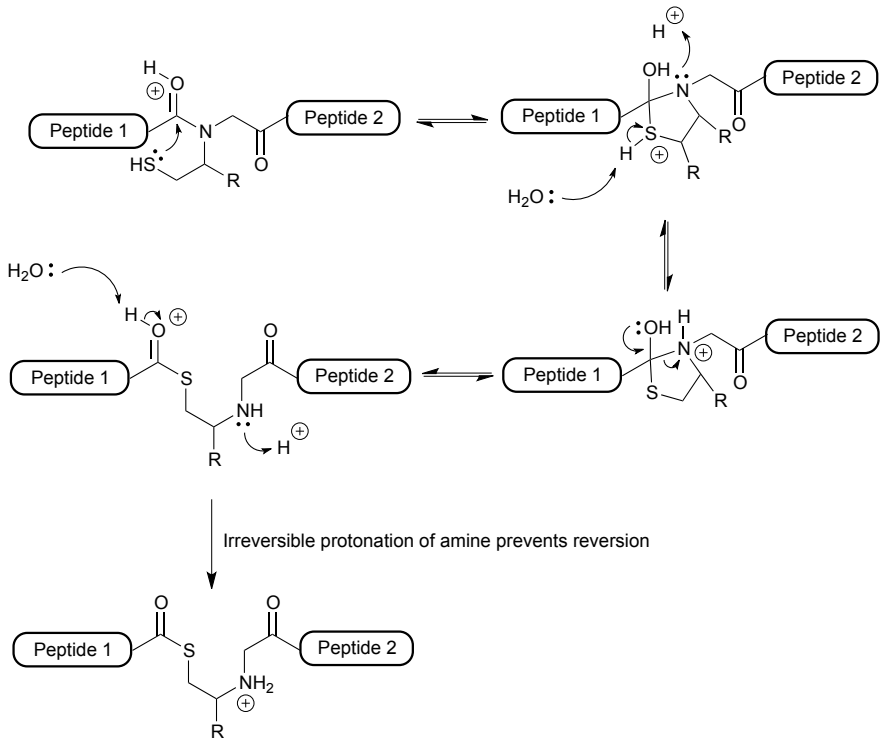

4.1.6.1.2 Thiol Analogues and Desulfurization

The use of thiol auxiliaries to extend NCL to non-cysteine residues has largely been surpassed by the development of Dawson's desulfurization technique.[217] Dawson realised that if an internal cysteine in a peptide chain were to be desulfurized after NCL then this would transform the cysteine into an alanine residue. To check the viability of this approach a model cyclic peptide Microcin J25 was chosen as a target because it contained a Gly-Ala junction and no cysteine residues. To prepare Microcin J25 SPPS was used to make the linear peptide with the target alanine residue replaced with a cysteine. NCL was then used to cyclise the peptide. Subsequent desulfurization by $Pd/C/H_2$ converted the cysteine into the native alanine residue to form the target Microcin J25 peptide (Scheme 4.24).

Scheme 4.24: NCL followed by desulfurization developed by Dawson. In the final step a Cys residue is transformed into an Ala residue.[217]

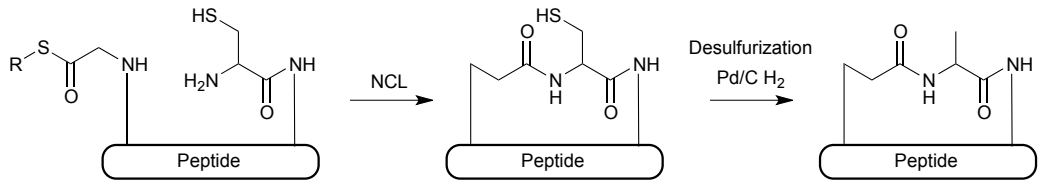

Dawson's method was initially limited to peptides with no cysteine residues as the desulfurization reaction removed all thiols present. Later developments allowed the preparation of peptides with multiple cysteine residues via thiol protection with acetamidomethyl (Acm). Raney nickel could be used to desulfurize the peptide followed by deprotection to reveal the cysteine residues.[218] A metal free desulfurization technique using the trialkylphosphine tris(2-carboxyethyl)phosphine (TCEP) has been developed by Danishefsky and has largely replaced the original Dawson methodology due to a simpler reaction setup and greater tolerance of protected cysteine and methionine residues.[219]

Since the first desulfurization report, further studies have increased the scope of desulfurization to thiol analogues of a variety of other native amino acids including phenylalanine,[220] valine,[206,221] lysine,[222,223] leucine,[224,225] threonine,[226] proline,[227,228] glutamine,[229] arginine[230] and aspartate[231] (Scheme 4.25).

Scheme 4.25: Examples of thiol analogues of native amino acids for use in NCL.

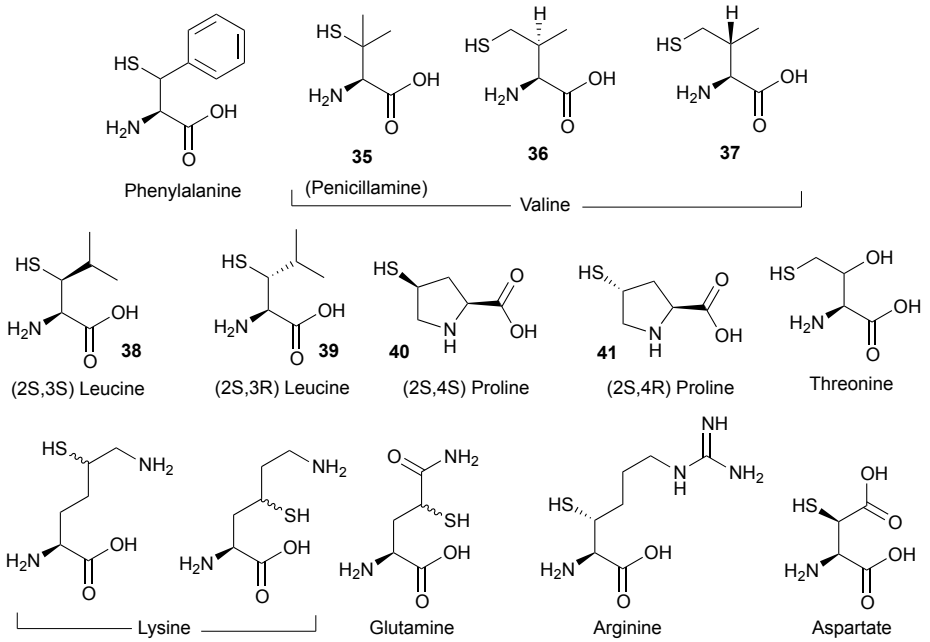

The use of penicillamine **35** as a thiol analogue of valine in NCL was demonstrated by Seitz in ligations with a range of different C-terminal amino acid thioesters: glycine, histidine, methionine, and leucine.[221] With the extra steric bulk around the thiol group in penicillamine the ligations took typically 3-fold longer to go to completion compared to cysteine. The longer reaction times did mean that a small amount of racemisation at the C-terminal thioester was observed. Undertaking the reaction at a lower pH of 7.5 vs. 8.5 could reduce this.

Danishefsky has reported an alternative thiol analogue of valine, **36**, with the thiol located on one of the methyl groups to create a primary as opposed to a secondary thiol **35**.[206] The reduced sterics of this primary thiol resulted in ligations that were 9-fold faster than for penicillamine. Ligations with **37** an epimer of **36** were ~ 2-fold slower presumably because of a hindering *cis*-1,2 interaction between the β-methyl group and amide in the N-to-S acyl transfer.

Unlike thiol analogues of valine, the epimers of a leucine thiol analogue **38** and **39** were found to show substantially different completion times for ligation.[225] A competition experiment between N-terminal **38** and **39** peptides highlighted that the ligation product ratio favoured **39** by 20 : 1 (Scheme 4.26). Suggested explanations for the product ratio focused on the *cis* / *trans* relationship between the *iso*-propyl group and the peptide chain (Scheme 4.27). The additional steric interactions for the *cis*-

relationship in **38** is believed to destabilise this route relative to **39**, which has a *trans*-relationship. This could be manifested in the transthioesterification step where *trans*-**39** allows for easier intramolecular deprotonation of the thiol by the amine than in *cis*-**38** (Scheme 4.27a). Also the *cis* / *trans* relationship could slow the S-to-N acyl shift reaction in *cis*-**38** compared to *trans* **39** (Scheme 4.27b).

Scheme 4.26: Competition experiment for the NCL of two different epimers **38** and **39** of leucine.[225]

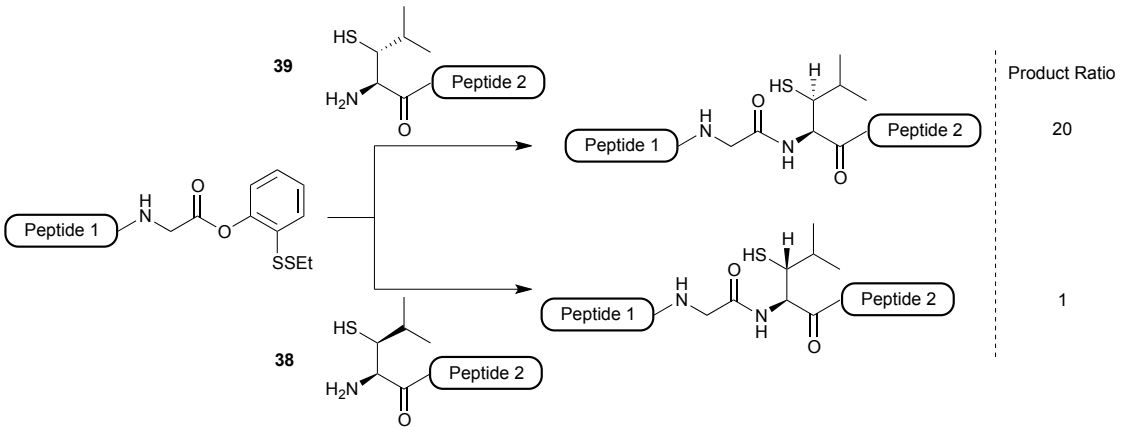

Scheme 4.27: How the *cis* / *trans* relationship between the *iso*-propyl and 'Peptide 2' could cause the difference in the product ratios for the NCL of two leucine epimers **38** and **39**.[225] a) Transthioesterification step, b) S-to-N acyl shift step.

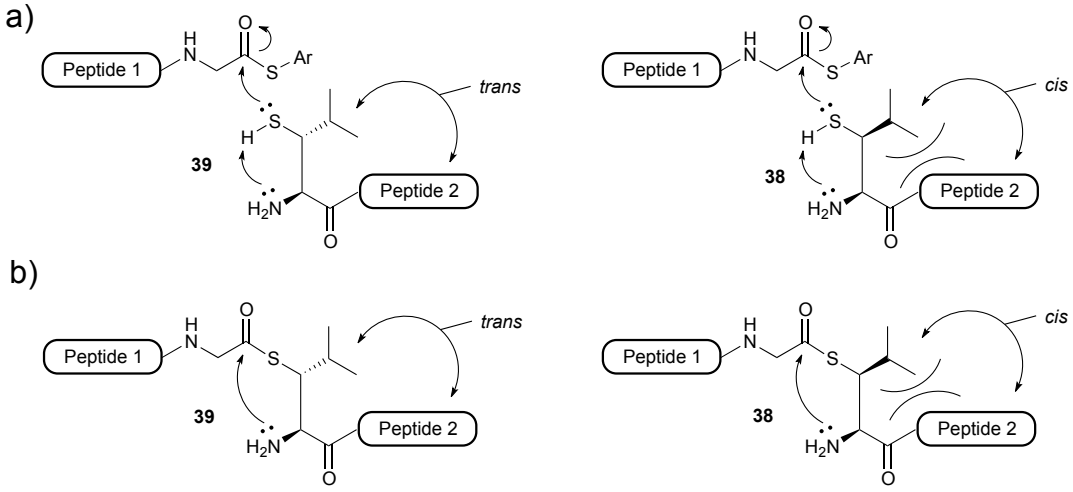

The possibility of differences in ligation rates between a N-terminal cysteine vs. a N-terminal leucine thiol analogue was next probed. The product ratio for ligation of a

cysteine N-terminal peptide vs. a N-terminal leucine peptide was favoured by 4 : 1. This ratio was smaller than would be expected from the differences in steric bulk (quantified through 'A values') between the thiol analogues of cysteine and leucine. Danishefsky proposed that the smaller difference observed was due to a Thorpe–Ingold effect in the transition state (Scheme 4.28). The *iso*-propyl substituent in leucine enforces a larger angle between itself and all vicinal groups compared to the H substituents in cysteine, i.e. angle 'y' is greater than angle 'x' in Scheme 4.28. This therefore compresses the thioester S and the amine closer together in leucine relative to cysteine i.e. angle 'b' is smaller than angle 'a' in Scheme 4.28. Therefore in the tetrahedral intermediate prior to S-to-N acyl shift the amine of leucine is in closer proximity to the thioester than that of the cysteine.[xlii] This is proposed to make the S-to-N acyl shift more labile than in the leucine peptide. This explanation assumes that the S-to-N acyl shift is the rate determining step of the reaction, which is unlikely given that this is an intramolecular reaction and all previous mechanistic studies have suggested that either the thiol-thioester exchange or transthioesterification is the rate determining. It would be more likely that the differences in reactivity arise from the transthioesterification reaction.

Scheme 4.28: Proposed Thorpe-Ingold effect in the transition state for S-to-N acyl shift.[225]

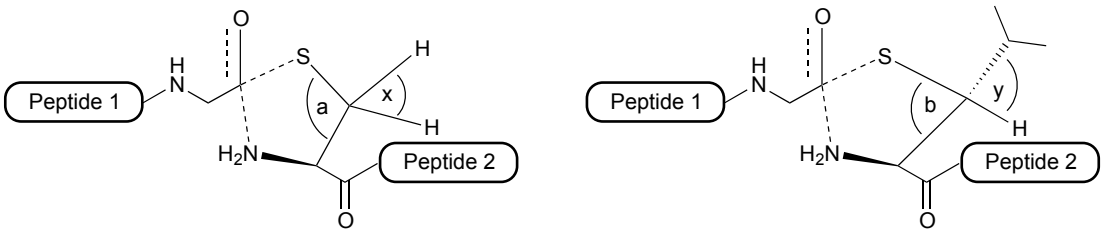

This difference in the reactivity of cysteine and leucine thiol analogues was harnessed to do the first N-terminal selective kinetic ligation (see Section 4.1.6.2) (Scheme 4.29). The ligation between N-terminal cysteine peptide **43** and N-terminal leucine thiol analogue peptide **42** proceeded smoothly to give peptide **44** with no

[xlii] This explanation also assumes that the compression does not affect the ability of the amine to adopt the Bürgi-Dunitz angle for nucleophilic attack of the thioester carbonyl carbon.

homo-ligation of **42** observed. After 30 min addition of peptide **45** to cap peptide **44** resulted in a 61 % yield of the target peptide **46**.

Scheme 4.29: N-terminal selective kinetic ligation that relies upon the differences in ligation rate between cysteine N-terminal peptide **43** and thiol analogue of leucine thiol analogue N-terminal peptide **42**.[225]

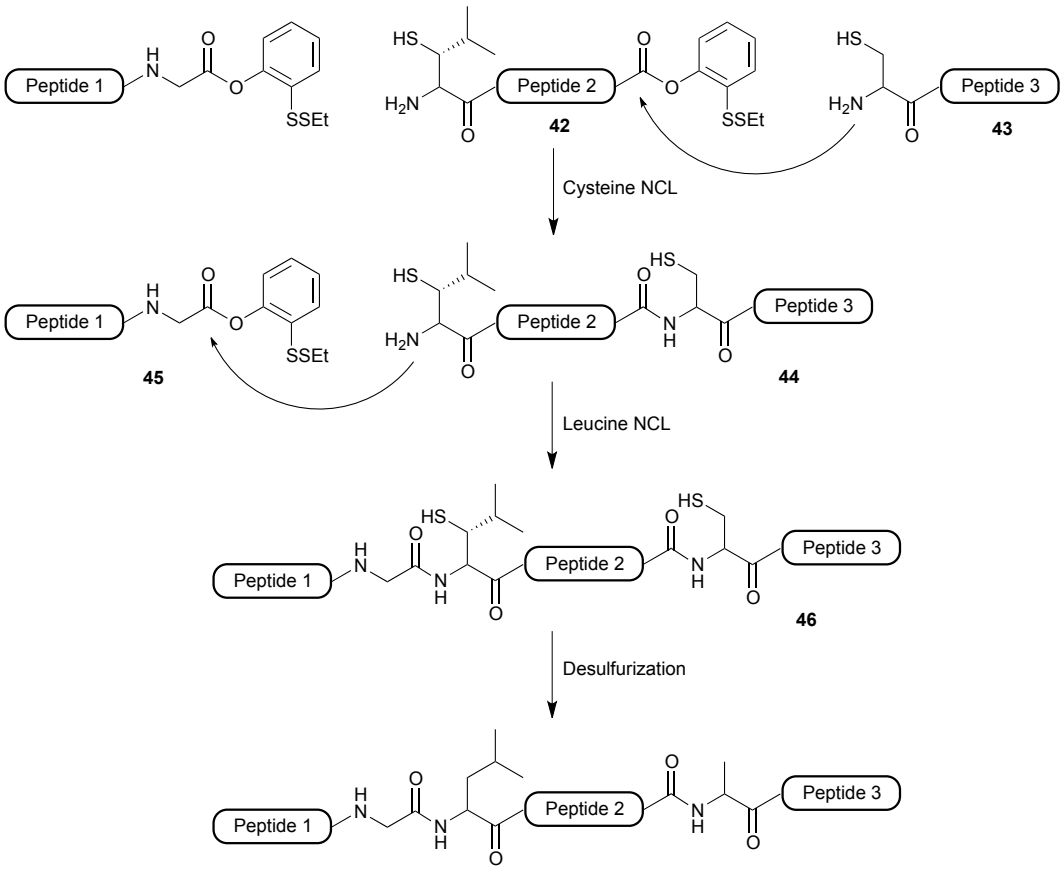

Danishefsky also found differences in completion times for epimers of a thiol analogue of proline **40** and **41** (Scheme 4.25).[227,228] The rate determining step in this case changed from transthioesterification, which is relatively fast for both epimers, to the S-to-N acyl shift. The S-to-N acyl shift is especially slow for **40** compared to **41** due to steric interactions between the two peptide chains, both of which reside on the same face of the pyrrolidine ring (Scheme 4.30). This N-terminal thiol analogue of proline **41** can be used to avoid the difficulty in ligating a C-terminal prolyl thioester.

Scheme 4.30: The (2*S*, 4*S*) prolyl **40** has interactions both peptide chains on the same face of the pyrrolidine ring while the (2*S*, 4*R*) prolyl **41** has peptide chains on opposite faces of the pyrrolidine ring.[227]

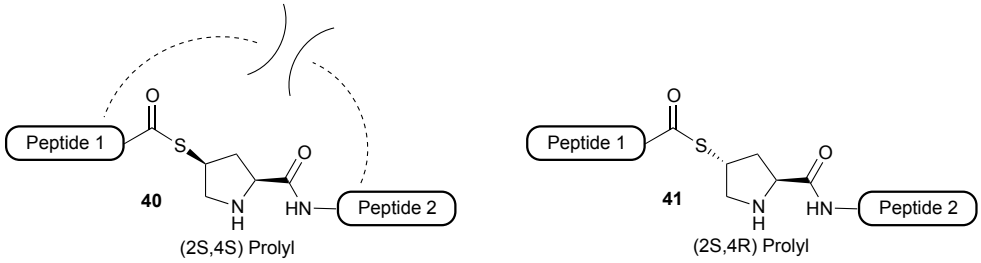

The use of thiol analogues of lysine (Scheme 4.25) in NCL is complicated by the presence of two amine groups both of which could partake in the N-to-S acyl shift. The side chain amine is likely to be the more nucleophilic because it is both further removed from the electron withdrawing amide bond and less sterically hindered because of no branching at the vicinal carbon. Consequently, the rate of peptide branching would likely be larger than the rate of peptide chain extension. Brik used the thiol analogue of lysine to perform side chain branching to prepare the peptide Ubiquitin. The thiol analogue of lysine was incorporated into the peptide chain in SPPS with the side chain amine protected.[222] Subsequent deprotection of the side chain allowed NCL of the side chain to give a branched peptide. Computational calculations for the pK_a of the side chain thiol placed it at pK_a = 9.74, which is above the calculated pK_a 9.1 for cysteine amide. Liu used an N-terminal lysine with a protected side chain to perform a chain extension NCL followed by a branching NCL after deprotection of the side chain.[223]

Thiol analogues of various amino acids have greatly extended the applicability of NCL. However, the multi-step synthesis and lack of commercial availability for many of these thiolated amino acids has limited their widespread application to date.[231]

4.1.6.2 Kinetically Controlled Ligations

NCL can be applied to the synthesis of peptides using either a N-to-C or a C-to-N approach (Scheme 4.31). In the former a peptide is prepared starting with the N-terminus of the peptide and then iteratively ligating towards the C-terminus (Scheme 4.31a). In the latter the reverse approach is used where preparation of a peptide starts

from the C-terminus and successive ligations build towards the N-terminus (Scheme 4.31b).

Scheme 4.31: N-to-C and C-to-N strategies to peptide chain extension via NCL. PG = Protecting Group.

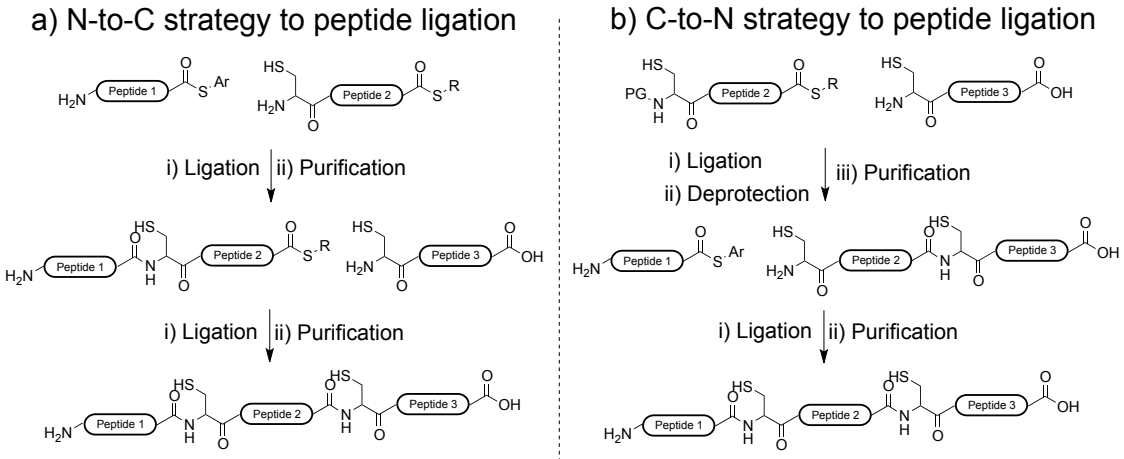

The N-to-C terminus approach is instinctively easier with NCL as the peptide can be steadily built via a repeated ligation and purification steps. Protection of an N-terminal cysteine allows access to a C-to-N NCL strategy of ligation, deprotection, purification, ligation.[232] However, the extra deprotection step required in the C-to-N process make it both more time consuming and more susceptible to material loss. To overcome these limitations Kent developed a C-to-N strategy based upon differences in the reactivity of thioesters that allow for the one pot synthesis of up to three peptide fragments together (Scheme 4.32).[233]

Scheme 4.32: Kinetically Controlled Ligation (KCL) developed by Kent for the synthesis of Crambin. Ligation 1 and Ligation 3 takes place in the presence of both an aryl and an alkyl thioester C-terminal. Thiophenol is a better leaving group than the alkyl thiol and therefore ligation occurs exclusively at the C-terminal aryl thioester.[233]

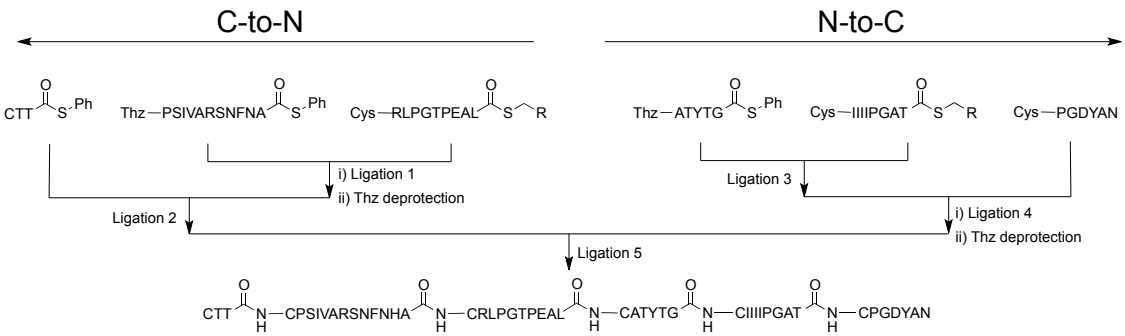

The lower reactivity of alkyl thioesters compared to aryl thioesters was harnessed to carry out a Kinetically Controlled Ligation (KCL) of the peptide Crambin (Scheme 4.32: Ligation 1 and 3).[xliii] In the C-to-N strategy three peptides were prepared: an N-terminus peptide with an aryl thioester, a middle peptide with a Thz protected N-terminal cysteine and a C-terminal aryl thioester and a C-terminus peptide with a N-terminal cysteine and a C-terminal alkyl thioester (Scheme 4.32: LHS). In Ligation 1 the middle and C-terminus peptides were linked together in the absence of a thiol additive, and as anticipated no homoligation at the alkyl thioester C-terminus was observed. The deprotection of the Thz N-terminal of the middle peptide was performed in the reaction mixture to reveal a cysteine, which, after purification, was reacted in Ligation 2 with the N-terminus peptide aryl thioester to give the C-to-N peptide. This again occurred without ligation at the alkyl thioester C-terminus.

In the N-to-C strategy three peptides were prepared: an N-terminus peptide with a Thz protected N-terminal cysteine and a C-terminal aryl thioester, a middle peptide with a N-terminal cysteine and an alkyl thioester C-terminal and a C-terminus peptide with an N-terminal cysteine (Scheme 4.32: RHS). In Ligation 3 a KCL of the N-terminus and middle peptides proceeded without ligation at the alkyl thioester. Ligation 4 was performed in the same reaction mixture upon addition of the C-terminus peptide and an aryl thiol additive to give the N-to-C peptide.

Finally, after Thz deprotection of the N-terminus of the N-to-C fragment the peptide Crambin was prepared in Ligation 5. The removal of multiple purification steps by the use of KCL enabled a high yield of Crambin despite the synthesis containing five ligations and two deprotections. The KCL approach also allowed Kent to make multiple large peptides including the 203 residue HIV-1 Protease which was at the time the largest peptide ever prepared chemically.[234]

Despite the benefits of KCL, there are drawbacks. A thiolactone (cyclic thioester) forming cyclisation reaction between a cysteine residue in the middle of a peptide chain with the C-terminal alkyl thioesters can slow the rate of ligations. Thiolactone formation also proved adverse for aryl thioesters.[235] This side reaction could be suppressed in the presence of an alkyl thiol reagent for the alkyl thioesters but this is not possible for aryl thioesters because it would prevent KCL. Careful choice of

[xliii] C-terminus and N-terminus refer to the C and N ends in the final peptide. C-terminal and N-terminal refer to the C and N ends of a peptide segment

the C-terminal amino acid for the alkyl and aryl thioesters was exercised in the Crambin synthesis. The presence of a slowly ligating amino acid at the C-terminal of the aryl thioester and a facile ligating amino acid at the alkyl thioester C-terminal has the potential to interfere with KCL as the alkyl thioester reaction may either compete or outcompete the ligation of the aryl thioester.

Pentelute and Bang have explored which C-terminal amino acids in the aryl and alkyl thioesters may be used in tandem during KCL.[236] Model ligations were undertaken using the peptide system in Scheme 4.33 to probe the product ratio and rate of KCL. The identity of Xaa1 and Xaa2 were varied between a representative amino acid in three out of the four groupings identified by Dawson (Section 4.1.4) (≤ 4 h = glycine, ≤ 9 h = alanine, and ≥ 48 h = valine). By monitoring the disappearance of the aryl thioester, second order rate constants for the ligation reactions were obtained (Table 4.1). The product distribution between the intermolecular ligations and intramolecular cyclisation was also examined (Table 4.1).

Scheme 4.33: Model peptides used to probe the effect of the C-terminal amino acid upon KCL. The cyclisation side reaction is also shown.[236]

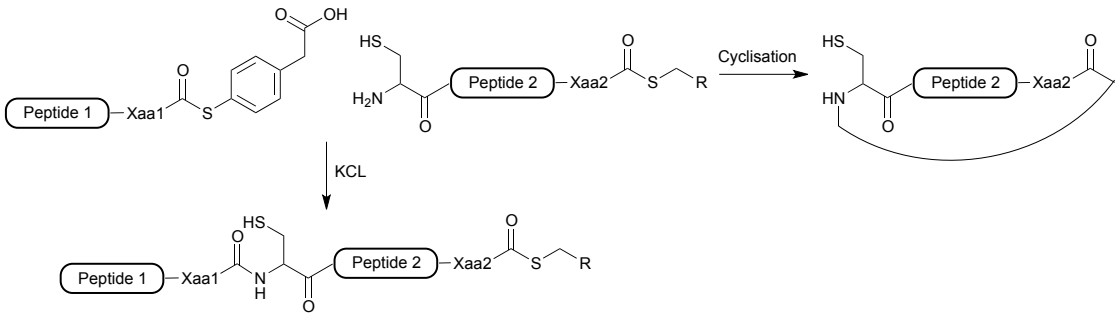

Table 4.1: The yield of cyclised and ligated peptides and observed second order rate constants for KCL for the model reaction between Peptide-Xaa1-aryl thioester and Peptide-Xaa2-alkyl thioester (Scheme 4.37).[236]

Cyclised Peptide / Ligated Peptide (%) k_{obs} (M^{-1} s^{-1}) R^2 value		Peptide-**Xaa2**-alkyl thioester		
		Gly	Ala	Val
Peptide-**Xaa1**-aryl thioester	Gly	22 / 71 2.00×10^{-7} 0.62	22 / 74 4.17×10^{-6} 0.92	0 / 90 2.33×10^{-6} 0.98
	Ala	11 / 50 1.37×10^{-8} 0.89	13 / 68 6.50×10^{-8} 0.95	0 / 70 1.67×10^{-8} 0.98
	Val	19 / 34 6.83×10^{-9} 0.81	25 / 24 9.67×10^{-9} 0.94	0 / 34 1.30×10^{-8} 0.99

The identity of Xaa1 in the aryl thioester was shown to have the greatest impact upon both the rate of ligation and the quantity of cyclisation product. Sterically more bulky residues were shown to decrease the observed second order rate constants for ligation. When Xaa1 was glycine the rate of ligation (2.00×10^{-7} M^{-1} s^{-1}) was 1 – 2 orders of magnitude greater than Xaa1 = alanine (1.37×10^{-8} M^{-1} s^{-1}) and 2 – 3 orders of magnitude larger than Xaa1 = valine (6.83×10^{-9} M^{-1} s^{-1}) (Table 4.1).

The impact of varying Xaa2 in the alkyl thioester upon ligation was smaller than for Xaa1. The observed second order rate constants for ligation increased when more sterically bulky amino acids are included at Xaa2. It was suggested that a more hindered C-terminal of the alkyl thioester decreases the competing rate of intramolecular cyclisation and results in a faster intermolecular reaction due to an increased concentration of active non-cyclised species. However, the concentration of peptide in solution should have no effect upon the magnitude of the second order rate constants, which are by definition concentration independent. Potentially, a bulkier Xaa2 also restricts folding of the peptide chain and therefore the thiolate of the cysteine is a better nucleophile as it is less hindered.

The ligation yields and product distribution were affected by the identity of Xaa1 in the aryl thioester and Xaa2 in the alkyl thioester. For Xaa1 the ligation yields

increased as the steric bulk of Xaa1 decreased with a 71 – 90 % yield for glycine, 50 – 70 % yield for alanine and 19 – 34 % yield for valine (Table 4.1). The amount of cyclisation product was dependent upon both Xaa1 and Xaa2. The dependence on Xaa1 was not a linear correlation. Increased steric bulk around the aryl thioester C-terminal should slow the intermolecular reaction and therefore increase the relative concentration of Xaa2 peptide in solution thus increasing the rate of the cyclisation reaction. While this trend holds when moving from glycine to valine, when Xaa1 = alanine the yield of the cyclisation is lower than for glycine; the cause of this remains unexplained. The rate of the cyclisation reaction is only slightly sensitive to small changes in steric bulk at Xaa2 as the cyclisation yield is approximately the same when Xaa2 = glycine or alanine. The large changes in steric bulk for Xaa2 = valine prevents the cyclisation reaction from occurring.

The kinetic experiments performed indicate that the highest intermolecular ligation yields in KCL are obtained when the aryl-thioester (Xaa1) is sterically unhindered and the alkyl thioester (Xaa2) is sterically hindered. While informative the above kinetic analysis had a number of flaws. The second order rate constants for ligation were obtained from reactions where the two peptides were added in an equimolar amount. This would be acceptable if no side reactions were present, however, owing to the competing cyclisation reaction, many of the fittings to find the second order rate constants for ligation have unacceptably low R^2 values (Table 4.1). To determine accurate second order rate constants for ligation, the rate constants for cyclisation must be determined independently with a highly dilute solution of Xaa2 peptide, and then be correctly factored into the overall kinetic scheme. In addition to the cyclisation reaction, a small amount of trimer product was also observed from the reaction between the internal thiol of the intended ligated product and Xaa1 peptide, which should also be accounted for in the overall kinetic scheme.

4.1.6.3 Cryptothioesters

The preparation of thioesters for NCL is a challenging process. Thioesters are prone to hydrolysis in acidic conditions and epimerisation at the α-carbon occurs more readily for thioesters than at oxoesters and amides as the pK_a of the α-protons is lower (ethyl thioacetate pK_a = 20.4 – 21.5,[237] ethyl acetate pK_a = 25.6[238] and acetamide pK_a = 28.4[239]). In order to overcome these limitations, cryptothioester methodology has been

developed involving an ester or amide group that can be readily converted into a thioester prior to or during NCL. The first example was developed by Danishefsky and was based upon a phenol ester with a disulfide protected *ortho*-thiol **47**.[240-242] Smooth NCL of **47** was observed when the thiol was deprotected in the presence of an N-terminal cysteine peptide (Scheme 4.34).

Scheme 4.34: The use of cryptothioesters in NCL.[240,241]

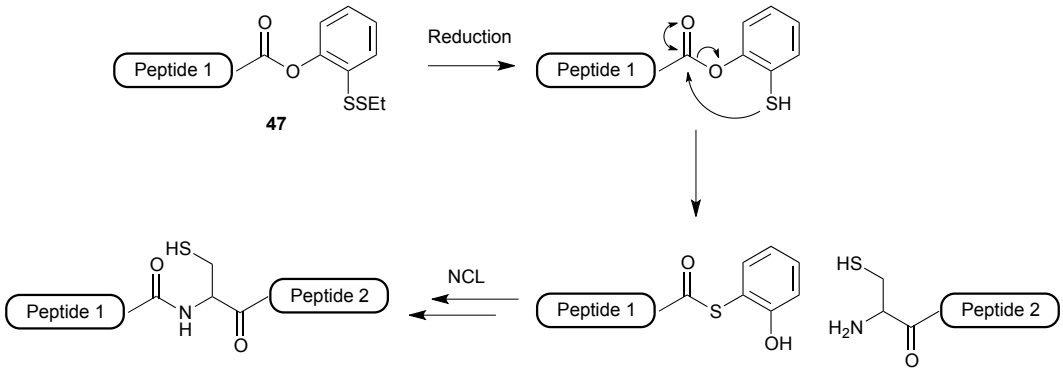

A number of other cryptothioesters have been developed (Scheme 4.35) including an alkyl carboxyethyl ester with a β-thiol **48**,[243,244] a sulfonamide with a protected thiol **49**,[216] a thiol oxazolidinone **50**,[245] a pyrrolidine **51**,[246,247] a alkyl thiol amide,[248] a bis(2-sulfanylethyl) amino (SEA) amide **52** and a *N*-aminoacyl-*N*-sulfanylethylaminobenzoic acid **53**.[253-255]

Scheme 4.35: A selection of Cryptothioesters developed to date.

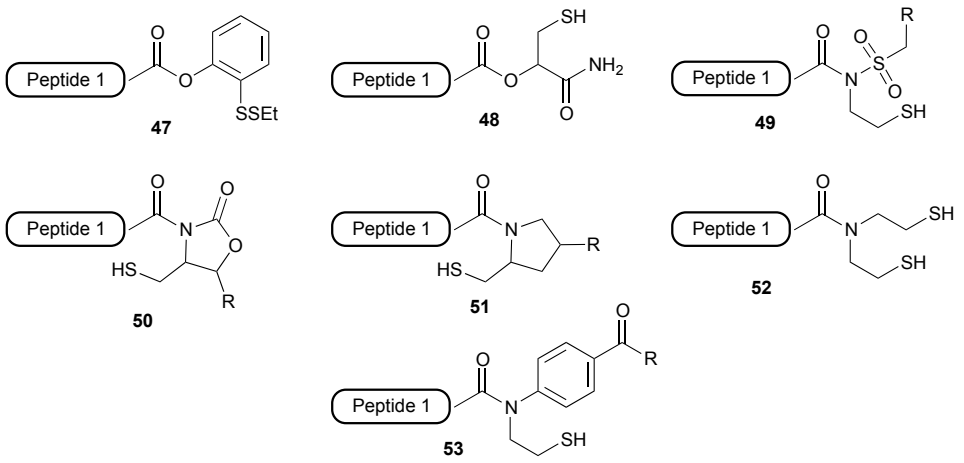

The O-to-S and N-to-S rearrangements in the ester and amide cryptothioesters can be controlled by adjusting reaction conditions. For the *N*-aminoacyl-*N*-

sulfanylethylaminobenzoic cryptothioester **53** developed by Otaka the N-to-S acyl shift reaction to generate the thioester prior to ligation was initially triggered under strong acidic conditions (4 M HCl / DMF).[253] This was likely due to protonation of the secondary amine group in acidic conditions preventing reversion back to the more stable amide. However, upon further examination of the conditions Otaka found that the presence of phosphate buffer also initiated the N-to-S acyl shift – potentially via a general acid catalysis mechanism. The greater control afforded by the cryptothioester allowed access to KCLs with C-terminal residues (e.g. Gly) that were previously inaccessible via Kent's alkyl / aryl thioester strategy (Scheme 4.36).[255]

Scheme 4.36: KCL with a *N*-aminoacyl-*N*-sulfanylethylaminobenzoic cryptothioester. Under the conditions of Ligation 1 no N-to-S acyl shift occurs rendering the C-terminal of Peptide 2 inert. In Ligation 2 N-to-S acyl shift is activated allowing ligation of Peptide 3.[255]

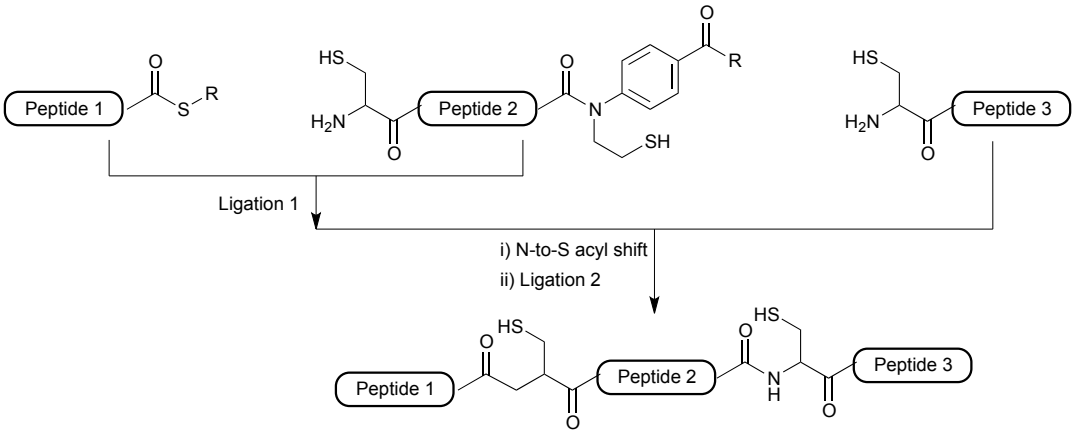

This methodology has been further extended by Otaka to prepare bovine insulin C through a one-pot dual KCL that combined the differences in reactivity at the N-terminus between a cysteine and a 4*R*-mercaptoproline and the differences in reactivity at the C-terminal between an alkyl thioester and a *N*-aminoacyl-*N*-sulfanylethylaminobenzoic cryptothioester (Scheme 4.37).[254] The cysteine on 'Peptide 2' ligates more rapidly than the (4*R*)-mercaptoproline on Peptide 3 with the alkyl thioester on 'Peptide 1'. The cryptothioester on Peptide 2 in amide form deactivates the C-terminal to ligation. The ligation between the (4*R*)-mercaptoproline and the cryptothioester can then be activated upon the addition of phosphate buffer to the reaction mixture. Thus two kinetically selective ligations were used to prepare the three

fragment peptide followed by desulfurization to give the final bovine insulin C product. This protocol was later applied to the synthesis of a glycopeptide.[256]

Scheme 4.37: One pot dual KCL for the synthesis of bovine Insulin C.[254]

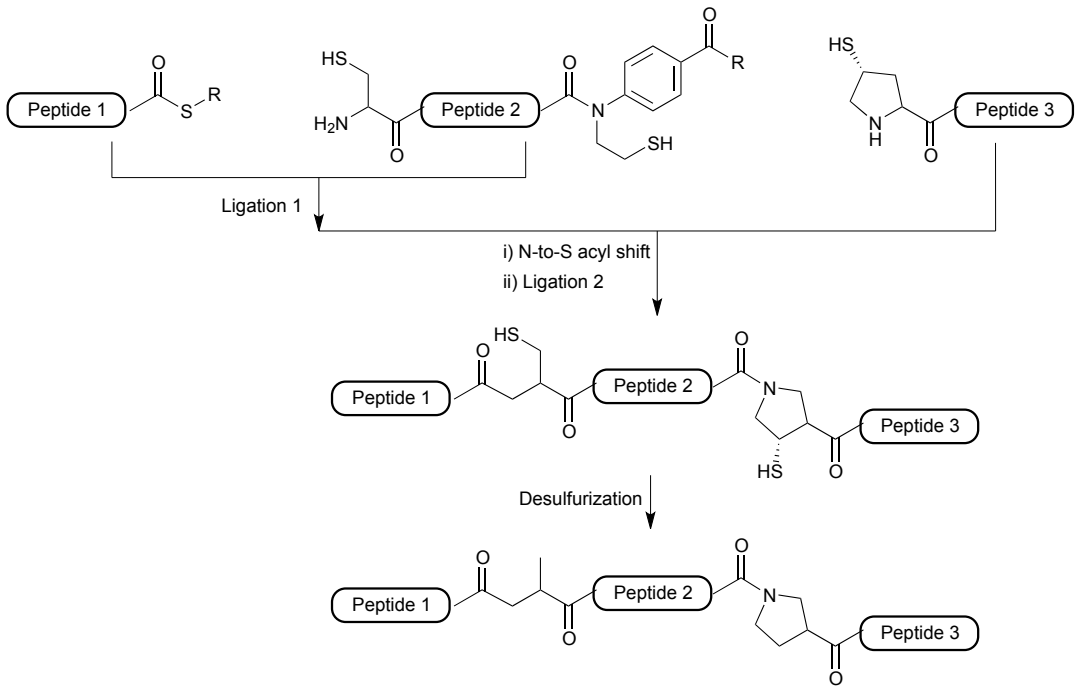

For the *bis*(2-sulfanylethyl) amino (SEA) amide cryptothioester **52** developed concomitantly by Melnyk and Liu the N-to-S acyl shift rearrangement is also favoured under acidic conditions because protonation of the released amine makes the reaction irreversible.[249,250] The added advantage of this cryptothioester is that the conversion to thioester can be controlled by oxidation / reduction of the thiol groups. This makes the cryptothioester amenable to one pot N-to-C ligations as the cryptothioester can be kept inactive while the ligation between the first two peptide fragments takes place (Scheme 4.38).[257] Ligation to the third fragment can then occur after reduction of the disulfide bridge.

Scheme 4.38: One pot N-to-C ligation strategy for the synthesis of peptides using a *bis*(2-sulfanylethyl) amino (SEA) amide cryptothioester.[257]

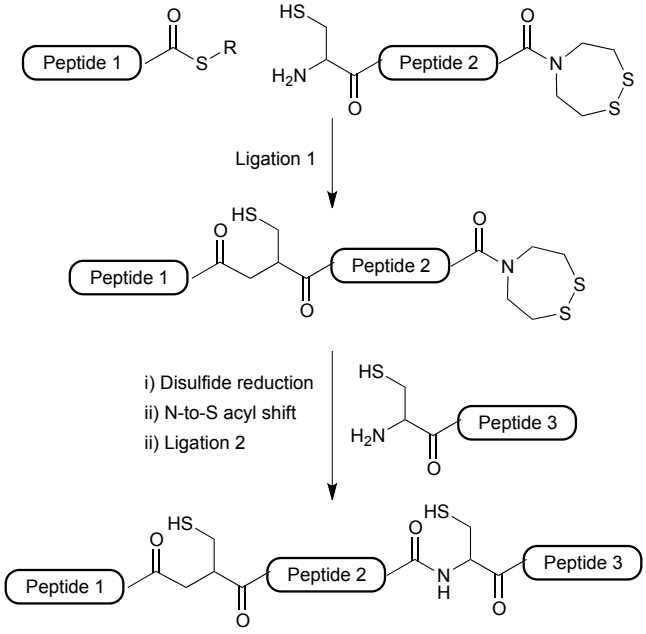

4.1.7 Peptide Synthesis Strategies with NCL

Over the last 20 years the developments in NCL have substantially widened the scope of its application. Peptide chemists frequently use combinations of the various ligation techniques above in the total chemical synthesis of peptides and proteins. Several detailed reviews exist for the use of NCL in peptide synthesis. An excellent review by Raibaut, Ollivier and Melnyk details the various C-to-N and N-to-C strategies developed to date for the three segment peptide synthesis by NCL.[258]

The majority of the strategies developed are dependent upon differences in reactivity at the C-terminal and apart from work done by Danishefsky[225] and Otaka[254] there have been very few attempts at developing a strategy that relies upon differences in reactivity at the N-terminal.

One area that has so far received scant attention is the differences in nucleophilicity of the thiolate group in the various thiol analogues used in the desulfurization methodology (Scheme 4.25). Danishefsky has demonstrated that alterations in chemical structure near the thiol group affect the nucleophilicity of thiol analogues (Scheme 4.29). In a competition experiment the product ratio for leucine thiol analogue N-terminus **39** vs. a cysteine N-terminus peptide favoured the cysteine product by 4 : 1. This was predominantly attributed to the change in sterics around the

thiol group. However, a change in sterics will not be the only contributing factor to nucleophilicity that will be affected by a change in structure. The placement of electron-donating or -withdrawing groups adjacent to the thiol will also affect the electronic properties of the thiolate nucleophile. This therefore raises the possibility of carrying out N-terminal-selective kinetically controlled ligations based upon the variation in nucleophilicity of thiol analogues with their structure.

The pK_a of the thiol may be used to establish how the nucleophilicity of thiol analogues varies with changes in structure. The pK_a of a nucleophile is usually a good predictor of its nucleophilicity (and in particular the nucleophiles electronic properties) as the transfer of a proton between an acid (leaving group) and a base (nucleophile) is also a nucleophilic substitution reaction (Chapter 1: Section 1.3). It is envisioned that an N-terminal kinetically controlled ligation that is based upon differences in the pK_a of thiolate nucleophiles will be subject to control by pH. In a solution containing several peptides each with a different N-terminal thiol analogue careful pH control could potentially be used to decide which of the peptides can undergo a ligation reaction. As a first step to assess the possibility of N-terminal-selective kinetically controlled ligation, we have undertaken a series of UV-Vis spectrophotometric studies to determine the pK_a of the thiol group for a variety of thiol analogues of amino acids (termed ‘cysteine derivatives’ hereafter).

4.2 Results

A selection of cysteine derivatives were initially examined including cysteine **54**, penicillamine (mercaptovaline) **55** and (4*S*)-mercaptoproline **56** methyl esters to determine the pK_a of the thiol (Scheme 4.39). Owing to their ready availability methyl esters were used to approximate the effect of an amide group on the amino acid. The validity of this assumption was later tested via a cysteine-glycine dipeptide **58,** cysteine peptide (H-Cys-Gly-Phe-NH_2) **59** and penicillamine peptide (H-Pen-Gly-Phe-NH_2) **60**. The parent amino acid cysteine **57** was also examined.

Scheme 4.39: Cysteine derivatives examined in this study.

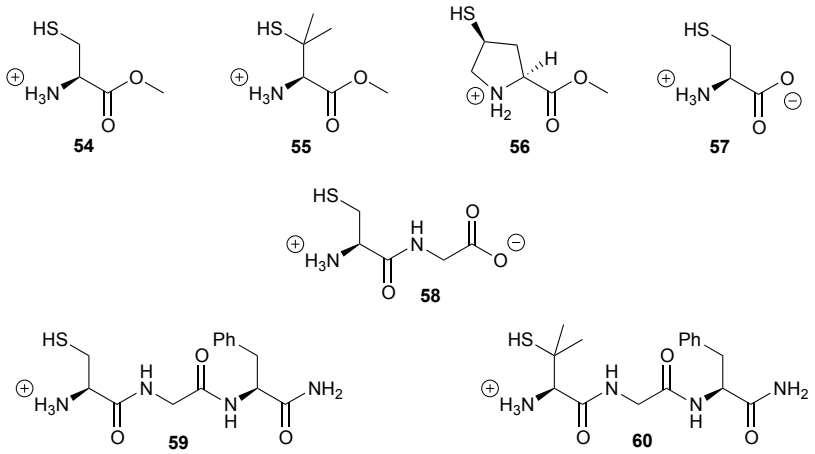

Previous investigations of NCL, and related discussion, have always assumed a single pK_a for the thiol group of cysteine (pK_a = 9.2).[258] At the N-terminus, however, cysteine residues have two possible ionization sites at the thiol and the ammonium groups. The typical pK_as of an alkyl thiol (10.6 – 11.8) and amino acid ammonium (9.1 – 9.7) are in sufficiently close proximity that up to four species may be present in solution depending upon the pH: a cationic (^+H_3N-R-SH), zwitterionic (^+H_3N-R-S^-), neutral (H_2N-R-SH) and anionic species (H_2N-R-S^-) (Scheme 4.40). *Due to the presence of four species in solution it is not strictly correct to quote a single pK_a for either the thiol or ammonium group*. The concentration of each species in solution at a given pH is mediated by the four dissociation constants K_A, K_B, K_C and K_D.

Scheme 4.40: The four possible ionization states of cysteine methyl ester that may be present in solution: cationic ($^{+}H_3N$-R-SH), zwitterionic ($^{+}H_3N$-R-S^{-}), neutral (H_2N-R-SH) and anionic (H_2N-R-S^{-}) species; and the acid dissociation constants K_A, K_B, K_C and K_D.

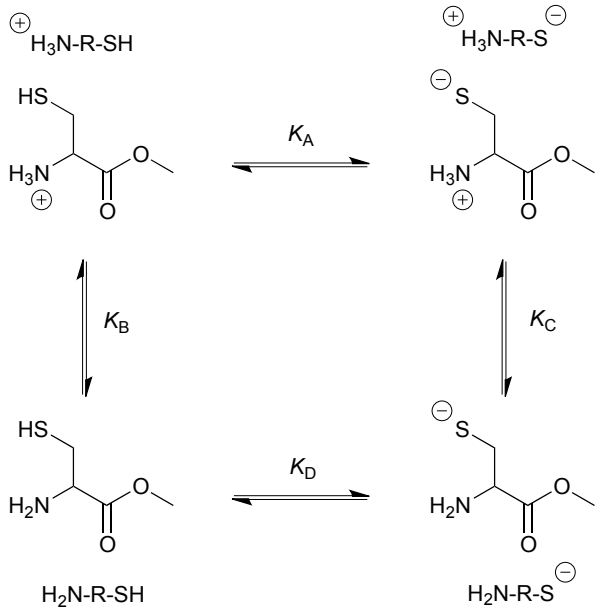

Benesch and Benesch have determined the dissociation constants K_A – K_D for cysteine and cysteine derivatives using a UV-Vis spectrophotometric method.[259] Ferrer-Sueta used an alternative method based upon the rate of reaction of a cysteine with a monobromobimane electrophile to determine the dissociation constants K_A – K_D (Scheme 4.40).[260] Due to its greater simplicity, the UV-Vis spectrophotometric method was chosen to determine K_A – K_D. The dissociation constants are determined by monitoring how the absorbance from an n to σ* transition on the thiolate (λ_{max} ~ 237 nm) varied with pH. This method is based on a number of assumptions detailed below along with explanations for why each should not affect the results:

1. The molar extinction coefficients of thiolates in $^{+}H_3N$-R-S^{-} and H_2N-R-S^{-} are assumed to be identical. Benesch and Benesch reported that the molar extinction coefficient of β-mercaptoethylamine remained constant over the pH range 9.9 – 12.0.[259] Within this pH range both the ammonium and thiol groups will transition from their conjugate acid and acid form to their base and conjugate base forms, respectively. Thus the molar extinction coefficients of the thiolate in both species: ^{-}S-$CH_2CH_2NH_3^{+}$ and ^{-}S-$CH_2CH_2NH_2$, are equivalent – or at least approximately equivalent that no discernable change was observed.

2. The molar extinction coefficients between the different cysteine derivative molecules examined are assumed to be approximately equivalent. This is imperative for the comparisons between speciation for the various cysteine methyl esters to be valid. This was experimentally verified to be the case (Section 4.2.4).
3. The observed absorbance at λ_{max} is solely due to the thiolate. This was again studied by Benesch and Benesch for alanine who found that negligible absorbances were observed at pH 7 when the amine is protonated and pH 12 when in base form.[259] This gives confidence that any absorbance changes are due to changes at the thiolate and do not originate from any other moiety.
4. There are no competing reactions, such as oxidation or acid/base catalysed hydrolysis of ester / amide bonds occurring that will affect the absorbance changes. The impact of oxidation of thiolate to form disulfide bonds will be discussed below. Acid and base catalysed hydrolyses are not expected to be relevant because reaction half lives for both of these reactions are significantly longer than the timescale (~ 2 min) of the UV-Vis spectrophotometric experiments:
    i. The second order rate constant for base catalysed hydrolysis of the ester ethyl acetate is k_{HO} = 0.087 M^{-1} s^{-1} which, at pH 11.8 an ester concentration of 0.2 mM, corresponds to a value of $k_{obs} \sim 1.11 \times 10^{-7}$ s^{-1} and a half life of ~ 72 days.
    ii. The second order rate constant for acid catalysed hydrolysis of the ester ethyl acetate is k_{H+} = 1.07 M^{-1} s^{-1} which at pH 1.5 and an ester concentration 0.2 mM corresponds to a value of $k_{obs} = 6.77 \times 10^{-6}$ s^{-1} and a half life of ~ 28.5 h.

The following sections present the results of the UV-Vis spectrophotometric experiments and the $K_A - K_D$ values determined for each of the cysteine derivatives in Scheme 4.39.

4.2.1 Determination of dissociation constants K_A – K_D for cysteine methyl ester

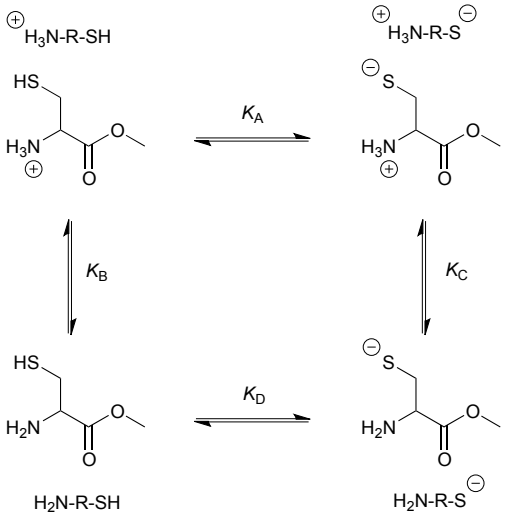

The UV-Vis spectra between 220 and 280 nm for cysteine methyl ester in the pH range 2.07 – 11.85 at 25 °C and ionic strength I = 0.3 M are shown in Figure 4.3. Background absorbances due to buffer have been subtracted from the observed spectra.

Figure 4.3: UV-Vis spectra for cysteine methyl ester (0.2 mM) in buffer solutions covering the pH range 2.07 – 11.85 at 25 °C and ionic strength I = 0.3 M (NaCl).

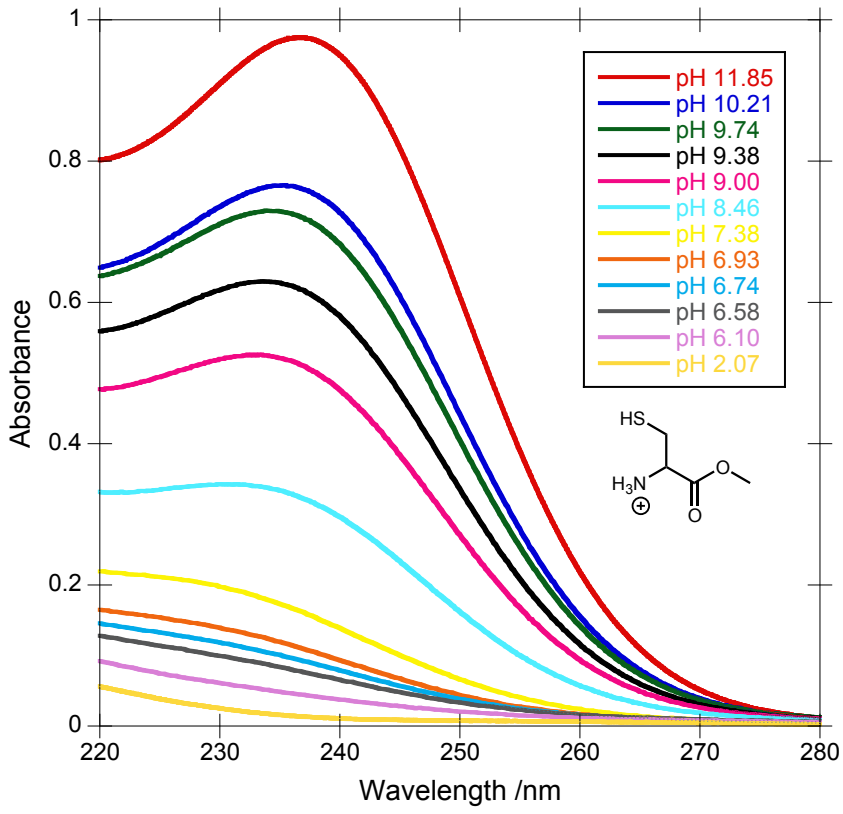

The wavelength of maximum absorbance at each pH over the range pH = 2.07 – 11.85 was then identified as λ_{max} = 235 – 237 nm for thiolate and was observed to blue shift with decreasing pH, which is attributed to $^{+}H_3N$-R-S^{-} absorbing at shorter wavelengths than H_2N-R-S^{-}. A single wavelength spectrum was then recorded at the appropriate λ_{max} for the pH of the buffer solution (Figure 4.4) to give the observed absorbance, A_{obs}. As well as leading to more accurate A_{obs} values these single wavelength measurements allow for detection of changes in A_{obs} over the time.

Figure 4.4: UV-Vis spectra monitored at a single wavelength (λ = 237 nm) for 0.2 mM cysteine methyl ester in buffer solutions covering the pH range 1.39 – 12.47 at 25 °C and ionic strength I = 0.3 M (NaCl).

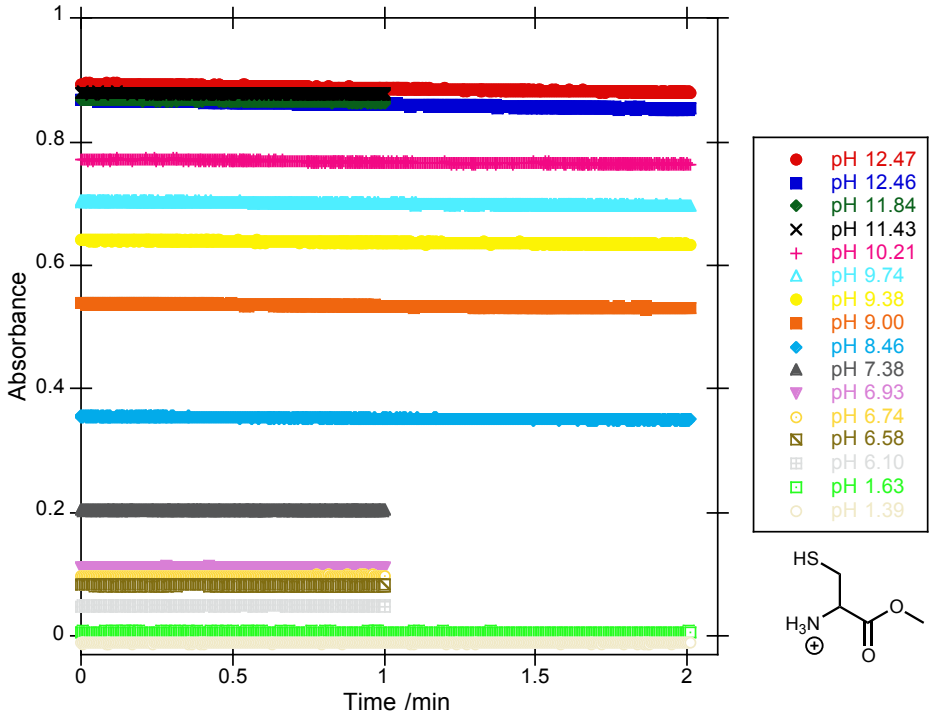

At pHs above 7.38 a slight decrease (~1.5 % loss) in A_{obs} over 2 minutes was observed. It is postulated that this is a result of a side reaction most likely disulfide bond formation between cysteine methyl esters. This initially was not a significant problem due to the small magnitude of the effect but subsequently became a more significant issue (see below).

The Benesch method uses the fraction of total thiol in thiolate form, f_{RS^-}, in the calculation of the dissociation constants K_A – K_D. At pH 12.47, it can be reasonably assumed that the observed absorbance is due to thiolate form only, $(A_{obs})_{max.}$ The f_{RS^-} of

thiolate present in solution at lower pHs may then be determined relative to $(A_{obs})_{max.}$ At lower pHs there may also be a small contribution to the absorbance at λ_{max} from the thiol in acid form (R–SH). In order to correct for this, the absorbance value at 237 nm for a solution at pH 1.63, A_{237}^{RSH}, (where it is reasonable to assume that all the thiol is in acid form) was subtracted from each observed absorbance in Figure 4.4 prior to the determination of f_{RS^-}. The absorbance contribution from R–SH to A_{obs} will decrease as the pH increases from 9.3 % at pH 6.53 to < 0.7 % at pH 11.84. Values for f_{RS^-} as a function of pH were calculated using Equation 4.1 and are listed in Table 4.2:

$$f_{RS^-} = \frac{[RS^-]}{[RS^-]_{max}} = \frac{Abs(RS^-)}{Abs(RS^-)_{max}} = \frac{(A_{obs} - A_{237}^{RSH})}{(A_{obs} - A_{237}^{RSH})_{max}}$$

$$f_{RS^-} = \frac{[H_2N-R-S^-]+[H_3N^+-R-S^-]}{[H_2N-R-S^-]+[H_3N^+-R-S^-]+[H_2N-R-SH]+[H_3N^+-R-SH]} \quad \text{(Equation 4.1)}$$

A plot of the f_{RS^-} against pH is shown Figure 4.5.

Table 4.2: A_{obs}, $A_{obs} - A_{237}^{RSH}$ and f_{RS^-} at each pH for cysteine methyl ester at 25 °C and ionic strength I = 0.3 M (NaCl).

Buffer	pH	A_{obs}	$A_{obs} - A_{237}^{RSH}$	f_{RS^-}
50 mM NaOH	12.47	0.893	0.886 [b]	1.00
50 mM NaOH	12.46	0.868	0.861	0.97
30 mM NaOH	11.84	0.869	0.862	0.97
10 mM NaOH	11.40	0.879	0.872	0.98
90 % fb 0.1 M NH_4Cl	10.21	0.771	0.764	0.86
90 % fb 0.1 M $Na_2B_4O_7$	10.07	0.792	0.786	0.89
80 % fb 0.1 M $Na_2B_4O_7$	9.86	0.771	0.764	0.86
70 % fb 0.1 M NH_4Cl	9.74	0.704	0.697	0.79
70 % fb 0.1 M $Na_2B_4O_7$	9.50	0.739	0.732	0.83
50 % fb 0.1 M NH_4Cl	9.38	0.641	0.634	0.72
60 % fb 0.1 M $Na_2B_4O_7$	9.27	0.679	0.672	0.76
50 % fb 0.1 M $Na_2B_4O_7$	9.12	0.645	0.639	0.72
30 % fb 0.1 M NH_4Cl	9.00	0.538	0.532	0.60
40 % fb 0.1 M $Na_2B_4O_7$	8.92	0.542	0.535	0.60
30 % fb 0.1 M $Na_2B_4O_7$	8.75	0.468	0.462	0.52
20 % fb 0.1 M $Na_2B_4O_7$	8.61	0.405	0.399	0.45
10 % fb 0.1 M NH_4Cl	8.46	0.355	0.349	0.39
10 % fb 0.1 M $Na_2B_4O_7$	8.22	0.351	0.344	0.39
80 % fb 0.1 M KH_2PO_4	7.38	0.204	0.197	0.22
60 % fb 0.1 M KH_2PO_4	6.93	0.148	0.142	0.16
50 % fb 0.1 M KH_2PO_4	6.74	0.127	0.120	0.14
40 % fb 0.1 M KH_2PO_4	6.58	0.109	0.102	0.12
20 % fb 0.1 M KH_2PO_4	6.10	0.069	0.062	0.07
20 % fb 0.1 M KH_2PO_4	6.10	0.070	0.063	0.07
90 % fb 0.1 M H_3PO_4	2.95	0.015	0.008	0.01
90 % fb 0.1 M H_3PO_4	2.95	0.015	0.008	0.01
30 mM HCl	1.65	0.007 [a]	0.000	0.00

[a] Value used for A_{237}^{RSH}. [b] Value used for $(A_{obs} - A_{237}^{RSH})_{ma4}$.

Figure 4.5: The variation of the fraction of thiol in thiolate form, f_{RS^-}, as a function of pH for cysteine methyl ester at 25 °C and ionic strength I = 0.3 M (NaCl). $K_C = 2.53 \times 10^{-9}$ M. The dotted line is the fit of Equation 4.2 to the f_{RS^-}.

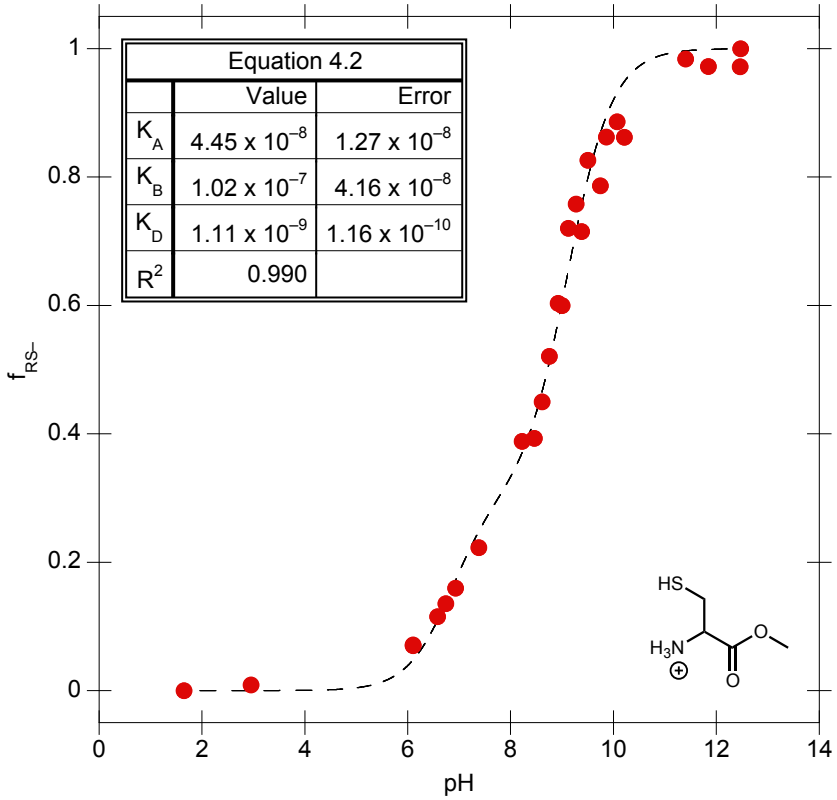

Equation 4.1 may be rearranged to give Equation 4.2. Values for the dissociation constants K_A, K_B and K_D are estimated from a fitting of data points (●) to Equation 4.2 (fit shown as dotted line in Figure 4.5).

$$f_{RS^-} = \frac{(A_{obs} - A_{237}^{RSH})}{(A_{obs} - A_{237}^{RSH})_{max}} = \frac{K_A/K_B + K_D/[H^+]}{[H^+]/K_B + K_A/K_B + K_D/[H^+] + 1} \qquad \text{(Equation 4.2)}$$

The dissociation constant K_C may then be calculated from the relationship:

$$\frac{K_A}{K_B} = \frac{K_D}{K_C} \qquad \text{(Equation 4.3)}$$

Attempts were also made to fit the data to two alternative "Two pK_a + Three Species" models, where the pK_as of the thiol and ammonium are independent of each other (> 2 pK units apart) – see Appendix III.11. However, the fittings were always

inferior to the "Four pK_a + Four Species" model used above (Scheme 4.40 and Equation 4.2).

4.2.2 Interference from disulfide bond formation

Initially, no attempt was made to prevent the formation of disulfide. The risk of disulfide bond formation was initially considered low because the cysteine methyl ester stock solution was prepared fresh for each experiment from solid cysteine methyl ester and the final concentration of cysteine methyl ester in the cuvette was relatively low (0.2 mM). The results using this method for cysteine methyl ester were in accordance with data from Benesch for a cysteine ethyl ester. It was noticed, however, during UV-Vis experiments for 4*R*-mercaptoproline methyl ester, that the λ_{max} began to significantly shift to higher wavelengths (λ_{max} ~ 253 nm) as the pH increased (Figure 4.6).

Figure 4.6: UV-Vis spectra for 4*R*-mercaptoproline methyl ester (0.2 mM) in buffer solutions covering the pH range 1.37 – 11.87 at 25 °C and ionic strength I = 0.3 M (NaCl).

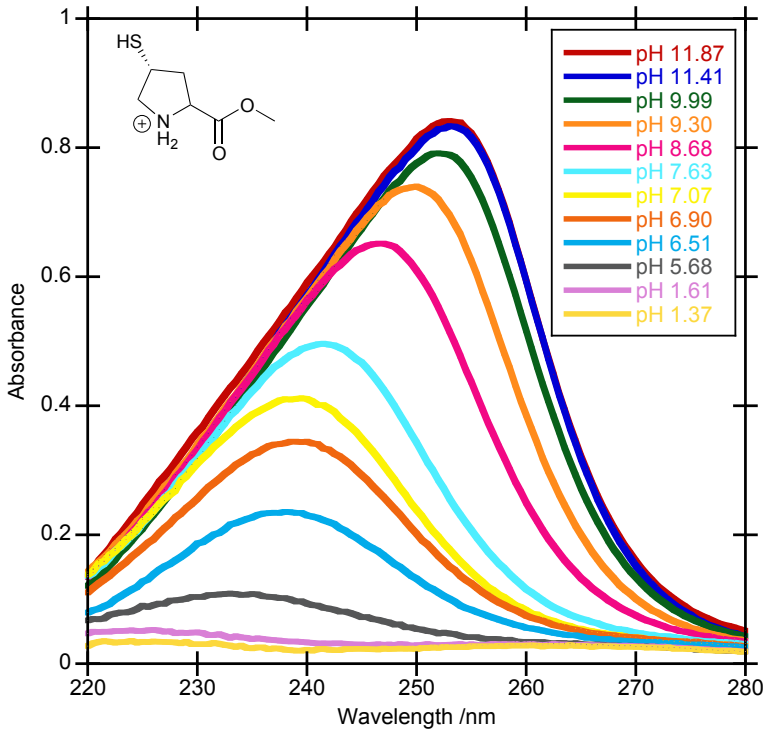

Subsequent, repeats with cysteine methyl ester also displayed a significant shift of the λ_{max} towards higher wavelengths at higher pH values (254 – 260 nm), albeit to a smaller degree, and the λ_{max} was also observed to be dependent upon the concentration of cysteine methyl ester in solution (Figure 4.7).

Figure 4.7: UV-Vis spectra for a series of different cysteine methyl ester concentrations in a 50 mM NaOH solutions (pH 12.06) at 25 °C and ionic strength $I = 0.3$ M (NaCl).

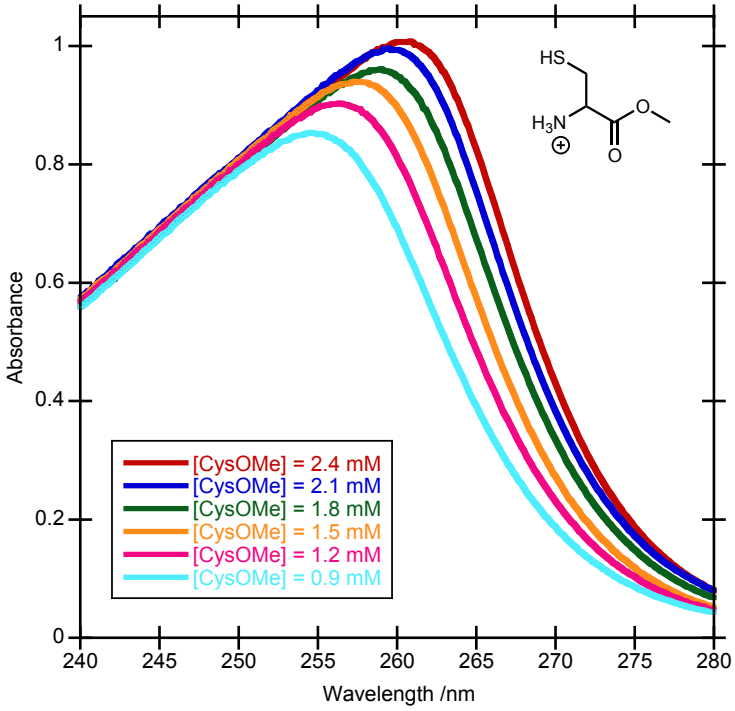

In principle, the λ_{max} should be independent of the concentration of cysteine methyl ester and therefore this observation required further explanation. The UV-Vis spectrum of dimethyl disulfide was recorded and a λ_{max} of 254 nm at pH 12.02 (Appendix III: Figure III.1) indicating that the change in λ_{max} could be due the formation of disulfide bonds between cysteine methyl esters. The exact cause as to why disulfide bond formation became an issue in later experiments is unknown. Coincidently, the filters used in the departmental apparatus for water purification were replaced, which may have altered the oxygen content of the deionised water used in our experiments thereby creating a more oxidizing environment.

In order to counteract oxidation the trialkylphosphine reducing agent *tris*(2-carboxyethyl)phosphine (TCEP) was chosen due to its high solubility and its regular

use in NCL (Scheme 4.41).[261] One concern regarding TCEP is that it is known to also oxidise relatively rapidly under basic conditions (Figure 4.8). However, the timescale for oxidation was substantially longer (hours) than our experimental timescale (minutes) (Figure 4.8). A solution of an oxidised cysteine methyl ester dimer was prepared and an aliquot added to a 50 mM NaOH solution (pH 12.48) in a cuvette to give a final concentration of 2.0 mM. The UV-Vis spectrum was then taken which showed very low absorbance in the 237 nm region (Figure 4.9). A spectrum taken immediately after addition of TCEP (20 mM) showed a significant increase in absorbance at 237 nm, and a further increase 20 minutes after addition (Figure 4.9). These experiments identified that TCEP was still active at higher pH values.

Scheme 4.41: a) The structure of the reducing agent *tris*(2-carboxyethyl)phosphine (TCEP), and b) a possible mechanism for the TCEP-mediated cleavage of disulfide bonds.

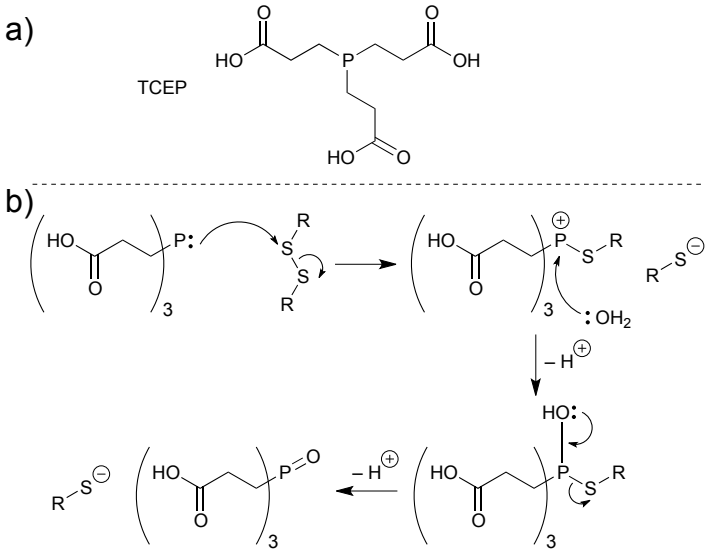

Figure 4.8: The percentage of TCEP oxidised as a function of time in solutions of different pH for a 5 mM TCEP followed by ^{31}P NMR.[261] Reproduced with permission from the ACS.

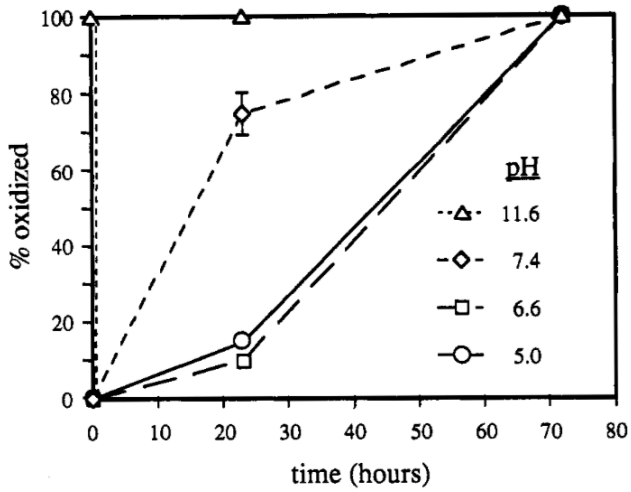

Figure 4.9: UV-Vis spectra for an oxidised cysteine methyl ester dimer solution (2.0 mM) in a 50 mM NaOH solutions (pH 12.48) before and after the addition of TCEP (20 mM) at 25 °C and ionic strength I = 0.3 M (NaCl).

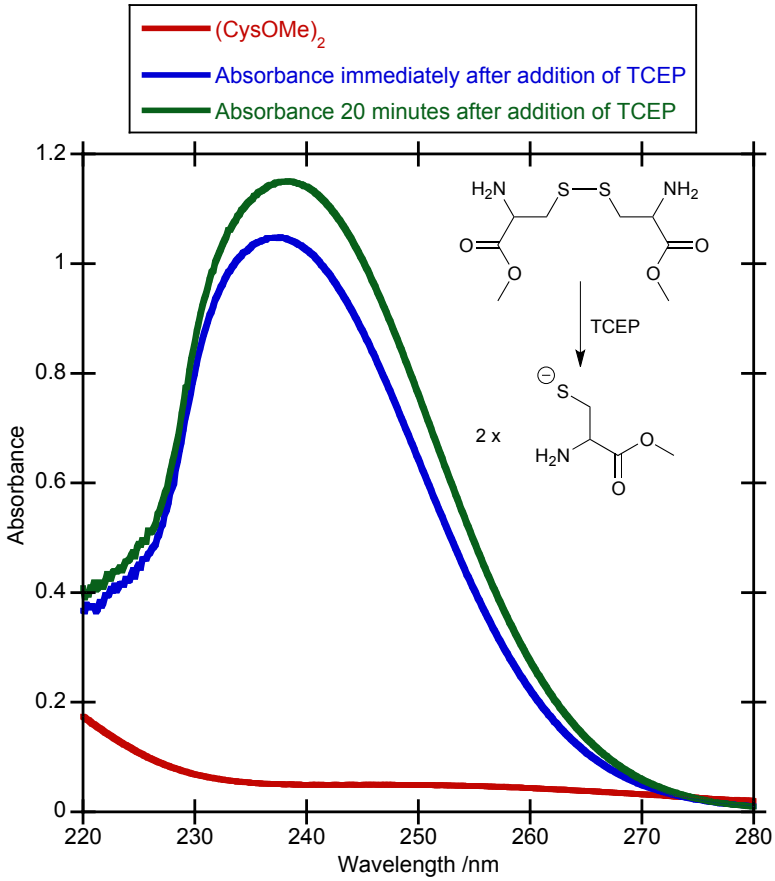

With the confirmation that TCEP was active even in highly basic conditions the above method for acquiring the absorbance changes with pH for the cysteine methyl esters was adapted. The TCEP concentration (2.0 mM) in the cuvette was maintained at 10-fold excess relative to the concentration of cysteine methyl ester. The absorbance from this TCEP and buffer solution was initially taken and this spectrum was manually subtracted from the spectrum of the cysteine methyl ester to give the absorbance due to thiolate only. The absorbance changes monitored by single wavelength at the λ_{max} now did not change over the time course of the measurements.

Measurements of K_A, K_B, K_C and K_D for the cysteine methyl ester and penicillamine methyl ester were repeated under reducing conditions. The evaluation of the acid dissociation constants for cysteine, cysteine glycine, H-Cys-Gly-Phe-NH_2 and H-Pen-Gly-Phe-NH_2 were all performed in reducing conditions.

All UV-Vis spectral overlays used in the determination of λ_{max} and the subsequent the single wavelength absorbance measurements at λ_{max} for cysteine methyl ester, penicillamine methyl ester, (4*S*)-mercaptoproline methyl ester, cysteine, cysteine glycine, H-Cys-Gly-Phe-NH_2 and H-Pen-Gly-Phe-NH_2 are located in the Appendix III. The final plots of f_{RS^-} against pH are shown below.

4.2.3 Determination of dissociation constants K_A – K_D for cysteine derivatives under reducing conditions

4.2.3.1 Cysteine Methyl Ester

Values of dissociation constants, $K_A = 4.30 \times 10^{-8}$ M, $K_B = 2.16 \times 10^{-7}$ M, $K_C = 4.99 \times 10^{-9}$ M, $K_D = 9.94 \times 10^{-10}$ M were determined for cysteine methyl ester by fitting of the data in Figure 4.10 to Equation 4.2 as described above. K_C was determined using Equation 4.3. A repeat experiment had values of $K_A = 5.63 \times 10^{-8}$ M, $K_B = 2.77 \times 10^{-7}$ M, $K_C = 5.37 \times 10^{-9}$ M, $K_D = 1.10 \times 10^{-9}$ M (Figure 4.11). These values are in good agreement with each other.

Scheme 4.42: Dissociation constants $K_A - K_D$ for cysteine methyl ester.

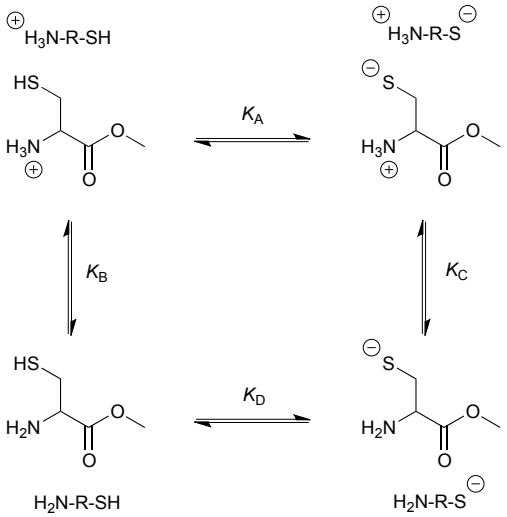

Figure 4.10: The variation of the fraction of thiol in thiolate form, f_{RS^-}, as a function of pH for cysteine methyl ester (0.2 mM) with TCEP (2.0 mM) at 25 °C and ionic strength $I = 0.3$ M (NaCl).

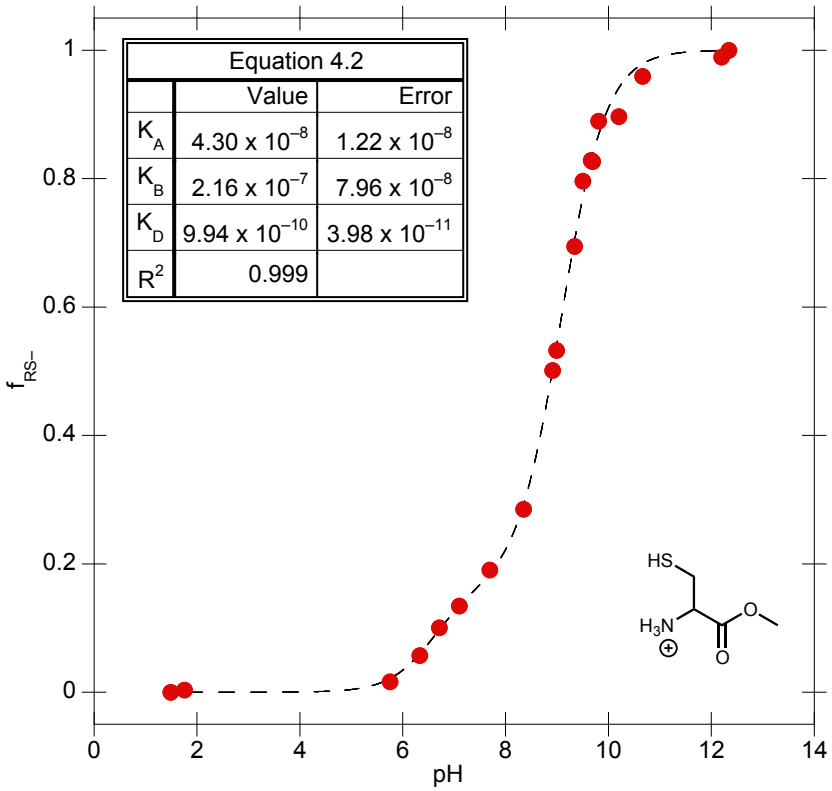

Figure 4.11: Repeat experiment for the variation of the fraction of thiol in thiolate form, f_{RS^-}, as a function of pH for cysteine methyl ester (0.2 mM) with TCEP (2.0 mM) at 25 °C and ionic strength I = 0.3 M (NaCl).

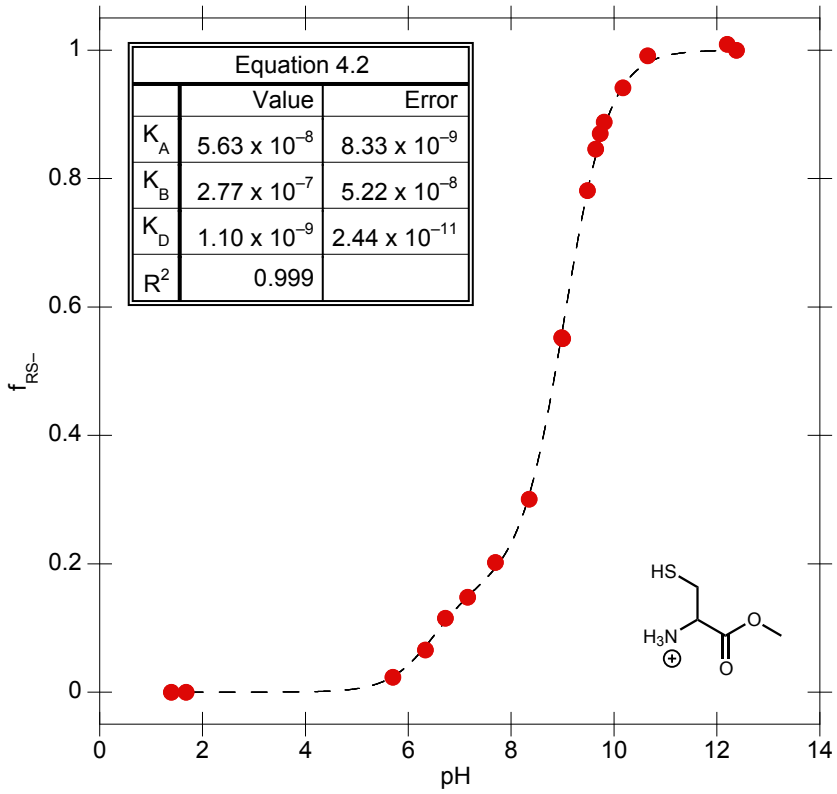

4.2.3.2 Penicillamine Methyl Ester

Values of dissociation constants, K_A = 2.15 × 10^{-8} M, K_B = 8.52 × 10^{-8} M, K_C = 1.95 × 10^{-10}, K_D = 4.86 × 10^{-10} M were determined under non-reducing conditions for penicillamine methyl ester by fitting of the data in Figure 4.12 to Equation 4.2 as described above. K_C was determined using Equation 4.3. When repeated under TCEP reducing conditions had values of K_A = 4.13 × 10^{-8} M, K_B = 2.44 × 10^{-7} M, K_C = 2.51 × 10^{-9} M, K_D = 4.21 × 10^{-10} M (Figure 4.13).

Scheme 4.43: Dissociation constants $K_A - K_D$ for penicillamine methyl ester.

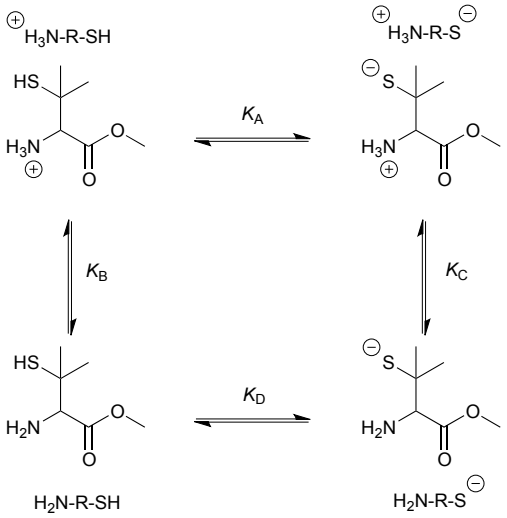

Figure 4.12: The variation of the fraction of thiol in thiolate form, f_{RS^-}, as a function of pH for penicillamine methyl ester (0.2 mM) at 25 °C and ionic strength $I = 0.3$ M (NaCl). Attempt to fit this data to a two pK_a and three species fitting failed to converge upon a solution.

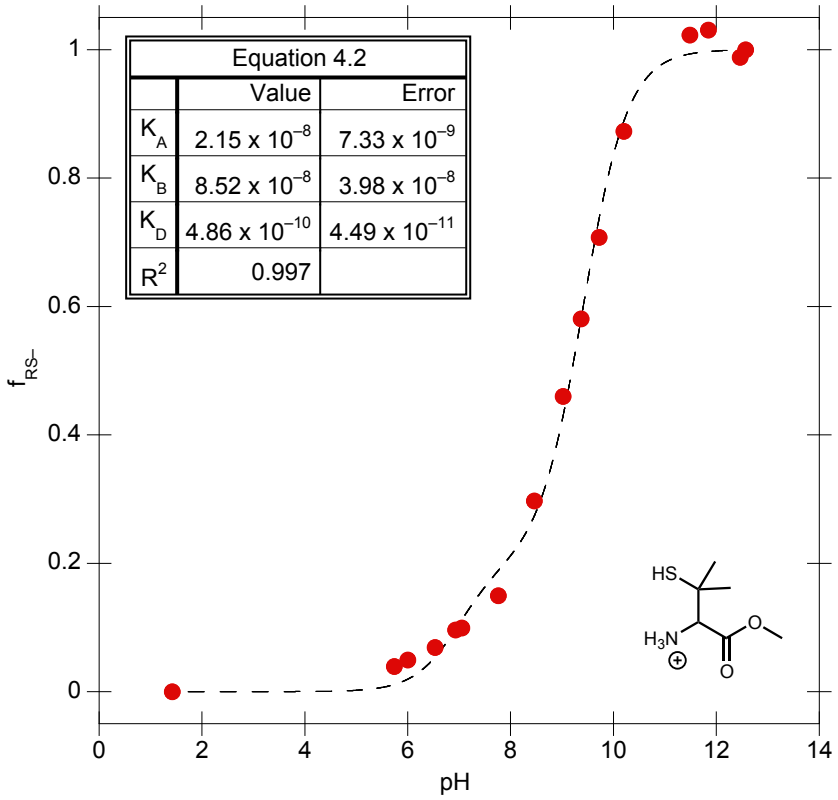

Figure 4.13: The variation of the fraction of thiol in thiolate form, f_{RS^-}, as a function of pH for penicillamine methyl ester (0.2 mM) with TCEP (2.0 mM) at 25 °C and ionic strength I = 0.3 M (NaCl).

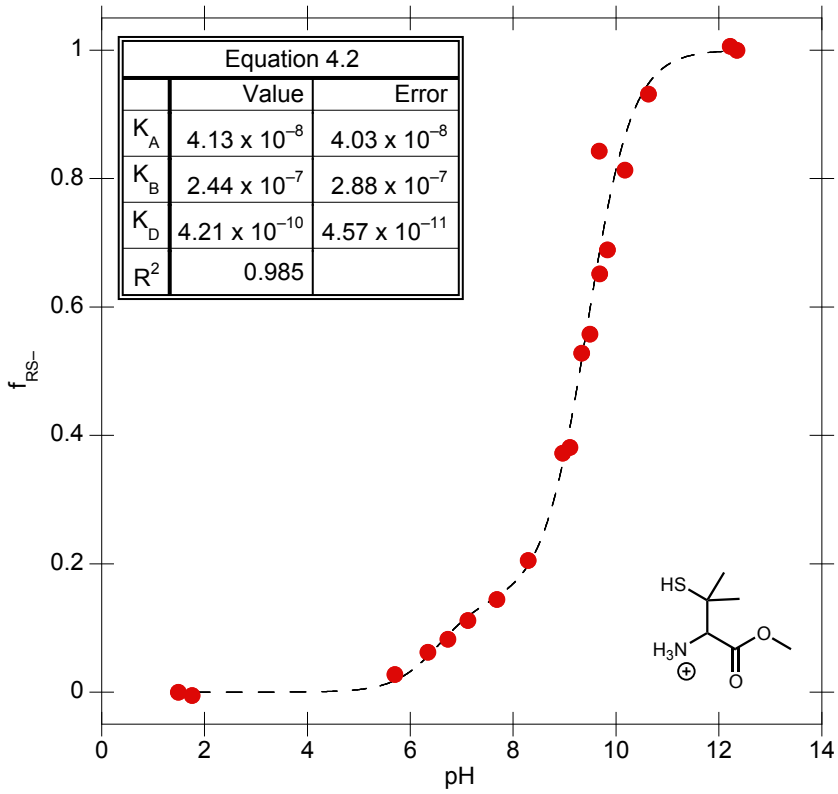

4.2.3.3 (4*S*)-Mercaptoproline Methyl Ester

Values of dissociation constants, K_A = 7.62 × 10^{-8} M, K_B = 1.28 × 10^{-7} M, K_C = 3.02 × 10^{-9}, K_D = 1.82 × 10^{-9} M were determined under non-reducing conditions for (4*S*)-mercaptoproline methyl ester by fitting of the data in Figure 4.14 to Equation 4.2 as described above. K_C was determined using Equation 4.3.

Scheme 4.44: Dissociation constants K_A – K_D for (4*S*)-mercaptoproline methyl ester.

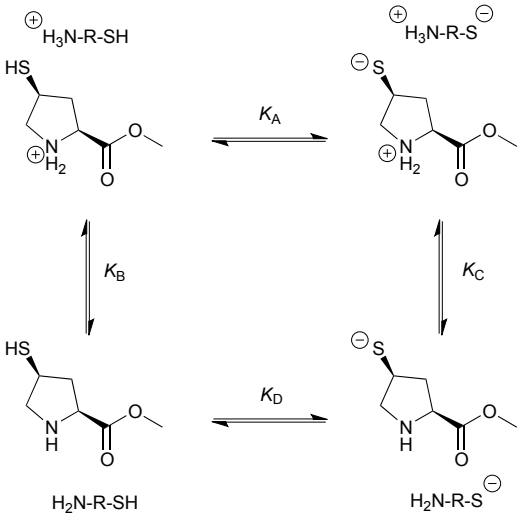

Figure 4.14: The variation of the fraction of thiol in thiolate form, f_{RS^-}, as a function of pH for (4*S*)-mercaptoproline methyl ester (0.2 mM) at 25 °C and ionic strength $I = 0.3$ M (NaCl).

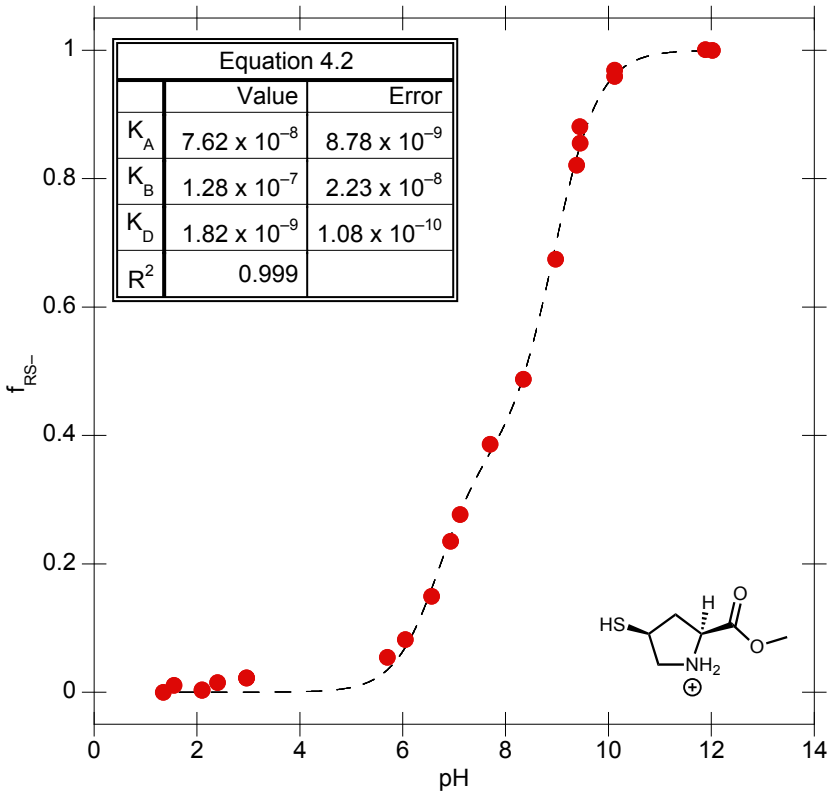

4.2.3.4 Cysteine

Values of dissociation constants, $K_A = 3.88 \times 10^{-9}$ M, $K_B = 3.44 \times 10^{-9}$ M, $K_C = 1.32 \times 10^{-10}$, $K_D = 1.50 \times 10^{-10}$ M were determined under reducing conditions for cysteine by fitting of the data in Figure 4.15 to Equation 4.2 as described above. K_C was determined using Equation 4.3.

Scheme 4.45: Dissociation constants $K_A - K_D$ for cysteine.

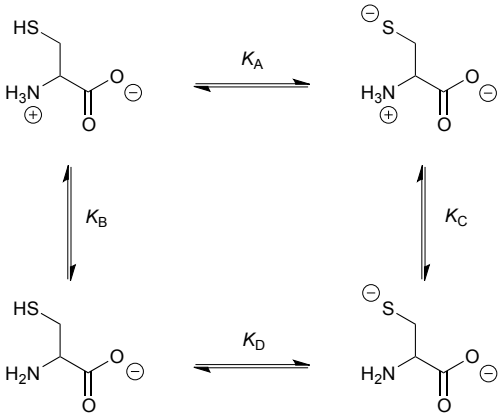

Figure 4.15: The variation of the fraction of thiol in thiolate form, f_{RS^-}, as a function of pH for cysteine (0.2 mM) with TCEP (2.0 mM) at 25 °C and ionic strength $I = 0.3$ M (NaCl).

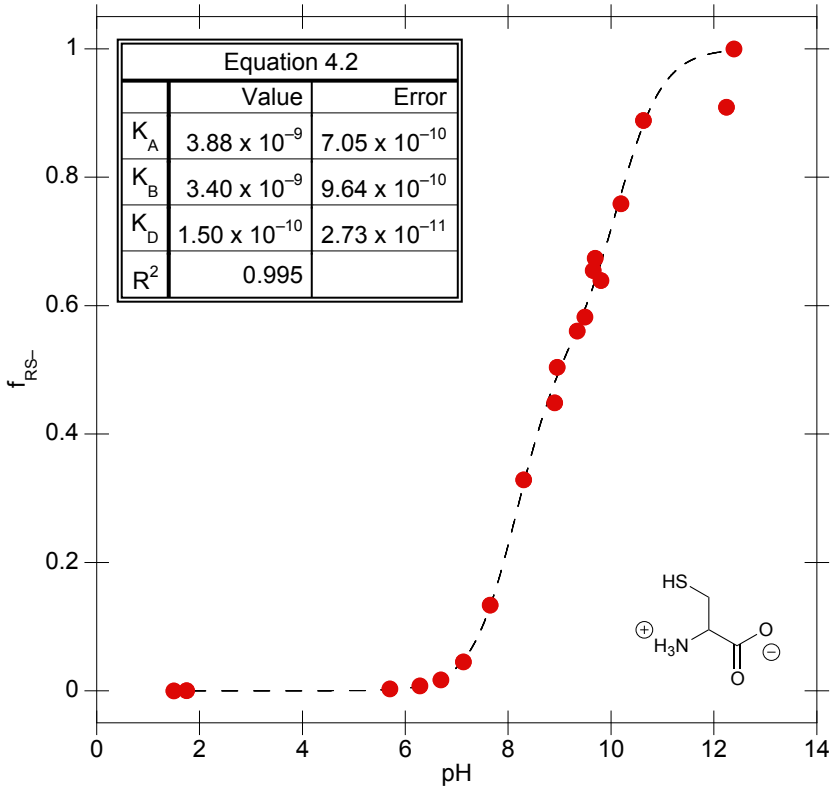

4.2.3.5 H-Cys-Gly-OH Peptide

Values of dissociation constants, $K_A = 1.07 \times 10^{-8}$ M, $K_B = 9.68 \times 10^{-8}$ M, $K_C = 4.57 \times 10^{-9}$, $K_D = 5.04 \times 10^{-10}$ M were determined under reducing conditions for H-Cys-Gly-OH by fitting of the data in Figure 4.16 to Equation 4.2 as described above. K_C was determined using Equation 4.3.

Scheme 4.46: Dissociation constants $K_A - K_D$ for H-Cys-Gly-OH.

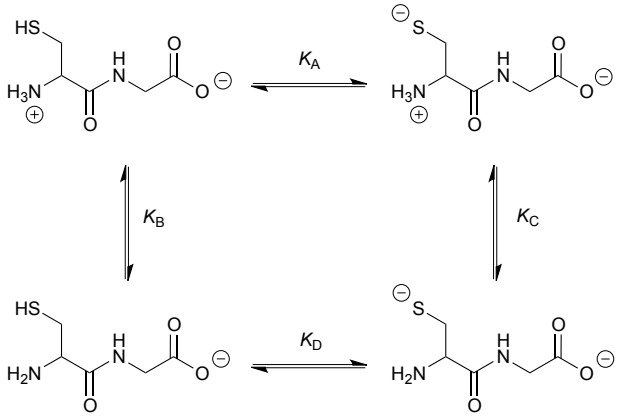

Figure 4.16: The variation of the fraction of thiol in thiolate form, f_{RS^-}, of pH for H-Cys-Gly-OH (0.2 mM) with TCEP (2.0 mM) at 25 °C and ionic strength $I = 0.3$ M (NaCl).

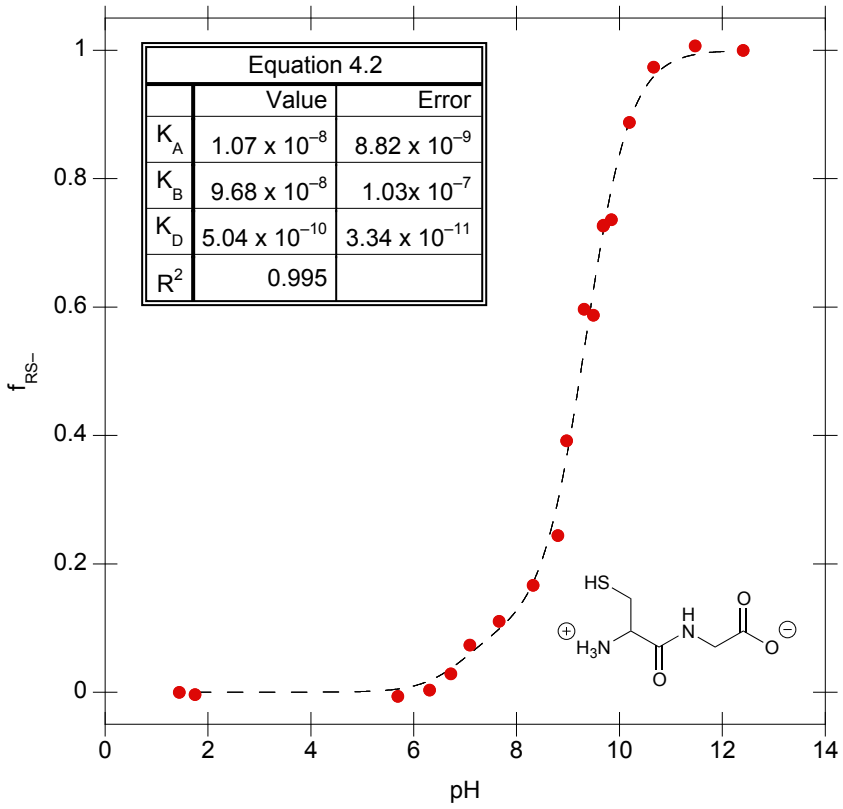

4.2.3.6 H-Cys-Gly-Phe-NH_2 Peptide

The peptide H-Cys-Gly-Phe-NH_2 was successfully prepared using solid phase peptide synthesis (See Experimental 4.5.12 for details).

Values of dissociation constants, $K_A = 7.46 \times 10^{-8}$ M, $K_B = 3.15 \times 10^{-8}$ M, $K_C = 3.80 \times 10^{-9}$, $K_D = 9.05 \times 10^{-10}$ M were determined under reducing conditions for H-Cys-Gly-Phe-NH_2 by fitting of the data in Figure 4.17 to Equation 4.2 as described above. K_C was determined using Equation 4.3.

Scheme 4.47: Dissociation constants $K_A - K_D$ for H-Cys-Gly-Phe-NH_2.

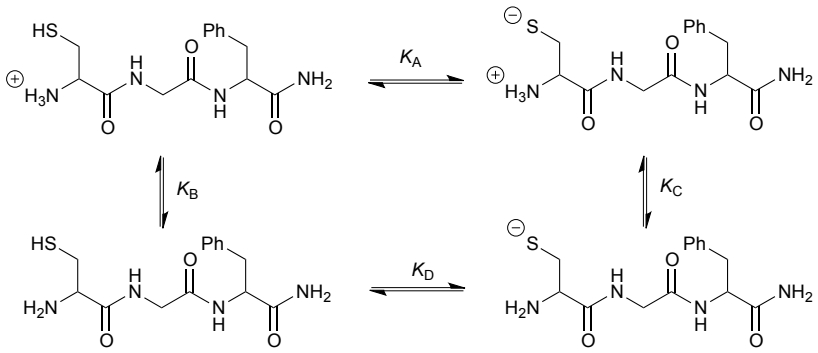

Figure 4.17: The variation of the fraction of thiol in thiolate form, f_{RS^-}, as a function of pH for H-Cys-Gly-Phe-NH_2 (0.2 mM) with TCEP (2.00 mM) at 25 °C and ionic strength $I = 0.3$ M (NaCl).

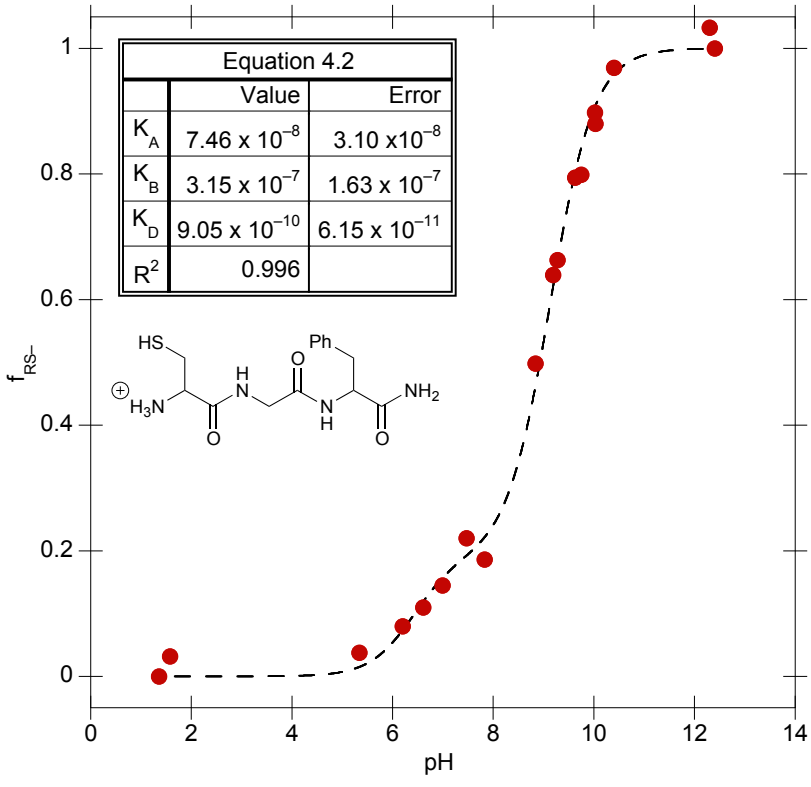

4.2.3.7 H-Pen-Gly-Phe-NH_2 Peptide

The peptide H-Pen-Gly-Phe-NH_2 was successfully prepared using solid phase peptide synthesis (See Experimental 4.5.13 for details).

Values of dissociation constants, $K_A = 3.60 \times 10^{-8}$ M, $K_B = 4.45 \times 10^{-7}$ M, $K_C = 4.07 \times 10^{-9}$, $K_D = 3.27 \times 10^{-10}$ M were determined under reducing conditions for H-Pen-Gly-Phe-NH_2 by fitting of the data in Figure 4.18 to Equation 4.2 as described above. K_C was determined using Equation 4.3.

Scheme 4.48: Dissociation constants $K_A - K_D$ for H-Pen-Gly-Phe-NH_2.

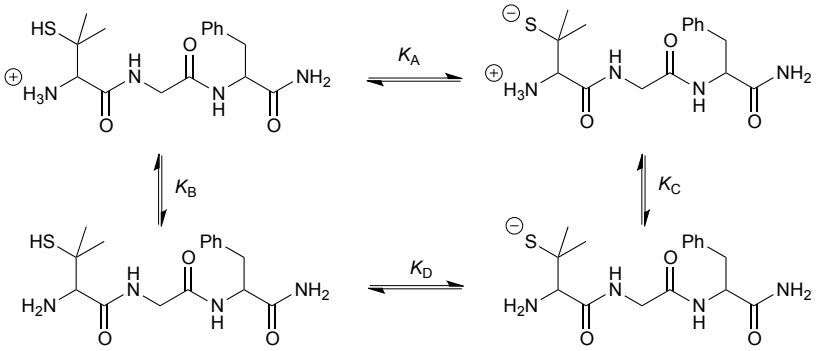

Figure 4.18: The variation of the fraction of thiol in thiolate form, f_{RS^-}, as a function of pH for H-Pen-Gly-Phe-NH_2 (0.2 mM) with TCEP (2.0 mM) at 25 °C and ionic strength $I = 0.3$ M (NaCl).

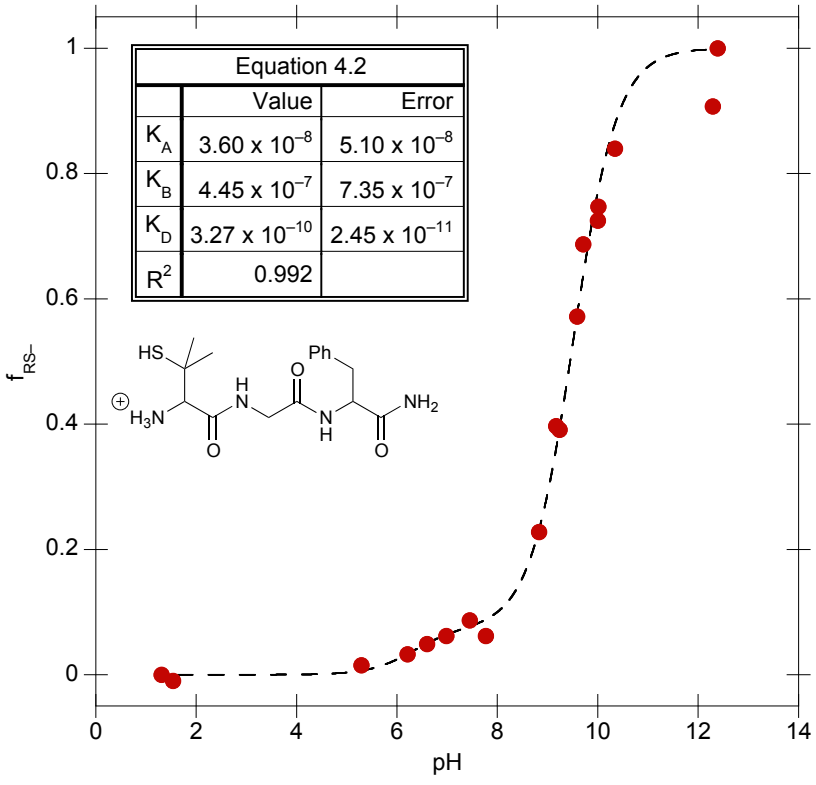

4.2.4 The molar extinction coefficients of cysteine derivatives

One of the main assumptions behind this UV-Vis approach to determining the acid dissociation constants is that the molar extinction coefficients between the different cysteine derivative molecules examined are approximately equivalent. This is imperative for the comparisons between speciation for the various cysteine methyl esters to be valid. To check whether this assumption was valid the molar extinction coefficients for cysteine, cysteine methyl ester, penicillamine methyl ester and (4*S*)-mercaptoproline methyl ester were determined.

Molar extinction coefficients are determined using the Beer Lambert Law:

$$A = c.\varepsilon.l \qquad \text{(Equation 4.4)}$$

where A is the absorption, c is the concentration of the compound in solution, ε is the molar extinction coefficient and l is the path length the light travels through in solution.

UV-Vis spectra were recorded in a 30 mM NaOH solution, in order to ensure that all thiol groups were in thiolate form, and in the presence of the reducing agent TCEP (2.00 mM), in order to prevent oxidative disulfide bond formation. Figure 4.21 includes an overlay of UV-Vis spectra for cysteine methyl ester over the concentration range 0.05 – 0.12 mM and Table 4.3 shows the wavelength of λ_{max} (= 236 – 237 nm) and the absorbance at λ_{max} as a function of concentration. The molar extinction coefficient could then determined as the slope of a plot of absorbance against concentration using the Beer Lambert Law in Figure 4.22. The analogous UV-Vis spectral overlays and tabulated data for cysteine, penicillamine methyl ester and 4*S*-mercaptoproline methyl ester are shown in the Appendix III: Figures III.20 – III.22 and Table III.10 – III.12 and the final Beer-Lambert plots Figure 4.23 – 4.25 below.

Figure 4.21: UV-Vis spectra for 0.05 mM – 0.12 mM cysteine methyl ester in 30 mM NaOH solution with TCEP (2.0 mM) at 25 °C and ionic strength $I = 0.3$ M (NaCl).

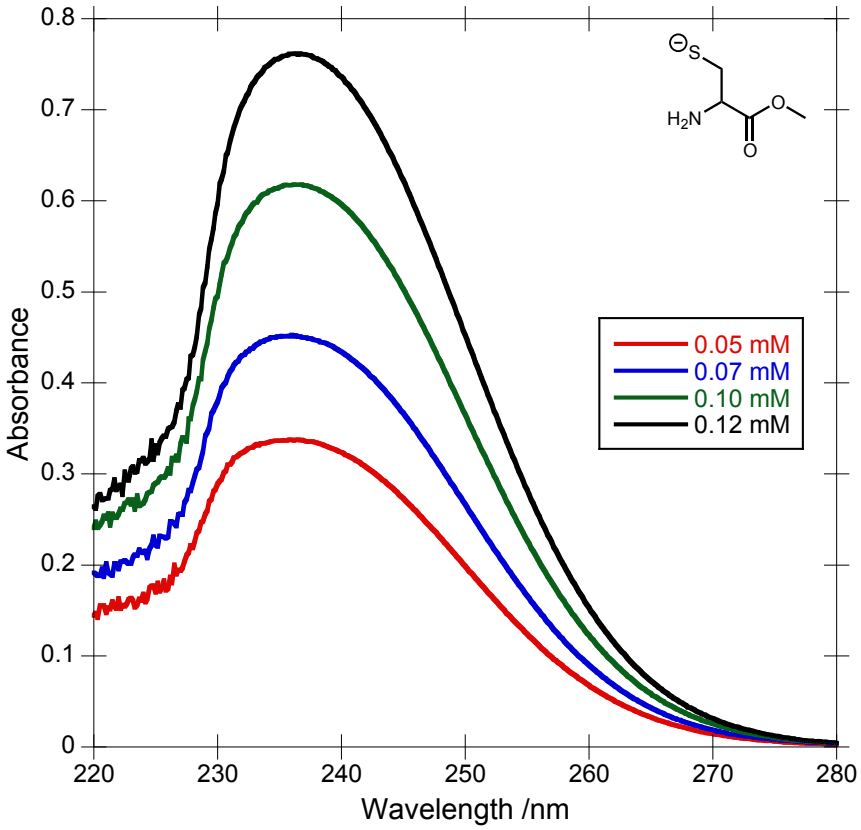

Table 4.3: The pH, λ_{max} and absorbance at λ_{max} values for different concentrations of cysteine methyl ester used to determine the molar extinction coefficient at 25 °C and ionic strength $I = 0.3$ M (NaCl).

[Cysteine methyl ester] /mM	pH	λ_{max} /nm	Absorbance at λ_{max}
0.05	12.19	236	0.338
0.07	12.19	236	0.453
0.10	12.19	237	0.618
0.12	12.19	236	0.762

Figure 4.22: Plot of maximum absorbance for 0.05 mM – 0.12 mM cysteine methyl ester against concentration in 30 mM NaOH solution with TCEP (2.0 mM) at 25 °C and ionic strength $I = 0.3$ M (NaCl).

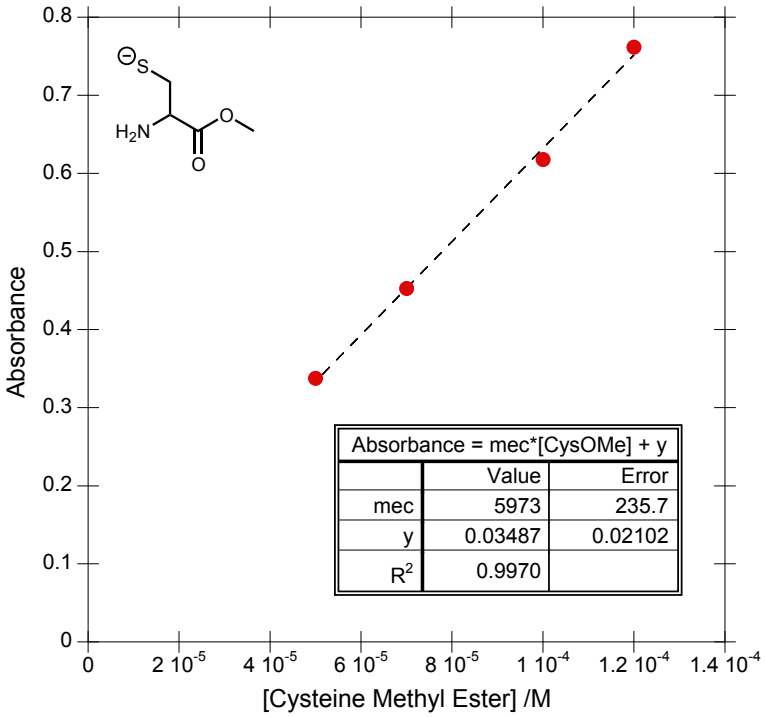

Figure 4.23: Plot of maximum absorbance for 0.05 mM – 0.12 mM penicillamine methyl ester against concentration in 30 mM NaOH solution with TCEP (2.0 mM) at 25 °C and ionic strength $I = 0.3$ M (NaCl).

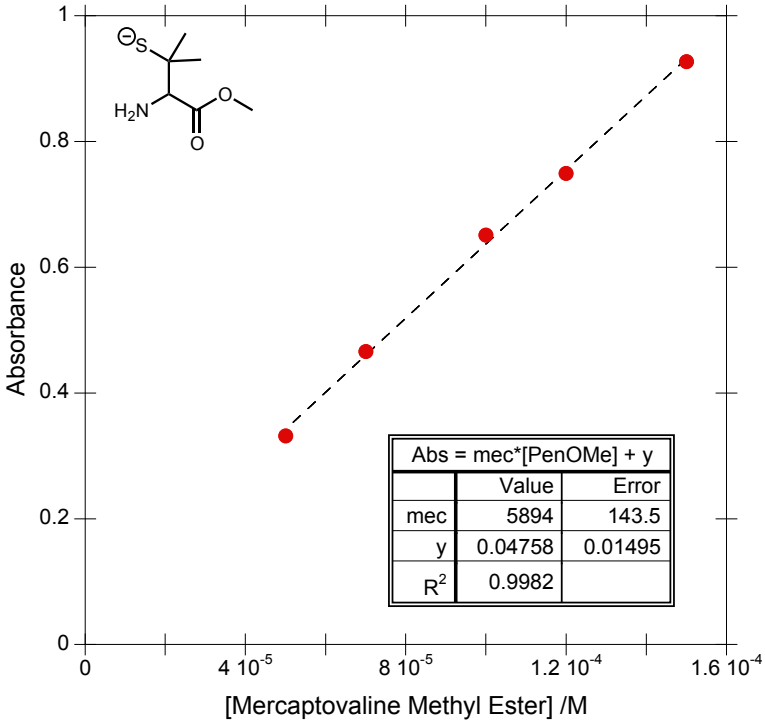

Figure 4.24: Plot of maximum absorbance for 0.05 mM – 0.12 mM (4*S*)-mercaptoproline methyl ester against concentration in 30 mM NaOH solution with TCEP (2.0 mM) at 25 °C and ionic strength I = 0.3 M (NaCl).

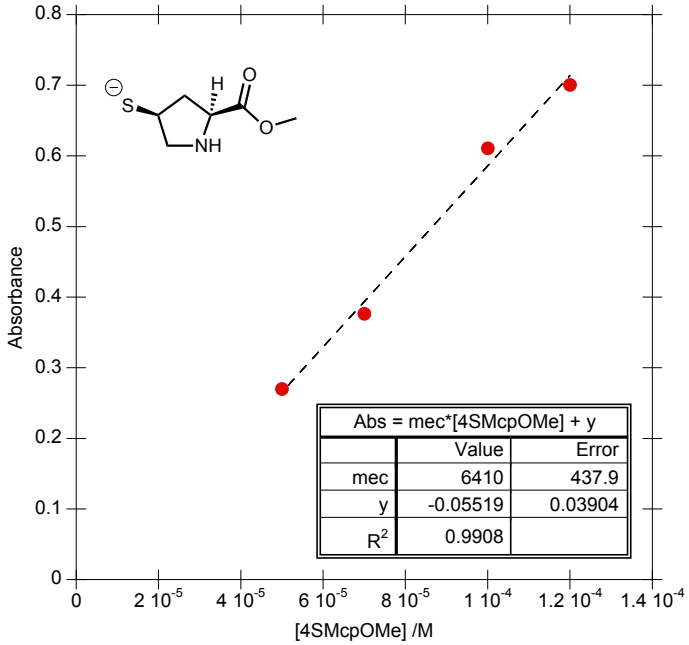

Figure 4.25: Plot of maximum absorbance for 0.05 mM – 0.12 mM cysteine against concentration in 30 mM NaOH solution with TCEP (2.0 mM) at 25 °C and ionic strength I = 0.3 M (NaCl).

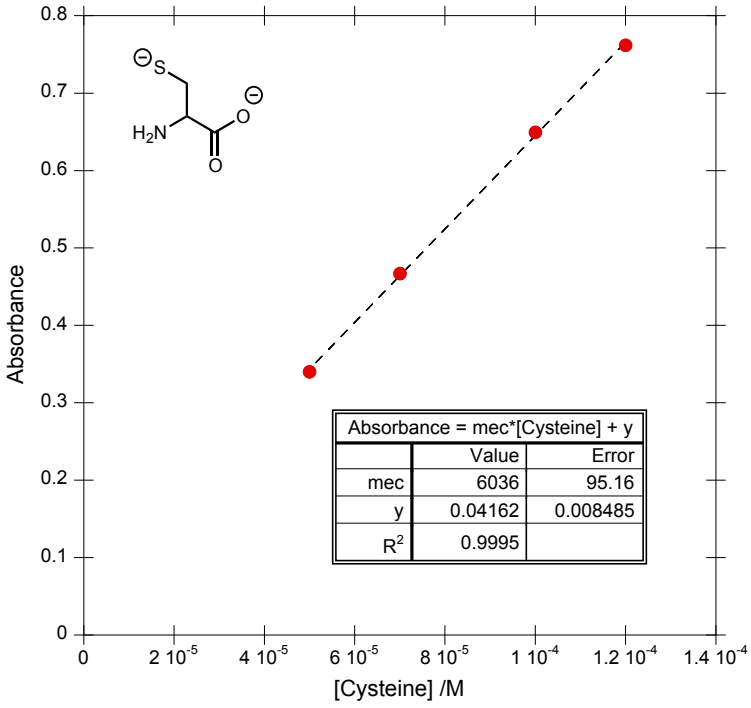

Table 4.4: Molar Extinction Coefficients for cysteine, cysteine methyl ester, penicillamine methyl ester and (4*S*)-mercaptoproline methyl ester at 25 °C and ionic strength I = 0.3 M (NaCl).

Compound	Molar Extinction Coefficient /M^{-1} cm^{-1}
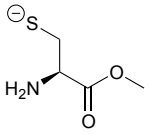	5973
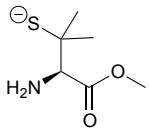	5894
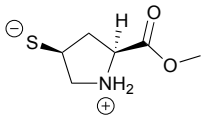	6410
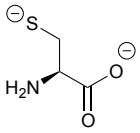	6036

The molar extinction coefficients, ε, for cysteine, cysteine methyl ester and penicillamine methyl ester are closely similar (± 3 %). The ε value for (4*S*)-mercaptoproline methyl ester has a < 9 % difference compared to the other values. The molar extinction coefficient determined for cysteine, ε = 6036 M^{-1} cm^{-1}, is in accordance with the literature value of ~ 6000 M^{-1} s^{-1}.[259]

4.3 Discussion

A summary of the pK_a values, pK_A – pK_D, for each cysteine derivative, obtained via UV-Vis spectrophotometry, is shown in Table 4.5. Table 4.5 also includes values recorded by Benesch for comparison.[259] For a given cysteine derivative, the values of pK_A, pK_B, pK_C and pK_D typically span 2.00 – 3.10 pK_a units. Repeat measurements of pK_A – pK_D under identical conditions in three cases indicated that the error limit in the pK_a values is ≤ 0.15 pK_a units. Repeat measurements were not possible for every cysteine derivative due to limitations in the quantity of material available. Between the different cysteine derivatives the values of pK_A, pK_B, pK_C or pK_D vary by 0.35 – 2.00 pK_a units.

pK values were measured in both non-reducing and reducing conditions as outlined in Section 4.2.3 and are shown in Table 4.5. All data from Benesch was measured under non-reducing conditions. The discussion will focus on a comparison of pK observed under reducing conditions with the exception of 4*S*-mercaptoproline methyl ester where it was not possible to measure pK_A – pK_D under reducing conditions due to limitations of material. It is important to note that it is not strictly correct to quote a single pK_a for either the ammonium or thiol group as a result of the speciation.

Table 4.5: Summary of the pK_A – pK_D for a range of cysteine derivatives at 25 °C and ionic strength I = 0.3 M (NaCl). pK_A, pK_B and pK_D values were obtained from a fit of the fraction of thiol in thiolate form, f_{RS^-}, to Equation 4.2 and K_C was determined using Equation 4.3.

Cysteine Derivative	pK_A $^{\oplus}H_3N\text{-}R\text{-}SH \rightleftharpoons {}^{\oplus}H_3N\text{-}R\text{-}S^{\ominus}$	pK_B $^{\oplus}H_3N\text{-}R\text{-}SH \rightleftharpoons H_2N\text{-}R\text{-}SH$	pK_C $^{\oplus}H_3N\text{-}R\text{-}S^{\ominus} \rightleftharpoons H_2N\text{-}R\text{-}S^{\ominus}$	pK_D $H_2N\text{-}R\text{-}SH \rightleftharpoons H_2N\text{-}R\text{-}S^{\ominus}$
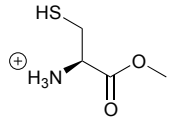	7.37 [a] 7.25 [a] [7.35] [b] (7.45) [c]	6.70 [a] 6.56 [a] [6.99] [b] (6.77) [c]	8.30 [a] 8.27 [a] [8.60] [b] (8.41) [c]	9.00 [a] 8.96 [a] [8.95] [b] (9.09) [c]
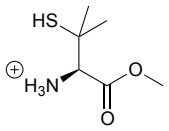	7.38 [a] [7.67] [b]	6.61 [a] [7.07] [b]	8.60 [a] [8.71] [b]	9.38 [a] [9.31] [b]
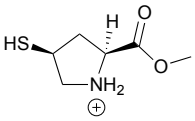	[7.12] [b]	[6.89] [b]	[8.52] [b]	[8.74] [b]
H-Cys-Gly-Phe-NH_2	7.13 [a]	6.50 [a]	8.42 [a]	9.04 [a]
H-Pen-Gly-Phe-NH_2	7.44 [a]	6.35 [a]	8.39 [a]	9.49 [a]
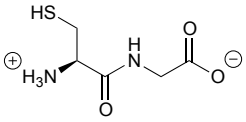	7.97 [a] (7.87) [d]	7.01 [a] (7.14) [d]	8.34 [a] (8.75) [d]	9.30 [a] (9.48) [d]
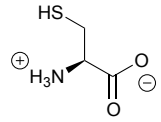	8.41 [a] (8.53) [d]	8.47 [a] (8.86) [d]	9.88 [a] (10.36) [d]	9.83 [a] (10.03) [d]

[a] Under reducing conditions (TCEP). [b] [pK_a] values in square brackets were obtained under non-reducing conditions. [c] For a cysteine ethyl ester with data acquired from Benesch under non-reducing conditions. [d] Data acquired from Benesch under non-reducing conditions.

4.3.1 Order of dissociation constants

For all cysteine derivatives in Table 4.5 the pK_as are consistently in the order:

$$pK_B < pK_A < pK_C < pK_D$$

with the exception of the parent amino acid cysteine where the order is:

$$pK_A < pK_B < pK_D < pK_C$$

pK_B and pK_C both refer to the ionization at the ammonium (NH_3^+ to NH_2) with neutral (SH) and anionic (S^-) sulfur substituents respectively. pK_C is between 1.33 – 2.04 pK units larger than pK_B for the various cysteine derivatives in Table 4.5. The higher pK_C will be partly due to the loss of favourable intramolecular electrostatic interactions between the ammonium group and thiolate in the zwitterionic reactant. Furthermore, a reduction in favourable intermolecular interactions with solvent water is expected in moving from the reactant ^+H_3N-R-S^- to the anionic H_2N-R-S^-. By contrast, for the ionization associated with pK_B, the only major loss is the intermolecular interaction between the ammonium and solvent water upon formation of conjugate base. In addition, due to the lesser stability of the localised negative charge in H_2N-R-S^-, the anionic product H_2N-R-S^- in pK_C should be less stable than neutral product H_2N-R-SH in pK_B. Overall, the greater stability of reactant and lesser stability of product accounts for pK_C being larger than pK_B.

pK_A and pK_D both refer to the ionization at the thiol (SH to S^-) with cationic and neutral amino substituents respectively. pK_A is 1.33 – 2.04 pK units smaller than pK_D for the various cysteine derivatives in Table 4.5. In pK_A product stabilisation is expected to be greater than in pK_D due to stabilisation of product ^+H_3N-R-S^- in pK_A through favourable electrostatic interactions between the ammonium and thiolate groups, in addition to the possibility for greater interactions with solvent water. By comparison, the anionic product H_2N-R-S^- in pK_D is expected to be relatively unstable due to the absence of stabilising intramolecular interactions and fewer solvent interactions.

For the parent amino acid cysteine the change in the order in of pK_A, pK_B, pK_C and pK_D reflects the unfavourable impact of losing the cationic charge from a species that has an anionic charge at the carboxylate in solutions whose pH is above 1.71. This will be discussed in more detail in Section 4.3.3.3.

4.3.2 Comparison between the p*K*s of cysteine derivatives

One of our primary goals was to explore the relative effect of local substitution near the thiol on pK_a. Potentially, any significant pK_a differences could be exploited towards an N-terminal selective native chemical ligation. The following sections compare the differences in pK_A – pK_D values. As repeat pK_A – pK_D measurements show values to be reproducible to ≤ 0.15 units only pK_a differences > 0.15 will be considered significant.

4.3.2.1 Comparison of p*K*s of the cysteine methyl esters

Table 4.6: Relative differences in pK_A – pK_D values for the methyl esters of cysteine derivatives measured relative to cysteine methyl ester at 25 °C and ionic strength I = 0.3 M (KCl).

	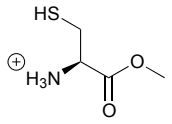	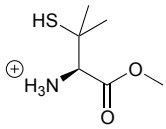	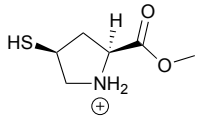
ΔpK_A [a]	0.00	0.07 [b] [0.32] [c]	- 0.19 [d] [- 0.23] [c]
ΔpK_B [a]	0.00	- 0.02 [b] [0.08] [c]	0.26 [d] [- 0.10] [c]
ΔpK_C [a]	0.00	0.32 [b] [0.11] [c]	0.24 [d] [- 0.08] [c]
ΔpK_D [a]	0.00	0.40 [b] [0.36] [c]	- 0.24 [d] [- 0.21] [c]

[a] ΔpK_X = pK_X(cysteine derivative) – pK_X(cysteine methyl ester). [b] Under reducing conditions, ΔpK_X calculated using reduced values. [c] Under non-reducing conditions, ΔpK_X calculated using non-reduced values. [d] ΔpK_X = pK_X(4*S*-mercaptoproline methyl ester, non-reduced) – pK_X(cysteine methyl ester, reduced).

Table 4.6 shows pK values relative to cysteine methyl ester for the three amino acid methyl esters studied. In comparison to the cysteine methyl ester the di-methylation adjacent to the thiol in the penicillamine methyl ester has no significant effect on the thiol pK_A (ΔpK_A = 0.07) and increases pK_D by 0.40 units (Table 4.6). The increase in pK_D could be attributed to the inductive destabilisation of the thiolate anion

by the methyl groups. The insignificant change in pK_A suggests that the inductive destabilisation of the thiolate by the methyl groups is counteracted by favourable electrostatic interactions between the cationic ammonium and the thiolate in $^{+}H_3N$-R-S^{-} that are possibly enhanced through the presence of the methyl groups.

For the (4*S*)-mercaptoproline methyl ester, pK_A and pK_D of the thiol decrease by 0.19 and 0.24 respectively, in comparison to the cysteine methyl ester. In all esters the thiol substituent is in a β-position relative to the electron withdrawing amine/ammonium groups. However, the thiol in (4*S*)-mercaptoproline methyl ester is in a γ-position relative to the ester group verses a β-position in the other methyl esters. If the electron withdrawing effect of the ester were dominant then an increase in pK_A and pK_D in (4*S*)-mercaptoproline methyl ester would be expected. Instead a significant decrease is observed for both pK_A and pK_D; it is proposed that this may be a result of a combination of ring conformation and stereoelectronic effects, which will be discussed further in Section 4.3.2.2.

For cysteine and penicillamine methyl ester a comparison between pK_B and pK_C of the ammonium, show a 0.02 decrease and a 0.32 increase, respectively. The absence of a significant change in pK_B suggests that the methyl groups are too remote to affect the stability of the ammonium. If this were the case then the increase in pK_C would reflect the greater loss of stability in penicillamine than cysteine from removal of the intramolecular electrostatic stabilisation between the thiolate and the ammonium rather than stabilisation of the ammonium *per se*.

For the secondary ammonium group in (4*S*)-mercaptoproline methyl ester pK_B and pK_C are 0.26 and 0.24 pK units higher compared to the primary ammonium in cysteine methyl ester. Typically acyclic secondary amines have higher pK_as than primary analogues due to greater inductive stabilisation of the parent secondary ammonium e.g. $Et_2NH_2^+$ has a pK_a of 10.98[262] while $EtNH_3^+$ has a pK_a of 10.63[262] and our results also demonstrate this expected trend.

4.3.2.2 Contribution of ring conformation and stereoelectronic effects to thiol p*K* for (4*S*)-mercaptoproline methyl ester

The pyrrolidine ring in proline and derivatives has two major conformations including a C^{γ}-*endo* pucker or a C^{γ}-*exo* pucker (Scheme 4.49).[263] The preferred conformation of the pyrrolidine ring is dependent upon a combination of

stereoelectronic effects, the minimisation of unfavourable dipole-dipole interactions and whether configuration at C^{γ} is *R* (R_1 = X, R_2 = H) or *S* (R_1 = H, R_2 = X).

Scheme 4.49: The two major conformations of the pyrrolidine ring in proline and proline derivatives.

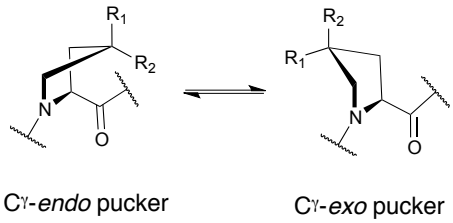

Proline residues in proteins such as collagen typically prefer to adopt the C^{γ}-*endo* pucker, however, for proline derivatives with electron withdrawing substituents, such as (4*R*)-hydroxyproline, a C^{γ}-*exo* pucker is favoured.[264] The preference for the C^{γ}-*exo* pucker in the latter case is in part due to the gauche effect, which places the C-O and the C-N bond in a *syn* relationship (Scheme 4.50). As a result the electron withdrawing C-O bond and C-N bond are in an *anti* relationship to vicinal C-H bonds. This conformation allows stereoelectronic stabilisation of the molecule as electron density from the respective vicinal σ_{C-H} bond is transferred into the σ^*_{C-N} and σ^*_{C-O} bonds thus stabilising the C^{γ}-*exo* pucker. The C^{γ}-*endo* pucker places the hydroxyl C-O bond *anti* to the amide C-N bond and provides no additional stabilisation. The preference for the C^{γ}-*exo* pucker is important in the protein collagen as it aids the formation of $n \rightarrow \pi^*$ interactions between the carbonyls of N-terminal and C-terminal amide bonds. This preorganises the protein and stabilises the collagen triple helix.[265]

Scheme 4.50: Illustration of the gauche effect in (4*R*)-hydroxyproline and the stereoelectronic stabilisation of the C$^{\gamma}$-*exo* pucker.

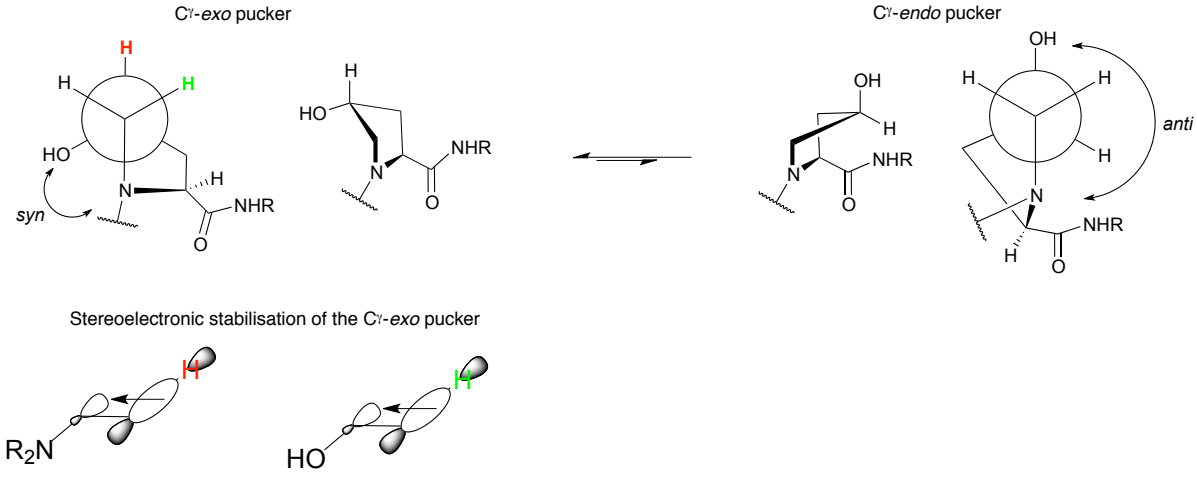

In addition to stereoelectronic effects Moroder has proposed that the 4*R*-hydroxyproline C$^{\gamma}$-*exo* pucker also minimises the unfavourable antiparallel interaction between the dipole at the substitution site in the pyrrolidine ring and the dipole of the C-terminal amide bond by placing the dipoles perpendicular to each other (Scheme 4.51).[266]

Scheme 4.51: Illustration of the minimisation of unfavourable antiparallel dipole dipole interactions. Mpc = Mercaptoproline, Hyp = Hydroxyproline, Flp = 4-Fluoroproline. "Optimized geometries of the L-proline derivatives as *trans*-amide conformers: The strength and direction of the X–C^{γ} bond dipoles μ are indicated by arrows. The atomic partial charges are indicated by a color code ranging from red (negative) through white (neutral) to blue (positive); adjacent red and blue atoms represent dipoles. The spheres represent "compound atoms"; the charges of hydrogen atoms are added to those of the neighboring heavy atoms. The experimentally observed conformers are marked by boxes."[266] Reproduced with permission from Wiley.

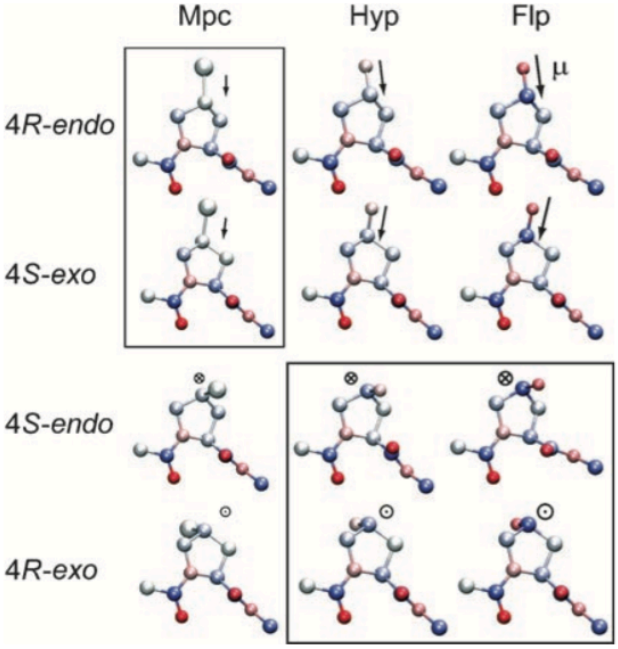

The inversion of the substituent site in (4*S*)-hydroxyproline requires the C^{γ}-*endo* pucker in order to access both the gauche effect and the minimisation of unfavourable antiparallel dipole-dipole interactions. In addition, Raines has observed the formation of a transannular hydrogen bond in the C^{γ}-*endo* pucker between the hydroxyl group and the C-terminal amide carbonyl in nonpolar aprotic solvents (Scheme 4.51) which adds ~ 3 kcal mol^{-1} of stability to the conformation.[267] In water a hydrogen bond is formed with bulk solvent rather than the carbonyl group; however, the C^{γ}-*endo* pucker remains intact.

Scheme 4.51: Intramolecular transannular hydrogen bond in C$^{\gamma}$-*endo* pucker of (4*S*)-hydroxyproline.

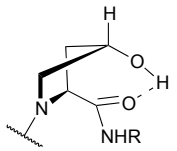

The mercaptoprolines prefer the opposite conformations to their hydroxyproline analogues.[266] (4*R*)-mercaptoproline favours the C$^{\gamma}$-*endo* pucker while (4*S*)-mercaptoproline prefers the C$^{\gamma}$-*exo* pucker. Moroder attributed this result to the weak dipole moment at the substituent site of mercaptoproline (electronegativity of C and S are almost identical, 2.55 and 2.58 respectively) which therefore imposes no energetic penalty upon the formation of the C$^{\gamma}$-*endo* pucker in 4*R*-Mcp and the C$^{\gamma}$-*exo* pucker in 4*S*-Mcp (Scheme 4.52).

Scheme 4.52: The major two conformations of the pyrrolidine ring in (4*R*)- and (4*S*)-mercaptoproline. The favoured conformations are marked by boxes.

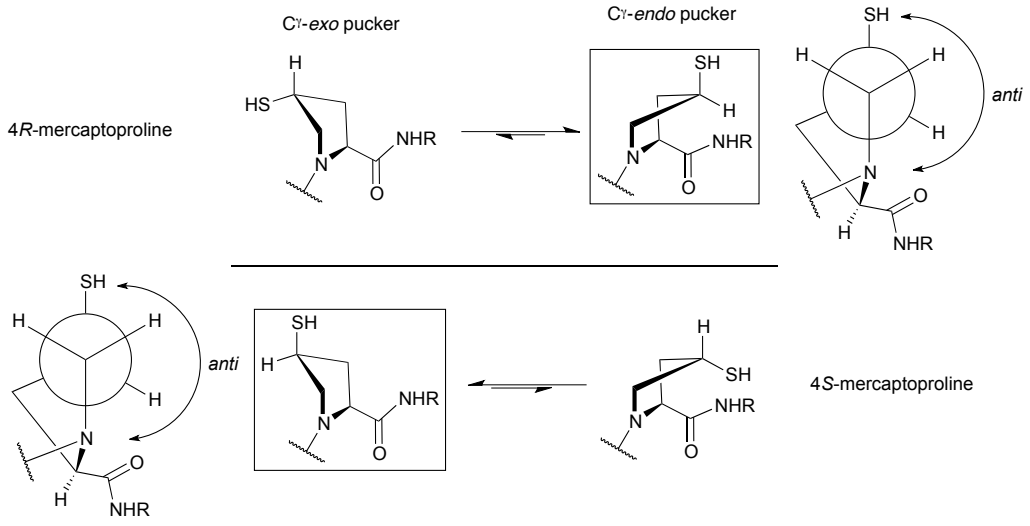

No gauche effect is observed for the mercaptoprolines as the C$^{\gamma}$-*endo* pucker in (4*R*)-mercaptoproline and the C$^{\gamma}$-*exo* pucker in (4*S*)-mercaptoproline place the thiol C-S bond and the C-N bond in an *anti* relationship (Scheme 4.52). It is proposed that this *anti* relationship is responsible for the observed lowering of the p*K*s of the thiol group in (4*S*)-mercaptoproline methyl ester with respect to the cysteine and penicillamine methyl esters (Table 4.6). Stereoelectronic donation of electron density from the σ_{C-S}

bond into the σ^*_{C-N} bond could stabilise the thiolate anion conjugate base which would therefore lower the pK_A and pK_D of the thiol (Scheme 4.53).

Scheme 4.53: Proposed stereoelectronic stabilisation of the thiolate anion in (4*S*)-mercaptoproline methyl ester (Scheme 4.52).

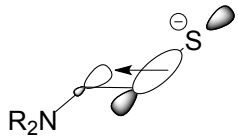

It should be noted that in the majority of previous studies upon the conformation of the pyrrolidine ring in proline and proline derivatives the N has been functionalised as an amide (usually via acetylation). However, the N in (4*S*)-mercaptoproline examined in this study is in the amine form. The change from an sp^2 hybridisation of N to an sp^3 hybridised amine N could alter the geometry of the pyrrolidine ring. However, a previous study on the gas phase geometry of the amino acids (4*R*)-hydroxyproline and (4*S*)-hydroxyproline with an amine N the pyrrolidine ring displayed a retention of the respective C^γ-*exo* pucker and C^γ-*endo* puckers.[268] It is not anticipated the transfer from gas to solvent phase will affect this result. Therefore it assumed that for this study the ring conformation preferences for (4*S*)-mercaptoproline methyl ester are identical to that of the previously studied acetylated (4*S*)-mercaptoproline methyl ester.

4.3.2.3 Comparison of p*K*s of the cysteine and penicillamine peptides

Table 4.7: Relative differences in $pK_A - pK_D$ values between H-Cys-Gly-Phe-NH_2 and H-Pen-Gly-Phe-NH_2 measured relative to H-Cys-Gly-Phe-NH_2 at 25 °C and ionic strength I = 0.3 M (KCl). All values determined are under reducing conditions.

	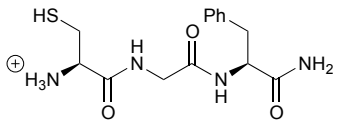 H-Cys-Gly-Phe-NH_2	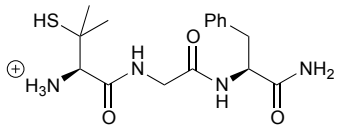 H-Pen-Gly-Phe-NH_2
ΔpK_A [a]	0.00	0.31
ΔpK_B [a]	0.00	- 0.15
ΔpK_C [a]	0.00	- 0.03
ΔpK_D [a]	0.00	0.45

[a] $\Delta pK_X = pK_X$(cysteine derivative) – pK_X(H-Cys-Gly-Phe-NH_2).

For H-Cys-Gly-Phe-NH_2 and H-Pen-Gly-Phe-NH_2 the thiol pK_A and pK_D are 0.31 and 0.45 respectively higher in H-Pen-Gly-Phe-NH_2 (Table 4.7). The higher value of pK_D can be attributed to the inductive thiolate destabilisation from the methyl groups, as observed in the comparison between the penicillamine and cysteine methyl ester. The significant increase in pK_A in the present case demonstrates that the destabilisation from the methyl groups is significant in the peptide systems, unlike in the methyl esters where the stabilising electrostatic interaction between the thiolate and ammonium counteracted the inductive effect. In the present case, the zwitterionic resonance form of the amide may reduce the electrostatic interactions between thiolate and ammonium (Scheme 4.54).

pK_D values can also be used to estimate the leaving group ability of the various cysteine derivatives in the S-to-N acyl shift step. While this intramolecular reaction is fast and non-rate determining and therefore difficult to probe by experiment, the relative pK_D values may help inform and evaluate computational studies of this step.

Scheme 4.54: Possible resonance forms of the amide bond in the H-Cys-Gly-Phe-NH_2 (and H-Pen-Gly-Phe-NH_2 – not shown) peptide.

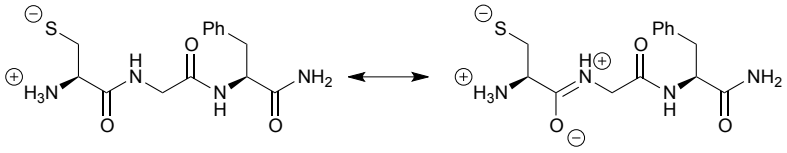

The ammonium pK_B and pK_C for H-Pen-Gly-Phe-NH_2 relative to H-Cys-Gly-Phe-NH_2 decrease by 0.15 and 0.03 respectively. Both of these changes are within the error limit of the experiment which suggests that there is little change in the ammonium pK_a in the peptide system upon moving from a cysteine to a penicillamine. This indicates that the additional methyl groups in penicillamine have no significant effect upon the ammonium pK_B and pK_C.

4.3.2.4 Comparison between cysteine and penicillamine peptides and their respective methyl esters

Table 4.8: Relative differences in pK_A – pK_D values between cysteine methyl ester and H-Cys-Gly-Phe-NH_2; and relative differences in pK_A – pK_D values between penicillamine methyl ester and H-Pen-Gly-Phe-NH_2 at 25 °C and ionic strength I = 0.3 M (KCl). All values used are under reducing conditions.

	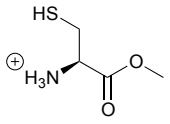	H-Cys-Gly-Phe-NH_2	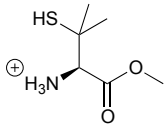	H-Pen-Gly-Phe-NH_2
ΔpK_A [a]	0.00	- 0.18	0.00	0.06
ΔpK_B [a]	0.00	- 0.13	0.00	- 0.16
ΔpK_C [a]	0.00	0.14	0.00	- 0.21
ΔpK_D [a]	0.00	0.06	0.00	0.11

[a] $\Delta pK_X = pK_X$(methyl ester) – pK_X(peptide).

Comparing the H-Cys-Gly-Phe-NH_2 with the cysteine methyl ester it can be seen that the thiol pK_A decreases by 0.18 units (although only just outside of error) and there is no significant change in pK_D (ΔpK_D = 0.06) upon moving to the peptide system. The pK_A decrease indicates that the thiol in the peptide is marginally more acidic in the

methyl ester. Comparing H-Pen-Gly-Phe-NH_2 with penicillamine methyl ester there is no change in the thiol pK_A or pK_D (0.06 and 0.11 increase) upon moving to the peptide system. Overall the effect of the ester to amide change on pK_A or pK_D is relatively small.

For the ammonium pK_B and pK_C there is a 0.13 decrease and a 0.14 increase, respectively, for H-Cys-Gly-Phe-NH_2 in comparison with the cysteine methyl ester, which are within error. Comparing H-Pen-Gly-Phe-NH_2 with penicillamine methyl ester, the corresponding changes are 0.16 and 0.21 decreases, respectively, in the peptide system. This is counterintuitive as an amide will be less electron withdrawing than an ester, which therefore ought to stabilise the ammonium to a greater extent and thus raise the pK_a.

4.3.3 Overview of Substituent Effects

The pK_A – pK_D values may be converted into Gibbs free energies which allows insight into the magnitude of various substituent effects. The Gibbs free energy (ΔG) of acid dissociation may be determined from:

$$\Delta G = - RT \ln K_X \qquad \text{(Equation 4.5)}$$

where R is the molar gas constant, T is the temperature and K_X is whichever acid dissociation constant is under examination. The Gibbs free energy for each species of the cysteine derivatives are shown in Table 4.9. The error in the free energy values is ± 0.9 kJ mol^{-1}.

Table 4.9: Gibbs free energies of the cysteine derivatives determined from Equation 4.5 and the $pK_A - pK_D$ values.

	pK_A Gibbs Free Energy /kJ mol^{-1}	pK_B Gibbs Free Energy /kJ mol^{-1}	pK_C Gibbs Free Energy /kJ mol^{-1}	pK_D Gibbs Free Energy /kJ mol^{-1}
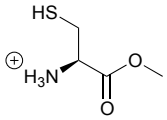	41.7	37.8	47.3	51.3
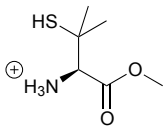	42.1	37.7	49.1	53.5
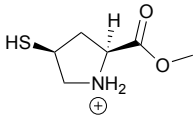	40.6	39.3	48.6	49.9
H-Cys-Gly-Phe-NH_2	40.7	37.1	48.1	51.6
H-Pen-Gly-Phe-NH_2	42.5	36.2	47.9	54.2
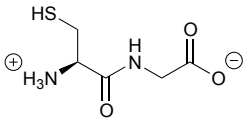	45.5	40.0	47.6	53.1
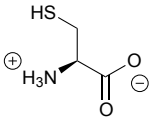	48.0	48.3	56.4	56.1

4.3.3.1 The intramolecular electrostatic interaction between thiolate anion and ammonium cation

The intramolecular electrostatic interaction between thiolate anion and ammonium cation affects the stability of both the thiolate and the ammonium. The difference between the free energies of pK_D and pK_A indicates that the electrostatic interaction contributes between 7.6 – 11.7 kJ mol^{-1} of stability (depending upon the cysteine derivative) to the formation of the thiolate. The difference in ammonium cation pK_C and pK_B values allow an alternative estimation of the energy of electrostatic interaction between an ammonium cation and thiolate anion in these systems of 7.6 – 11.6 kJ mol^{-1} of stability depending upon the cysteine derivative. Both values are in good agreement with each other. It should be stated that the values here would perhaps

be more adequately described as representing the maximum possible intramolecular interaction as the values will also incorporate an enhanced interaction with solvent from an additional charged substituent in the zwitterionic species. The effect of solvent could also reduce the intramolecular interaction directly via solvent shielding.

4.3.3.2 The effect of the dimethyl groups on penicillamine on the stability of the thiolate and ammonium

The magnitude of inductive destabilisation of the thiolate by the methyl groups in penicillamine can be quantified using the difference in the free energies for pK_D between cysteine methyl ester and penicillamine methyl ester. The free energy destabilisation from the methyl groups is 2.2 kJ mol^{-1} [= 53.5 kJ mol^{-1} – 51.3 kJ mol^{-1}] i.e. 1.1 kJ mol^{-1} per methyl group. While in pK_D the full force of inductive destabilisation is unattenuated, in pK_A the intramolecular electrostatic interaction between thiolate and ammonium masks the impact of inductive destabilisation on the thiolate. The inductive donation of electron-density from the methyl groups will have two opposing effects upon the thiolate in $^{+}H_3N$-R-S^{-}. It will both destabilise the thiolate by increasing the concentration of negative charge but this will also increase the magnitude of the electrostatic interaction. The difference in the pK_A free energies shows that the penicillamine methyl ester is 0.4 kJ mol^{-1} [= 42.1 kJ mol^{-1} – 41.7 kJ mol^{-1}] less stable than the cysteine methyl ester. The inductive destabilisation from the methyl groups is therefore larger than the enhanced electrostatic interaction from increased negative charge at the thiolate. The magnitude of the enhanced electrostatic interaction generated by the methyl groups can be found by taking the difference in pK_A free energies from the difference in pK_D free energies. The methyl groups therefore contribute 1.9 kJ mol^{-1} [= 2.3 kJ mol^{-1} – 0.4 kJ mol^{-1}] in stabilisation to the electrostatic interaction between the thiolate anion and the ammonium cation.[xliv]

[xliv] An alternative way of arguing this is to look at the difference in the free energy difference between pK_A and pK_D for cysteine methyl ester and penicillamine methyl ester. For cysteine methyl ester the pK_A pK_D difference is 9.54 kJ mol^{-1} [= 51.26 kJ mol^{-1} – 41.72 kJ mol^{-1}] and for penicillamine methyl ester the pK_A pK_D difference is 11.42 kJ mol^{-1} [= 53.54 kJ mol^{-1} – 42.12 kJ mol^{-1}]. The difference of differences in the free energies of pK_A and pK_D is therefore 1.88 kJ mol^{-1} [= 11.42 kJ mol^{-1} – 9.54 kJ mol^{-1}] which is the free energy contribution that the methyl groups make to enhancing the electrostatic interaction in penicillamine methyl ester.

For the ammonium in the cysteine and penicillamine methyl esters the effect of the methyl groups on free energy for pK_B is small at - 0.1 kJ mol^{-1} [= 37.7 kJ mol^{-1} – 37.8 kJ mol^{-1}]. The impact of the methyl groups on the intramolecular electrostatic interaction on the ammonium can be calculated from the differences in free energy between pK_C, 1.8 kJ mol^{-1} [= 49.1 kJ mol^{-1} – 47.3 kJ mol^{-1}], and pK_B, - 0.1 kJ mol^{-1}. The methyl groups therefore contribute 1.9 kJ mol^{-1} in extra stability to the ammonium, which is in close agreement with the value calculated for the thiolate. The increase in stability from the electrostatic interaction when methyl groups present is probably due to the inductively donating methyl groups increasing the electron density in the thiolate which therefore increases the magnitude of the electrostatic interaction.

For the peptides H-Cys-Gly-Phe-NH_2 and H-Pen-Gly-Phe-NH_2 the magnitude of the destabilisation of the thiolate from the methyl groups (pK_D) is 2.6 kJ mol^{-1} [= 54.2 kJ mol^{-1} – 51.6 kJ mol^{-1}]. For pK_A the free energy difference between H-Cys-Gly-Phe-NH_2 and H-Pen-Gly-Phe-NH_2 is greater than that of the methyl esters at 1.8 kJ mol^{-1} [= 42.5 kJ mol^{-1} – 40.7 kJ mol^{-1}]. The methyl groups therefore only contribute an extra 0.8 kJ mol^{-1} [= 2.6 kJ mol^{-1} – 1.8 kJ mol^{-1}] in the electrostatic stabilisation, which is lower than the methyl esters (1.9 kJ mol^{-1}). The lower contribution may in part be due to the change from the ester to the amide group which is less electron withdrawing and therefore the cationic charge at the ammonium end is likely to be decreased thus reducing the electrostatic interaction. The extra contribution of the zwitterionic resonance form of the amide (Scheme 4.54) could also reduce the need for the ammonium N-terminus to stabilise the thiolate.

The methyl groups destabilise the ammonium in the peptides H-Cys-Gly-Phe-NH_2 and H-Pen-Gly-Phe-NH_2, which is counterintuitive. However, both decreases in stability are small (pK_B = 0.9 kJ mol^{-1} and pK_C = 0.2 kJ mol^{-1}) and are within error.

4.3.3.3 The effect of an anionic carboxylate C-terminus relative to a neutral C-terminus

The effect of an anionic C-terminus relative to a neutral C-terminus on the ammonium and thiol p*K*s can be studied by comparing H-Cys-Gly-OH and H-Cys-Gly-Phe-NH_2. For H-Cys-Gly-OH in pHs above pH = 2.34 the C-terminal carboxylic acid will be deprotonated and therefore there is an additional anionic charge on the peptide.

For H-Cys-Gly-Phe-NH_2 the amide C-terminus has a pK_a ~ 17 and therefore remains neutral in the pH ranges studied.

For H-Cys-Gly-OH the acid form in pK_B is a zwitterion and therefore deprotonation causes a loss of favourable electrostatic interactions between the ammonium and the carboxylate.[xlv] The acid form of H-Cys-Gly-Phe-NH_2 is cationic and therefore there is no intramolecular electrostatic interaction present. The electrostatic interaction in zwitterionic H-Cys-Gly-OH causes a 0.51 rise in pK_B relative to cationic H-Cys-Gly-Phe-NH_2. This is equivalent to a 2.9 kJ mol^{-1} [= 40.0 kJ mol^{-1} – 37.1 kJ mol^{-1}] free energy stabilisation of the ammonium in zwitterionic H-Cys-Gly-OH by the carboxylate C-terminus.

For the other ammonium pK, pK_C, there is 0.08 decrease, which is within error, upon moving from H-Cys-Gly-Phe-NH_2 to H-Cys-Gly-OH. In pK_C H-Cys-Gly-Phe-NH_2 has a zwitterionic conjugate acid form and an anionic base form, thus deprotonation of the ammonium causes a loss of the favourable electrostatic interaction between the ammonium and the thiolate.

In pK_C H-Cys-Gly-OH has an overall anionic conjugate acid form (one cation and two anions) and a dianionic base form. The lack of significant change in pK_C for H-Cys-Gly-OH relative to H-Cys-Gly-Phe-NH_2 despite the extra anionic charge on H-Cys-Gly-OH would suggest that the benefit of an additional electrostatic interaction between the ammonium cation and the thiolate anion in the conjugate acid form is equivalent to the enhanced destabilisation of the anion-anion repulsion between the thiolate and carboxylate in the base form such that the overall equilibrium K_C is unaffected by the additional anionic charge. Thus the net loss of electrostatic interactions in anion H-Cys-Gly-OH is equivalent to the loss of electrostatic interactions in H-Cys-Gly-Phe-NH_2.

The effect of the anionic C-terminus upon the thiol pKs is to increase pK_A by 0.84 and increase pK_D by 0.26 pK units when comparing H-Cys-Gly-OH with H-Cys-Gly-Phe-NH_2. The increase in both pKs for H-Cys-Gly-OH relative to H-Cys-Gly-Phe-NH_2 is from the formation of a repulsive electrostatic interaction between the two anionic charges which destabilise the base form. The introduction of an anionic charge in H-Cys-Gly-OH clearly has a greater effect upon moving from a zwitterionic to a net monoanionic species (pK_A) than it does upon moving from a monoanionic to a

[xlv] There is also the possibility of hydrogen bonding between the ammonium and carboxylate.

dianionic species (pK_D). The magnitude of the destabilisation from solely the repulsive interaction between the two anionic charges is found by comparing the free energies of the pK_D values of H-Cys-Gly-OH and H-Cys-Gly-Phe-NH_2 and is 1.5 kJ mol^{-1} [= 53.1 kJ mol^{-1} – 51.6 kJ mol^{-1}]. The subtraction of the free energy of H-Cys-Gly-Phe-NH_2 here separates the destabilisation caused by forming a thiolate anion from the extra destabilisation caused by the thiolate-carboxylate anion-anion repulsion.

For pK_A the free energy difference between H-Cys-Gly-OH and H-Cys-Gly-Phe-NH_2 shows that deprotonation of the zwitterionic H-Cys-Gly-OH thiol is 4.8 kJ mol^{-1} [= 45.5 kJ mol^{-1} – 40.7 kJ mol^{-1}] less stable than deprotonation of the cationic H-Cys-Gly-Phe-NH_2 thiol. It should be noted that this value is in fact a net destabilisation as it includes the favourable electrostatic interactions between the cationic ammonium and both the thiolate and the carboxylate anions – therefore the total free energy of destabilisation will be even higher. The thiolate-carboxylate anion-anion repulsion in the base form can account for 1.5 kJ mol^{-1} of this destabilisation but there is a further 3.3 kJ mol^{-1} [= 4.8 kJ mol^{-1} – 1.5 kJ mol^{-1}] of destabilisation from the introduction of an anionic C-terminus that must be accounted for. A maximum of 2.9 kJ mol^{-1} (from pK_B, see above) could come from the reduction in electrostatic interactions between the ammonium and the carboxylate in H-Cys-Gly-OH by the introduction of shielding from the anionic charge on the thiolate. However, this value is clearly an overestimate, as the ammonium-carboxylate interaction still exists, albeit likely reduced because repulsive interactions between the thiolate and carboxylate will push the carboxylate further away from the ammonium. Thus a source for a minimum of 0.4 kJ mol^{-1} of destabilisation (again, almost certainly higher) is required. The location of the two anions on opposite ends of the molecule will favour a linear as opposed to folded conformations and this could potentially cause an increase in hydrophobic surface area presented to solvent.

4.3.3.4 The effect of the proximity of carboxylate on thiolate and ammonium

The differences between the thiol pK_as, pK_A and pK_D, in cysteine and H-Cys-Gly-OH can be used to measure of how the proximity of the carboxylate affects the stability of the thiolate. For pK_A the difference between cysteine and H-Cys-Gly-OH is 2.5 kJ mol^{-1} [= 48.0 kJ mol^{-1} – 45.5 kJ mol^{-1}] while for pK_D the difference is 3.0 kJ

mol^{-1} [= 56.1 kJ mol^{-1} – 53.1 kJ mol^{-1}]. The smaller difference for pK_A than pK_D between cysteine and H-Cys-Gly-OH indicates that the presence of the ammonium in pK_A reduces the destabilisation caused by placing the thiolate and carboxylate closer together by 0.5 kJ mol^{-1}. The increase in the favourable electrostatic interaction between the ammonium and the carboxylate is therefore greater than the increase in the unfavourable interaction between the thiolate and carboxylate upon bringing the carboxylate closer.

The impact of the proximity of the carboxylate on the ammonium may be found by comparing pK_B and pK_C for cysteine and H-Cys-Gly-OH. For pK_B the cysteine ammonium is more stable by 8.3 kJ mol^{-1} [= 48.3 kJ mol^{-1} – 40.0 kJ mol^{-1}] while for pK_C cysteine ammonium is more stable by 8.8 kJ mol^{-1} [= 56.4 kJ mol^{-1} – 47.6 kJ mol^{-1}]. The proximity of the carboxylate has a greater effect on the stability of the ammonium when there is an additional anionic charge (from the thiolate) present in the molecule. The magnitude of this enhanced interaction is 0.5 kJ mol^{-1}, which is, gratifyingly, in good agreement with the value of the electrostatic interaction measured via pK_A and pK_D.

4.3.4 Concentration of Species in a variety of pHs

The percentage abundance for each of the four possible species $^{+}H_3N$-R-SH, $^{+}H_3N$-R-S^{-}, H_2N-R-SH and H_2N-R-S^{-} for the cysteine derivatives over the pH range 0 – 14 is shown in Figure 4.26 – 4.32. Table 4.10 shows the percentage abundances for the various cysteine derivatives over a breadth of pHs at which native chemical ligations have been performed. The error in the values is ± 6 %.

Figure 4.26: The percentage abundance in solution of each of the four species in the pH range 0 – 14 for cysteine methyl ester at 25 °C and ionic strength I = 0.3 M (KCl).

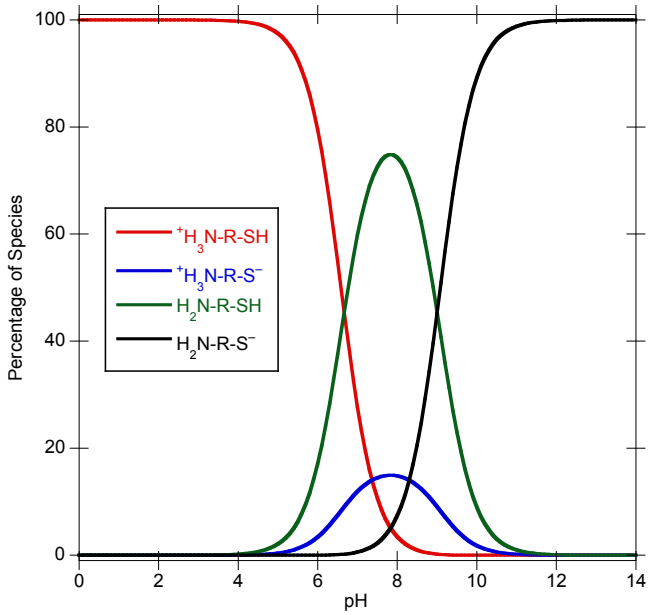

Figure 4.27: The percentage abundance in solution of each of the four species in the pH range 0 – 14 for penicillamine methyl ester at 25 °C and ionic strength I = 0.3 M (KCl).

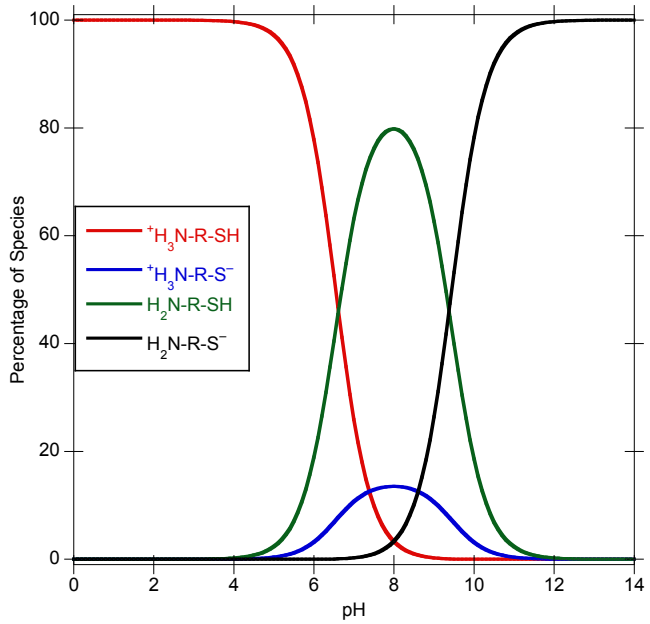

Figure 4.28: The percentage abundance in solution of each of the four species in the pH range 0 – 14 for (4*S*)-mercaptoproline methyl ester at 25 °C and ionic strength $I = 0.3$ M (KCl).

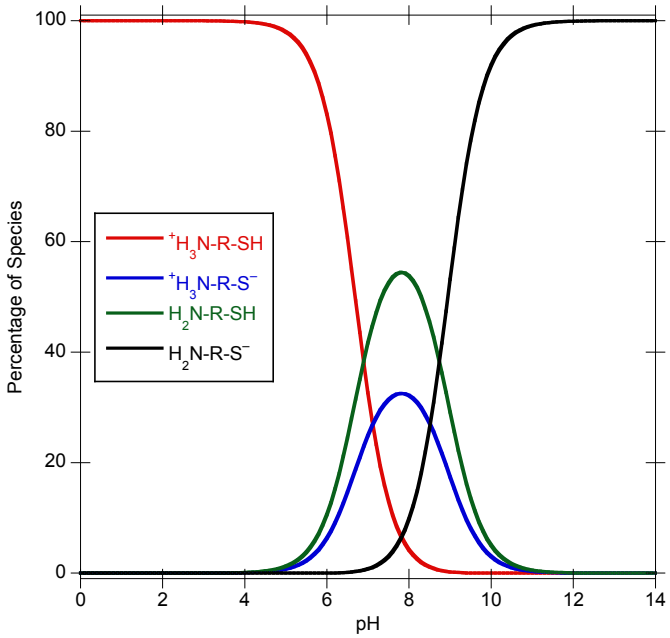

Figure 4.29: The percentage abundance in solution of each of the four species in the pH range 0 – 14 for H-Cys-Gly-Phe-NH_2 at 25 °C and ionic strength $I =$ 0.3 M (KCl).

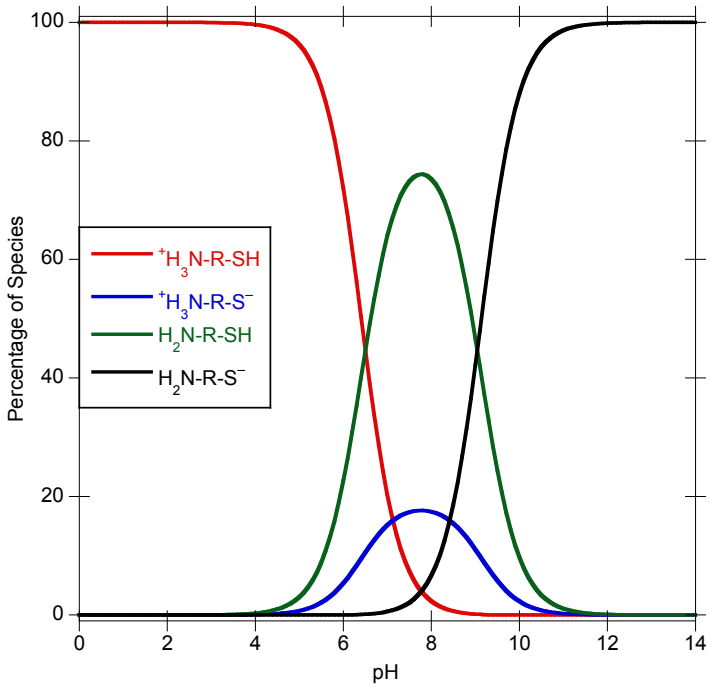

Figure 4.30: The percentage abundance in solution of each of the four species in the pH range 0 – 14 for H-Pen-Gly-Phe-NH_2 at 25 °C and ionic strength I = 0.3 M (KCl).

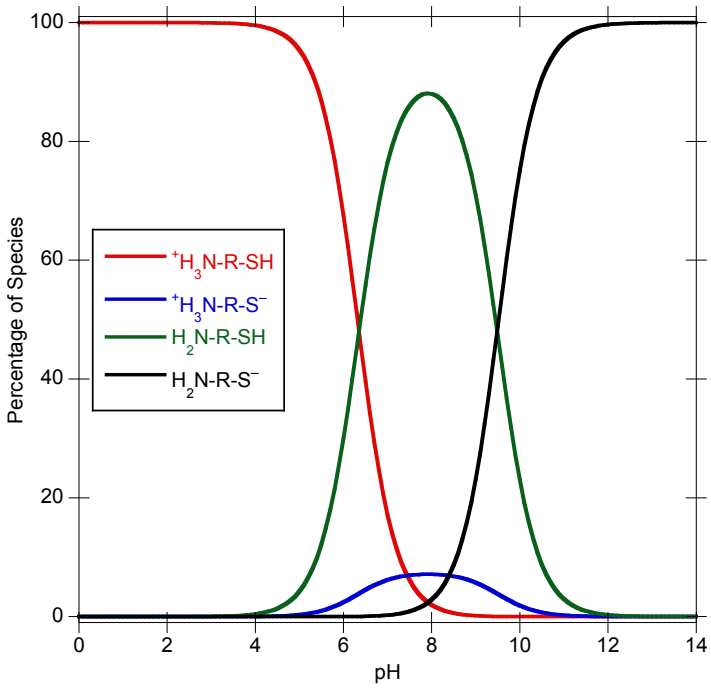

Figure 4.31: The percentage abundance in solution of each of the four species in the pH range 0 – 14 for cysteine at 25 °C and ionic strength I = 0.3 M (KCl).

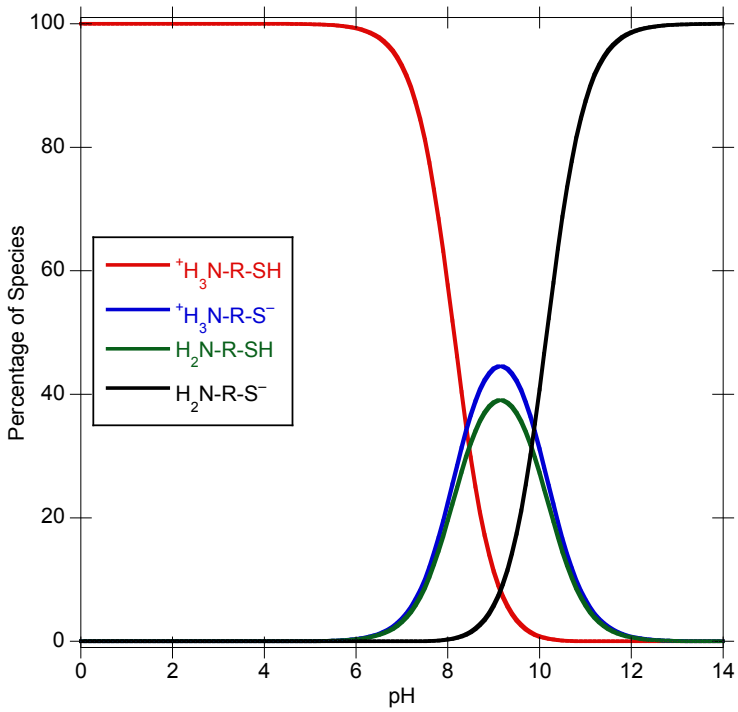

Figure 4.32: The percentage abundance in solution of each of the four species in the pH range 0 – 14 for H-Cys-Gly-OH at 25 °C and ionic strength $I = 0.3$ M (KCl).

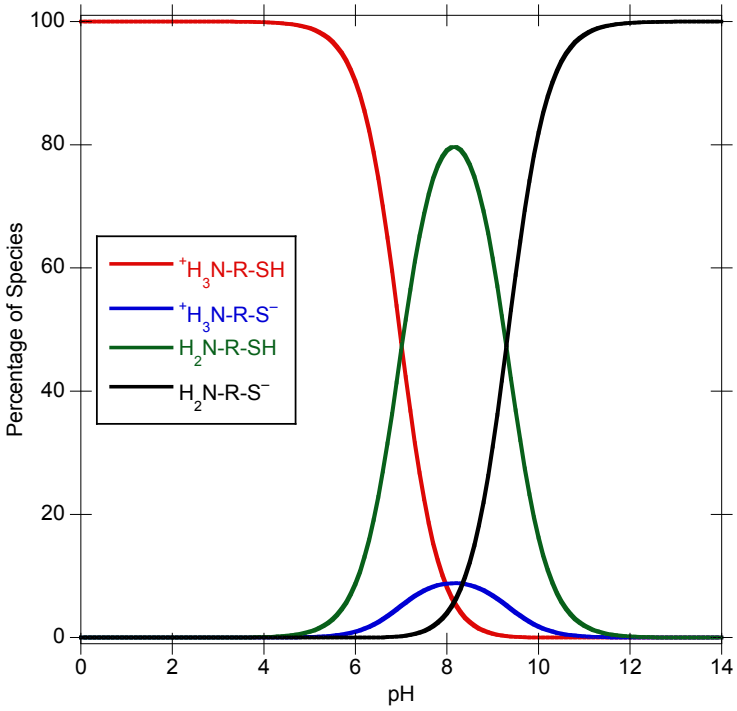

Table 4.10: The percentage abundance of each species for a range of representative pHs for cysteine derivatives studied in this work.[a]

Molecule	Species	pH 5	pH 6	pH 7	pH 8	pH 9
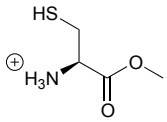	$^{+}H_3N$-R-SH	97	78	26	3	0
	$^{+}H_3N$-R-S^{-}	0	4	13	15	9
	H_2N-R-SH	2	18	61	74	44
	H_2N-R-S^{-}	0	0	1	8	46
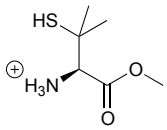	$^{+}H_3N$-R-SH	97	78	26	3	0
	$^{+}H_3N$-R-S^{-}	0	3	11	14	11
	H_2N-R-SH	2	19	63	80	63
	H_2N-R-S^{-}	0	0	0	3	26
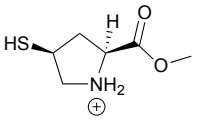	$^{+}H_3N$-R-SH	98	83	33	4	0
	$^{+}H_3N$-R-S^{-}	1	6	25	32	17
	H_2N-R-SH	1	11	42	54	29
	H_2N-R-S^{-}	0	0	1	10	53
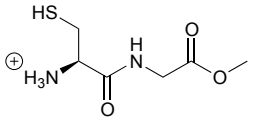	$^{+}H_3N$-R-SH	83	34	5	0	0
	$^{+}H_3N$-R-S^{-}	1	4	6	6	3
	H_2N-R-SH	15	62	88	81	37
	H_2N-R-S^{-}	0	0	1	13	60
H-Cys-Gly-Phe-NH_2	$^{+}H_3N$-R-SH	96	72	20	2	0
	$^{+}H_3N$-R-S^{-}	1	5	15	17	11
	H_2N-R-SH	3	23	64	74	47
	H_2N-R-S^{-}	0	0	1	7	42
H-Pen-Gly-Phe-NH_2	$^{+}H_3N$-R-SH	95	68	17	2	0
	$^{+}H_3N$-R-S^{-}	0	2	6	7	6
	H_2N-R-SH	4	30	76	88	71
	H_2N-R-S^{-}	0	0	0	3	23
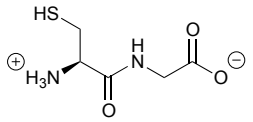	$^{+}H_3N$-R-SH	99	90	48	8	1
	$^{+}H_3N$-R-S^{-}	0	1	5	9	7
	H_2N-R-SH	1	9	47	79	62
	H_2N-R-S^{-}	0	0	0	4	31
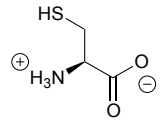	$^{+}H_3N$-R-SH	100	99	93	58	11
	$^{+}H_3N$-R-S^{-}	0	0	4	22	44
	H_2N-R-SH	0	0	3	20	39
	H_2N-R-S^{-}	0	0	0	0	6

[a] The error in the values is ± 6 %.

NCL is typically undertaken around pH 7.00, and in the case of the methyl esters and the peptides the concentration of the four species at this pH is:

$$H_2N\text{-}R\text{-}SH > {}^{+}H_3N\text{-}R\text{-}SH > {}^{+}H_3N\text{-}R\text{-}S^{-} >> H_2N\text{-}R\text{-}S^{-}$$

For methyl esters the total percentage of species in thiolate form at pH 7 is 14 % for the cysteine methyl ester, 11 % for the penicillamine methyl ester and 26 % for the (4*S*)-mercaptoproline methyl ester (Table 4.10).

For the peptides at pH 7 the percentage of thiolate for H-Cys-Gly-Phe-NH_2, 16 %, is much greater than that of the H-Pen-Gly-Phe-NH_2, 6 %. The abundance of thiolate for H-Cys-Gly-Phe-NH_2 is relatively insensitive to the change from ester to amide while H-Pen-Gly-Phe-NH_2 shows a much greater dependence, the abundance of thiolate approximately halves upon the switch to the amide. The difference in the response to the presence of the amide bond means that, unfortunately, the exact quantitative trends seen in the methyl esters do not appear to be applicable to the peptide systems. However, the qualitative trend of higher thiolate concentration in cysteine than penicillamine is valid and therefore it is not unreasonable to expect that the (4*S*)-mercaptoproline peptide would have a higher thiolate concentration than the cysteine peptide.

The implications for NCL are that in typical conditions of pH 7 only ~ 16 % of the total concentration of peptide is ever in the active thiolate form to react with the C-terminal thioester.[xlvi] Of the two thiolate species present the zwitterionic ${}^{+}H_3N\text{-}R\text{-}S^{-}$ species is dominant. This implies that prior to formation of the native amide bond via S-to-N acyl shift a deprotonation of the ammonium in the thioester ligated peptide is required.

At pH 8 for the methyl esters the abundance of thiolate increases to 23 % for

[xlvi] The total percentage of thiolate form will be affected by the ionic strength of the solution. In typical NCL conditions the ionic strength is $I \sim 0.2$. An $I = 0.3$ was used for the results shown here. Thus the percentage of thiolate found in our experiments will be approximately the same as that for normal NCL conditions. The overall impact of changes in ionic strength is believed to be small for the thiols on cysteine derivative as Friedman has shown that for the reaction between the thiol group on cysteine and acrylonitrile when the ionic strength is changed from $I = 0.15$ to $I = 1.55$ the change in the rate of the reaction is only 6 % higher in $I = 1.55$ (Friedman, M.; Cavins, J. F.; Wall, J. S. *J. Am. Chem. Soc.* **1965**, *87*, 3672 – 3682).

cysteine methyl ester, 17 % for penicillamine methyl ester and 42 % for (4*S*)-mercaptoproline methyl ester (Table 4.10). For the peptides the percentage of thiolate is 24 % for H-Cys-Gly-Phe-NH_2 and for H-Pen-Gly-Phe-NH_2 it is 10 %. In all cases the zwitterionic form $^{+}H_3N$-R-S^{-} of the thiolate is still dominant in solution over the anionic form H_2N-R-S^{-}. For the majority of cysteine derivatives the anionic form will be more abundant only when pH > 8.3.

At pH 6 for all cysteine derivatives the abundance of thiolate decreases significantly to between 2 – 6 % and only the zwitterionic $^{+}H_3N$-R-S^{-} species is present in solution (Table 4.10).

Knowing the abundance of each thiolate species present in solution is vital to establishing accurate rate constants for the reaction between an nucleophilic cysteine derivative thiolate and an electrophile, as will seen below.

4.3.5 Nucleophilicities of Thiols

The differences in the pK_as between the cysteine derivatives will, along with differences in steric and polar factors, contribute to differences in the nucleophilicities of the respective thiolates. For any cysteine derivative the differences in nucleophilicity between the $^{+}H_3N$-R-S^{-} and H_2N-R-S^{-} species will be directly related to the difference between pK_A and pK_D due to the similarity in sterics for both species.

A typical reaction between a cysteine derivative nucleophile and an electrophile will be composed of two parallel reactions that lead to an identical product which will only differ in the protonation state of the amine (Scheme 4.55).

Scheme 4.55: The two parallel reactions between a cysteine derivative nucleophile and an electrophile for the two thiolate species $^{+}H_3N$-R-S^{-} and H_2N-R-S^{-} species.

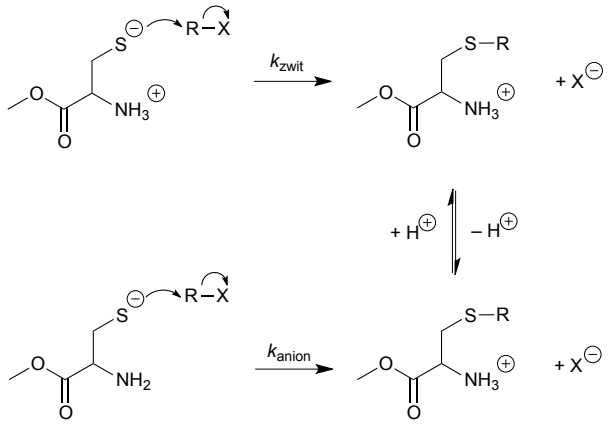

The rate equation for this reaction will be:

$$\text{Rate} = (k_{\text{zwit}}[^{+}\text{H}_3\text{NRS}^{-}] + k_{\text{anion}}[\text{H}_2\text{NRS}^{-}])\,[\text{Electrophile}] \quad \text{(Equation 4.6)}$$

where k_{zwit} is the second order rate constant for the reaction between the zwitterionic $^{+}H_3N$-R-S^{-} thiolate species and an electrophile and k_{anion} is the second order rate constant for the reaction between the anionic H_2N-R-S^{-} thiolate species and an electrophile.

4.3.5.1 Nucleophilicity estimates with acrylonitrile

Friedman has measured the nucleophilicity of the thiolate for both the species $^{+}H_3N$-R-S^{-} and H_2N-R-S^{-} for a variety of cysteine based thiol nucleophiles (including both primary thiolates, e.g. cysteine, and tertiary thiolates, e.g. penicillamine) via their reaction with the α,β-unsaturated carbon double bond in acrylonitrile (Scheme 4.56).[198] Second order observed rate constants, k_2, were measured through microamperometric titration with $AgNO_3$ and the dependence of these values upon pH is shown in Figure 4.33. The observed rate constant of the reaction increases linearly with pH as the fraction of thiolate in solution increases. At the pH where all the thiol is converted to thiolate the rate of reaction reaches a plateau allowing the determination of the second order rate constant for the reaction of the anionic H_2N-R-S^{-} with acrylonitrile, k_{RS2-} (equivalent to k_{anion} in Equation 4.6).

Scheme 4.56: The reaction between cysteine and acrylonitrile used by Friedman to probe the nucleophilicities of cysteine derivatives.[198]

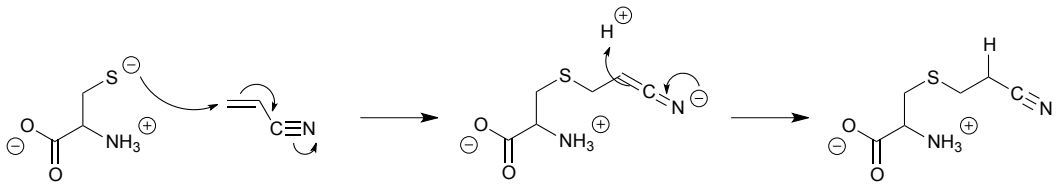

Figure 4.33: pH rate (k_2) profile for the reaction of β-mercaptoacetic acid, penicillamine, β-mercapto-isoleucine and glutathione with acrylonitrile at 30 °C and ionic strength I = 0.3 M. The plateaus at high pH are where $k_2 = k_{RS2-}$. Used with permission from the ACS.[198]

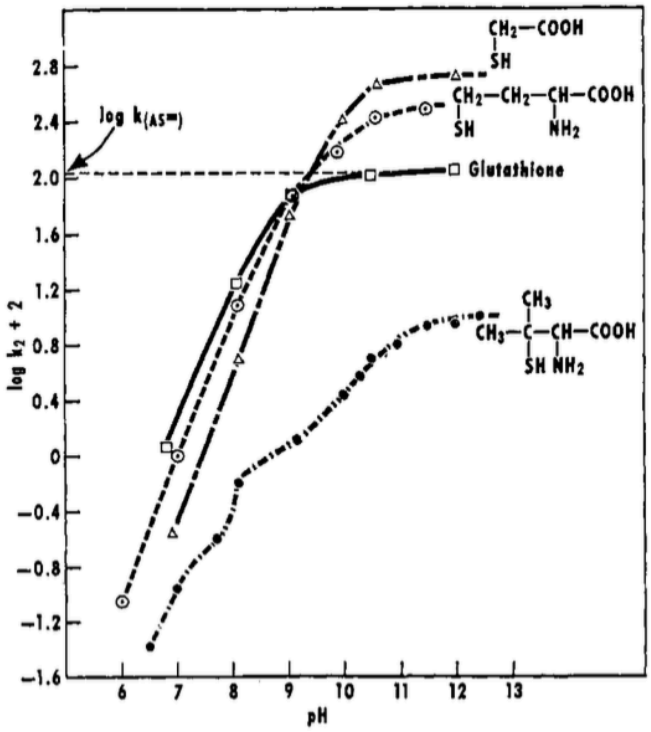

The onset of the plateau for penicillamine in Figure 4.35 (the lowest pH-rate trace shown in Figure 4.35) occurs at a higher pH than for β-mercaptoacetic acid, β-mercapto-isoleucine or glutathione, which indicates that the pK_D value for penicillamine is higher than for the other thiol nucleophiles. Based upon k_{RS2-} the second order rate constants for the reaction of the zwitterionic $^{+}H_3N$-R-S^{-} with acrylonitrile, k_{HRS-} (equivalent to k_{zwit} in Equation 4.6), could be calculated.

A Brønsted linear free energy relationship (Equation 4.7) can be used to determine the dependence of the rate constant for a reaction on the basicity of a nucleophile (Chapter 1: Section 1.3).

$$\log k = \beta_{nuc}\, pK_a + c \qquad \text{(Equation 4.7)}$$

where k is the rate constant, the pK_a is that of the conjugate acid of the nucleophile and β_{nuc} is the Brønsted nucleophilicity parameter which shows how sensitive the reaction is to the basicity of the nucleophile.

Friedman had determined k_{RS2-} and calculated k_{HRS-} values and, whilst aware of $K_A - K_D$, did not use these individual values for the basicity of the nucleophiles but instead relied upon the two titration constants, K_1 and K_2, where:

$$K_1 = K_A + K_B = \frac{[H^+]([^+H_3NRS^-]+[H_2NRSH])}{[^+H_3NRSH]} \quad \text{(Equation 4.8)}$$

$$K_2 = \frac{K_C K_D}{K_C + K_D} = \frac{[H^+][H_2NRS^-]}{[^+H_3NRS^-]+[H_2NRSH]} \quad \text{(Equation 4.9)}$$

where K_1 is the combined equilibrium constant for the dissociation of a proton from reactant ^+H_3N-R-SH to form both ^+H_3N-R-S^- and H_2N-R-SH products and K_2 is the combined equilibrium constant for the dissociation of a proton from reactant ^+H_3N-R-S^- and H_2N-R-SH to form H_2N-R-S^- product. Friedman assumed that $K_1 \sim K_A$ in order to determine the relationship between k_{HRS-} and the basicity of the thiolate in the zwitterionic ^+H_3N-R-S^-, and also that $K_2 \sim K_D$ for assessing the relationship between k_{RS2-} and the basicity of the thiolate in the anionic H_2N-R-S^-.

The Brønsted plot of log k_{S-} vs. pK_{SH} is shown in Figure 4.34, *where* log k_{S-} *refers to either* log k_{HRS-} *or* log k_{RS2-} *and* pK_{SH} *refers to either* pK_1 *or* pK_2. The upper plot in Figure 4.34 is for the reaction between acrylonitrile and a primary thiolate while the lower plot is for the reaction with a tertiary thiolate. The plots show that there is a continuous relationship between the nucleophilicities of ^+H_3N-R-S^- and H_2N-R-S^-, as log k_{HRS-} and pK_1, and, log k_{RS2-} and pK_2 align, which is unsurprising as there is little difference in sterics between ^+H_3N-R-S^- and H_2N-R-S^-. The upper plot for primary thiolates has a Brønsted relationship of:

$$\log k_{S-} = 0.456\ pK_{SH} - 4.139 \quad \text{(Equation 4.10)}$$

while the lower plot for tertiary thiolates has a Brønsted relationship of:

$$\log k_{S-} = 0.416\ pK_{SH} - 5.324 \quad \text{(Equation 4.11)}$$

Figure 4.34: Brønsted plot of log k_{HRS-} and log k_{RS2-}vs. pK_1 and pK_2 respectively for the reaction between primary and tertiary thiolates with acrylonitrile at 30 °C and ionic strength I = 0.3 M. Data taken from Friedman, M.; Cavins, J. F.; Wall, J. S. *J. Am. Chem. Soc.* **1965**, *87*, 3672 – 3682.

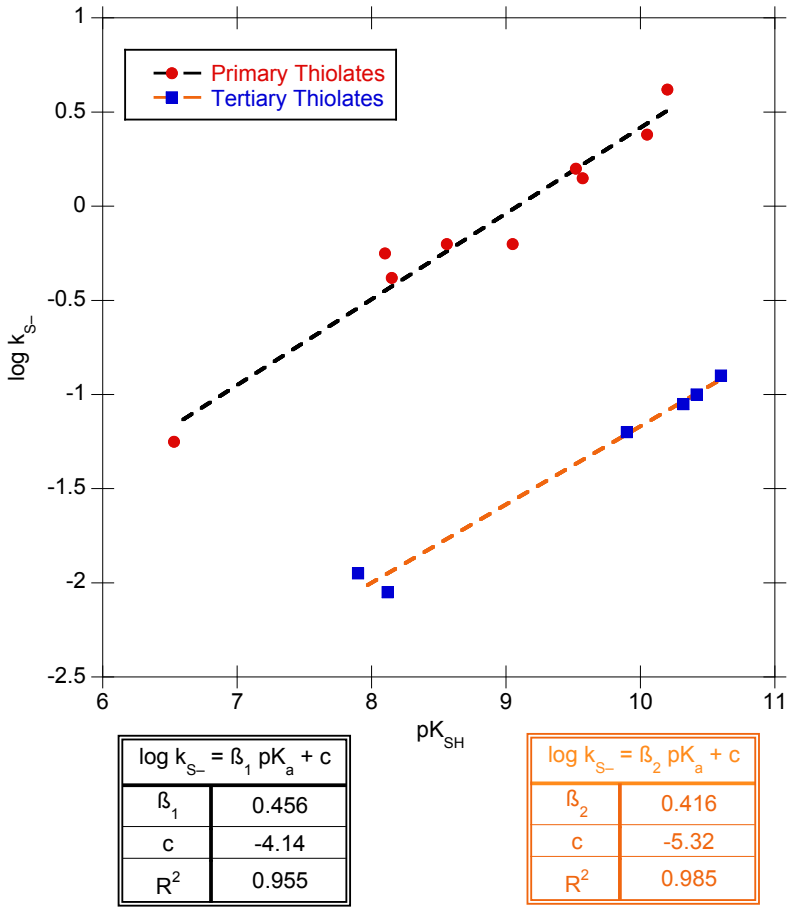

log k_{S-} = ß$_1$ pK_a + c	
ß$_1$	0.456
c	-4.14
R^2	0.955

log k_{S-} = ß$_2$ pK_a + c	
ß$_2$	0.416
c	-5.32
R^2	0.985

The Brønsted linear free energy relationship above could be used to interpolate estimates for k_{RS2-} and k_{HRS-} values for the reaction between the cysteine derivatives and acrylonitrile. This would first require converting the K_A and K_D values into K_1 and K_2 values. However, upon doing this it was found that the difference between K_1 and K_A, and, K_2 and K_D, was in some cases over 10-fold. Therefore Friedman's assumption that $K_1 \sim K_A$ and $K_2 \sim K_D$ was incorrect.

To adjust for this, the K_A and K_D values for the cysteine derivatives measured by us were combined with Friedman's k_{RS2-} and k_{HRS-} values and used to re-determine the Brønsted relationship between log k_{HRS-} and pK_A, and, log k_{RS2-} and pK_D. The experimental conditions used by Friedman and us were approximately the same, as both were performed at ionic strength I = 0.3, but k_{HRS-} and k_{RS2-} were determined at 30 °C while pK_A and pK_D were determined at 25 °C. In addition, as no pK_A and pK_D values

were recorded by us for penicillamine, the difference between cysteine methyl ester and cysteine pK_As and pK_Ds was used to estimate pK_A and pK_D for penicillamine from the pK_A and pK_D values of the penicillamine methyl ester. The new Brønsted plot is shown in Figure 4.35.

Figure 4.35: Brønsted plot of log k_{HRS-} and log k_{RS2-} vs. pK_A and pK_D respectively for the reaction between primary and tertiary thiolates with acrylonitrile at 30 °C and ionic strength I = 0.3 M. Data taken from Friedman, M.; Cavins, J. F.; Wall, J. S. *J. Am. Chem. Soc.* **1965**, *87*, 3672 – 3682 and Table 4.5.

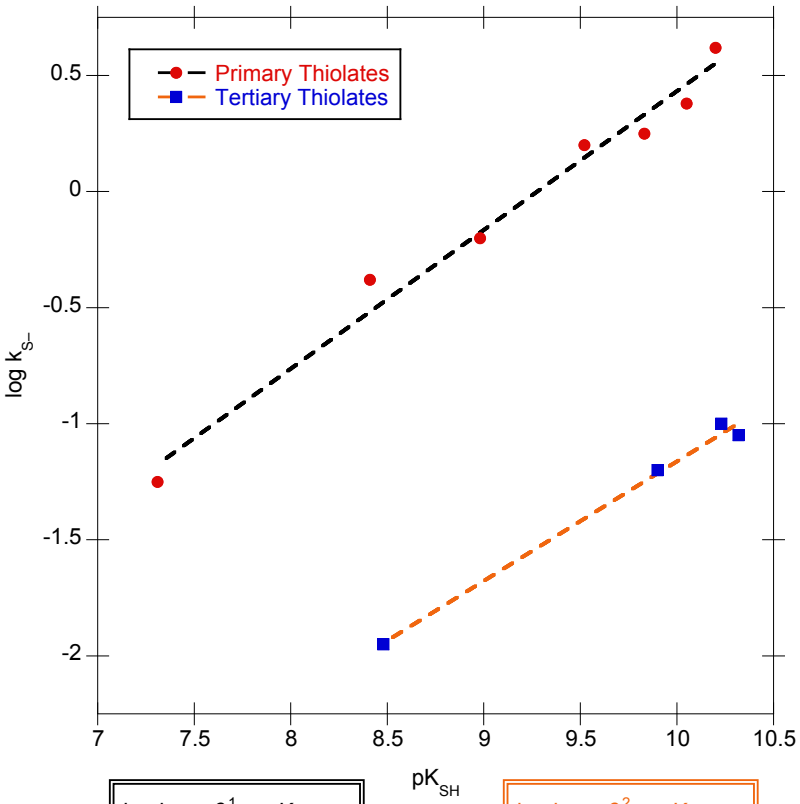

$\log k_{S-} = \beta^1_{nuc} pK_{SH} + c$	
β^1_{nuc}	0.598
c	-5.55
R^2	0.981

$\log k_{S-} = \beta^2_{nuc} pK_{SH} + c$	
β^2_{nuc}	0.515
c	-6.31
R^2	0.992

The new Brønsted relationship between k_{HRS-} and k_{RS2-} and the basicity (pK_A and pK_D) of the primary thiolate (upper plot) has a β^1_{nuc} = 0.598:

$$\log k_{S-} = 0.598\ pK_{SH} - 5.55 \qquad \text{(Equation 4.12)}$$

The new Brønsted relationship between k_{HRS^-} and k_{RS2^-} and the basicity (pK_A and pK_D) of the tertiary thiolate (lower plot) has a $\beta^2_{nuc} = 0.515$:

$$\log k_{S^-} = 0.515\ pK_{SH} - 6.31 \qquad \text{(Equation 4.13)}$$

The Brønsted linear free energy relationship (LFER) in the upper plot is composed of thiolates with a variety of C-terminals including carboxylates (e.g. cysteine) and ethyl esters (e.g. cysteine ethyl ester) (Table 4.11 Entries 1 – 5). The observation of a good correlation implies that while the C-terminal structure may affect the pK_{SH} of the species the relationship between pK_{SH} and k_{S^-} within the primary thiolate series is unaffected. Thus, k_{RS2^-} and k_{HRS^-} values for the reaction between acrylonitrile and the cysteine derivatives examined here may be interpolated from Equation 4.12 using the values for pK_A and pK_D determined above (Table 4.11 Entries 6 – 9).

Values of k_{RS2^-} and k_{HRS^-} for penicillamine methyl ester and peptide and 4*S*-mercaptoproline methyl ester may also be found using Equation 4.13. It is assumed that the differing C-terminals between the tertiary thiolates that compose the Brønsted LFER (Table 4.11 Entries 10 – 12), which are all carboxylates, and the tertiary thiolates examined here (Table 4.11 Entries 13 – 15), which are esters and amides, does not affect the relationship between pK_{SH} and k_{S^-}.

Table 4.11: pK_A, pK_D, k_{RS2-}, k_{HRS-} and interpolated k_{RS2-} and k_{HRS-} values for the reaction between primary and tertiary thiolates and acrylonitrile at 30 °C and ionic strength $I = 0.3$ M.

Entry	Molecule	pK_A	pK_D	k_{HRS-} /M^{-1} s^{-1}	k_{RS2-} /M^{-1} s^{-1}
1	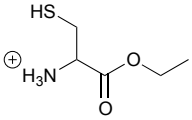	7.31 [d]	8.98 [d]	5.62×10^{-2} [c]	6.31×10^{-1} [c]
2	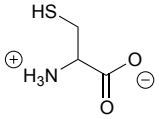	8.41 [d]	9.83 [d]	4.17×10^{-1} [c]	1.78 [c]
3	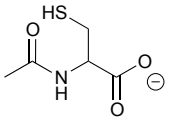	-	9.52 [c]	-	1.58 [c]
4	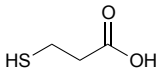	-	10.05 [c]	-	2.40 [c]
5	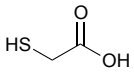	-	10.20 [c]	-	4.17 [c]
6	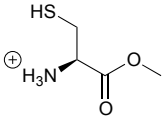	7.31 [d]	8.98 [d]	6.7×10^{-2} [a]	6.7×10^{-1} [a]
7	H-Cys-Gly-Phe-NH_2	7.13 [d]	9.04 [d]	5.3×10^{-2} [a]	7.2×10^{-1} [a]
8	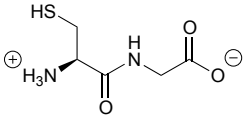	7.97 [d]	9.30 [d]	1.7×10^{-1} [a]	1.0 [a]
9	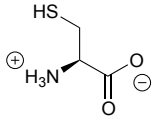	8.41 [d]	9.83 [d]	3.0×10^{-1} [a]	2.1 [a]
10	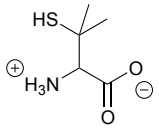	8.48 [e]	10.23 [e]	1.1×10^{-2} [c]	1.0×10^{-1} [c]
11	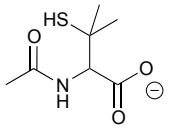	-	9.90 [c]	-	6.31×10^{-2} [c]
12	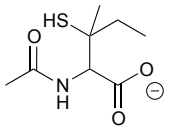	-	10.32 [c]	-	8.91×10^{-2} [c]
13	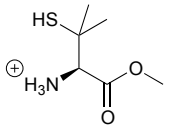	7.38 [d]	9.38 [d]	3.1×10^{-3} [b]	3.3×10^{-2} [b]

14	H-Pen-Gly-Phe-NH_2	7.44 [d]	9.49 [d]	3.3×10^{-3} [b]	3.8×10^{-2} [b]
15	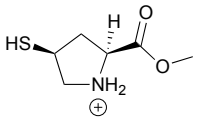	7.12 [d]	8.74 [d]	2.3×10^{-3} [b]	1.6×10^{-2} [b]

[a] Interpolated from Equation 4.12. [b] Interpolated from Equation 4.13. [c] Data from Friedman, M.; Cavins, J. F.; Wall, J. S. *J. Am. Chem. Soc.* **1965**, *87*, 3672 – 3682. [d] Data from Table 4.5. [e] Estimate for pK_A and pK_D of penicillamine found from: the difference between cysteine methyl ester and cysteine pK_As and pK_Ds added onto the pK_A and pK_D of the penicillamine methyl ester.

The estimates for k_{HRS^-} and k_{RS2^-} serve as an indication of the different nucleophilicities of the thiolates towards reaction at the β-alkenyl carbon of acrylonitrile (Table 4.11 Entries 6 – 9). The anionic species H_2N-R-S^- for the primary thiolates of cysteine methyl ester and H-Cys-Gly-Phe-NH_2 is estimated to be between 10- to 14-fold more nucleophilic than the zwitterionic ^+H_3N-R-S^-. This is in good agreement with Friedman's observations whose measurement of k_{HRS^-} and k_{RS2^-} for cysteine ethyl ester indicated an 11.2-fold higher reactivity for H_2N-R-S^-. For cysteine and H-Cys-Gly-OH, which both have carboxylate C-terminals, H_2N-R-S^- is estimated to be only 6.2- and 7.1-fold more nucleophilic than ^+H_3N-R-S^-, which is higher than the 4.3-fold increase found by Friedman.

For the tertiary thiolates of penicillamine methyl ester and H-Pen-Gly-Phe-NH_2, the k_{RS2^-} value for H_2N-R-S^- is 11-fold larger than k_{HRS^-} for ^+H_3N-R-S^- (Table 4.11 Entries 14 and 15). This is greater than the 8.9-fold difference found by Friedman for penicillamine and is likely due to the differing C-terminals (neutral vs. carboxylate). The estimates for k_{HRS^-} and k_{RS2^-} for (4*S*)-mercaptoproline methyl ester indicate a 6.8-fold increase in reactivity for H_2N-R-S^- compared to ^+H_3N-R-S^-.

Comparing k_{HRS^-} values of cysteine methyl ester and penicillamine methyl ester predicts that ^+H_3N-R-S^- of cysteine methyl ester is predicted to be 22-fold more nucleophilic than the ^+H_3N-R-S^- of penicillamine methyl ester. In a comparison of k_{RS2^-} values, the H_2N-R-S^- of cysteine methyl ester is predicted to be 20-fold more nucleophilic than the H_2N-R-S^- of penicillamine methyl ester. In the comparison between (4*S*)-mercaptoproline methyl ester and cysteine methyl ester the k_{HRS^-} and k_{RS2^-} values are 73-fold and 67-fold higher for the cysteine methyl ester. A comparison of H-Cys-Gly-Phe-NH_2 and H-Pen-Gly-Phe-NH_2 predicts that the H-Cys-Gly-Phe-NH_2 k_{HRS^-} and k_{RS2^-} will be 16- and 19-fold more reactive, respectively. Friedman's results

indicated that k_{HRS^-} and k_{RS2-} values are 37- and 18-fold larger, respectively, for cysteine than penicillamine, which is not substantially different to that predicted for the corresponding methyl esters and peptides. Overall, although the reaction between thiolates and acrylonitrile is informative on the relative nucleophilicities of the different cysteine derivatives towards an α,β-unsaturated carbon double bond, it is not directly comparable to NCL as the latter involves reaction at a thioester carbonyl carbon.

4.3.5.2 Relative nucleophilicity differences between thiolates of cysteine derivatives towards aryl thioesters

A better estimate for the difference in nucleophilicities of the various cysteine derivative thiolates typically employed in NCL may be gained using a study by Jencks of the second order rate constants for the reaction between primary thiolates and *p*-nitrophenyl thioacetate.[201] Figure 4.36 shows the Brønsted plot for the reaction between various thiolates and *p*-nitrophenyl thioacetate.

Figure 4.36: Brønsted plot for the reaction of a series of thiolate nucleophiles with *p*-nitrophenyl acetate thioester at 25 °C and ionic strength I = 1.0 M (KCl). Reproduced with permission from the ACS.[201]

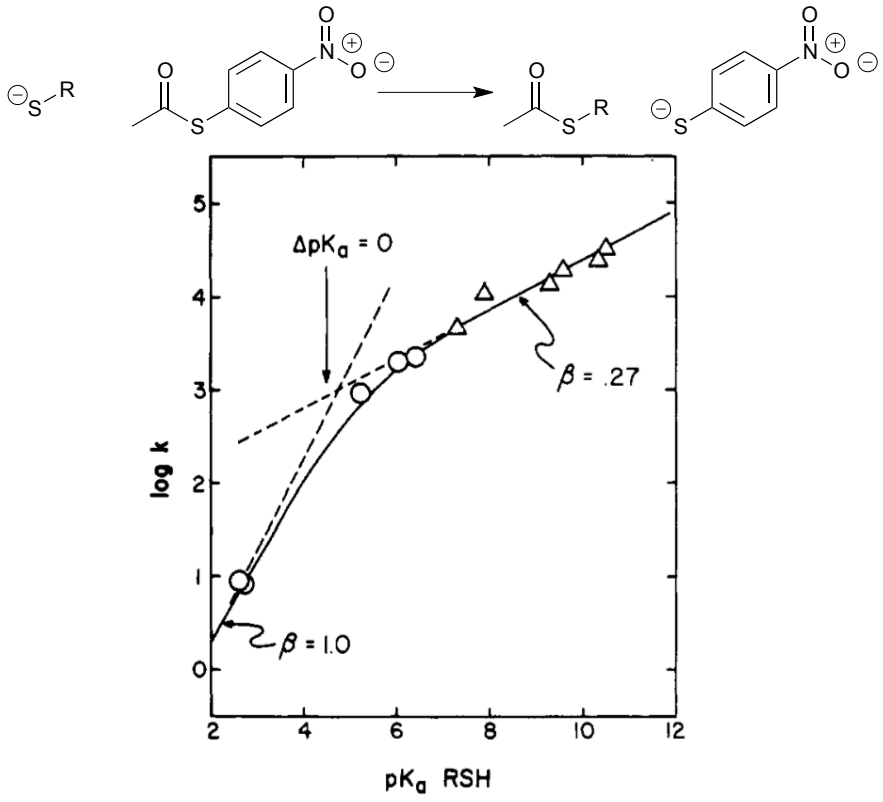

The Brønsted relationship between the second order rate constant for the reaction, k_{PNTPA}, and the pK_a of the thiol nucleophile is:

$$\log k_{PNTPA} = 0.27\ pK_a + 1.70 \qquad \text{(Equation 4.14)}$$

The rate constants for the thiol-thioester exchange reaction between *p*-nitrophenyl thioacetate and both $^{+}H_3N\text{-}R\text{-}S^{-}$ (k_{PNTPA}) and $H_2N\text{-}R\text{-}S^{-}$ (k_{PNTPA}') species of the cysteine derivatives may be predicted from Equation 4.14 using the pK_A and pK_D values determined herein (Table 4.5). Predicted k_{PNTPA} and k_{PNTPA}' values for the reaction of the cysteine derivatives with *p*-nitrophenyl thioacetate are found in Table 4.12. The estimates for k_{PNTPA} and k_{PNTPA}' values for the tertiary thiolates of penicillamine and (4*S*)-mercaptoproline in Table 4.12 were predicted using the differences in reactivity between primary cysteine and tertiary thiolates established by Friedman above.[xlvii]

[xlvii] k_{PNTPA} 21.6-fold difference between methyl esters of Cys and Pen, k_{PNTPA} 15.7-fold for peptides, k_{PNTPA}' 20.1-fold for methyl esters and k_{PNTPA}' 19.1-fold for peptides. k_{PNTPA} 72.8-fold and k_{PNTPA}' 66.6-fold for (4*S*)-mercaptoproline methyl ester.

Table 4.12: Predicted rate constants for the reaction between *p*-nitrophenyl thioacetate and cysteine derivatives at 25 °C and ionic strength I = 1.0 M (KCl). Equation 4.14 was used to determine the values of k_{PNTPA} and k_{PNTPA}'.

Molecule	pK_A	k_{PNTPA} /M^{-1} s^{-1}	pK_D	k_{PNTPA}' /M^{-1} s^{-1}
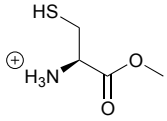	7.31	79	8.98	222
H-Cys-Gly-Phe-NH_2	7.13	70	9.04	230
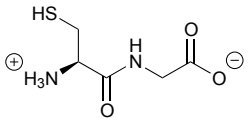	7.97	119	9.30	271
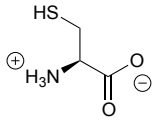	8.41	156	9.83	377
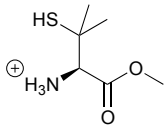	7.38	3.6	9.38	11
H-Pen-Gly-Phe-NH_2	7.44	4.5	9.49	12
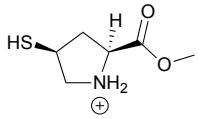	7.12	1.1	8.74	3.3

Compared to the reaction with acrylonitrile the predicted difference in reactivity between $^{+}H_3N$-R-S^{-} and H_2N-R-S^{-} is smaller with a 2.3 – 3.3-fold difference in reactivity for the primary thiolates and a 2.7 – 3.1-fold difference for the tertiary thiolates.

The reactions between primary thiol nucleophiles and thioesters, and, the reaction between primary thiol nucleophiles and oxoesters have been found by Jencks to both have a consistent Brønsted relationship[xlviii] with a β_{nuc} = 0.27 provided that nucleophilic attack of the thiolate was rate limiting (Figure 4.36). The existence of a consistent Brønsted relationship for thiol nucleophiles means that the differences in nucleophilicity between $^{+}H_3N$-R-S^{-} and H_2N-R-S^{-} shown above in Table 4.12 will be

[xlviii] Brønsted relationship between the second order rate constant for thiol-(thio/oxo)ester exchange and the pK_a of the primary thiol.

applicable to the transthioesterification step of NCL, where the thiol additive (usually MPAA) is displaced by the thiolate on the N-terminal cysteine.

Jencks probed the differences in reactivities of *p*-nitrophenyl thioacetate and the analogous oxoester *p*-nitrophenyl acetate with a series of primary thiolates. For *p*-nitrophenyl acetate, when nucleophilic attack of the thiolate is rate limiting, the Brønsted relationship between the second order rate constant for the reaction, k_{PNPA}, and the pK_a of the thiol nucleophile is:

$$\log k_{PNPA} = 0.27\ \mathrm{p}K_a + 0.33 \qquad \text{(Equation 4.15)}$$

A comparison of this to the Brønsted relationship for *p*-nitrophenyl thioacetate (Equation 4.14) shows that there is a difference in the y-intercepts of 1.37, which translates as a 23.4-fold increase in the second order rate constant upon moving from an oxoester to a thioester. This difference is to do with the intrinsic differences in reactivity between an oxoester and a thioester. This is attributed to a greater loss of delocalization energy in the oxoester compared to the thioester and a greater stabilisation of the transition state in a thioester via a stronger a $p_S \rightarrow \sigma^*_{C\text{-}Nu}$ interaction than the equivalent $p_O \rightarrow \sigma^*_{C\text{-}Nu}$ interaction in an oxoester.[269]

Jencks also determined the Brønsted relationship for the reaction between phenyl acetate and various thiolates:

$$\log k_{PA} = 0.27\ \mathrm{p}K_a - 0.58 \qquad \text{(Equation 4.16)}$$

where k_{PA} is the second order rate constant for the reaction with phenyl acetate and pK_a is that of the thiol nucleophile. Unfortunately, these studies did not include the reactions between thiolate nucleophiles and phenyl thioacetate, which would be akin to the thiol-thioester exchange and the transthioesterification reaction in NCL.

However, the intrinsic differences between a similar oxoester, *p*-nitrophenyl acetate, and a similar thioester, *p*-nitrophenyl thioacetate, are known. By taking Equation 4.16 and, assuming the same 23.4-fold difference in reactivity between *p*-nitrophenyl acetate and *p*-nitrophenyl thioacetate from above, the predicted Brønsted relationship for phenyl thioacetate when nucleophilic attack of the thiolate is rate determining will therefore be:

$$\log k_{PTA} = 0.27\ pK_a + 0.79 \qquad \text{(Equation 4.17)}$$

where k_{PTA} is the second order rate constant for the reaction of the thiolate with the phenyl thioacetate and pK_a is that of the thiol nucleophile. This allows for an estimate of k_{PTA} (for pK_A) and k_{PTA}' (for pK_D) for the reaction between phenyl thioacetate and the various cysteine derivatives (Table 4.13). For the tertiary thiolates of penicillamine and 4*S*-mercaptoproline estimates for k_{PTA} and k_{PTA}' in Table 4.13 were predicted using the differences in reactivity between cysteine and tertiary thiolate established by Friedman above.[xlix]

[xlix] k_{PTA} 21.6-fold difference between methyl esters of Cys and Pen, k_{PTA} 15.7-fold for peptides, k_{PTA}' 20.1-fold for methyl esters and k_{PTA}' 19.1-fold for peptides. k_{PTA} 72.8-fold and k_{PTA}' 66.6-fold for 4*S*-mercaptoproline methyl ester.

Table 4.13: Predicted rate constants for the reaction between phenyl thioacetate and the cysteine derivatives at 25 °C and ionic strength I = 1.0 M (KCl). [a] Equation 4.17 was used to determine the values of k_{PTA} and k_{PTA}'.

Molecule	pK_A	k_{PTA} /M^{-1} s^{-1} (~ k_{zwit})	pK_D	k_{PTA}' /M^{-1} s^{-1} (~ k_{anion})
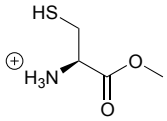	7.31	9.7	8.98	27
H-Cys-Gly-Phe-NH_2	7.13	8.7	9.04	28
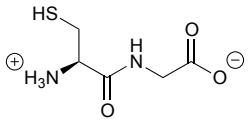	7.97	15	9.30	33
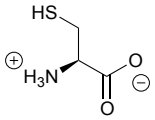	8.41	19	9.83	46
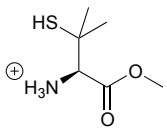	7.38	4.9×10^{-1}	9.38	1.4
H-Pen-Gly-Phe-NH_2	7.44	5.5×10^{-1}	9.49	1.5
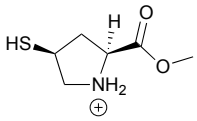	7.12	1.3×10^{-1}	8.74	4.1×10^{-1}

[a] The ionic strength in which pK_A and pK_D were measured at was I = 0.3 while the second order rate constants were measured at I = 1.0.

4.3.5.3 Implications of predicted reactivity differences of cysteine derivatives for Native Chemical Ligation

Values of k_{PTA} and k_{PTA}' can be used to give insight into the transthioesterification reaction between an aryl thioester and an N-terminal cysteine thiolate in NCL. The applicability of k_{PTA} and k_{PTA}' to NCL will depend upon whether the phenyl thioacetate is a good model system for a peptide thioester. The pK_a of the widely used aryl thiol additive MPAA is identical to that of thiophenol (pK_a = 6.60) and therefore the electronic effects from the aryl thiol at the carbonyl electrophilic centre are expected to be identical. Provided that the carboxylate group on MPAA does not sterically or electrostatically interfere with the approaching thiolate nucleophile then

phenyl thiolate is a good model system for a MPAA thioester. However, the presence of an electron withdrawing amide group alpha to the thioester in the peptide thioester will be expected to slightly increase the value of k_{PTA} and k_{PTA}' in the peptide system. Nevertheless, the values for k_{PTA} and k_{PTA}' in Table 4.13 should allow for a reasonable estimate for the second order rate constants of the transthioesterification reaction.

The rate equation for the transthioesterification reaction is:

$$\text{Rate} = (k_{zwit}[^{+}H_3NRS^{-}] + k_{anion}[H_2NRS^{-}])\ [\text{Peptide Aryl Thioester}] \quad \text{(Equation 4.18)}$$

$$= (k_{zwit}\, f_{zwit}[\text{Cysteine Peptide}] + k_{anion}\, f_{anion}[\text{Cysteine Peptide}])\ [\text{Peptide Aryl Thioester}]$$

$$k_{NCL} = k_{zwit}\, f_{zwit} + k_{anion}\, f_{anion} \quad \text{(Equation 4.19)}$$

where k_{anion} is the second order rate constant for the reaction between H_2N-R-S^{-} and peptide aryl thioester, k_{zwit} is the second order rate constant for the reaction between $^{+}H_3N$-R-S^{-} and peptide aryl thioester, f_{anion} is the fraction of cysteine peptide in H_2N-R-S^{-} form,[l] f_{zwit} is the fraction of cysteine peptide in $^{+}H_3N$-R-S^{-} form[li] and k_{NCL} is the observed second order rate constant for NCL.

NCL is typically undertaken at pH 7.0 and with the concentration of peptide aryl thioester and cysteine C-terminal peptide at 0.5 – 2.0 mM. In the comparisons below a concentration of 0.5 mM is used for peptide aryl thioester and cysteine C-terminal peptide, which are identical to those used in a kinetic study by Bang and Pentelute (introduced in Section 4.1.6.2).[236] Assuming that $k_{anion} \sim k_{PTA}$' and $k_{zwit} \sim k_{PTA}$ and the percentage of H-Cys-Gly-Phe-NH_2 present as the species $^{+}H_3N$-R-S^{-} (14 %) and H_2N-R-S^{-} (0 %) (Figure 4.29) at pH 6.8 then the second order rate constant for NCL can be estimated to be:

$$k_{NCL} = 8.65\ M^{-1}\ s^{-1} \times 0.14 + 28.36\ M^{-1}\ s^{-1} \times 0.00$$
$$= 1.58\ M^{-1}\ s^{-1}$$

[l] $f_{anion} = \dfrac{\frac{K_B K_D}{10^{-pH}}}{1+\frac{K_A}{10^{-pH}}+\frac{K_B}{10^{-pH}}+\frac{K_B K_D}{(10^{-pH})^2}}$

[li] $f_{zwit} = \dfrac{\frac{K_A}{10^{-pH}}}{1+\frac{K_A}{10^{-pH}}+\frac{K_B}{10^{-pH}}+\frac{K_B K_D}{(10^{-pH})^2}}$

and the initial rate of the NCL is predicted to be:

$$\text{Rate} = [8.65\ M^{-1}\ s^{-1}\ (0.14 \times 0.5\ mM) + 28.36\ M^{-1}\ s^{-1}\ (0.00 \times 0.5\ mM)] \times 0.5\ mM$$
$$= 3.03 \times 10^{-7}\ M\ s^{-1}$$

The values of k_{NCL} measured by Bang and Pentelute were between 1.30×10^{-8} – 2.33×10^{-6} M^{-1} s^{-1} depending upon the identity of the residue at the C-terminal (Valine and Glycine respectively). These values are significantly different to the estimated k_{NCL} = 1.58 M^{-1} s^{-1} based upon Jencks work. The reaction between *p*-nitrophenyl thioacetate and alkyl thiolates studied by Jencks has second order rate constants, k_{PNTPA}, between 19.8×10^{3} – 32.7×10^{3} M^{-1} s^{-1}. It is highly unlikely that removal of the nitro group to give a thiophenol could cause a drop in the second order rate constant of between 10^{12} – 10^{14} M^{-1} s^{-1}, particularly when Jencks found that the second order rate constants for the reaction between alkyl thiolates and phenyl acetate are only 15 – 27-fold smaller than for the reaction between alkyl thiolates and *p*-nitrophenyl acetate.

One observation is that the lower end of the experimental k_{NCL} values reported by Bang and Pentelute are similar to our initial rate estimate of 3.03×10^{-7} M s^{-1}. The explanation for this discrepancy is that Bang and Pentelute appear to have obtained their k_{NCL} values by plotting concentration against time rather than 1/concentration ($1/C_t$) against time, which would be required for a second order rate constant. The initial concentrations of peptide aryl thioester and cysteine C-terminal peptide were 0.5 mM and therefore the y-axis of the plots of $1/C_t$ vs. time ought to be in the 1000's. However, it can be seen from Figure 4.37 that the y-axis is in units of 0.001, which equates to concentration values. Therefore the lines plotted would measure initial rates rather than k_{NCL} values. Our predicted initial rate of 3.03×10^{-7} M s^{-1} is in reasonable accordance with the initial rates of 1.30×10^{-8} – 2.33×10^{-6} M^{-1} s^{-1} measured by Bang and Pentelute.

Figure 4.37: Kinetic data analysis by Bang and Pentelute showing how k_{NCL} values were obtained from plots of 1/[Concentration] vs. time. However, the plots appear to be for [Concentration] vs. time. Plot b) is a magnified version of the lower values in a).[236]

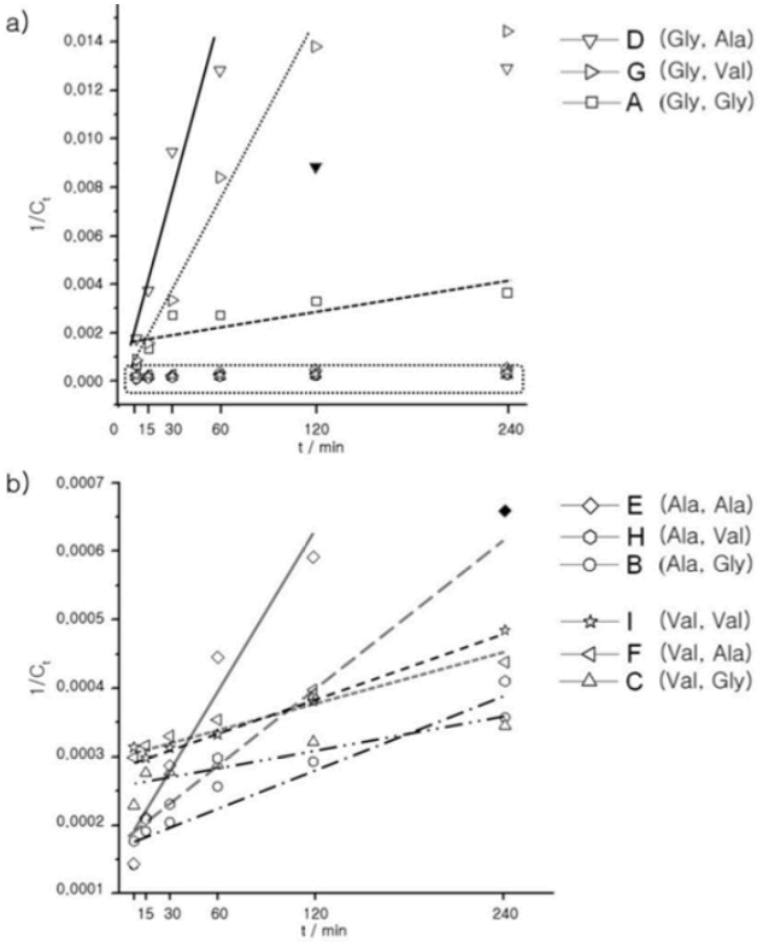

Calculated rates of NCL may be made using Equation 4.18 and the predicted values for k_{zwit} and k_{anion} and calculated f_{zwit} and f_{anion} values, based on our pK_as. These rates may be used to construct concentration vs. time profiles for NCL that may then be compared with experiment. Figure 4.38 shows how the concentration of cysteine C-terminal peptide decreases and the concentration of ligated product increases over time using the Brad and Pentelute conditions mentioned above and Equation 4.18. Note that because the reaction between cysteine C-terminal peptide and peptide aryl thioester has a 1 : 1 stoichiometry the decrease in concentration of peptide aryl thioester will be equivalent to that of cysteine C-terminal peptide.

Figure 4.38: Predicted changes in the concentration of cysteine C-terminal peptide and ligated product is predicted to change over time during a NCL. Conditions are [cysteine C-terminal peptide] = 0.5 mM and [peptide aryl thioester] = 0.5 mM, pH 6.8 and 25 °C with $k_{anion} \sim k_{PTA}$' and $k_{zwit} \sim k_{PTA}$ (Table 4.13) and the percentage of species $^{+}H_3N$-R-S^{-} (14 %) and H_2N-R-S^{-} (0 %) for H-Cys-Gly-Phe-NH_2 (Figure 4.29).

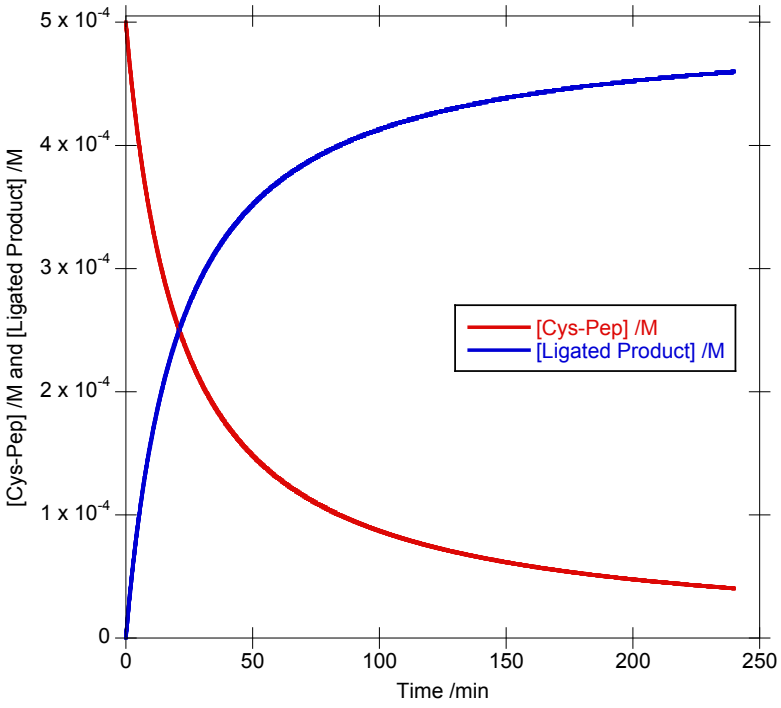

The majority of peptide chemists typically follow NCL via monitoring the percentage of ligated product present over time. For the reaction in Figure 4.38 the corresponding percentage of ligated product is shown in Figure 4.39 alongside the experimental plot from Bang and Pentelute.

Figure 4.39: The percentage of ligated product for the modeled reaction in Figure 4.39. Conditions are [cysteine C-terminal peptide] = 0.5 mM and [peptide aryl thioester] = 0.5 mM, pH 6.8 (red) and pH 7.0 (green) and 25 °C with $k_{anion} \sim k_{PTA}$' and $k_{zwit} \sim k_{PTA}$ (Table 4.13) and the percentage of species $^{+}H_3N$-R-S^{-} (pH 6.8 = 14 %, pH 7.0 = 15 %) and H_2N-R-S^{-} (pH 6.8 = 0 %, pH 7.0 = 1 %) for H-Cys-Gly-Phe-NH_2 (Figure 4.29). The experimental data from Bang and Pentelute for the reaction between an N-terminal Cysteine (0.5 mM) and a C-terminal glycine thioester (0.5 mM) at pH 6.8 and 25 °C is also plotted (blue).

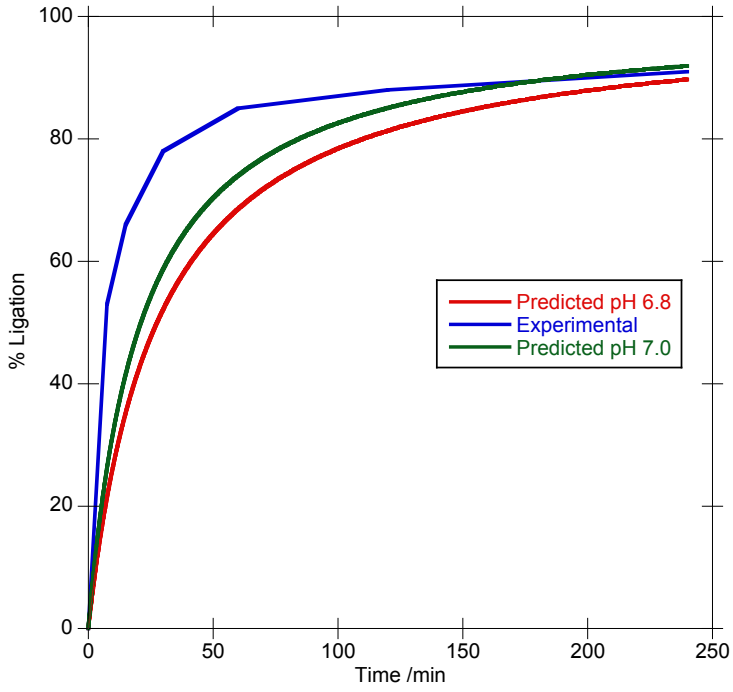

The model NCL in Figure 4.39 gives a reasonable prediction for the percentage of ligated product observed by experiment. Bang and Pentelute recorded that at 60 min the percentage of ligated product was 82 % for the reaction between a peptide with a C-terminal glycine thioester while for the modeled reaction the predicted percentage of ligated product at 60 min is 69 %. The lower percentage of ligation in the modeled reaction may possibly be due to the absence of an electron withdrawing amide group alpha to the thioester. In the peptide systems the amide group will increase the electrophilicity of the thioester and therefore is expected to increase the rate of ligation, hence the higher percentage completion.

The percentage of ligated product at pH 7.0 is also shown in Figure 4.39, as at this pH there is 1 % of H_2N-R-S^{-} present in solution and at 60 min 74 % ligation is

predicted. The experimental NCL results were measured at a higher ionic strength than the $pK_A - pK_D$ and therefore it is not inconceivable that a small amount of $H_2N\text{-}R\text{-}S^-$ species may be present in solution. As k_{anion} is about 3.3-fold larger than k_{zwit}, the reaction with the $H_2N\text{-}R\text{-}S^-$ has a larger impact on the percentage of ligation observed (Table 4.13).

The percentage of ligated product from the predicted rate constants for H-Pen-Gly-Phe-NH_2 is shown in Figure 4.40 alongside the experimental percentage of ligation measured by Seitz.[221]

Figure 4.40: The predicted percentage of ligated product for the modeled reaction between H-Pen-Gly-Phe-NH_2 with a peptide aryl thioester (phenyl thioacetate used to approximate). Conditions are [cysteine C-terminal peptide] = 5 mM and [peptide aryl thioester] = 5 mM, pH 8.5 and 25 °C with $k_{anion} \sim k_{PTA}$' and $k_{zwit} \sim k_{PTA}$ (Table 4.13) and the percentage of species $^+H_3N\text{-}R\text{-}S^-$ (7 %) and $H_2N\text{-}R\text{-}S^-$ (9 %) for H-Pen-Gly-Phe-NH_2 (Figure 4.30). The experimental data is from Seitz for the reaction between an N-terminal penicillamine (5 mM) and a C-terminal glycine thioester (5 mM) at pH 8.5 and 37 °C.[221]

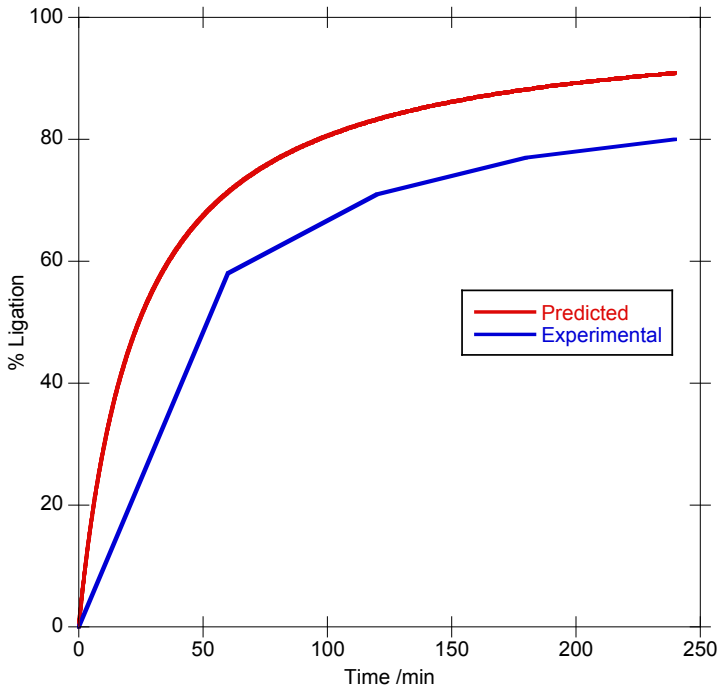

It is apparent that the estimates for k_{anion} and k_{zwit} are above the experimental values as the percentage of ligation predicted is above that of the experimental. Seitz's

NCL was undertaken at 37 °C while the predicted model is at 25 °C which means that the discrepancy between predicted and experimental is even larger than that shown in Figure 4.40. The overestimate is likely due to the sterics not being properly accounted for in penicillamine. Estimates for k_{anion} and k_{zwit} were made based upon the differences in the second order rate constants k_{HRS^-} and k_{RS2^-} for the reaction between cysteine and penicillamine and acrylonitrile. Acrylonitrile has less steric bulk around the electrophilic C-terminus of the double bond than an aryl thioester does around the carbonyl carbon. Thus, the extra steric bulk from the two adjacent methyl groups in penicillamine is expected to have a larger impact on the reaction between the thiolate and the thioester than the thiolate with acrylonitrile.

For (4*S*)-mercaptoproline Danishefsky identified that the rate determining step for ligation was not transthioesterification but the S-to-N acyl shift.[227] Consequently, the predicted second order rate constants, k_{anion} and k_{zwit} in Table 4.13 cannot be used to model the ligation between an N-terminal (4*S*)-mercaptoproline peptide and a peptide aryl thioester. Ligations with (4*S*)-mercaptoproline will have a pre-equilibrium formation of the transthioesterification product. Thus, in conjunction with a partition experiment to determine the reverse rate constant for the transthioesterification reaction the k_{anion} and k_{zwit} values could be used to determine the pre-equilibrium constant.

4.3.6 N-terminal Kinetically Controlled Ligations

The differences in structure between cysteine derivatives has been clearly shown to affect pK_A and pK_D and hence alter the concentration of the active thiolate species present in solution. The different concentrations of thiolate species in conjunction with the predicted differences in nucleophilicity shown above, raise the possibility of conducting N-terminal kinetically controlled ligations (KCL).

A possible one-pot procedure for the synthesis of a peptide from three segments via N-terminal KCL is shown in Scheme 4.57. The three segment peptides are 1) an N-terminus peptide segment, with a C-terminal thioester, 2) a middle peptide segment, with the more nucleophilic cysteine derivative N-terminal and a less reactive thioester at the C-terminal, and 3) a C-terminus segment, with a less reactive cysteine derivative N-terminal. The N-terminal KCL is conceived to proceed in the N-to-C direction with an initial reaction between the more nucleophilic cysteine derivative on the middle segment and the N-terminus segment C-terminal thioester. The C-terminus peptide

segment will then ligate to this peptide via reaction between the less reactive cysteine derivative and the less reactive thioester.

Scheme 4.57: Proposed procedure for a three segment N-terminal Kinetically Controlled Ligation. In Ligation 1 the more nucleophilic cysteine derivative reacts with the more reactive thioester. In Ligation 2 the less reactive cysteine derivative reacts with the less reactive thioester.

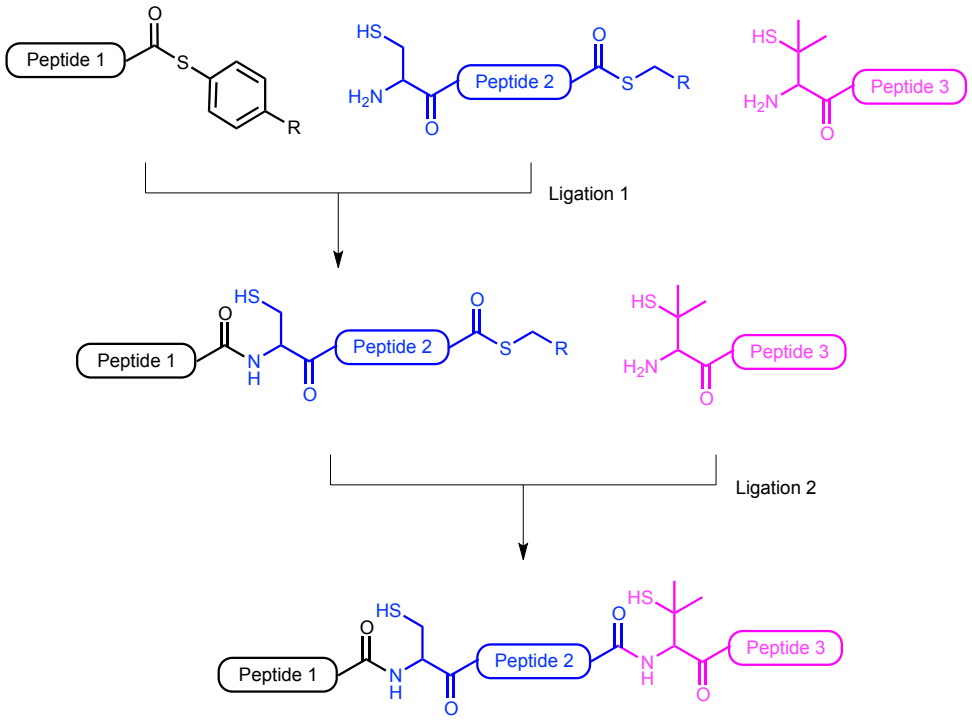

In order for N-terminal KCL to be viable suitable conditions must be found in which one N-terminal cysteine derivative is considerably more reactive than the other to ensure that there is not a mixture of ligated peptide formed. One possible way to control N-terminal KCL would be careful pH control of the reaction in order to harness the differences in the concentration of thiolate species between cysteine derivatives at different pHs. Figure 4.41 shows how the percentage of ligated product is predicted to vary over time at pH 7.0 and pH 8.5 for H-Cys-Gly-Phe-NH_2 and H-Pen-Gly-Phe-NH_2.

Figure 4.41: The predicted percentages of ligation for H-Cys-Gly-Phe-NH_2 and H-Pen-Gly-Phe-NH_2 at pH 7.0 and 8.5. Conditions are [cysteine derivative C-terminus peptide] = 1 mM and [peptide aryl thioester] = 1 mM and 25 °C with $k_{anion} \sim k_{PTA}$' and $k_{zwit} \sim k_{PTA}$ (Table 4.13). The percentage of species for H-Cys-Gly-Phe-NH_2 $^{+}H_3N$-R-S^{-} (pH 7.0 = 15 %; pH 8.5 = 15 %) and H_2N-R-S^{-} (pH 7.0 = 1 %; pH 8.5 = 19 %) (Figure 4.29). The percentage of species for H-Pen-Gly-Phe-NH_2 $^{+}H_3N$-R-S^{-} (pH 7.0 = 6 %; pH 8.5 = 7 %) and H_2N-R-S^{-} (pH 7.0 = 0 %; pH 8.5 = 9 %) (Figure 4.30).

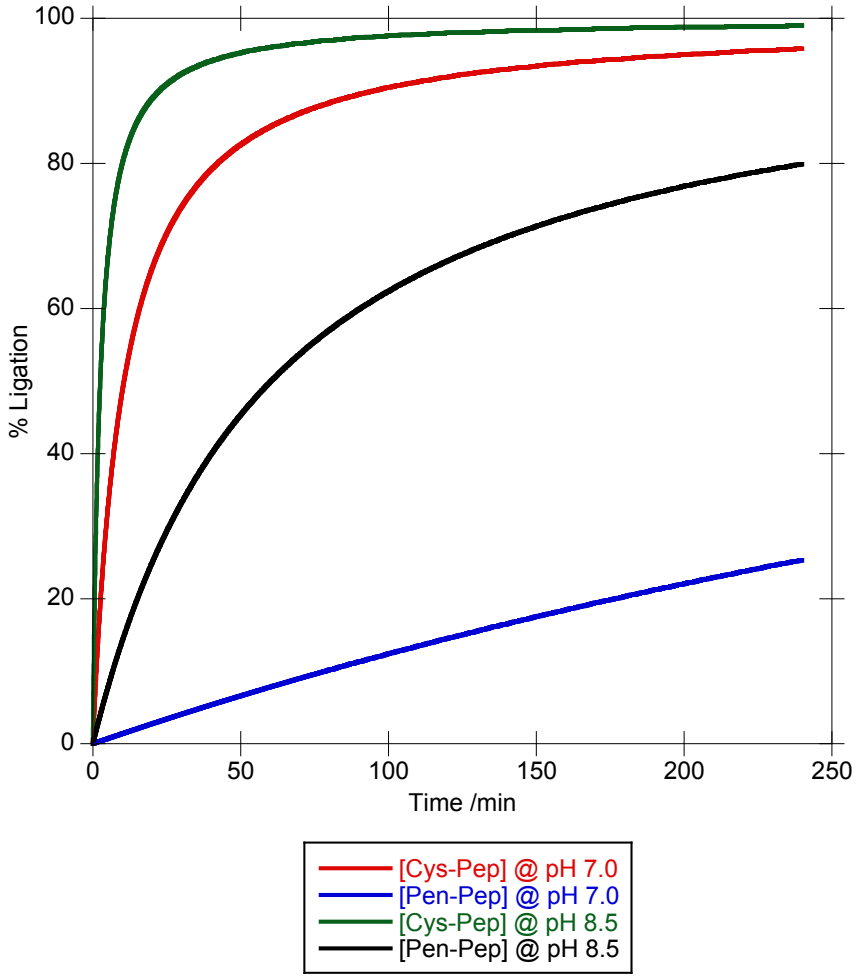

The predictions here are caveated by the above comparisons with experimental that indicate that the values for k_{anion} and k_{zwit} in Table 4.13 for H-Cys-Gly-Phe-NH_2 are underestimates and for H-Pen-Gly-Phe-NH_2 are overestimates. Nevertheless it is clear that the differences in percentage ligation for H-Cys-Gly-Phe-NH_2 vs. H-Pen-Gly-Phe-

NH_2 are greater at lower pHs, e.g. at 60 min in pH 7.0 Cys is at 85 % while Pen is at 8 % ligation, whereas at pH 8.0 Cys is at 96 % while Pen is at 50 % ligation.

Figure 4.41 suggests that lowering the pH can maximise the differences in reactivity between cysteine derivatives. The implications for a N-terminal KCL are twofold. First, that the more reactive ligation should take place at a low pH in order to prevent a mixture of ligation products from forming, and second, that after the first ligation is complete the second ligation can then be easily activated by a pH jump to the higher pH.

4.4 Conclusions

The acid dissociation constants K_A – K_D for a series of cysteine derivatives have been measured using UV-Vis spectrophotometry at 25 °C and ionic strength I = 0.3. The two dissociation constants for the thiol, K_A and K_D, have values in the range of pK_A (^+H_3N-R-SH ⇆ ^+H_3N-R-S^-) = 7.13 – 7.97 and pK_D (H_2N-R-SH ⇆ H_2N-R-S^-) = 8.96 – 9.49. The two dissociation constants for the ammonium, K_B and K_C, have values in the range of pK_B (^+H_3N-R-SH ⇆ H_2N-R-SH) = 6.35 – 7.01 and pK_C (^+H_3N-R-S^- ⇆ H_2N-R-S^-) = 8.27 – 8.60. There are clear differences in K_A – K_D values between the cysteine derivatives and justifications for the observed changes have been proposed based upon the alterations in structure between derivatives.

The free energy changes associated with the dissociation constants have been used to quantify the effect that various substituents (e.g. methyl groups and anionic carboxylates) have upon the stability of thiolate and ammonium groups.

The measurement of K_A – K_D values have also been used to determine the percentage of each of the four possible species (^+H_3N-R-SH, ^+H_3N-R-S^-, H_2N-R-SH and H_2N-R-S^-) in solution as a function of pH. At pH = 7.0, the typical conditions for NCL, the concentration of peptide in thiolate form is small, only 6 – 16 % depending upon the cysteine derivative.

Previously determined Brønsted relationships between the reactions of thiolate nucleophiles with various electrophiles have been used to estimate the nucleophilicities of the cysteine derivatives' two thiolate species, ^+H_3N-R-S^- and H_2N-R-S^- using the thiol K_A and K_D values. The predicted second order rate constants k_{zwit} and k_{anion} for the reaction between a thiolate nucleophile and a thioester have been used in conjunction with the concentration of both thiolate species to calculate how the differences in structure between cysteine derivatives might affect the rate of NCL. The possibility of N-terminal Kinetically Controlled Ligation has been explored and it is predicted based upon the k_{zwit}, k_{anion}, K_A and K_D values that adjusting the pH of the solution can be used to control which ligation reaction occurs.

4.5 Experimental

4.5.1 General

4.5.1.1 Instrumentation

UV-Vis Spectrophotometry: A Cary 100 UV-Vis spectrophotometer with a temperature regulated cuvette holder and attached heating unit was used to collect all absorbance spectra.

pH Measurement: A MeterLab^{TM} PHM 290 pH-Stat Controller equipped with a radiometer combination electrode filled with saturated KCl solution was used to measure pH.

Chromatography: Chromatography was performed with a Sunfire C18 column on a Perkin Elmer Series 200 HPLC Apparatus with Autosampler, Pump, UV-Vis Detector and Chromatography Interface.

Mass Spectrometry: Low resolution mass spectrometry was performed on a TQD mass spectrometer. High resolution mass spectrometry was performed on a Thermo-Finnigan LTQ FT mass spectrometer.

4.5.1.2 Materials

UV-Vis Spectrophotometry: *L*-Cysteine methyl ester, *L*-cysteine methyl ester dimer, *L*-penicillamine methyl ester and H-Cys-Gly-OH were purchased from Sigma Aldrich. *Tris*(2-carboxyethyl)phosphine (TCEP) was purchased from TCI UK. Volumetric 1 M sodium hydroxide and volumetric hydrochloric acid were purchased from Fisher Scientific UK. All other chemicals used were reagent grade and used without further purification. Prof. Steven Cobb donated (4*S*)-mercaptoproline methyl ester and Prof. Neil Cameron donated cysteine.

Peptide Synthesis: Rink amide resin, DMF, piperidine, *N*,*N*-Diisopropylethylamine, (benzotriazol-1-yloxy)-tripyrrolidinophosphonium hexafluorophosphate (PyBOP), trifluoroacetic acid, triisopropylsilane, Fmoc-Phe-OH, Fmoc-Gly-OH, Fmoc-Cys(Trt)-OH and Fmoc-Pen(Trt)-OH were all provided by the Cobb laboratory.

4.5.2 Determination of dissociation constants K_A – K_D for cysteine methyl ester

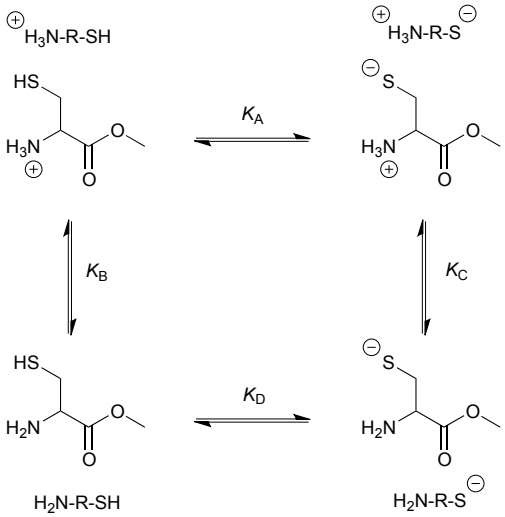

A 0.1 M stock solution of cysteine methyl ester was prepared from 85.76 mg (0.500 mmol) of cysteine methyl ester.HCl and 5.00 mL of deionised water. A series of HCl, H_3PO_4, KH_2PO_4, NH_4Cl, $KHCO_3$ and NaOH solutions with varying percentages of free base were prepared and maintained at a constant ionic strength I = 0.3 M (KCl or NaCl). A 0.1 M stock solution of TCEP was prepared using 2.86 mg (9.98×10^{-6} mol) and 100 μL of deionised water. Inorganic buffers were necessary as organic buffers absorb at the same wavelengths as the λ_{max} of the n to σ* transition on the thiolate (λ_{max} ~ 237 nm).

Absorbance spectra were measured with a Cary 100 UV-Vis spectrophotometer. The buffer solutions were added to 1.0 mL cuvettes and the cuvettes were placed in a temperature regulated cuvette holder of the UV-Vis spectrophotometer. The solutions were allowed to equilibrate to 25 °C prior to the recording of the absorbance spectrum over the wavelength range 200 – 300 nm (the UV-Vis spectrophotometer had been zeroed against air). 20 μL of 0.1 M TCEP solution was added to the cuvette give a 2.0 mM solution and the absorption spectrum of the TCEP and buffer solution was recorded. 2 μL of 0.1 M cysteine methyl ester stock solution was added to the cuvette to give a 0.2 mM solution and the absorption spectrum of the cysteine methyl ester was

recorded and the absorbance from the solution was manually subtracted in Figure 4.3. This process was repeated for every buffer solution.

The wavelength of maximum absorbance, λ_{max}, at each pH was identified. A single wavelength spectrum was then recorded at the appropriate λ_{max} for the pH of the buffer solution using an identical procedure as above (Figure 4.4). The largest value for A_{obs} at the single wavelength recorded was used to determine the acid dissociation constants $K_A - K_D$. The largest A_{obs} value was usually the initial A_{obs} except in the cases where there was significant oxidation of thiolates.

4.5.3 Determination of dissociation constants $K_A - K_D$ for penicillamine methyl ester

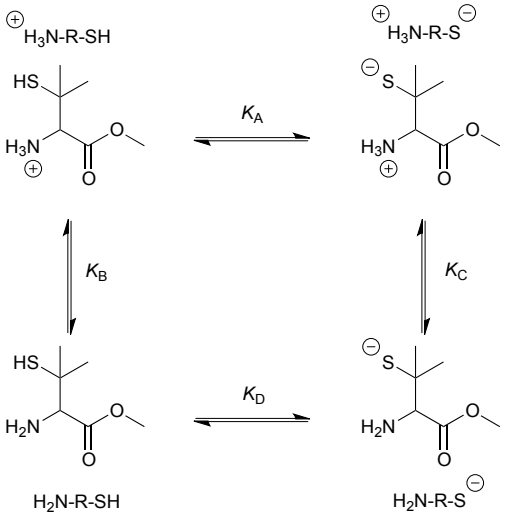

A 0.1 M solution of penicillamine methyl ester was prepared from 7.99 mg (4.00×10^{-5} M) of penicillamine methyl ester.HCl and 400 μL of deionised water. An identical procedure to that for cysteine methyl ester was used for determining the dissociation constants $K_A - K_D$ for penicillamine methyl ester.

4.5.4 Determination of dissociation constants K_A – K_D for the (4*S*)-mercaptoproline methyl ester

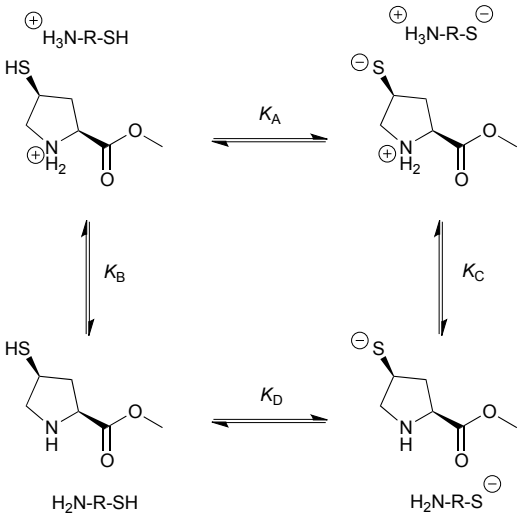

A 0.1 M solution of (4*S*)-mercaptoproline methyl ester was prepared from 7.91 mg (4.00×10^{-5} M) of (4*S*)-mercaptoproline methyl ester.HCl and 400 μL of deionised water. An identical procedure to that for cysteine methyl ester was used for determining the dissociation constants K_A – K_D for (4*S*)-mercaptoproline methyl ester.

4.5.5 Determination of dissociation constants K_A – K_D for the peptide H-Cys-Gly-Phe-NH_2

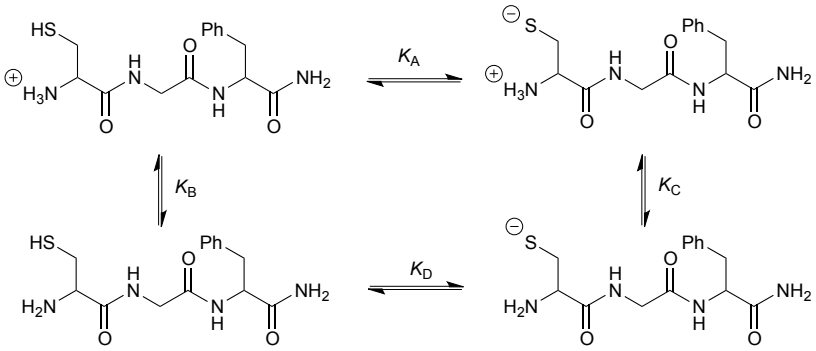

A 0.1 M solution of H-Cys-Gly-Phe-NH_2 was prepared from 3.24 mg (9.99×10^{-6} M) of H-Cys-Gly-Phe-NH_2 and 100 μL of deionised water. An identical procedure to that for cysteine methyl ester was used for determining the dissociation constants K_A – K_D for H-Cys-Gly-Phe-NH_2.

4.5.6 Determination of the dissociation constants $K_A - K_D$ for the peptide H-Pen-Gly-Phe-NH_2

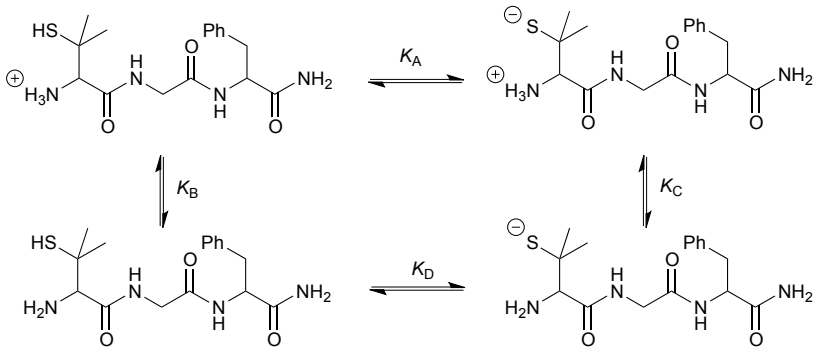

A 0.1 M solution of H-Pen-Gly-Phe-NH_2 was prepared from 3.52 mg (1.00×10^{-5} mol) of H-Pen-Gly-Phe-NH_2 and 100 μL of deionised water. An identical procedure to that for cysteine methyl ester was used for determining the dissociation constants $K_A - K_D$ for H-Pen-Gly-Phe-NH_2.

4.4.7 Determination of dissociation constants $K_A - K_D$ for cysteine

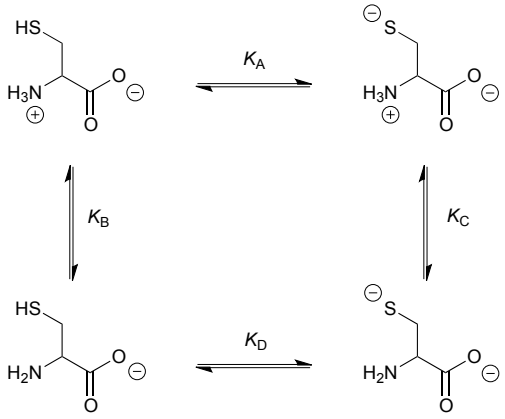

A 0.1 M solution of cysteine was prepared from 4.86 mg (4.00×10^{-5} M) of cysteine and 400 μL of deionised water. An identical procedure to that for cysteine methyl ester was used for determining the dissociation constants $K_A - K_D$ for cysteine.

4.5.8 Determination of molar extinction coefficient for cysteine methyl ester

A 0.1 M stock solution of cysteine methyl ester was prepared from 1.72 mg (1.00×10^{-5} mol) of cysteine methyl ester.HCl and 100 μL of deionised water, a 0.100 M solution of *tris*(2-carboxyethyl)phosphine (TCEP) was prepared from 2.87 mg (1.00×10^{-4} mol) of TCEP and 100 μL of deionised water and a 10 mL solution of 30 mM NaOH at ionic

strength I = 0.3 M (NaCl) was prepared from a 1.0 M volumetric NaOH standard solution.

As above, absorbance spectra between 200 – 300 nm were measured with a Cary 100 UV-Vis spectrophotometer thermostated at 25 °C. The background absorbance within the spectrophotometer was zeroed against air. 0.98 mL of the 30 mM NaOH solution was placed in 1.0 mL quartz cuvette and the absorbance spectrum of the solution was recorded. 20 μL of 0.1 M TCEP solution was added to give a 2.0 mM TCEP solution; the absorbance of the TCEP-containing solution was then determined. Different volume aliquots between 0.5 – 1.2 μL of the 0.1 M stock solution of cysteine methyl ester were added to the cuvette to give 5.0×10^{-5} – 1.2×10^{-4} M solution of cysteine methyl ester. The absorption spectrum of cysteine methyl ester was recorded and the absorbance from the 2.0 mM TCEP solution was manually subtracted (Figure 10).

The maximum absorbance (λ_{max} = 236) was plotted against concentration of cysteine methyl ester and the linear fit of the data gave the molar extinction coefficient (Figure 11 and Table 1).

4.5.9 Determination of molar extinction coefficient for penicillamine methyl ester

A 0.1 M stock solution of penicillamine methyl ester was prepared from 2.00 mg (1.00×10^{-5} mol) of penicillamine methyl ester.HCl and 100 μL of deionised water. The molar extinction coefficient was determined using the above method for cysteine methyl ester.

4.5.10 Determination of molar extinction coefficient for the (4*S*)-mercaptoproline methyl ester

A 0.1 M stock solution of (4*S*)-mercaptoproline methyl ester was prepared from 1.98 mg (1.00×10^{-5} mol) of (4*S*)-mercaptoproline methyl ester.HCl and 100 μL of deionised water. The molar extinction coefficient was determined using the above method for cysteine methyl ester.

4.5.11 Determination of molar extinction coefficient for cysteine

A 0.1 M stock solution of cysteine was prepared from 1.21 mg (1.00×10^{-5} mol) of cysteine and 100 μL of deionised water. The molar extinction coefficient was determined using the above method for cysteine methyl ester.

4.5.12 Synthesis of H-Cys-Gly-Phe-NH_2

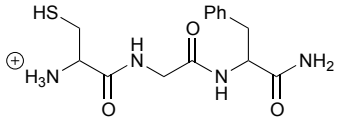

Solid Phase Peptide Synthesis (SPPS) was used to prepare H-Cys-Gly-Phe-NH_2. Rink amide (0.82 mmol/g) resin was weighted (0.28 g, 0.23 mmol) into a SPPS plastic vessel containing a Frit. DMF (3 mL) was added and the resin was left to swell for 1 h. The DMF was drained and 20% (v/v) piperidine/DMF solution (3 mL) was added and the flask was placed on a shaker for 5 min in order to activate the resin. The solution was drained and a further amount of 20% (v/v) piperidine/DMF solution (3 mL) was added and the flask placed on the shaker for 10 min and then drained and washed with DMF.

0.23 g (0.60 mmol) of Fmoc-Phe-OH, 0.31 g (0.60 mmol) of PyBOP and 0.21 mL (1.21 mmol) of *N*,*N*-diisopropylethylamine (DIPEA) dissolved in DMF (3 mL) was added to the resin and the flask placed on the shaker for 1 h. The solution was then drained and the resin washed 3 × with DMF (3 mL). This process was repeated to ensure all sites on the rink amide resin had Fmoc-Phe attached.

The Fmoc was deprotected by the addition of 20 % (v/v) piperidine/DMF solution (3 mL) and placed on shaker for 5 min. The solution was drained and a further amount of 20 % (v/v) piperidine/DMF solution (3 mL) was added and the flask placed on the shaker for 10 min and then drained and washed with DMF (3 mL).

0.18 g (0.61 mmol) of Fmoc-Gly-OH, 0.34 g (0.66 mmol) of PyBOP and 0.21 mL (1.21 mmol) of DIPEA dissolved in DMF (3 mL) was added to the resin in the flask and then placed on the shaker for 1 h. The solution was then drained and the resin washed 3 × with DMF (3 mL). This process was repeated to ensure all peptide chains had Fmoc-Gly attached.

The Fmoc was deprotected by the addition of 20 % (v/v) piperidine/DMF solution (3 mL) and placed on the shaker for 5 min. The solution was drained and a further amount

of 20 % (v/v) piperidine/DMF solution (3 mL) was added and the flask placed on the shaker for 10 min and then drained and washed with DMF (3 mL).

The resin was divided in two and half carried forward to prepare H-Cys-Gly-Phe-NH_2 and the other half to prepare H-Pen-Gly-Phe-NH_2.

0.06 g (0.11 mmol) of Fmoc-Cys(Trt)-OH, 0.18 g (0.34 mmol) of PyBOP and 0.10 mL (0.57 mmol) of DIPEA dissolved in DMF (3 mL) was added to the resin in the flask and then placed on the shaker for 1 h. The solution was then drained and the resin washed 3 × with DMF (3 mL). This process was repeated to ensure all peptide chains had Fmoc-Cys(Trt) attached.

The Fmoc-deprotection was achieved by the addition of 20 % (v/v) piperidine/DMF solution (3 mL) and the flask was placed on shaker for 5 min. The solution was drained and a further amount of 20 % (v/v) piperidine/DMF solution (3 mL) was added and the flask placed on the shaker for 10 min and then drained and washed with DMF (3 mL).

The resin was then shrunk by the addition of diethyl ether (3 mL) and shaking for 1 h. The diethyl ether was then drained and the resin washed 3 × with diethyl ether (3 mL).

The peptide was cleaved from the resin via the addition of 95 % (v/v) trifluoroacetic acid, 2.5 % water and 2.5 % triisopropylsilane (3 mL) and placing on the shaker for 4 h. The solution was removed under vacuum at 50 °C to leave the peptide as a yellow solid.

The peptide was purified using preparatory HPLC. The peptide was dissolved in a 9 : 1 H_2O : MeOH solution (1.5 mL). The peptide was isolated using a gradient of 95 : 5 H_2O : MeOH to 50 : 50 H_2O : MeOH with a flow rate of 3 mL min^{-1} on a Sunfire C18 column attached to a Waters HPLC instrument. The peptide eluted with a retention time of 7 – 10 min.

The solvent was removed via freeze-drying to give the isolated H-Cys-Gly-Phe-NH_2 peptide as a white solid (15 mg, 4.6 × 10^{-5} mol, 41 % yield) ***m/z*** (ES+): 276 ($[M–H]^+$, 100%); **HRMS** (ES+): $[M–H]^+$ $C_{14}H_{21}N_4O_3S$ requires 325.1334, found 325.1346 (Figure 4.42).

Figure 4.42 High resolution mass spectrum of H-Cys-Gly-Phe-NH_2.

Elemental Composition Report **Page 1**

Single Mass Analysis
Tolerance = 5.0 PPM / DBE: min = -1.5, max = 50.0
Element prediction: Off
Number of isotope peaks used for i-FIT = 3

Monoisotopic Mass, Even Electron Ions
569 formula(e) evaluated with 2 results within limits (up to 500 best isotopic matches for each mass)
Elements Used:
C: 0-60 H: 0-90 N: 0-6 O: 0-6 S: 0-1 154Gd: 0-1

Peter Quinn

30-Mar-2016
PQ_OM1 114 (0.980) Cm (114:119)

1: TOF MS ES+
1.47e+004

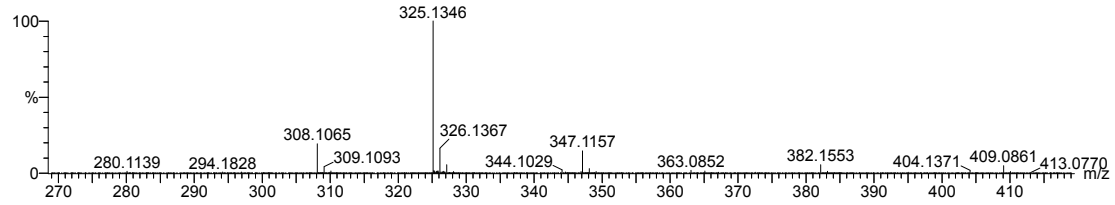

Minimum:				-1.5			
Maximum:		3.0	5.0	50.0			
Mass	Calc. Mass	mDa	PPM	DBE	i-FIT	i-FIT (Norm)	Formula
325.1346	325.1334	1.2	3.7	6.5	285.0	0.0	C14 H21 N4 O3 S
	325.1341	0.5	1.5	15.5	295.2	10.2	C22 H17 N2 O

4.5.13 Synthesis of H-Pen-Gly-Phe-NH_2

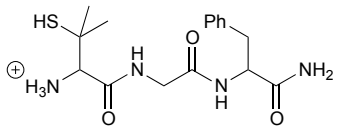

The H-Gly-Phe-NH-Resin was prepared as described for H-Cys-Gly-Phe-NH_2. 0.06 g (0.01 mmol) of Fmoc-Pen(Trt)-OH, 0.17 g (0.33 mmol) of PyBOP and 0.10 mL (0.57 mmol) of DIPEA dissolved in DMF (3 mL) was added to the resin in the flask and then placed on the shaker for 1 h. The solution was then drained and the resin washed 3 × with DMF (3 mL). This process was repeated to ensure all peptide chains had Fmoc-Pen(Trt) attached.

The Fmoc was deprotected by the addition of 20 % (v/v) piperidine/DMF solution (3 mL) and placed on shaker for 5 min. The solution was drained and a further amount of 20 % (v/v) piperidine/DMF solution (3 mL) was added and the flask placed on the shaker for 10 min and then drained and washed with DMF (3 mL).

The resin was then shrunk by the addition of diethyl ether (3 mL) and shaking for 1 h. The diethyl ether was drained and the resin washed 3 × with diethyl ether (3 mL). The peptide was then cleaved from the resin via the addition of 95 % (v/v) trifluoroacetic acid, 2.5 % water and 2.5 % triisopropylsilane (3 mL) and placing on the shaker for 4

h. The solution was then removed under vacuum at 50 °C to leave the peptide as a yellow solid.

The peptide was purified using preparatory HPLC. The peptide was dissolved in of 9 : 1 H_2O : MeOH solution (1.5 mL). The peptide was isolated using a gradient of 95 : 5 H_2O : MeOH to 50 : 50 H_2O : MeOH with a flow rate of 3 mL min^{-1} on a Sunfire C18 column attached to a Waters HPLC machine. The peptide eluted with a retention time of 7 – 10 min.

The solvent was removed via freeze-drying to give the isolated H-Pen-Gly-Phe-NH_2 peptide as a white solid (12 mg, 3.4×10^{-5} mol, 30 % yield) ***m/z*** (ES+): 353 ($[M–H]^+$, 100%); **HRMS** (ES+): $[M–H]^+$ $C_{16}H_{25}N_4O_3S$ requires 353.1647, found 353.1644 (Figure 4.43).

Figure 4.43 High resolution mass spectrum of H-Pen-Gly-Phe-NH_2.

Elemental Composition Report **Page 1**

Single Mass Analysis
Tolerance = 3.0 mDa / DBE: min = -1.5, max = 50.0
Element prediction: Off
Number of isotope peaks used for i-FIT = 3

Monoisotopic Mass, Even Electron Ions
4418 formula(e) evaluated with 17 results within limits (up to 50 best isotopic matches for each mass)
Elements Used:
C: 0-50 H: 0-100 N: 0-10 O: 0-10 P: 0-1 S: 0-3 96Ru: 0-1

Oliver Maguire
OMxPEPx002x007 175 (1.446) Cm (175:179)

1: TOF MS ES+
2.10e+004

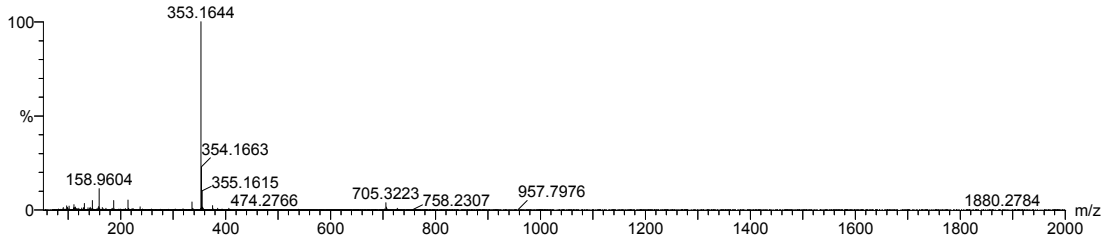

Mass	Calc. Mass	mDa	PPM	DBE	i-FIT	i-FIT (Norm)	Formula
Minimum:				-1.5			
Maximum:		3.0	5.0	50.0			
353.1644	353.1654	-1.0	-2.8	2.5	327.4	0.6	C9 H25 N10 O S2
	353.1637	0.7	2.0	2.5	328.7	1.9	C10 H26 N8 O2 P S
	353.1647	-0.3	-0.8	6.5	329.0	2.2	C16 H25 N4 O3 S
	353.1643	0.1	0.3	0.5	329.5	2.7	C16 H33 O2 S3
	353.1621	2.3	6.5	7.5	329.6	2.7	C12 H21 N10 O S
	353.1634	1.0	2.8	1.5	330.4	3.6	C15 H29 O7 S
	353.1616	2.8	7.9	1.5	330.9	4.1	C12 H29 N6 S3
	353.1664	-2.0	-5.7	1.5	331.1	4.3	C14 H30 N2 O4 P S
	353.1630	1.4	4.0	6.5	337.9	11.1	C17 H26 N2 O4 P
	353.1644	0.0	0.0	11.5	337.9	11.1	C18 H22 N6 P
	353.1654	-1.0	-2.8	15.5	338.0	11.1	C24 H21 N2 O
	353.1670	-2.6	-7.4	10.5	338.1	11.3	C22 H26 O2 P
	353.1672	-2.8	-7.9	2.5	338.3	11.5	C12 H25 N4 O8
	353.1646	-0.2	-0.6	3.5	338.4	11.6	C8 H21 N10 O6
	353.1632	1.2	3.4	-1.5	338.7	11.9	C7 H25 N6 O10
	353.1669	-2.5	-7.1	0.5	338.9	12.1	C15 H33 N2 O 96Ru
	353.1662	-1.8	-5.1	-1.5	339.1	12.3	C6 H26 N8 O7 P

4.6 References:

(178) Kent, S. B. H. *Chem Soc Rev* **2009**, *38*, 338.

(179) Kent, S. B. H. *Annu Rev Biochem* **1988**, *57*, 957.

(180) Merrifield, R. B. *J Am Chem Soc* **1963**, *85*, 2149.

(181) Dawson, P. E.; Muir, T. W.; Clark-Lewis, I.; Kent, S. B. H. *Science* **1994**, *266*, 776.

(182) Goodman, M.; Cai, W. B.; Smith, N. D. *J Pept Sci* **2003**, *9*, 594.

(183) Marshall, G. R. *J Peptide Sci* **2007**, *90*, 190

(184) Fischer, E.; Fourneau, E. *Ber Dtsch Chem Ges* **1901**, *34*, 2868.

(185) Fischer, E. *Ber Dtsch Chem Ges* **1907**, *40*, 1754.

(186) du Vigneaud, V.; Ressler, C.; Swan, J. M.; Roberts, C. W.; Katsoyannis, P. G.; Gordon, S. *J Am Chem Soc* **1953**, *75*, 4879.

(187) Yajima, H.; Fujii, N. *Biopolymers* **1981**, *20*, 1859.

(188) Hendrickson, J. B. *J Am Chem Soc* **1977**, *99*, 5439.

(189) Schnolzer, M.; Kent, S. B. H. *Science* **1992**, *256*, 221.

(190) Rose, K. *J Am Chem Soc* **1994**, *116*, 30.

(191) Dawson, P. E.; Churchill, M. J.; Ghadiri, M. R.; Kent, S. B. H. *J Am Chem Soc* **1997**, *119*, 4325.

(192) Johnson, E. C. B.; Kent, S. B. H. *J Am Chem Soc* **2006**, *128*, 6640.

(193) Hackeng, T. M.; Griffin, J. H.; Dawson, P. E. *Proc Natl Acad Sci USA* **1999**, *96*, 10068.

(194) Pollock, S. B.; Kent, S. B. H. *Chem Commun* **2011**, *47*, 2342.

(195) Nakamura, T.; Shigenaga, A.; Sato, K.; Tsuda, Y.; Sakamoto, K.; Otaka, A. *Chem Commun* **2014**, *50*, 58.

(196) Wang, C.; Guo, Q. X.; Fu, Y. *Chem-Asian J* **2011**, *6*, 1241.

(197) Danehy, J. P.; Noel, C. J. *J Am Chem Soc* **1960**, *82*, 2511.

(198) Friedman, M.; Cavins, J. F.; Wall, J. S. *J Am Chem Soc* **1965**, *87*, 3672.

(199) Castro, E. A.; Ureta, C. *J Org Chem* **1989**, *54*, 2153.

(200) Castro, E. A.; Ibanez, F.; Santos, J. G.; Ureta, C. *J Chem Soc Perk Trans 2* **1991**, 1919.

(201) Hupe, D. J.; Jencks, W. P. *J Am Chem Soc* **1977**, *99*, 451.

(202) Castro, E. A. *Chem Rev* **1999**, *99*, 3505.

(203) Douglas, K. T.; Yaggi, N. F.; Mervis, C. M. *J Chem Soc Perk Trans 2* **1981**, 171.

(204) Douglas, K. T.; Alborz, M. *J Chem Soc Chem Comm* **1981**, 551.

(205) Douglas, K. T. *Accounts Chem Res* **1986**, *19*, 186.

(206) Chen, J.; Wan, Q.; Yuan, Y.; Zhu, J. L.; Danishefsky, S. J. *Angew Chem Int Ed* **2008**, *47*, 8521.

(207) Canne, L. E.; Bark, S. J.; Kent, S. B. H. *J Am Chem Soc* **1996**, *118*, 5891.

(208) Botti, P.; Carrasco, M. R.; Kent, S. B. H. *Tetrahedron Lett* **2001**, *42*, 1831.

(209) Low, D. W.; Hill, M. G.; Carrasco, M. R.; Kent, S. B. H.; Botti, P. *Proc Natl Acad Sci USA* **2001**, *98*, 6554.

(210) Offer, J.; Dawson, P. E. *Org Lett* **2000**, *2*, 23.

(211) Marinzi, C.; Bark, S. J.; Offer, J.; Dawson, P. E. *Bioorgan Med Chem* **2001**, *9*, 2323.

(212) Kawakami, T.; Akaji, K.; Aimoto, S. *Org Lett* **2001**, *3*, 1403.

(213) Offer, J.; Boddy, C. N. C.; Dawson, P. E. *J Am Chem Soc* **2002**, *124*, 4642.

(214) Macmillan, D. *Angew Chem Int Ed* **2006**, *45*, 7668.

(215) Wu, B.; Chen, J. H.; Warren, J. D.; Chen, G.; Hua, Z. H.; Danishefsky, S. J. *Angew Chem Int Ed* **2006**, *45*, 4116.

(216) Ollivier, N.; Behr, J. B.; El-Mahdi, O.; Blanpain, A.; Melnyk, O. *Org Lett* **2005**, *7*, 2647.

(217) Yan, L. Z.; Dawson, P. E. *J Am Chem Soc* **2001**, *123*, 526.

(218) Pentelute, B. L.; Kent, S. B. H. *Org Lett* **2007**, *9*, 687.

(219) Wan, Q.; Danishefsky, S. J. *Angew Chem Int Ed* **2007**, *46*, 9248.

(220) Crich, D.; Banerjee, A. *J Am Chem Soc* **2007**, *129*, 10064.

(221) Haase, C.; Rohde, H.; Seitz, O. *Angew Chem Int Ed* **2008**, *47*, 6807.

(222) Kumar, K. S. A.; Haj-Yahya, M.; Olschewski, D.; Lashuel, H. A.; Brik, A. *Angew Chem Int Ed* **2009**, *48*, 8090.

(223) Yang, R. L.; Pasunooti, K. K.; Li, F. P.; Liu, X. W.; Liu, C. F. *J Am Chem Soc* **2009**, *131*, 13592.

(224) Harpaz, Z.; Siman, P.; Kumar, K. S. A.; Brik, A. *ChemBioChem* **2010**, *11*, 1232.

(225) Tan, Z. P.; Shang, S. Y.; Danishefsky, S. J. *Angew Chem Int Ed* **2010**, *49*, 9500.

(226) Chen, J.; Wang, P.; Zhu, J. L.; Wan, Q.; Danishefsky, S. J. *Tetrahedron* **2010**, *66*, 2277.

(227) Shang, S. Y.; Tan, Z. P.; Dong, S. W.; Danishefsky, S. J. *J Am Chem Soc* **2011**, *133*, 10784.

(228) Townsend, S. D.; Tan, Z. P.; Dong, S. W.; Shang, S. Y.; Brailsford, J. A.; Danishefsky, S. J. *J Am Chem Soc* **2012**, *134*, 3912.

(229) Siman, P.; Karthikeyan, S. V.; Brik, A. *Org Lett* **2012**, *14*, 1520.

(230) Malins, L. R.; Cergol, K. M.; Payne, R. J. *ChemBioChem* **2013**, *14*, 559.

(231) Thompson, R. E.; Chan, B.; Radom, L.; Jolliffe, K. A.; Payne, R. J. *Angew Chem Int Ed* **2013**, *52*, 9723.

(232) Bang, D.; Kent, S. B. H. *Angew Chem Int Ed* **2004**, *43*, 2534.

(233) Bang, D.; Pentelute, B. L.; Kent, S. B. H. *Angew Chem Int Ed* **2006**, *45*, 3985.

(234) Torbeev, V. Y.; Kent, S. B. H. *Angew Chem Int Ed* **2007**, *46*, 1667.

(235) Durek, T.; Torbeev, V. Y.; Kent, S. B. H. *Proc Natl Acad Sci USA* **2007**, *104*, 4846.

(236) Lee, J.; Kwon, Y.; Pentelute, B. L.; Bang, D. *Bioconjugate Chem* **2011**, *22*, 1645.

(237) Amyes, T. L.; Richard, J. P. *J Am Chem Soc* **1992**, *114*, 10297.

(238) Amyes, T. L.; Richard, J. P. *J Am Chem Soc* **1996**, *118*, 3129.

(239) Richard, J. P.; Williams, G.; O'Donoghue, A. C.; Amyes, T. L. *J Am Chem Soc* **2002**, *124*, 2957.

(240) Warren, J. D.; Miller, J. S.; Keding, S. J.; Danishefsky, S. J. *J Am Chem Soc* **2004**, *126*, 6576.

(241) Chen, J. H.; Warren, J. D.; Wu, B.; Chen, G.; Wan, Q.; Danishefsky, S. J. *Tetrahedron Lett* **2006**, *47*, 1969.

(242) Chen, G.; Warren, J. D.; Chen, J. H.; Wu, B.; Wan, Q.; Danishefsky, S. J. *J Am Chem Soc* **2006**, *128*, 7460.

(243) Botti, P.; Villain, M.; Manganiello, S.; Gaertner, H. *Org Lett* **2004**, *6*, 4861.

(244) Zheng, J. S.; Cui, H. K.; Fang, G. M.; Xi, W. X.; Liu, L. *ChemBioChem* **2010**, *11*, 511.

(245) Ohta, Y.; Itoh, S.; Shigenaga, A.; Shintaku, S.; Fujii, N.; Otaka, A. *Org Lett* **2006**, *8*, 467.

(246) Nagaike, F.; Onuma, Y.; Kanazawa, C.; Hojo, H.; Ueki, A.; Nakahara, Y.; Nakahara, Y. *Org Lett* **2006**, *8*, 4465.

(247) Kawakami, T.; Aimoto, S. *Tetrahedron Lett* **2007**, *48*, 1903.

(248) Hojo, H.; Onuma, Y.; Akimoto, Y.; Nakahara, Y.; Nakahara, Y. *Tetrahedron Lett* **2007**, *48*, 25.

(249) Ollivier, N.; Dheur, J.; Mhidia, R.; Blanpain, A.; Melnyk, O. *Org Lett* **2010**, *12*, 5238.

(250) Hou, W.; Zhang, X. H.; Li, F. P.; Liu, C. F. *Org Lett* **2011**, *13*, 386.

(251) Dheur, J.; Ollivier, N.; Vallin, A.; Melnyk, O. *J Org Chem* **2011**, *76*, 3194.

(252) Yang, R. L.; Hou, W.; Zhang, X. H.; Liu, C. F. *Org Lett* **2012**, *14*, 374.

(253) Tsuda, S.; Shigenaga, A.; Bando, K.; Otaka, A. *Org Lett* **2009**, *11*, 823.

(254) Ding, H.; Shigenaga, A.; Sato, K.; Morishita, K.; Otaka, A. *Org Lett* **2011**, *13*, 5588.

(255) Sato, K.; Shigenaga, A.; Tsuji, K.; Tsuda, S.; Sumikawa, Y.; Sakamoto, K.; Otaka, A. *ChemBioChem* **2011**, *12*, 1840.

(256) Sato, K.; Shigenaga, A.; Kitakaze, K.; Sakamoto, K.; Tsuji, D.; Itoh, K.; Otaka, A. *Angew Chem Int Ed* **2013**, *52*, 7855.

(257) Ollivier, N.; Vicogne, J.; Vallin, A.; Drobecq, H.; Desmet, R.; El Mahdi, O.; Leclercq, B.; Goormachtigh, G.; Fafeur, V.; Melnyk, O. *Angew Chem Int Ed* **2012**, *51*, 209.

(258) Raibaut, L.; Ollivier, N.; Melnyk, O. *Chem Soc Rev* **2012**, *41*, 7001.

(259) Benesch, R. E.; Benesch, R. *J Am Chem Soc* **1955**, *77*, 5877.

(260) Sardi, F.; Manta, B.; Portillo-Ledesma, S.; Knoops, B.; Comini, M. A.; Ferrer-Sueta, G. *Anal Biochem* **2013**, *435*, 74.

(261) Burns, J. A.; Butler, J. C.; Moran, J.; Whitesides, G. M. *J Org Chem* **1991**, *56*, 2648.

(262) Hall, H. K. *J Am Chem Soc* **1957**, *79*, 5441.

(263) Shoulders, M. D.; Raines, R. T. *Annu Rev Biochem* **2009**, *78*, 929.

(264) Bretscher, L. E.; Jenkins, C. L.; Taylor, K. M.; DeRider, M. L.; Raines, R. T. *J Am Chem Soc* **2001**, *123*, 777.

(265) Jenkins, C. L.; Bretscher, L. E.; Guzei, I. A.; Raines, R. T. *J Am Chem Soc* **2003**, *125*, 6422.

(266) Cadamuro, S. A.; Reichold, R.; Kusebauch, U.; Musiol, H. J.; Renner, C.; Tavan, P.; Moroder, L. *Angew Chem Int Ed* **2008**, *47*, 2143.

(267) Shoulders, M. D.; Kotch, F. W.; Choudhary, A.; Guzei, I. A.; Raines, R. T. *J Am Chem Soc* **2010**, *132*, 10857.

(268) Lesarri, A.; Cocinero, E. J.; Lopez, J. C.; Alonso, J. L. *J Am Chem Soc* **2005**, *127*, 2572.

(269) Yang, W.; Drueckhammer, D. G. *J Am Chem Soc* **2001**, *123*, 11004.

5 Conclusions and Future Work

5.1 Overview

This thesis has explored two different aspects of proton transfer in peptide systems: the carbon acidity of peptide systems and the acidity of cysteine derivatives used in native chemical ligation. Detailed studies of both kinetic and thermodynamic acidity have been used to advance an understanding of the fundamentals behind chemical reactivity and to develop a quantitative understanding of a widely employed chemical reaction.

5.2 Carbon acidity of Diketopiperazines and Triketopiperazines

The carbon acidity of α-carbonyl systems plays an essential role in a host of biochemical and synthetic reactions. The two cyclic peptide systems, diketopiperazines and triketopiperazines, studied within this thesis have been used to explore how a number of different fundamental aspects of chemical reactivity affect carbon acidity.

5.2.1 Carbon acidity of Diketopiperazines

Scheme 5.1: The range of DKP substrates utilised for H-D exchange experiments.

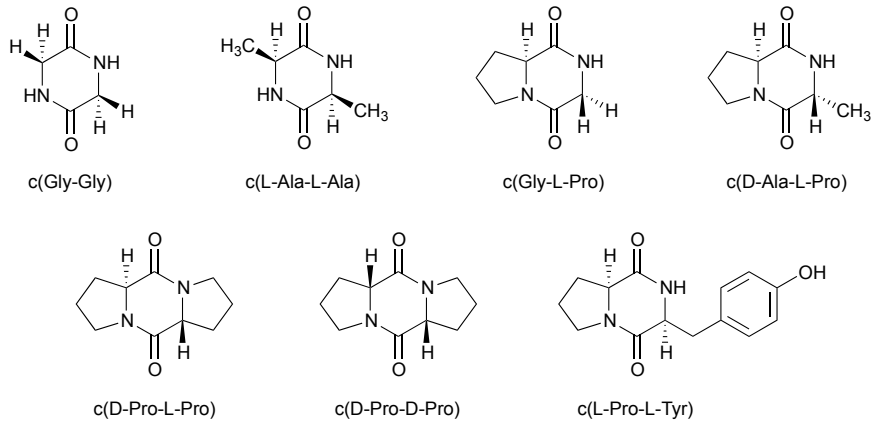

Hydrogen deuterium exchange reactions monitored by ^{1}H NMR spectroscopy have been used to measure the second order rate constants for the deuteroxide catalysed exchange, k_{DO} (M^{-1} s^{-1}), of the α-protons in a series of diketopiperazines at 25 ºC and ionic strength I = 1.00 (KCl) (Scheme 5.1). Kinetic acidities in the range of k_{DO} = 1.87 × 10^{-1} – 2.09 × 10^{-3} M^{-1} s^{-1} have been determined. The order of average kinetic acidity

for the amino acid residues studied was found to be Prolyl (1.12×10^{-1} M^{-1} s^{-1}) > Glycyl (3.42×10^{-2} M^{-1} s^{-1}) > Alanyl (4.71×10^{-3} M^{-1} s^{-1}) > Tyrosyl (1.02×10^{-3} M^{-1} s^{-1}).

The order of kinetic acidity Glycyl > Alanyl > Tyrosyl could be readily explained. The poor carbon acidity of the tyrosyl residue was attributed to inductive destabilisation from the aryl group and the hydrophobic phenol ring being forced out into bulk solvent upon formation of a tyrosyl enolate. The electron donating methyl group on the alanyl residue will destabilise the alanyl enolate relative to the glycyl residue. The absence of destabilising interactions and lack of steric hindrance surrounding the glycyl α-protons made them on average 7- and 34-fold more acidic than the alanyl and tyrosyl residue, respectively.

The two α-protons on the glycyl residue in c(Gly-L-Pro) were found to have a 3-fold difference in their k_{DO} values – with the α-proton spatially closest to the prolyl α-proton having a higher kinetic acidity. This indicated the existence of a stereoelectronic effect where one of the α-protons has a stronger overlap between the σ_{C-H} and the $\pi^*_{C=O}$ of the adjacent amide carbonyl, which could lower the barrier to enolate formation.

The prolyl α-proton was found to have a higher than expected kinetic acidity. This was also predominantly attributed to a stereoelectronic effect where the interaction between the conformation of the pyrrolidine ring and the DKP ring locks the prolyl α-proton into a favourable position for deprotonation.

The k_{DO} values for DKP α-protons are up to 144-fold more acidic than the α-protons of *N*-acyl-glycine amide, a linear peptide system that is akin to an uncyclised DKP. This difference in acidity is proposed to be a result of the aforementioned stereoelectronic effect and stabilising electrostatic interactions from within the DKP ring.

The hydrogen deuterium exchange in DKPs appears to proceed via a mechanism in which both deprotonation of the carbon acid by deuteroxide and solvent reorganisation to place a deuterium in the reactive position are partially rate limiting. The evidence for this is twofold with: i) an absence of buffer catalysed exchange – which eliminates the deprotonation of the carbon acid by deuteroxide from being solely rate limiting, and ii)

the magnitude of the k_{DO} values for DKPs being ~ 300-fold greater than the k_{DO} values for other similar α-carbonyl carbon acids which have rate limiting solvent reorganisation – which eliminates solvent reorganisation from being the solely rate limiting step. Consequently, an intermediate secondary solvent isotope effect of k_{DO} / k_{HO} = 2.0 was used to convert the k_{DO} values into second order rate constants for hydroxide catalysed deprotonation, k_{HO} (M^{-1} s^{-1}).

Estimates for the pK_as of the α-protons were interpolated from a Brønsted relationship for simple neutral α-carbonyl carbon acids and the DKP α-protons were found to have pK_as in the range of pK_a = 18.8 – 23.7. The pK_as of the residues studied are prolyl pK_a = 18.8 – 22.6 (with the majority of those prolyl residue studied pK_a ≤ 20.0), glycyl pK_a = 19.9 – 21.2, alanyl pK_a = 22.6 – 22.7 and tyrosyl pK_a = 23.7. These pK_as are ~ 3.3 p*K*a units lower than previous computational estimates for the pK_a of DKPs and demonstrate that the DKP enolates are ~ 4.4 kcal mol^{-1} more stable than previously thought.

The relevance of these results to enzyme catalysis has been explored. It is suggested that the role of stereoelectronic effects highlighted could help lower the barrier to enolate formation in proline racemases, which catalyse the epimerisation reaction of proline in the absence of a cofactor.

5.2.2 Carbon acidity of Triketopiperazines

Scheme 5.2: Glycyl TKP and Prolyl TKP studied.

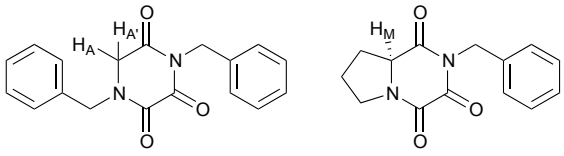

The carbon acidity of two triketopiperazine systems was also studied via hydrogen deuterium exchange experiments (Scheme 5.2). The second order rate constants for deuteroxide catalysed and buffer catalysed exchange, k_{DO} and k_{A-}, for the α-protons on a glycyl TKP were $k_{DO} = 5.09 \times 10^5$ M^{-1} s^{-1} and $k_{A-} = 1.61 \times 10^{-2}$ M^{-1} s^{-1} and were $k_{DO} = 8.99 \times 10^6$ M^{-1} s^{-1} and $k_{A-} = 1.21 \times 10^{-2}$ M^{-1} s^{-1} for a prolyl TKP at 25 ºC

and ionic strength $I = 0.06 – 0.20$ (KCl) in 60 : 40 D_2O : d3-MeCN. The greater kinetic acidity of the prolyl TKP α-proton relative to the glycyl TKP α-protons was attributed to both reactant destabilisation of the prolyl TKP by the interaction between the pyrrolidine ring and the TKP ring and to the stereoelectronic effect where the $\sigma_{C–H}$ and the $\pi^*_{C=O}$ orbitals are in a more optimal alignment for enolate formation in the prolyl TKP.

In order to compare the k_{DO} values to those determined for other carbon acids in 100 % D_2O solutions a 5.4-fold correction was applied to the k_{DO} values. This gave $k_{DO} = 9.43 \times 10^4$ M^{-1} s^{-1} for the glycyl TKP and $k_{DO} = 1.66 \times 10^6$ M^{-1} s^{-1} for the prolyl TKP in 100 % D_2O.

The effect of an additional carbonyl group on a DKP ring in the TKPs is an increase in the kinetic acidity, k_{DO}, of the α-protons of ~ 10^6-fold, although there were differences in ionic strength between the DKP and TKP experiments.

The mechanism for proton transfer in TKPs was found to be different to that of DKPs. Unlike in the DKP systems the TKPs displayed clear evidence for buffer catalysed exchange. This indicates that the rate determining step in the proton transfer is the initial deprotonation of the carbon acid. Thus, a secondary solvent isotope effect of $k_{DO} / k_{HO} = 1.46$ was used to convert the k_{DO} values into second order rate constants for hydroxide catalysed deprotonation, k_{HO}, as proton transfer is only partially complete at the transition state of the rate determining step.

The kinetic acidity, k_{HO} (M^{-1} s^{-1}), of the TKPs (glycyl TKP $k_{HO} = 6.40 \times 10^4$; prolyl TKP $k_{HO} = 1.14 \times 10^6$ M^{-1} s^{-1}) is similar to that of carbon acids that have aromatic enolates. An aromatic enolate structure is feasible for TKPs but would require considerable reorganisation of both charge and the solvent shell. The Principle of Non-perfect Synchronisation was invoked to explain that if significant early development of product stabilising aromaticity occurs at the transition state for deprotonation then this would considerably lower the barrier to deprotonation of the α-proton(s) despite the need for considerable solvent and charge reorganisation. Prior experimental and computational evidence from Bernasconi that indicated that the development of aromaticity occurs ahead of charge transfer was used to support the idea that TKPs

have aromatic enolates. This could account for the significantly enhanced kinetic acidity of the TKPs relative to both their DKP counterparts and other simple α-carbonyl carbon acids.

A Brønsted relationship for the kinetic acidity, k_{HO}, and pK_a of carbon acids with aromatic enolates was constructed for the first time and used to estimate the pK_a of the TKPs as glycyl TKP pK_a = 4.15 – 4.39 and prolyl TKP pK_a = - 3.35.

5.2.3 Future directions in Carbon acidity of DKPs and TKPs

Substantive experimental studies of the carbon acidity of DKP systems have been performed and further experimental studies are probably unnecessary. A computational examination of the DKPs may be worthwhile in order to probe the plausibility of the stereoelectronic effect via calculation of the orbital energies and the spatial orientation of the σ_{C-H} and the $\pi^*_{C=O}$ orbitals.

The full impact on the carbon acidity of the incorporation of additional of carbonyls could be assessed by determining the carbon acidity of the α-protons of a cyclic six-membered ring system with a single amide carbonyl (Scheme 5.3). This could provide experimental insight into the impact of electrostatic interactions within the DKP and TKP rings.

Scheme 5.3: Proposed hydrogen deuterium exchange experiment to evaluate the carbon acidity of the α-protons in a six-membered ring with a single carbonyl group.

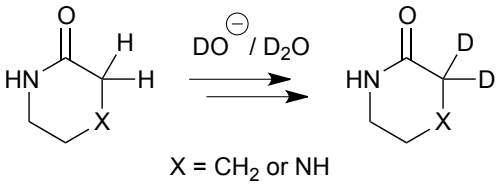

Further hydrogen deuterium exchange experiments are required to confirm the k_{DO} and pK_a estimations of the glycyl TKP. In addition, hydrogen deuterium exchange experiments could also be performed on a range of other TKPs which incorporate other

amino acid residues in order to probe the effect that altering the amino acid α-substituent has on k_{DO} in TKPs.

Further evidence is required to assess the plausibility of an aromatic enolate for the TKPs. A computational assessment of the stability of the aromatic enolate relative to the non-aromatic enolate resonance structure would be helpful. An attempt to observe the aromatic enolate via UV-Vis spectrophotometry was tried (data not shown). However, this failed because of a presumed ring opening reaction (with evidence of a ring-opened product found). Stopped flow spectrophotometry could potentially be used to observe the supposed aromatic TKP enolate before significant TKP ring hydrolysis occurs. Alternatively, a time resolved IR experiment could also be used to detect the aromatic enolate in solution – this setup is not available in our department but we do have a collaborator with access to one. The stopped flow UV-Vis and time resolved IR experiments could potentially also be used to determine the reverse rate of protonation of the TKPs. This would allow an alternative estimate for the pK_a to be made (See Chapter 1: Section 1.3.2.2).

In summary, the study of the carbon acidity of diketopiperazines and triketopiperazines has been used to develop a greater understanding of how a number of different fundamental aspects of chemical reactivity, such as stereoelectronic effects, principle of non-perfect synchronisation and aromaticity in a transition state, affect carbon acidity.

5.3 Cysteine Derivative Acidity and Native Chemical Ligation

The range of peptides that can now be prepared via total chemical synthesis has been substantially expanded by the invention of native chemical ligation. While there have been multiple developments in extending the applicability of NCL there has to date been little detailed quantitative examination of the reaction itself and the fundamental reactivity differences between various cysteine derivative containing peptides. The work undertaken in this thesis goes someway to addressing this gap in our understanding of the NCL reaction.

5.3.1 The acidity of the thiol and ammonium in Cysteine Derivatives

The examination of the acid dissociation constants here has highlighted the need to consider that for cysteine derivatives there are up to four different species present in solution depending upon the ionisation states of the thiol and ammonium group: the cationic $^{+}H_3N$-R-SH, the zwitterionic $^{+}H_3N$-R-S^{-}, the neutral H_2N-R-SH and the anionic H_2N-R-S^{-}.

Scheme 5.4: Cysteine derivatives examined in this study.

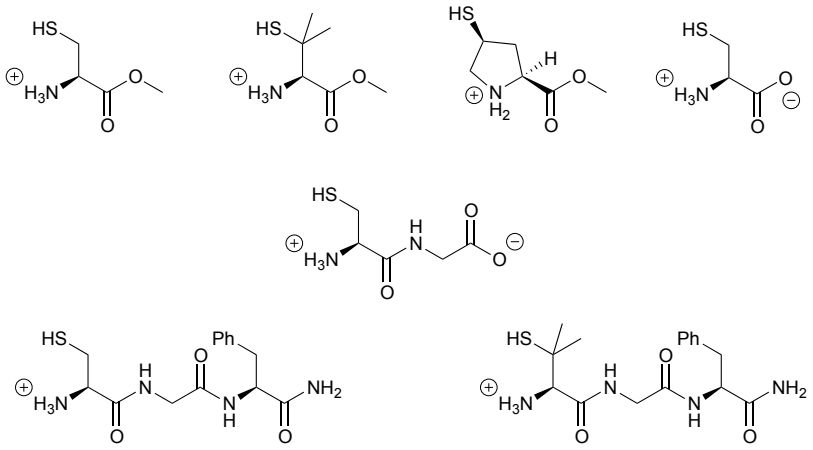

The acid dissociation constants K_A – K_D for a series of cysteine derivatives (Scheme 5.4) have been measured using UV-Vis spectrophotometry at 25 °C and ionic strength I = 0.3 (NaCl). The two dissociation constants for the thiol, K_A and K_D, have values in the range of pK_A ($^{+}H_3N$-R-SH ⇆ $^{+}H_3N$-R-S^{-}) = 7.13 – 7.97 and pK_D (H_2N-R-SH ⇆ H_2N-R-S^{-}) = 8.96 – 9.49. The two dissociation constants for the ammonium, K_B and K_C, have values in the range of pK_B ($^{+}H_3N$-R-SH ⇆ H_2N-R-SH) = 6.35 – 7.01 and pK_C ($^{+}H_3N$-R-S^{-} ⇆ H_2N-R-S^{-}) = 8.27 – 8.60. The overall order of the pKs for a cysteine derivative is pK_B < pK_A < pK_C < pK_D. This can be explained by a consideration of reactant and product stabilisation/destabilisation arising from the presence or absence of charge stabilisation via intramolecular electrostatic interactions and interactions with solvent.

There are clear differences in K_A – K_D values between the cysteine derivatives and justifications for the observed changes have been proposed based upon the alterations in structure between derivatives. For example, the thiol pK_D of penicillamine methyl ester is destabilised by 0.40 pK units relative the cysteine methyl ester via the presence

of the two methyl groups adjacent to the thiol. The thiol pK_A and pK_D of a (4*S*)-mercaptoproline methyl ester were unexpectedly lower than predicted. This was attributed to a stereoelectronic stabilisation of the thiolate by the amine/ammonium in the pyrrolidine ring. A comparison between the methyl ester and peptide systems studied showed that the p*K* values for both were broadly similar.

The free energy changes associated with the dissociation constants have been used to quantify the effect that various substituents (e.g. methyl groups and anionic carboxylates) have upon the stability of thiolate and ammonium groups. The free energy contribution to stability of the electrostatic interaction between the thiolate and the ammonium in the zwitterionic species was found to be between 7.59 – 11.70 kJ mol^{-1} depending upon the cysteine derivative. The inductive destabilisation of an adjacent methyl group upon a thiolate was quantified as being 1.14 kJ mol^{-1}. The effect of an anionic carboxylate C-terminus relative to a neutral ester terminus upon was found to stabilise the ammonium by 2.91 kJ mol^{-1} and to destabilise the thiolate by 1.48 – 4.79 kJ mol^{-1}. The effect that the proximity of a carboxylate has upon the stability of an ammonium and thiolate was also explored. The ammonium was found to be 8.33 – 8.79 kJ mol^{-1} more stable when the carboxylate was located one amino acid residue closer. Meanwhile, the thiolate was destabilised by 2.51 – 3.03 kJ mol^{-1} upon bringing the carboxylate one amino acid residue closer.

5.3.2 The application of Cysteine Derivative acidity to NCL

The K_A – K_D values determined in this study have also been used to shed light on a number of different aspects of NCL that have received scant attention in the literature to date.

The measurement of K_A – K_D values was used to determine the percentage of each of the four possible species (^+H_3N-R-SH, ^+H_3N-R-S^-, H_2N-R-SH and H_2N-R-S^-) in solution as a function of pH for each of the cysteine derivatives studied. At the typical NCL pH = 7.0, the order of the concentration of each species was H_2N-R-SH > ^+H_3N-R-SH > ^+H_3N-R-S^- >> H_2N-R-S^-. At pH = 7.0 the percentage of thiol in the active form thiolate form for NCL is small at only 6 – 16 % depending upon the cysteine derivative.

Previously determined Brønsted relationships between the reactions of thiolate nucleophiles with various electrophiles have been used in conjunction with the thiol K_A and K_D values to estimate the thiolate nucleophilicities of the cysteine derivatives, $^{+}H_3N$-R-S^{-} and H_2N-R-S^{-}. A study by Friedman into the reaction between amino acid thiolate nucleophiles and an acrylonitrile electrophile had determined two different Brønsted relationships: one for primary thiolates and another for tertiary thiolates. These relationships were used with the K_A and K_D values to estimate the differences in reactivity between the primary and tertiary thiolates of the cysteine derivatives in this study. Jencks had previously determined a Brønsted relationship for the reaction between primary thiolate nucleophiles and a thioester electrophile. This Brønsted relationship was then combined with the K_A and K_D values to estimate the second order rate constants for the native chemical ligations of the primary cysteine derivatives. Two different second order rate constants were predicted: k_{zwit}, for the reaction between a primary $^{+}H_3N$-R-S^{-} and a thioester, and k_{anion}, for the reaction between a primary H_2N-R-S^{-} and a thioester. Values for k_{zwit} and k_{anion} of tertiary cysteine derivatives were then estimated from the differences in reactivity determined by Friedman.

In the majority of NCL reactions with an aryl thiol additive the rate determining step in the mechanism is the transthioesterification reaction between the N-terminal cysteine and the C-terminal thioester. Therefore the k_{zwit} and k_{anion} values could be combined with the concentration of the thiolate species $^{+}H_3N$-R-S^{-} and H_2N-R-S^{-} at a given pH to predict the ligation rates of the cysteine derivatives. The predicted rates of ligation showed good agreement with experimental results.

The predicted second order rate constants k_{zwit} and k_{anion} showed that the changes in structure around the thiol in different cysteine derivatives could affect the rate of ligation. This opens up the possibility of undertaking N-terminal kinetically controlled ligations where a one-pot procedure could be used to prepare a peptide from several different peptide fragments without the need for purification of intermediate peptides. The importance of pH to control the kinetic ligations was shown – with the greatest disparities in ligation rates between different cysteine derivatives seen at low pHs.

This work has highlighted the versatility of pK_a measurements and how they can be used to not only determine the acidity of molecular systems but also may be used to

give a detailed understanding of the speciation of molecules and predict chemical reactivity.

5.3.3 Future Directions in Cysteine Derivative acidity and NCL

Looking forward, this study on the acidity of cysteine derivatives has opened the way to both a more detailed mechanistic understanding of native chemical ligation and how this can be harnessed to develop new ligation techniques.

The priority for the future of this project should be to undertake model kinetic studies on the native chemical ligations of N-terminal cysteine derivative peptides in order to quantify the second order rate constants k_{zwit} and k_{anion} experimentally. These reactions should use an HPLC set-up and monitor disappearance of the C-terminal thioester peptide and the N-terminal cysteine derivative peptide and the formation of ligated product via UV-Vis and mass spectrometry.

If and when optimal conditions are found, an N-terminal kinetically controlled native chemical ligation should be trialed to explore the feasibility of undertaking one-pot reactions to prepare a peptide from several peptide fragments whereby the order of ligations is controlled by the identity of the cysteine derivative at the N-terminal. It would be easiest to first demonstrate this with the two cysteine derivatives that are found to have the greatest disparity in ligation rates.

This study has focused on three of the eleven cysteine derivatives that have previously been used in native chemical ligation. There is a wider diversity of structure surrounding the thiol group in the other eight cysteine derivatives that has not been explored here. For example, an adjacent carboxylate in an aspartate thiol analogue or an amine/ammonium *beta* to the thiol in a lysine thiol analogue are expected to significantly affect the stability of the thiolate. UV-Vis spectrophotometric measurements of the $K_A - K_D$ values of these other cysteine derivatives should therefore been undertaken.

The ligation of peptides has also been performed with a series of selenium-based analogues of amino acids.[270] A subsequent deselenization reaction can then be used to

transform the selenium analogue into the natural amino acid residue. A more detailed understanding of the selenium-analogue ligations may be found by determining the acidity of the selenol group. Selenol groups are known to be a considerably more acidic than thiol groups [pK_a(Selenocysteine) = 5.4[271] vs. pK_a(cysteine) = 8.2; both of these values make the mistake of quoting a single pK_a for the selenol and thiol] and therefore a high proportion of selenol will be in selenolate form at a given pH than for the corresponding thiol. The effect of this upon the nucleophilicity of the selenolates may in part be found through the determination of the K_A – K_D values for selenium derivative peptide analogues.

It may be of benefit to determine the pK values of the cysteine derivatives via an alternative technique in order to confirm the validity of the K_A – K_D values in this work. Potentiometric titration is a possible candidate; however, the extraction of multiple K_A – K_D values from a titration curve is not a trivial process.

Finally, the plethora of bioconjugate techniques that have been develop in recent years could also benefit from detailed mechanistic investigations.[272-277] The physical organic techniques used hereinbefore are well placed to shed further light on these reactions.

5.4 Final Word

In conclusion, I hope this thesis has highlighted that physical organic chemistry has an important role to play in not just developing an understanding of chemical reactions at a fundamental, or perhaps, what is sometimes regarded as, an esoteric, level; but that a deep knowledge of underlying chemical reactivity can play a vital role in the development new methodologies in applied chemical research.

5.5 References

(270) Malins, L. R.; Mitchell, N. J.; Payne, R. J. *J Pept Sci* **2014**, *20*, 64.

(271) Arnold, A. P.; Tan, K. S.; Rabenstein, D. L. *Inorg Chem* **1986**, *25*, 2433.

(272) Borrmann, A.; van Hest, J. C. M. *Chem Sci* **2014**, *5*, 2123.

(273) Koniev, O.; Wagner, A. *Chem Soc Rev* **2015**, *44*, 5495.

(274) Monbaliu, J. C. M.; Katritzky, A. R. *Chem Commun* **2012**, *48*, 11601.

(275) Stephanopoulos, N.; Francis, M. B. *Nat Chem Biol* **2011**, *7*, 876.

(276) Tang, W.; Becker, M. L. *Chem Soc Rev* **2014**, *43*, 7013.

(277) Verzele, D.; Madder, A. *ChemBioChem* **2013**, *14*, 1032.

I Appendix I

I.1 Deuterium exchange of c(D-Pro-L-Pro)

I.1.1 c(D-Pro-L-Pro) Prolyl α-proton buffer catalysis

Table I.1: Reaction data and observed first order rate constants (k_{ex}) for the deuterium exchange of the prolyl α-protons H_A in c(D-Pro-L-Pro) (5.0 mM) monitored via $H_D/H_{D'}$ pyrrolidine protons on c(D-Pro-D-Pro) / c(L-Pro-L-Pro) in 70 % free base $KDCO_3$ (0.07 – 0.37 M, pD = 10.85 – 10.98) buffered D_2O solution, I = 1.0 (KCl) and 25 °C.

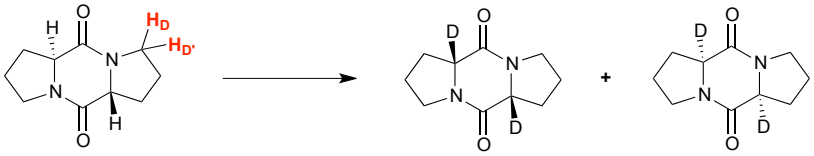

[$KDCO_3$] /M	[CO_3^{2-}] /M	[DO^-] /M	Time /s	f(s)	k_{ex} /s^{-1}
0.37	0.259	1.48×10^{-4}	1.06×10^{3}	1.00	1.39×10^{-5}
		(pD = 10.98)	7.38×10^{4}	0.43	
			8.85×10^{4}	0.24	
			1.68×10^{5}	0.11	
0.25	0.175	1.37×10^{-4}	1.06×10^{3}	1.00	1.32×10^{-5}
		(pD = 10.95)	5.02×10^{4}	0.53	
			8.91×10^{4}	0.32	
			1.43×10^{5}	0.16	
			2.62×10^{5}	0.04	
			3.07×10^{5}	0.03	
			5.66×10^{5}	0.00	
0.185	0.1295	1.29×10^{-4}	1.06×10^{3}	1.00	1.26×10^{-5}
		(pD = 10.92)	4.92×10^{4}	0.55	
			8.92×10^{4}	0.35	
			1.45×10^{5}	0.18	
			2.63×10^{5}	0.05	
			3.06×10^{5}	0.03	
			5.66×10^{5}	0.00	
0.13	0.091	1.22×10^{-4}	1.06×10^{3}	1.00	1.17×10^{-5}
		(pD = 10.90)	5.14×10^{4}	0.59	
			8.86×10^{4}	0.39	
			1.51×10^{5}	0.21	

			2.62×10^5	0.07	
			3.06×10^5	0.05	
			5.65×10^5	0.00	
0.07	0.049	1.09×10^{-4}	1.06×10^3	1.00	1.03×10^{-5}
		(p*D* = 10.85)	7.38×10^4	0.49	
			8.85×10^4	0.42	
			1.68×10^5	0.20	
			2.62×10^5	0.09	
			3.06×10^5	0.06	
			5.65×10^5	0.00	

Table I.2: Reaction data and observed first order rate constants (k_{ex}) for the deuterium exchange of the prolyl α-protons H_A in c(D-Pro-L-Pro) (5.0 mM) monitored via $H_4/H_{4'}$ pyrrolidine protons on c(D-Pro-D-Pro) / c(L-Pro-L-Pro) in 70 % free base $KDCO_3$ (0.07 – 0.37 M, p*D* = 10.85 – 10.98) buffered D_2O solution, *I* = 1.0 (KCl) and 25 °C.

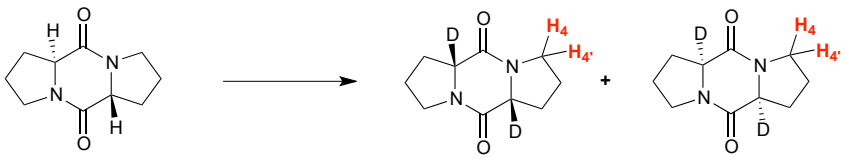

$[KDCO_3]$ /M	$[CO_3^{2-}]$ /M	$[DO^-]$ /M	Time /s	*f*(s)	k_{ex} /s^{-1}
0.37	0.259	1.48×10^{-4}	1.06×10^3	0.97	1.39×10^{-5}
		(p*D* = 10.98)	7.38×10^4	0.41	
			8.85×10^4	0.23	
			1.68×10^3	0.10	
			2.62×10^5	0.02	
			3.06×10^5	0.02	
			5.65×10^5	0.00	
0.25	0.175	1.37×10^{-4}	1.06×10^3	0.97	1.32×10^{-5}
		(p*D* = 10.95)	5.02×10^4	0.51	
			8.91×10^4	0.31	
			1.43×10^5	0.15	
			2.62×10^5	0.02	
			3.07×10^5	0.03	
			5.66×10^5	0.00	
0.185	0.1295	1.29×10^{-4}	1.06×10^3	0.97	1.26×10^{-5}
		(p*D* = 10.92)	4.92×10^4	0.54	
			8.92×10^4	0.32	
			1.45×10^5	0.16	
			2.63×10^5	0.04	

			3.06×10^5	0.02	
			5.66×10^5	0.00	
0.13	0.091	1.22×10^{-4}	1.06×10^3	0.97	1.17×10^{-5}
		(p*D* = 10.90)	5.14×10^4	0.56	
			8.86×10^4	0.36	
			1.51×10^5	0.15	
			2.62×10^5	0.01	
			3.06×10^5	0.07	
			5.65×10^5	0.00	
0.07	0.049	1.09×10^{-4}	1.06×10^3	0.97	1.03×10^{-5}
		(p*D* = 10.85)	7.38×10^4	0.47	
			8.85×10^4	0.41	
			1.68×10^5	0.17	
			2.62×10^5	0.05	
			3.06×10^5	0.03	
			5.65×10^5	0.00	

I.2 Deuterium exchange of c(D-Pro-D-Pro)

I.2.1 c(D-Pro-D-Pro) Prolyl α-proton

Table I.3: Reaction data and observed first order rate constants (k_{ex}) for the deuterium exchange of the prolyl α-protons H_A in c(D-Pro-D-Pro) (5.0 mM) in $KDCO_3$ (0.185 M, p*D* = 10.16 – 10.81) buffered D_2O solution, *I* = 1.0 (KCl) and 25 °C.

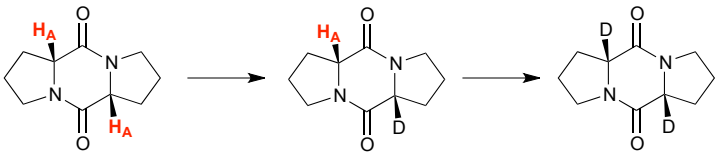

Experiment	Proton Chemical Shift /ppm	[DO^-] /M	Time /s	*f*(s)	k_{ex} /s^{-1}
70% fb	H_A	9.90×10^{-5}	1.19×10^3	1.00	8.80×10^{-7}
		(p*D* 10.81)	1.57×10^4	1.00	
			2.29×10^4	0.97	
			8.13×10^4	0.95	
			9.70×10^4	0.90	
			1.71×10^5	0.87	
			1.95×10^5	0.85	
			2.55×10^5	0.80	
			2.83×10^5	0.79	
			3.44×10^5	0.73	

			6.04×10^{5}	0.58	
50% fb	H_A	6.10×10^{-5}	1.19×10^{3}	1.00	5.67×10^{-7}
		(p*D* 10.60)	1.19×10^{4}	0.96	
			1.90×10^{4}	0.95	
			7.74×10^{4}	0.94	
			9.31×10^{4}	0.93	
			1.67×10^{5}	0.88	
			1.91×10^{5}	0.88	
			2.51×10^{5}	0.86	
			2.79×10^{5}	0.82	
			3.49×10^{5}	0.81	
			6.00×10^{5}	0.68	
			6.88×10^{5}	0.64	
			7.69×10^{5}	0.64	
			8.59×10^{5}	0.62	
			9.60×10^{5}	0.57	
			1.21×10^{6}	0.51	
			1.29×10^{6}	0.49	
			1.39×10^{6}	0.45	
			1.47×10^{6}	0.46	
			1.56×10^{6}	0.42	
			1.82×10^{6}	0.36	
			1.90×10^{6}	0.35	
			1.99×10^{6}	0.32	
			2.16×10^{6}	0.31	
			2.38×10^{6}	0.28	
20% fb	H_A	3.99×10^{-5}	1.19×10^{3}	1.00	4.13×10^{-7}
		(p*D* 10.41)	7.22×10^{4}	0.99	
			1.53×10^{5}	0.95	
			2.50×10^{5}	0.92	
			3.46×10^{5}	0.86	
			5.94×10^{5}	0.75	
			6.74×10^{5}	0.73	
			7.80×10^{5}	0.70	
			8.60×10^{5}	0.68	
			9.49×10^{5}	0.65	
			1.21×10^{6}	0.62	
			1.29×10^{6}	0.59	
			1.38×10^{6}	0.56	
			1.63×10^{6}	0.54	
			1.89×10^{6}	0.50	
22% fb	H_A	2.24×10^{-5}	1.19×10^{3}	1.00	2.60×10^{-7}
		(p*D* 10.16)	7.22×10^{4}	0.99	

		1.55×10^5	0.98
		2.62×10^5	0.93
		3.47×10^5	0.87
		5.94×10^5	0.82
		6.76×10^5	0.81
		7.80×10^5	0.80
		8.61×10^5	0.79
		1.21×10^6	0.75
		1.29×10^6	0.71
		1.38×10^6	0.69
		1.54×10^6	0.68
		1.81×10^6	0.66

I.3 Deuterium exchange of c(D-Ala-L-Pro)

I.3.1 c(D-Ala-L-Pro) Prolyl α-proton

Table I.4: Reaction data and observed first order rate constants (k_{ex}) for the deuterium exchange of the prolyl α-protons H_D in c(D-Ala-L-Pro) (5.0 mM) in $KDCO_3$ (0.185 M, p*D* = 10.12 – 10.98) buffered D_2O solution, *I* = 1.0 (KCl) and 25 °C.

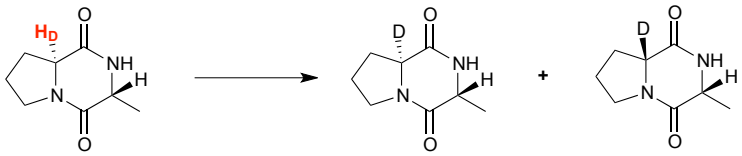

Experiment	Proton Chemical Shift /ppm	[DO^-] /M	Time /s	*f*(s)	k_{ex} /s^{-1}
70% 2nd	4.26 – 4.33	9.90×10^{-5}	5.40×10^2	1.00	8.57×10^{-6}
	H_D	(p*D* 10.81)	1.31×10^4	0.88	
			2.38×10^4	0.83	
			8.09×10^4	0.49	
			9.32×10^4	0.44	
			1.07×10^5	0.41	
			1.71×10^5	0.23	
			1.94×10^5	0.18	
			3.63×10^5	0.06	
			4.44×10^5	0.04	
60%	4.26 – 4.33	9.79×10^{-5}	1.06×10^3	1.00	9.46×10^{-6}
	H_D	(p*D* 10.80)	1.46×10^4	0.86	
			7.75×10^4	0.46	
			1.01×10^5	0.36	

			1.64×10^5	0.21	
			2.52×10^5	0.12	
			2.72×10^5	0.08	
			3.35×10^5	0.09	
			3.58×10^5	0.08	
			5.97×10^5	0.05	
			7.68×10^5	0.08	
50%fb	4.26 – 4.33	5.90×10^{-5}	1.07×10^3	1.00	4.62×10^{-6}
	H_D	(p*D* 10.58)	5.10×10^4	0.77	
			1.38×10^5	0.51	
			2.25×10^5	0.32	
			4.01×10^5	0.15	
			4.85×10^5	0.13	
			5.73×10^5	0.08	
			6.59×10^5	0.09	
			7.45×10^5	0.08	
			8.40×10^5	0.05	
			1.01×10^6	0.06	
			1.09×10^6	0.05	
			1.19×10^6	0.04	
20%	4.26 – 4.33	4.27×10^{-5}	1.06×10^3	1.00	3.42×10^{-6}
	H_D	(p*D* 10.44)	7.49×10^4	0.77	
			3.29×10^5	0.33	
			4.04×10^5	0.22	
			4.89×10^5	0.19	
			5.81×10^5	0.14	
			6.70×10^5	0.12	
			9.44×10^5	0.07	
			1.02×10^6	0.04	
			1.11×10^6	0.03	
			1.19×10^6	0.03	
35%	4.26 – 4.33	3.24×10^{-5}	1.06×10^3	1.00	2.70×10^{-6}
	H_D	(p*D* 10.32)	8.42×10^4	0.80	
			1.53×10^5	0.68	
			4.07×10^5	0.34	
			4.89×10^5	0.24	
			5.73×10^5	0.19	
			6.65×10^5	0.16	
			7.51×10^5	0.14	
			1.02×10^6	0.08	
			1.10×10^6	0.09	
			1.18×10^6	0.03	
			1.27×10^6	0.08	

22%fb	4.26 – 4.33	2.04×10^{-5}	1.19×10^{3}	1.00	1.59×10^{-6}
	H_D	(p*D* 10.12)	1.60×10^{4}	0.98	
			1.01×10^{5}	0.87	
			1.57×10^{5}	0.80	
			2.44×10^{5}	0.68	
			3.30×10^{5}	0.57	
			5.91×10^{5}	0.38	
			6.77×10^{5}	0.33	
			8.50×10^{5}	0.26	
			9.35×10^{5}	0.20	
			1.19×10^{6}	0.15	
			1.29×10^{6}	0.13	
			1.37×10^{6}	0.12	
			1.46×10^{6}	0.10	
			1.54×10^{6}	0.09	
			1.81×10^{6}	0.08	
			1.89×10^{6}	0.09	
			1.98×10^{6}	0.09	

Table I.5: Reaction data and observed first order rate constants (k_{ex}) for the deuterium exchange of the prolyl α-protons H_D in c(D-Ala-L-Pro) (5.0 mM) monitored via H_1 methyl protons on c(D-Ala-D-Pro) in $KDCO_3$ (0.185 M, p*D* = 10.12 – 10.98) buffered D_2O solution, *I* = 1.0 (KCl) and 25 °C.

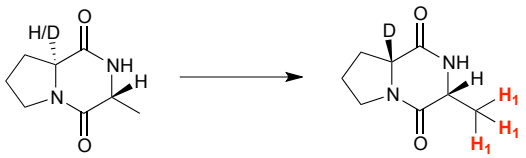

Experiment	Proton Chemical Shift /ppm	[DO^-] /M	Time /s	*f*(s)	k_{ex} /s^{-1}
70% 2nd	1.27 – 1.31	9.90×10^{-5}	5.40×10^{2}	1.00	1.07×10^{-5}
	H_1	(p*D* 10.81)	1.31×10^{4}	0.86	
			2.38×10^{4}	0.75	
			8.09×10^{4}	0.43	
			9.32×10^{4}	0.39	
			1.07×10^{5}	0.32	
			1.71×10^{5}	0.15	
			1.94×10^{5}	0.13	
			3.63×10^{5}	0.01	
			4.44×10^{5}	0.00	
60%	1.27 – 1.31	9.79×10^{-5}	1.06×10^{3}	1.00	1.24×10^{-5}
	H_1	(p*D* 10.80)	1.46×10^{4}	0.82	

			7.75×10^{4}	0.38	
			1.01×10^{5}	0.29	
			1.64×10^{5}	0.14	
			2.52×10^{5}	0.03	
			2.72×10^{5}	0.02	
			3.35×10^{5}	0.00	
50%fb	1.27 – 1.31	5.90×10^{-5}	1.07×10^{3}	1.00	6.26×10^{-6}
	H_1	(pD 10.58)	5.10×10^{4}	0.71	
			1.38×10^{5}	0.44	
			2.25×10^{5}	0.25	
			4.01×10^{5}	0.08	
			4.85×10^{5}	0.02	
			5.73×10^{5}	0.00	
			6.59×10^{5}	0.00	
			7.45×10^{5}	0.01	
			8.40×10^{5}	-0.02	
			1.01×10^{6}	0.02	
			1.09×10^{6}	0.03	
			1.19×10^{6}	0.04	
20%	1.27 – 1.31	4.27×10^{-5}	1.06×10^{3}	1.00	4.37×10^{-6}
	H_1	(pD 10.44)	7.49×10^{4}	0.71	
			3.29×10^{5}	0.24	
			4.04×10^{5}	0.18	
			4.89×10^{5}	0.11	
			5.81×10^{5}	0.08	
			6.70×10^{5}	0.04	
			9.44×10^{5}	0.02	
			1.02×10^{6}	0.01	
			1.11×10^{6}	0.02	
			1.19×10^{6}	0.00	
35%	1.27 – 1.31	3.24×10^{-5}	1.06×10^{3}	1.00	3.60×10^{-6}
	H_1	(pD 10.32)	8.42×10^{4}	0.72	
			1.53×10^{5}	0.58	
			4.07×10^{5}	0.23	
			4.89×10^{5}	0.19	
			5.73×10^{5}	0.13	
			6.65×10^{5}	0.09	
			7.51×10^{5}	0.05	
			1.02×10^{6}	0.04	
			1.10×10^{6}	0.02	
			1.18×10^{6}	0.01	
			1.27×10^{6}	0.00	

22%fb	1.27 – 1.31	2.04×10^{-5}	1.19×10^{3}	1.00	2.23×10^{-6}
	H_1	(p*D* 10.12)	1.60×10^{4}	0.94	
			1.01×10^{5}	0.76	
			1.57×10^{5}	0.66	
			2.44×10^{5}	0.58	
			3.30×10^{5}	0.48	
			5.91×10^{5}	0.28	
			6.77×10^{5}	0.23	
			8.50×10^{5}	0.14	
			9.35×10^{5}	0.16	
			1.19×10^{6}	0.07	
			1.29×10^{6}	0.07	
			1.37×10^{6}	0.06	
			1.46×10^{6}	0.04	
			1.54×10^{6}	0.03	
			1.81×10^{6}	0.01	
			1.89×10^{6}	0.03	
			1.98×10^{6}	0.00	

I.3.2 c(D-Ala-L-Pro) Prolyl α-proton buffer catalysis

Table I.6: Reaction data and observed first order rate constants (k_{ex}) for the deuterium exchange of the prolyl α-protons H_D in c(D-Ala-L-Pro) (5.0 mM) in 70 % free base $KDCO_3$ (0.07 – 0.37 M, p*D* = 10.85 – 10.98) buffered D_2O solutions, I = 1.0 (KCl) and 25 °C.

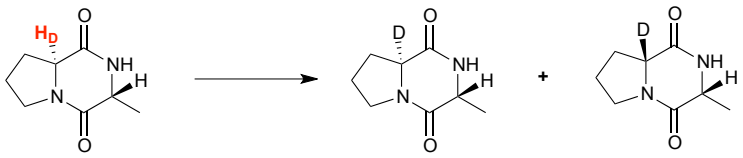

$[KDCO_3]$ /M	$[CO_3^{2-}]$ /M	$[DO^-]$ /M	Time /s	*f*(s)	k_{ex} /s^{-1}
0.37	0.259	1.48×10^{-4}	1.06×10^{3}	1.00	1.35×10^{-5}
		(p*D* 10.98)	2.43×10^{4}	0.72	
			8.10×10^{4}	0.33	
			1.11×10^{5}	0.23	
			2.68×10^{5}	0.04	
			3.41×10^{5}	0.00	
0.25	0.175	1.37×10^{-4}	1.06×10^{3}	1.00	1.23×10^{-5}
		(p*D* 10.95)	2.01×10^{4}	0.78	
			7.29×10^{4}	0.38	
			1.03×10^{5}	0.28	
			2.60×10^{5}	0.05	
			3.33×10^{5}	0.06	

			3.67×10^5	0.10	
			4.43×10^5	0.05	
			5.19×10^5	0.05	
			6.07×10^5	0.08	
			6.91×10^5	0.04	
			8.68×10^5	0.06	
0.185	0.1295	1.29×10^{-4}	1.06×10^3	1.00	9.68×10^{-6}
		(p*D* 10.92)	2.44×10^4	0.77	
			9.00×10^4	0.42	
			1.20×10^5	0.30	
			2.77×10^5	0.08	
			3.57×10^5	0.06	
			3.84×10^5	0.04	
			5.19×10^5	0.04	
			6.30×10^5	0.05	
			7.09×10^5	0.03	
			8.86×10^5	0.04	
0.13	0.091	1.22×10^{-4}	1.06×10^3	1.00	9.79×10^{-6}
		(p*D* 10.90)	2.30×10^4	0.81	
			8.33×10^4	0.41	
			1.12×10^5	0.32	
			2.69×10^5	0.10	
			3.49×10^5	0.08	
			4.22×10^5	0.03	
			5.11×10^5	0.04	
			6.28×10^5	0.06	
			7.01×10^5	0.04	
			8.77×10^5	0.04	
0.07	0.049	1.09×10^{-4}	1.06×10^3	1.00	8.94×10^{-6}
		(p*D* 10.85)	1.89×10^4	0.84	
			7.94×10^4	0.48	
			1.06×10^5	0.39	
			2.62×10^5	0.11	
			3.58×10^5	0.05	
			4.16×10^5	0.03	
			5.05×10^5	0.02	
			6.23×10^5	0.02	
			6.96×10^5	0.04	
			8.71×10^5	0.02	

Table I.7: Reaction data and observed first order rate constants (k_{ex}) for the deuterium exchange of the prolyl α-protons H_D in c(D-Ala-L-Pro) (5.0 mM) in 20 % free base $KDCO_3$ (0.07 – 0.37 M, p*D* = 10.59 – 10.66) buffered D_2O solutions, I = 1.0 (KCl) and 25 °C.

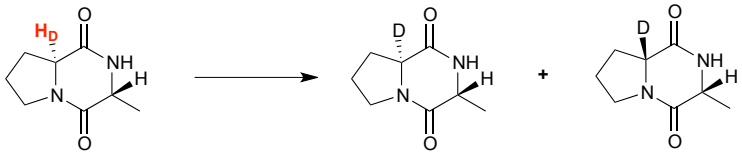

[$KDCO_3$] /M	[CO_3^{2-}] /M	[DO^-] /M	Time /s	*f*(s)	k_{ex} /s^{-1}
0.37	0.074	7.01×10^{-5}	1.06×10^{3}	1.00	6.19×10^{-6}
		(p*D* 10.66)	7.13×10^{4}	0.63	
			1.57×10^{5}	0.38	
			2.41×10^{5}	0.22	
			3.28×10^{5}	0.14	
			6.75×10^{5}	0.04	
			7.62×10^{5}	0.05	
			8.48×10^{5}	0.05	
0.25	0.05	6.85×10^{-5}	1.06×10^{3}	1.00	5.67×10^{-6}
		(p*D* 10.65)	7.11×10^{4}	0.67	
			1.56×10^{5}	0.40	
			2.41×10^{5}	0.24	
			3.28×10^{5}	0.16	
			6.94×10^{5}	0.04	
			7.62×10^{5}	0.05	
			8.50×10^{5}	0.06	
0.185	0.037	6.25×10^{-5}	1.06×10^{3}	1.00	5.25×10^{-6}
		(p*D* 10.61)	7.10×10^{4}	0.67	
			1.59×10^{5}	0.44	
			2.41×10^{5}	0.26	
			3.28×10^{5}	0.18	
			6.94×10^{5}	0.05	
			7.64×10^{5}	0.06	
			8.50×10^{5}	0.05	
0.13	0.026	6.25×10^{-5}	1.06×10^{3}	1.00	5.39×10^{-6}
		(p*D* 10.61)	7.10×10^{4}	0.67	
			1.62×10^{5}	0.41	
			2.42×10^{5}	0.27	
			3.28×10^{5}	0.16	
			6.94×10^{5}	0.06	
			7.65×10^{5}	0.06	
			8.50×10^{5}	0.05	

0.07	0.014	5.97×10^{-5}	1.06×10^{3}	1.00	4.94×10^{-6}
		(p*D* 10.59)	7.02×10^{4}	0.70	
			1.60×10^{5}	0.44	
			2.39×10^{5}	0.30	
			3.25×10^{5}	0.20	
			6.91×10^{5}	0.05	
			7.62×10^{5}	0.05	
			8.49×10^{5}	0.06	

Table I.8: Reaction data and observed first order rate constants (k_{ex}) for the deuterium exchange of the prolyl α-protons H_D in c(D-Ala-L-Pro) (5.0 mM) monitored via H_1 methyl protons on c(D-Ala-D-Pro) in 70 % free base $KDCO_3$ (0.07 – 0.37 M, p*D* = 10.85 – 10.98) buffered D_2O solution, I = 1.0 (KCl) and 25 °C.

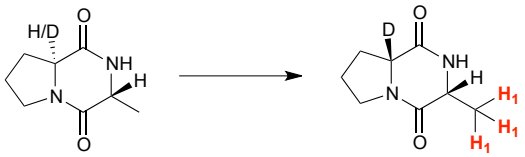

$[KDCO_3]$ /M	$[CO_3^{2-}]$ /M	$[DO^-]$ /M	Time /s	*f*(s)	k_{ex} /s^{-1}
0.37	0.259	1.48×10^{-4}	1.06×10^{3}	1.00	1.69×10^{-5}
		(p*D* 10.98)	2.43×10^{4}	0.64	
			8.10×10^{4}	0.27	
			1.11×10^{5}	0.15	
			2.68×10^{5}	0.00	
0.25	0.175	1.37×10^{-4}	1.06×10^{3}	1.00	1.43×10^{-5}
		(p*D* 10.95)	2.01×10^{4}	0.72	
			7.29×10^{4}	0.37	
			1.03×10^{5}	0.23	
			2.60×10^{5}	0.00	
0.185	0.1295	1.29×10^{-4}	1.06×10^{3}	1.00	1.22×10^{-5}
		(p*D* 10.92)	2.44×10^{4}	0.72	
			9.00×10^{4}	0.34	
			1.20×10^{5}	0.25	
			2.77×10^{5}	0.01	
			3.57×10^{5}	0.02	
			3.84×10^{5}	0.00	
0.13	0.091	1.22×10^{-4}	1.06×10^{3}	1.00	1.18×10^{-5}
		(p*D* 10.90)	2.30×10^{4}	0.74	
			8.33×10^{4}	0.38	

			1.12×10^5	0.28	
			2.69×10^5	0.03	
			3.49×10^5	0.00	
			4.22×10^5	0.00	
0.07	0.049	1.09×10^{-4}	1.06×10^3	1.00	1.09×10^{-5}
		(p*D* 10.85)	1.89×10^4	0.81	
			7.94×10^4	0.43	
			1.06×10^5	0.33	
			2.62×10^5	0.04	
			3.58×10^5	0.01	
			4.16×10^5	0.00	
			5.05×10^5	0.00	

Table I.9: Reaction data and observed first order rate constants (k_{ex}) for the deuterium exchange of the prolyl α-protons H_D in c(D-Ala-L-Pro) (5.0 mM) monitored via H_1 methyl protons on c(D-Ala-D-Pro) in 20 % free base $KDCO_3$ (0.07 – 0.37 M, p*D* = 10.59 – 10.66) buffered D_2O solution, I = 1.0 (KCl) and 25 °C.

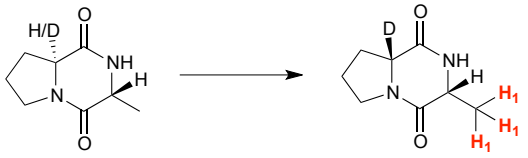

$[KDCO_3]$ /M	$[CO_3^{2-}]$ /M	$[DO^-]$ /M	Time /s	*f*(s)	k_{ex} /s^{-1}
0.37	0.074	7.01×10^{-5}	1.06×10^3	1.00	7.66×10^{-6}
		(p*D* 10.66)	7.13×10^4	0.57	
			1.57×10^5	0.31	
			2.41×10^5	0.15	
			3.28×10^5	0.08	
			6.75×10^5	0.00	
0.25	0.05	6.85×10^{-5}	1.06×10^3	1.00	7.20×10^{-6}
		(p*D* 10.65)	7.11×10^4	0.58	
			1.56×10^5	0.34	
			2.41×10^5	0.18	
			3.28×10^5	0.09	
			6.94×10^5	0.01	
			7.62×10^5	0.00	
0.185	0.037	6.25×10^{-5}	1.06×10^3	1.00	6.90×10^{-6}
		(p*D* 10.61)	7.10×10^4	0.57	
			1.59×10^5	0.36	
			2.41×10^5	0.20	

			3.28×10^5	0.11	
			6.94×10^5	0.02	
			7.64×10^5	0.01	
			8.50×10^5	0.00	
0.13	0.026	6.25×10^{-5}	1.06×10^3	1.00	6.35×10^{-6}
		(p*D* 10.61)	7.10×10^4	0.62	
			1.62×10^5	0.35	
			2.42×10^5	0.22	
			3.28×10^5	0.15	
			6.94×10^5	0.00	
0.07	0.014	5.97×10^{-5}	1.06×10^3	1.00	6.10×10^{-6}
		(p*D* 10.59)	7.02×10^4	0.64	
			1.60×10^5	0.38	
			2.39×10^5	0.23	
			3.25×10^5	0.14	
			6.91×10^5	0.02	
			7.62×10^5	0.01	
			8.49×10^5	0.00	

I.3.3 c(D-Ala-L-Pro) Alanyl α-proton

Table I.10: Reaction data and observed first order rate constants (k_{ex}) for the deuterium exchange of the alanyl α-protons H_B in c(D-Ala-L-Pro) (5.0 mM) in $KDCO_3$ (0.185 M, p*D* = 10.12 – 10.98) buffered D_2O solution, *I* = 1.0 (KCl) and 25 °C.

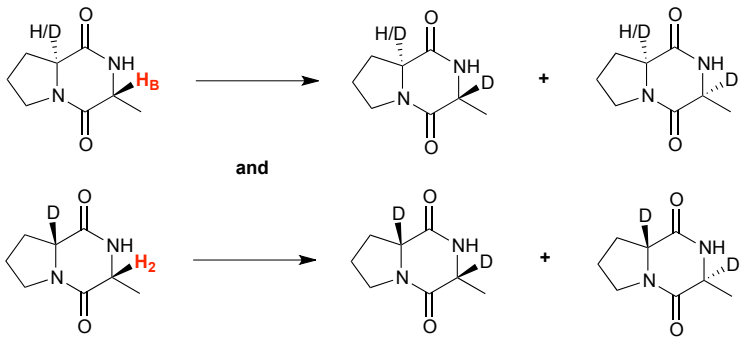

Experiment	Proton Chemical Shift /ppm	[DO^-] /M	Time /s	*f*(s)	k_{ex} /s^{-1}
70% fb BC	3.92–4.00	1.48×10^{-4}	1.06×10^3	1.00	7.81×10^{-7}
	+ 4.18–4.24	(p*D* 10.98)	2.43×10^4	0.80	
	H_B+H_2		8.10×10^4	0.51	
			1.11×10^5	0.44	
			2.68×10^5	0.27	
			3.41×10^5	0.23	

			3.73×10^5	0.22	
			4.46×10^5	0.20	
			5.19×10^5	0.20	
			6.15×10^5	0.18	
			6.87×10^5	0.17	
			8.76×10^5	0.16	
70% 2nd	3.92–4.00	9.90×10^{-5}	5.40×10^2	1.00	4.94×10^{-7}
	+ 4.18–4.24	(p*D* 10.81)	1.31×10^4	0.86	
	H_B+H_2		2.38×10^4	0.75	
			8.09×10^4	0.43	
			9.32×10^4	0.38	
			1.07×10^5	0.33	
			1.71×10^5	0.13	
			1.94×10^5	0.16	
			3.63×10^5	0.08	
			4.44×10^5	0.05	
			5.14×10^5	0.06	
			6.02×10^5	0.00	
60%	3.92–4.00	9.79×10^{-5}	1.06×10^3	1.00	6.06×10^{-7}
	+ 4.18–4.24	(p*D* 10.80)	1.46×10^4	0.97	
	H_B+H_2		7.75×10^4	0.94	
			1.01×10^5	0.91	
			1.64×10^5	0.89	
			2.52×10^5	0.85	
			2.72×10^5	0.83	
			3.35×10^5	0.82	
			3.58×10^5	0.79	
			5.97×10^5	0.68	
			7.68×10^5	0.65	
20% BC	3.92–4.00	7.01×10^{-5}	1.06×10^3	1.00	4.34×10^{-7}
	+ 4.18–4.24	(p*D* 10.66)	7.13×10^4	0.95	
	H_B+H_2		1.57×10^5	0.93	
			2.41×10^5	0.88	
			3.28×10^5	0.86	
			6.75×10^5	0.73	
			7.62×10^5	0.74	
			8.48×10^5	0.70	
50%fb	3.92–4.00	5.90×10^{-5}	1.07×10^3	1.00	2.53×10^{-7}
	+ 4.18–4.24	(p*D* 10.58)	5.10×10^4	0.99	
	H_B+H_2		1.38×10^5	0.98	
			2.25×10^5	0.91	
			4.01×10^5	0.88	

			4.85×10^5	0.89	
			5.73×10^5	0.87	
			6.59×10^5	0.84	
			7.45×10^5	0.82	
			8.40×10^5	0.82	
			1.01×10^6	0.76	
			1.09×10^6	0.77	
			1.19×10^6	0.74	
35% 0.37M	3.92–4.00	5.14×10^{-5}	1.19×10^3	1.00	3.25×10^{-7}
	+ 4.18–4.24	(p*D* 10.52)	6.70×10^4	0.96	
	H_B+H_2		1.50×10^5	0.93	
			2.35×10^5	0.89	
			4.96×10^5	0.82	
			5.84×10^5	0.81	
			6.73×10^5	0.82	
			7.76×10^5	0.79	
			8.43×10^5	0.74	
			1.10×10^6	0.73	
20%	3.92–4.00	4.27×10^{-5}	1.06×10^3	1.00	2.22×10^{-7}
	+ 4.18–4.24	(p*D* 10.44)	7.49×10^4	0.98	
	H_B+H_2		3.29×10^5	0.97	
			4.04×10^5	0.87	
			4.89×10^5	0.81	
			5.81×10^5	0.87	
			6.70×10^5	0.88	
			9.44×10^5	0.82	
			1.02×10^6	0.80	
			1.11×10^6	0.77	
			1.19×10^6	0.81	
35% (version 1)	3.92–4.00	3.24×10^{-5}	1.06×10^3	1.00	1.63×10^{-7}
	+ 4.18–4.24	(p*D* 10.32)	8.42×10^4	1.02	
	H_B+H_2		1.53×10^5	0.96	
			4.07×10^5	0.93	
			4.89×10^5	0.91	
			5.73×10^5	0.89	
			6.65×10^5	0.90	
			7.51×10^5	0.87	
			1.02×10^6	0.80	
			1.10×10^6	0.84	
			1.18×10^6	0.88	
			1.27×10^6	0.82	
22%fb	3.92–4.00	2.04×10^{-5}	1.19×10^3	1.00	1.03×10^{-7}

+ 4.18–4.24	(p*D* 10.12)	1.60×10^4	1.00
H_B+H_2		1.01×10^5	1.00
		1.57×10^5	1.03
		2.44×10^5	0.99
		3.30×10^5	0.96
		5.91×10^5	0.95
		6.77×10^5	0.93
		8.50×10^5	0.92
		9.35×10^5	0.88
		1.19×10^6	0.89
		1.29×10^6	0.86
		1.37×10^6	0.86
		1.46×10^6	0.84
		1.54×10^6	0.86
		1.81×10^6	0.85
		1.89×10^6	0.83
		1.98×10^6	0.83

I.4 Deuterium exchange of c(L-Pro-L-Tyr)

I.4.1 c(L-Pro-L-Tyr) Prolyl α-proton

Table I.11: Reaction data and observed first order rate constants (k_{ex}) for the deuterium exchange of the prolyl α-proton H_F in c(L-Pro-L-Tyr) (5.0 mM) in $KDCO_3$ (0.185 M, p*D* = 10.30 – 10.81) buffered D_2O solution, *I* = 1.0 (KCl) and 25 °C.

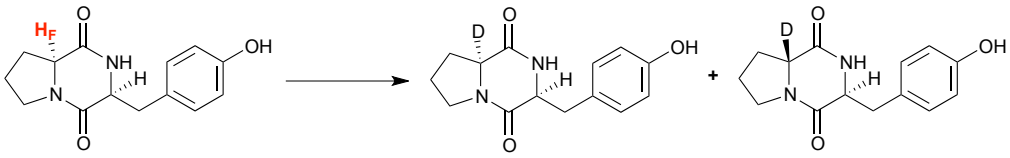

Experiment	Proton Chemical Shift /ppm	[DO^-] /M	Time /s	*f*(s)	k_{ex} /s^{-1}	k_{ex}/f_{OH} /s^{-1}
70% fb 2nd c	3.88 – 3.96	9.90×10^{-5}	5.40×10^2	1.00	4.47×10^{-6}	1.04×10^{-5}
	H_F	(p*D* 10.81)	1.23×10^4	0.96		
			2.30×10^4	0.92		
			7.94×10^4	0.70		
			9.18×10^4	0.66		
			1.06×10^5	0.61		
			1.71×10^5	0.47		
			1.92×10^5	0.43		
			3.61×10^5	0.20		
			4.42×10^5	0.13		
			5.13×10^5	0.10		
			5.97×10^5	0.07		

			6.85×10^5	0.05		
			7.71×10^5	0.04		
			1.03×10^6	0.00		
50% fb	3.88 – 3.96	5.76×10^{-5}	1.07×10^3	1.00	2.85×10^{-6}	5.05×10^{-6}
	H_F	(p*D* 10.57)	5.09×10^4	0.86		
			1.38×10^5	0.65		
			2.25×10^5	0.53		
			4.01×10^5	0.31		
			4.86×10^5	0.25		
			5.73×10^5	0.19		
			6.58×10^5	0.16		
			7.44×10^5	0.13		
			8.40×10^5	0.09		
			1.01×10^6	0.06		
			1.09×10^6	0.04		
			1.19×10^6	0.04		
20% fb	3.88 – 3.96	3.99×10^{-5}	1.06×10^3	1.00	2.05×10^{-6}	3.13×10^{-6}
	H_F	(p*D* 10.41)	7.60×10^4	0.86		
			3.40×10^5	0.50		
			4.12×10^5	0.43		
			4.96×10^5	0.36		
			5.88×10^5	0.32		
			6.79×10^5	0.24		
			9.52×10^5	0.15		
			1.02×10^6	0.12		
			1.11×10^6	0.11		
			1.19×10^6	0.08		
35% fb	3.88 – 3.96	3.10×10^{-5}	1.06×10^3	1.00	1.75×10^{-6}	2.48×10^{-6}
	H_F	(p*D* 10.30)	8.40×10^4	0.87		
			1.57×10^5	0.75		
			4.10×10^5	0.48		
			4.88×10^5	0.42		
			5.73×10^5	0.37		
			6.65×10^5	0.30		
			7.51×10^5	0.28		
			1.02×10^6	0.17		
			1.10×10^6	0.15		
			1.19×10^6	0.13		
			1.27×10^6	0.12		

I.4.2 c(L-Pro-L-Tyr) Prolyl α-proton buffer catalysis

Table I.12: Reaction data and observed first order rate constants (k_{ex}) for the deuterium exchange of the prolyl α-proton H_F in c(L-Pro-L-Tyr) (5.0 mM) in 70 % free base $KDCO_3$ (0.13 – 0.37 M, p*D* = 10.83 – 10.94) buffered D_2O solution, I = 1.0 (KCl) and 25 °C.

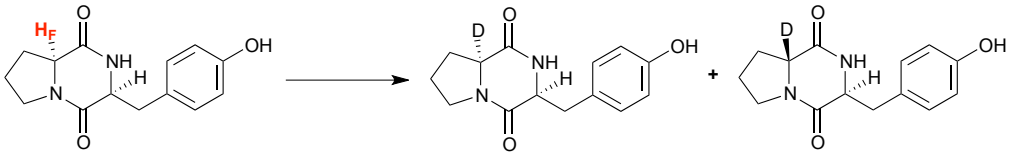

$[KDCO_3]$ /M	$[CO_3^{2-}]$ /M	$[DO^-]$ /M	Time /s	*f*(s)	k_{ex} /s^{-1}	k_{ex}/f_{OH} /s^{-1}
0.37	0.26	1.35×10^{-4}	1.06×10^{3}	1.00	6.74×10^{-6}	1.89×10^{-5}
		(p*D* 10.94)	5.90×10^{4}	0.68		
			9.03×10^{4}	0.55		
			1.48×10^{5}	0.37		
			2.38×10^{5}	0.20		
			2.64×10^{5}	0.16		
			3.38×10^{5}	0.10		
			4.97×10^{5}	0.03		
			5.23×10^{5}	0.02		
			5.82×10^{5}	0.02		
			6.80×10^{5}	0.01		
0.25	0.18	1.28×10^{-4}	1.26×10^{3}	1.00	5.83×10^{-6}	1.58×10^{-5}
		(p*D* 10.92)	5.91×10^{4}	0.71		
			8.63×10^{4}	0.60		
			1.48×10^{5}	0.42		
			1.75×10^{5}	0.36		
			2.49×10^{5}	0.24		
			4.05×10^{5}	0.09		
			4.32×10^{5}	0.08		
			4.93×10^{5}	0.06		
			5.85×10^{5}	0.04		
			6.66×10^{5}	0.02		
0.185	0.13	1.10×10^{-4}	1.06×10^{3}	1.00	5.23×10^{-6}	1.29×10^{-5}
		(p*D* 10.85)	5.90×10^{4}	0.75		
			9.02×10^{4}	0.63		
			1.48×10^{5}	0.45		
			2.40×10^{5}	0.28		
			2.64×10^{5}	0.25		
			3.38×10^{5}	0.17		
			5.00×10^{5}	0.07		

			5.23×10^5	0.06		
			5.82×10^5	0.04		
			6.72×10^5	0.03		
			7.53×10^5	0.02		
0.13	0.09	1.04×10^{-4}	1.06×10^3	1.00	4.81×10^{-6}	1.15×10^{-5}
		(p*D* 10.83)	5.88×10^4	0.76		
			9.02×10^4	0.64		
			1.48×10^5	0.49		
			2.47×10^5	0.30		
			2.64×10^5	0.29		
			3.38×10^5	0.20		
			5.01×10^5	0.09		
			5.23×10^5	0.08		
			5.82×10^5	0.05		
			6.73×10^5	0.05		
			7.53×10^5	0.03		

Table I.13: Reaction data and observed first order rate constants (k_{ex}) for the deuterium exchange of the prolyl α-proton H_F in c(L-Pro-L-Tyr) (5.0 mM) in 20 % free base $KDCO_3$ (0.13 – 0.37 M, p*D* = 10.19 – 10.28) buffered D_2O solution, I = 1.0 (KCl) and 25 ºC.

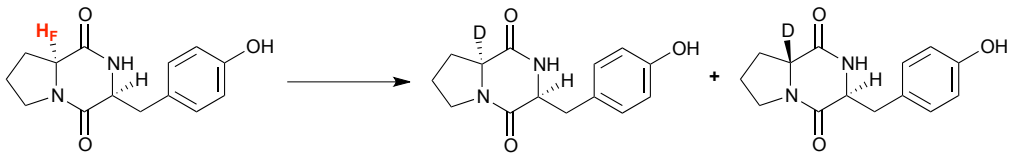

$[KDCO_3]$ /M	$[CO_3^{2-}]$ /M	$[DO^-]$ /M	Time /s	f(s)	k_{ex} /s^{-1}	k_{ex}/f_{OH} /s^{-1}
0.370	0.074	7.42×10^{-5}	1.06×10^3	1.00	3.59×10^{-6}	5.00×10^{-6}
		(p*D* 10.28)	7.47×10^4	0.76		
			1.61×10^5	0.56		
			2.47×10^5	0.41		
			5.22×10^5	0.15		
			5.95×10^5	0.12		
			6.87×10^5	0.09		
			7.67×10^5	0.06		
			8.53×10^5	0.05		
0.250	0.050	6.85×10^{-5}	1.06×10^3	1.00	3.18×10^{-6}	4.33×10^{-6}
		(p*D* 10.25)	7.65×10^4	0.78		
			1.74×10^5	0.58		
			2.47×10^5	0.47		
			5.21×10^5	0.18		
			5.94×10^5	0.15		

			6.87×10^5	0.12		
			7.66×10^5	0.08		
			8.52×10^5	0.06		
0.185	0.037	6.62×10^{-5}	1.06×10^3	1.00	2.99×10^{-6}	4.05×10^{-6}
		(p*D* 10.23)	8.24×10^4	0.79		
			1.72×10^5	0.61		
			2.44×10^5	0.47		
			5.18×10^5	0.21		
			5.91×10^5	0.17		
			6.85×10^5	0.13		
			7.63×10^5	0.10		
			8.49×10^5	0.08		
0.120	0.024	6.04×10^{-5}	1.06×10^3	1.00	2.67×10^{-6}	3.52×10^{-6}
		(p*D* 10.19)	8.02×10^4	0.82		
			1.71×10^5	0.63		
			2.56×10^5	0.50		
			5.17×10^5	0.25		
			5.89×10^5	0.21		
			6.83×10^5	0.17		
			7.63×10^5	0.13		
			8.47×10^5	0.10		

I.4.3 c(L-Pro-L-Tyr) Tyrosyl α-proton

Table I.14: Reaction data and observed first order rate constants (k_{ex}) for the deuterium exchange of the tyrosyl α-protons H_D in c(L-Pro-L-Tyr) and H_4 in c(D-Pro-L-Tyr) (5.0 mM) in $KDCO_3$ (0.185 M, p*D* = 10.23 – 10.85) buffered D_2O solution, I = 1.0 (KCl) and 25 ºC.

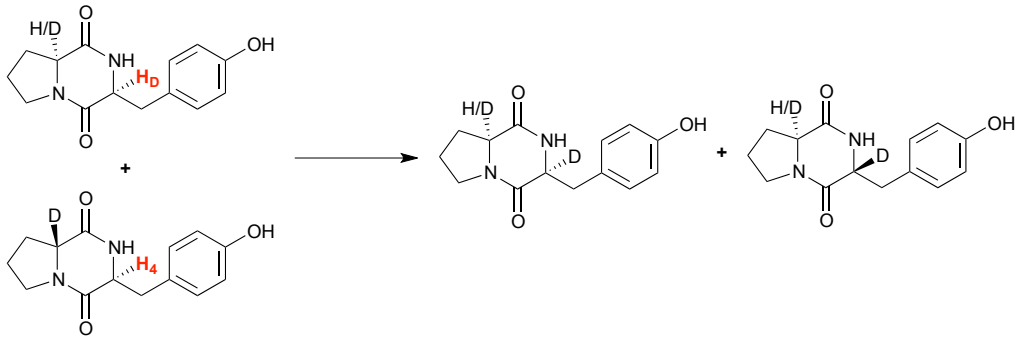

Experiment	$[DO^-]$ /M	Time /s	f(s)	k_{ex} /s^{-1}	k_{ex}/f_{OH} /s^{-1}
70%	9.90×10^{-5}	5.40×10^2	1.00	1.08×10^{-7}	4.66×10^{-7}
	(p*D* 10.81)	1.23×10^4	1.01		
		2.30×10^4	1.02		

		7.94×10^4	0.99		
		9.18×10^4	0.99		
		1.06×10^5	1.00		
		1.71×10^5	0.99		
		1.92×10^5	0.98		
		3.61×10^5	0.98		
		4.42×10^5	0.94		
		5.13×10^5	0.94		
		5.97×10^5	0.94		
		6.85×10^5	0.93		
		7.71×10^5	0.93		
		1.03×10^5	0.88		
70% BC	1.10×10^{-4}	1.06×10^3	1.00	1.28×10^{-7}	5.98×10^{-7}
	(p*D* 10.85)	5.90×10^4	1.01		
		9.02×10^4	0.96		
		1.48×10^5	0.96		
		2.40×10^5	0.97		
		2.64×10^5	0.97		
		3.38×10^5	0.94		
		5.00×10^5	0.93		
		5.23×10^5	0.93		
		5.82×10^5	0.93		
		6.72×10^5	0.92		
		7.53×10^5	0.89		
		1.06×10^6	0.87		
		1.14×10^6	0.86		
		1.23×10^6	0.88		
50%	5.76×10^{-5}	1.07×10^3	1.00	1.17×10^{-7}	3.43×10^{-7}
	(p*D* 10.57)	5.09×10^4	0.98		
		1.38×10^5	0.97		
		2.25×10^5	0.96		
		4.01×10^5	0.95		
		4.86×10^5	0.92		
		5.73×10^5	0.96		
		6.58×10^5	0.96		
		7.44×10^5	0.90		
		8.40×10^5	0.89		
		1.01×10^6	0.90		
		1.09×10^6	0.88		
		1.19×10^6	0.87		
20%	3.99×10^{-5}	1.06×10^3	1.00	8.01×10^{-8}	1.87×10^{-7}
	(p*D* 10.41)	7.60×10^4	1.01		
		3.40×10^5	1.00		

		4.12×10^5	0.96		
		4.96×10^5	0.95		
		5.88×10^5	1.01		
		6.79×10^5	0.94		
		9.52×10^5	0.93		
		1.02×10^6	0.92		
		1.11×10^6	1.00		
		1.19×10^6	0.91		
35%	3.10×10^{-5}	1.06×10^3	1.00	8.44×10^{-8}	1.72×10^{-7}
	(p*D* 10.30)	8.40×10^4	0.97		
		1.57×10^5	0.96		
		4.10×10^5	0.96		
		4.88×10^5	0.94		
		5.73×10^5	0.96		
		6.65×10^5	0.94		
		7.51×10^5	0.94		
		1.02×10^6	0.94		
		1.10×10^6	0.91		
		1.19×10^6	0.90		
		1.27×10^6	0.91		
20% BC	2.63×10^{-5}	1.06×10^3	1.00	1.09×10^{-7}	2.06×10^{-7}
	(p*D* 10.23)	8.24×10^4	0.98		
		1.72×10^5	0.96		
		2.44×10^5	0.97		
		5.18×10^5	0.94		
		5.91×10^5	0.96		
		6.85×10^5	0.93		
		7.63×10^5	0.92		
		8.49×10^5	0.90		

I.5 Deuterium exchange of c(Gly-L-Pro)

I.5.1 c(Gly-L-Pro) Prolyl α-proton

Table I.15: Reaction data and observed first order rate constants (k_{ex}) for the deuterium exchange of the prolyl α-proton H_A in c(Gly-L-Pro) (5.0 mM) in $KDCO_3$ (0.185 M, p*D* = 10.39 – 10.83) buffered D_2O solution, I = 1.0 (KCl) and 25 ºC.

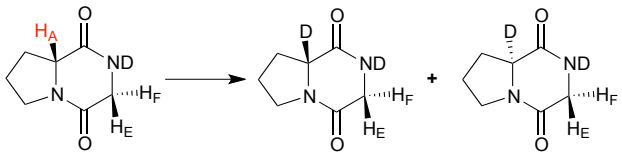

Experiment	Proton Chemical Shift /ppm	[DO^-] /M	Time /s	*f*(s)	k_{ex} /s^{-1}
70% fb	H_A	4.13×10^{-5}	1.75×10^{3}	1.00	7.63×10^{-6}
	4.21-4.28	(p*D* 10.83)	7.47×10^{4}	0.57	
			1.61×10^{5}	0.28	
			2.55×10^{5}	0.15	
			6.91×10^{5}	0.03	
			7.57×10^{5}	0.03	
			8.34×10^{5}	0.03	
60% fb	H_A	2.66×10^{-5}	1.06×10^{3}	1.00	4.40×10^{-6}
	4.21-4.28	(p*D* 10.64)	7.54×10^{4}	0.70	
			1.67×10^{5}	0.48	
			2.55×10^{5}	0.32	
			6.90×10^{5}	0.08	
			7.57×10^{5}	0.06	
			8.36×10^{5}	0.06	
50% fb	H_A	2.04×10^{-5}	1.06×10^{3}	1.00	3.64×10^{-6}
	4.21-4.28	(p*D* 10.52)	8.34×10^{4}	0.73	
			1.67×10^{5}	0.52	
			2.55×10^{5}	0.37	
			6.90×10^{5}	0.13	
			7.57×10^{5}	0.09	
			8.36×10^{5}	0.08	
48% fb	H_A	1.82×10^{-5}	1.06×10^{3}	1.00	3.23×10^{-6}
	4.21-4.28	(p*D* 10.47)	8.34×10^{4}	0.75	
			1.67×10^{5}	0.56	
			2.55×10^{5}	0.43	
			6.90×10^{5}	0.11	

			7.58×10^5	0.11	
			8.36×10^5	0.11	
20% fb	H_A	1.59×10^{-5}	1.06×10^3	1.00	2.74×10^{-6}
	4.21-4.28	(p*D* 10.41)	8.43×10^4	0.79	
			1.67×10^5	0.63	
			2.55×10^5	0.48	
			7.39×10^5	0.14	
			8.36×10^5	0.12	
22% fb	H_A	1.52×10^{-5}	1.06×10^3	1.00	2.70×10^{-6}
	4.21-4.28	(p*D* 10.39)	8.38×10^4	0.80	
			1.67×10^5	0.64	
			2.55×10^5	0.49	
			8.36×10^5	0.12	

I.5.2 c(Gly-L-Pro) Glycyl α-protons

Table I.16: Reaction data and observed first order rate constants (k_{ex}) for the deuterium exchange of the glycyl α-proton H_E in c(Gly-L-Pro) (5.0 mM) in $KDCO_3$ (0.185 M, p*D* = 10.39 – 10.83) buffered D_2O solution, I = 1.0 (KCl) and 25 °C.

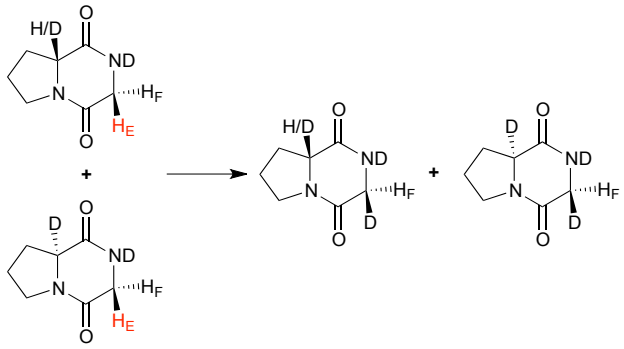

Experiment	Proton Chemical Shift /ppm	[DO^-] /M	Time /s	*f*(s)	k_{ex} /s^{-1}
70% fb	H_E	4.13×10^{-5}	1.75×10^3	1.00	7.91×10^{-7}
	3.75-3.79+3.80-3.83	(p*D* 10.43)	7.47×10^4	0.95	
			1.61×10^5	0.84	
			2.55×10^5	0.79	
			6.91×10^5	0.57	
			7.57×10^5	0.56	
			8.34×10^5	0.54	
60% fb	H_E	2.66×10^{-5}	1.06×10^3	1.00	4.36×10^{-7}
	3.75-3.79+3.80-3.83	(p*D* 10.24)	7.54×10^4	0.94	

			1.67×10^5	0.93	
			2.55×10^5	0.88	
			6.90×10^5	0.74	
			7.57×10^5	0.72	
			8.36×10^5	0.71	
50% fb	H_E	2.04×10^{-5}	1.06×10^3	1.00	3.28×10^{-7}
	3.75-3.79+3.80-3.83	(p*D* 10.12)	8.34×10^4	0.99	
			1.67×10^5	0.93	
			2.55×10^5	0.91	
			6.90×10^5	0.80	
			7.57×10^5	0.78	
			8.36×10^5	0.76	
48% fb	H_E	1.82×10^{-5}	1.06×10^3	1.00	2.91×10^{-7}
	3.75-3.79+3.80-3.83	(p*D* 10.07)	8.34×10^4	0.98	
			1.67×10^5	0.94	
			2.55×10^5	0.95	
			6.90×10^5	0.81	
			7.58×10^5	0.80	
			8.36×10^5	0.79	
20% fb	H_E	1.59×10^{-5}	1.06×10^3	1.00	2.77×10^{-7}
	3.75-3.79+3.80-3.83	(p*D* 10.01)	8.43×10^4	0.98	
			1.67×10^5	0.94	
			2.55×10^5	0.95	
			7.39×10^5	0.81	
			8.36×10^5	0.80	
22% fb	H_E	1.52×10^{-5}	1.06×10^3	1.00	2.24×10^{-7}
	3.75-3.79+3.80-3.83	(p*D* 9.99)	8.38×10^4	1.00	
			1.67×10^5	0.98	
			2.55×10^5	0.93	
			8.36×10^5	0.83	

Table I.17: Reaction data and observed first order rate constants (k_{ex}) for the deuterium exchange of the glycyl α-proton H_F in c(Gly-L-Pro) (5.0 mM) in $KDCO_3$ (0.185 M, p*D* = 10.39 – 10.83) buffered D_2O solution, *I* = 1.0 (KCl) and 25 °C.

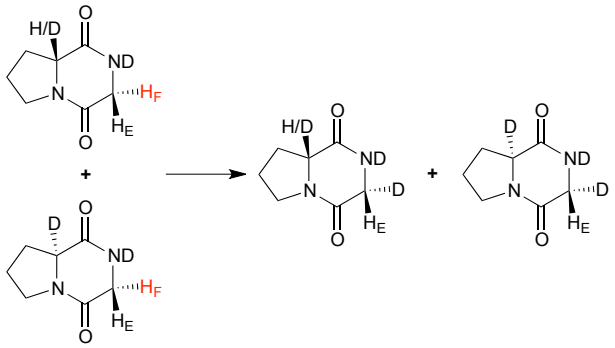

Experiment	Proton Chemical Shift /ppm	[DO^-] /M	Time /s	*f*(s)	k_{ex} /s^{-1}
70% fb	H_F	4.13×10^{-5}	1.75×10^{3}	1.00	2.75×10^{-6}
	4.05-4.09+4.09-4.13	(p*D* 10.43)	7.47×10^{4}	0.81	
			1.61×10^{5}	0.62	
			2.55×10^{5}	0.48	
			6.91×10^{5}	0.16	
			7.57×10^{5}	0.14	
			8.34×10^{5}	0.12	
60% fb	H_F	2.66×10^{-5}	1.06×10^{3}	1.00	1.68×10^{-6}
	4.05-4.09+4.09-4.13	(p*D* 10.24)	7.54×10^{4}	0.84	
			1.67×10^{5}	0.74	
			2.55×10^{5}	0.64	
			6.90×10^{5}	0.31	
			7.57×10^{5}	0.29	
			8.36×10^{5}	0.27	
50% fb	H_F	2.04×10^{-5}	1.06×10^{3}	1.00	1.38×10^{-6}
	4.05-4.09+4.09-4.13	(p*D* 10.12)	8.34×10^{4}	0.89	
			1.67×10^{5}	0.77	
			2.55×10^{5}	0.68	
			6.90×10^{5}	0.39	
			7.57×10^{5}	0.37	
			8.36×10^{5}	0.32	
48% fb	H_F	1.82×10^{-5}	1.06×10^{3}	1.00	1.22×10^{-6}
	4.05-4.09+4.09-4.13	(p*D* 10.07)	8.34×10^{4}	0.90	
			1.67×10^{5}	0.80	
			2.55×10^{5}	0.73	
			6.90×10^{5}	0.42	

			7.58×10^5	0.41	
			8.36×10^5	0.38	
20% fb	H_F	1.59×10^{-5}	1.06×10^3	1.00	1.06×10^{-6}
	4.05-4.09+4.09-4.13	(p*D* 10.01)	8.43×10^4	0.90	
			1.67×10^5	0.83	
			2.55×10^5	0.76	
			7.39×10^5	0.46	
			8.36×10^5	0.42	
22% fb	H_F	1.52×10^{-5}	1.06×10^3	1.00	1.00×10^{-6}
	4.05-4.09+4.09-4.13	(p*D* 9.99)	8.38×10^4	0.93	
			1.67×10^5	0.85	
			2.55×10^5	0.77	
			8.36×10^5	0.43	

I.6 Deuterium exchange of c(Gly-Gly)

I.6.1 c(Gly-Gly) Glycyl α-proton

Table I.18: Reaction data and observed first order rate constants (k_{ex}) for the deuterium exchange of the glycyl α-proton H_A in c(Gly-Gly) (20.0 mM) in 3Cl-Quinuclidine (0.15 M, p*D* = 10.19 – 10.82) at 25 °C and *I* = 1.0 M (KCl).

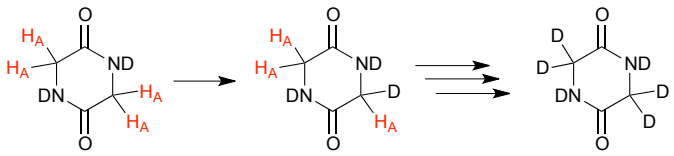

Experiment	Proton Chemical Shift /ppm	[DO^-] /M	Time /s	*f*(s)	k_{ex} /s^{-1}
90%fb	4.01-4.05	1.02×10^{-4}	1.06×10^3	1.00	6.81×10^{-6}
	H_A	(p*D* 10.82)	1.08×10^5	0.44	
			1.69×10^5	0.31	
			2.79×10^5	0.16	
			3.59×10^5	0.11	
			4.26×10^5	0.08	
			5.11×10^5	0.05	
			5.93×10^5	0.03	
			6.85×10^5	0.03	
70%fb	4.01-4.05	2.29×10^{-5}	1.06×10^3	1.00	2.04×10^{-6}
	H_A	(p*D* 10.17)	7.02×10^4	0.87	

			3.43×10^5	0.49	
			5.12×10^5	0.35	
			5.91×10^5	0.30	
			6.76×10^5	0.25	
			8.67×10^5	0.18	
			9.48×10^5	0.15	
50%fb	4.01-4.05 H_A	6.04×10^{-6} (p*D* 9.59)	1.06×10^3	1.00	7.68×10^{-7}
			7.48×10^4	0.96	
			1.84×10^5	0.87	
			4.36×10^5	0.70	
			5.90×10^5	0.63	
			6.75×10^5	0.60	
			7.66×10^5	0.55	
			1.14×10^6	0.43	
30%fb	4.01-4.05 H_A	3.47×10^{-6} (p*D* 9.35)	1.06×10^3	1.00	4.59×10^{-7}
			8.29×10^4	0.96	
			2.72×10^5	0.88	
			3.38×10^5	0.86	
			4.21×10^5	0.83	
			5.07×10^5	0.79	
			6.75×10^5	0.73	
			9.40×10^5	0.65	

I.7 Deuterium exchange of c(L-Ala-L-Ala)

I.7.1 c(L-Ala-L-Ala)Alanyl α-proton

Table I.19: Reaction data and observed first order rate constants (k_{ex}) for the deuterium exchange of the alanyl α-proton H_A in c(L-Ala-L-Ala) (20.0 mM) in 3Cl-Quinuclidine (0.15 M, p*D* = 9.35 – 10.81), at 25 °C and *I* = 1.0 M (KCl).

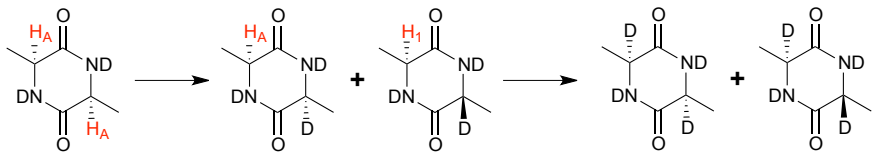

Experiment	Proton Chemical Shift ppm	[DO–] /M	Time /s	f(s)	kex /s–1
90 % fb	4.11-4.17	1.00×10^{-4}	1.06×10^3	1.00	8.52×10^{-7}

	H_A	(p*D* 10.81)	1.08×10^5	0.91	
			1.68×10^5	0.86	
			2.79×10^5	0.79	
			3.58×10^5	0.74	
			4.26×10^5	0.70	
			5.11×10^5	0.65	
50 % fb	4.11-4.17	6.32×10^{-6}	1.06×10^3	1.00	1.44×10^{-7}
	H_A	(p*D* 9.61)	7.49×10^4	0.97	
			1.84×10^5	0.97	
			4.36×10^5	0.95	
			5.90×10^5	0.92	
			6.75×10^5	0.91	
			8.52×10^5	0.89	
			1.14×10^6	0.84	
30 % fb	4.11-4.17	3.47×10^{-6}	1.06×10^3	1.00	7.77×10^{-8}
	H_A	(p*D* 9.35)	8.27×10^4	1.00	
			2.72×10^5	0.98	
			3.38×10^5	0.98	
			4.21×10^5	0.96	
			5.08×10^5	0.96	
			6.76×10^5	0.95	
			9.41×10^5	0.93	

II Appendix II

II.1 Buffer Catalysis of the α-protons in Glycyl TKP

Figure II.1: Plot of the fraction of unexchanged α-protons H_A and $H_{A'}$ against time for the glycyl TKP (**10**) in 75 % fb 0.0250 M KOAc with 40 % d_3-MeCN co-solvent, I = 0.06 (KCl) and 25 ºC.

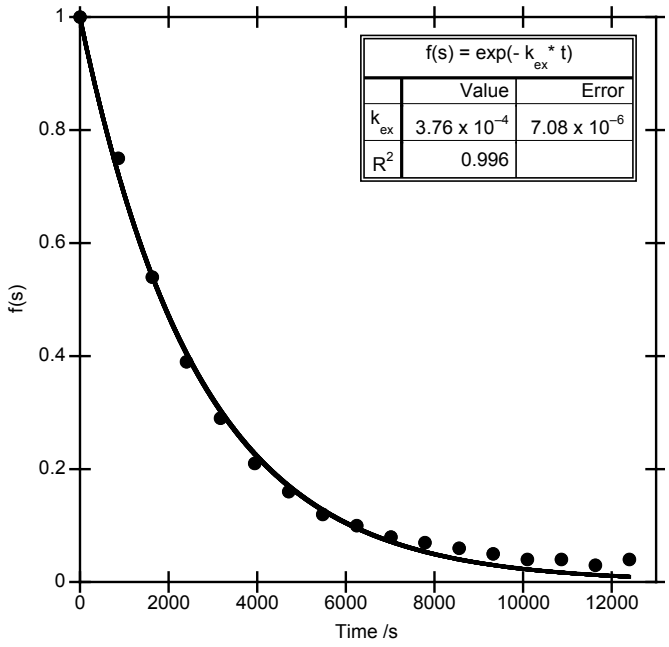

Figure II.2: Plot of the fraction of unexchanged α-protons H_A and $H_{A'}$ against time for the glycyl TKP (**10**) in 75 % fb 0.0500 M KOAc with 40 % d_3-MeCN co-solvent, I = 0.06 (KCl) and 25 ºC.

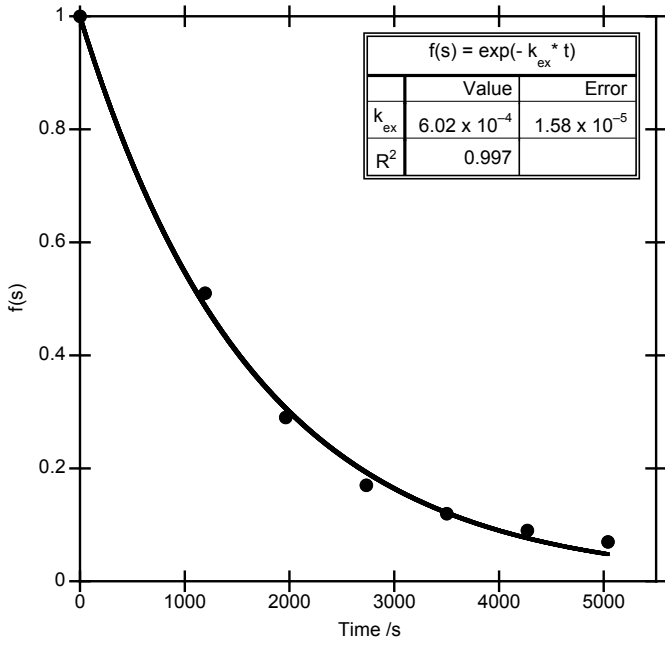

II.2 Deuterium exchange of the α-protons in Prolyl TKP

Table II.1: Reaction data and observed first order rate constants (k_{ex}) for the deuterium exchange of the α-proton H_M in prolyl TKP (**11**) in 15 % free base KOAc solutions with 40 % d_3-MeCN co-solvent, I = 0.2 (KCl) and 25 ºC.

[KOAc] /M	[fb KOAc] /M	[DO^-] /M	Time /s	f(s)	k_{ex} /s^{-1}
0.200	0.03 (15 % fb)	8.95×10^{-12} (pD 4.76)	624	0.75	4.06×10^{-4}
			1497	0.63	
			1923	0.53	
			2346	0.39	
			2763	0.29	
			3183	0.25	
			3598	0.24	
			4019	0.17	
			4442	0.13	
			4858	0.09	
0.150	0.023 (15 % fb)	9.05×10^{-12} (pD 4.76)	624	0.78	4.21×10^{-4}
			1061	0.65	
			1478	0.56	
			1895	0.43	
			2312	0.38	
			2728	0.36	
			3146	0.27	
			3566	0.22	
			3984	0.15	
			4399	0.13	
			4817	0.15	
			5233	0.08	
0.125	0.019 (15 % fb)	8.95×10^{-12} (pD 4.76)	504	0.84	4.18×10^{-4}
			937	0.62	
			1353	0.59	
			1767	0.44	
			2182	0.40	
			2602	0.31	
			3016	0.27	
			3437	0.24	
			3850	0.24	

			4266	0.16	
			4685	0.14	
			5105	0.17	
			5534	0.12	
			5982	0.10	
			624	0.79	
			1051	0.69	
			1467	0.64	
			1882	0.52	
			2379	0.43	
			2799	0.40	
			3219	0.33	
0.100	0.015 (15 % fb)	8.85×10^{-13} (p*D* 4.75)	3641	0.29	3.41×10^{-4}
			4055	0.22	
			4472	0.23	
			4887	0.20	
			5305	0.18	
			5725	0.14	
			6143	0.12	
			6560	0.10	

Figure II.3: Plot of the fraction of unexchanged α-proton H_M against time for the prolyl TKP (**11**) in 15 % fb 0.200 M KOAc with 40 % d_3-MeCN co-solvent, I = 0.2 (KCl) and 25 ºC.

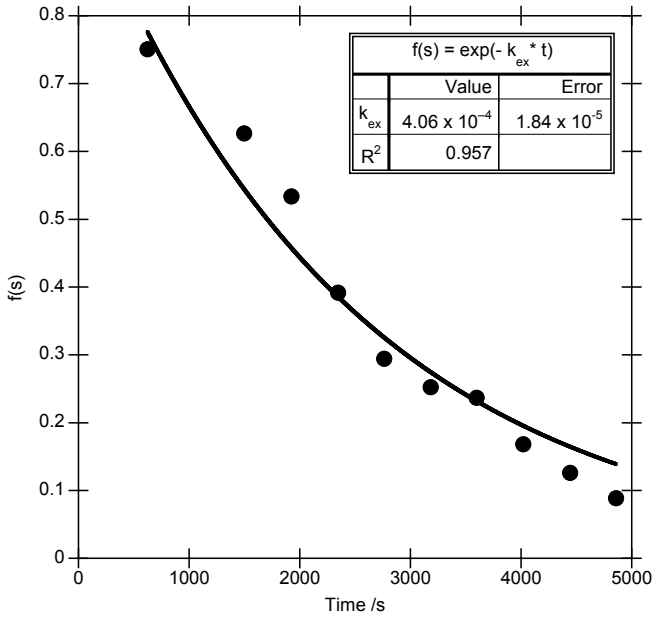

Figure II.4: Plot of the fraction of unexchanged α-proton H_M against time for the prolyl TKP (**11**) in 15 % fb 0.150 M KOAc with 40 % d_3-MeCN co-solvent, $I = 0.2$ (KCl) and 25 ºC.

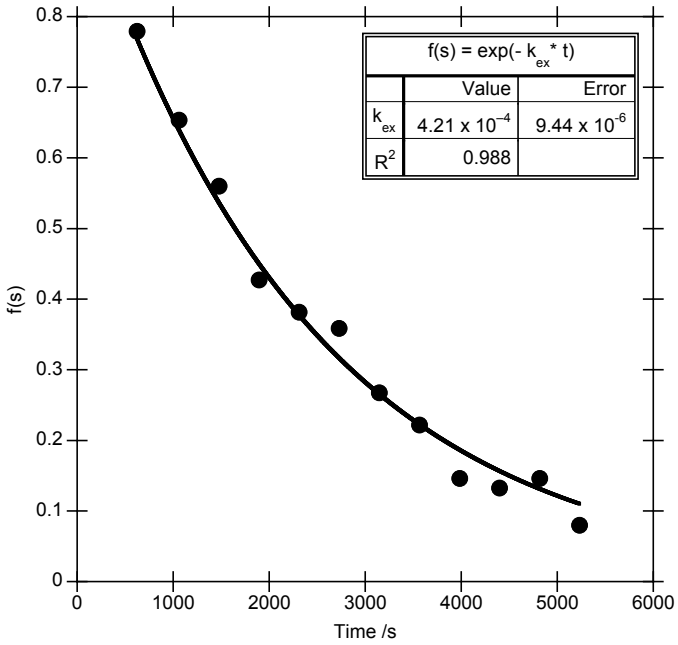

Figure II.5: Plot of the fraction of unexchanged α-proton H_M against time for the prolyl TKP (**11**) in 15 % fb 0.125 M KOAc with 40 % d_3-MeCN co-solvent, $I = 0.2$ (KCl) and 25 ºC.

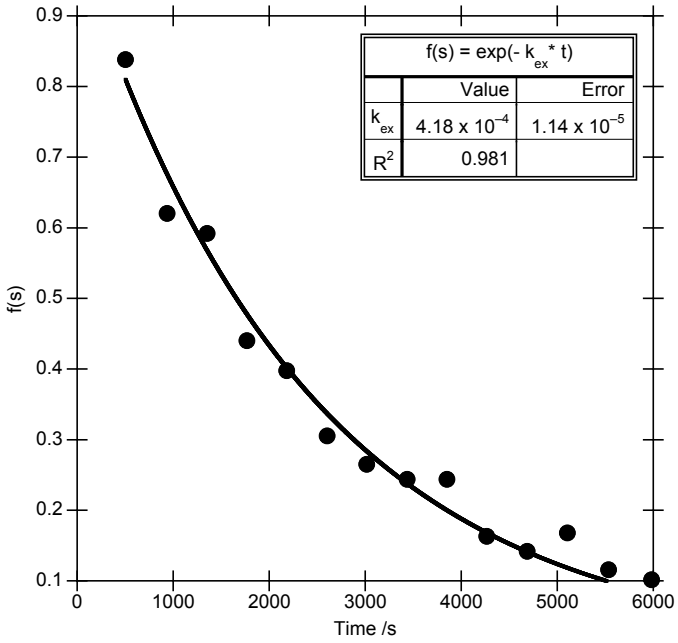

Figure II.6: Plot of the fraction of unexchanged α-proton H_M against time for the prolyl TKP (**11**) in 15 % fb 0.100 M KOAc with 40 % d_3-MeCN co-solvent, I = 0.2 (KCl) and 25 ºC.

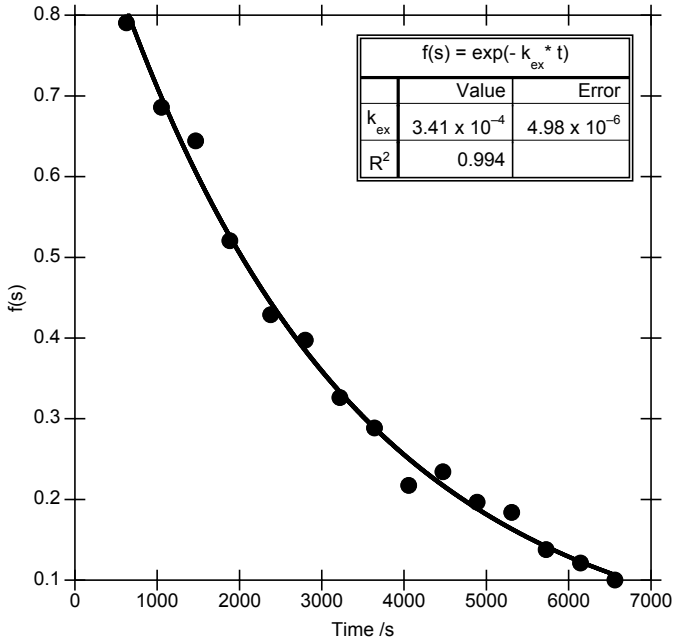

Table II.2: Reaction data and observed first order rate constants (k_{ex}) for the deuterium exchange of the α-proton H_M in prolyl TKP (**11**) in 20 % free base KOAc solutions with 40 % d_3-MeCN co-solvent, I = 0.2 (KCl) and 25 ºC.

[KOAc] /M	[fb KOAc] /M	[DO^-] /M	Time /s	f(s)	k_{ex} /s^{-1}
0.200	0.04 (20 % fb)	1.50×10^{-11} (pD 4.98)	624	0.54	8.93×10^{-4}
			1048	0.40	
			1466	0.27	
			1882	0.19	
			2313	0.14	
			2736	0.08	
			3155	0.07	
			3577	0.06	
0.150	0.03 (20 % fb)	1.49×10^{-11} (pD 4.98)	624	0.67	7.53×10^{-4}
			1048	0.43	
			1466	0.30	
			1883	0.24	
			2303	0.17	
			2724	0.15	

			3145	0.11	
			3564	0.05	
			504	0.69	
			932	0.50	
			1352	0.40	
			1770	0.29	
0.125	0.025 (20 % fb)	1.47×10^{-11} (p*D* 4.97)	2186	0.24	6.96×10^{-4}
			2605	0.16	
			3021	0.11	
			3441	0.10	
			3863	0.07	
			4287	0.06	
			624	0.70	
			1045	0.60	
			1491	0.48	
			1914	0.35	
			2340	0.28	
			2755	0.22	
0.100	0.02 (20 % fb)	1.49×10^{-11} (p*D* 4.98)	3174	0.16	5.42×10^{-4}
			3590	0.12	
			4013	0.10	
			4428	0.07	
			4852	0.08	
			5277	0.06	
			5698	0.06	

Figure II.7: Plot of the fraction of unexchanged α-proton H_M against time for the prolyl TKP (**11**) in 20 % fb 0.200 M KOAc with 40 % d_3-MeCN co-solvent, I = 0.2 (KCl) and 25 ºC.

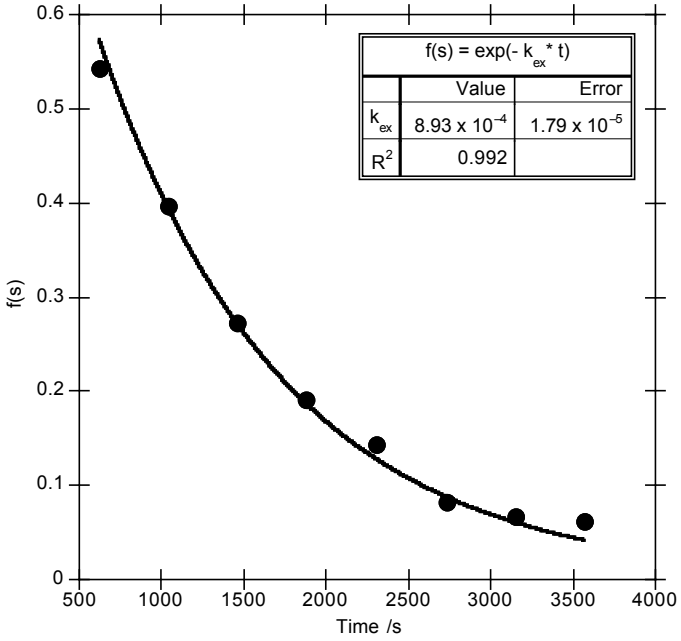

Figure II.8: Plot of the fraction of unexchanged α-proton H_M against time for the prolyl TKP (**11**) in 20 % fb 0.150 M KOAc with 40 % d_3-MeCN co-solvent, I = 0.2 (KCl) and 25 ºC.

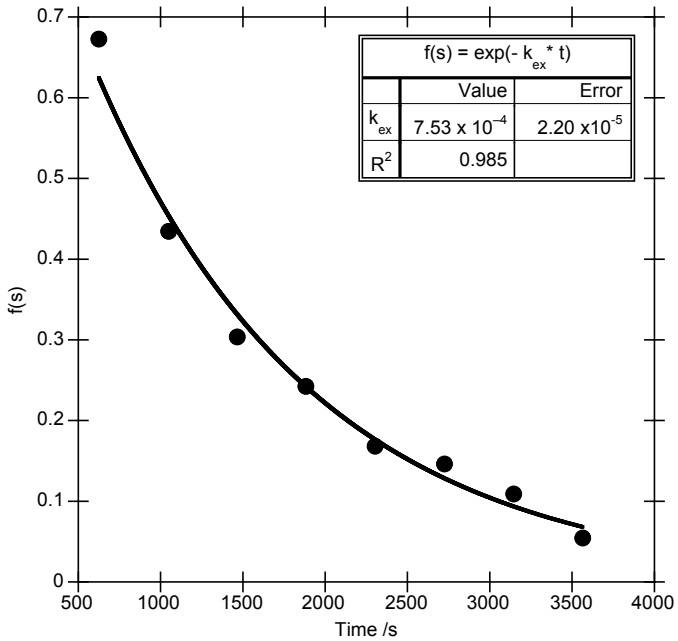

Figure II.9: Plot of the fraction of unexchanged α-proton H_M against time for the prolyl TKP (**11**) in 20 % fb 0.125 M KOAc with 40 % d_3-MeCN co-solvent, I = 0.2 (KCl) and 25 ºC.

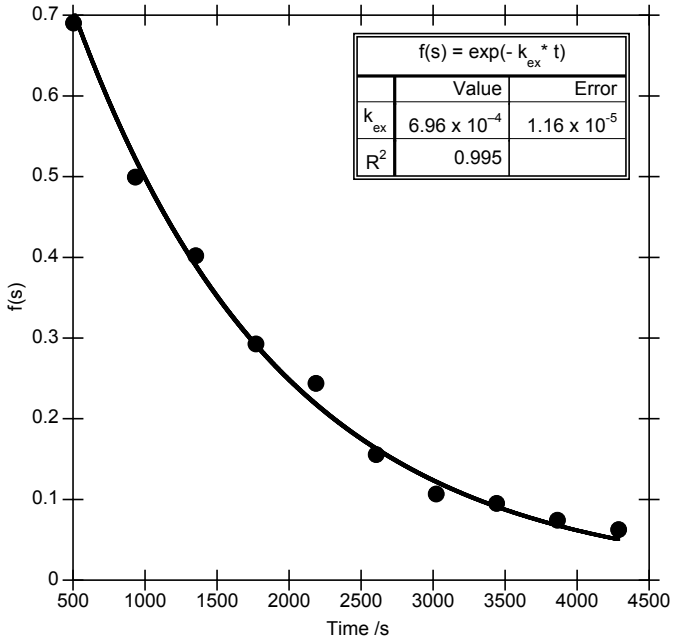

Figure II.10: Plot of the fraction of unexchanged α-proton H_M against time for the prolyl TKP (**11**) in 20 % fb 0.100 M KOAc with 40 % d_3-MeCN co-solvent, I = 0.2 (KCl) and 25 ºC.

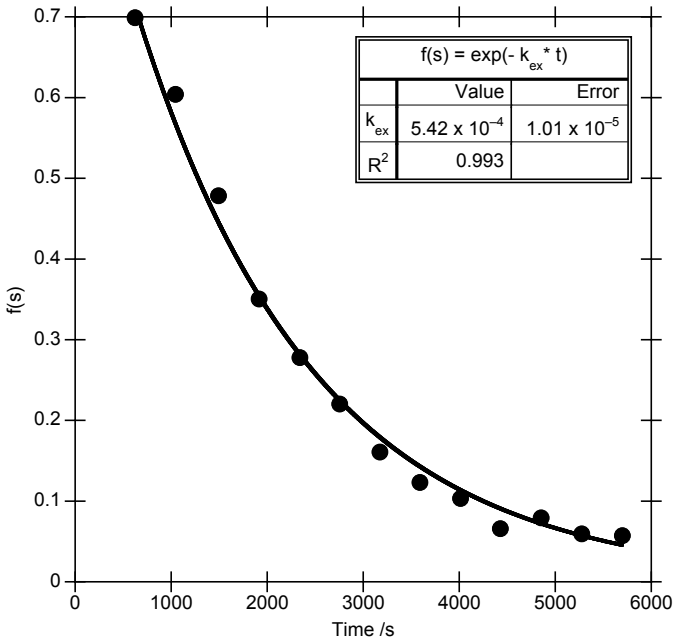

Table II.3: Reaction data and observed first order rate constants (k_{ex}) for the deuterium exchange of the α-proton H_M in prolyl TKP (**11**) in 25 % free base KOAc solutions with 40 % d_3-MeCN co-solvent, I = 0.2 (KCl) and 25 °C.

[KOAc] /M	[fb KOAc] /M	[DO^-] /M	Time /s	f(s)	k_{ex} /s^{-1}
0.200	0.05 (25 % fb)	2.25×10^{-11} (pD 5.16)	624	0.56	9.73×10^{-4}
			1041	0.39	
			1464	0.21	
			1881	0.15	
			2337	0.10	
			2752	0.06	
0.150	0.038 (25 % fb)	2.17×10^{-11} (pD 5.14)	624	0.60	9.22×10^{-4}
			1036	0.38	
			1456	0.24	
			1877	0.16	
			2296	0.12	
			2717	0.07	
			3135	0.06	
			3552	0.05	
0.125	0.031 (25 % fb)	2.15×10^{-11} (pD 5.14)	624	0.62	8.12×10^{-4}
			1044	0.43	
			1462	0.31	
			1878	0.20	
			2294	0.14	
			2711	0.12	
			3126	0.09	
			3550	0.06	
0.10	0.025 (25 % fb)	2.15×10^{-11} (pD 5.14)	624	0.67	7.22×10^{-4}
			1042	0.46	
			1457	0.34	
			1875	0.26	
			2331	0.17	
			2755	0.15	
			3172	0.09	
			3592	0.06	
			4009	0.05	

Figure II.11: Plot of the fraction of unexchanged α-proton H_M against time for the prolyl TKP (**11**) in 25 % fb 0.200 M KOAc with 40 % d_3-MeCN co-solvent, I = 0.2 (KCl) and 25 ºC.

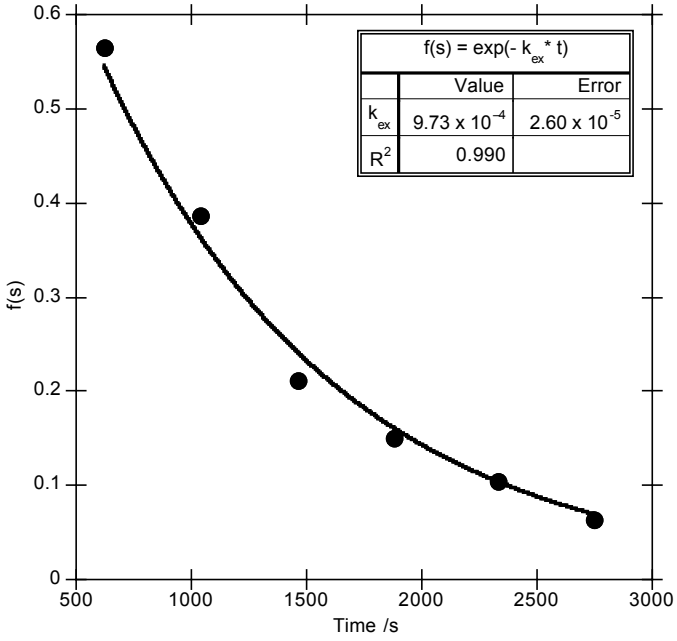

Figure II.12: Plot of the fraction of unexchanged α-proton H_M against time for the prolyl TKP (**11**) in 25 % fb 0.150 M KOAc with 40 % d_3-MeCN co-solvent, I = 0.2 (KCl) and 25 ºC.

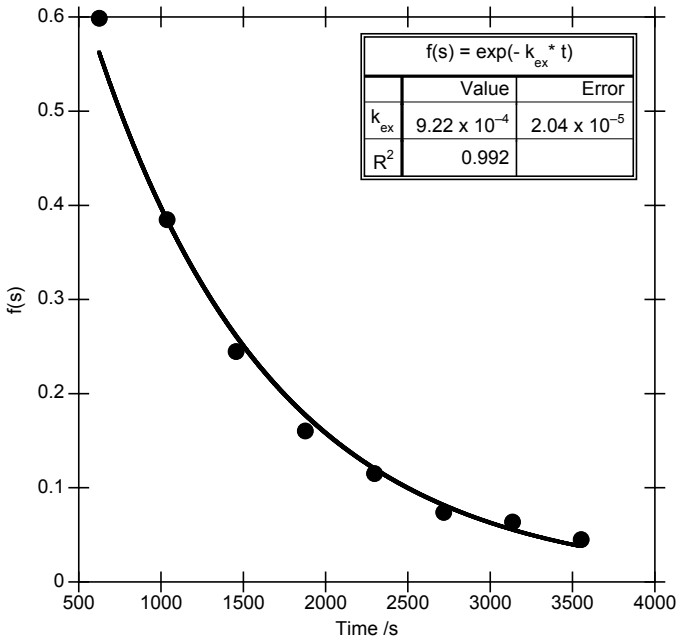

Figure II.13: Plot of the fraction of unexchanged α-proton H_M against time for the prolyl TKP (**11**) in 25 % fb 0.125 M KOAc with 40 % d_3-MeCN co-solvent, I = 0.2 (KCl) and 25 ºC.

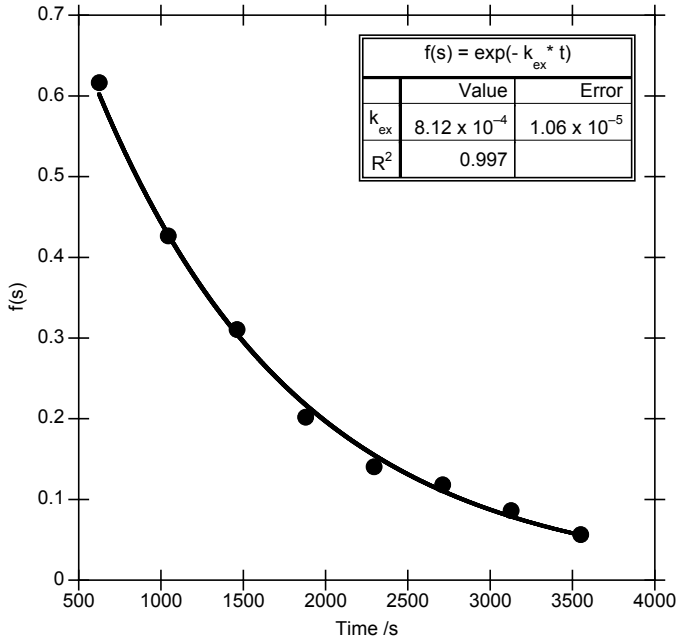

Figure II.14: Plot of the fraction of unexchanged α-proton H_M against time for the prolyl TKP (**11**) in 25 % fb 0.100 M KOAc with 40 % d_3-MeCN co-solvent, I = 0.2 (KCl) and 25 ºC.

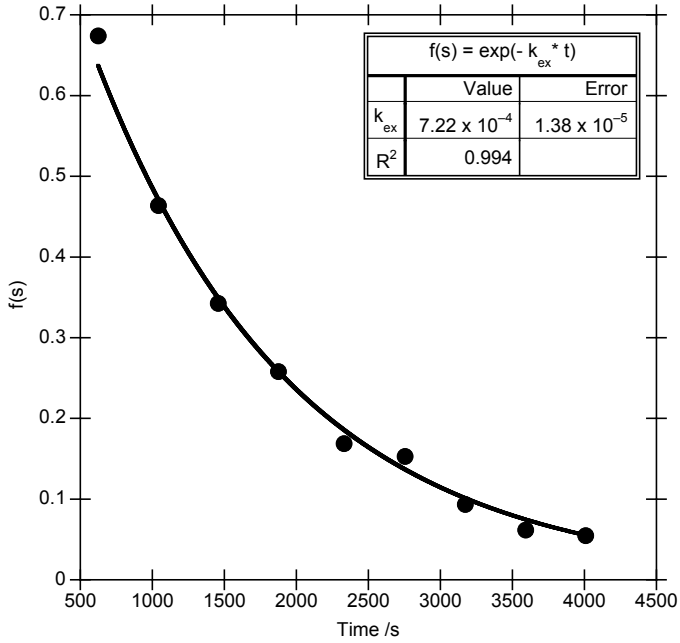

Table II.4: Reaction data and observed first order rate constants (k_{ex}) for the deuterium exchange of the α-proton H_M in prolyl TKP (**11**) in 30 % free base KOAc solutions with 40 % d_3-MeCN co-solvent, I = 0.2 (KCl) and 25 °C.

[KOAc] /M	[fb KOAc] /M	[DO^-] /M	Time /s	f(s)	k_{ex} /s^{-1}
0.200	0.06 (30 % fb)	3.03×10^{-11} (pD 5.29)	744	0.38	1.34×10^{-3}
			1548	0.10	
			2352	0.07	
			3161	0.00	
0.150	0.045 (30 % fb)	3.00×10^{-11} (pD 5.28)	564	0.53	1.14×10^{-3}
			981	0.31	
			1410	0.18	
			1839	0.14	
			2264	0.09	
			2714	0.07	
0.125	0.038 (30 % fb)	2.93×10^{-11} (pD 5.27)	624	0.58	9.68×10^{-4}
			1084	0.34	
			1543	0.20	
			1965	0.14	
			2385	0.10	
			2806	0.05	
			3227	0.05	
			3971	0.03	
0.100	0.03 (30 % fb)	2.90×10^{-11} (pD 5.27)	564	0.61	8.67×10^{-4}
			984	0.42	
			1401	0.29	
			1819	0.21	
			2242	0.14	
			2673	0.11	
			3093	0.07	
			3510	0.05	
			3939	0.04	
			4378	0.02	

Figure II.15: Plot of the fraction of unexchanged α-proton H_M against time for the prolyl TKP (**11**) in 30 % fb 0.200 M KOAc with 40 % d_3-MeCN co-solvent, I = 0.2 (KCl) and 25 ºC.

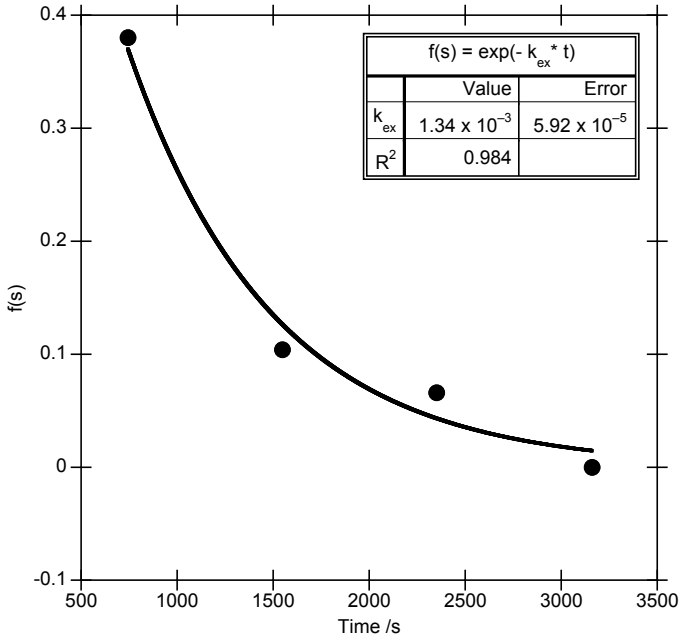

Figure II.16: Plot of the fraction of unexchanged α-proton H_M against time for the prolyl TKP (**11**) in 30 % fb 0.150 M KOAc with 40 % d_3-MeCN co-solvent, I = 0.2 (KCl) and 25 ºC.

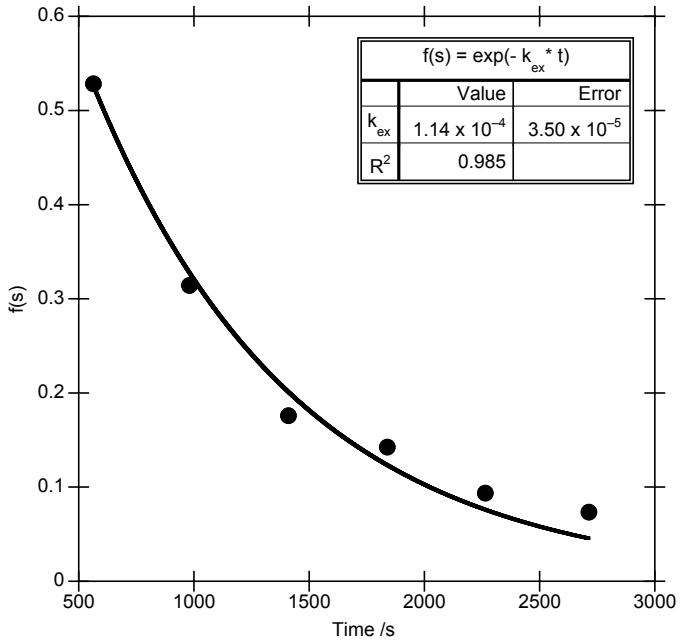

Figure II.17: Plot of the fraction of unexchanged α-proton H_M against time for the prolyl TKP (**11**) in 30 % fb 0.125 M KOAc with 40 % d_3-MeCN co-solvent, I = 0.2 (KCl) and 25 ºC.

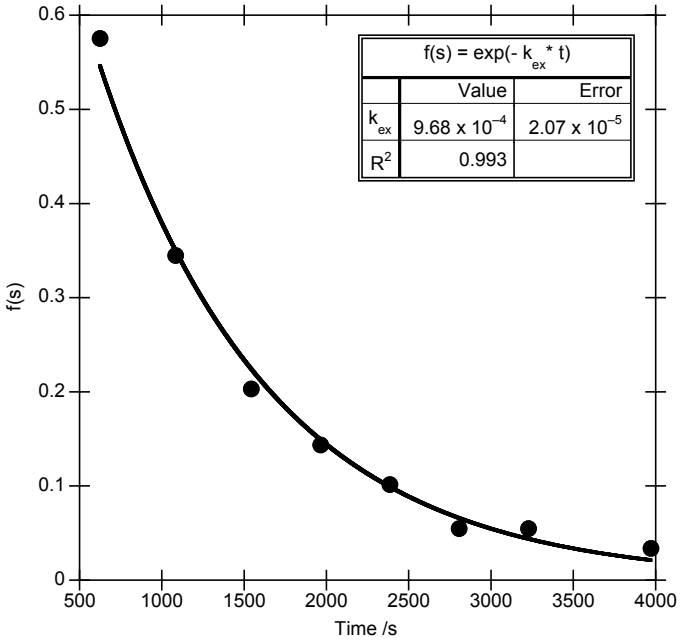

Figure II.18: Plot of the fraction of unexchanged α-proton H_M against time for the prolyl TKP (**11**) in 30 % fb 0.100 M KOAc with 40 % d_3-MeCN co-solvent, I = 0.2 (KCl) and 25 ºC.

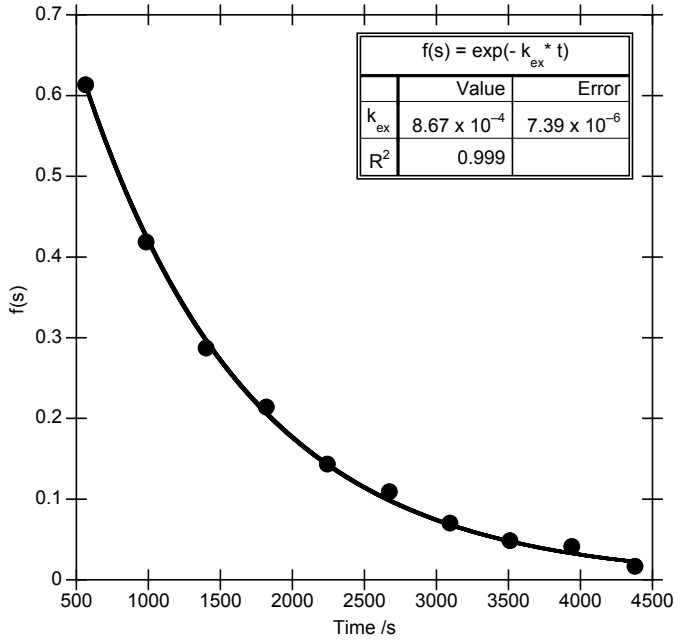

III Appendix III

Figure III.1: UV-Vis spectra for a dimethyl disulfide solution in a 50 mM NaOH solutions (pH 12.02) at 25 °C and ionic strength $I = 0.3$ M (NaCl).

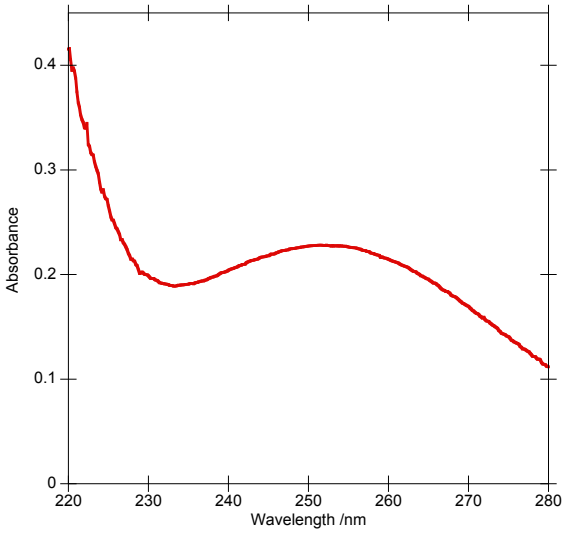

III.1 Determination of dissociation constants K_A – K_D for cysteine methyl ester

Figure III.2: UV-Vis spectra for 0.2 mM cysteine methyl ester in buffer solutions covering the pH range 1.76 – 12.34 with 2.0 mM TCEP at 25 °C and ionic strength $I = 0.3$ M (NaCl).

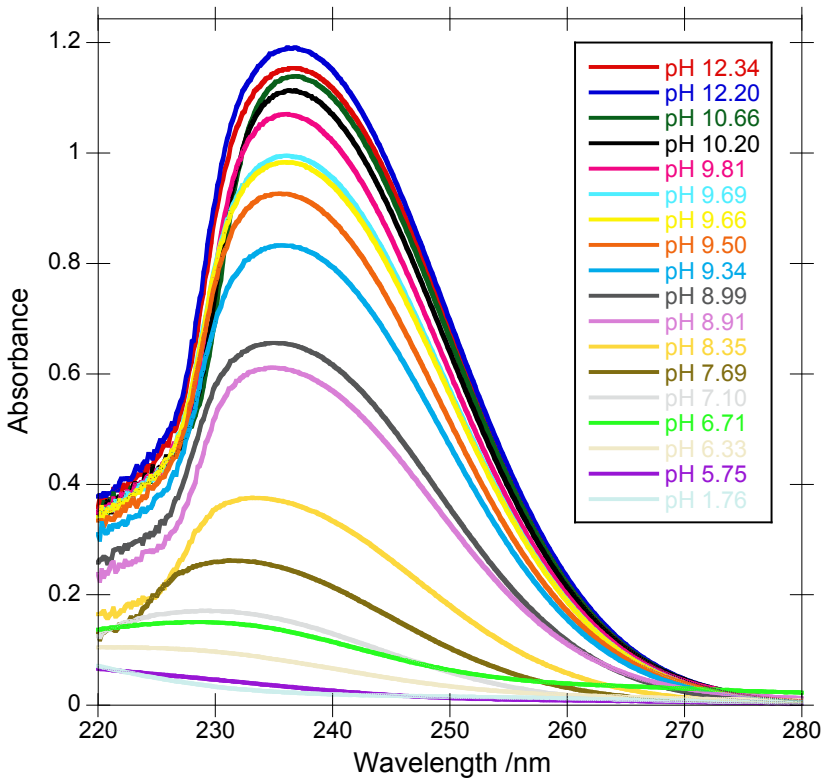

Figure III.3: UV-Vis spectra monitored at a single wavelength (λ = 237 nm) for 0.2 mM cysteine methyl ester in buffer solutions covering the pH range 1.49 – 12.34 with 2.0 mM TCEP at 25 °C and ionic strength I = 0.3 M (NaCl).

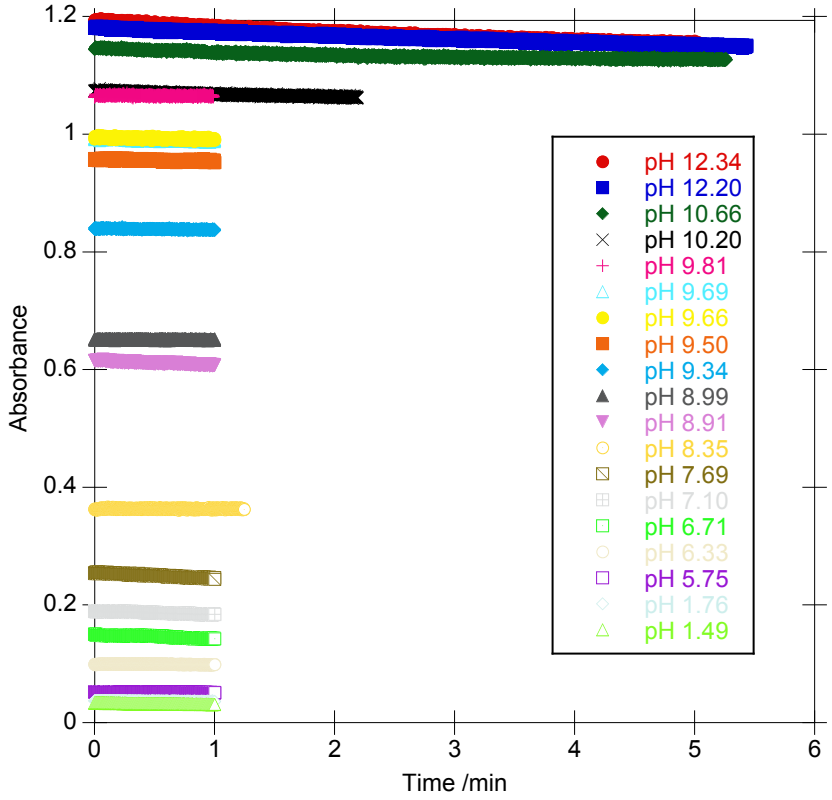

Table III.1: A_{obs}, $A_{obs} - A_{237}^{RSH}$ and f_{RS-} at each pH for cysteine methyl ester at 25 °C and ionic strength I = 0.3 M (NaCl).

Solution	pH	A_{obs}	$A_{obs} - A_{237}^{RSH}$	f_{RS-}
50 mM NaOH	12.34	1.194	1.160 [b]	1.00
30 mM NaOH	12.20	1.181	1.148	0.99
90% fb 0.1 M K_2CO_3	10.66	1.146	1.113	0.96
70% fb 0.1 M K_2CO_3	10.20	1.074	1.040	0.90
50% fb 0.1 M K_2CO_3	9.81	1.066	1.032	0.89
90% fb 0.1 M NH_4Cl	9.69	0.993	0.959	0.83
70% fb 0.1 M NH_4Cl	9.66	0.995	0.961	0.83
30% fb 0.1 M K_2CO_3	9.50	0.958	0.924	0.80
50% fb 0.1 M NH_4Cl	9.34	0.839	0.806	0.70
30% fb 0.1 M NH_4Cl	8.99	0.651	0.618	0.53
10% fb 0.1 M K_2CO_3	8.91	0.615	0.582	0.50
10% fb 0.1 M NH_4Cl	8.35	0.364	0.331	0.29
90% fb 0.1 M KH_2PO_4	7.69	0.255	0.221	0.19
70% fb 0.1 M KH_2PO_4	7.10	0.189	0.156	0.13
50% fb 0.1 M KH_2PO_4	6.71	0.150	0.117	0.10
30% fb 0.1 M KH_2PO_4	6.33	0.100	0.066	0.06
10% fb 0.1 M KH_2PO_4	5.75	0.052	0.019	0.02
30 mM HCl	1.76	0.037	0.004	0.003
50 mM HCl	1.49	0.034 [a]	0.000	0.00

[a] Value used for A_{237}^{RSH}. [b] Value used for $(A_{obs} - A_{237}^{RSH})_{max.}$

Figure III.4: UV-Vis spectra for 0.2 mM cysteine methyl ester in buffer solutions covering the pH range 5.70 – 12.38 with 2.0 mM TCEP at 25 °C and ionic strength I = 0.3 M (NaCl).

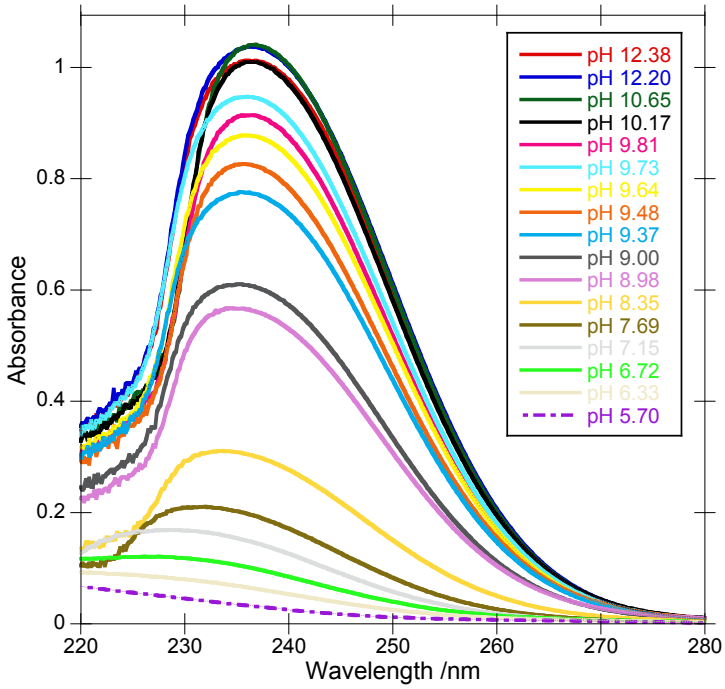

Figure III.5: UV-Vis spectra monitored at a single wavelength (λ = 237 nm) for 0.2 mM cysteine methyl ester in buffer solutions covering the pH range 1.39 – 12.38 with 2.0 mM TCEP at 25 °C and ionic strength I = 0.3 M (NaCl).

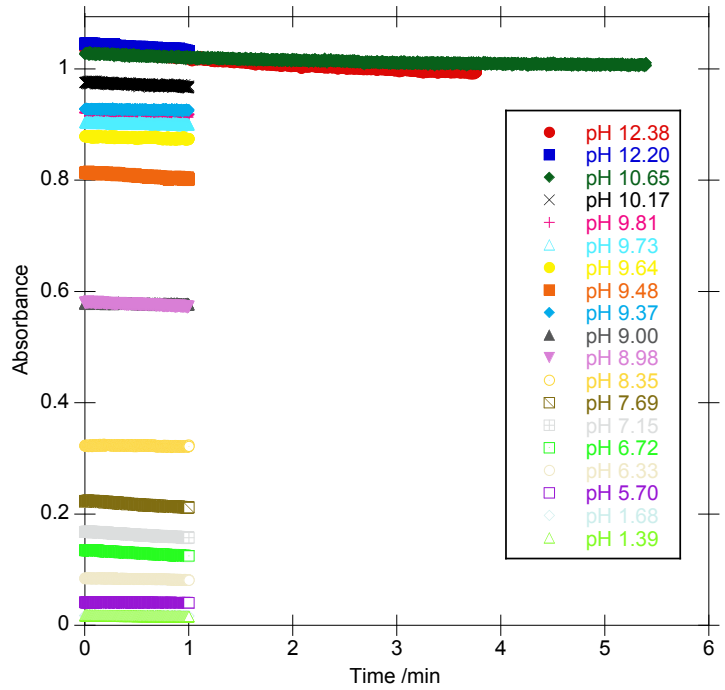

Table III.2: A_{obs}, $A_{obs} - A_{237}^{RSH}$ and f_{RS-} at each pH for cysteine methyl ester at 25 °C and ionic strength I = 0.3 M (NaCl).

Solution	pH	A_{obs}	$A_{obs} - A_{237}^{RSH}$	f_{RS-}
50 mM NaOH	12.38	1.036	1.018 [b]	1.00
30 mM NaOH	12.20	1.045	1.027	1.01
90% fb 0.1 M K_2CO_3	10.65	1.027	1.010	0.99
70% fb 0.1 M K_2CO_3	10.17	0.977	0.959	0.94
50% fb 0.1 M K_2CO_3	9.81	0.922	0.904	0.89
70% fb 0.1 M NH_4Cl	9.73	0.904	0.886	0.87
90% fb 0.1 M NH_4Cl	9.64	0.879	0.861	0.85
30% fb 0.1 M K_2CO_3	9.48	0.813	0.796	0.78
50% fb 0.1 M NH_4Cl	9.37	0.928	0.910	0.89
30% fb 0.1 M NH_4Cl	9.00	0.579	0.561	0.55
10% fb 0.1 M K_2CO_3	8.98	0.580	0.563	0.55
10% fb 0.1 M NH_4Cl	8.35	0.324	0.306	0.30
90% fb 0.1 M KH_2PO_4	7.69	0.224	0.206	0.20
70% fb 0.1 M KH_2PO_4	7.15	0.168	0.150	0.15
50% fb 0.1 M KH_2PO_4	6.72	0.135	0.117	0.12
30% fb 0.1 M KH_2PO_4	6.33	0.085	0.067	0.07
10% fb 0.1 M KH_2PO_4	5.70	0.041	0.024	0.02
30 mM HCl	1.68	0.018	0.000	0.00
50 mM HCl	1.39	0.018 [a]	0.000	0.00

[a] Value used for A_{237}^{RSH}. [b] Value used for $(A_{obs} - A_{237}^{RSH})_{max.}$

III.2 Determination of dissociation constants K_A – K_D for penicillamine methyl ester

Figure III.6: UV-Vis spectra for 0.2 mM penicillamine methyl ester in buffer solutions covering the pH range 1.42 – 11.82 at 25 °C and ionic strength I = 0.3 M (NaCl).

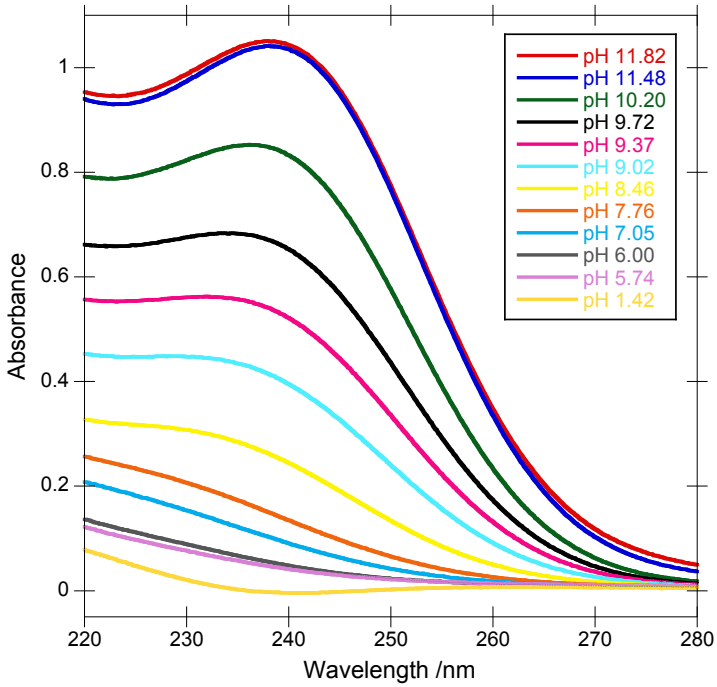

Figure III.7: UV-Vis spectra monitored at a single wavelength (λ = 237 nm) for 0.2 mM penicillamine methyl ester in buffer solutions covering the pH range 1.42 – 12.57 at 25 °C and ionic strength I = 0.3 M (NaCl).

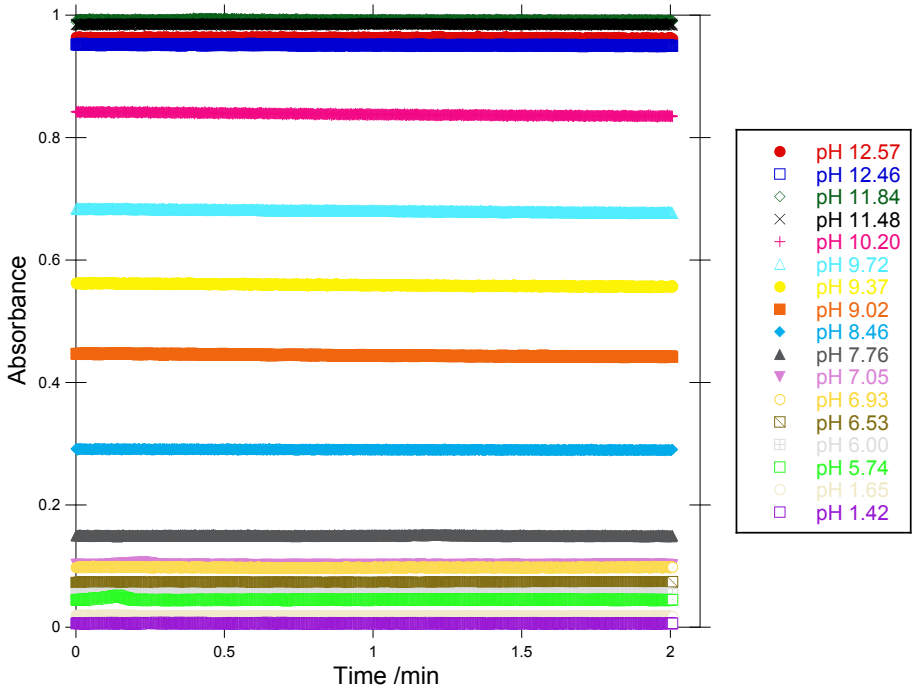

Table III.3: A_{obs}, $A_{obs} - A_{237}^{RSH}$ and f_{RS^-} at each pH for penicillamine methyl ester at 25 °C and ionic strength I = 0.3 M (NaCl).

Solution	pH	A_{obs}	$A_{obs} - A_{237}^{RSH}$	f_{RS^-}
50 mM NaOH	12.57	0.963	0.956 [b]	1.00
40 mM NaOH	12.46	0.952	0.945	0.99
30 mM NaOH	11.84	0.992	0.985	1.03
10 mM NaOH	11.49	0.985	0.978	1.02
90% fb 0.1 M NH_4Cl	10.20	0.842	0.835	0.87
70% fb 0.1 M NH_4Cl	9.72	0.684	0.677	0.71
50% fb 0.1 M NH_4Cl	9.37	0.562	0.555	0.58
30% fb 0.1 M NH_4Cl	9.02	0.447	0.440	0.46
10% fb 0.1 M NH_4Cl	8.46	0.291	0.284	0.30
90% fb 0.1 M KH_2PO_4	7.76	0.150	0.143	0.15
70% fb 0.1 M KH_2PO_4	7.05	0.102	0.095	0.10
60% fb 0.1 M KH_2PO_4	6.93	0.098	0.092	0.10
40% fb 0.1 M KH_2PO_4	6.53	0.073	0.066	0.07
20% fb 0.1 M KH_2PO_4	6.00	0.054	0.047	0.05
10% fb 0.1 M KH_2PO_4	5.74	0.045	0.038	0.04
90% fb 0.1 M H_3PO_4	2.97	0.099	0.093	0.10
90% fb 0.1 M H_3PO_4	2.97	0.099	0.092	0.10
70% fb 0.1 M H_3PO_4	2.42	0.099	0.093	0.10
90% fb 0.1 M H_3PO_4	2.42	0.099	0.092	0.10
30 mM HCl	1.42	0.007 [a]	0.000	0.00

[a] Value used for A_{237}^{RSH}. [b] Value used for $(A_{obs} - A_{237}^{RSH})_{max.}$

Figure III.8: UV-Vis spectra for 0.2 mM penicillamine methyl ester in buffer solutions covering the pH range 1.49 – 12.35 with 2.0 mM TCEP at 25 °C and ionic strength I = 0.3 M (NaCl).

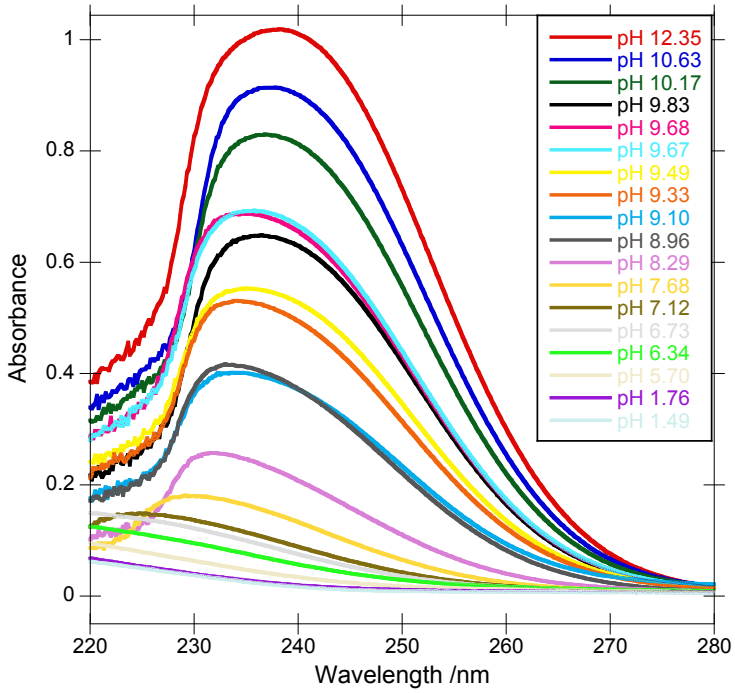

Figure III.9: UV-Vis spectra monitored at a single wavelength (λ = 237 nm) for 0.2 mM penicillamine methyl ester in buffer solutions covering the pH range 1.49 – 12.35 with 2.0 mM TCEP at 25 °C and ionic strength I = 0.3 M (NaCl).

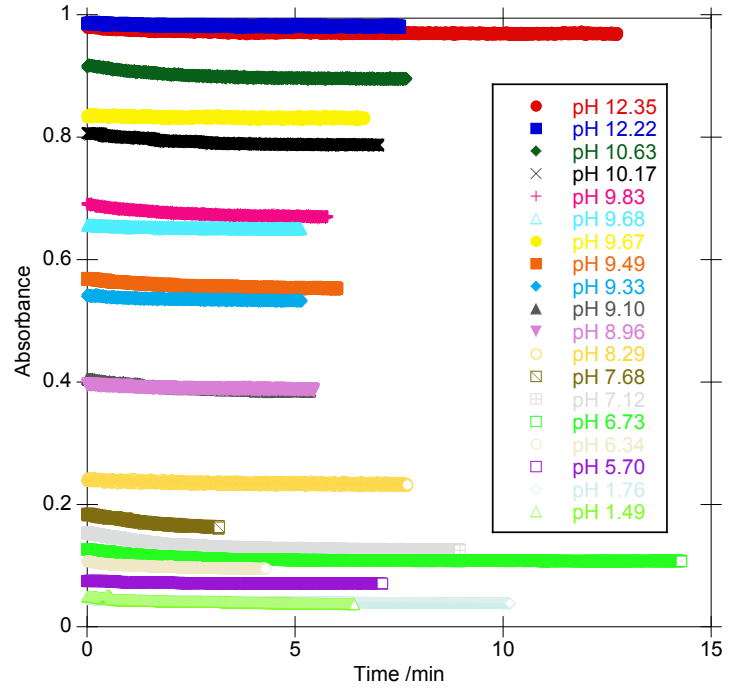

Table III.4: A_{obs}, $A_{obs} - A_{237}^{RSH}$ and f_{RS^-} at each pH for penicillamine methyl ester with TCEP (2.0 mM) at 25 °C and ionic strength I = 0.3 M (NaCl).

Solution	pH	A_{obs}	$A_{obs} - A_{237}^{RSH}$	f_{RS^-}
50 mM NaOH	12.35	0.980	0.931 [b]	1.00
30 mM NaOH	12.22	0.986	0.937	1.01
90% fb 0.1 M K_2CO_3	10.63	0.917	0.868	0.93
70% fb 0.1 M K_2CO_3	10.17	0.807	0.757	0.81
50% fb 0.1 M K_2CO_3	9.83	0.691	0.642	0.69
90% fb 0.1 M NH_4Cl	9.68	0.656	0.607	0.65
70% fb 0.1 M NH_4Cl	9.67	0.834	0.785	0.84
30% fb 0.1 M K_2CO_3	9.49	0.569	0.519	0.56
50% fb 0.1 M NH_4Cl	9.33	0.541	0.492	0.53
10% fb 0.1 M K_2CO_3	9.10	0.404	0.355	0.38
30% fb 0.1 M NH_4Cl	8.96	0.396	0.347	0.37
10% fb 0.1 M NH_4Cl	8.29	0.240	0.191	0.21
90% fb 0.1 M KH_2PO_4	7.68	0.184	0.135	0.14
70% fb 0.1 M KH_2PO_4	7.12	0.153	0.104	0.11
50% fb 0.1 M KH_2PO_4	6.73	0.126	0.077	0.08
30% fb 0.1 M KH_2PO_4	6.34	0.107	0.058	0.06
10% fb 0.1 M KH_2PO_4	5.70	0.075	0.026	0.03
30 mM HCl	1.76	0.045	-0.005	-0.01
50 mM HCl	1.49	0.049 [a]	0.000	0.00

[a] Value used for A_{237}^{RSH}. [b] Value used for $(A_{obs} - A_{237}^{RSH})_{max.}$

III.3 Determination of dissociation constants K_A – K_D 4*S*-mercaptoproline methyl ester

Figure III.10: UV-Vis spectra for 0.2 mM 4*S*-mercaptoproline methyl ester in buffer solutions covering the pH range 1.36 – 12.09 at 25 °C and ionic strength I = 0.3 M (NaCl).

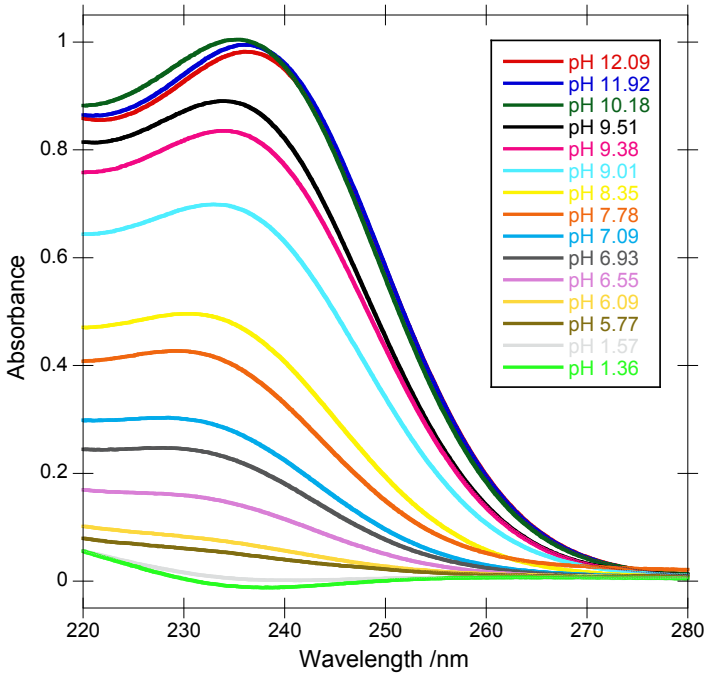

Figure III.11: UV-Vis spectra monitored at a single wavelength (λ = 230 – 236 nm) for 0.2 mM 4*S*-mercaptoproline methyl ester in buffer solutions covering the pH range 1.34 – 12.02 at 25 °C and ionic strength I = 0.3 M (NaCl).

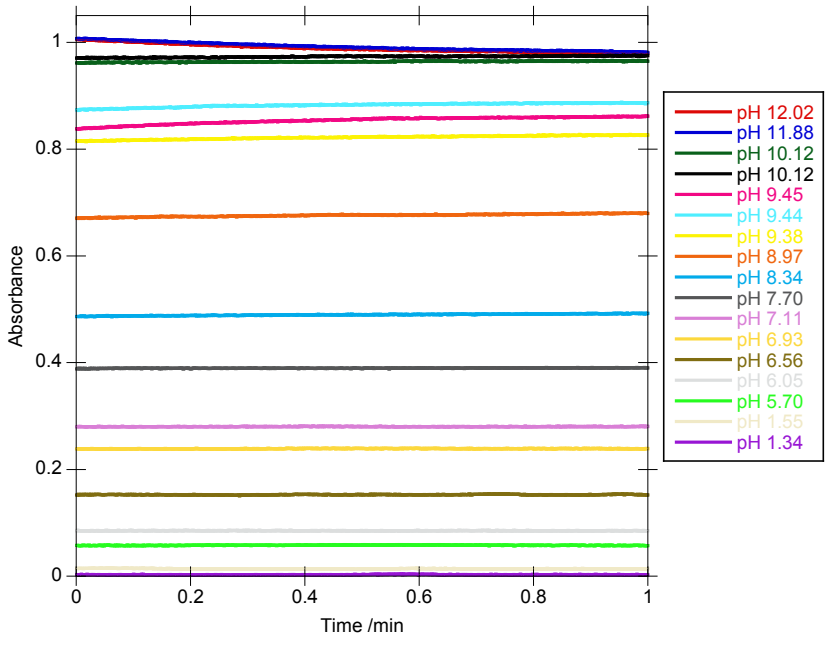

Table III.5: A_{obs}, $A_{obs} - A_{237}^{RSH}$ and f_{RS-} at each pH for 4*S*-mercaptoproline methyl ester at 25 °C and ionic strength I = 0.3 M (NaCl).

Solution	pH	A_{obs}	$A_{obs} - A_{237}^{RSH}$	f_{RS-}
50 mM NaOH	12.02	1.006	1.003 [b]	1.00
30 mM NaOH	11.88	1.007	1.004	1.00
90% fb 0.1 M NH_4Cl	10.12	0.965	0.963	0.96
90% fb 0.1 M NH_4Cl	10.12	0.975	0.972	0.97
70% fb 0.1 M NH_4Cl	9.45	0.861	0.858	0.86
70% fb 0.1 M NH_4Cl	9.44	0.887	0.884	0.88
50% fb 0.1 M NH_4Cl	9.38	0.826	0.824	0.82
30% fb 0.1 M NH_4Cl	8.97	0.680	0.677	0.67
10% fb 0.1 M NH_4Cl	8.34	0.492	0.489	0.49
90% 0.1 M KH_2PO_4	7.70	0.390	0.388	0.39
70% fb 0.1 M KH_2PO_4	7.11	0.280	0.278	0.28
60% fb 0.1 M KH_2PO_4	6.93	0.239	0.236	0.24
40% fb 0.1 M KH_2PO_4	6.56	0.153	0.150	0.15
20% fb 0.1 M KH_2PO_4	6.05	0.085	0.083	0.08
10% fb 0.1 M KH_2PO_4	5.70	0.058	0.055	0.05
90% fb 0.1 M H_3PO_4	2.96	0.025	0.023	0.02
90% fb 0.1 M H_3PO_4	2.96	0.025	0.022	0.02
70% fb 0.1 M H_3PO_4	2.40	0.018	0.015	0.02
70% fb 0.1 M H_3PO_4	2.40	0.018	0.015	0.02
50% fb 0.1 M H_3PO_4	2.10	0.006	0.003	0.00
50% fb 0.1 M H_3PO_4	2.10	0.007	0.004	0.00
30% fb 0.1 M H_3PO_4	1.85	-0.005	-0.007	-0.01
30% fb 0.1 M H_3PO_4	1.85	-0.005	-0.008	-0.01
30 mM HCl	1.55	0.013	0.011	0.01
50 mM HCl	1.34	0.003 [a]	0.000	0.00

[a] Value used for A_{237}^{RSH}. [b] Value used for $(A_{obs} - A_{237}^{RSH})_{max.}$

III.4 Determination of dissociation constants K_A – K_D H-Cys-Gly-Phe-NH_2

Figure III.12: UV-Vis spectra for 0.2 mM H-Cys-Gly-Phe-NH_2 in buffer solutions covering the pH range 1.58 – 12.40 with 2.0 mM TCEP at 25 °C and ionic strength I = 0.3 M (NaCl).

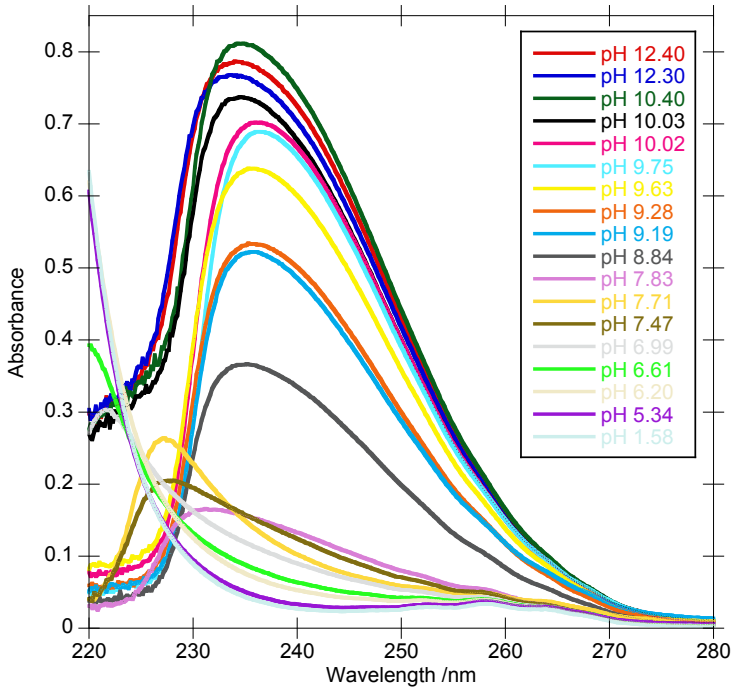

Figure III.13: UV-Vis spectra monitored at a single wavelength (λ = 230 – 236 nm) for 0.2 mM H-Cys-Gly-Phe-NH_2 in buffer solutions covering the pH range 1.36 – 12.40 with 2.0 mM TCEP at 25 °C and ionic strength I = 0.3 M (NaCl).

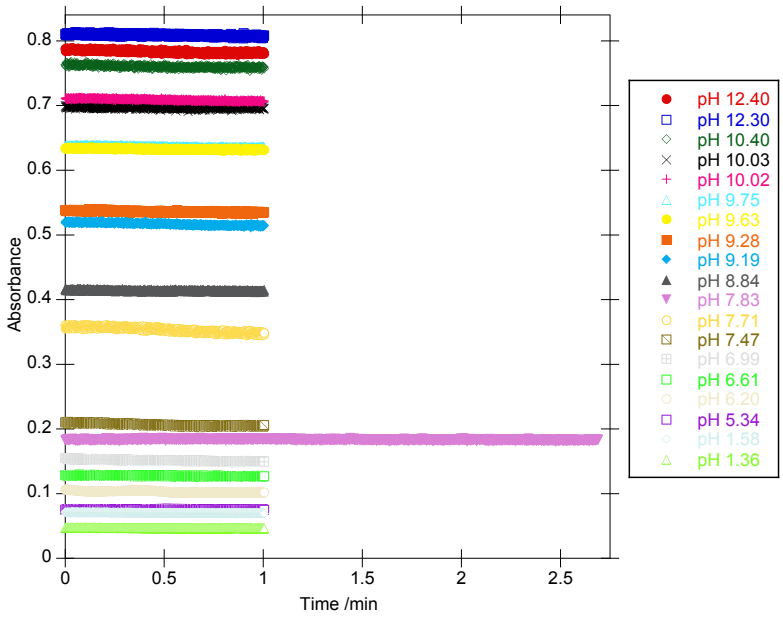

Table III.6: A_{obs}, $A_{obs} - A_{237}^{RSH}$ and f_{RS-} at each pH for H-Cys-Gly-Phe-NH_2 at 25 °C and ionic strength I = 0.3 M (NaCl).

Solution	pH	A_{obs}	$A_{obs} - A_{237}^{RSH}$	f_{RS-}
50m M NaOH	12.40	0.787	0.739 [b]	1.00
40 mM NaOH	12.30	0.811	0.764	1.03
90% fb 0.1 M K_2CO_3	10.40	0.764	0.716	0.97
70% fb 0.1 M K_2CO_3	10.03	0.698	0.651	0.88
90% fb 0.1 M NH_4Cl	10.02	0.711	0.664	0.90
50% fb 0.1 M K_2CO_3	9.75	0.638	0.591	0.80
70% fb 0.1 M NH_4Cl	9.63	0.634	0.587	0.79
50% fb 0.1 M NH_4Cl	9.28	0.538	0.491	0.66
30% fb 0.1 M K_2CO_3	9.19	0.520	0.472	0.64
30% fb 0.1 M NH_4Cl	8.84	0.416	0.368	0.50
10% fb 0.1 M NH_4Cl	7.83	0.185	0.137	0.19
10% fb 0.1 M K_2CO_3	7.71	0.359	0.312	0.42
90% fb 0.1 M KH_2PO_4	7.47	0.210	0.162	0.22
70% fb 0.1 M KH_2PO_4	6.99	0.155	0.108	0.15
50% fb 0.1 M KH_2PO_4	6.61	0.129	0.081	0.11
30% fb 0.1 M KH_2PO_4	6.20	0.107	0.059	0.08
10% fb 0.1 M KH_2PO_4	5.34	0.076	0.028	0.04
30 mM HCl	1.58	0.071	0.024	0.03
50 mM HCl	1.36	0.047 [a]	0.000	0.00

[a] Value used for A_{237}^{RSH}. [b] Value used for $(A_{obs} - A_{237}^{RSH})_{max.}$

III.5 Determination of dissociation constants K_A – K_D H-Pen-Gly-Phe-NH_2

Figure III.14: UV-Vis spectra for 0.2 mM H-Pen-Gly-Phe-NH_2 in buffer solutions covering the pH range 1.54 – 12.39 with 2.0 mM TCEP at 25 °C and ionic strength I = 0.3 M (NaCl).

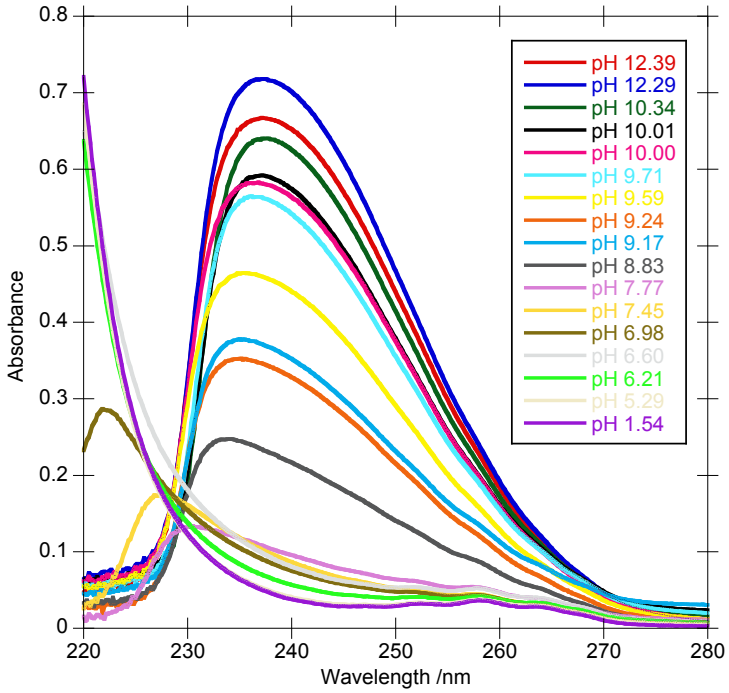

Figure III.15: UV-Vis spectra monitored at a single wavelength (λ = 230 – 236 nm) for 0.2 mM H-Pen-Gly-Phe-NH_2 in buffer solutions covering the pH range 1.31 – 12.39 with 2.0 mM TCEP at 25 °C and ionic strength I = 0.3 M (NaCl).

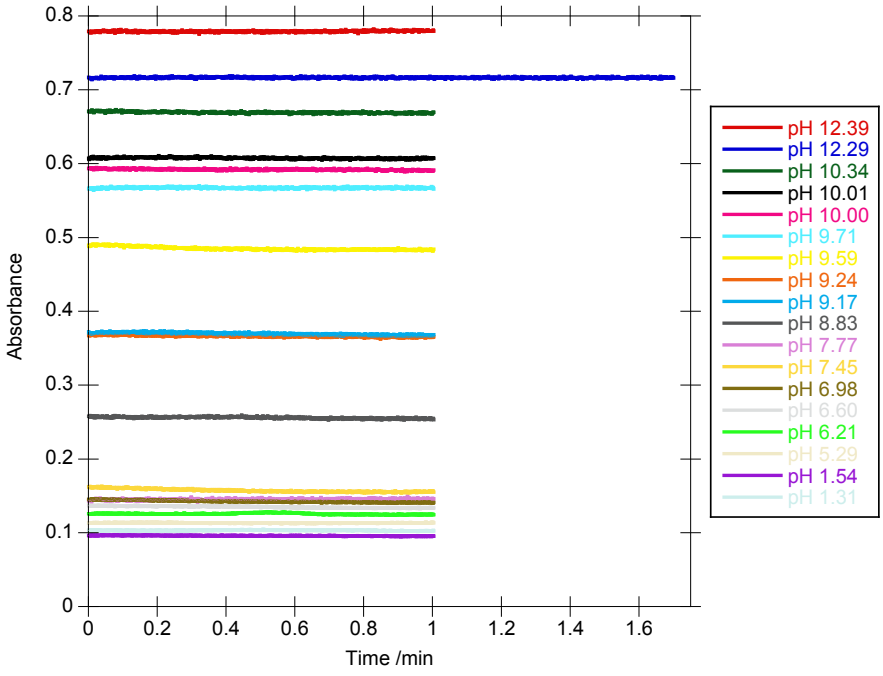

Table III.7: A_{obs}, $A_{obs} - A_{237}^{RSH}$ and f_{RS-} at each pH for H-Pen-Gly-Phe-NH_2 at 25 °C and ionic strength I = 0.3 M (NaCl).

Solution	pH	A_{obs}	$A_{obs} - A_{237}^{RSH}$	f_{RS-}
50m M NaOH	12.39	0.779	0.676 [b]	1.00
40 mM NaOH	12.29	0.717	0.613	0.91
90% fb 0.1 M K_2CO_3	10.34	0.671	0.568	0.84
70% fb 0.1 M K_2CO_3	10.01	0.609	0.505	0.75
50% fb 0.1 M K_2CO_3	9.71	0.568	0.464	0.69
30% fb 0.1 M K_2CO_3	9.17	0.372	0.268	0.40
90% fb 0.1 M NH_4Cl	10.00	0.594	0.490	0.73
70% fb 0.1 M NH_4Cl	9.59	0.490	0.386	0.57
50% fb 0.1 M NH_4Cl	9.24	0.368	0.264	0.39
30% fb 0.1 M NH_4Cl	8.83	0.258	0.154	0.23
10% fb 0.1 M NH_4Cl	7.77	0.145	0.042	0.06
90% fb 0.1M KH_2PO_4	7.45	0.162	0.059	0.09
70% fb 0.1 M KH_2PO_4	6.98	0.145	0.042	0.06
50% fb 0.1 M KH_2PO_4	6.60	0.137	0.033	0.05
30% fb 0.1 M KH_2PO_4	6.21	0.126	0.023	0.03
10% fb 0.1 M KH_2PO_4	5.29	0.114	0.010	0.02
30 mM HCl	1.54	0.097	-0.007	-0.01
50 mM HCl	1.31	0.103 [a]	0.000	0.00

[a] Value used for A_{237}^{RSH}. [b] Value used for $(A_{obs} - A_{237}^{RSH})_{max.}$

III.6 Determination of dissociation constants K_A – K_D H-Cys-Gly-OH

Figure III.16: UV-Vis spectra for 0.2 mM H-Cys-Gly-OH in buffer solutions covering the pH range 1.44 – 12.42 with 2.0 mM TCEP at 25 °C and ionic strength I = 0.3 M (NaCl).

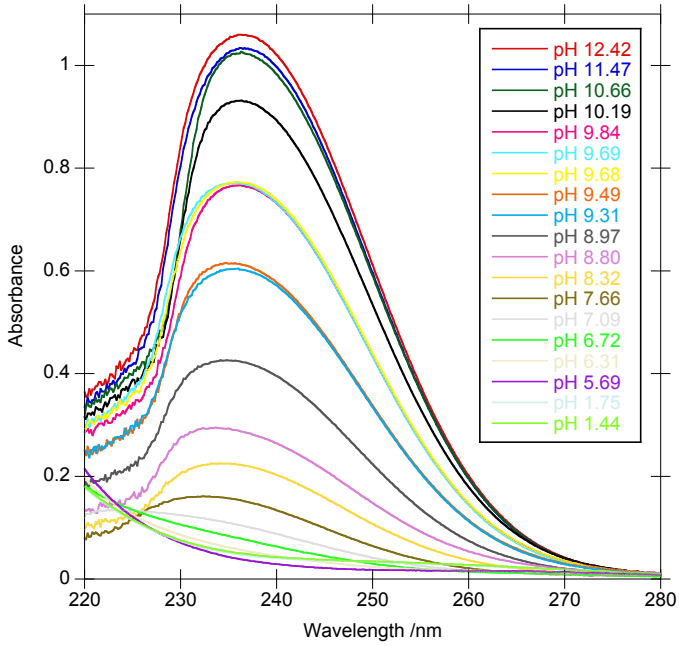

Figure III.17: UV-Vis spectra monitored at a single wavelength (λ = 230 – 236 nm) for 0.2 mM H-Cys-Gly-OH in buffer solutions covering the pH range 1.44 – 12.40 with 2.0 mM TCEP at 25 °C and ionic strength I = 0.3 M (NaCl).

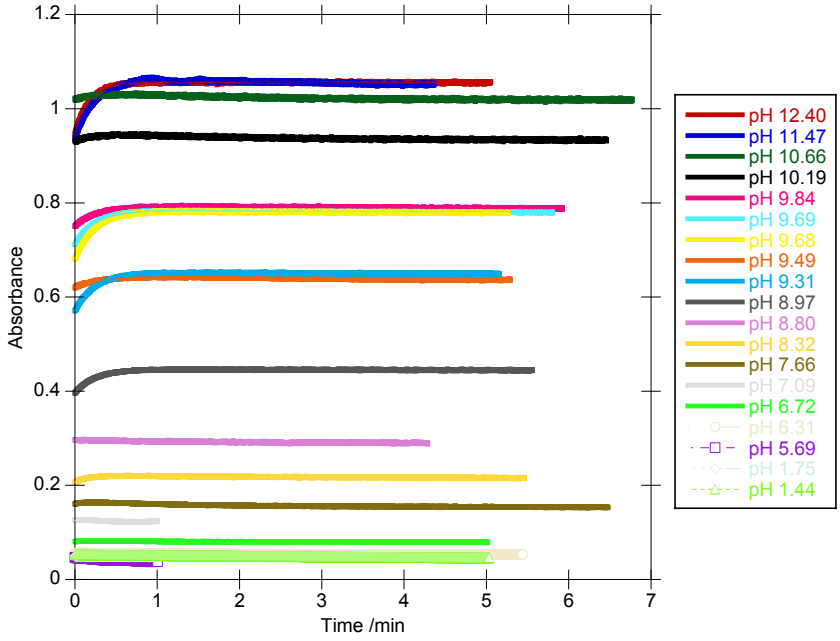

Table III.8: A_{obs}, $A_{obs} - A_{237}^{RSH}$ and f_{RS^-} at each pH for H-Cys-Gly-OH at 25 °C and ionic strength $I = 0.3$ M (NaCl).

Solution	pH	A_{obs}	$A_{obs} - A_{237}^{RSH}$	f_{RS^-}
50m M NaOH	12.40	1.056	1.004 [b]	1.00
40 mM NaOH	11.47	1.063	1.011	1.01
90% fb 0.1 M K_2CO_3	10.66	1.030	0.977	0.97
70% fb 0.1 M K_2CO_3	10.19	0.944	0.891	0.89
50% fb 0.1 M K_2CO_3	9.84	0.792	0.739	0.74
30% fb 0.1 M K_2CO_3	9.49	0.642	0.590	0.59
10% fb 0.1 M K_2CO_3	8.80	0.298	0.245	0.24
90% fb 0.1 M NH_4Cl	9.69	0.783	0.730	0.73
70% fb 0.1 M NH_4Cl	9.68	0.782	0.729	0.73
50% fb 0.1 M NH_4Cl	9.31	0.652	0.599	0.60
30% fb 0.1 M NH_4Cl	8.97	0.446	0.393	0.39
10% fb 0.1 M NH_4Cl	8.32	0.220	0.167	0.17
90% fb 0.1 M KH_2PO_4	7.66	0.164	0.111	0.11
70% fb 0.1 M KH_2PO_4	7.09	0.127	0.074	0.07
50% fb 0.1 M KH_2PO_4	6.72	0.082	0.029	0.03
30% fb 0.1 M KH_2PO_4	6.31	0.056	0.003	0.00
10% fb 0.1 M KH_2PO_4	5.69	0.047	-0.006	-0.01
30 mM HCl	1.75	0.049	-0.004	0.00
50 mM HCl	1.44	0.053 [a]	0.000	0.00

[a] Value used for A_{237}^{RSH}. [b] Value used for $(A_{obs} - A_{237}^{RSH})_{max.}$

III.7 Determination of dissociation constants K_A – K_D cysteine

Figure III.18: UV-Vis spectra for 0.2 mM cysteine in buffer solutions covering the pH range 6.69 – 12.39 with 2.0 mM TCEP at 25 °C and ionic strength I = 0.3 M (NaCl).

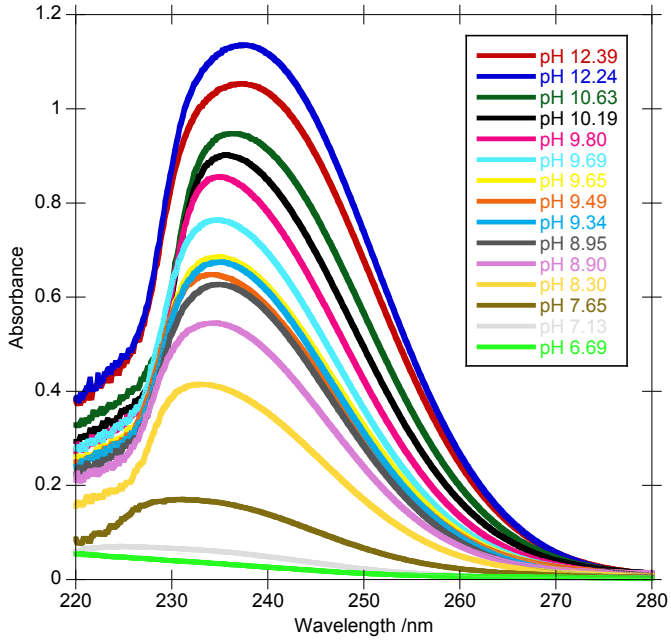

Figure III.19: UV-Vis spectra monitored at a single wavelength (λ = 230 – 236 nm) for 0.2 mM cysteine in buffer solutions covering the pH range 1.50 – 12.39 with 2.0 mM TCEP at 25 °C and ionic strength I = 0.3 M (NaCl).

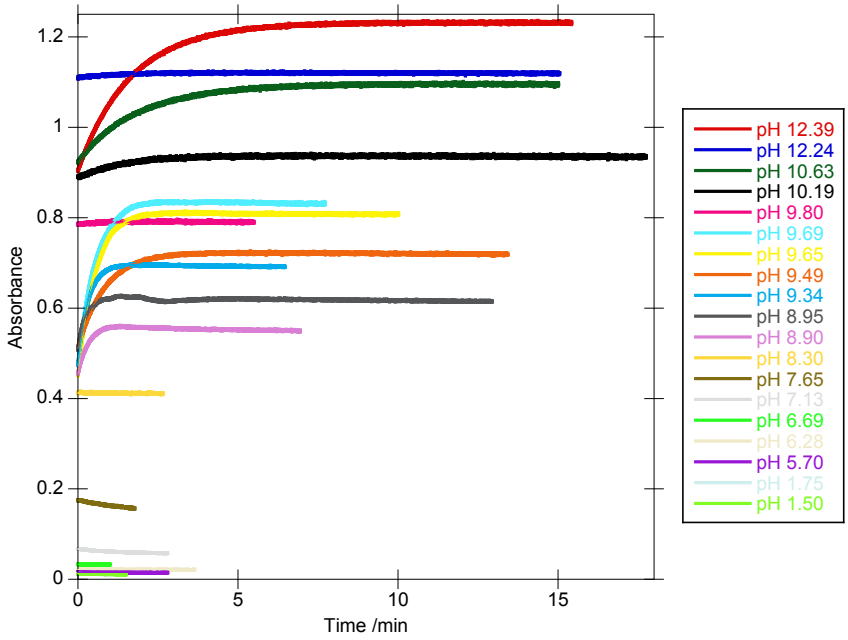

The rise in absorbance over time observed at higher pHs in Figure III.19 indicates that the cysteine had oxidised in solution. The rise in absorbance as the experiment progressed is a result of the TCEP reducing the disulfide bonds.

Table III.9: A_{obs}, $A_{obs} - A_{237}^{RSH}$ and f_{RS^-} at each pH for cysteine at 25 °C and ionic strength I = 0.3 M (NaCl).

Solution	pH	A_{obs}	$A_{obs} - A_{237}^{RSH}$	f_{RS^-}
50 mM NaOH	12.39	1.231	1.219 [b]	1.00
30 mM NaOH	12.24	1.121	1.108	0.91
90% fb 0.1 M K_2CO_3	10.63	1.095	1.083	0.89
70% fb 0.1 M K_2CO_3	10.19	0.937	0.925	0.76
50% fb 0.1 M K_2CO_3	9.80	0.792	0.779	0.64
90% fb 0.1 M NH_4Cl	9.69	0.834	0.822	0.67
70% fb 0.1 M NH_4Cl	9.65	0.811	0.799	0.66
30% fb 0.1 M K_2CO_3	9.49	0.722	0.710	0.58
50% fb 0.1 M NH_4Cl	9.34	0.696	0.683	0.56
30% fb 0.1 M NH_4Cl	8.95	0.626	0.614	0.50
10% fb 0.1 M K_2CO_3	8.90	0.559	0.547	0.45
10% fb 0.1 M NH_4Cl	8.30	0.413	0.401	0.33
90% fb 0.1 M KH_2PO_4	7.65	0.175	0.163	0.13
70% fb 0.1 M KH_2PO_4	7.13	0.067	0.055	0.04
50% fb 0.1 M KH_2PO_4	6.69	0.033	0.021	0.02
30% fb 0.1 M KH_2PO_4	6.28	0.022	0.010	0.01
10% fb 0.1 M KH_2PO_4	5.70	0.016	0.004	0.003
30 mM HCl	1.75	0.012	0.000	0.000
50 mM HCl	1.50	0.012 [a]	0.000	0.000

[a] Value used for A_{237}^{RSH}. [b] Value used for $(A_{obs} - A_{237}^{RSH})_{max.}$

III.8 Determination of molar extinction coefficient for penicillamine methyl ester

Figure III.20: UV-Vis spectra for 0.05 mM – 0.15 mM penicillamine methyl ester in 30 mM NaOH solution with 2.0 mM TCEP at 25 °C and ionic strength *I* = 0.3 M (NaCl).

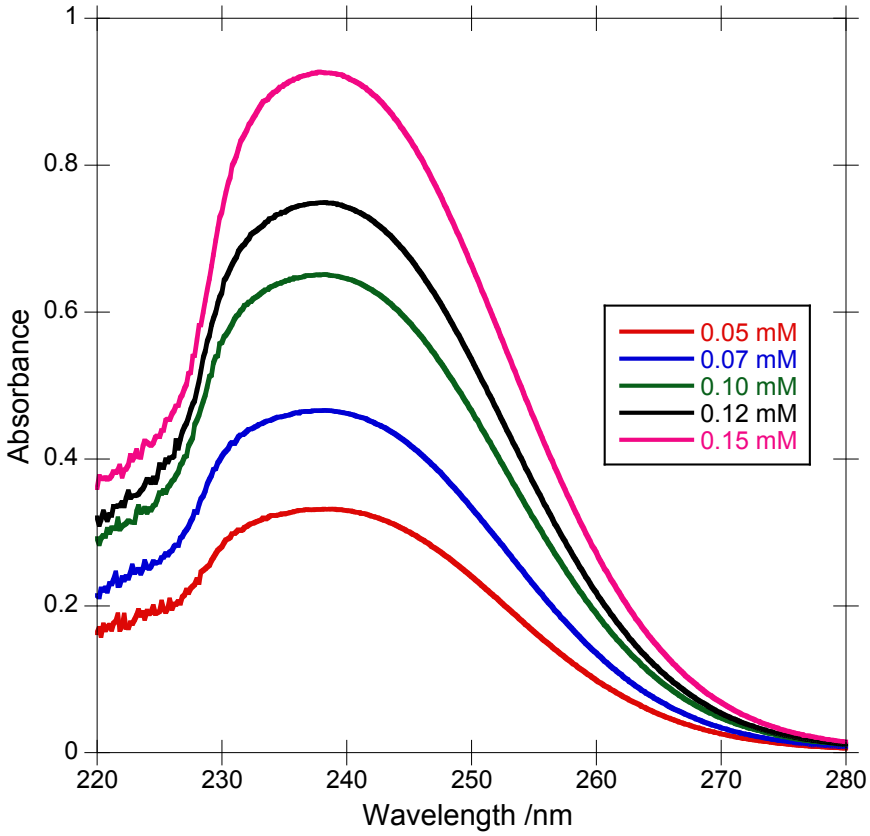

Table III.10: pH, λ_{max} and Absorbance values for different concentrations of penicillamine methyl ester used to determine the molar extinction coefficient.

[Penicillamine methyl ester] /mM	pH	λ_{max} /nm	Absorbance
0.05	12.27	238	0.332
0.07	12.27	238	0.466
0.10	12.27	238	0.651
0.12	12.28	238	0.749
0.15	12.27	238	0.927

III.9 Determination of molar extinction coefficient for the 4*S*-mercaptoproline methyl ester

Figure III.21: UV-Vis spectra for 0.05 mM – 0.12 mM 4*S*-mercaptoproline methyl ester in 30 mM NaOH solution with 2.0 mM TCEP at 25 °C and ionic strength I = 0.3 M (NaCl).

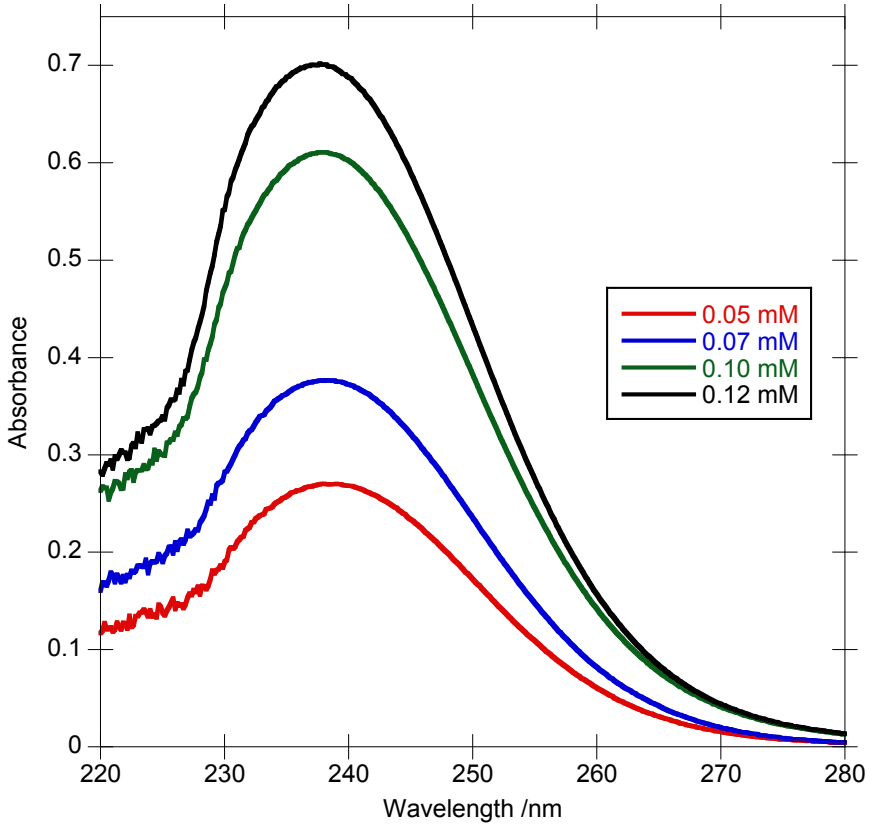

Table III.11: pH, λ_{max} and Absorbance values for different concentrations of 4*S*-mercaptoproline methyl ester used to determine the molar extinction coefficient.

[4*S*-mercaptoproline methyl ester] /mM	pH	λ_{max} /nm	Absorbance
0.05	12.22	238	0.701
0.07	12.24	238	0.611
0.10	12.22	238	0.377
0.12	12.22	238	0.270

III.10 Determination of molar extinction coefficient for cysteine

Figure III.22: UV-Vis spectra for 0.05 mM – 0.12 mM cysteine in 30 mM NaOH solution with 2.0 mM TCEP at 25 °C and ionic strength I = 0.3 M (NaCl).

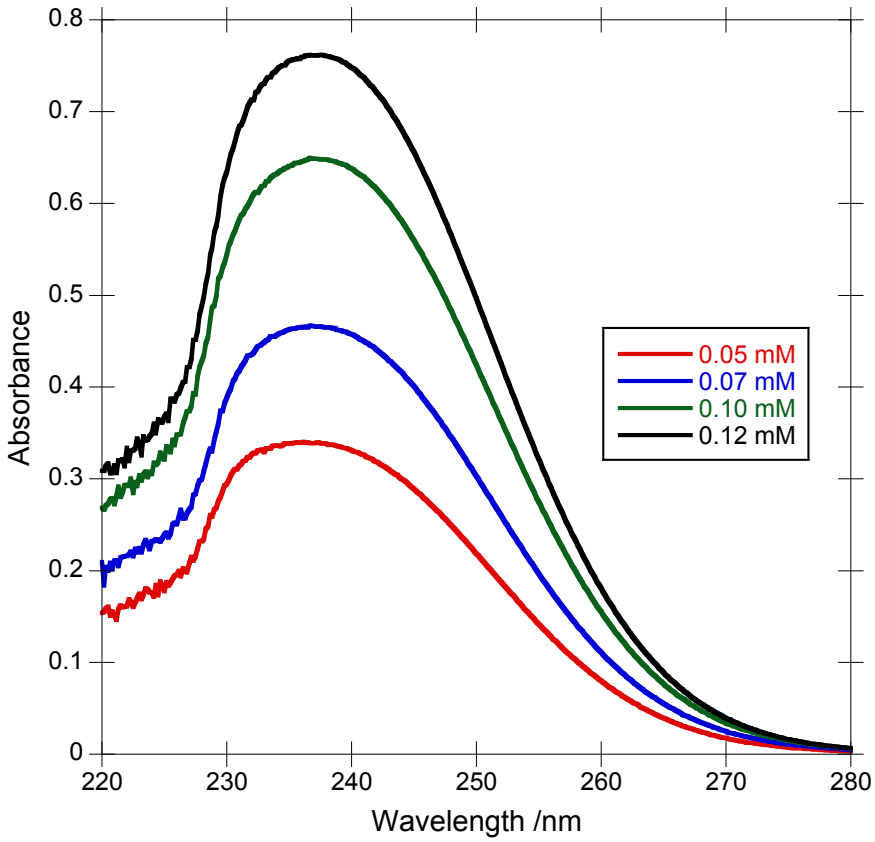

Table III.12: pH, λ_{max} and Absorbance values for different concentrations of cysteine used to determine the molar extinction coefficient.

[Cysteine] /mM	pH	λ_{max} /nm	Absorbance
0.05	12.23	236	0.340
0.07	12.24	236	0.467
0.10	12.22	236	0.650
0.12	12.24	237	0.762

III.11 An Alternative Speciation Model

A speciation model with four pK_as and four possible species in solution has been used to determine the pK of the thiol and ammonium (K_A – K_D) on the cysteine derivatives (Scheme 4.40 and Equation 4.2). Two alternative "Two pK_a + Three Species" models do exist where the pK_as of the thiol and ammonium are independent of each other (> 2 pK units apart).

The first of these "Two pK_a + Three Species" models has the ammonium pK_a below that of the thiol such that only a single thiolate species (H_2N-R-S^-) is present in solution (Scheme III.1)

Scheme III.1: "Two pK_a + Three Species" with the ammonium pK_a lower than that of the thiol.

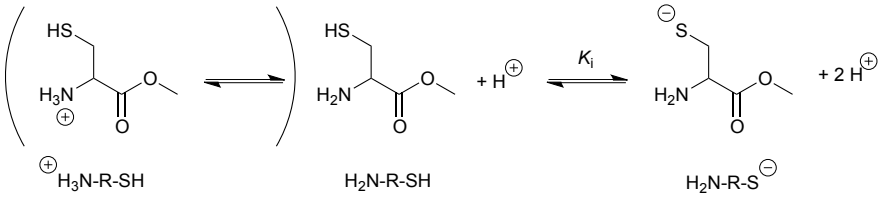

Consequently, the K_a of the thiol (K_i) may be found from Equation III.1:

$$K_{\mathrm{i}} = \frac{\left[\mathrm{H_2N{-}R{-}S^-}\right][\mathrm{H^+}]}{[\mathrm{H_2N{-}R{-}SH}]} \qquad \text{(Equation III.1)}$$

The fraction of thiol in thiolate form may therefore be found from Equation III.2:

$$f_{\mathrm{RS^-}} = \frac{\frac{K_{\mathrm{i}}}{[\mathrm{H^+}]}}{\frac{K_{\mathrm{i}}}{[\mathrm{H^+}]} + 1} \qquad \text{(Equation III.2)}$$

The fit of the data for a penicillamine methyl ester to Equation III.2 is shown in Figure III.23 (labeled as: 2 pK_a + 3 Species NH_3^+). The poor fit of the data to Equation III.2 will be discussed below.

The second "Two pK_a + Three Species" model has the thiol pK_a below that of the ammonium such that two thiolate species (^+H_3N-R-S$^-$ and H_2N-R-S$^-$) may be present in solution (Scheme III.2).

Scheme III.2: "Two pK_a + Three Species" with the thiol pK_a (K_I) lower than that of the ammonium (K_{II}).

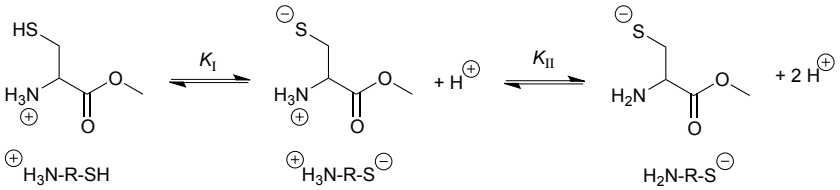

The concentration of both thiolate species at a given pH is therefore dependent upon the K_a of the thiol (K_I) (Equation III.3) and the K_a of the ammonium (K_{II}) (Equation III.4).

$$K_{\mathrm{I}} = \frac{\left[\mathrm{H_3N^+{-}R{-}S^-}\right][\mathrm{H^+}]}{[\mathrm{H_3N^+{-}R{-}SH}]} \qquad \text{(Equation III.3)}$$

$$K_{\mathrm{II}} = \frac{\left[\mathrm{H_2N{-}R{-}S^-}\right][\mathrm{H^+}]}{\left[\mathrm{H_3N^+{-}R{-}S^-}\right]} \qquad \text{(Equation III.4)}$$

The fraction of thiol in thiolate form may therefore be found from Equation III.5:

$$f_{\mathrm{RS^-}} = \frac{\frac{K_{\mathrm{I}}K_{\mathrm{II}}}{[\mathrm{H^+}]^2} + \frac{K_{\mathrm{I}}}{[\mathrm{H^+}]}}{\frac{K_{\mathrm{I}}K_{\mathrm{II}}}{[\mathrm{H^+}]^2} + \frac{K_{\mathrm{I}}}{[\mathrm{H^+}]} + 1} \qquad \text{(Equation III.5)}$$

The fit of the data for a penicillamine methyl ester to Equation III.5 is shown in Figure III.23 (labeled as: 2 pK_a + 3 Species SH). The fit of the data to Equation III.5 will be discussed below.

Figure III.23: The variation of the fraction of thiol in thiolate form, f_{RS^-}, as a function of pH for penicillamine methyl ester (0.2 mM) at 25 °C and ionic strength I = 0.3 M (NaCl). The fit of the data to the three possible pK_a and speciation models (Equation 4.2, Equation III.2 and Equation III.5) are shown.

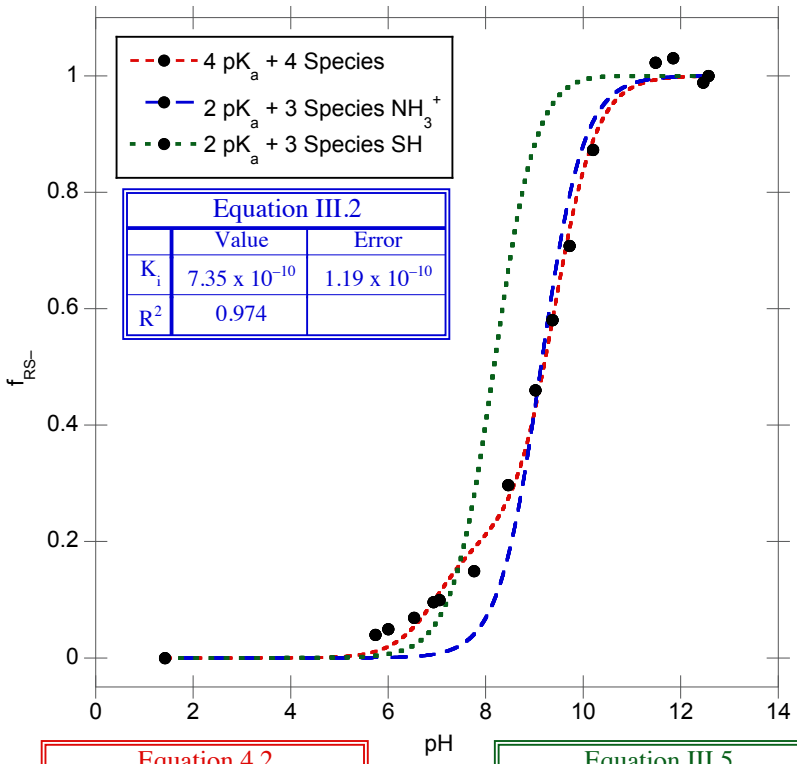

Equation III.2		
	Value	Error
K_i	7.35×10^{-10}	1.19×10^{-10}
R^2	0.974	

Equation 4.2		
	Value	Error
K_A	2.15×10^{-8}	7.33×10^{-9}
K_B	8.52×10^{-8}	3.98×10^{-8}
K_D	4.86×10^{-10}	4.49×10^{-11}
R^2	0.997	

Equation III.5		
	Value	Error
K_I	6.66×10^{-9}	5.06×10^{-9}
K_{II}	1.09×10^{-10}	1.62×10^{-9}
R^2	0.777	

The data for penicillamine methyl ester was chosen for Figure III.23 because it demonstrated one of the poorest correlations to the "Four pK_a and Four Species" model, particularly in the pH region 5.9 – 7.9. Figure III.23 confirms that the "Four pK_a and Four Species" model is superior to both of the "Two pK_a + Three Species" models as the R^2 value for the fit is higher (0.997 vs. 0.974 and 0.777). The "Two pK_a + Three Species" model with a single thiolate species (Equation III.2, K_i) has a better fit than that of the model with two thiolate species (Equation III.5, K_I and K_{II}). However, in the pH range 6.0 – 8.0 the fit of the "Two pK_a + Three Species" model with a single thiolate species is inferior to that of the "Four pK_a and Four Species" model. Attempts to fit the data of the other cysteine derivatives to either "Two pK_a + Three Species" models resulted in poor fits or in some cases failed to converge upon a solution.